A Study of Variability in the Ultraviolet Spectra of Galactic Wolf-Rayet Stars

by

Nicole St-Louis

A Thesis Submitted to
THE UNIVERSITY OF LONDON
for the Degree of
DOCTOR OF PHILOSOPHY

University College London November 1990

A mes parents

Abstract

The results of an archival search for ultraviolet spectroscopic variability of all galactic, single-lined Wolf-Rayet (WR) stars observed more than once with IUE are presented. At least 35 % of stars are found to be variable; a large proportion considering that, in many cases, the available datasets are not ideally suited for this type of study. For each star, spectra have been co-added to form a mean spectrum with an improved signal-to-noise. The resulting spectra are presented as and atlas of high resolution IUE spectra for 28 galactic WR stars.

A detailed study of the ultraviolet spectroscopic variability for the WR stars HD 192163 (WR 136) and HD 50896 (WR 6) has been conducted, using high resolution IUE spectra. For HD 192163, significant variability is found in the C IV λ1550, He II λ1640 and N IV λ1718 P Cygni profiles, over a period of $\sim$ 1 day. Enhanced absorption is observed at velocities exceeding the usual maximum wind outflow velocity. Weak variability is also detected in the emission components of the P Cygni profiles on a similar timescale as the variability found in the absorption components. In the case of HD 50896, variations are observed in the absorption and emission components of the N V λ1240, C IV λ1550, He II λ1640 and N IV λ1718 P Cygni profiles as well as for a series of Fe V and Fe VI lines. As for HD 192163, the changes in the absorption components occur at velocities in excess of the terminal velocity of the wind. As a result of the excellent time resolution of the dataset for this star, it has been established that the absorption component variability takes place on a timescale of $\sim$ 1 day and has a similar recurrence timescale. The variations found in the emission components have a smaller amplitude and occur on a much longer timescale, indicating that the mechanism causing the changes is not occurring on the scale of the wind but is much more localised. For both stars, the amplitude and character of the P Cygni profile variability is found to alter with epoch. In each case, it is concluded that the observed variations cannot be interpreted as effects of a compact companion orbiting in the dense stellar wind, and therefore, the ultraviolet variability does not support previous claims that these stars are WR + compact binary systems. Instead, the ultraviolet spectroscopic variability of HD 192163 and HD 50896 are considered to be intrinsic to the WR stellar winds. Models incorporating radiatively driven

wind instabilities are found to, at least qualitatively, account for the variations observed at the highest outflow velocities.

The line of sight towards HD 192163 and other stars in Cygnus has been investigated. High-velocity components have been detected in HI-type and highly-ionised species towards 10 out of 13 stars in the sample and are interpreted as arising in an expanding supershell enveloping the Cyg OB1 association.

A study of the phase-dependent ultraviolet variability observed in high resolution *Copernicus* and IUE spectra of the well-known WR+O spectroscopic binary γ Velorum is presented. Changes in the P Cygni profiles of resonance and low-excitation transitions are confirmed as being partly caused by selective eclipses of the O star continuum light by the WR wind. The appearance of a high velocity wing in the absorption component of N V λ1240, Si IV λ1396 and C IV λ1550, at phases when the O star companion is in front of the WR star, is attributed to the formation of a region of shocked gas, following the collision between the two stellar winds. A broad absorption in the eclipse spectrum between $\sim$ 1410–1910 Å is found to be due to a large number of Fe IV transitions and reveals that the density distribution of this ion in the wind of the WR star is asymmetric. A similar pattern of ultraviolet line profile variability is found in the binary systems V444 Cygni (WN5 + O5) and CV Serpentis (WC8 + O9).

Table of Contents

Errata

Page 59 : In Figure 2.3, the Si IV λ1402.770 component is plotted in the top part of the graph and the Si IV λ1393.755 component is plotted in the bottom part of the graph. Therefore, the labels need to be interchanged.

Page 203 : In Section 5.3.2.2, LWR 1359 should be changed for SWP 1359.

Page 204 : In the figure caption, LWR 1359 should be changed for SWP 1359.

Page 205 : In the figure caption, LWR 1359 should be changed for SWP 1359.

List of Tables

Chapter 5

UV Observations of Selective Wind Eclipses in γ Velorum

List of Figures

Chapter 4

New Results on the Ultraviolet Variability of HD 50896

Chapter 5

UV Observations of Selective Wind Eclipses in γ Velorum

Acknowledgements

First, I wish to thank my supervisor, Allan Willis, for his support and encouragement during the course of my Ph.D. studies and for providing me with the opportunity to work on such an interesting area of astronomy. It is also a great pleasure to thank Linda Smith; her guidance, patience and expertise are largely responsible for making this project a very gratifying experience.

I have benefited from many rewarding conversations with Ian Howarth and Raman Prinja. I also thank them for useful comments on parts of this thesis.

Many thanks to Paul Crowther for calculating line formation regions in the wind of HD 50896 and to Ian Stevens for providing me with a program to calculate the shape of the shock surface for colliding winds and for evaluating the expected X-ray flux for HD 192163. I also thank them for reading parts of this thesis.

I am especially grateful to René Doyon for his constant support and for many fruitful discussions.

Financial support from the Formation des Chercheurs at Aide à la Recherche of Québec and from the Physics and Astronomy department of University College London is gratefully acknowledged.

Preface

Since their discovery by C.J.E. Wolf and G. Rayet in 1867, our understanding of Wolf-Rayet (WR) stars has considerably improved. Quantities such as absolute visual magnitudes, chemical composition and mass-loss rates are now relatively well-known, although the tremendous complexity of the physical phenomena taking place in these stars renders the determination of other quantities such as effective temperatures or luminosities more controversial (for a recent review of Wolf-Rayet stars, see Abbott and Conti 1987). As our general knowledge of WR stars increased, more detailed aspects began to be explored. For instance, the advent of a new generation of scientific instruments capable of providing data with improved signal-to-noise and resolution revealed that a large proportion of WR stars showed variability, at varying degrees, in their continuum light and emission-line fluxes. Not all these variations can be attributed to effects in binary systems and therefore alternative interpretations have to be sought.

This work is concerned with various aspects of the variability observed in the ultraviolet spectra of galactic WR stars. As an introduction, Chapter 1 presents a brief review of the photometric, spectroscopic and polarimetric variability observed and predicted theoretically for WR stars. Most of the data employed in this work have been acquired with the *International Ultraviolet Explorer* (IUE) satellite. Over the past ten years, a large number of observations have been secured with this telescope which are made widely available to the international astronomical community through an extensive archive. In Chapter 2, the results of an archival search for spectroscopic variability for all galactic WR stars observed more than once with IUE are described. The aims are to provide a general description of the data already available in the archive at the time this work began and to try to assess the ubiquity of the phenomenon of ultraviolet spectroscopic variability of WR stars. The third and fourth chapters of this thesis consist of a study of ultraviolet variability in the spectra of the Wolf-Rayet stars WR 136 (HD 192163) and WR 6 (HD 50896), respectively. These stars have been suggested as candidates for WR + compact companion (neutron star or black hole) binaries. Such systems are expected to exhibit very distinctive phase-dependent changes in their ultraviolet P Cygni profiles. For both stars, an extensive set of IUE observations has been acquired with the specific aim of searching for variability. In each case, the variations are assessed

in order to determine if they can be ascribed to a compact companion and thus provide support for the binary hypothesis or alternatively if the changes are intrinsic to the WR star itself. In the latter context, the nature and timescale of the variability can help determine the mechanisms responsible and provide further insight into the basic physical properties of the hot and dense stellar wind. In the final part of this thesis, a different kind of variability is investigated. The behaviour, as a function of orbital phase, of the ultraviolet spectrum of the well-known WR+O binary, γ Velorum, is analysed. The mechanisms generating the changes are identified and information on the phenomena taking place in the binary system and on the chemical composition of the WR stellar wind is derived.

Chapter 1

Variability of Wolf-Rayet Stars

1.1 Observed Intrinsic Variability

In this section, I will present a brief summary of the variations observed in the light and spectra of Wolf-Rayet (WR) stars which are thought to be intrinsic to the star rather than caused by the effects of a companion in a binary system. Two reviews have previously been published on this subject, the first by Vreux (1987) and the other by Moffat and Robert (1991).

1.1.1 OPTICAL PHOTOMETRY

It is well known that some apparently single Wolf-Rayet stars show small scale (Δm $\sim$ 0.01–0.1) light variations at optical wavelengths. In the past, this has often been explained in terms of the presence of a compact companion. The occurrence of WR+compact binary systems has been theoretically proposed to represent one stage in the evolution of massive close binaries (see the review by van den Heuvel 1976) which can be illustrated schematically as follows:

$$O+O \longrightarrow WR+O \longrightarrow compact+O \longrightarrow compact+WR \longrightarrow compact+compact$$

Moffat (1982) has suggested a list of 11 candidate WR+c systems with periods in the range 2–10 days and low mass functions using the criteria that they show

optical light and spectral variations; have an unusually large z-distance and/or runaway velocity; and are associated with ring nebulae (ejected during a phase of rapid mass transfer from the O star to its compact companion). However, to date, none of these candidates have been reliably confirmed. Vreux (1985) has suggested that all the published periods, which are of the order of a few days, can easily be related to each other and thus could perhaps be attributed to non-radial pulsations. However, Matthews and Beech (1987) demonstrated that the periods are consistent with a random distribution and therefore, no observational evidence is currently available for non-radial pulsations occurring in Wolf-Rayet stars. The amplitude of the light curves and spectroscopic orbits of these candidates are often very low; the scatter around the curves cannot, in most cases, be accounted for by instrumental uncertainties and therefore, in any case, another process has to be invoked. More importantly, in most cases the periods suggested cannot be reproduced in subsequent datasets.

In recent years, it has been questioned whether the photometric variations observed in apparently single Wolf-Rayet stars can be attributed to effects in compact binary systems. In order to try to shed some light on the origin of these changes, several authors have carried out extensive photometric monitoring of groups or samples of Wolf-Rayet stars. Such studies have the potential of revealing general trends and patterns in the observed changes and thus provide new clues as to how they originate. Moffat and Shara (1986) have observed a complete magnitude-limited sample of 20 northern Wolf-Rayet stars including 6 well-established spectroscopic binaries. They find that at least half of the stars observed (in the B band) show continuum light variability with a amplitude of > 0.02 magnitudes. Excluding the predictable changes associated with the well known binary systems, they were not able to identify the source of the variations. However, they do remark that the WN 8 stars in their sample show the highest level of random noise. A similar result was found one year later by Lamontagne and Moffat (1987) who observed, in broadbands V and I, a group of 8 southern Wolf-Rayet stars that are known or suspected to show large photometric variations. These results suggest a singular characteristic of WN 8 stars compared to other subtypes. Over the years, it has been found that these stars show a number of distinctive properties such as narrower emission lines, strong P Cygni profiles (even in the optical), a higher runaway frequency and the fact that none has been found in a binary system (Moffat 1983). Lamontagne

and Moffat (1987) also reach broader conclusions. They find that in general the WN stars have a larger variation amplitude than the WC stars and that for both classes the amplitude increases towards later subtypes.

In a very high precision Walraven VBLUW photometric monitoring program of 7 Wolf-Rayet stars, van Genderen, van der Hucht and Steemers (1987) not only found light variations but also colour variations. They conclude that when the amplitude of the light variations is low (< 0.03 magnitude), the colour changes are difficult to detect but when the amplitude is higher, B-L,B-U and U-W colour variations are easily detectable with amplitudes between 5-10 times smaller than the light amplitudes. The B-L and B-U colours for many stars vary in phase with each other as a function of brightness (becoming bluer with increasing brightness) while U-W seems to show the opposite behaviour. The fact that the correlation between colour and brightness changes is so similar for stars of different spectral type, together with the fact that although the L and U bandpasses have the smallest content in emission lines, they show the largest variations, led the authors to conclude that the changes were continuum, not emission line variations. The authors suggest that they can probably be attributed to temperature effects such as hot blobs in the wind or eddies in a turbulent envelope allowing us to see deeper into the hotter layers.

Balona, Egan and Marang (1989) secured an extensive set of Johnson-B filter photometry of 17 of the brightest southern Wolf-Rayet stars over a period of three years. Only 5 stars in the sample were found to be constant. The authors found 3 cases of semi-periodic variations, or periods that are only temporarily present in the light curve. Their dataset was also appropriate for searching for very short timescale changes. Not a single case was found of such variations which could have been attributed to pulsations. However, short timescale changes have recently been detected by Monderen *et al.* (1988) and van Genderen, van der Hucht and Larsen (1990) for WR 46, WR 50 and WR 86. These stars were found to show variations with a timescale of $\sim$ 3 hours and a amplitude of 0.05–0.1 magnitude. For the two latter stars, the authors conclude that the changes are mainly caused by emission line strength variations while for WR 46 the main cause is thought to be continuum changes with emission line strength variations contributing only a few hundreths of a magnitude. In all three cases the time coverage was insufficient to determine if the variations are

strictly periodic, semi-periodic or completely irregular, which makes it difficult to suggest an origin or causes for the variability.

1.1.2 FLUX CHANGES AT OTHER WAVELENGTHS

Short timescale variability has been reported in the *Einstein* IPC X-ray flux of the WN 5 star WR 6 by White and Long (1986). However, formal statistical tests by Pollock (1989) on the data obtained in the hard energy band (0.8–4.5 kev), taking into account Poissonian statistics, have shown that the statistical significance of the variability is low. It is necessary to use Poissonian as opposed to Gaussian statistics in this case due to the low count rate of the sources. Pollock (1989) has also applied these tests to IPC observations of 8 other WR stars and found little evidence for variability on timescales from 200 seconds to a few thousand seconds. There was, however, one exception in a 1979 observation of WR 25 where a steady decrease in the intensity was observed on a timescale of $\sim$ 5000 seconds. The variations reported by Moffat *et al.* (1982) for WR 6 on a timescale of 3.8 days also turned out to be statistically significant at the few percent level. These variations are consistent with the period of 3.766 days often associated with this star, although the phase coverage in only $\sim$ 3 %.

Hogg (1989) has monitored the radio flux at 4885 MHz of five thermally emitting WR stars using the VLA between 1980 and 1987 with the aim of searching for variability. Also included in his study are the observations of Abbott *et al.* (1986) and Dickel, Habing and Isaacman (1980). For all five sources, the observations are found to be constant within 20 % of the mean value. For the four stars WR 6, WR 79, WR 134 and WR 136 no consistent pattern of change was found and therefore the sources are considered to be constant with variability greater than 20 % ruled out. For the WN7 star WR 78, however, a steady increase in the flux of 10 % per year was detected between 1981 and 1985, although the author does stress that this conclusion is tentative and that more observations are required to confirm the variability of this star at 4885 MHz.

1.1.3 OPTICAL SPECTROSCOPY

Reports of intrinsic wind variability observed in the strong optical emission lines of Wolf-Rayet stars have only recently begun to appear. This is mainly because of their very small amplitudes ($\sim$ 1 % of the total equivalent width) which requires extremely high signal-to-noise and spectral resolution. Moffat

et al. (1988) have monitored two bright Cygnus WR stars, WR 134 (HD 191765) and WR 136 (HD 192163), during one night in July 1986 over the spectral region covering the He II λ5411.524 transition. Although WR 136 showed little change during that night, several bumps were found superposed on the broad emission line for WR 134. These features have a width of FWHM$\approx$2–10 Å and a height $\leq$ 10 % of the continuum and move across the profile with a timescale of $\leq$ 8 hours. One important characteristic of these changes is that bumps that are initially redshifted with respect to the rest wavelength of the transition become even more redshifted with time whereas those that are initially blueshifted become even more blueshifted. Moffat *et al.* interpret the variations in terms of condensations of material or 'blobs' being accelerated outwards in the WR wind, with the timescale reflecting the time that wind material takes to flow through the He II emitting region. McCandliss (1988) in a more extensive study of WR 134 has obtained 152 spectra over a much larger spectral range (3940–6610 Å) and time period (12 nights). All the major lines in this spectral range were found to be variable. This includes the He II Pickering series, He II λ4200,4686, He I λ4471,5876, N IV λ4058, N V λ4945 and the blend of He II and N III at 4100 Å. The He II λ4686 line was found to vary the most and the variability in the Pickering lines increased with increasing wavelength. Hillier (1987) showed, in a model of the WN5 star WR 6, that the lower members of the Pickering series formed at progressively larger radii and that He II λ4686 line was formed even further out. By extending this to WR 134, McCandliss concluded that the outer regions of the wind were more variable than the inner regions and therefore predicted that the He II Pickering line at 10124 Å, which Hillier showed is formed approximately in the same region as He II λ4686 line, should show a particularly high level of variability. In addition to the narrow features moving across the broad emission line, McCandliss concluded that there were also non-periodic global line flux and line position variations. Finally, Underhill *et al.* (1990) have also found variations in the peak of the He II λ5411 and C IV λ5805 emission lines of WR 134, although they claim that they cannot detect any of the systematic changes found by Moffat *et al.* (1988) or McCandliss (1988). They interpret their observations in terms of a rotating wheel-like structure in which the "spokes" consist of filamentary tubes of plasma.

For WR 134, Moffat and Robert (1991) have compared the observed variation of the velocity of the narrow features as a function of time with model predictions. These were evaluated by assuming that the 'blob' ejection is radial and that the inhomogeneities follow a velocity law of the form $v_w = v_\infty(1 - R_*/r)^\beta$ where v_∞ is the terminal velocity of the wind and R_* is the radius of the WR core. A blob ejected at an angle θ with respect to the direction towards the observer would therefore be detected at a velocity of $v = v_w cos\theta$. Comparing the predicted and observed values can in principle yield the ejection angle and β if one assumes values for v_∞ and R_*. They conclude that, as expected, the blobs seem to be emitted at random angles but that their progression cannot be described by a velocity law with $\beta \approx 1$, as generally expected for winds of hot stars. They speculate that this is either because the regions of the wind probed by the blobs have larger β values or that the blobs are simply moving more slowly than the wind.

1.1.4 ULTRAVIOLET SPECTROSCOPY

As mentioned in Section 1.1.1, the interpretation of radial velocity and photometric variability of single-lined Wolf-Rayet stars in terms of the presence of a compact companion (neutron star or black hole) had become increasingly popular in the first half of the 1980s. Confirmation of the existence of such companions for WR stars was therefore actively sought. One observational consequence of a compact companion orbiting in the dense WR wind was suggested theoretically by Hatchett and McCray (1977). The accretion of wind material onto the neutron star produces a high X-ray flux, which will ionise the gas in a region around the X-ray source to higher ionisation stages. This could have an observable effect on the ultraviolet P Cygni profiles of resonance lines such as N Vλ1240, C IV λ1550 and Si IV λ1396. When the companion is in front of the WR star, the material giving rise to the absorption component is affected. The reduction in the number of scatterers should cause a weakening of the absorption. At opposite phases, the normal state of the wind is restored and the P Cygni absorption reflects once again the undisturbed wind density and velocity structure. Such changes were subsequently observed with IUE in several massive X-ray binaries (*e.g.* for Vela X–1 by Dupree *et al.* 1980) confirming the basic Hatchett and McCray model for such systems. In complementary programmes, extensive datasets of IUE ultraviolet high resolution spectra have

been secured for two WR+c candidates, WR 6 (HD 50896) and WR 40 (HD 96548) to search for variability akin to the Hatchett and McCray effect.

WR 40 is a WN8 star which was suggested as a WR+c candidate by Moffat and Isserstedt (1980). From an extensive narrow-band photoelectric photometry and optical photographic spectroscopy dataset, they proposed an orbital period of 4.762 days with a semi amplitude of 0.02 magnitude in the light curve and of 8–10 km s^{-1} in the radial velocity curve. Smith, Lloyd and Walker (1985) presented a study of 14 archival IUE high resolution spectra obtained between 1979–1982. The spectra contain many emission lines and P Cygni profiles from ions ranging from Fe II to N V. Variability was found in *all* the emission lines although the largest changes were observed in the absorption components of the C IV λ1550 and Si IV λ1396 resonance doublets. The variations were, however, inconsistent with the proposed orbital period although more data were required to confirm this assertion. Additional observations were obtained in 1983, 1985 and 1986 and a preliminary analysis of the data was presented by Smith *et al.* (1986). In contrast with the earlier archival spectra, only the Si IV λ1396 and N IV λ1718 lines were found to show significant variability. This strongly suggests that the changes in the ultraviolet spectra are epoch dependent. The nature of the changes were also quite revealing. The blue absorption edge of the Si IV P Cygni profile was found to gradually decrease by 400 km s^{-1} over a five day period in 1985. This corroborated the earlier claim that the variations do not have the required phase-dependence to be caused by the Hatchett and McCray effect. Instead, the authors suggest that the changes are more likely caused by intrinsic variations within the WR stellar wind.

WR 6 (HD 50896) is presently the best candidate for a WR+c system mainly because of the well-established 3.766 day period often associated with it. This periodicity was first announced by Firmani *et al.* (1980) in a set of photometric and spectroscopic observations and McLean (1980) using polarimetry, but was later refined by Lamontagne, Moffat and Lamarre (1986) using five years of optical photometry. WR 6 has been very extensively observed at high resolution with IUE. Observations have been obtained over several epochs including an extensive sequence of 46 spectra over 7 consecutive days in September 1983. These data were discussed by Willis *et al.* (1989) with a preliminary analysis presented a few years earlier (Willis *et al.* 1986a). Substantial variability has been found in the absorption and emission components of the N V λ1240,

C IV λ1550, He II λ1640 and N IV λ1718 P Cygni profiles as well as in numerous other lines which are thought to be blends of Fe IV and Fe V transitions. One feature that immediately became clear was that the ultraviolet variations were epoch-dependent. While spectra obtained at random epochs showed large scale differences, the extensive 1983 dataset appeared to reflect a relatively quiescent period. The changes that were found are mainly confined to the P Cygni absorption components, in particular to the soft blue edge. Willis *et al.* (1989) suggested a (poorly-determined) ultraviolet variability timescale of ~ 1 day, with some evidence for time-delay effects in different ions, possibly resulting from stratification effects. No significant phase-dependence was found and therefore the changes could not be ascribed to the Hatchett and McCray effect. As for WR 40, the ultraviolet variability is thought to be intrinsic to the WR wind, probably caused by changes in the wind, density or ionisation structure.

1.1.5 LINEAR POLARIZATION

Intensive monitoring of Wolf-Rayet stars in visible linear polarization has only recently been started. The first survey of variability in the polarized light of WR stars was presented by St-Louis *et al.* (1987), Drissen *et al.* (1987) and Robert *et al.* (1989). For single stars, the variability is always found to be stochastic in nature with no significant periodicity. Therefore these changes are thought to be intrinsic to the dense WR wind. The winds of WR stars are strongly ionised and thus contain a large number of free electrons which can polarize the starlight through single Thomson scattering of photons. For a completely uniform and spherically symmetric electron density distribution with the illuminating star at the centre, there will be no net polarization but any asymmetry in the position of the light source or in the density distribution will yield a net polarization. This is thought to be the main cause of polarization in WR winds. Such a process should produce wavelength-independent polarization; a confirmation that this is the case for WR star polarization variations is presented by Robert and Moffat (1989). This study also ruled out electrons gyrating in a magnetic field as a cause for the changes, due to the complete lack of variations in circular polarization ($\Delta V/\Delta P \leq 0.06$) while large changes in linear polarization are observed. The main conclusion of this initial survey, in the case of single stars, was that for the 26 stars studied, the faster WR winds show the smallest amplitudes of intrinsic variations. A relatively tight correlation with spectral type was also found; WN stars in general have

larger amplitudes than WC stars and in a given subclass the later spectral types (WN8 and WC9) are found to present the largest variations. The changes were interpreted as ejection of mass-conserving blobs of material at random angles in the wind. Following the work of Owocki, Castor and Rybicki (1988), Robert *et al.* (1989) have attempted to understand the changes in terms of radiative instabilities that would create a blob-like structure. The polarization dispersion was assumed to be proportional to $e^{k(\overline{v}/v_{th})}$ with $\overline{v}$ the velocity of the wind at the radius where τ=1, v_{th} is the thermal velocity and k is a constant. This is similar to that which Owocki, Castor and Rybicki (1988) derived for a velocity amplitude growth. Unfortunately, uncertainties in parameters such as the mass loss rate, the stellar radius and the thermal and terminal velocities hindered a definite conclusion on the validity of this model. They have also tried another model based on the assumption that the growth rate of the perturbation is proportional to the magnitude of the perturbation. They find that this works well but that uncertainties in WR star parameters are still a limiting factor. Finally, it is worth mentioning that these polarization measurements are not capable of distinguishing between mass-conserving blobs or disturbances in the velocity or ionisation structure of the wind and therefore this latter interpretation should also be taken into account.

Schulte-Ladbeck and van der Hucht (1989) have monitored four Wolf-Rayet stars of which two were found to show variability. For one of these stars, WR 151, the changes are attributed to the fact that the star is a binary while in the other case, WR 103, the variations are thought to be intrinsic to the WR wind. These authors suggest that the polarization variability is associated with the photometric variability; the main layer in which most of the continuum is formed has dynamical instabilities resulting in the formation of temporarily hotter eddies or blobs. This in turn produces the variable linear polarization.

1.2 Theory of Intrinsic Variability

In this section, I will present a short outline of the current state of the theory for the three main processes capable of generating the intrinsic variability of Wolf-Rayet stars.

1.2.1 RADIATIVELY DRIVEN BLOBS

The propagation or ejection of mass-conserving inhomogeneities or blobs of wind material has been suggested by some authors as the origin of intrinsic wind variability. A model for the wind of hot stars including such a population of blobs was proposed by Lucy and White (1980). Initially, this model was developed to explain the X-ray emission from the wind of hot O and B stars as well as the presence of relatively high ionisation stages such as O VI and N V. The basis of the model is the unstable nature of line-driven flows which are thought to be the dominant process for driving the O, B and WR stellar winds. This unstable nature is a consequence of the sensitive dependence of the line-force on velocity. In such a case, a small increase in the radial velocity of an element of gas with respect to the surrounding medium shifts the local line frequency out of the absorption shadow of intervening material and therefore increases the line force. This will increase the velocity of the element even further leading to an instability. Lucy and White suggested that as a consequence of the instability, the final state of the stellar wind could be described as a number of radiatively driven blobs moving through the ambient gas which is not itself radiatively driven because it is shadowed by the blob population. This component nevertheless flows away from the star because of the drag force between the blobs and the ambient gas. The shocks preceeding these blobs emit the required X-rays in their cooling zones.

More recently, Antokhin, Kholtygin and Cherepashchuk (1988) have calculated the ionisation structure of a WR wind and claim that the simultaneous existence of regions with different ionisation states is only possible for a restricted range of core temperatures, which is inconsistent with the present observations. They therefore suggest that the wind is divided into a large number of blobs of higher density than the ambient medium, which can easily accommodate the simultaneous existence of several ionisation states over a wide range of temperatures.

Finally, it is worthwhile mentioning that ejection of mass-conserving inhomogeneities was not found to be a suitable interpretation for the narrow absorption components seen moving across the Si IV resonance profile of the O star 68 Cygni [O7.5 III((f))] by Prinja and Howarth (1988). In a study of three well-monitored consecutive sequences of progressive opacity enhancements, they found that the propagation of the blob would follow a very slow velocity law and predict that substantial absorption features should be detected at velocities much smaller than are actually observed. Therefore, they conclude that blob ejection is inadequate to explain their observations. Instead, they suggest that wind material is passing *through* perturbations in the flow. Although the variations found for O star winds are not exactly the same as those observed for WR stars, it is judicious to bear in mind the results of studies of intrinsic variability in the winds of O stars. As they are the progenitors of WR stars and both types of stars probably have the same wind driving mechanism, it is not unreasonable to expect similar processes generating the changes.

1.2.2 RADIATIVE INSTABILITIES IN LINE-DRIVEN FLOWS

It is generally accepted that the driving mechanism for the winds of O, B and WR stars is line-scattering of the star's continuum radiation flux. Because of the unstable nature of this process, described in Section 1.2.1, these winds are expected to be highly structured and variable rather than smooth and constant as is usually assumed in steady state models. There is some observational evidence suggesting that this is indeed the case. Besides the fact that observed variations in the light and spectra of WR stars are increasingly being interpreted as intrinsic to the star, some properties of these flows such as superionisation, X-ray emission, non-thermal radio emission and black absorption troughs are difficult to explain in uniform line-driven outflows. The first linear stability analyses were based on simple assumptions and led to very different conclusions. MacGregor, Hartmann and Raymond (1979) and Carlberg (1980) assumed that the perturbations were optically thin and neglected the dynamical effect of the diffuse radiation field. This leads to a perturbed force which is proportional to the perturbed velocity, $\delta g_{abs} \propto \delta v$, and thus the flow is unstable as the net work done by the force amplifies the velocity perturbation. Abbott (1980) also neglected the diffuse radiation field but assumed that the perturbation followed the Sobolev approximation, $\delta g_{abs} \propto \delta v'$. In this case, there is a 90° phase difference between the perturbed force and velocity and therefore the perturbation

is stable. Owocki and Rybicki (1984) solved this apparent discrepancy by presenting a linear stability analysis in which they made no assumptions about the behaviour of the perturbed force, although they still neglected the effect of the diffuse radiation field. They found that the perturbed force could be expressed as :

$$\delta g_{abs} = \Omega_b \frac{ik}{\chi_b + ik} \delta v$$

where Ω_b is the instability growth rate, k is the wavenumber and $\chi_b^{-1} \simeq$L/2 with L being the Sobolev length. Therefore, for long-wavelengths ($k \ll \chi_b$) this equation is equivalent to Abbott's expression using the Sobolev approximation and thus the flow is stable while for short-wavelengths ($k \gg \chi_b$) the expression is equivalent to making the optically thin approximation and thus the flow is unstable. The growth rate of these instabilities was found to be so large (cumulative effect of 100 e-folds through the wind) that any small linear perturbation in the wind would rapidly become nonlinear.

The possible dynamical effect of the diffuse radiation field was first investigated by Lucy (1984). He concluded that in contrast to what occurs in the mean flow in which the diffuse radiation has a roughly fore-aft symmetry and therefore exerts no net force on the flow, the diffuse radiation field exerted a net drag force on the perturbations. Owocki and Rybicki (1985) have studied the magnitude of this effect by considering a diffuse field with complete redistribution and a Doppler profile. They found that at the base of the wind, where the flow can be considered as plane parallel, the instability growth rate is greatly reduced but that as the flow moves outwards, the effect decreases rapidly. At 1 R_*, the growth rate is 50 % of its value in the case of pure absorption and at large radii it can reach almost 80 % of its approximate value. Another conclusion which they have reached in this study is that the diffuse radiation field tends to dampen horizontal velocity perturbations. Therefore, in general, the instability problem can be reduced to one dimension (radial direction) which greatly simplifies the calculations.

Efforts have been made to include these instabilities in simple wind models. Lucy (1982) presented a model in which the structure of the wind was assumed to consist of a series of forward shocks. Consequently, the velocity structure of the wind had a ramped sawtooth character. In this model, the fast material is pushed against the slow material which gives rise to a shock. This shock sweeps up and accelerates the slow material and therefore the post-shock

flow can be characterised by high velocity material at high density and high temperature. One appealing feature of this model is that it naturally explains the saturated or 'black' P Cygni absorption components observed in the spectra of hot stars. In uniform line-driven flows, the absorption component is partially filled in by forward scattered radiation received from the wind's approaching side. Lucy (1982) found that a wind with the assumed structure preferentially *backscatters* photospheric radiation. Therefore the forward scattered radiation is greatly reduced and the absorption components are not filled in. This model has, however, the disadvantage of not being set on a solid physical base, as the structure of the wind is hypothetical. Owocki, Castor and Rybicki (1988) have developed a numerical, radiation-hydrodynamics code that simulates the evolution of instabilities in line-driven flows and therefore determines the likely structure of the resulting wind. In contrast with Lucy's model, they found that the strongest shocks are *reverse* shocks which decelerate high-speed, rarefied gas as it impacts onto slower material which has been compressed into denser shells. Therefore, in this model, the high speed material has a very low density which is the opposite of what is found in Lucy's model.

In their wind model, Owocki, Castor and Rybicki (1988) introduced an explicit perturbation at the base of the wind and examined its evolution as a function of time. However, Owocki, Poe and Castor (1990) and Poe, Owocki and Castor (1990) have shown that line-driven flows can be *intrinsically* variable. This property was found to depend on the ratio of the thermal speed to the sound speed (v_{th}/a). For $v_{th}/a \lesssim 1/2$, there exists a well defined steady solution which allows a time-dependent model to relax to the associated state and thus to become stable. For $v_{th}/a \gtrsim 1/2$, a whole series of solutions exists and therefore the wind never settles down. Instead, it oscillates continuously among the degenerate family of possible steady solutions. The timescale for this oscillation is $\sim 1/2$ day which is much longer that the growth time for individual small scale instabilities ($\sim$ 1 hour). This, however, compares well with the propagation timescale for narrow absorption components observed in the saturated P Cygni absorption components of O stars.

1.2.3 RADIAL AND NONRADIAL PULSATIONS

As evidence accumulated for an intrinsic rather than binary-related origin for the variability observed in the light and spectra of several Wolf-Rayet stars, some authors began to suggest that pulsations might be a possible source for the

variations. This, together with the suggestion that pulsations might contribute to the driving of the WR wind, led to a series of theoretical investigations into the vibrational instability of WR stars in various phases of evolution.

Maeder (1985) presented a study of the vibrational stability to radial pulsations of very massive stars (85 $M_\odot$ and 120 $M_\odot$) through various evolutionary stages, using observed mass-loss rates. For WR stars, he found that the nuclear energizing of the pulsations in the central He-burning core largely dominated the radiative damping in the envelope and therefore that WR stars are vibrationally unstable to radial modes. This unstable phase begins when the hydrogen to helium ratio at the surface is H/He=0.3 and remains throughout the subsequent WR evolutionary stages. Processes such as overshooting, turbulent diffusion or mixing by nonradial oscillations would enhance even further the vibrational instability. However, the periods predicted by Maeder's models were relatively short (15–60 minutes) and did not correspond to the timescales of the observed variability. Noels and Scuflaire (1986) suggested that one way to reduce the discrepancy was to consider g^+ modes of nonradial pulsations. They investigated this type of instability for a 100 $M_\odot$ star in the adiabatic case and showed that there existed a vibrational instability towards nonradial pulsations starting after the exhaustion of H in the centre but when H-burning still remained in a shell, distant from the centre. Although the predicted periods of several hours were generally in agreement with some of the observed timescales, the duration of the unstable phase was so short ($\sim$ 6000 years) that it was doubtful that it could be responsible for the observed variability. Recently, Cox and Cahn (1988) have made more accurate nonadiabatic calculations for a series of representative radial and nonradial pulsational modes of 5 WR star models. Although Maeder's conclusions remained correct for radial oscillation modes, Cox and Cahn found no unstable nonradial modes, in contrast with Noels and Scuflaire's work. They suggest that this is probably a result of the quasiadiabatic approximation in the hydrogen shell burning region which is not valid during pulsations.

In conclusion, it appears that only radial pulsations can be invoked to explain intrinsic variability of WR stars. Therefore, only very short timescale changes ($<$ 1 hour) could be attributed to this mechanism. As the observed timescales are generally much longer, it is clear that some other process in playing a major role in the production of the variability. Finally, despite the fact

that radial modes are possible for WR stars, it is not clear how the extended non-static wind will respond to the inner oscillations. Perhaps this type of variability will be very difficult to observe. Only with very high time resolution datasets will we be able to ascertain if pulsations are a significant contributor to the intrinsic variability of WR stars.

1.3 Binary Related Changes

In this section, both observational and theoretical aspects of the variations of WR stars caused by the presence of a companion will be discussed. This is not intended as a complete review of the subject, which is very broad, but rather as a brief overview of the most important topics.

1.3.1 OPTICAL PHOTOMETRY

For any type of binary system with a sufficiently large orbital inclination, there will be eclipses of the continuum emitting cores of the two stars. For WR+O binaries, the O star light can also be eclipsed by the dense WR envelope. Kopal and Shapley (1946) were the first to attempt to study the nature and structure of absorption processes in the extended WR winds, using phase-dependent variations in optical photometry. For the well-known WR+O binary V444 Cygni, they found that the opacity causing the continuum variations increased towards the centre of the WR star but they were not able to detect a sharp core larger than 11 $R_{\odot}$. Consequently, they concluded that the opacity was caused by a large envelope and they went on to suggest that the dominant effect was scattering by free electrons. This led them to predict that the primary eclipse would be wavelength independent which was later confirmed by Hiltner (1949).

Since these pioneering efforts, many individual WR+O optical light curves have been secured. Moffat and Shara (1986) have obtained observations for a complete magnitude-limited sample of northern Wolf-Rayet stars and found that all well established binaries in their sample had a light curve with a minimum at phase 0.0, when the WR star is in front of the O star. For the truly core-eclipsing systems, two light minima are observed separated by 0.5 in phase (for circular orbits). In this case, the dips are found to be relatively deep and sharp. Lamontagne *et al.* (1991) have studied all galactic WR+O systems for which only one minimum at phase 0.0 is observed in the light curve. They have developed a simple model in which the light from the companion is scattered by

free electrons in the WR wind. As the O star orbits to the far side of the WR wind, the line of sight crosses an increasingly large column density of electrons and thus the opacity increases. The optical depth in this case is given by a relatively simple expression:

$$d\tau = \sigma_e n_e(r) dz$$

where σ_e is the Thomson electron scattering coefficient and $n_e(r)$ is the electron density. By using the equation of mass conservation $\dot{M} = 4\pi r^2 \rho(r) v(r)$ and a parametric velocity law of the form $v(r) = v_\infty(1 - R_*/r)^\beta$, the optical depth integrated over the line of sight is given by

$$\tau = \int_{z=z_0}^{\infty} \frac{\alpha \sigma_e}{4\pi m_p v_\infty} \frac{\dot{M}}{r^2(1 - R_*/r)^\beta} dz$$

where α is the number of electrons per baryon mass and $z_0 = -(a\,sini)cos2\pi\phi$, with ϕ being the orbital phase. Therefore, the shape and amplitude of the minimum yields estimates of $\dot{M}$ and i.

Lamontagne *et al.* (1991) have presented fitted light curves for all non-core-eclipsing WR binaries for which optical photometry is available and with orbital periods < 30 days. The mass-loss rates determined from these fitted curves show a general trend with spectral type, in the sense that more luminous stars have higher mass-loss rates, in agreement with previous results (Abbott *et al.* 1986, St-Louis *et al.* 1988).

1.3.2 PHASE-DEPENDENT PHOTOMETRIC CHANGES AT OTHER WAVELENGTHS

The great majority of WR+O binary systems have been discovered by the detection of periodic variability in photometric or spectroscopic observations at optical wavelengths. One remarkable exception has been the Wolf-Rayet system WR 140 (HD 193793). It was known as early as 1947 that absorption lines are present in the spectrum of this star and that they show a significant range in radial velocities, although no periodicity could be established (McDonald 1947). Lamontagne, Moffat and Seggewiss (1984) presented an optical radial velocity orbit with a period of ~ 3 years but this was not reproduced in the dataset of Conti *et al.* (1984) and thus was considered to be spurious. Williams *et al.* (1978) reported an increase in the infrared flux of WR 140 between 1976 and 1977 which they attributed to the formation of a 4 $\times 10^{-8}$ $M_\odot$ shell of graphite dust grains. A new shell was observed to be forming in 1985 (Williams

and Smith 1985) which lead Williams *et al.* (1987) to suggest that these events were cyclic with a period of $\sim$ 7.9 years and that they were most likely a consequence of orbital motion. Moffat *et al.* (1987) re-analysed all the optical radial velocity observations and confirmed that WR 140 was a WR+O binary with an extremely high eccentricity ($e = 0.7 - 0.8$).

Williams *et al.* (1990a) presented a summary of most infrared, X-ray, radio and optical observations previously published together with new observations at infrared, X-ray and radio wavelengths. An analysis of the now extensive dataset of infrared photometry yielded a period of P=2900$\pm$10 days which they then used to re-analyse all the optical radial velocities and provide improved estimates of the orbital elements of this system. WR 140 is the strongest X-ray emitting WR star, with a flux two orders of magnitude higher than usually observed from normal emission in hot star winds. This strongly suggests the presence of a X-ray producing shocked region between the two stellar winds. The variability in the X-ray flux is consistent with varying free-free extinction as a consequence of the changes in ion and electron column densities along the line of sight as the O star orbits through the dense WR wind. The authors used this varying circumstellar extinction together with the orbital parameters to determine a fractional carbon abundance in the wind of n_C $\sim$0.06. The radio flux was found to consist of two components, the normal free-free emission from the WR wind and a non thermal source which, as the X-ray flux, suffers varying amounts of attenuation with orbital phase. However, they were not able to reconcile the observations with an isotropic WR wind and suggest that the discrepancy is caused by the presence of a low density cone in the shadow of the O star in which the extinction is much smaller than in the undisturbed WR wind.

In summary, in the case of WR 140 the infrared photometry was crucial in establishing the binary nature of this star. As extensive observations already exist, this type of data can also be used to improve the period and for measuring more precisely the duration of the dust formation process by obtaining a new set of observations during the next predicted event. Finally, it is worth mentioning that X-ray observations of such binary systems provide an independent means of determining the chemical composition of WR winds and that radio observations can provide information on the density distribution. Two other candidates for

this type of binary system, WR 48a and WR 137, have been suggested but more systematic observing is required to establish their exact nature.

1.3.3 ULTRAVIOLET SPECTROSCOPY

Phase-dependent variations in the intensity of spectral features in the ultraviolet have been detected for 3 WC+O and 5 WN+O binary systems. The changes are observed in a large number of transitions and are typically described as a gradual strengthening of the absorption components of P Cygni profiles accompanied by a weakening of emission features when the bright O-type companion orbits to the far side of the dense WR wind. The most widespread interpretation for these changes is that the WR wind absorbs or scatters the O star light at wavelengths corresponding to transitions in which the lower level is sufficiently populated. The effect becomes stronger as the O star moves to the back of the WR wind because the light beam encounters an increasingly larger column density of material. Alternative interpretations have also been put forward. Kuhi (1968) explained changes in the optical emission lines of V444 Cygni by suggesting that the distribution of emitting atoms in the WR envelope was asymmetric, *i.e.* that the part facing the O star was considerably brighter as a consequence of gas flowing through the Lagrangian points of the gravitational equipotentials. Another interesting suggestion is that of Shore and Brown (1988) and Brandi, Ferrer and Sahade (1989) in which wind material being accelerated to high velocities along a shock front caused by the interaction between the two stellar winds is invoked to explain some aspects of the variability.

The detailed study of such phase-dependent spectral line variations has the potential of yielding valuable information on the structure and composition of Wolf-Rayet winds. The ultraviolet wavelength range includes a great wealth of spectral features which is a definite advantage in this type of study. Resonance lines such as C IVλ1550 and Si IVλ1396, that can originate in relatively low density gas, provide information on the outer regions of the wind while excited transitions such as He IIλ1640 and N IVλ1718 probe higher density regions closer to the core. The presence or absence of variations in these various spectral lines provides information on the actual location of the changes within the envelope.

The three WC+O systems for which ultraviolet phase-dependent variations have been reported are γ Velorum (WC8+O9 I, Willis and Wilson 1976 and

Willis *et al.* 1979), CV Serpentis (WC8+08-09IV, Howarth, Willis and Stickland 1982 and Eaton, Cherepashchuk and Khaliullin 1985a) and HD 97152 (WC7+O7V, Auer, Colomé and Koenigsberger 1988). Most of these studies are based on low resolution IUE spectra with the exception of the earlier work of Willis and Wilson (1976) in which spectra from the S2/68 experiment were used. Changes were detected in a large number of isolated transitions from a wide variety of ions including He II, C II– IV and Si II– IV. In addition to these well identified individual lines, Eaton, Cherepashchuk and Khaliullin (1985a) reported a broad depression in the eclipse spectrum of CV Serpentis around 1200–1470 Å which they interpreted as being caused by a large number of Fe IV transitions between the $d^4 4s$ and $d^4 4p$ levels. They proposed that the lower level may be populated by ultraviolet radiation near 500 Å which would provide evidence for the existence of radiation below the Lyman limit. A similar broad absorption was also detected for HD 97152 by Auer, Colomé and Koenigsberger (1988).

Koenigsberger and Auer (1985) (see also Auer and Koenigsberger 1982) were the first to report phase-dependent ultraviolet spectroscopic variations for WN binaries. Using an extensive set of low resolution IUE spectra, they find changes for the 5 WN+O systems V444 Cygni, HD 90657, HD 94546, HD 186943 and HD 211853. The authors detect variations in all major P Cygni profiles which are of similar nature and amplitude for all systems, which include WR stars of spectral types ranging from WN 4 to WN 6. This strongly suggests a common origin for the changes observed in the five systems. Using the flux measured in the N IVλ1718 line at various orbital phases, they derived an optical depth distribution of the form $\tau \propto r^{-1}$ for $r > 14\ R_\odot$. Koenigsberger and Auer (1985) also report that the "continuum" shortward of $\sim$ 1500 Å is depressed at phases when the O star is behind the WR wind. As in the case of WC binaries, they interpret this as being caused by a large number of Fe lines although this time Fe V and Fe VI lines are invoked. Another interesting result from this work is that the C IVλ1550 emission shows a decrease in intensity at phases when the WR star is in front while at the same time the absorption component becomes narrower instead of broader. This was interpreted as evidence of wind-wind interaction; the WR outflow, which is much more massive, dominates the O star wind in the region between the two stars preventing it from reaching its maximum velocity. Therefore, we can only see the full extent of the O star

wind when the O star is in front of the WR star. Note that there was no mention in this study of the formation of a shock front. It would be surprising if this did not occur in view of the high density of the two stellar winds as well as their relative velocities. The study of Koenigsberger and Auer (1985), although including 5 stars, was mainly concentrated on the N IVλ1718 line. Eaton, Cherepashchuk and Khaliullin (1985a) simultaneously examined one of these 5 binaries, V444 Cygni, but included all spectral lines. They concluded that the material generating the opacity in the WR wind was distributed in shells with the central hole being caused by the fact that the upper levels of the transitions are being populated which increases stimulated emission and reduces the optical depth. This requires temperatures of $\sim 10^5$ K which would be sufficient to drive the dense stellar wind.

The discovery of Fe as a source of opacity in the winds of galactic WR stars led to the study of WR binaries in the Small Magellanic Cloud (SMC). As radiation pressure depends on heavy element abundances, an analysis of WR winds in different metallicity environments may provide information on the role radiation pressure plays in driving these winds. Koenigsberger, Moffat and Auer (1987) obtained low resolution IUE spectra of the SMC binary HD 5980 (WN4+O7I:). They find selective atmospheric eclipses in transitions of N IV$-$V, He II and C IV of similar amplitude as in galactic WN binaries but they do not detect any changes < 1500 Å. This is most likely the result of the lower heavy element abundances in the SMC. Similar results were found for the WO binary Sk 188 (WO4+O4V) by Koenigsberger, Moffat and Auer (1988) and Moffat, Koenigsberger and Auer (1989).

Clearly, a large amount of valuable information on the composition, structure and nature of WR stellar winds can be deduced from the detailed study of phase-dependent changes in the ultraviolet. Much more observational and theoretical work is necessary for development of this relatively young field.

1.3.4 POLARIMETRIC VARIATIONS

As mentioned in Section 1.1.5, the large number of free electrons present in WR winds will linearly polarize the light from the star through simple Thomson scattering of photons. For a single WR star with a spherically symmetric and highly uniform wind, no net linear polarization will be observed, as the contributions from all the electrons cancel out. In the case of a WR+O binary, the O star constitutes an additional illuminating source with respect to

which the electron density distribution (WR wind) is highly asymmetric. This will produce significant levels of polarization which will change with orbital phase as the companion orbits the WR wind. The basic theory describing these phase-dependent variations has been developed by Brown, McClean and Emslie (1978). These authors have derived the following general expressions for the normalised Stokes parameters of linear polarization (Q,U) as a function of orbital phase Φ $(=\lambda/2\pi)$:

$$Q = \tau_0(1-3\gamma_0)sin^2i + (\tau_0\gamma_1 sin^2i)cos\lambda + (-\tau_0\gamma_2 sin^2i)sin\lambda$$
$$+ (-\tau_0\gamma_3(1+cos^2i))cos2\lambda + (\tau_0\gamma_4(1+cos^2))sin2\lambda$$
$$U = (2\tau_0\gamma_2 sini)cos\lambda + (2\tau_0\gamma_1 sini)sin\lambda$$
$$+ (-2\tau_0\gamma_4 cosi)cos2\lambda + (-2\tau_0\gamma_3 cosi)sin2\lambda$$

where i is the orbital inclination, τ_0 is the effective Thomson optical depth integrated over all directions and ($\tau_0\gamma_1, \tau_0\gamma_2, \tau_0\gamma_3$ and $\tau_0\gamma_4$) are the four moments over the density distribution. Therefore, by fitting expressions of the form:

$$Q = q_0 + q_1 cos\lambda + q_2 sin\lambda + q_3 cos2\lambda + q4 sin2\lambda$$
$$U = u_0 + u_1 cos\lambda + u_2 sin\lambda + u_3 cos2\lambda + q4 sin2\lambda$$

to observed normalized Stokes parameters as a function of orbital phase, information on the density distribution of the electrons as well as the orbital inclination can be obtained. The determination of the orbital inclination is of crucial importance for the evaluation of the masses of the Wolf-Rayet stars in WR+O binaries as for non-eclipsing systems, only the minimum masses ($Msin^3i$) are available from the spectroscopic data.

Although this type of analysis has been applied for many years to isolated WR binaries, intense monitoring of such systems have only recently begun to be carried out (St-Louis *et al.* 1987, 1988; Schulte-Ladbeck and van der Hucht 1989; Robert *et al.* 1989, 1990). Evidence that these binary-type polarization variations are wavelength independent (Luna 1982; Piirolla and Linnaluoto 1988) as well as a complete lack of associated circular polarization variations, strongly support electron scattering as the source of polarization.

One application of the basic theory developed by Brown, McClean and Emslie is a new way to derive the mass-loss rate of WR stars ($\dot{M}_{WR}$) in binary systems (St-Louis *et al.* 1988). This method is based on the fact that the amplitude of the linear polarization variations (A_p) is related to the electron

density and thus to the mass-loss rate of the WR star. Using the mass conservation law $\dot{M} = 4\pi r^2 \rho(r) v(r)$ and a parameterised wind velocity law of the form $v(r) = v_\infty(1 - R_*/r)^\beta$ where v_∞ is the terminal velocity and R_* is the radius of the WR star, St-Louis *et al.* (1988) find the following expression for the mass-loss rate:

$$\dot{M}(M_\odot yr^{-1}) = \frac{2.33 \times 10^{-7} A_p a(R_\odot) v_\infty(km\ s^{-1})}{(1 + cos^2 i) f_c I}$$

where a is the orbital separation, f_c is the fraction of the total light coming from the companion star and I is the value of an integral, evaluated numerically, which depends on the parameter β of the velocity law and on the value of the radius at which the scattering envelope becomes optically thin.

These authors have used this expression to determine $\dot{M}$ for 10 galactic WR+O binaries. Combining this with the values of the masses of the WR stars (M_{WR}) deduced from the spectroscopic variations and the orbital inclination (also deduced from the polarization variations) lead to a confirmation of the correlation of $\dot{M}_{WR}$ with M_{WR} first proposed by Abbott *et al.* (1986).

Thus, there is a total of 10 WR stars with O-type companions for which reasonably accurate values of the masses have been determined from linear polarization variations. Schulte-Ladbeck (1989) has compared these masses with massive-binary evolution models with and without convective-core overshooting and found that the best agreement was obtained for non-conservative models with classical cores. However, the author suggests that this is a consequence of the amount of overshooting being too large in the only available set of models with convective-core overshooting.

1.3.5 COLLIDING WINDS

Winds from hot stars (O, B, WR) have been recognised and studied for some time. Nevertheless, investigations into the effects of binarity on these strong stellar outflows have only recently started. In a binary system where both components have a significant stellar wind, such as many WR+O binaries, interesting dynamical phenomena can take place. Because the mean free path of a wind particle through the opposing stellar wind is relatively short, the two winds will not diffuse into one another. Instead, a shocked region will be formed. The region will, in fact, consist of two shocks separated by a contact discontinuity. Between the shocks and the contact discontinuity, the gas is shock-heated

and becomes very hot. Prilutskii and Usov (1976) and Cherepashchuk (1976) suggested that this hot gas would emit X-rays with a characteristic spectrum. The varying column of wind material as a function of orbital phase would then give rise to phase dependent variations in the X-ray flux.

The first calculations of collisions between two stellar winds were done using the thin-shell approximation. This basically consists of treating the shocked region as a two-dimensional surface. It is equivalent to assuming that the dynamics of the region are only dependent on momentum conservation or that the cooling time in both winds is much shorter than the characteristic flow timescale. In such a case, the mechanical energy from the inelastic collision between the two stellar winds is efficiently radiated away by the shocked region which will quickly collapse into a very thin sheet. In particular, Girard and Willson (1987) (see also Shore and Brown 1988), using a general formulation by Giuliani (1982) have established the basic set of differential equations governing the geometry, mass distribution and internal velocity structure of the shocked region. The basic equations that need to be considered are the conservation of momentum parallel and perpendicular to the shocked surface and the mass conservation equation. Girard and Willson found that most of the shock surface can be described by a simple truncated cone with an apex angle which, remarkably, depends only on the product of the ratio of the two star's wind velocities and the ratio of their mass-loss rates.

Luo, McCray and Mac Low (1990) have recently presented models for colliding winds in which the thin-shell approximation was not used. These authors made detailed numerical simulations of the hydrodynamics and X-ray emission for two systems in particular; one binary in which the winds are identical in strength and the other with one wind completely dominating the wind of the companion. The agreement between the predicted and observed X-ray luminosities was found to be very good. However, one assumption made by Luo, McCray and Mac Low's model was that the shocked region remained adiabatic or, in other words, that the radiative cooling time was much longer that the dynamical timescale. Pollock, Blondin and Stevens (1991) have presented similar two-dimensional hydrodynamic calculations of colliding winds but have included the effects of cooling on the shock structure. They conclude that cooling effects are very important for systems in which the cooling timescale is smaller than

the dynamical timescale, which will be the case for systems in which the orbital separation is relatively small.

Clearly, this is a very young and dynamic field of study. New observations with the recently launched ROSAT satellite will allow for more detailed comparison with predicted X-ray fluxes and spectra and therefore should prove to be a good test for the recently developed models.

Chapter 2

An IUE Archival Survey of Variability in Wolf-Rayet Stars

2.1 Introduction

The *International Ultraviolet Explorer* (IUE) satellite was launched from Cape Canaveral, Florida on the 26 of January 1978. It is a joint project between the American National Aeronautics Space Administration (NASA), the European Space Agency (ESA) and the UK Science and Engineering Research Council (SERC) and has been one of the most successful scientific space missions, lasting at least four times longer than planned and providing a big step forward in our understanding of the universe. Its geosynchronous elliptical orbit allows for continuous contact with the ground which is one of the major attributes of IUE, making it the first observatory-type satellite. Its scientific instrument consists of a 45 cm Ritchey-Chrétien telescope feeding either of two echelle-grating spectrographs for the high resolution mode ($\Delta\lambda \sim 0.1 - 0.3$ Å). A low resolution mode ($\Delta\lambda \sim 6 - 7$ Å) is also available by rotating a plane mirror in front of the echelle. Each spectrograph (Short Wavelength : $\sim$ 1150 $-$ 1950 Å; Long Wavelength $\sim$ 1850 $-$3200 Å) is associated with a primary (SWP, LWP) and a redundant (SWR, LWR) camera which use SEC Vidicon detectors. A detailed description of the satellite and its inflight performance

can be found in Boggess *et al.* (1978a, 1978b) and a commemorative book describing the major scientific results obtained with IUE was published in 1987 (*Exploring the Universe with the IUE Satellite*).

During the last twelve years, a considerable amount of data has been secured on a wide variety of targets from planetary bodies to very distant galaxies. All these data contain valuable information and are archived by the three participating agencies. The primary NASA archive is located at the Goddard Space Flight Center at the National Space Science Data Center (NSSDC). It is supplemented by two regional data analysis facilities (RDAF), one at Goddard and the other at the University of Colorado. The ESA archive is located in the European ground station at Villafranca del Castillo (VILSPA) near Madrid while the SERC archive is maintained in the World Data Centre at the Rutherford Appleton Laboratory (RAL). After a preliminary period of six months during which the data are reserved for the observer, the spectra are widely made available to the whole international astronomical community. For each observation, the archive contains three files. The raw image, the photometrically corrected image (PHOT or GPHOT) and the extracted spectrum (IUESIPS).

Over the many years of operation of IUE, the processing software has continually evolved and the various instruments have often been recalibrated. Consequently, the archives do not constitute a completely homogeneously processed dataset. In order to correct the situation, the IUE project has recently undertaken the major task of reprocessing the entire low and high resolution archive. The final product will be a collection of IUE images with much improved signal to noise and accuracy, presented in a convenient and easily accessible form. The main ameliorations in the various new outputs will arise mainly from improvements in the data processing algorithms. One of the most important is the one concerned with the alignment of the science images to the rapidly varying sensitivity patterns across the detector. The photometric correction of an IUE image is achieved by using a pixel-by-pixel Intensity Transfer Function (ITF) which converts the raw signal data numbers (DN), which have a non-linear response to exposure time, to IUE linearized flux numbers (FN). It is important to associate each pixel with its correct response curve because there is reproducible spatial structure to the detector response even down to the single pixel level. Failure to align the pixels correctly introduces fixed pattern noise in the data . This is one of the major problems in IUE spectra as it

increases the general noise level and limits the improvements in signal to noise achievable when multiple images of the same source are co-added. The new technique consists in identifying fixed patterns in the background between the orders and cross-correlating them with corresponding patterns in a suitably exposed "flat field image". An accuracy of approximately $\frac{1}{8}$ of a pixel is expected with the new algorithm compared with $\frac{1}{4}$ presently achieved. Other important ameliorations include new ITFs for the SWP, LWP and LWR cameras as well as an improved resampling technique for the image. Preliminary studies have shown that the signal to noise in one given spectrum is generally increased by 10 – 30 % but improvements by up to 50 % have been obtained for some regions of underexposed spectra. The fixed pattern noise is also significantly reduced. For example, adding sixteen images of the star BD+284211 with the new method has led to a 50 % improvement in signal-to-noise over the same summation using current processing techniques. Improvements are also expected in spectral resolution as well as in absolute calibrations, which will be completely rederived. The final reprocessing of the $\sim 10^5$ images in the archive is expected to begin in early 1991 and take approximately three years. The low resolution spectra will be done before the high resolution spectra but all the images will be processed similarly. The final outputs will be in standard FITS format and will be stored on optical disks.

The basic role of the archive is to supply data to the astronomical community rapidly and efficiently. A typical UK retrieving procedure begins by the drawing-up of a list of desired images. For this, the astronomer needs to consult an on-line index of images named the IUE Merged Observing Log which contains, for each observation, astronomical information about the target (identification, coordinates, object class, etc.), data on the instrument configuration and processing information about the calibration and the algorithm used. This is followed by the submission of a batch job, requesting the desired images, to the main computer at RAL. Once the copying job to the previously allocated magnetic tape is performed, the user is notified and if no further observations are required the data in VICAR format are dispatched by postal service. This last step is usually the limiting factor in determining the time required to obtain data from the archive. However, It is presently the only way to transmit high resolution data to the user as their size is usually measured in tens of megabytes.

The IUE wavelength range includes the resonance lines of many of the most cosmically abundant elements in the universe. Hot stars in particular have a very rich ultraviolet spectra. In the case of Wolf-Rayet (WR) stars, there are so many features that it is often difficult to distinguish a continuum level and many of the observed features do not have a secure identification. In the past few years, evidence has begun to emerge for variability in some of the well known ultraviolet P Cygni profiles as well as in some less familiar metallic transitions of these stars. In particular, extensive changes have been found in the ultraviolet spectra of two WR+compact candidates, HD 50896 (Willis *et al.* 1986a, 1989) and HD 96548 (Smith *et al.* 1985, 1986). The variations are not periodic and are thus more likely to be intrinsic to the dense WR wind than caused by the presence of a companion. A study of the nature and timescale of such variations can help determine the mechanisms responsible and provide further insight into the basic physical properties of the hot and dense WR stellar wind. In order to try to assess the ubiquity of this phenomenon, I have taken advantage of the enormous potential of the IUE archive to carry out an extensive archival search for spectroscopic variability for all galactic WR stars observed more than once at high resolution. The results of this survey are described in this chapter.

2.2 Observational Data

I have consulted the IUE merged observing log in order to assess the content of the IUE archive with regards to spectra of galactic WR stars. As of 12 January 1990 there were some 1600 spectra of population I galactic Wolf-Rayet stars in the IUE archives of which almost half were secured in the high resolution mode. Table 2.1 lists the number of spectra secured in high ($\delta\lambda \sim 0.1$ Å, HIRES) and low ($\delta\lambda \sim 5$ Å, LORES) resolution mode for each of the three cameras used (SWP; Short Wavelength Prime, LWP; Long Wavelength Prime, LWR; Long Wavelength Redundant) for each star observed. Also given are the WR and HD numbers and the spectral types and v magnitudes taken from van der Hucht *et al.* (1988). No SWR images are listed as this camera has never been available to Guest Observers due to the intermittent failure of its read-out section since launch.

Table 2.1

IUE Archival Spectra of Galactic Wolf-Rayet Stars

WR Number	HD Number	Spectral Type	v (mag)	LORES SWP	LORES LWR	LORES LWP	HIRES SWP	HIRES LWR	HIRES LWP
WR 1	4004	WN5	10.51	4	3	0	0	0	0
WR 2	6327	WN2	11.33	3	2	2	1	0	0
WR 3	9974	WN3+abs (SB1)	10.70	5	3	0	0	0	0
WR 4	16523	WC5	10.53	3	3	0	0	0	0
WR 5	17638	WC6	11.02	2	2	0	0	0	0
WR 6	50896	WN5	6.94	20	6	0	206	28	4
WR 7	56925	WN4	11.75	2	2	0	0	0	0
WR 8	62910	WN6–WC4	10.56	2	2	0	1	1	0
WR 10	65865	WN4.5	11.08	2	2	1	1	0	0
WR 11	68273	WC8+O9 I	1.74	1	0	1	41	34	0
WR 14	76536	WC6	9.42	6	4	0	4	0	0
WR 15	79573	WC6	11.73	2	0	2	0	0	0
WR 16	86161	WN8	8.43	4	2	0	1	0	0
WR 17	88500	WC5	11.11	2	1	0	0	0	0
WR 18	89358	WN5	11.20	3	4	0	0	0	0
WR 21	90657	WN4+O4-6	9.80	37	3	0	0	0	0
WR 22	92740	WN7+abs (SB1)	6.44	5	3	2	11	3	0
WR 23	92809	WC6	9.71	4	2	0	4	3	0
WR 24	93131	WN7+abs	6.49	4	2	2	32	2	0
WR 25	93162	WN7+abs	8.17	6	3	2	8	1	0
WR 30	94305	WC6+O6-8	11.73	5	2	0	0	0	0
WR 31	94546	WN4+O8 V	10.69	8	2	0	0	0	0
WR 33	95435	WC5	12.34	2	1	0	0	0	0
WR 40	96548	WN8	7.85	12	16	0	70	6	32
WR 42	97152	WC7+O7 V	8.25	17	3	0	6	1	1
WR 43	97950	WN6+O5	9.66	6	2	0	0	0	0
WR 44		WN4	12.96	1	1	0	0	0	0
WR 46	104994	WN3pec	10.96	6	3	1	1	0	0
WR 47	E311884	WN6+O5 V	11.09	9	1	1	0	0	0
WR 48	113904	WC6+O9.5 I	5.69	5	3	0	13	12	0
WR 50		WC6+abs	12.49	1	1	0	0	0	0
WR 52	115473	WC5	9.98	3	3	0	1	0	0
WR 53	117297	WC8	11.06	1	1	0	0	0	0
WR 55	117688	WN7	10.87	3	2	0	0	0	0
WR 56		WC7	13.97	2	1	0	0	0	0
WR 57	119078	WC7	10.11	2	2	0	3	0	0
WR 61		WN4.5	12.56	3	1	0	0	0	0

Table 2.1 (Continued)

IUE Archival Spectra of Galactic Wolf-Rayet Stars

WR Number	HD Number	Spectral Type	v (mag)	LORES SWP	LORES LWR	LORES LWP	HIRES SWP	HIRES LWR	HIRES LWP
WR 69	136488	WC9	9.43	7	4	1	1	0	1
WR 70	137603	WC9+B0 I	10.15	1	0	1	0	0	0
WR 71	143414	WN6	10.22	2	2	0	1	0	0
WR 75	147419	WN6	11.42	3	3	0	0	0	0
WR 77	150136	WC8	13.16	0	0	0	1	1	0
WR 78	151932	WN7	6.61	3	2	1	19	4	3
WR 79	152270	WC7+O5-8	6.95	10	3	0	8	1	5
WR 86	156327	WC7	9.73	3	0	4	0	0	0
WR 90	156385	WC7	7.45	5	4	1	4	3	0
WR 92	157451	WC9	10.60	2	2	0	1	0	2
WR 103	164270	WC9	9.01	4	4	0	2	1	1
WR 104		WC9	13.54	1	0	1	0	0	0
WR 106	E313643	WC9	12.33	1	0	1	0	0	0
WR 110	165688	WN6	10.30	1	1	0	0	0	0
WR 111	165763	WC5	8.23	4	6	0	2	3	0
WR 113	168206	WC8+O8-9 IV	9.43	31	24	0	2	0	0
WR 123	177230	WN8	11.26	5	2	0	0	0	0
WR 124		WN8	11.58	0	4	0	0	0	0
WR 127	186943	WN4+O9.5 V	10.36	17	3	0	0	0	0
WR 128	187282	WN4	10.54	4	2	1	2	0	0
WR 133	190918	WN4.5+O9.5 Ib	6.70	2	3	0	4	1	0
WR 134	191765	WN6	8.23	6	5	1	14	2	0
WR 135	192103	WC8	8.36	4	2	0	3	2	0
WR 136	192163	WN6	7.65	12	7	3	46	7	31
WR 137	192641	WC7+OB	8.15	12	2	16	7	0	3
WR 138	193077	WN6+abs	8.10	9	1	1	7	0	1
WR 139	193576	WN5+O6	8.10	66	13	1	26	2	0
WR 140	193793	WC7+O4-5	7.07	20	12	15	10	1	7
WR 141	193928	WN6 (SB1)	10.14	1	1	0	0	0	0
WR 148	197406	WN7 (SB1)	10.46	7	2	0	0	0	1
WR 151		WN5+O8 V	12.37	3	0	0	0	0	0
WR 152	211564	WN3	11.67	2	2	0	0	0	0
WR 153	211853	WN6+O	9.08	25	7	0	5	0	0
WR 154	213049	WC6	11.54	1	1	0	0	0	0
WR 155	214419	WN7 (SB1)	8.75	49	39	0	2	1	0
WR 156		WN8	11.09	1	1	0	0	0	0
WR 157	219460	WN4.5	9.91	1	1	0	0	0	0

Excluding the well-known SB1 and SB2 spectroscopic binaries, there are seventeen WR stars with more than one high resolution spectrum obtained with a given camera. WR 136 and WR 6 will be the subjects of chapters 3 and 4 respectively and WR 40 will be analysed in detail elsewhere. Therefore, these stars will not be discussed here. All the spectra for the remaining fourteen stars were obtained from the IUE archive at RAL, following the procedure described in the previous section.

Because of the inhomogeneity of the extracted data currently provided by the IUE project (IUESIPS), all the spectra were extracted directly from the PHOT or GPHOT images using the highly successful IUEDR software package (Giddings 1983, Giddings and Rees 1989) available on the UK STARLINK network of VAX computers. This extraction technique uses a centroid tracking algorithm which locates the echelle orders with precision and reproducibility. Other advantages over the current extracted spectra include a better ripple correction as well as an improved determination of the interorder background based on the algorithm of Bianchi and Bohlin (1983) for the correction of high dispersion order overlap, a well-known problem of IUE spectra. All subsequent measurements and analysis were performed with the DIPSO software package (Howarth and Murray 1990) also available on Starlink.

2.3 Results

For most stars, only a very small number of spectra are available for a given camera. These represent only glimpses of the star's spectra in time and are therefore not ideally suited for the search of intrinsic variability. In order to claim that there is evidence for line profile variability, I will generally require that (i) any changes are present in more than one line or in both components of a doublet and that (ii) they occur at roughly the same velocities. These are quite conservative criteria and should prevent any spurious claims. Each star will now be discussed in turn.

WR 14 (HD 76536)

For this star four large aperture SWP spectra are available. They were secured in September 1980 over a period of only three days. In this short time, no variations are apparent in the ultraviolet spectra.

WR 23 (HD 92809)

Four SWP spectra of WR 23 are found in the archive. They were all obtained in 1981 over a period of approximately nine months. The last of these spectra shows a very small difference with the others in the blue edge of the absorption component of Si IV λ1393. However, the change is very small and is not detected in the other component of the doublet. Therefore, the evidence for variability in the SWP spectra of this star is marginal.

Three LWR spectra are also available for this star. These were obtained in 1981 at the same time as three of the SWP spectra. No differences are found between these spectra.

WR 24 (HD 93131)

The WN 7 star WR 24 is situated in the Carina Nebula and appears to be single. Moffat and Seggewiss (1978) detected no significant radial velocity variations in a set of 15 photographic plates obtained in 1976 and 1977. From a photometric dataset obtained during 37 days in 1975, they also conclude that WR 24 is constant in brightness, colour and line strength. Conti, Niemela and Walborn (1979) obtained an extensive set of optical spectrograms between 1970 and 1977 but found no periodic motion in the radial velocities, although some random fluctuations were detected. Linear polarization observations by Drissen *et al.* (1987) show only stochastic changes with no significant periodicity. The changes are thought to be related to inhomogeneities in the dense WR wind.

Twenty-nine IUE SWP spectra of WR 24 were obtained over a period of five consecutive days in December 1985 with the specific aim of searching for intrinsic variability. A preliminary analysis of eleven of these spectra together with three archival spectra was presented by Smith *et al.* (1986). These authors find no evidence for any significant variations in the major P Cygni profiles.

In order to insure a uniform dataset, I have extracted all the spectra available for this star, including the observations previously discussed by Smith *et al.* (1986). Most spectra show no significant variability but two of the archival observations (SWP 1591, 15132) do present some small scale differences. These are most easily seen in the C IV λ1550 doublet but are also detected, at a weaker level, in the He II λ1640 and Si IV λ1396 transitions. No variations are

detected in the two other major P Cygni profiles (N V λ1240 and N IV λ1718) or in any of the subordinate transitions observed in the ultraviolet spectrum of this star. The spectra for which no changes were found have been merged together to form a mean of higher signal-to-noise. This mean is compared with SWP 1591 and SWP 15132 in Figure 2.1 for the C IV resonance doublet. Note that because SWP 1591 was obtained with the small aperture, which does not retain the photometric precision, it was scaled with the other spectra in order to facilitate comparison.

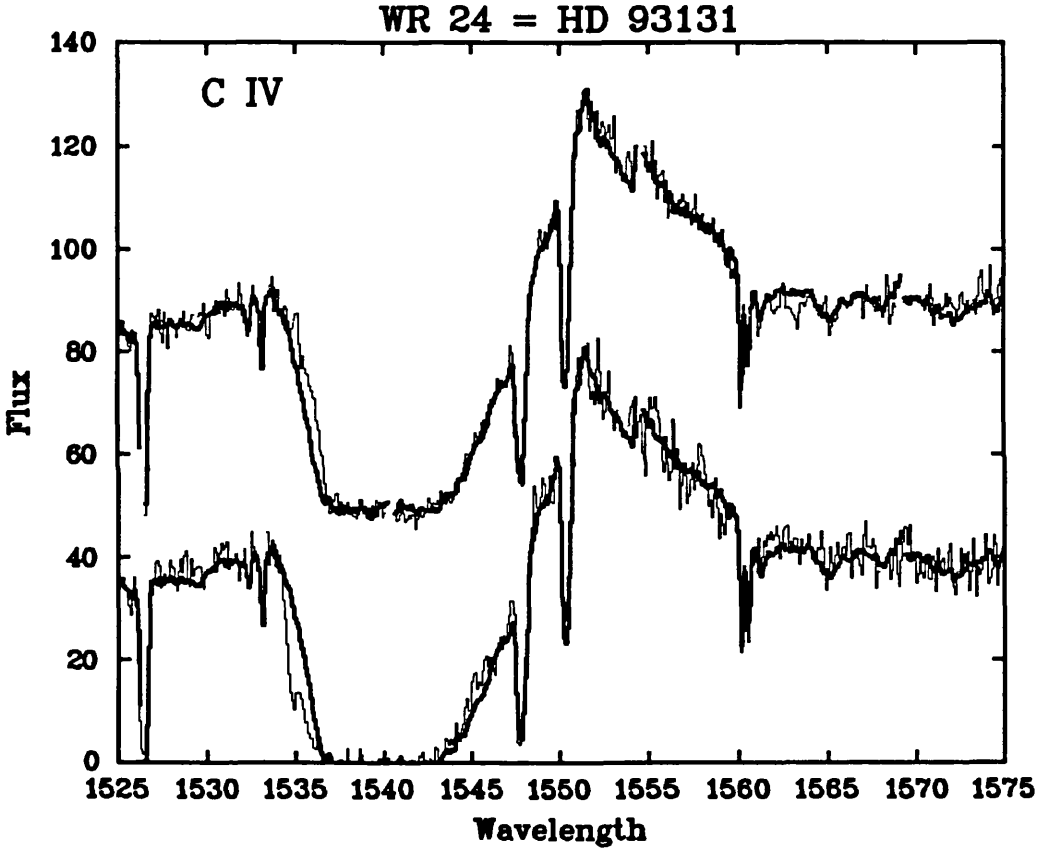

Figure 2.1 : Archival Spectra SWP 1591 (bottom) and SWP 15132 (top) compared to the mean (thick line) for the C IV λ1550 P Cygni profile. For clarity, the two top spectra have been shifted in ordinate by 50 flux units.

The changes occur in the blue edge of the absorption component at velocities of -2200 – -2700 km s^{-1}, well in excess of the wind terminal velocity of 2155 km s^{-1}, estimated from the violet edge of the black absorption of the C IV λ1550 P Cygni profile (Prinja, Barlow and Howarth 1990). SWP 1591 was obtained in May 1978 while SWP 15132 was obtained in September 1981. There is another archival spectra secured in February 1979 which shows no significant differences with the extensive set of observations obtained in December 1985. As for HD 50896 (WR 6) and HD 96548 (WR 40) (see Chapter 1, Section 1.1.4) the changes are clearly epoch dependent. However, many more observations are required to draw any conclusion on the specific nature of the changes.

Two LWR spectra, obtained 9 months apart, are also found in the archive for this star. The spectra were compared but no significant variations were found.

WR 25 (HD 93162)

WR 25 is another WN 7 star in Carina which has been claimed to be single. One interesting characteristic of this star is its extremely bright X-ray flux [L_X(0.2–4.0 KeV)=137.$\pm$9.] (Pollock 1987). It is the WR star with the highest IPC count rate detected by the *Einstein Observatory* and there is even evidence for variability in one of the *Einstein* observations (Pollock 1989). However, as for WR 24, Moffat (1978) found no evidence for variability in the radial velocities of this star from a series of 15 photographic plates obtained over a period of 15 days in February 1977. This author has also obtained a narrow-band photoelectric photometry dataset over a period of 37 days in February/March 1975 which shows no significant variability in the continuum and emission bands. Conti, Niemela and Walborn (1979) report only random fluctuations in their extensive radial velocity dataset. The linear polarization observations of Drissen *et al.* (1987) generally show stochastic variations with a certain level of organization in the Q-U plane. The authors indicate that this may suggest that this star is a long-period binary or that the star shows active rotating regions.

Eight IUE SWP spectra are available from the archive for WR 25. The observations were secured in September 1979, February 1980, May 1981 (2 spectra), September 1981 and finally December 1988 (3 spectra). The first

spectrum was obtained with the small aperture and thus needed to be scaled to the others. No variations are found between the February 1980, the September 1981 and the three December 1988 observations but some changes are detected for the three others in the C IV λ1550 P Cygni profile. Although the variations are of a similar nature for all three spectra, the differences are much smaller for the two spectra obtained in May 1981. The changes for the September 1979 (SWP 6609) observation are illustrated in Figure 2.2 where this spectrum is compared to a mean, consisting of the 5 spectra which show no variations, for the C IV resonance doublet.

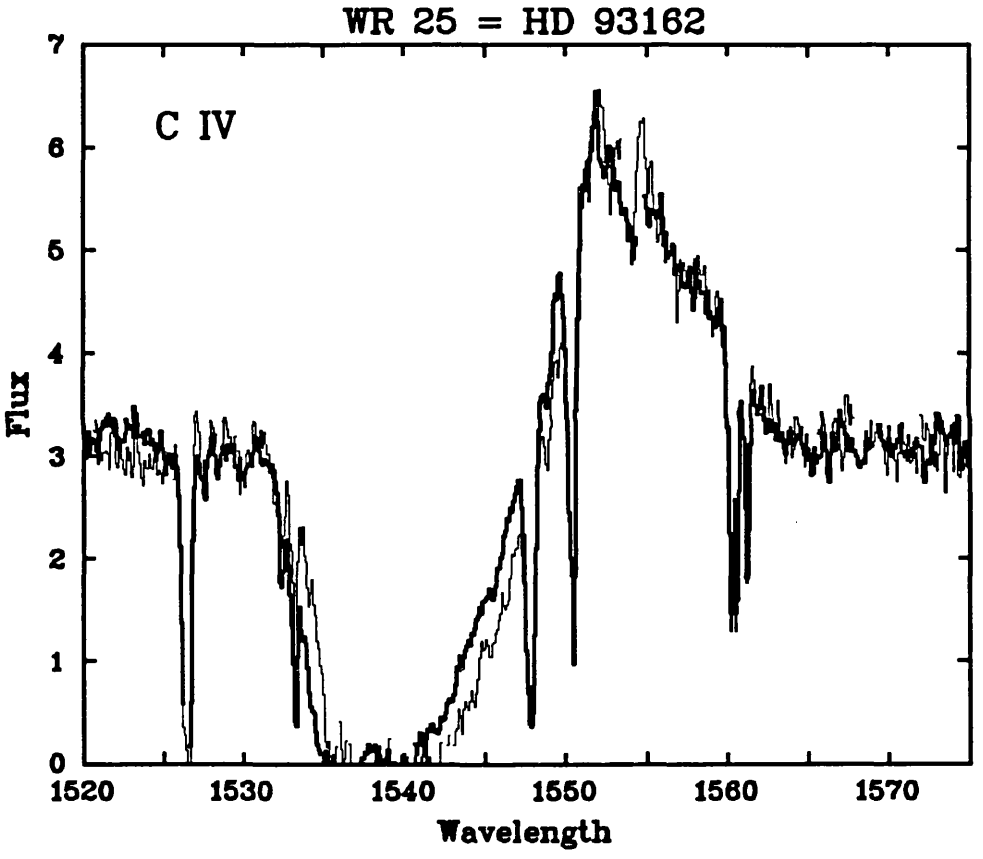

Figure 2.2 : Variations in the C IV λ1550 resonance doublet between SWP 6609 (thin line) and the mean (thick line) for WR 25.

The variations in the C IV P Cygni profile of SWP 6609 are observed as a decrease in absorption at high negative velocities accompanied by an increase in absorption at lower negative velocities. Unfortunately, the absorption component of C IV is saturated, which prevents us from obtaining information about the changes over the full velocity range. Variations of a similar nature were previously observed for HD 50896 (WR 6) in the C IV λ1550, He II λ1640 and N IV λ1718 P Cygni profiles. Although the variations between the two spectra appear to be relatively large, the total equivalent width of the P Cygni profile does not change very much. I have measured the equivalent widths for both spectra using a fixed wavelength range embracing the entire P Cygni profile and found that the difference is not more than 4 %. Perhaps this indicates that the opacity is simply redistributed in velocity space with no real total increase or decrease. Unfortunately, the changes are not detected in any other line but their scale is large enough to be confident in their reality. As for WR 24, more observations are required in order to reach any conclusion on the nature of the changes. Bearing in mind its exceptionally high X-ray flux as well as the variations found in the radial velocities, X-ray flux, linear polarization and ultraviolet P Cygni profiles, this star is an excellent candidate for future variability studies.

WR 57 (HD 119078)

Three large aperture SWP spectra can be found in the archive for this star, two obtained in March 1982 and one 16 months later in June 1983. The first spectrum is particularly noisy due to the exposure time which is approximately ten times too low. On the other hand, the last spectrum seems to be slightly overexposed causing the peaks of the strong emission lines to be saturated and thus removed from the extracted spectrum. These problems render the search for variability rather difficult. Nevertheless, there is no evidence for significant differences between these three spectra.

WR 78 (HD 151932)

WR 78 is a WN 7 star for which spectroscopic and polarimetric changes have been detected in the optical, making it a particularly good candidate for

a variability search in the ultraviolet. Seggewiss (1974) found that the radial velocities for the optical emission lines of this star were constant but that the blue-shifted absorption lines of He I λ3889,4026, which he found to be split into two components, showed variability. The N III λ4097 line was also found to be variable. The author claimed that the radial velocity changes in these lines described a double-wave with a period of about 3.5 days, which he interpreted as caused by an oscillating outer envelope. Later, Seggewiss and Moffat (1979), from a new extensive set of observations, concluded that the radial velocity variations in the He I P Cygni absorptions were epoch-dependent with no apparent periodicity. More recently, Vreux *et al.* (1987) reported variations in the absorption components of He I λ3889,4026 as well as in the Si IV λ4089 emission line, in a new set of high and low dispersion optical spectra. Finally, in linear polarization, blue broad band observations by Drissen *et al.* (1987) show stochastic variations with no significant periodicity. In summary, WR 78 has a long history of showing profile variations at visible wavelengths but with no obvious periodicity. Lack of emission line radial velocity variations indicate that WR 78 is probably single (Seggewiss and Moffat 1979) and thus the observed variability is thought to be intrinsic to the star.

Originally, only 3 SWP and 4 LWR IUE spectra were available for this star. However, as part of this work, 16 SWP and 3 LWP high resolution spectra were secured over a period of four days in May 1988 with the specific aim of searching for intrinsic variability. A log of these new observations together with the 7 archival spectra is presented in Table 2.2. Listed are the camera type, the image number, the Julian Date at the beginning of the exposure, the exposure time and the aperture used.

All the spectra for a given camera were meticulously compared to one another. In particular, the major P Cygni profiles in the SWP spectra (Si IV λ1396, C IV λ1550, He II λ1640 and N IV λ1718) were closely inspected. The 16 SWP spectra obtained in 1988 show no significant variability. Consequently, a mean of these observations was created in order to obtain a spectrum with a much higher signal-to-noise ratio. This mean spectrum was then compared to the SWP archival data. Two of these were obtained with the small aperture and thus needed to be scaled to the others by a constant factor. Variability has been detected in the two components of the Si IV doublet between the mean

Table 2.2

IUE High Resolution Spectra of WR 78

Camera	Image Number	Julian Date 2440000+	Exposure Time (s)	Aperture
SWP	1603	3651.352	3000	S
LWR	1542	3651.395	3600	S
LWR	1923	3720.191	900	S
SWP	2154	3720.213	2100	S
LWR	2305	3759.417	6300	S
SWP	4334	3926.926	1140	L
LWR	3828	3926.943	780	L
SWP	33449	7286.490	1200	L
LWP	13166	7286.516	900	L
SWP	33450	7286.538	1200	L
SWP	33451	7286.577	1200	L
SWP	33452	7286.612	1200	L
SWP	33461	7287.652	1200	L
LWP	13169	7287.671	900	L
SWP	33462	7287.693	1200	L
SWP	33463	7287.727	1200	L
SWP	33464	7287.761	1200	L
SWP	33472	7288.511	1200	L
SWP	33473	7288.549	1200	L
SWP	33474	7288.588	1020	L
SWP	33475	7288.619	900	L
SWP	33482	7289.503	1200	L
LWP	13180	7289.522	900	L
SWP	33483	7289.544	1200	L
SWP	33484	7289.579	1200	L
SWP	33485	7289.611	1200	L

1988 spectrum and these three archival spectra. The changes have similar characteristics but are much larger for SWP 4334. The variations for the latter are shown in Figure 2.3, where each component of the doublet is presented in velocity space. The 1988 mean spectrum appears to show a weak excess of absorption compared to the earlier 1980 spectrum. The fact that the changes are observed in both components of the doublet at the same velocities (~ -1650 to -2000

kms^{-1}) is a convincing argument in favour of the reality of the changes. The LWR and LWP spectra were also closely compared but no significant changes were detected.

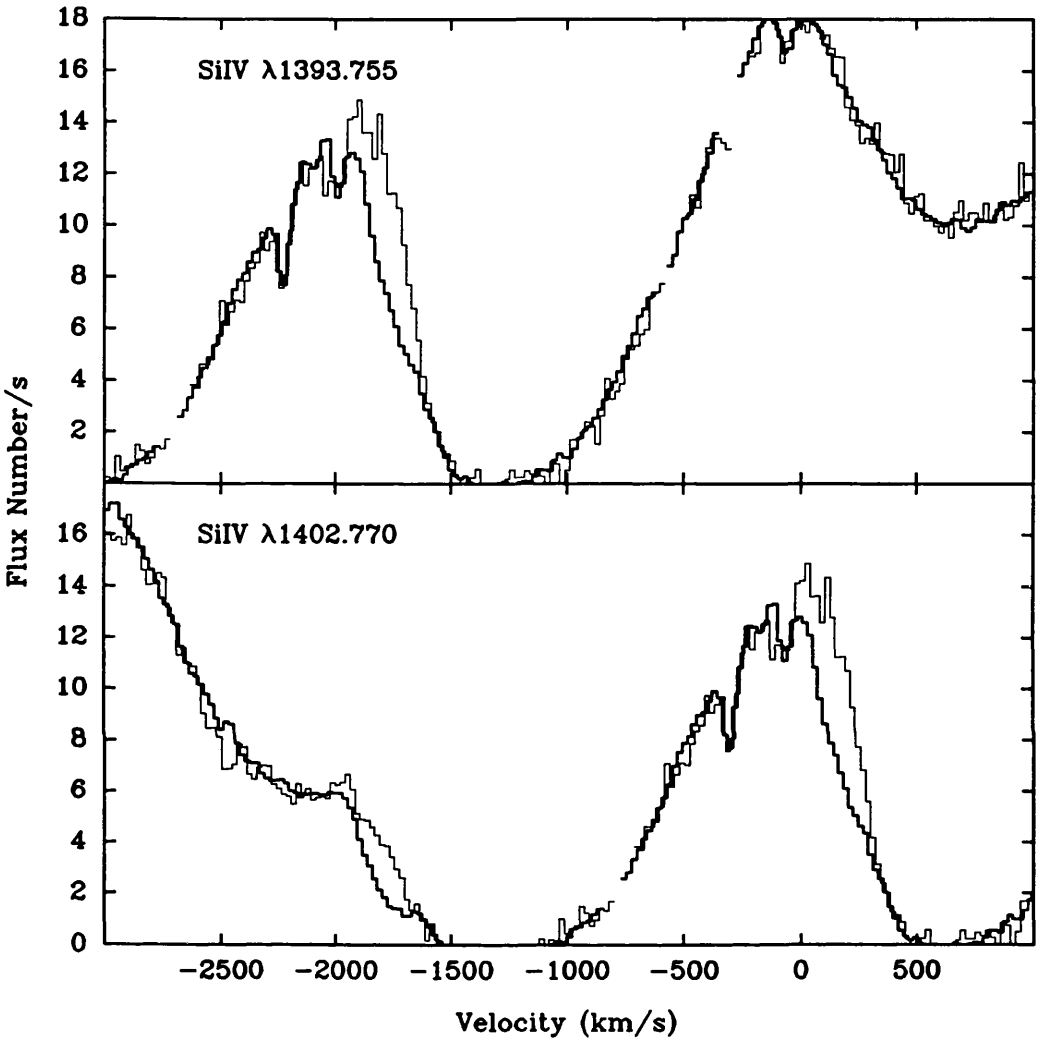

Figure 2.3 : P Cygni profiles in velocity space of the Si IV resonance doublet for SWP 4334 (thin line) and the 1988 mean (thick line).

The profile variations that have been detected in the ultraviolet spectra of WR 78 between 1980 and 1988 is reminiscent of those previously observed for other WR stars. As for HD 50896 and HD 96548 (see Chapter 1, Section 1.1.4), the changes are observed in the soft blue edge of the absorption component, at velocities which are well in excess of the wind terminal velocity of 1365 km s^{-1}, estimated from the violet edge of the black absorption of the CIV λ1550 P

Cygni profile (Prinja, Barlow and Howarth 1990). Also in common with the two WR stars mentioned above, is the fact that the ultraviolet variability in WR 78 appears to be epoch-dependent. No variations are found in the 16 spectra obtained over 4 days in 1988. In comparison with optical spectra, Seggewiss and Moffat (1979) found large velocity changes in the He I P Cygni absorption components in 1971 over 3.5 days, no changes in 1975 and slow velocity changes in 1977. One major difference between the variations in the spectra of WR 78 and the ones detected for other WR stars is the velocity range over which they occur. The variation detected here is confined to a very narrow velocity range ($\sim$ 350 kms^{-1}) whereas for the other stars it extends over $\sim$1000 kms^{-1}.

It is of interest to note that the velocity variations observed in the optical spectra of 1971 are very reminiscent of the discrete absorption components seen moving through the ultraviolet P Cygni absorption profiles in O stars (e.g. Prinja and Howarth 1986). For WR 78 the 1971 data show that the He I P Cygni absorption is split into two components; the lower velocity component gradually increases in velocity until it merges with the higher velocity component after $\sim$ 3.5 days.

Although the data presented here are clearly insufficient to provide any new insights into variability in WR winds, WR 78 is a good candidate for future, more detailed observations at ultraviolet and optical wavelengths.

WR 90 (HD 156385)

Four SWP spectra can be found in the archive for this star. Three were obtained in April, September and October 1978 using the small aperture and one was obtained three years later with the large aperture. Because the transmission of the small aperture is approximately half that of the large aperture, the three 1978 spectra were scaled to match the large aperture spectrum. No significant variability was found. The peaks of the strongest emission lines do not always reproduce very well but this is most likely due to uncertainties in the fluxes which are in the non-linear part of the ITF.

Three LWR spectra are available for WR 90. They were all obtained in 1978 over a period of six months at the same time as the three 1978 SWP spectra. Again, the small aperture was used. Because the throughput of the small aperture is not constant, one spectrum was chosen as a template and

the other two were multiplied by constants to match it. I find no significant differences between these three spectra.

WR 92 (HD 157451)

Two large aperture LWP spectra are available for this star. They were obtained on the 31 August 1988 at an interval of only $\sim$ 150 minutes. In this very short period, no significant variations are detected.

WR 103 (HD 164270)

Only two SWP spectra separated by a period of seventeen months have been obtained for WR 103. One was secured with the small aperture and thus was scaled to the other. No significant variations are detected between the two spectra although they are both relatively noisy.

WR 111 (HD 165763)

The only two SWP spectra available for this star were both obtained with the small aperture. One was multiplied by a constant to match the other and they were closely compared. Variability appears to be present in the C III λ1247 P Cygni profile as illustrated in Figure 2.4. This type of change has never been observed for any WR star in the past. The difference occurs in the part of the absorption component which is normally saturated, and indeed SWP 2872 has a black profile. The material producing the opacity in the case of SWP 2518 must be rarified as the optical depth at these wavelengths is very high. Unfortunately, no changes are found in any other line. Moreover, this line is situated in a rather difficult region of the SWP camera as the orders are very closely spaced, making the determination of the interorder background imprecise. I conclude that the evidence for variability in the SWP spectra of this star is marginal.

There are three LWR spectra of WR 111 in the archive. Two were obtained in 1978 1 month apart (LWR 2303, LWR 2548) and the other (LWR 10490) in May 1981. The two 1978 spectra were scaled to the 1981 spectra as they were obtained with the small aperture. LWR 10490 is not a very good

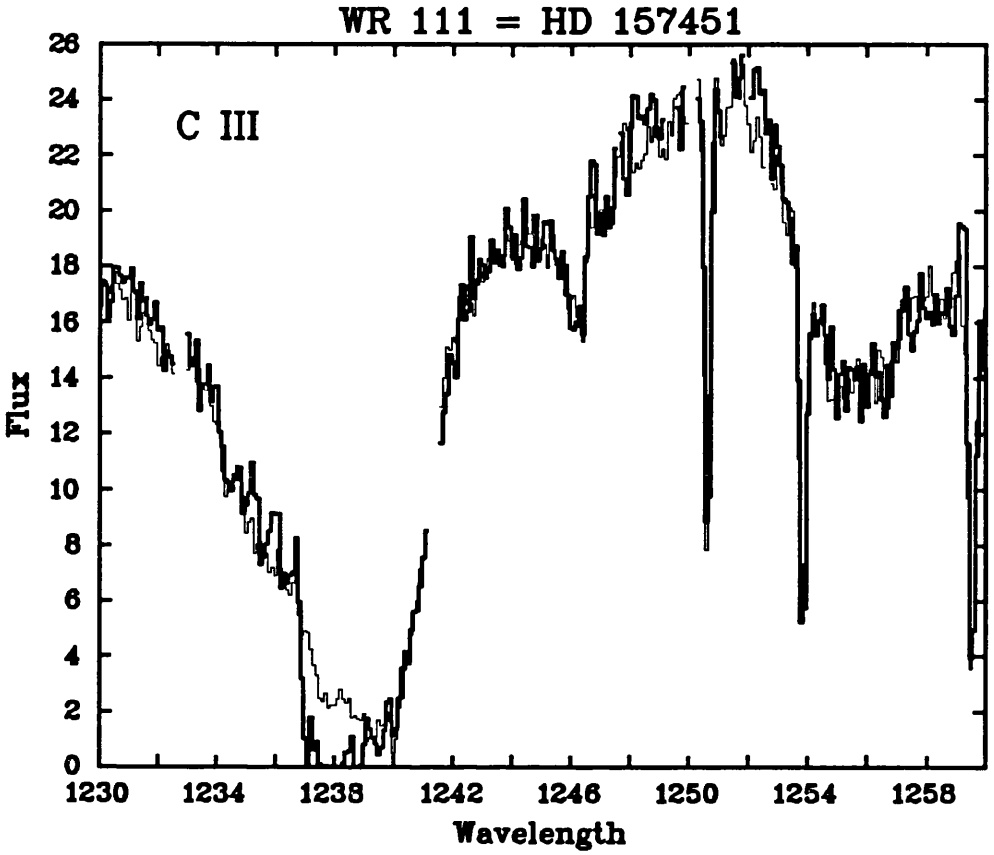

Figure 2.4 : C III λ1247 P Cygni profiles for SWP 2518 (thin line) and SWP 2872 (thick line).

spectrum. First, many of the peaks of the strong emission lines are saturated and were therefore removed during the extraction procedure. Also, below ~ 2150 Å , there are regular drop-outs in the flux which seem to be caused by an instrumental effect. All these problems render a search for variability rather difficult. Nevertheless, no variations are found in the parts of the spectrum which are not affected. The two 1978 spectra also show no variability

WR 128 (HD 187282)

The data for this star consist of only two SWP spectra obtained one year apart. No significant differences are found in any parts of the spectra.

Moffat *et al.* (1988) have recently reported substantial variability in the He II λ5411 emission line of WR 134. Bumps of FWHM $\approx$ 2–10 Å and a height of $\leq$ 10 % of the continuum are found superimposed on the general wind profile. The features that are redshifted when first detected become even more redshifted with time, whilst the features that are blueshifted become even more blueshifted on a timescale of $\leq$ 8 hours. The authors attribute the changes to blobs or condensations of wind material being accelerated outwards. In a more elaborate work, McCandliss (1988) obtained 152 optical spectra of this star covering 3940–6610 Å over a period of 12 nights. He found that all the major lines in the spectrum were significantly variable in the flux level as well as in the line position. No convincing period was found in these observations. McCandliss concludes that the changes have a double nature : discrete components moving outwards from the line center and non-periodic global line flux and line position variations.

WR 134 has, in fact, an extensive history of variability in the optical. Photometric observations by Antokhin, Aslanov and Cherepashchuk (1982) and Antokhin and Cherepashchuk (1984) reveal changes with an amplitude of 0.04 mag in the optical continuum with a suggested period of 7.483 days. The low mass function resulting from the derived orbit led them to suggest this star as a candidate for a WR + c (c=compact companion: neutron star or black hole) binary system. Moffat and Shara (1986) find no evidence for variability in a set of broadband B photometric observations obtained in 1983 but definite changes with an amplitude of 0.02 mag and a period of 1.81 days in another set secured in 1984. This period is similar to the 1.7844 day period found by Lamontagne (1983) in radial velocity data. More recently, Antokhin and Volkov (1987) secured photometric observations indicating clearly irregular variations on a timescale of a month.

Broadband blue light polarization data by Robert *et al.* (1989) also show extensive variability. These changes have an amplitude of 0.043 % and are thought to be of random nature, as no convincing periodicity is visible in the observations. However, there is marginal evidence for a preferred plane for the variations which is reminiscent of the results of Schmidt (1988). They find that the polarization in the lines is unusually weak compared to the polarization of the continuum which they interpret as a disk-shape envelope.

In view of its broad history of optical variability, WR 134 was an excellent candidate for a variability study in the ultraviolet. Therefore, as part of this work, 12 new IUE SWP spectra were obtained in November/December 1989 over a period of seven days with the aim of searching for variability. The IUE archive contains only two SWP HIRES spectra of WR 134. These were secured at two different epochs, with radically different exposure times, one with the small aperture and the other with the large aperture. In table 2.3, a log of the new spectra together with the two archival spectra is presented. Listed are the SWP Image Number, the Julian Date at the beginning of the exposure the exposure time as well as the aperture used.

Table 2.3

IUE SWP High Resolution Spectra of WR 134

SWP Image Number	Julian Date 2440000+	Exposure Time (s)	Aperture
2873	3788.738	4800	S
4088	3904.068	2700	L
37705	7861.079	2400	L
37707	7861.200	2400	L
37718	7862.994	2400	L
37720	7863.113	2400	L
37725	7863.967	2400	L
37727	7864.084	2400	L
37734	7865.122	2400	L
37735	7865.170	2400	L
37748	7865.958	2400	L
37750	7866.081	2400	L
37755	7866.962	2400	L
37757	7867.090	2400	L

No variations have been found in the 14 SWP spectra. For the 1989 observations two spectra, separated by $\sim$ 3 hours, were generally obtained each night . We can thus conclude that the variations observed in the optical over a period of $\sim$ 8 hours are not reproduced in the ultraviolet or that the variability is epoch-dependent and the observations were obtained during a quiescent epoch.

The two LWR spectra available for this star were obtained 4 months apart and show no significant variability.

WR 135 (HD 192103)

The data for this star consists of three SWP and two LWR spectra. A first pair of observations (one in each camera) was obtained in October 1978, a second pair four months later and an extra SWP spectrum was secured in April 1984. No significant variations are found.

WR 138 (HD 193077)

Seven SWP spectra are listed in the IUE merged observing log for this star. However for one of the observations (SWP 7000), obtained in October 1979, the GPHOT image was temporarily inaccessible with only the IUESIPS extracted spectrum available. As it is important for a variability search to use a uniformly extracted dataset, I decided to exclude this image from the study. The six other spectra were obtained over a period of 7 days in November/December 1981. In this period no significant differences are apparent between the spectra.

2.4 Discussion and Conclusion

Of the fourteen stars included in this archival survey of intrinsic variability, three have been found to be definitely variable, a proportion of 21 %. This is quite a large percentage considering that the datasets available are far from ideally suited for such a study. In fact, the spectra are usually very few in number and obtained with a sporadic and often highly restricted time coverage. When the two stars discussed in Chapters 3 and 4 as well as WR 40 (which all show variability) are added to this list, the fraction of Wolf-Rayet stars for which ultraviolet spectral variability is found is raised to 35 %. Finally, if I include the two stars with marginal evidence for variability, a total of almost 50 % is obtained. The fact that variability is usually found for the stars that have been intensively monitored and that the observations used in this study cannot in themselves rule out stellar wind variability, strongly suggests that the real proportion of variable WR winds is much higher. This is not, in fact, very surprising. Theorist studying the winds of hot stars have long predicted that these line-driven flows should be dynamically unstable. In order to obtain a complete understanding of the winds, these time-dependant phenomena must be included in the models. It is now crucial for observers to carry out detailed investigations of these variations in order to establish their timescale and general characteristics to provide firm constraints for the line-driven instability models or any other models which can be invoked to interpret the ultraviolet variability.

A large number of the IUE high resolution spectra of WR stars used in this chapter do not, however, show variability. For a given star, multiple spectra can therefore be co-added to obtain a higher signal-to-noise mean spectrum. For each star discussed in this survey, I have merged all the spectra which proved to be non variable. For stars with only marginal evidence for variability, the spectra were also added to form a mean. To this, I have added the SB1 binaries listed in Table 2.1 as well as the three stars WR 6, WR 40 and WR 136 which have been claimed by some authors to be WR+compact systems. The result is an atlas of high resolution and relatively good signal-to-noise ultraviolet spectra of galactic WR stars which are presently believed to be single or for which only one set of spectral lines are visible. The mean spectra have been created in the following way. First, in order not to decrease the resolution, it was necessary to make sure that no wavelength shifts exist between the spectra. This was achieved by aligning a selection a well isolated strong interstellar lines. The

spectra were then merged using the exposure times as a weighting factor. In the case of small aperture spectra, because the transmission factor of the aperture is approximately half that of the large aperture, the exposure times were divided by the scaling factor to the large aperture spectra. For completeness, I have also included in this atlas the stars for which only one spectrum is available. Unfortunately, some images in the archive are temporarily unavailable. WR 46 and WR 77 have one SWP high resolution spectrum listed in the IUE merged observing log but these were inaccessible at the time this work was performed. WR 103 has a LWP spectrum which I was not able to obtain. In the case of WR 71 and WR 92, the PHOT or GPHOT images were unavailable but I was able to obtain the IUESIPS spectrum which was used in the atlas. Finally, one spectra of WR 22 was unusable due to the fact that half of the image was missing.

Table 2.4 presents a list of the 28 stars included in this atlas. Listed are the WR and HD numbers, the spectral type, the v magnitude, the colour excess (from van der Hucht *et al.* 1988) as well as the number of spectra included in each mean spectrum for the SWP, LWR and LWP cameras. The stars have a broad distribution in spectral type. There are 1 WN2, 1 WN4, 1 WN4.5, 1 WN5, 4 WN6, 6 WN7, 2 WN8 and 2 WC5, 2 WC6, 2 WC7, 2 WC8, 3 WC9 as well as one star with a combined WN6–WC4 spectral type.

Plots of all the mean spectra are presented in the Appendix. These are displayed in chronological order of WR numbers with the SWP wavelength range plotted first followed by the LWP or LWR spectrum. Willis *et al.* (1986b) have presented the first atlas of high resolution IUE spectra of WR stars. The work presented in this chapter represents an update on this atlas. The major improvements include a higher signal-to-noise level achieved by co-adding multiple spectra and the availability of better software analysis packages. Also, stars which had not previously been observed at high resolution with IUE and for which a spectrum has since been obtained have been added, resulting in a larger total number of stars.

The spectral atlas, also available on magnetic tape, should form an important dataset for further studies of the chemical composition, terminal velocity and interstellar spectra of galactic WR stars, as well as detailed comparison with the ultraviolet spectra of extragalactic WR stars when these become available at high spectral resolution.

Table 2.4

Wolf-Rayet Stars with IUE High Resolution Spectra

WR Number	HD Number	Spectral Type	v Magnitude	E(B-V)†	SWP	LWR	LWP
2	6327	WN 2	11.33	0.48	1		
6	50896	WN 5	6.94	0.24	16		3
8	62910	WN 6 - WC 4	10.56	0.82	1	1	
10	65865	WN 4.5	11.08	0.57	1		
14	76536	WC 6	9.42	0.51	4		
16	86161	WN 8	8.43	0.63	1		
22	92740	WN 7 + abs (SB1)	6.44	0.28	6	3	
23	92809	WC 6	9.71	0.38	4	3	
24	93131	WN 7 + abs	6.49	0.24	28	2	
25	93162	WN 7 + abs	8.17	0.68	5	1	
40	96548	WN 8	7.85	0.46	4		4
52	115473	WC 5	9.98	0.51	1		
57	119078	WC 7	10.11	0.59	3		
69	136488	WC 9	9.43	0.67	1		1
71	143414	WN 6	10.22	0.41	1		
77	150136	WC 8	13.16	1.19		1	
78	151932	WN 7	6.61	0.52	16	4	3
90	156385	WC 7	7.45	0.23	4	3	
92	157451	WC 9	10.60	0.57	1		2
103	164270	WC 9	9.01	0.53	2	1	
111	165763	WC 5	8.23	0.30	2	2*	
128	187282	WN 4	10.54	0.32	2		
134	191765	WN 6	8.23	0.58	14	2	
135	192103	WC 8	8.36	0.42	3	2	
136	192163	WN 6	7.65	0.59	31		35
138	193077	WN 6 + abs	8.10	0.63	6		1
148	197406	WN 7 (SB1)	10.46	0.76			1
155	214419	WN 7 (SB1)	8.75	0.76	1	1	

† E(B–V)=1.212 E(b–v), from Turner (1982).

* LWR 10490 was not included in the mean spectrum due to its poor quality.

Chapter 3

IUE Observations of Variability in the WN6 star HD 192163

3.1 Introduction

Over the last few years our understanding of O stars has changed considerably following observations at various wavelengths indicating that the winds contain extensive structure and are usually variable. For example, radio observations have shown that some O stars are nonthermal sources (Abbott, Bieging and Churchwell, 1984); UV observations have shown that the winds are often inhomogeneous and vary with time (Prinja and Howarth, 1986, 1988); and optical observations have shown that many O stars are nonradial pulsators (Baade 1988). These observations have led to new time-dependent stellar wind models incorporating radiatively-driven wind instabilities (see Chapter 1, Section 1.2.2). How Wolf-Rayet (WR) stars, the descendants of massive O stars, fit into this model is not clear. At optical wavelengths, it is well known that some apparently single WR stars show both light and spectral variations but this has traditionally been explained in terms of a compact companion. (A WR+compact binary is an expected stage in the evolution of massive close binaries; see Chapter 1, Section 1.1.1). The recent observations of variability in single O stars have naturally led to a re-appraisal of the cause of variability in WR stars.

Ultraviolet observations have the potential of discriminating between binary-related changes and intrinsic wind variations. For the binary case, we would expect to see phase-related ultraviolet profile variations as a result of the Hatchett and McCray (1977) effect; X-rays produced by the accretion of stellar wind material on to the neutron star will strongly modify the ionization structure of the wind as a function of phase (for details see Chapter 1, Section 1.1.4). This has led to the extensive work described in Section 1.1.4 of Chapter 1 on two WR + compact object candidates; HD 50896 and HD 96548 as well as to the study presented in this chapter.

HD 192163 is a single-lined WN6 star which largely fulfils the criteria for WR+compact candidacy; it is associated with the ring nebula NGC 6888 and shows spectral and light variations at optical wavelengths. It does not, however, have an unusually large z-distance (77 pc) and is, in fact, a member of the Cyg OB1 association (van der Hucht *et al.*, 1988). Koenigsberger, Firmani and Bisiacchi (1980) first reported emission line and radial velocity variability in HD 192163 and suggested a period of 4.5 days. Further spectroscopic observations of HD 192163 by Aslanov and Cherepashchuk (1981) confirmed the 4.5 day period although the radial velocity curves are noisy and have an amplitude of only 20 km s^{-1} or 1% of the width of the emission lines.

More recently, Vreux, Andrillat and Gosset (1985) analysed all the published radial velocity data together with a new more extensive set of observations. They find that radial velocity variations are definitely present and periodic. They derive a much shorter period of 0.45 days and suggest that the star may be undergoing nonradial pulsations. Matthews and Beech (1987) have, however, questioned the validity of the frequency analysis employed in the Vreux *et al.* paper for their period determination. They find that the 4.5 day period (which is an alias of the 0.45 day period) gives an acceptable fit to the Vreux *et al.* data if one datum point is removed and suggest that it was premature of them to identify the 0.45 day period as the correct one. In addition, Cox and Cahn (1988) have examined theoretically the pulsational stability of WR stars and find no unstable g-type nonradial modes in any of their models.

Concerning photometric variations, Aslanov (1982) found weak variations in HD 192163 with a 4.5 day period. Further photometric observations by Antokhin and Cherepashchuk (1985) showed that HD 192163 is slightly variable at the 0.01 magnitude level with a period of 4.554 ± 0.006 days. Moffat and

Shara (1986), on the other hand, find only weak evidence for variability in their 1983 dataset and virtually none in their 1984 dataset. Finally, Robert *et al.* (1989) find that their blue broadband linear polarization data show only small amplitude variations with no significant periodicity.

To summarise, the available observations of variability in HD 192163 and the resulting periods do *not* present overwhelming evidence for the star being a binary. A similar situation prevails for most of the other WR+compact candidates with the possible exception of HD 50896 which has a well established period of 3.76 days. One serious objection to this whole scenario is the lack of observed X-rays arising from the accretion of wind material by the compact companion. A recent detailed analysis of HD 50896 by Stevens and Willis (1988) has shown that, while the dense WR wind will absorb a large fraction of the X-rays emitted, the observed X-ray luminosity should be considerably higher than that actually observed by *Einstein*, which can be attributed to intrinsic wind emission. Similarly for HD 192163, *Einstein* observations (Pollock, 1987) over the 0.2–4 keV range give an X-ray luminosity of $6 \pm 6 \times 10^{31}$ ergs s^{-1} which is entirely compatible with intrinsic weak wind emission. This problem is addressed in more detail in Section 3.4.

In this chapter an extensive set of new IUE observations of HD 192163 together with data drawn from the IUE archive will be presented. These observations are described in Section 3.2 and, in Section 3.3, the spectra are compared and the observed line profile variations are discussed. In Section 3.4, the variations are discussed in terms of binary-induced changes and this hypothesis is tested by examining the computation of the expected X-ray luminosity of HD 192163 and comparing the observed variations with those predicted by the Hatchett and McCray effect. The observed line variability is discussed in terms of intrinsic stellar wind variations in Section 3.5 and the results are compared with those obtained for O stars and other WR stars.

3.2 Observations

HD 192163 was observed over 48 hours in April 1987 with the IUE satellite. The observations were continuous apart from two periods of 6 and 10 hours when over-ride observations of SN1987a were made. The high resolution dataset obtained for HD 192163 consists of 24 SWP (Short Wavelength Prime: $\lambda\lambda 1150-2050$ Å; $\Delta\lambda \sim 0.1$ Å) and 24 LWP (Long Wavelength Prime: $\lambda\lambda 1850 - 3200$ Å; $\Delta\lambda \sim 0.2$ Å) spectra. I have also obtained all available SWP (22 images) and LWP (7 images) spectra from the IUE archive at the Rutherford Appleton Laboratory (Giaretta, Mead and Benvenuti, 1987; Stickland and Harvey, 1987). These spectra consist of three distinct groups: 8 SWP and 7 LWP spectra obtained over 27 hours in 1983; 5 SWP spectra obtained over 21 hours in 1982; and 9 individual spectra, representing glimpses of the star's spectrum in time, acquired between 1978 and 1987. The details of these 46 SWP and 31 LWP spectra are given in Tables 3.1 and 3.2 respectively; listed are the image number, the Julian Date at the beginning of the exposure, the exposure time and the aperture (S = Small $\sim$ 3 arcsec radius; L = Large $\sim 10 \times 20$ arcsec).

The spectra have been uniformly extracted from either the GPHOT or PHOT images using the IUEDR package (Giddings, 1983; Giddings and Rees, 1989) available on the UK SERC STARLINK network of VAX computers. The advantages of the IUEDR extracted spectra over the IUESIPS output provided by the IUE project are described by Willis *et al.* (1989). The reduced spectra (mapped at 0.1 and 0.2 Å intervals for the SWP and LWP ranges respectively) have been analysed using the interactive data analysis software DIPSO (Howarth and Murray, 1990), also available on STARLINK.

Table 3.1

IUE SWP High Resolution Images of HD 192163

SWP Image Number	Julian Date 2440000+	Exposure Time (s)	Aperture
1668	3658.571	2400	S
2517	3759.189	3600	S
2841	3785.488	3000	S
3419	3835.671	2400	S
3420	3835.727	1500	S
8812	4351.957	1500	L
14133	4756.144	1500	L
16089	4991.473	1500	L
18839	5324.187	1200	L
18840	5324.230	900	L
18846	5324.944	1200	L
18847	5324.981	2400	L
18849	5325.059	1200	L
21809	5688.119	2400	L
21810	5688.173	2400	L
21820	5688.937	2400	L
21821	5688.992	2400	L
21822	5689.044	2400	L
21824	5689.122	2400	L
21825	5689.171	2400	L
21826	5689.221	1800	L
30769	6899.589	2400	L
30770	6899.647	2400	L
30771	6899.704	2400	L
30772	6899.760	2400	L
30773	6899.824	2400	L
30774	6899.880	2400	L
30775	6899.937	2400	L
30776	6899.992	2400	L
30777	6900.049	2400	L
30778	6900.106	2400	L
30779	6900.162	2400	L
30781	6900.437	2400	L
30782	6900.493	2400	L
30783	6900.559	2400	L
30784	6900.612	2400	L
30785	6900.664	2400	L
30786	6900.717	2400	L
30787	6900.776	2400	L
30788	6900.829	2400	L
30790	6901.266	2400	L
30791	6901.320	2400	L
30792	6901.374	2400	L
30793	6901.429	2400	L
30794	6901.484	2400	L
32359	7483.747	1200	L

Table 3.2

IUE LWP High Resolution Images of HD 192163

LWP Image Number	Julian Date 2440000+	Exposure Time (s)	Aperture
2433	5688.151	1500	L
2434	5688.204	1500	L
2443	5688.970	1500	L
2444	5689.023	1500	L
2445	5689.074	1500	L
2446	5689.151	1500	L
2447	5689.201	1500	L
10551	6899.567	1500	L
10552	6899.620	3000	L
10553	6899.679	1500	L
10554	6899.737	1500	L
10555	6899.792	1500	L
10556	6899.857	1500	L
10557	6899.915	1500	L
10558	6899.969	1500	L
10559	6900.027	1500	L
10560	6900.082	1500	L
10561	6900.139	1500	L
10563	6900.470	1500	L
10564	6900.539	1500	L
10565	6900.591	1500	L
10566	6900.643	1500	L
10567	6900.696	1500	L
10568	6900.752	1500	L
10569	6900.806	1500	L
10570	6900.871	1500	L
10572	6901.298	1500	L
10573	6901.352	1500	L
10574	6901.407	1500	L
10575	6901.462	1500	L
10576	6901.516	1500	L

3.3 Comparison of the IUE Spectra

The IUE spectra reveal that HD 192163 is a typical WN6 star with numerous strong emission lines. The strongest line in the SWP spectrum is He II λ1640 and there are well developed P Cygni profiles in the N V λ1240, C IV λ1550, He II λ1640 and N IV λ1718 transitions. The ultraviolet spectrum has been presented and described by Willis *et al.* (1986b).

3.3.1 THE SWP SPECTRA

In order to compare the SWP spectra, a mean spectrum of higher signal-to-noise was formed to use as the basis for this comparison. The mean spectrum consists of 5 spectra (SWP 21810, 21824, 21825, 21826 and 30773) which are identical to within the noise level. Small wavelength shifts were corrected for by aligning the interstellar lines near the P Cygni profiles to match those in the mean spectrum. Spurious noise spikes due to cosmic ray events were removed from the individual spectra (pixels affected by reseaux, saturation or extrapolated intensity transfer tables were automatically removed during the extraction procedure).

In Figure 3.1, the nine individual "snapshot" spectra, taken between 1978 and 1987, covering the N IV P Cygni profile are shown in chronological order starting from the bottom. Each spectrum (thin line) is compared with the mean spectrum (thick line) and plotted in velocity space. The lower five spectra were taken with the small aperture and are scaled by constants to match the mean spectrum because this aperture has a transmission of $\sim$ 50% compared to the large aperture through which all the other observations were made. This figure shows that no obvious large scale variability is present in any of the nine spectra covering scattered epochs. There may, however, be small scale changes occurring in the extreme absorption edge as seen in the first three small aperture spectra (SWP 1668, 2517 and 2841). The He II P Cygni profiles for these three spectra show similar changes but no variations are discernible for C IV. The two epochs of spectra obtained in 1982 (5 spectra over 21 hours) and 1983 (8 spectra over 27 hours) are shown in Figures 3.2 and 3.3 for the N IV P Cygni profile as in Figure 3.1. The first spectrum in each series is plotted at the bottom of the figure and the time interval is indicated between each successive spectrum. It can be seen that there is no substantial variability present either within or between epochs for N IV and the same is also true for the He II and C IV P Cygni profiles. Finally, in Figures 3.4, 3.5 and 3.6 the 24 SWP spectra obtained over 48 hours in 1987 for N IV, He II and C IV are presented. (The time interval between successive spectra is indicated in Figure 3.4.) Inspection of Figures 3.4–3.6 reveals that the first half of the dataset (SWP 30769–SWP 30781) shows no differences to within the noise whereas for the second half of the dataset (SWP 30782–SWP 30794), it is immediately apparent that profile variations are present. For comparison purposes, it will be assumed that the mean spectrum represents the undisturbed, quiescent or

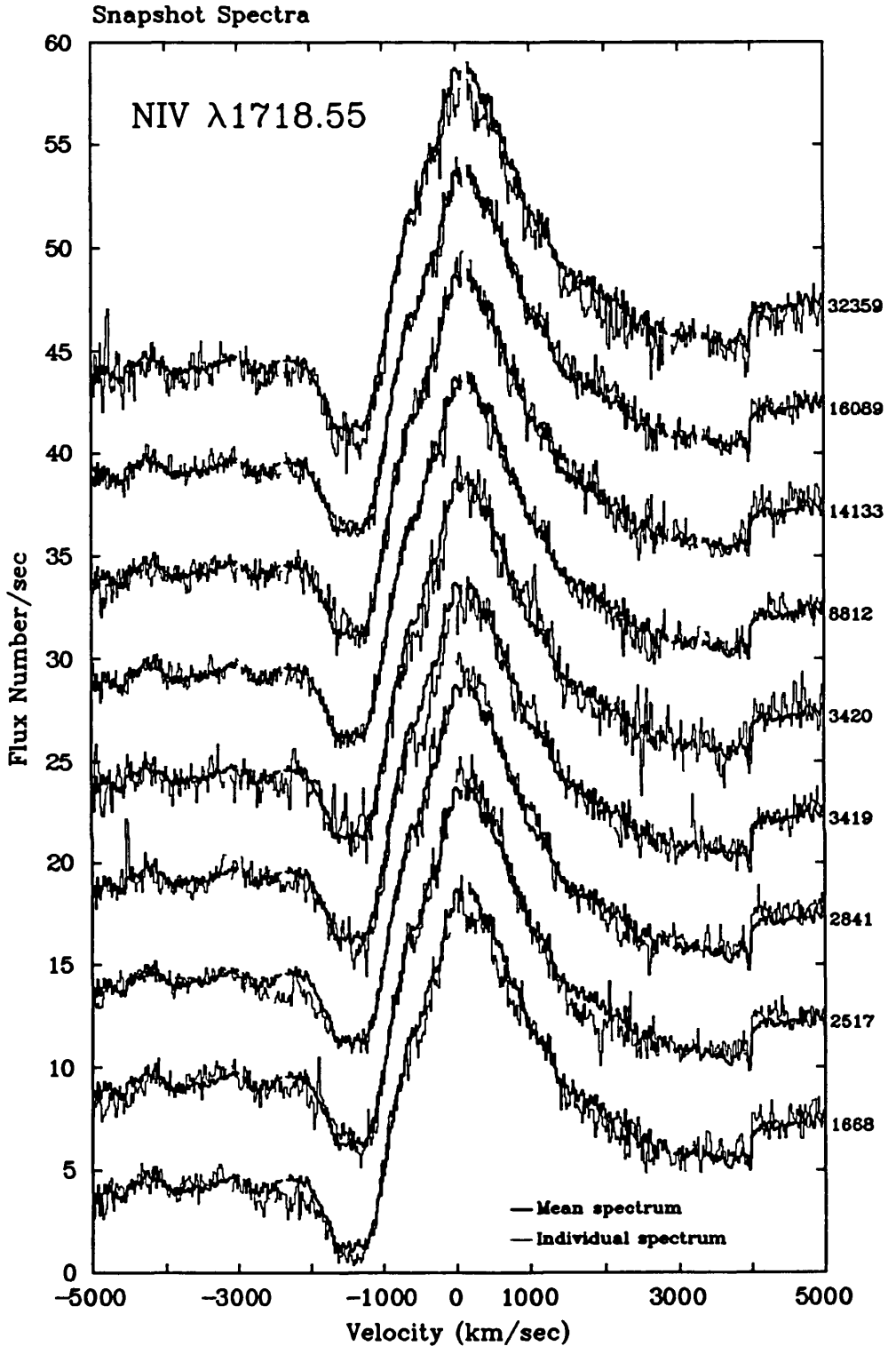

Figure 3.1: The nine "snapshot" spectra (thin line) taken between 1978 and 1987 compared with the mean spectrum (thick line) for the N IV λ1718 P Cygni profile. The spectra are arranged chronologically from the bottom; the SWP image numbers are given on the right hand side. Each spectrum (except the first) has been shifted by 5 ordinate units.

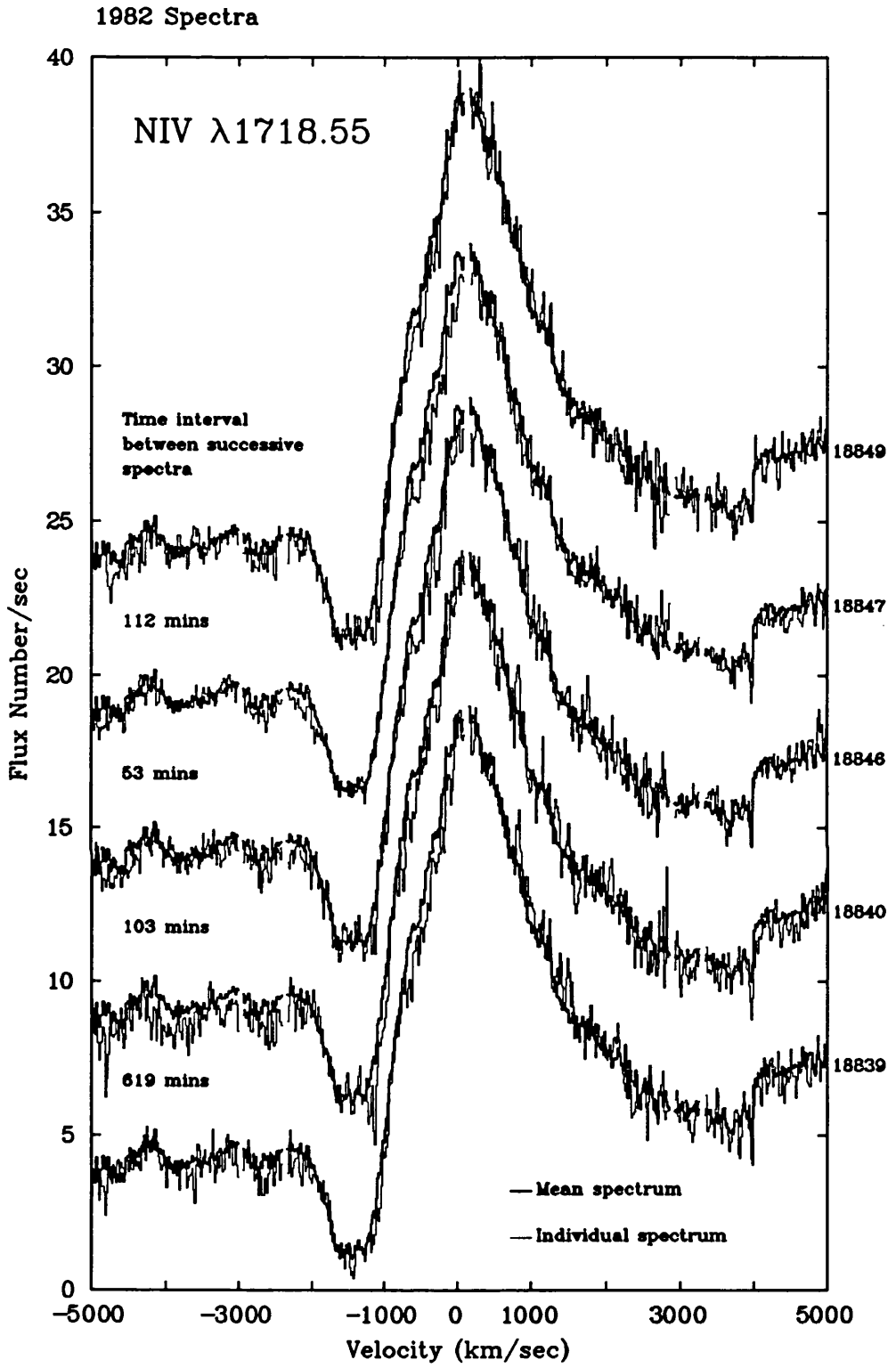

Figure 3.2: The five spectra taken over 21 hours in 1982 compared with the mean spectrum for the NIV λ1718 P Cygni profile. The time interval between successive spectra is indicated. Other details as for Figure 3.1.

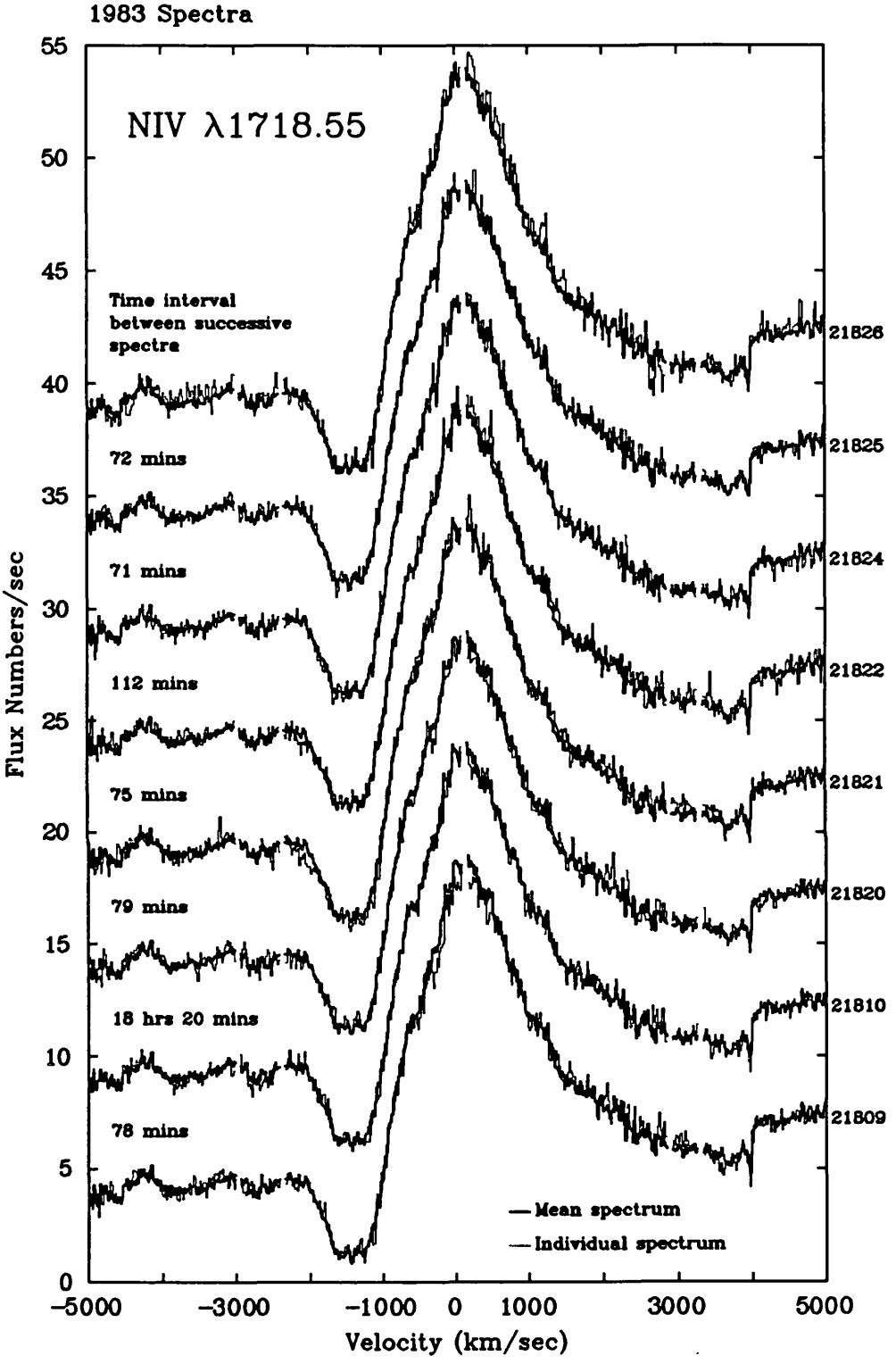

Figure 3.3: The eight spectra taken over 27 hours in 1983 compared with the mean spectrum for the N IV λ1718 P Cygni profile. Other details as for Figure 3.1.

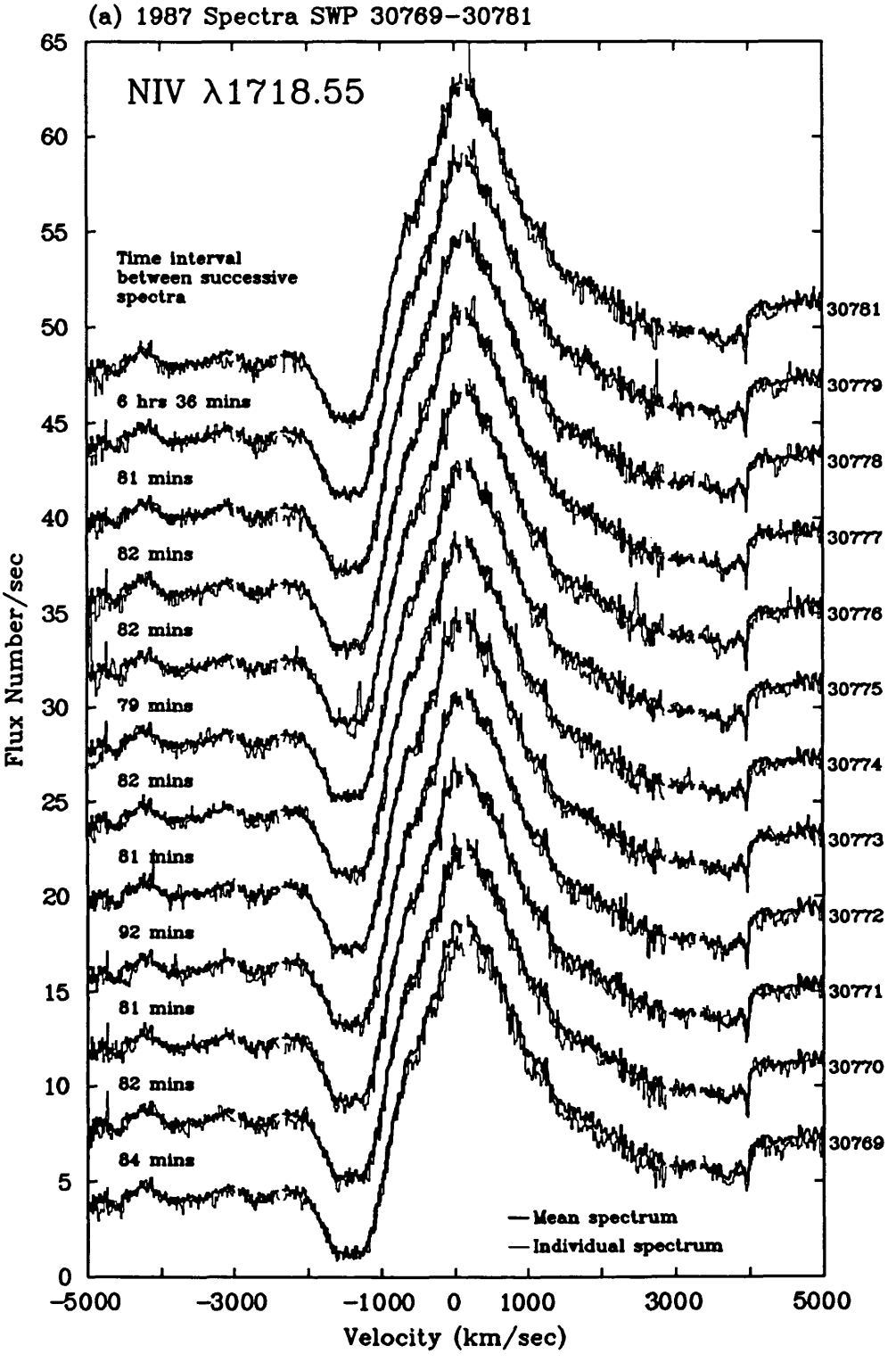

Figure 3.4a: First half of the 24 spectra comprising the extensive 1987 dataset which covers a total of 48 hours compared with the mean spectrum for the NIV λ1718 P Cygni profile. The time interval between successive spectra is indicated. Other details as for Figure 3.1.

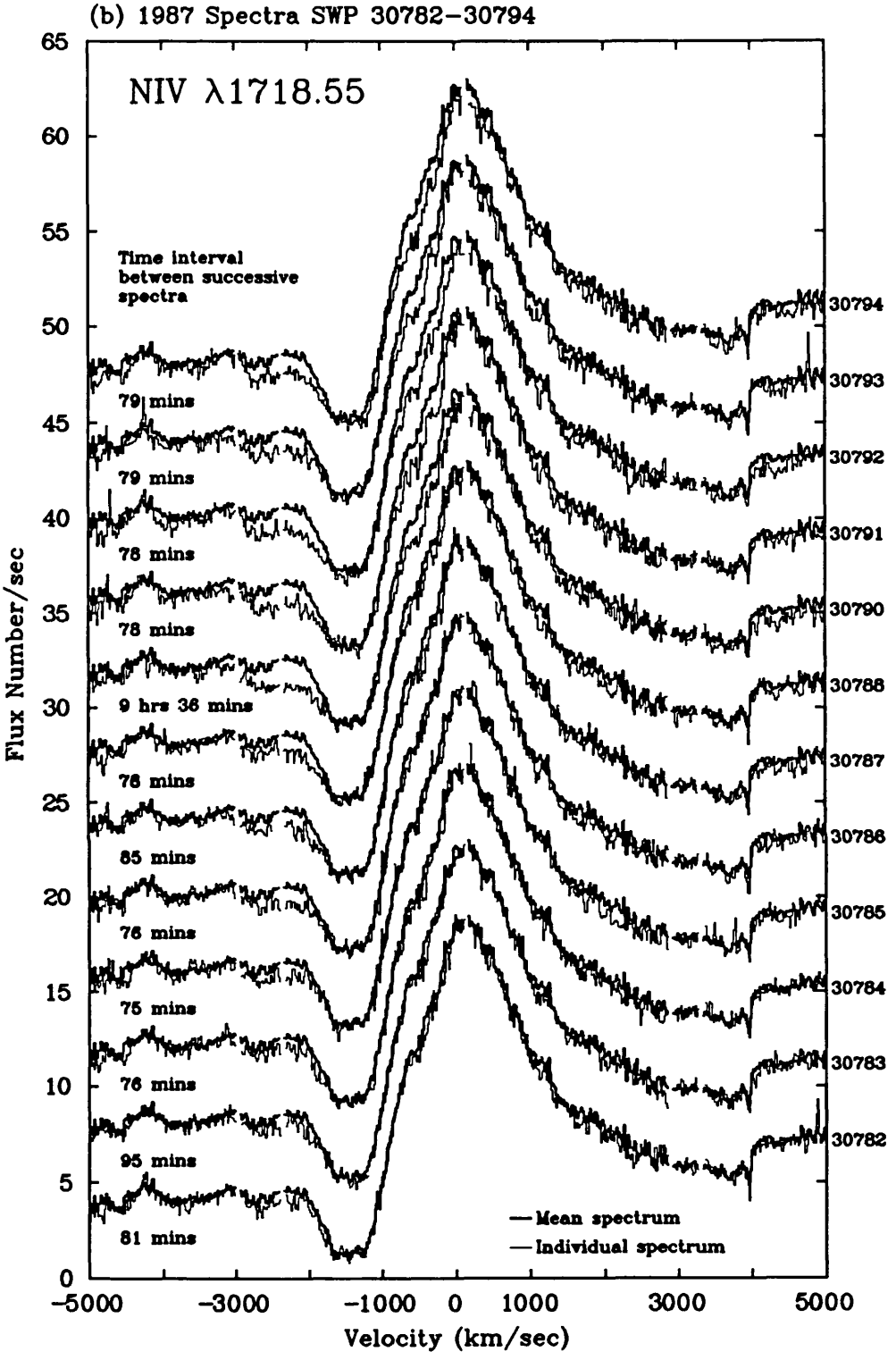

Figure 3.4b: Second half of the 24 spectra comprising the extensive 1987 dataset which covers a total of 48 hours compared with the mean spectrum for the NIV λ1718 P Cygni profile. The time interval between successive spectra is indicated. Other details as for Figure 3.1.

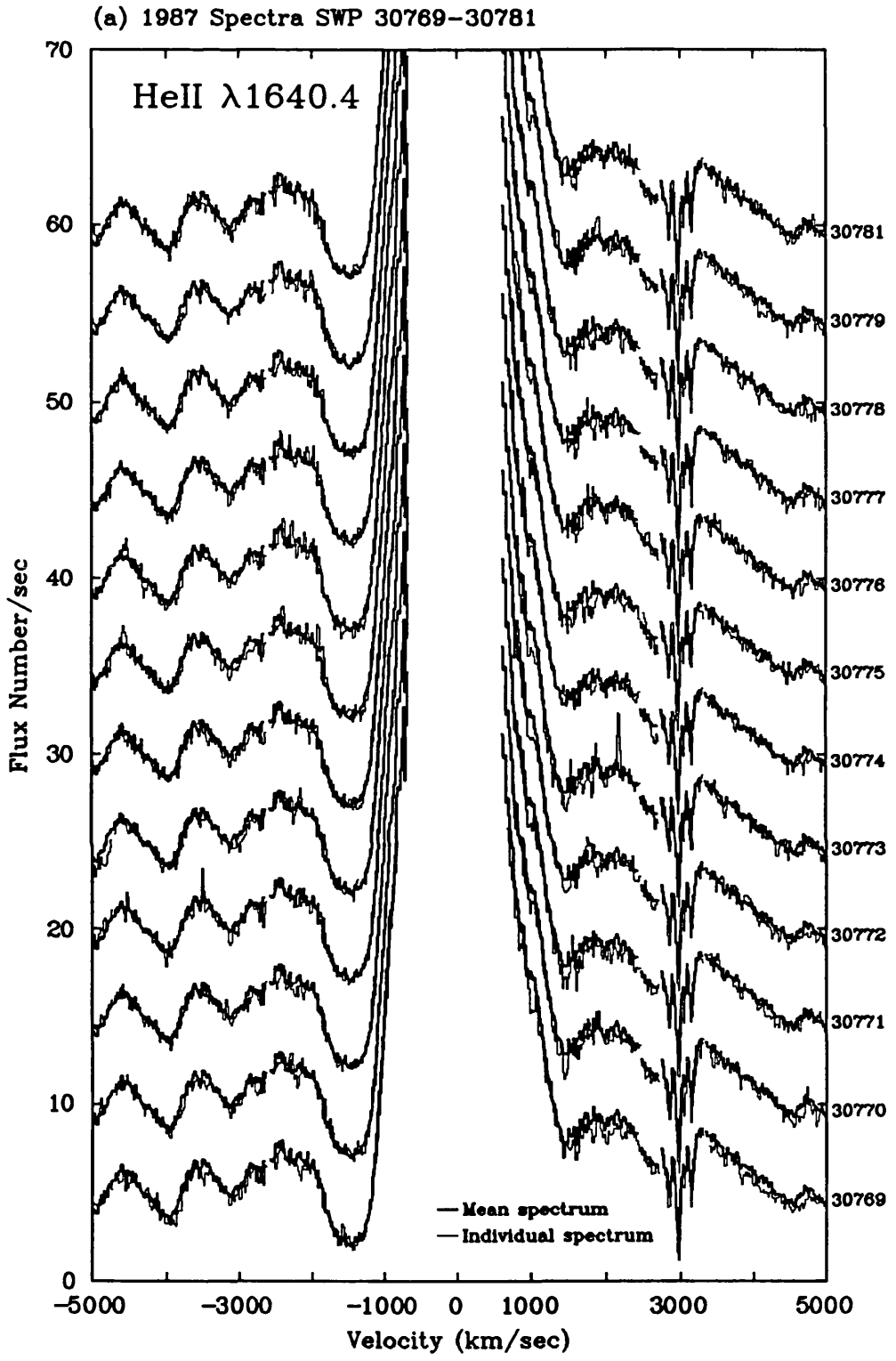

Figure 3.5a: First half of the 24 spectra comprising the extensive 1987 dataset which covers a total of 48 hours compared with the mean spectrum for the He II λ1640 P Cygni profile. The time interval between successive spectra is indicated in Figure 3.4. Other details as for Figure 3.1.

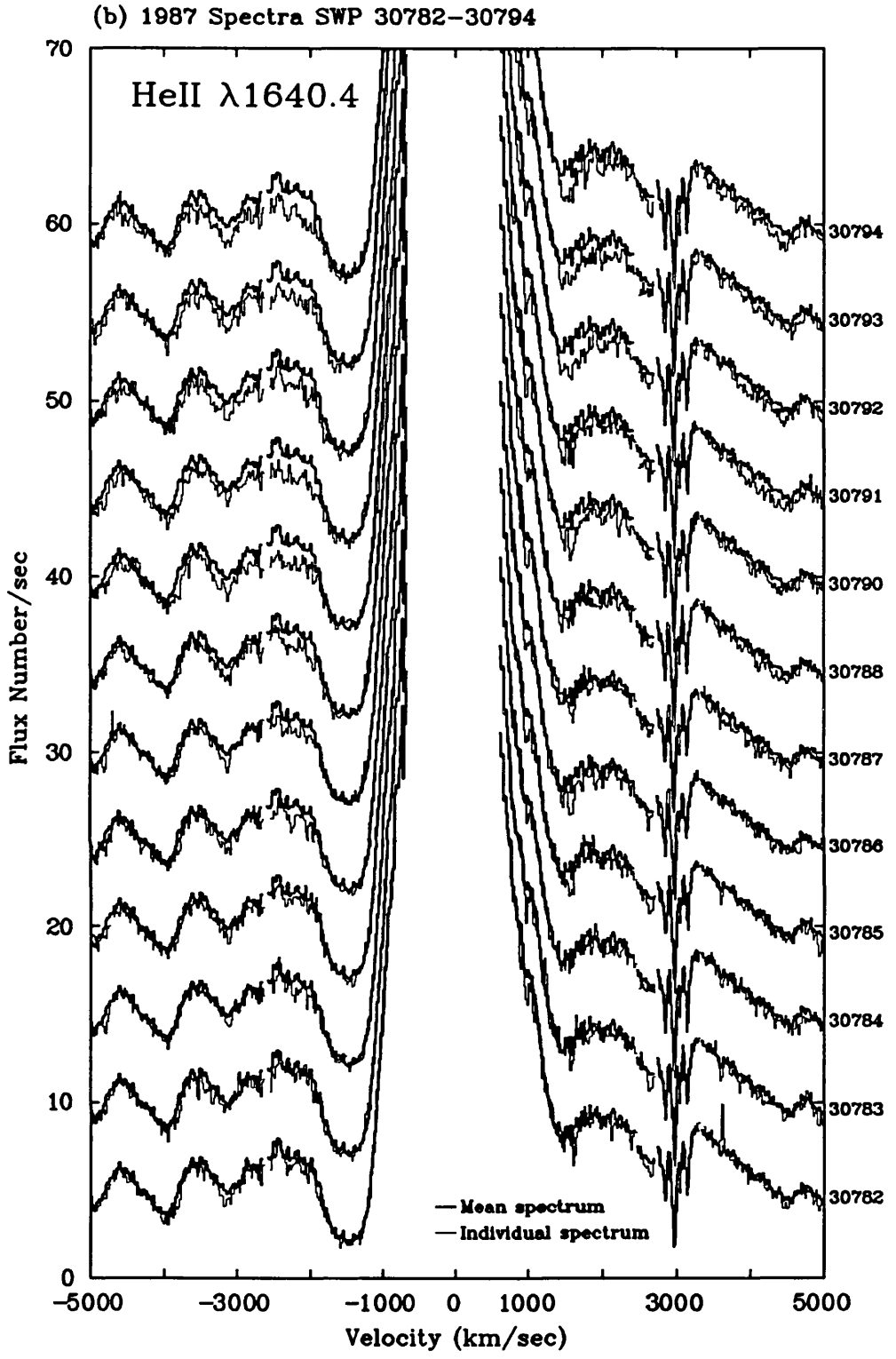

Figure 3.5b: Second half of the 24 spectra comprising the extensive 1987 dataset which covers a total of 48 hours compared with the mean spectrum for the He II λ1640 P Cygni profile. The time interval between successive spectra is indicated in Figure 3.4. Other details as for Figure 3.1.

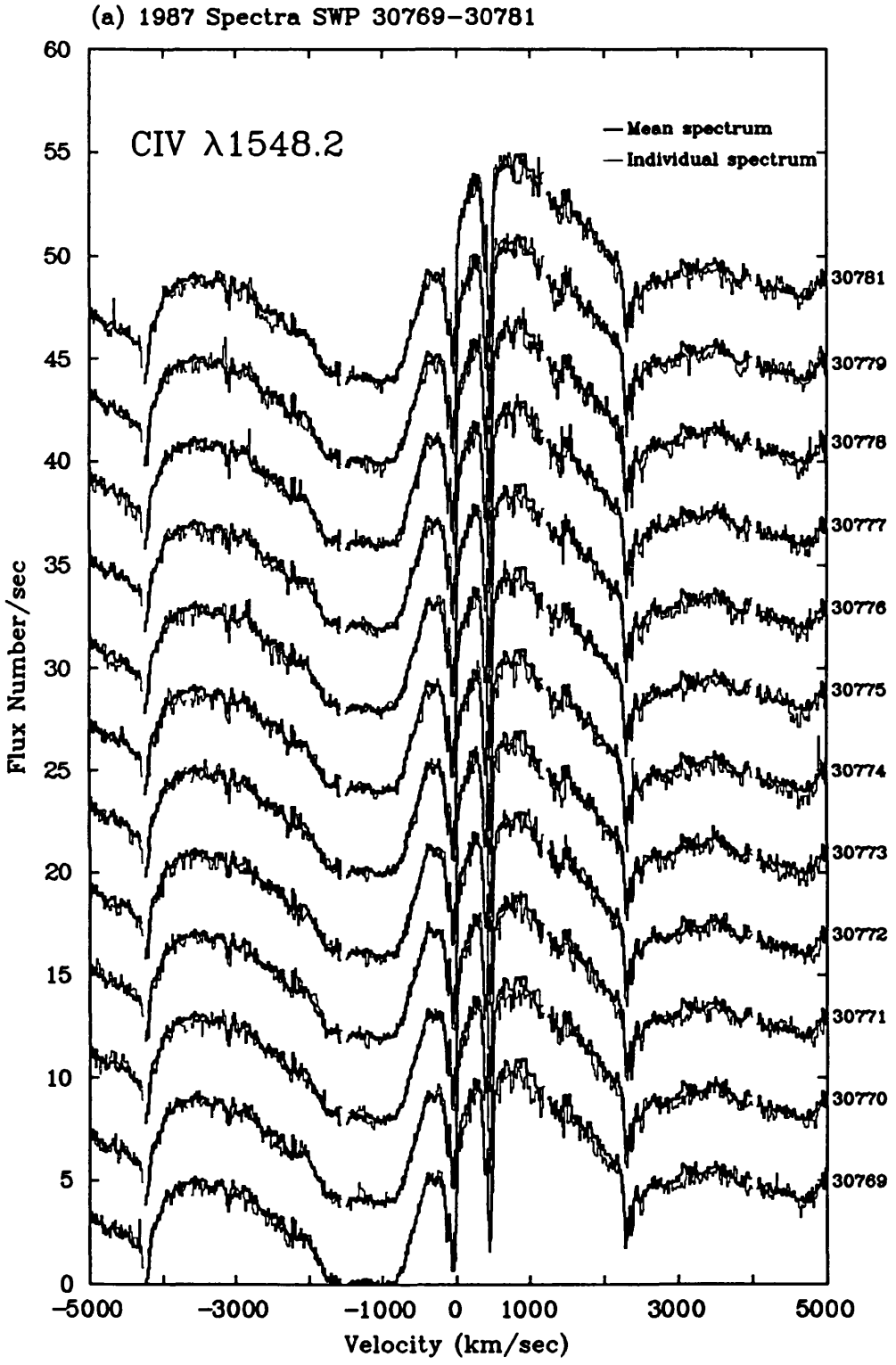

Figure 3.6a: First half of the 24 spectra comprising the extensive 1987 dataset which covers a total of 48 hours compared with the mean spectrum for the CIV λ1550 P Cygni profile. The time interval between successive spectra is indicated in Figure 3.4. Other details as for Figure 3.1.

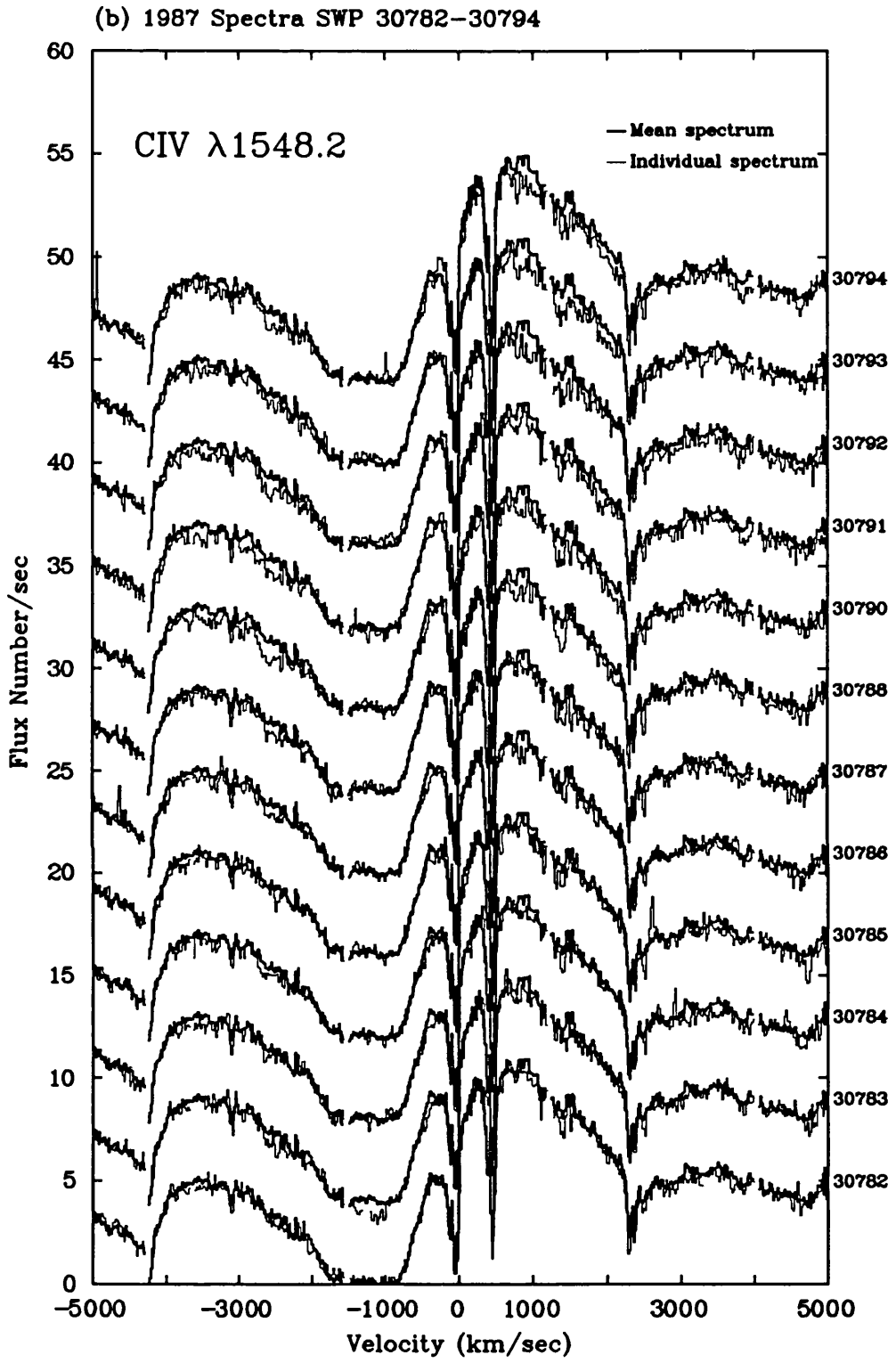

Figure 3.6b: Second half of the 24 spectra comprising the extensive 1987 dataset which covers a total of 48 hours compared with the mean spectrum for the C IV λ1550 P Cygni profile. The time interval between successive spectra is indicated in Figure 3.4. Other details as for Figure 3.1.

"normal" wind of HD 192163. This is substantiated by the fact that the archive spectra (*cf.* Figures 3.1–3.3) and the first half of the 1987 dataset agree well with the mean spectrum. The maximum edge velocities of the N IV, He II and C IV P Cygni absorption components measured from the mean spectrum are: −2050, −1950 and −2350 km s^{-1} respectively. These values agree well with those given by Willis (1982) who finds that the maximum outflow velocity for the wind of HD 192163 from IUE data is −2400 km s^{-1}, as determined by the point where the C IV absorption edge intersects the continuum.

The spectra displaying line profile variations shown in Figures 3.4–3.6 (SWP 30782–SWP 30794) cover a time span of 24 hours; there is a gap of 9.5 hours between SWP 30788 and SWP 37890 due to an intervening observation of SN1987a. Figure 3.4, covering the N IV λ1718.55 P Cygni profile, shows that, as time progresses, the P Cygni absorption edge deepens compared to the mean spectrum over the velocity range $\sim$ −1700 to $\sim$ −3100 km s^{-1}. This excess absorption is also seen simultaneously in He II (Figure 3.5) and to a lesser extent in C IV (Figure 3.6). In contrast to N IV, however, the He II absorption excess appears to extend up to $\sim$ −4000 km s^{-1}. The variation in the C IV absorption edge is much smaller but each spectrum from SWP 30790 to SWP 30794 in Figure 3.6 shows excess absorption up to the maximum velocity observed for He II. The maximum outflow velocities measured for all three ions in the 1987 series of spectra which show variations therefore exceed those encountered in the normal wind as defined by the mean spectrum. From Figures 3.4–3.6, it is also apparent that smaller variations are occurring in other regions of the P Cygni profiles. For N IV, excess absorption is apparent from $\sim$ 0 to −1100 km s^{-1} which, together with the excess absorption already noted at higher outflow velocities, implies that the whole wind, as seen in absorption through N IV, is varying (changes in the bottom of any of the P Cygni profiles are not expected as they are all too optically thick over this range). Unfortunately, no information is available about variations over this velocity range of 0 to −1100 km s^{-1} for He II because of saturation in the data through over-exposure of the IUE SWP camera. For C IV, no obvious variations are detected in the low velocity region of the profile to match those of N IV; this is not surprising since the higher velocity variations are much smaller compared to N IV. Variations also appear to be present at high positive velocities (1400 – 2500 km s^{-1}) in the electron scattering red wing of the He II emission profile. These are undoubtedly

real since they share the same pattern of growth as the absorption excess seen at high negative velocities. This variation or *emission deficit* is not observed in N IV but for C IV, the red emission wing does appear to weaken compared to the mean spectrum, particularly in the last three spectra.

In order to quantify these complex variations, I have measured the equivalent widths of the absorption excesses in the differenced spectra (individual − mean spectrum) for all three ions and these are given in Table 3.3. A fixed velocity range was used for each ion; -1690 km s^{-1} to -3130 km s^{-1} for N IV and -1690 km s^{-1} to -4000 km s^{-1} for He II and C IV. (These ranges were evaluated by taking the mean of the estimated cut-off velocities for each spectrum.) In Figure 3.7 the equivalent width of the absorption excess, measured in the N IV, He II and C IV lines, is plotted as a function of time for all the April 1987 observations. For N IV, there is a progressive increase in the strength of the absorption excess followed by a decrease (the peak is not observed because of the gap in the observations). For He II, however, only a rise in the strength of the absorption excess is observed and no decrease. The absorption excess measurements for C IV show that this ion exhibits a similar behaviour to N IV with a gradual rise in strength and then a decrease although the overall change is much less marked. An indication of the error associated with each measurement is given by the scatter of the first 11 points for each ion as these spectra are observed to show no variations (*cf.* Figures 3.4–3.6). The differing behaviour of the ions has been quantified by doing linear least squares fits to determine the rise and decay rates (as shown in Figure 3.7). For N IV, the rate of rise is 1.7 ± 0.2 Å/day and the rate of decay is -2.2 ± 0.5 Å/day. Thus, within the errors, the rise and decay rates are the same. Extrapolating these fits backwards and forwards in time, the total rise and decay timescales are each found to be $\sim$ 20 hours. The rate of increase in the absorption excess for He II is 2.5 ± 0.2 Å/day or slightly greater than that found for N IV. For C IV, the rate of increase is 1.4 ± 0.2 Å/day which is similar to that of N IV. The rate of decay for C IV is -1.9 ± 0.7 Å/day which is the same, to within the errors, as the rate of increase for this ion. Thus I conclude that the rise and decay rates are approximately the same for each ion irrespective of whether there is a rise and decay in the absorption excess (N IV, C IV) or just a rise (He II).

I have also measured the absorption excesses and emission deficits for the other velocity ranges undergoing variations; these are plotted against time

Table 3.3

Equivalent Width Measurements (Å) of the Absorption Excesses and Emission Deficits in the 1987 Spectra for HD 192163

SWP Image Number	N IV −1690 to −3130 km s^{-1}	He II −1690 to −4000 km s^{-1}	C IV −1690 to −4000 km s^{-1}	N IV −1690 to 0 km s^{-1}	He II +1415 to +2460 km s^{-1}	C IV +560 to +2235 km s^{-1}
30769	0.312	1.158	0.696	0.895	1.060	1.414
30770	0.380	0.711	0.446	0.576	0.562	0.843
30771	0.158	0.843	0.568	0.273	0.872	1.034
30772	0.229	0.578	0.234	0.528	0.562	0.144
30773	0.200	0.431	0.722	0.431	0.383	1.048
30774	0.122	0.641	0.323	0.421	0.236	1.007
30775	0.325	0.359	0.656	0.479	0.786	0.537
30776	0.176	0.638	0.361	0.338	0.344	0.652
30777	0.272	0.478	0.487	0.395	0.690	0.623
30778	0.419	0.504	0.387	0.393	0.757	0.601
30779	0.370	0.648	0.465	0.339	0.325	0.155
30781	0.518	0.891	0.525	0.491	0.336	0.792
30782	0.634	1.438	0.552	0.410	0.475	0.966
30783	0.648	1.373	0.639	0.403	0.379	0.939
30784	0.730	1.092	0.777	0.463	0.413	0.817
30785	0.827	1.354	0.878	0.294	0.554	1.181
30786	1.011	1.931	0.766	0.369	0.957	0.925
30787	1.173	1.603	0.957	0.678	0.511	1.103
30788	1.099	2.233	1.111	0.734	0.852	1.454
30790	1.737	3.237	1.813	1.430	1.418	1.814
30791	1.453	3.399	1.456	1.426	1.219	1.791
30792	1.513	3.284	1.567	1.529	1.766	1.925
30793	1.297	3.247	1.338	1.280	1.773	2.156
30794	1.221	3.692	1.357	1.583	1.461	2.051

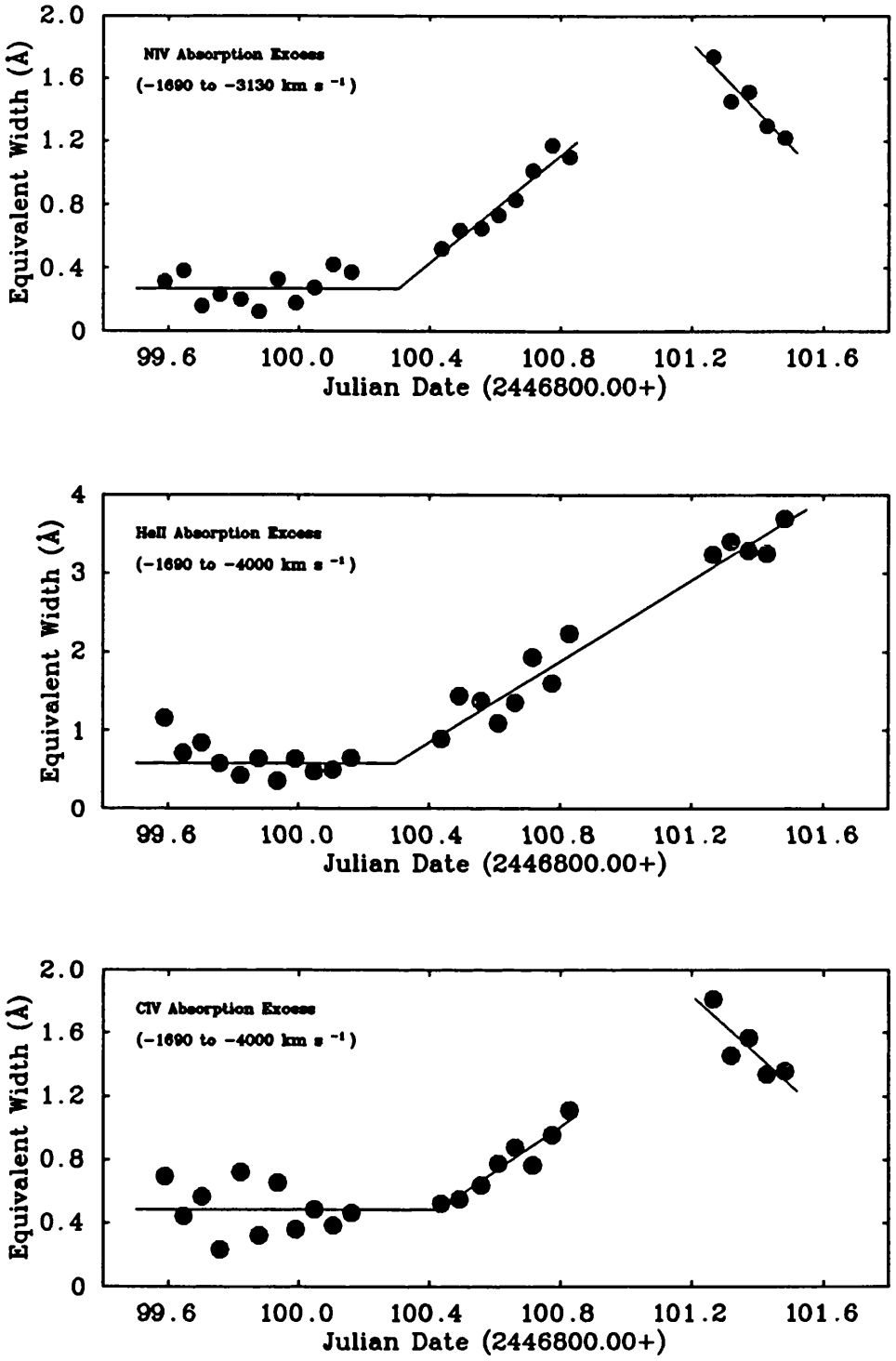

Figure 3.7: The equivalent widths of the absorption excesses for NIV, He II and CIV plotted against Julian Date for the 24 SWP spectra obtained over 48 hours in 1987. The velocity range for each measurement is indicated in the figures. The solid lines represent least squares fits to each dataset.

in Figure 3.8 for the 1987 spectra and listed in Table 3.3. The absorption excess variation for low outflow velocities in N IV (0 to -1090 km s^{-1}) shows a different behaviour to that found for higher outflow velocities in this ion; only an increase in the strength is observed and no corresponding decrease. The slope of this increase in strength is also slightly smaller; 1.2 ± 0.1 Å/day compared to 1.7 ± 0.2 Å/day over the -1690 to -3130 km s^{-1} velocity range. For He II and C IV the emission deficit measurements at positive velocities are shown in Figure 3.8. Again, only an increase in the strength is observed. The measured slopes are the same: 1.3 ± 0.1 Å/day for He II over the velocity range 1415 to 2460 km s^{-1}; and 1.3 ± 0.1 Å/day for C IV over the velocity range 560 to 2235 km s^{-1}. Thus these three velocity ranges all show very similar rates of increase that are smaller than those measured for the features at higher outflow velocities.

I have examined the rest of the SWP wavelength range to see if variations are present in any other emission lines. The only possible profile changes detected at scattered epochs occur in the N V λ1240 P Cygni profile. Unfortunately, this line occurs in a difficult wavelength region because the orders are very closely spaced, making the determination of the interorder background uncertain. Nevertheless, the 1987 series of spectra (with the exception of SWP 30792) show no evidence for any variability in the N V P Cygni absorption profile.

3.3.2 THE LWP SPECTRA

The LWP spectra have been reduced and analysed in the same way as the SWP spectra. No significant variations were found in the 7 archival and 24 1987 spectra although the individual spectra are considerably noisier than the SWP spectra. This result is not too surprising since the variations appear to be confined to the strong P Cygni profiles and there are no major P Cygni profiles in the LWP spectral region.

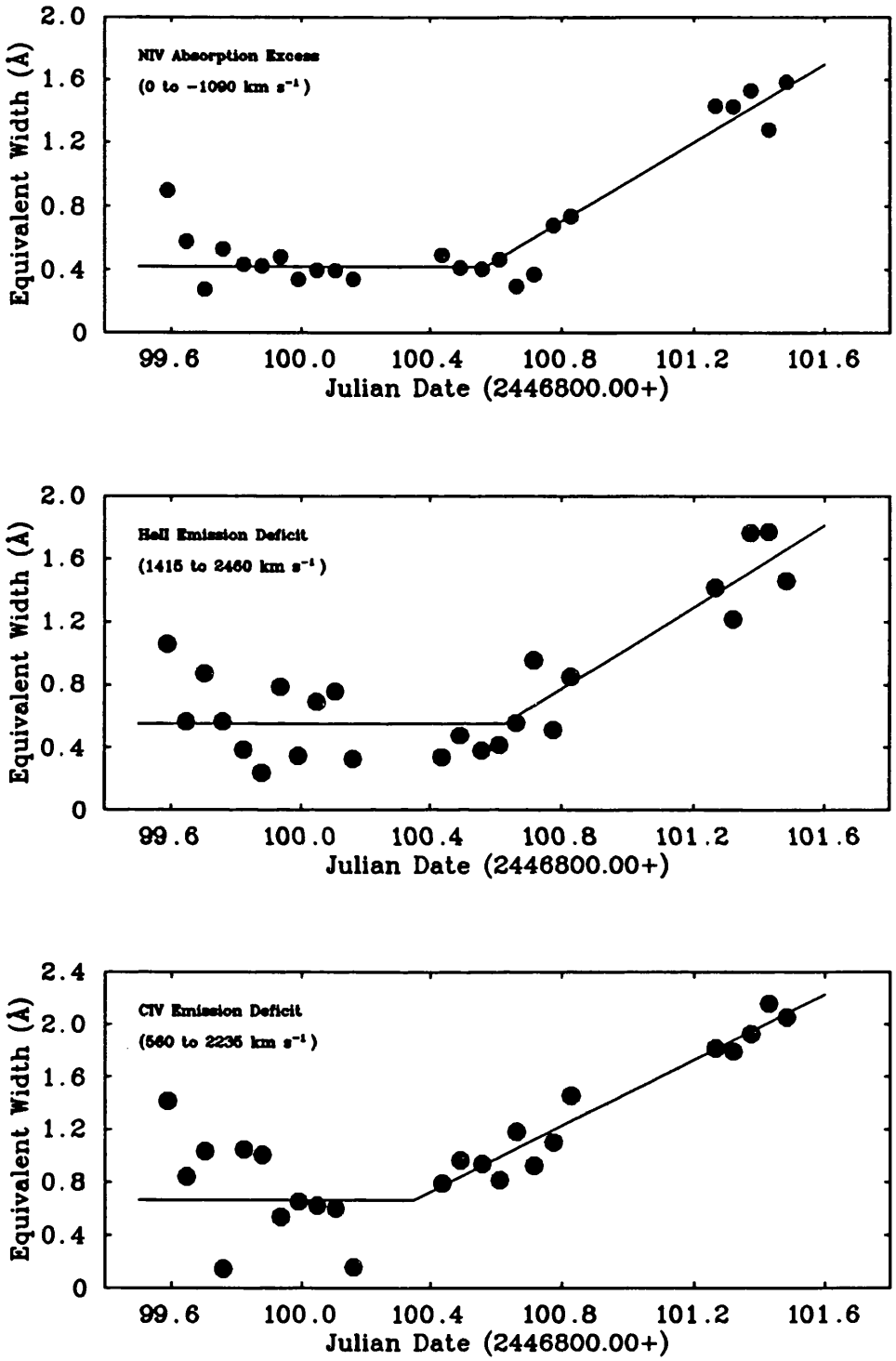

Figure 3.8: The equivalent widths of the absorption excess for N IV and emission deficits for He II and C IV plotted against Julian Date for the 24 SWP spectra obtained over 48 hours in 1987. The velocity range for each measurement is indicated in the figures. The solid lines represent least squares fits to each dataset.

3.4 A Compact Companion?

In the previous section, the complex P Cygni profile variations observed over 48 hours in 1987 were described. I now consider the possible causes of these variations in terms of binary-induced changes in this section and intrinsic stellar wind variations in Section 3.5. In Section 3.1, the observational evidence for HD 192163 being a binary was discussed and I concluded that it was tentative at best. If HD 192163 does have a compact companion, variations in the P Cygni absorption component not unlike those described in Section 3.3.1 would be expected. These variations or the "Hatchett and McCray effect" are critically phase-dependent; the binary hypothesis can thus be tested by determining if the observed P Cygni profile variations have the required phase-dependence. By analogy with X-ray binaries, an accreting neutron star should produce a high level of observable X-ray emission. Again, the neutron star hypothesis can be tested by computing the expected X-ray luminosity of the system as a function of phase. Both these tests require the parameters of the binary orbit of HD 192163. Unfortunately, these parameters are not very well known and therefore, in order to try to improve this situation, all the published optical radial velocities for this star have been re-analysed .

3.4.1 THE BINARY ORBIT

The radial velocity datasets of Koenigsberger *et al.* (1980), Vreux *et al.* (1985) and Aslanov and Cherepashchuk (1981) were examined to determine if any consistent period was present. The Fourier periodogram method (Scargle, 1982) and the period finding algorithm of Lafler and Kinman (1965) were used. It was generally found that the Lafler and Kinman technique was superior to the Fourier method because the datasets suffer from too few points and sampling aliases. The Koenigsberger *et al.* (1980) dataset gives periods between 4.0–5.0 d (depending on the emission line used) in a 4–6 day search region. The Aslanov and Cherepashchuk (1981) data for four emission lines give a mean period of 4.52 ± 0.06 d in a 4–6 day search interval. Vreux *et al.* (1985) found a period of 0.45 or 0.31 d for their dataset but Matthews and Beech (1987) showed that the removal of one or two discrepant points produced an additional period near 4.5 d. The ultraviolet data show that periods as short as 0.45 or 0.31 d can be ruled out because the variations, particularly in He II, show only a progressive increase over 0.9 d. Following Matthews and Beech, I find that the best period

between 4–6 days is either 4.55 or 4.62 d, depending on whether one or two data points are removed from the Vreux *et al.* data. It can therefore be concluded that, if any real period exists, it lies between 4.52–4.62 d.

Orbital solutions to the modified Vreux *et al.* data have been calculated using periods of 4.52, 4.55 and 4.62 d. The resulting parameters for each value of the period do not differ greatly. I therefore decided to adopt the solution for P= 4.55 d with errors that reflect the range of each parameter obtained for the three different solutions. These values are given in Table 3.4 and compared to the mean values of Aslanov and Cherepashchuk (1981) from their emission line analysis. It can be seen that, with the exception of the value for ω (the longitude of periastron), all the parameters agree remarkably well. Following the analysis of HD 50896 by Firmani *et al.* (1980), phase zero is defined to be the passage of the WR star through the γ-velocity from negative to positive velocities. Thus, using this definition, the WR star is in front as phase 0 and behind at phase 0.48; the periastron and apastron passages occur at phases 0.03 and 0.53; and the ascending and descending nodes for the WR star are at phases 0.16 and 0.82 respectively. The inclination of the orbit is unknown. If we take sin $i = 1$, the mass of the secondary is $\sim$ 1.1–1.8 $M_\odot$ for a WR mass of 10–20 $M_\odot$; this mass range is consistent with the secondary being a neutron star.

Table 3.4

IUE SWP High Resolution Images of HD 192163

Parameter	This Work	Aslanov & Cherepashchuk (1981)
Period, P (days)	4.55 ± 0.07	4.52 ± 0.06
Time of periastron passage, T_0 (JD)	2445591.765	—
Time of phase zero (WR in front), E (JD)	2445591.633	—
Orbital eccentricity, e	0.26 ± 0.10	0.29 ± 0.09
Velocity amplitude, K (km s^{-1})	30 ± 1	27 ± 9
Longitude of periastron, ω	$284 \pm 10°$	$196 \pm 23°$
Mass function ($M_\odot$)	0.012 ± 0.001	0.011 ± 0.001

3.4.2 THE EXPECTED X-RAY LUMINOSITY OF HD 192163

Stevens and Willis (1988) analysed the WN5 star HD 50896, which has also been postulated as a prospective WR+compact object binary, and showed that the observed level of X-ray emission from HD 50896 was inconsistent with the existence of an accreting neutron star companion. In this section, using relatively simple models, the hypothesis that HD 192163 has a neutron star companion will be tested by examining a computation of the expected X-ray luminosity of the system, kindly provided to me by Dr I.R. Stevens. For the purposes of the calculation, it was assumed that the WR star and neutron star have masses of 10 and 1.4 $M_\odot$ respectively. The semi-major axis of the system is then 26.0 $R_\odot$, the periastron separation (assuming the eccentricity to be 0.26) is 19.3 $R_\odot$, while at apastron, the separation is 32.8 $R_\odot$. Periastron passage occurs at phase $\Phi = 0.03$ when the neutron star is still largely behind the WR star from the point of view of an earthbound observer.

A mass loss rate of 1.1×10^{-4} $M_\odot$ yr^{-1} was adopted for HD 192163. This value has been calculated using the radio flux of Abbott *et al.* (1986); a distance of 1.8 kpc (van der Hucht *et al.*, 1988); a terminal velocity of 2400 km s^{-1} as derived from the CIV absorption edge by Willis (1982); and assuming that the main ion in the wind is He^+ (Schmutz, Hamann and Wessolowski, 1989). This mass loss rate, coupled with the relatively short orbital period, means that the proposed neutron star companion, if in fact it exists, will be enveloped in the dense wind of the WR star. The neutron star will thus accrete material from the wind giving rise to X-ray emission which will then be attenuated by the surrounding wind material. As a result of the high mass-loss rate, the equivalent column of material between the observer and the neutron star, which varies as a function of orbital phase, will be fairly high. In Figure 3.9, the equivalent column N_H (H cm^{-2}) is given as a function of orbital phase for a variety of orbital inclinations i. The wind is assumed to have a velocity law of the form (*cf.* Pauldrach *et al.*, 1985);

$$v(r) = v_\infty(1 - R_*/r)^{0.8}$$

where R_* is the stellar radius and is assumed to be 7 $R_\odot$ (Schmutz *et al.*, 1989). Figure 3.9 shows that, because of the high wind density, the column of material N_H will be substantial at all phases. The minimum column of material occurs when HD 192163 is behind the neutron star and is around 7×10^{23} H cm^{-2},

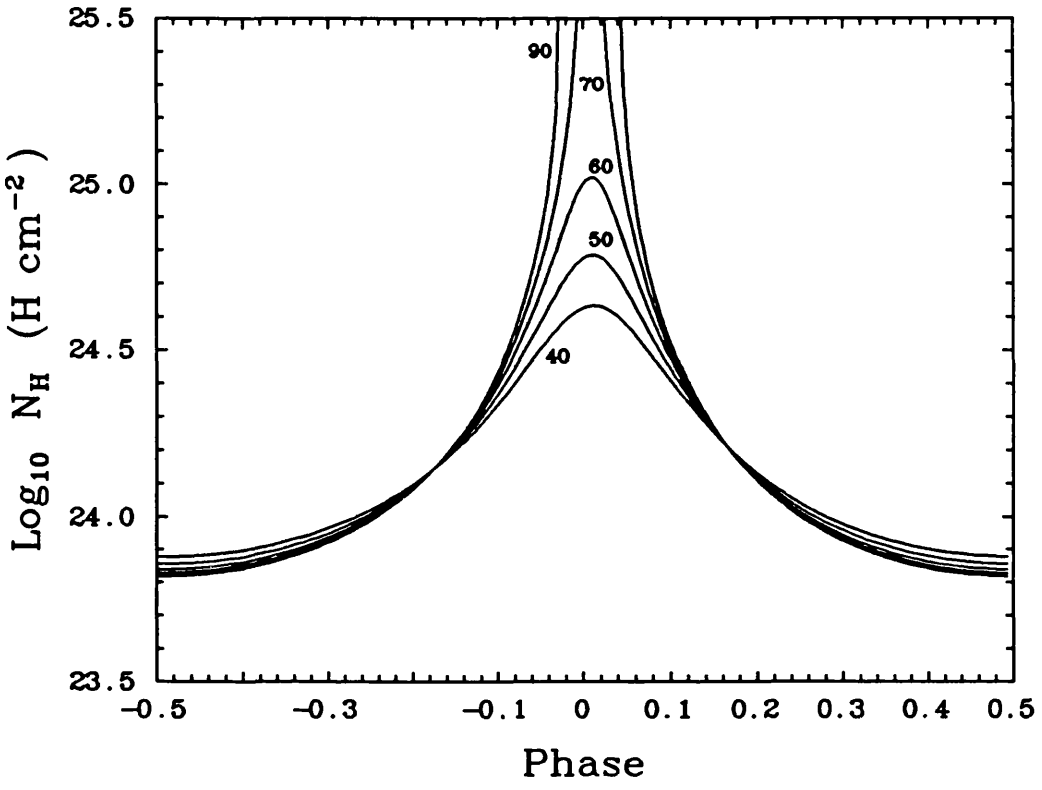

Figure 3.9: The calculated orbital variation of the absorbing column in HD 192163 for a variety of orbital inclinations.

while close to periastron N_H can be extremely large and for values of $i > 70°$ the WR star will occult the neutron star.

The intrinsic X-ray accretion luminosity can be calculated easily (e.g. Stevens, 1988) and is given in Figure 3.10 as a function of orbital phase; phase $\Phi = 0$ occurs when the WR star is in front of the companion and periastron occurs at phase $\Phi = 0.03$. The dense wind, in addition to giving large values of N_H, also gives rise to fairly high levels of X-ray emission, peaking at periastron at a level of over 7×10^{36} ergs s^{-1}, while the minimum which correspondingly occurs at apastron is still close to 2×10^{36} ergs s^{-1}. The dense WR wind will, however, attenuate these high levels of intrinsic X-ray emission. So, in order to compare the expected X-ray flux with observations, it is necessary to include the effects of wind attenuation. The method employed by Vanbeveren, Van Rensbergen and de Loore (1982) has been used. This is somewhat simpler than that used by Stevens and Willis (1988) for their models of HD 50896, but will suffice. In Figure 3.11 the attenuated X-ray luminosity in the 2.0–6.0 keV waveband (which corresponds to the detectors on the *Uhuru* satellite) and the

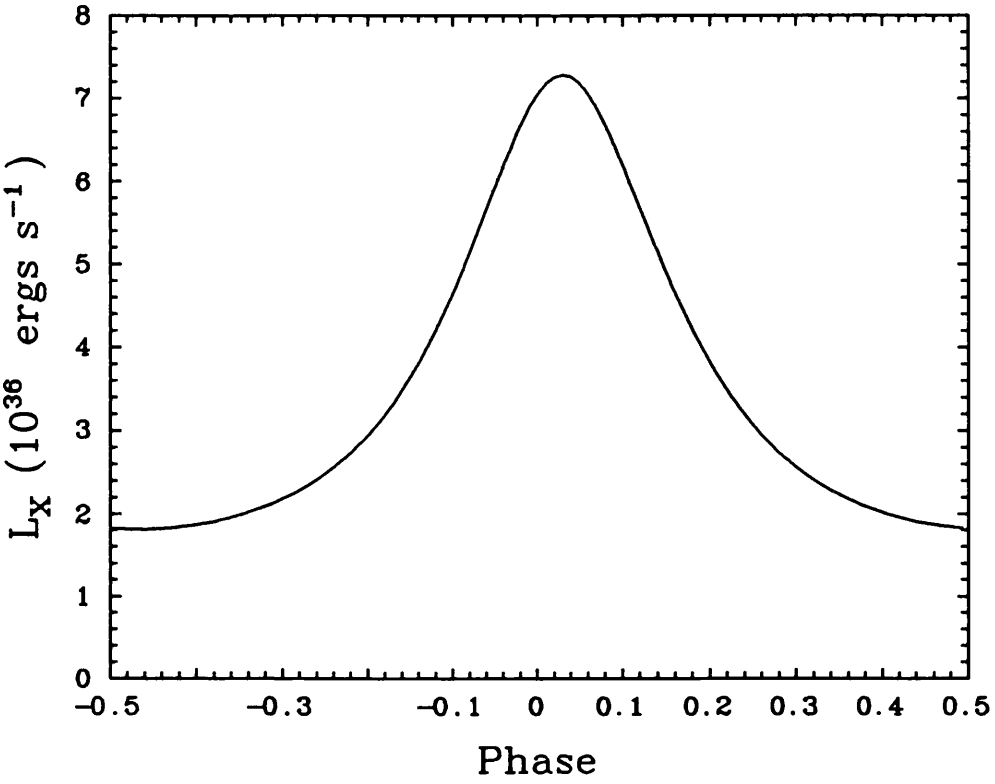

Figure 3.10: The calculated orbital variation of the intrinsic X-ray accretion luminosity of the postulated neutron star companion.

0.2–4.0 keV waveband (which corresponds to the *Einstein* satellite) is given as a function of orbital phase for a model with orbital inclination $i = 60°$. Figure 3.11 shows that for most of the orbit, the level of X-ray emission is $> 10^{34}$ ergs s^{-1} in the *Uhuru* waveband and $> 10^{33}$ ergs s^{-1} in the *Einstein* waveband. Close to $\Phi = 0$, when the intrinsic X-ray luminosity is at its maximum, the flux that would actually be observed in both the 2.0–6.0 keV and the 0.2–4.0 keV wavebands is, however, very low and is largely absorbed by the stellar wind. Note that lower energy X-ray photons will be preferentially photo-absorbed so that the flux degradation in the 0.2–4.0 keV waveband will be greater than that in the 2.0–6.0 keV waveband. In both wavebands the X-ray maximum occurs at phase $\Phi = 0.5$ when, although the intrinsic X-ray flux is at a minimum, the attenuation is also at minimum (*cf.* Figure 3.9).

The results presented in Figure 3.11 can now be compared with the actual X-ray observations of HD 192163 to test the hypothesis that it has a neutron star companion. The *Uhuru* satellite did not detect HD 192163; this gives an upper limit to the X-ray flux of about 1.2×10^{34} ergs s^{-1} (assuming a

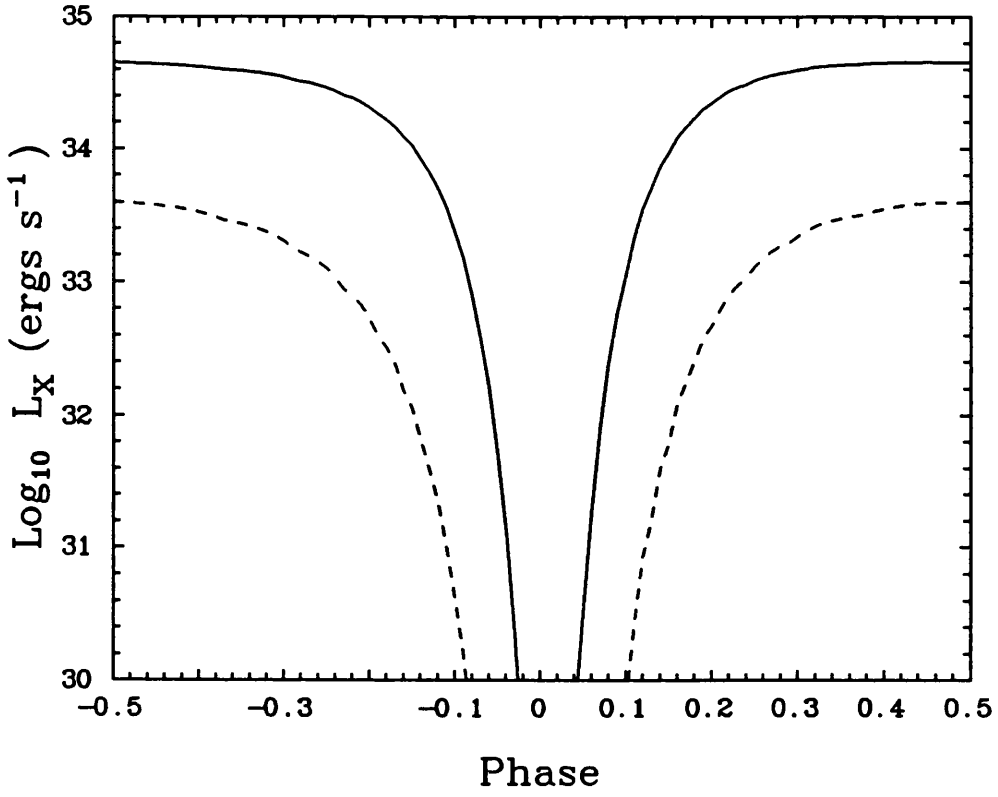

Figure 3.11: The calculated orbital variation of the observed X-ray luminosity in the Uhuru waveband (2.0–6.0 keV — solid line) and the Einstein waveband (0.2–4.0 keV — dashed line).

distance to HD 192163 of 1.8 kpc). HD 192163 has been observed by the *Einstein* satellite to have an X-ray luminosity of $6 \pm 6 \times 10^{31}$ ergs s^{-1} (Pollock, 1987) or $< 2 \times 10^{31}$ ergs s^{-1} (Bocharev, 1988). This low X-ray luminosity is comparable to other (presumably) single WR stars, suggesting that the X-rays observed are a consequence of shocks in the wind rather than an accreting neutron star. Comparison of the *Uhuru* upper limit with Figure 3.11 shows that, for a significant portion of the orbital cycle, HD 192163 should have been detected as an X-ray source by this satellite. The *Einstein* observation occurred at $\Phi = 0.71$ (using the ephemeris given in Table 3.4) and thus should have recorded an X-ray flux 30–70 times greater than that actually detected. Of course, the predicted X-ray fluxes from our model can only be considered a rough estimate since they are based on one binary orbit solution and an assumed inclination. Nevertheless, the fluxes are not expected to change by orders of magnitude for a different orbit solution because the controlling parameter is the

attenuation of the stellar wind. I therefore conclude that the lack of observed X-rays from HD 192163 points to the absence of a neutron star companion.

3.4.3 THE HATCHETT AND MCCRAY EFFECT

The compact companion hypothesis can be further tested by considering the P Cygni profile variations discussed in Section 3.3. If, indeed there is a neutron star companion, the X-rays from the neutron star will affect the ionization balance in a volume surrounding the compact object, which in turn will affect the ultraviolet P Cygni profiles (*cf.* Hatchett and McCray, 1977). To determine accurately the effect of the X-rays on the ionization balance and dynamics of the wind requires very extensive calculations, far beyond the scope of this chapter. Some insight can be obtained, however, by defining a wind ionization parameter ξ given by

$$\xi = \frac{L_x}{n r_x^2}$$

where L_x is the attenuated X-ray luminosity, n is the number density of the wind material and r_x is the distance from the neutron star. Curves of constant ξ give an indication of the zone of influence of the neutron star in the stellar wind. In Figure 3.12a, the contours of constant ξ are shown for HD 192163 at phase $\Phi = 0.0$, when the neutron star is nearly behind the WR star and the separation is close to $20R_\odot$. The WR star of radius $7R_\odot$ is also shown. Conversely, Figure 3.12b shows the contours of constant ξ for phase $\Phi = 0.5$ when the WR star is behind the neutron star and the separation is $33R_\odot$.

From the ionization models of Kallman and McCray (1982), generally, significant changes in ionization fraction only occur for values of $\log_{10}\xi > 1.6$. This X-ray ionization zone (*cf.* Figure 3.12) is small compared to the separation of the two stars because the attenuation of the wind localises the X-ray ionization effect. The question of what effect changes in the ionization fraction will have on the ultraviolet P Cygni profiles is complicated. When the WR star is in front, as in Figure 3.12a, the zone where $\log_{10}\xi > 1.6$ is largely occulted by the WR core and thus little, if any change, would be expected in the emission part of the P Cygni profile. In Figure 3.12b, the zone where $\log_{10}\xi > 1.6$ extends from 28–41 $R_\odot$ or a velocity range of -1900 to -2100 km s^{-1}. We would thus expect ions over this velocity range in the line of sight to be affected by the X-rays from the neutron star when $\Phi = 0.5$. The precise effect depends on the ionization balance of the undisturbed wind. Hillier (1988) has investigated the

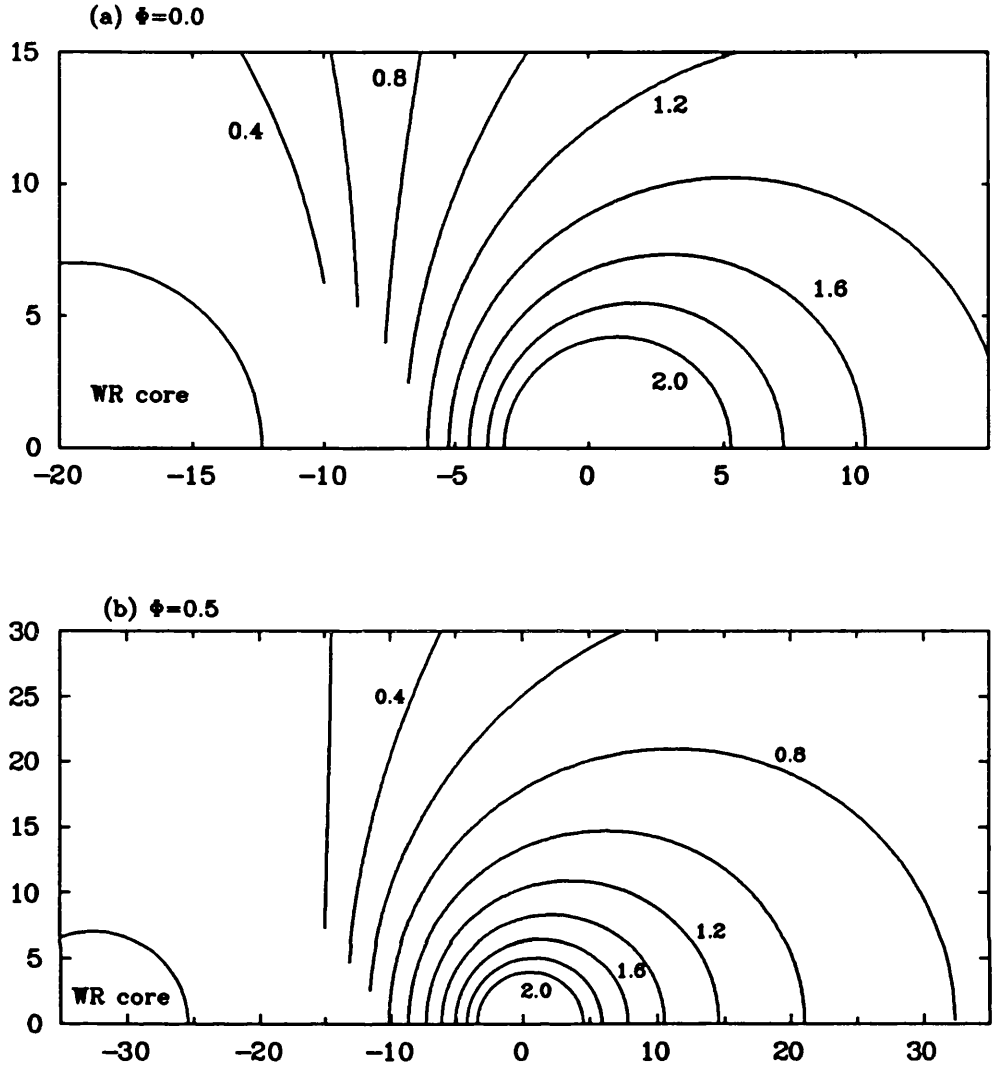

Figure 3.12: Contours of constant ξ, the ionization parameter at (a) phase $\Phi = 0.0$ and (b) phase $\Phi = 0.5$. The curves are labelled with $\log_{10}\xi$ and the neutron star is located at the origin. The x and y axes are in units of $R_\odot$.

formation of C and N lines in HD 50896 which is of a similar spectral type to HD 192163 (WN5 vs. WN6). His models show that the dominant ions in the WR wind will be C^{4+} and N^{4+} over the radii where $\log_{10}\xi > 1.6$. The N^{3+} and C^{3+} ions in the wind of HD 192163 will therefore be ionized to higher states and we should see reduced N IV and C IV absorption at $\Phi = 0.5$ over high negative outflow velocities.

To compare the predictions of the Hatchett and McCray effect, discussed above, with the P Cygni profile variations that are actually observed in HD

192163, I have measured the total equivalent width of the N IV P Cygni absorption component in all the SWP spectra. These measurements are plotted against phase (using the ephemeris given in Table 3.4) in Figure 3.13 and presented in Table 3.5. In general, Figure 3.13 shows that most of the archive data (1978–1983) were taken at phases $\Phi = 0.15 - 0.45$ whereas the extensive April 1987 observations are concentrated between $\Phi = 0.46 - 0.88$. The equivalent width variations do not appear to be consistent with the Hatchett and McCray effect; the peak occurs at $\Phi \approx 0.8$ and not 0.5 when the neutron star is in front. Furthermore, the archive data between $\Phi = 0.15 - 0.45$ show a broad scatter which, again, is not predicted by the Hatchett and McCray effect. Perhaps, however, the most serious objection to the neutron star hypothesis is the velocity range over which the variations occur. As noted in Section 3.3, the P Cygni absorption variations seen in N IV indicate that the entire wind from 0 to -3100 km s^{-1} is varying. It is impossible to reconcile this with the Hatchett and McCray effect because the attenuation of X-rays by the wind ensures that the X-ray ionization zone is very localised in velocity space. Futhermore, the variations occur at velocities in excess of the normal maximum outflow velocity of the wind, as measured in our mean spectrum. I therefore conclude that the Hatchett and McCray effect is not capable of explaining the observed P Cygni variations in HD 192163.

Phase dependent variations, caused by the Hatchett and McCray effect, have been searched for in two other WR+compact candidates. The IUE observations for HD 50896 (Willis *et al.*, 1989) are very extensive and cover two complete binary cycles of 3.76 days; no Hatchett and McCray effect is observed. Similarly, IUE data for HD 96548 (Smith *et al.*, 1985, 1986) show no phase dependence as required by the Hatchett and McCray effect although the period is not so well known for this star. Thus, to conclude this section, I have found no evidence for HD 192163 having a compact companion but more data are required to completely rule out this hypothesis.

Table 3.5

Equivalent Width Measurements of the NIV λ1718 P Cygni Absorption Component

SWP Image Number	Orbital Phase P=4.55d	NIV λ1718.55 W_a (Å)
1668	0.151	4.697
2517	0.265	3.840
2841	0.045	4.563
3419	0.074	3.609
3420	0.087	3.417
8812	0.544	3.419
14133	0.376	3.213
16089	0.097	3.386
18839	0.221	3.628
18840	0.230	3.337
18846	0.387	3.660
18847	0.395	3.822
18849	0.412	3.715
21809	0.206	3.410
21810	0.218	2.967
21820	0.385	3.143
21821	0.398	3.658
21822	0.409	3.291
21824	0.426	3.036
21825	0.437	3.049
21826	0.448	3.107
30769	0.463	3.262
30770	0.476	3.495
30771	0.488	3.399
30772	0.500	3.254
30773	0.515	3.350
30774	0.527	3.417
30775	0.539	3.253
30776	0.551	3.415
30777	0.564	3.263
30778	0.576	3.630
30779	0.589	3.403
30781	0.649	3.399
30782	0.662	3.521
30783	0.676	3.687
30784	0.688	3.911
30785	0.699	3.950
30786	0.711	4.061
30787	0.724	4.386
30788	0.735	4.113
30790	0.831	4.869
30791	0.843	4.391
30792	0.855	4.578
30793	0.867	4.186
30794	0.879	4.344
32359	0.849	4.045

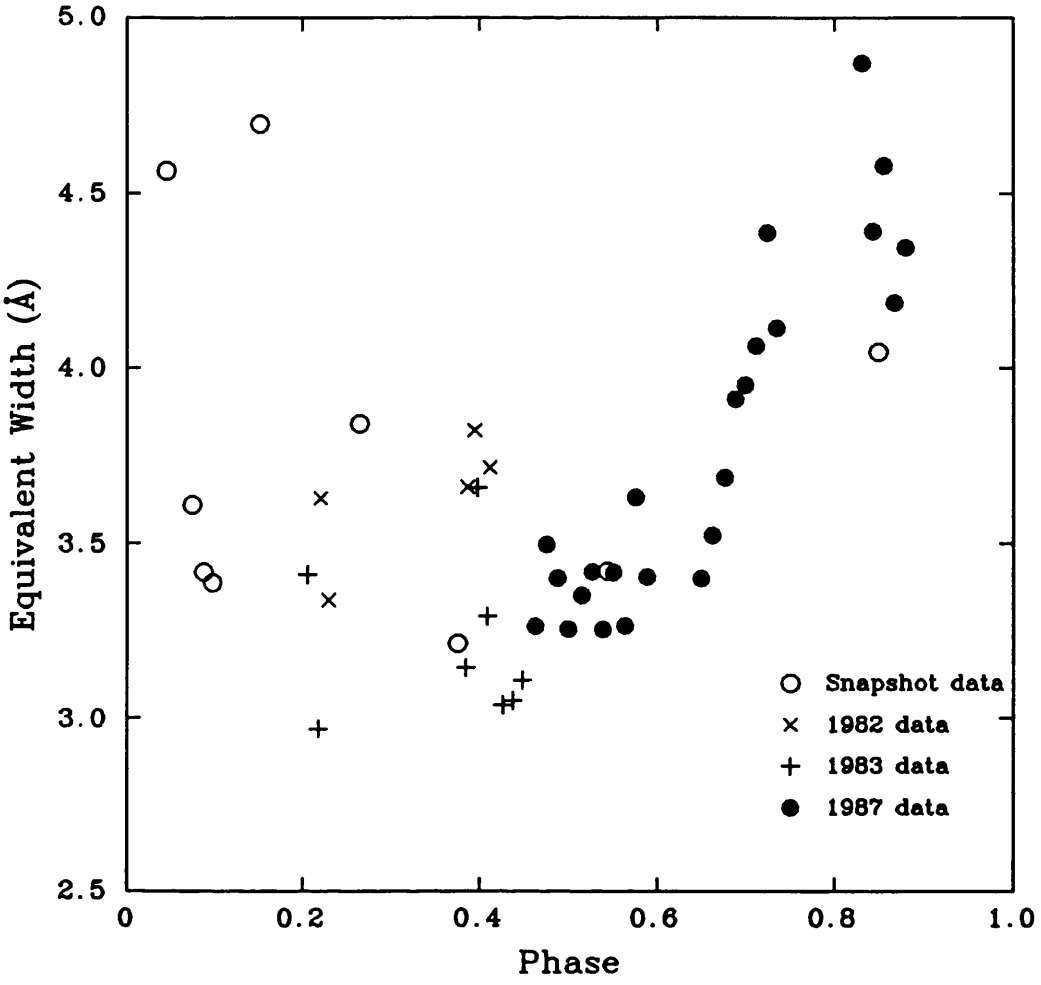

Figure 3.13: The equivalent widths of the N IV λ1718 P Cygni absorption component plotted as a function of phase for all the SWP spectra.

3.5 Intrinsic Stellar Wind Variations?

In this section I will consider the observed ultraviolet P Cygni variability of HD 192163 in terms of intrinsic stellar wind variations. Specifically, I need to try to explain:

(i) Enhanced P Cygni absorption in N IV λ1718, He II λ1640 and C IV λ1550 at velocities exceeding the normal maximum outflow velocities for these ions, as measured in the mean spectrum. The strength of this excess absorption is observed to increase at the same rate for N IV, He II and C IV and then decrease for N IV and C IV while He II continues to increase in strength. The rise and decay timescales for N IV and C IV are approximately 1 day. The maximum outflow velocity observed for each

ion appears to remain constant while the absorption feature changes in strength. The maximum equivalent width change we observe for the N IV P Cygni absorption component is 30%.

(ii) Weak variability is observed at low outflow velocities for N IV and at high positive velocities for He II and C IV. These features are only observed to increase in strength in contrast to the behaviour of the high negative velocity absorption enhancements.

The observed P Cygni profile variations summarised above share some similarities with those found in HD 50896 which appear to be intrinsic to the WN5 stellar wind (Willis *et al.*, 1989). The largest profile variations for HD 50896 occur in the C IV, N IV and He II lines and are characterised by enhanced absorption at velocities in excess of the maximum quiescent wind velocity. Smaller variations are seen at low outflow velocities in the form of reduced absorption; in HD 192163 we see enhanced absorption but at a much reduced level compared to HD 50896. Significant variability is also detected in N V λ1240 and in many subordinate emission lines in the SWP spectra of HD 50896 whereas for HD 192163, the variability is confined to C IV, N IV and He II.

The observed temporal behaviour of the P Cygni profile changes in HD 50896, seen over 3 days in 1980, seems to differ from that seen in HD 192163. In particular, the relative behaviour of the He II, C IV and N IV ions and their rise and decay rates may be different. This is difficult to assess, however, because the HD 50896 series of spectra cover a longer time interval but with a much poorer time resolution compared to HD 192163. For HD 50896, the He II and C IV excess absorptions are present at the beginning of the sequence of spectra and they are observed to reach a maximum and then gradually decay. The N IV excess absorption appears about one day later, reaches a maximum and then decays away over $\sim$ 11 hours. For HD 192163, the C IV and N IV ions share the same rise and decay characteristics but for He II, only an increase is observed. Another difference is that, for HD 50896, the edge velocity of the enhanced absorption decreases as the feature decays whereas in HD 192163 no such reduction is observed. The rise timescale of $\sim$ 1 day, however, appears to be similar for the two stars and probably reflects the flow timescale of the wind.

The other WR star that has been studied in detail at ultraviolet wavelengths is the WN8 star HD 96548 (Smith *et al.*, 1985, 1986). This star has a cooler wind with the most pronounced variability occurring in the Si IV λ1400 P

Cygni profile. A sequence of spectra taken over 5 days shows that the extreme absorption edges of the Si IV doublet gradually decrease in velocity over the observing period. Thus the timescale is much longer for HD 96548 compared to HD 192163 and HD 50896 and decaying rather than increasing absorption is observed. Overall, the broad similarity in the nature and timescale of the observed P Cygni profile variability in HD 192163 and HD 50896 suggests a common physical origin, which for HD 50896, appears to be intrinsic. The differences noted in the relative behaviour of the various ions for HD 192163, HD 50896 and HD 96548 could reflect differences in the levels of ionization, particles densities or velocity laws between the WN6, WN5 and WN8 winds.

One characteristic that all three stars appear to have in common is an epoch dependency for the variability. Archive data for HD 192163 taken over 2 days in 1982 and 1983 show no variations whereas the 1987 data covering the same interval of time do show variations. Similarly the IUE data for HD 50896 and HD 96548 show that these stars undergo periods of quiescence and activity in the extent of the P Cygni variability.

Ultraviolet P Cygni profile variations of intrinsic origin have been observed in many O stars (Prinja and Howarth, 1986). Lamers *et al.* (1988) suggest that the observed variability in α Cam (O9.5 Ia) is caused by blobs propagating outwards in the wind. On the other hand, Prinja and Howarth (1988) suggest that the extensive variability observed in 68 Cyg [O7.5 III((f))] is caused by material passing through perturbations in the flow where a given absorption enhancement is caused by different material at different times. Whatever the physical origin for the profile variability, it seems likely that the fundamental cause is radiatively driven wind instabilities. Lucy and White (1980) developed a phenomenological model based on radiatively driven wind instabilities in the form of blobs to explain the X-ray emission from the winds of hot stars. Later, Lucy (1982, 1983) extended these ideas and developed an heuristic model consisting of radiatively driven periodic shocks which has successfully explained many of the observed characteristics of O star winds. Very recently, Owocki *et al.* (1988) have used numerical simulations to study the nonlinear evolution of line driven flow instabilities and find that such instabilities will indeed lead to the extensive formation of shocks in a stellar wind. In particular, as discussed by Willis *et al.* (1989), this type of model is capable of explaining variations at velocities which appear to be in excess of the wind terminal velocity. As noted

by Abbott and Conti (1987), the proper definition of terminal velocity is the asymptotic velocity of the bulk of the outflow or the blueward extent of the saturated bottom of the P Cygni absorption profile. The observed excess or turbulent velocity as measured by the soft blue edge then arises from shocked gas moving at higher velocities which either has a small column density or small covering factor. Following Lucy (1983), a characteristic velocity amplitude of chaotic motions in the presence of a locally nonmonotonic flow can be estimated from the observed line profiles, such as postulated by Lucy and indicated, in a somewhat different form, by the numerical model of Owocki *et al.* (1988). For the N V, C IV, He II and N IV profiles in HD 192163, the mean extent of the saturation is 360 ± 40 km s^{-1} (correcting for the doublet separation) and this reflects the characteristic velocity amplitude of chaotic motions in the wind. The velocity of the blueward edge of the saturated portion of the C IV profile is -1950 km s^{-1}; this implies that the strongest shocks have propagation speeds of 450–2050 km s^{-1} when the velocity width of the variation of the soft blue edge is taken into account. Thus the variability that is observed in HD 192163 at velocities greater than the normal maximum absorption edge velocities for N IV, He II and C IV can be explained by increases in the propagation speeds of the shocks coupled with changes in column density/covering factor. This model does not, however, easily explain the variability that we observe at low outflow velocities.

The actual profile variability displayed by O stars is usually quite different to that seen in either HD 50896 or HD 192163. The unsaturated resonance lines of O stars (e.g. 68 Cyg; Prinja and Howarth, 1988) show discrete absorption components propagating through the line profiles on timescales of $\sim$ 1 day. Although the timescale is similar to HD 50896 and HD 192163, narrow absorption components are not observed because all the resonance lines in the IUE spectra are saturated. The O supergiant α Cam, however, has saturated resonance lines and the variability displayed by this star appears to be rather similar to that seen in HD 192163. Lamers *et al.* (1988) find changes at the 2% level in the absorption edges at velocities slightly greater than the normal maximum wind velocity of α Cam as well as variations at low outflow and high positive velocities. They suggest that the absorption component variations can be explained by outward accelerated blobs or shells in the line of sight and

the variable emission by a blob moving away from the observer and scattering photons into the line of sight.

Evidence is accumulating for local density enhancements in WR winds. Polarization studies (St-Louis *et al.*, 1987; Drissen *et al.*, 1987; Robert *et al.*, 1989) reveal that most WR stars have randomly variable intrinsic polarization (including HD 192163), indicating that the electron scatterers are distributed asymmetrically. They suggest this asymmetry is caused by blobs formed in an unstable, line-driven wind (Lucy and White 1980). Recently, Moffat *et al.* (1988) have probed the variability of fine structure in the emission lines of the two WN6 stars HD 192163 and HD 191765. They present high signal-to-noise data obtained over 8 hours for the He II λ5411 emission line. Both stars show variations although they are more pronounced for HD 191765 which shows narrow emission bumps moving through the line profile. Again, blobs of material are offered as the most likely explanation although perturbations in the flow may be equally plausible (*cf.* 68 Cyg; Prinja and Howarth, 1988).

The polarization studies of WR stars indicate that the electron scatterers are distributed asymmetrically and vary with time. It would be interesting to see what effect this would have on the electron scattering wings of a line profile since this may also go some way to explaining the P Cygni variability, particularly at the high outflow velocities that we observe in HD 192163. Castor, Smith and Van Blerkom (1970) first drew attention to the very strong electron scattering wings present in the N IV λ3483 P Cygni profile of HD 192163. Hillier (1984) has studied the influence of electron scattering on the He II line profiles in HD 50896 and finds that the electron scattering wings for He II λ1640 are very pronounced. We therefore might expect to observe strong wings on the He II profile in HD 192163, particularly since it has a much higher mass loss rate than HD 50896. If the emission line wing changes that we observe in He II are caused by variations in the electron scattering wings through asymmetries in the wind, we should see changes in the strength of the emission line itself. Unfortunately, no information is available on the He II emission line strength because it is saturated through overexposure of the IUE SWP camera.

I conclude that an intrinsic explanation for the observed variability in HD 192163 seems to be very plausible for the following reasons. First, WR stars including HD 192163 are observed to have asymmetric winds which in turn

suggests that inhomogeneities are present. The precise form of these inhomogeneities is not clear at present. Moffat and co-workers favour mass-conserving structures such as blobs but the data do not appear to rule out the possibility that the variations are being caused by material passing through perturbations in the flow (*cf.* Prinja and Howarth, 1988). Second, the model of Lucy and White (1980), incorporating radiatively driven blobs, or the propagating shock models of Lucy (1982, 1983) and Owocki *et al.* (1988) can at least qualitatively explain the variations observed at high negative outflow velocities. Again, it is not possible to choose between these models incorporating blobs or propagating disturbances until more detailed observations are obtained and three dimensional gas dynamic codes are available. In Section 3.4, the possibility that HD 192163 has a compact companion was examined. I concluded that the lack of observed X-rays points to the absence of a compact companion; the variations do not appear to have the required phase dependence to be caused by the Hatchett and McCray effect; and this effect cannot account for the observed variations in excess of the normal maximum wind velocity. Furthermore, the evidence that HD 192163 varies periodically is weak and contradictory. More data are, however, needed to completely rule out the binary hypothesis. Firstly, the question of whether HD 192163 is actually periodic needs to be settled by acquiring extensive optical radial velocity data. Secondly, if a period exists, the star should be observed at both X-ray and ultraviolet wavelengths over at least one binary cycle.

3.6 New IUE Observations of HD 192163

The analysis, described in Sections 3.1 – 3.5, of the extensive set of IUE observations of HD 192163 strongly suggests that the ultraviolet variations observed in the spectra of this star are intrinsic to the WR wind and not caused by the Hatchett and McCray effect. However, the unfortunate lack of overlap between the orbital phases of the archival data and the orbital phases of the new 1987 observations, prevented a definitive conclusion regarding the periodic nature of the changes. The fact that the origin of the variability is unlikely to be the Hatchett and McCray effect does not preclude the changes from being periodic. Other mechanisms such as pulsation and rotation can produce periodic

Table 3.6

New IUE SWP High Resolution Images of HD 192163

SWP Image Number	Julian Date 2440000+	Exposure Time (s)	Aperture
37704	7861.013	2400	L
37706	7861.140	2400	L
37717	7862.922	2400	L
37719	7863.053	2400	L
37721	7863.187	1200	L
37724	7863.903	2400	L
37726	7864.026	2400	L
37728	7864.147	2400	L
37733	7865.065	2400	L
37747	7865.897	2400	L
37749	7866.018	2400	L
37751	7866.152	2400	L
37754	7866.903	2400	L
37756	7867.029	2400	L
37758	7867.153	2400	L

variations and thus resolving this question would provide new insight into the problem. Therefore a new set of IUE observations of HD 192163 was acquired with the specific aim of determining if the ultraviolet variations are strictly periodic. For this purpose, it was important to obtain sufficient time coverage and temporal resolution, covering at least one complete cycle of the 4.55 days period.

The new data were obtained in December 1989 over a period of seven days, slightly less than two complete cycles. The observations were not continuous but a good proportion of the cycle was covered. The dataset consists of 15 SWP spectra for which details are given in Table 3.6. Listed are the image number, the Julian date at the beginning of the exposure, the exposure time and the aperture used for each new spectrum. The data have been extracted, in exactly the same way as the previous observations, from the PHOT images using the IUEDR software package. Subsequent analysis were performed using the DIPSO data analysis software.

In order to be consistent with the work presented in previous sections, the new set of observations were compared to the same template, which consists of the mean of 5 spectra obtained at various epochs (*cf.* Section 3.3.1). A preliminary analysis immediately revealed that three spectra (SWP 37704, SWP

37717 and SWP 37733) had systematically lower flux levels than the mean. The ratio of the mean to each of these spectra gives average values of 1.07, 1.05 and 1.05 respectively for SWP 37704, SWP 37717 and SWP 37733. It is not immediately clear if these differences represent real variations in the underlying continuum level or calibration problems due to instrumental effects. However, the first of these two options is very unlikely. The typical variations detected in optical photometry of this star is of the order of 0.01 magnitude which is at least five times smaller that the variations detected here. On the other hand, instrumental differences as big as these are unusual in IUE data for bright object with well exposed spectra and have not been encountered in the previous dataset of HD 192163 or in similar work on HD 50896 and HD 96548 (see Chapter 1). A study by the IUE project based on frequent monitoring of five low dispersion standard stars reveals no flux variations beyond $\sim$ 3 % scatter (Pérez, Oliversen, Garhart and Teays 1990). As the present study is more concerned with line profile variability than flux level changes, the three spectra will simply be scaled to the mean, using the above numbers as correction factors.

Figure 3.14 shows the fifteen new spectra, in chronological order starting from the bottom, for the N IVλ1718 P Cygni profile. Variations similar to the ones observed in the 1987 dataset are observed in the blue edge of the absorption component as well as in the emission component between the new spectra and the mean. However no significant variability seems to be present among the new spectra themselves. As for the 1987 dataset, similar changes are also visible in the He II λ1640 P Cygni profile and on a much smaller scale in the C IV λ1550 profile.

In order to quantify the changes and check their phase dependency, I have measured the total equivalent width of the N IV absorption component between -3130 and -1000 km s^{-1} for each new spectrum, in exactly the same way as for the previous dataset (*cf.* Section 3.4). These measurements are listed in Table 3.7 and plotted against orbital phase in Figure 3.15. Also reproduced are the corresponding measurements of the observations of HD 192163 at other epochs, taken from Figure 3.13. Figure 3.15 demonstrates that the spectra in the new dataset show no significant variability yet they cover all phases. This emphasizes the epoch-dependency of the changes; over a period of two days in 1987, an increase followed by a decrease of the absorption equivalent width

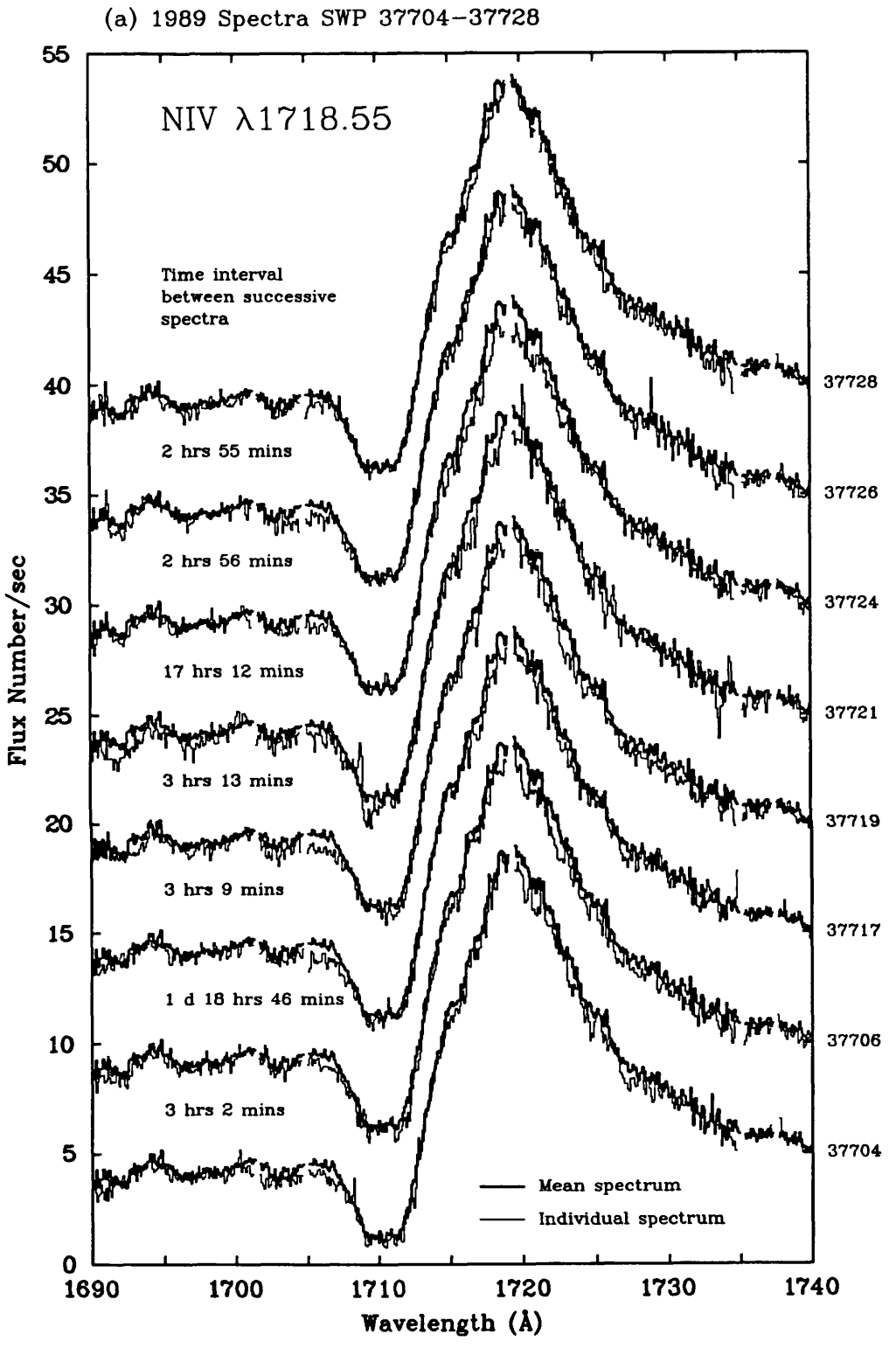

Figure 3.14a: First half of the 15 new spectra of HD 192163 compared with the mean spectrum for the NIVλ1718 P Cygni profile. The time interval between successive spectra is indicated. Other details as for Figure 3.1.

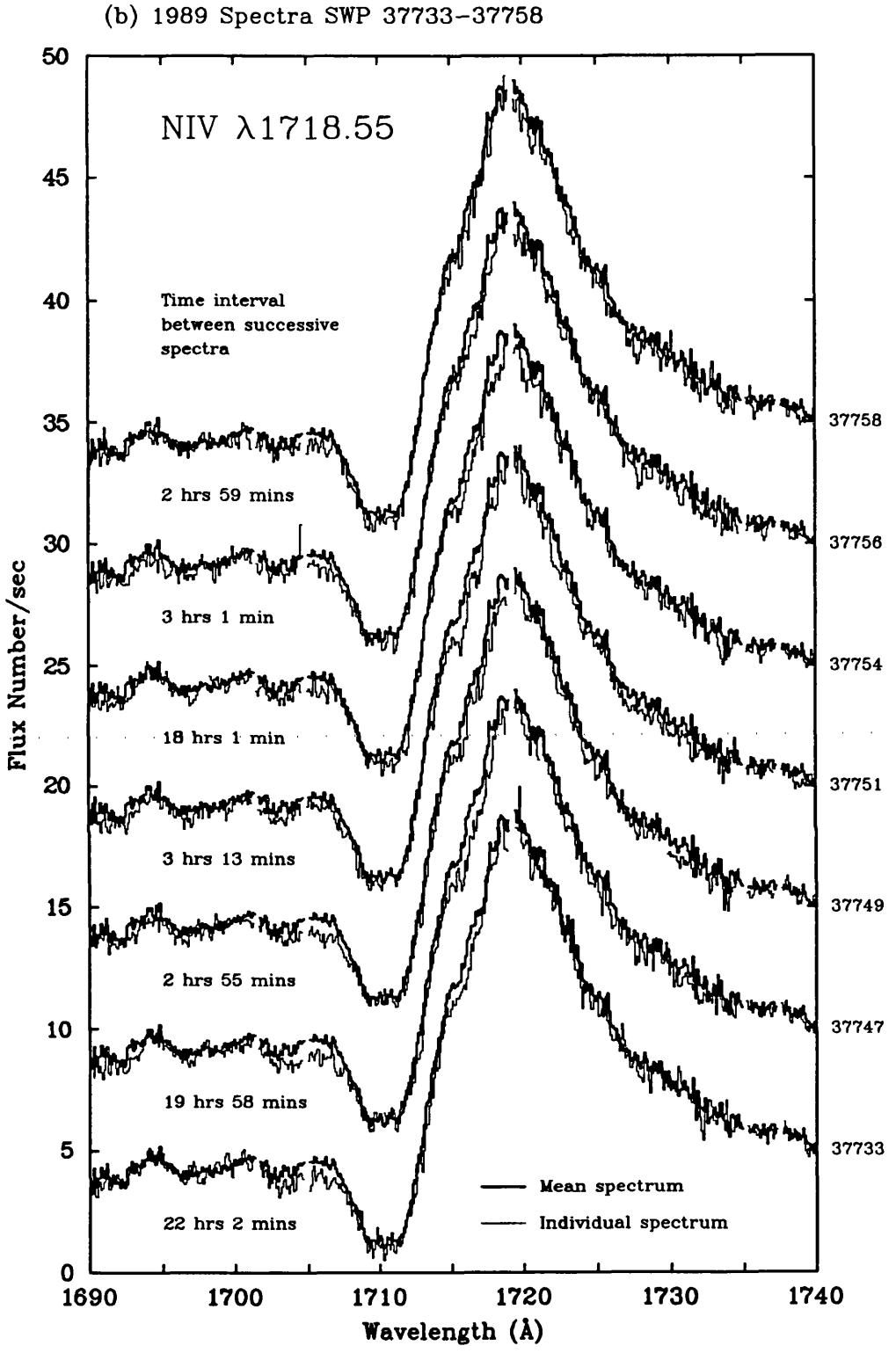

Figure 3.14b: Second half of the 15 new spectra of HD 192163 compared with the mean spectrum for the NIVλ1718 P Cygni profile. The time interval between successive spectra is indicated. Other details as for Figure 3.1.

Table 3.7

Equivalent Width Measurements of the NIV λ1718
P Cygni Absorption Component for the New 1989 Observations

SWP Image Number	Orbital Phase P=4.55d	NIV λ1718.55 W_a (Å)
37704	0.765	3.961
37706	0.793	3.867
37717	0.184	4.041
37719	0.213	4.075
37721	0.243	3.825
37724	0.400	3.704
37726	0.427	3.875
37728	0.454	3.540
37733	0.655	4.089
37747	0.838	3.974
37749	0.865	3.962
37751	0.894	3.944
37754	0.059	3.929
37756	0.087	3.756
37758	0.114	3.982

is observed while over a period of seven days in 1989 no significant changes are detected. Furthermore, compared to the subset of 1987 data which show no variations, the average equivalent width in the new dataset is significantly higher (3.9 Å compared to 3.4 Å) while the noise level is similar. This indicates that variations can occur on very different timescale for this star; while the 1987 dataset show variations on a timescale of the order of one day, the difference between the spectra obtained in 1989 and the non-variable spectra of 1987 demonstrates that variations on a much slower timescale are occuring.

I conclude that these observations strengthen the evidence for an intrinsic rather than binary origin for the ultraviolet variations detected in various P Cygni profiles of HD 192163.

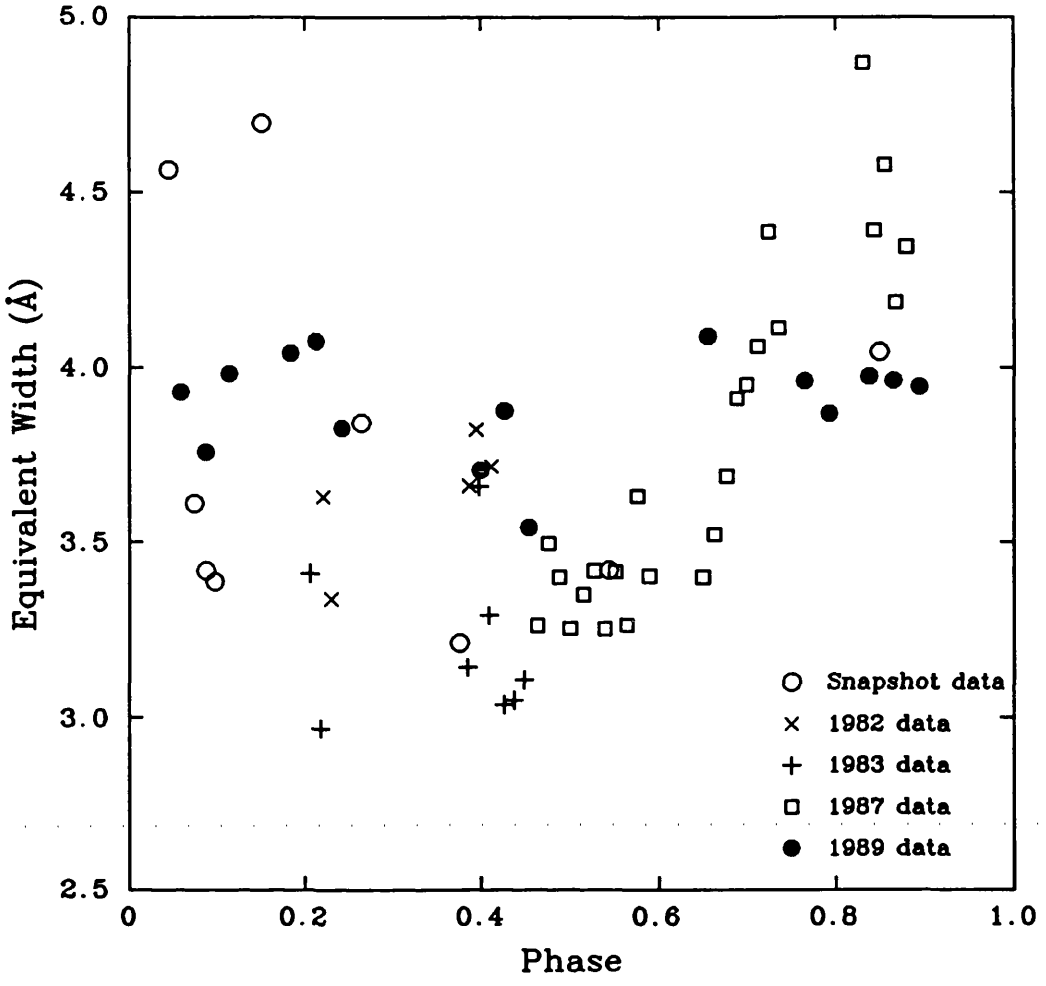

Figure 3.15: The equivalent widths of the N IV λ1718 P Cygni absorption component plotted as a function of phase for all the SWP spectra.

3.7 The Interstellar medium in the line of sight towards WR 136 and other stars in Cygnus

3.7.1 INTRODUCTION

It has long been recognized that the winds of hot massive stars play an important role in the structure and composition of the interstellar medium. Wolf-Rayet (WR) stars, in particular, can have a significant effect on their surrounding interstellar gas. As well as enriching their environments with nuclear-processed material, their energetic winds can produce important dynamical phenomena. The ring nebulae surrounding some WR stars are well observed examples of the interaction of the winds of these objects with interstellar material. On a much larger scale, giant shells formed by successive supernova explosions and/or the combined effects of strong stellar winds are observed around associations containing OB and WR stars. Well known examples include the supershells around Orion (Cowie, Songaila & York 1979) and Carina (Cowie *et al.* 1981).

In this section the results of an investigation into the existence of a supershell surrounding the Cygnus OB1 and OB3 associations is presented. I have used the technique of ultraviolet absorption line spectroscopy against association members to detect high velocity interstellar components. The survey area is a 4° × 4° box centred on the WN6 star WR 136 (HD 192163) and includes 5 WR and 7 OB stars which are members of the Cygnus OB1 and OB3 associations. WR 136 is surrounded by the ring nebula NGC 6888 which is the prototype of its class. The star is believed to be a member of the Cygnus OB1 association which is itself surrounded by the giant filamentary shell Cyg I of dimensions 95 × 125 pc (Brand & Zealey 1975). Moreover, Cash *et al.* (1980) discovered an X-ray superbubble, 450 pc in diameter, centred on the Cygnus OB2 association and coincident with previously known Hα filaments (Ikhsanov 1961; Dickel, Wendker & Bieritz 1969). (Cygnus OB2, one of the eight OB associations in Cygnus, is a compact cluster containing some of the most luminous stars in the Galaxy.) More recently, Bochkarev & Sitnik (1985) suggested that the Cygnus superbubble is not a single structure but rather is composed of discrete sources accounting for 50–75% of the X-ray emission. They suggested that the remaining 25–50% is due to coronal gas, created by stellar winds and supernovae, surrounding the individual associations which are seen projected

onto the ring of X-ray emission. In a recent study, Lozinskaya & Sitnik (1988) investigated the structure and kinematics of the Cyg OB1 gas-dust complex by analysing optical and radio data. They find a hierarchical system of mutually embedded shells composed of small-scale structures; two larger overlapping shells approximately centred on the young clusters NGC 6913 and IC 4996; and a common envelope (corresponding to Cyg I) surrounding the whole association.

Blue-shifted absorption components to the interstellar lines of C IV, Si IV and Al III were discovered by Huber *et al.* (1979) in the ultraviolet spectrum of WR 136 by using observations from the *International Ultraviolet Explorer* satellite (IUE). The authors associated this high velocity (-90 km s^{-1}) gas with the WR ring nebula NGC 6888. In a later paper, Phillips, Welsh & Pettini (1984; hereafter PWP) found similar high-velocity components towards three O stars which are also members of the Cygnus OB1 association. This discovery cast several doubts on the origin of the blue-shifted components observed towards WR 136. Instead, PWP proposed that the high-velocity components are formed in a large-scale expanding shell surrounding the Cygnus OB1 association. They did not, however, rule out a contribution to the blue-shifted components observed in the spectrum of WR 136 from NGC 6888. In this section I re-address the question of whether the high-velocity components observed towards WR 136 originate in NGC 6888 or in a much larger-scale feature.

I am now able to extend and improve the analyses of Huber *et al.* (1979) and PWP through the use of many more observations. As part of the study of P Cygni profile variability in WR 136 presented in the previous sections of this chapter, numerous spectra were obtained. These spectra can be added together to form a high signal-to-noise mean spectrum to provide more accurate velocities and column densities for the blue-shifted components. Also, IUE observations of more stars in the Cygnus OB associations are now available, allowing me to search for blue-shifted components in other stars near WR 136, and thus help to draw a better picture of the gas kinematics in this region. Finally, accurate measurements of the emission line velocities in NGC 6888 near WR 136 are now available (Marston & Meaburn 1988; Chu 1988). I can compare these more precisely with the velocities of the blue-shifted components observed towards WR 136. With these new observations it is now possible to obtain more insight, not only on the origin of the blue-shifted material observed in absorption towards WR 136, but also on a much larger region surrounding it.

3.7.2 Observations

In order to study the properties of the interstellar gas in the vicinity of WR 136, I used the IUE data archive at the Rutherford Appleton Laboratory (Stickland & Harvey 1987; Giaretta, Mead & Benvenuti 1987) to search for additional Cygnus OB stars having SWP high resolution spectra (Short Wavelength Prime, $\lambda\lambda$1150–2050 Å) in a $4° \times 4°$ box centred on WR 136. I found 5 WR stars, the 3 O stars studied by PWP and 4 early B stars, including P Cygni. The total sample thus consists of 13 stars; 3 are members of Cyg OB3 and the remaining 10 are members of Cyg OB1 (Humphreys 1978, van der Hucht *et al.* 1988). The observational parameters of these stars are listed in Table 3.8 together with the references for each parameter. I used the SIMBAD database of the Astronomical Data Centre in Strasbourg, France to assemble the data for the non-WR stars. I have checked that the O and B stars are genuine Cyg OB members by computing their photometric distances and find that two stars are doubtful members. The first, HD 193443, is believed to be a binary as it is composed of two stars of equal magnitude and has a variable radial velocity. Its photometric distance is 1 kpc and thus it may be a foreground star. The second star, HD 228519, has a photometric distance of 3.6 kpc, assuming a B0.5 III spectral type. The luminosity class may, however, be doubtful since Humphreys (1978) lists it as a B0.5 V although I can find no reference to this in the literature. Certainly, HD 228519 is more likely to be a member of Cyg OB1 if it is a main sequence star. The IUE spectra are unfortunately too noisy to draw any conclusions about the luminosity class. I will assume that it is a member of Cyg OB1 although it may be more distant. Figure 3.16 is a reproduction from the red Palomar sky survey showing the positions of the stars within the Cygnus region. The filamentary ring Cyg I (Brand & Zealey 1975) can be seen surrounding the Cyg OB1 association and the ring nebula NGC 6888.

3.7.2.1 Na I and Ca II Observations

In order to compare line velocities in the IUE spectra from each star, an absolute frame of reference is required. This is not usually possible for IUE spectra, principally because of the uncertainty in the position of the star within the spectrograph's large aperture. If the absolute velocities of the Na I and Ca II interstellar lines are known, however, I can assume that the neutral species

Table 3.8

Observational Parameters

Star	SpT	l	b	V	E(B-V)	Cluster or Association	Distance (kpc)	No. of SWP Images	References for Columns				
(1)	(2)	(3)	(4)	(5)	(6)	(7)	(8)	(9)	(2)	(5)	(6)	(7)	(8)
WR 134 (HD 191765)	WN6	73.5	1.6	8.31	0.58	Cyg OB3	2.1	2	1	1	1	10	10
WR 135 (HD 192103)	WC8	73.7	1.3	8.51	0.42	Cyg OB3	2.1	3	1	1	1	10	10
HD 191456	B0.5 II-III	73.7	2.1	7.44	0.36	Cyg OB3	2.1	1	2	6	9	11	10
WR 137 (HD 192641)	WC7+OB	74.3	1.1	8.18	0.54	Cyg OB1	1.8	3	1	1	1	10	10
HD 192639	O7 Ib (f)	74.9	1.5	7.11	0.63	Cyg OB1	1.8	1	3	7	9	11	10
WR 138 (HD 193077)	WN6	75.2	1.1	8.21	0.63	Cyg OB1	1.8	6	1	1	1	10	10
HD 192303	B1 III	75.4	2.3	8.93	0.59	Cyg OB1	1.8	1	4	8	9	11	10
WR 136 (HD 192163)	WN6	75.5	2.4	7.73	0.59	Cyg OB1	1.8	31	1	1	1	10	10
P Cygni	B1 Ia$^+$	75.8	1.3	4.82	0.63	IC 4996	1.8	5	5	5	5	5	5
HD 193443	O9 III	76.1	1.3	7.24	0.72	Cyg OB1	1.8	1	2	7	9	11	10
HD 228519	B0.5 III	76.2	2.3	9.46	0.43	Cyg OB1	1.8	1	4	8	9	11	10
WR 139 (V444 Cyg)	WN5+O6	76.6	1.4	8.27	0.82	Be 86/Cyg OB1	1.7	10	1	1	1	10	10
HD 193514	O7 Ib (f)	77.0	1.8	7.38	0.73	Cyg OB1	1.8	1	3	7	9	11	10

(1) van der Hucht *et al.* (1988); (2) Walborn (1971); (3) Walborn (1972); (4) Barbier (1962); (5) Lamers *et al.* 1983; (6) Nicolet (1978); (7) Hiltner (1956); (8) Bouigue *et al.* (1963); (9) Carnochan (1982); (10) Lundström & Stenholm (1984); (11) Humphreys (1978).

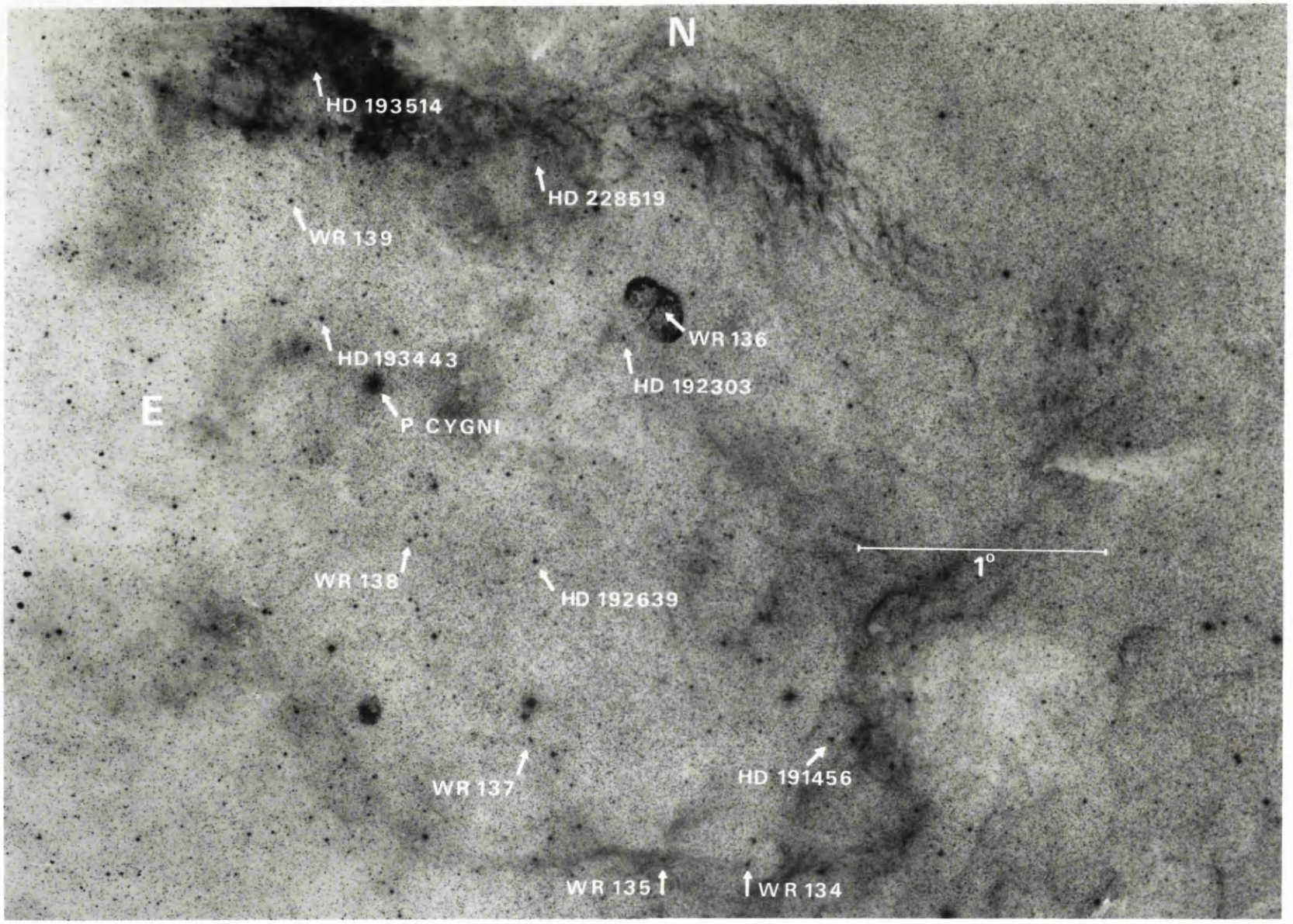

Figure 3.16 : Reproduction from the red Palomar sky survey showing the positions of the stars within the Cygnus region. North is top and east is left; the scale is indicated by the 1° long bar on the right-hand side.

in the IUE wavelength range share the same velocity distribution and thus transform the velocities to the local standard of rest (LSR) frame of reference (V_{LSR}=V_{Hel}+17.5 km s^{-1}). Therefore, as part of this work, high signal-to-noise optical spectra in the region of the Na I $\lambda\lambda$5889.950, 5895.924 and Ca II $\lambda\lambda$3933.663, 3968.468 doublets were obtained for 12 of the 13 stars in this study (P Cygni was excluded because the velocity of the Na I and Ca II lines are well known). The spectra were obtained during service time on the 1988 August 9–10 using the 500-mm camera of the Intermediate Dispersion Spectrograph (IDS) on the 2.5 m Isaac Newton Telescope (INT) of the Observatorio del Roque de Los Muchachos on La Palma. A 2400 lines mm^{-1} grating blazed at 4000Å was used in first order to give a dispersion of 8.0Å mm^{-1} at Ca II and 6.8Å mm^{-1} at Na I. The detector was a GEC CCD dye-coated to give an enhanced ultraviolet response. One 22μm CCD pixel coresponds to 13.3 km s^{-1} at Ca II and 7.6 km s^{-1} at Na I.

As the stars are very bright, the reduction procedure was fairly simple. All the raw images were divided by a normalised flat field and the bias was subtracted. The count rates from the sky were found to be negligible compared to the signal from the stars and thus no sky subtraction was necessary. The spectra were wavelength calibrated to an accuracy of better than 0.03Å using arcs taken before or after each stellar spectrum . The instrumental resolution achieved was 16 km s^{-1} for the Na I lines and 34 km s^{-1} for the Ca II lines as measured from the FWHM of emission lines from the arc spectra extracted in the same way as the data. Signal-to-noise ratios achieved for the continua in the regions of the Na I and Ca II lines range from 32–45.

3.7.2.2 IUE Observations

All the IUE spectra used in this work were uniformly extracted from the PHOT or GPHOT images using the IUEDR software package (Giddings 1983; Giddings & Rees 1989) available on the UK STARLINK network of VAX computers. This method of extraction provides significant advantages compared to the standard IUESIPS output produced by the IUE project. These include higher wavelength accuracy, a better determination of the interorder background and an improved ripple correction. The resulting spectra were mapped on to a 0.05Å wavelength grid. Subsequent measurements and analysis of the spectra were made using the DIPSO software package described by Howarth & Murray (1990), also available on STARLINK.

When multiple spectra were available for a particular star, they were added together to form a mean. In order not to degrade the resolution the spectra were carefully aligned before merging. This was achieved by cross-correlating a selection of well-isolated interstellar lines. The mean of the shifts of the different lines used was then adopted and the scatter around this mean was used to evaluate the error on an individual wavelength measurement. Typically, this was found to be 0.02Å in each individual spectrum. As the signal-to-noise was different in each spectrum, a weighting factor was used when performing the sum. Effects taken into consideration were the transmission factor of the aperture used [large ($\sim 10 \times 20$ arcsec) or small (~ 3 arcsec diameter)] and the exposure time. The equation can be found in Howarth & Phillips (1986). The number of SWP images used for each star is listed in Table 3.8.

3.7.3 RESULTS

3.7.3.1 Velocity Distribution of Na I and Ca II

The 13 stars in this study are highly reddened (*cf.* Table 3.8) and thus strong, saturated interstellar Na I and Ca II lines are expected to be present in the optical spectra. A montage of the spectra in the region of the Na I doublet is shown in Figure 3.17 for the 12 stars for which data were obtained. (The data have been rectified by fitting a polynomial to selected continuum regions.) Most of the stars exhibit just one strong, unresolved low-velocity component in each of Na I and Ca II. Equivalent widths and LSR velocities have been measured for both components of each doublet and are given in Table 3.9. (The 1σ errors quoted for the equivalent widths are derived from the r.m.s. deviation of the continuum fit to each line.) The 3σ detection limit for weak components is ~ 25 mÅ (Na I) and ~ 40 mÅ (Ca II). Weak, resolved high-velocity components are detected in WR 136 (-65 km s^{-1}), WR 135 (-50 km s^{-1}) and WR 137 (-54 km s^{-1}) for Na I λ5890. WR 135 and WR 136 also show unresolved components at $V_{LSR} \approx -20$ km s^{-1} in Na I and Ca II.

In order to determine more accurate velocities and column densities, I have fitted theoretical profiles to the Na I and Ca II doublets seen towards the 12 stars. The theoretical line profiles were calculated in the usual way based on the description of Strömgren (1948). Fit parameters (v: velocity; b: velocity dispersion; N: column density) were simultaneously adjusted for both components of a given doublet by trial and error until a satisfactory fit was

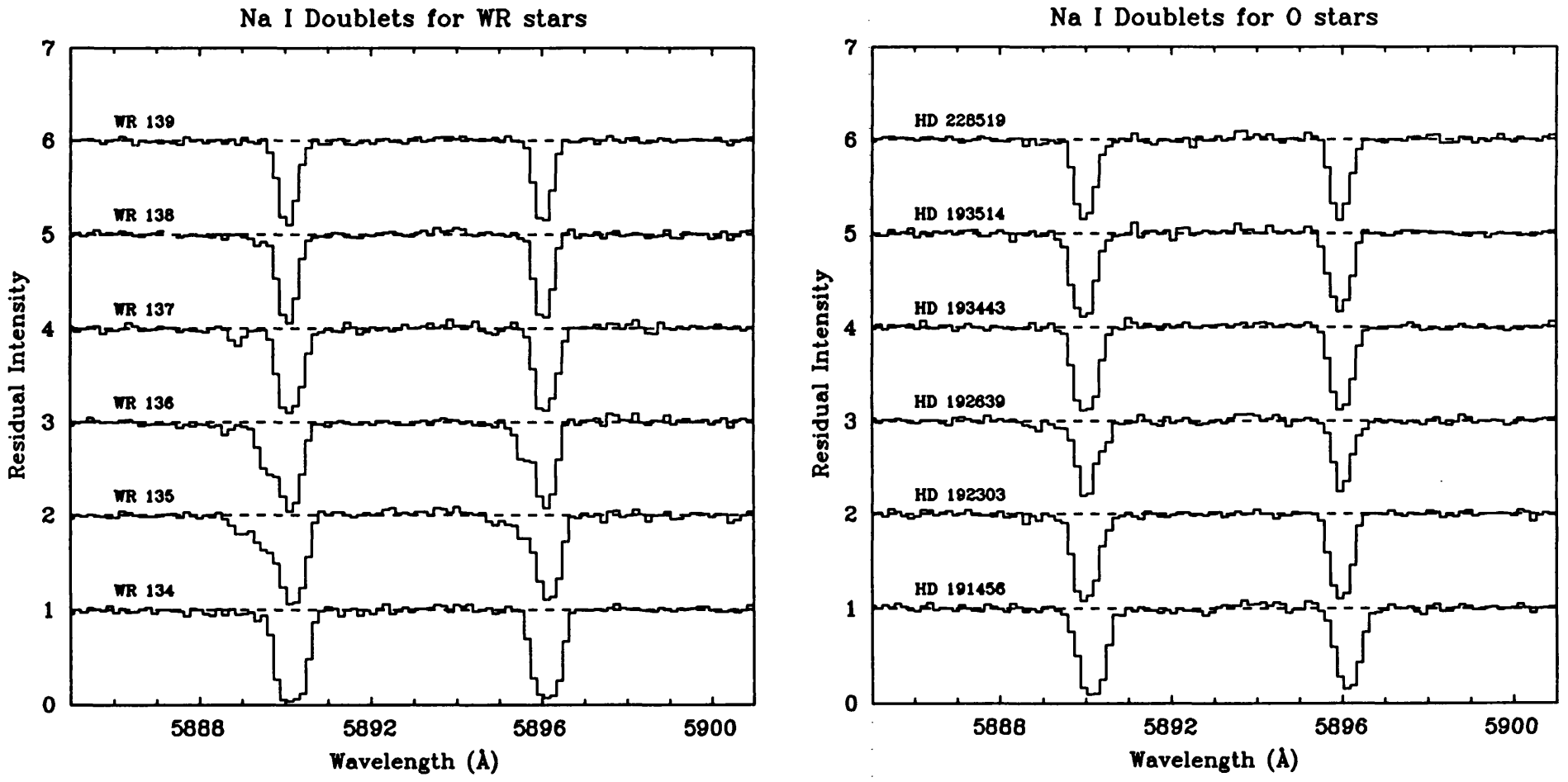

Figure 3.17 : Optical interstellar absorption lines of Na I for twelve of the stars in the sample.

Table 3.9

Velocities (km s^{-1}) and Equivalent Widths (mÅ) for Na I and Ca II Doublets

Star	Na I λ5889.950			Na I λ5895.924			Ca II λ3933.663			Ca II λ3968.468		
	V_{LSR}	Wλ	σ(Wλ)	V_{LSR}	Wλ	σ(Wλ)	V_{LSR}	Wλ	σ(Wλ)	V_{LSR}	Wλ	σ(Wλ)
WR 134	+10	804	12	+10	718	11	+14	368	14	+15	234	16
WR 135	+12	642	20	+13	550	20	+15	304	26	+17	184	26
	−50	104	20	...	...	...	...	...	...	...	...	...
HD 191456	+12	709	15	+12	575	14	+15	383	16	+17	280	19
WR 137	+8	606	14	+10	538	14	+15	313	17	+17	234	16
	−54	60	10	...	...	...	...	...	...	...	...	...
HD 192639	+4	452	16	+6	404	16	+14	318	14	+15	149	15
WR 138	+7	497	10	+7	434	10	+8	273	15	+12	214	16
HD 192303	+4	651	12	+3	547	12	+7	408	30	+9	280	16
WR 136	+9	602	17	+10	496	17	+15	264	26	+18	176	24
	−65	32	8	...	...	...	...	...	...	...	...	...
HD 193443	+4	629	11	+3	538	10	+7	275	21	+9	194	17
HD 228519	+3	501	12	+2	445	12	+7	303	17	+9	171	20
WR 139	+7	477	11	+6	424	11	+17	274	17	+17	205	15
HD 193514	+1	606	13	+1	499	12	+7	304	21	+9	245	19

obtained. In each case, the calculated profile was convolved with the appropriate instrumental resolution function, assumed to be Gaussian. Results are presented in Table 3.10 where the range in b and log N for which the fit was judged to be acceptable is given. Note, however, that the instrumental profiles are very broad [b=9.5 km s^{-1} (Na I); 20.5 km s^{-1} (Ca II)] and that the implicit assumption of a single absorbing cloud is almost certainly wrong for the low velocity components. This component probably consists of a number of unresolved components so the derived column densities should be viewed as lower limits. Conversely, the weak, high velocity components are optically thin and their b and N values are well constrained.

For most stars, the velocities found for the main component of the Ca II lines seem to be systematically larger than the ones obtained for the Na I lines. This velocity difference is most likely caused by insufficient resolution. Indeed, if a broad feature consists of a number of unresolved components with different proportions of Na I and Ca II, such a situation may well occur. If one species dominates in one velocity component and the other dominates in a different velocity component the measured velocities will be effectively different. However, only the *relative* LSR velocities of the stars are required for this study. Thus a systematic velocity difference between Na I and Ca II is unimportant. I will therefore adopt the Na I velocities as the resolution of these data is much higher.

Inspection of Table 3.10 shows that the velocities of the main Na I and Ca II components can be split into two groups which reflect the spatial distribution of the stars as shown in Figure 3.16. The four southernmost stars, WR 134, 135, 137 and HD 191456 have $\overline{V}_{LSR}$(Na I) = +10 ± 2 km s^{-1} and $\overline{V}_{LSR}$(Ca II) = +14±1 km s^{-1}. WR 136 also seems to belong to this group with V_{LSR}(Na I) = +9 km s^{-1} and V_{LSR}(Ca II) = +15 km s^{-1}. The 5 stars in the northern part of Figure 3.16 (HD 193514, HD 228519, HD 193443, P Cygni and HD 192303) have lower Na I and Ca II velocities; $\overline{V}_{LSR}$(Na I) = +2 ± 1 km s^{-1} and $\overline{V}_{LSR}$(Ca II) = +6 ± 2 km s^{-1}. Note that WR 136 and HD 192303 have quite different velocities even though they are only 4 pc apart. The remaining 3 stars, WR 138 and HD 192639 in the centre, and WR 139 in the north-east, have intermediate velocities and cannot easily be put into either group. Interstellar clouds distributed along the line of sight to Cyg OB1 and OB3 are expected to have LSR velocities between 0–9 km s^{-1} if they participate in the normal

Table 3.10

Profile Fit Parameters for Na I and Ca II Doublets

Star	Na I b (km s^{-1})	Na I V_{LSR} (km s^{-1})	Na I log N (cm^{-2})	Ca II b (km s^{-1})	Ca II V_{LSR} (km s^{-1})	Ca II log N (cm^{-2})
WR 134	12.5–15.5	+9.0	13.28–13.40	13.0–17.0	+13.0	12.78–12.80
WR 135	4.0–10.0	−50.0	11.70–11.75			
	8.5–14.0	−20.0	12.07–12.18			
	5.0–11.5	+12.5	13.15–15.20	8.5–16.0	+13.0	12.78–12.95
HD 191456	11.5–14.5	+10.5	13.03–13.10	11.5–16.5	+15.0	12.87–12.95
WR 137	2.0–7.0	−55.0	11.55–11.65			
	9.0–11.5	+9.0	13.05–13.25	7.5–13.0	+15.0	12.74–12.90
HD 192639	3.0–7.5	+3.0	12.93–15.00	9.0–17.5	+13.0	12.70–12.75
	3.0–12.0	+28.0:	11.70–11.80			
WR 138	4.5–9.0	+6.0	13.15–14.75	15.0–21.0	+10.0	12.68–12.70
HD 192303	9.0–12.0	+2.0	13.10–13.30	12.0–15.0	+8.0	12.86–12.90
WR 136	2.5–12.0	−65.0	11.50–11.60			
	4.0–6.5	−19.0	12.30–12.40	3.0–5.0	−20.0:	12.30–12.50
	4.5–9.0	+9.0	13.28–15.20	6.5–9.5	+15.0	12.78–12.98
P Cygni*	...	+3	...	...	+3	...
HD 193443	8.5–11.0	+3.0	13.07–13.30	5.0–9.0	+7.0	12.73–13.10
HD 228519	5.0–9.0	+1.5	13.10–13.24	9.5–16.5	+7.5	12.75–12.85
WR 139	3.5–8.5	+6.0	13.05–15.00	3.0–9.0	+17.0	12.90–14.85
HD 193514	10.0–13.0	+1.0	13.02–13.10	3.5–8.5	+6.5	13.00–14.75

* Velocities from Beals and Oke (1953)

galactic rotation. This range agrees well with the observed Na I velocities given above. Several stars show components with velocities outside this range: WR 135 ($-20, -50\,\mathrm{km\ s^{-1}}$); WR 137 ($-55\,\mathrm{km\ s^{-1}}$); HD 192639 ($+28\,\mathrm{km\ s^{-1}}$); and WR 136 ($-19, -65\,\mathrm{km\ s^{-1}}$). Overall, the optical data show that a single value cannot be adopted to characterise the velocity of the interstellar clouds along the line of sight to the Cygnus stars when correcting the IUE velocities.

3.7.3.2 The UV Interstellar Spectrum of WR 136

As a result of the large number of IUE spectra available for WR 136 (31 SWP images), it is possible to detect very weak interstellar lines not usually seen in single spectra. Consequently, it is worthwhile to carry out a more detailed analysis of the interstellar line of sight towards this star. For completeness, I have extracted 35 LWP spectra (Long Wavelength Prime, $\lambda\lambda$1850–3200 Å) of WR 136 using the same method as for the SWP data. The resulting spectra have been mapped on to a 0.1Å wavelength grid and added together using the same weighting algorithm applied to the SWP spectra.

Measurements of the interstellar lines identified in the mean spectrum of WR 136 are given in Table 3.11. Listed are the laboratory wavelength, the corresponding LSR velocity, the oscillator strength, the measured equivalent widths and the source for the atomic data. The errors quoted for the equivalent widths were estimated by taking into account the statistical uncertainties on the flux within the line and in the continuum placement. Systematic errors in the continuum placement were considered negligible as the "continuum" was found to change slowly and smoothly across most of the narrow interstellar lines. I also assumed that the spectrum extraction method used in this study rendered the systematic zero level error negligible. The algorithms are described in Howarth and Phillips (1986).

The mean SWP and LWP spectra have been measured at various wavelengths to determine representative values of the signal-to-noise ratio. This is more difficult in the SWP spectrum because the large number of emission lines present means that there are few stellar continuum regions. At the short wavelength end ($\lambda < 1200$Å) the signal-to-noise is about 25 and is consistently above 50 for the rest of the spectrum and reaches $\sim$ 75 near 1500Å. I estimate that the weakest lines that can be detected have an equivalent width of 10mÅ (excluding the interval 1150–1200Å where the value is closer to 25mÅ). This very high signal-to-noise ratio has been obtained by adding small and large aperture

Table 3.11

Observed interstellar lines in the mean spectrum of WR136

Ion	λ_{lab} (Å)	V_{LSR} (km s^{-1})	f	W_λ (mÅ)	Ref.	Comments
C I	1188.833	+3	0.0170	70±14	4	Blend with Cl I 1188.768
	1276.482	+9	0.0120	30±5	1	
	1277.245	+11	0.156	164±7	1	Blend with C I* 1277.282
	1280.135	+13	0.0278	144±9	1	
	1328.833	+9	0.0824	146±6	1	
	1560.310	+11	0.0810	216±7	1	
	1656.928	+10	0.136	254±7	1	Blend with C I** 1657.008
C I*	1277.513	+9	0.0390	68±6	1	Blend with C I** 1277.550
	1280.597	+15	0.00672	38±6	2	Blend of 3 lines
	1329.101	+9	0.0824	102±4	1	Blend of 3 lines
	1560.683	+10	0.0810	186±12	2	Blend of 2 lines
	1656.266	+6	0.0566	103±7	2	
	1657.380	+7	0.0340	94±17	2	
	1657.907	+8	0.0453	148±9	2	Blend with C I** 1658.122
C I**	1261.520	+7	0.0284	20±7	2	Blend of 2 lines
	1329.584	+9	0.0824	35±4	1	Blend of 2 lines
	1561.438	−0	0.0680	76±4	2	Blend of 2 lines
C II	1334.532	−6	0.118	564±8	1	
C II*	1335.703	−18	0.118	441±7	1	
C IV	1548.188	+17	0.194	365±13	1	
	"	−61	"	167±11		High velocity component
	1550.762	+14	0.097	277±7	1	
	"	−61	"	108±6		High velocity component
N I	1199.550	−1	0.133	348±16	1	
	1200.223	+1	0.0885	283±11	1	
N V	1238.808	−72	0.152	29±3	1	High velocity component
	1242.796	−65	0.0757	15±1	1	High velocity component
O I	1302.168	−6	0.0486	402±6	1	
Na I	5889.950	+9	0.655	575±12	2	
	"	−65	"	56±13	2	High velocity component
	5895.924	+9	0.327	505±14	2	
Mg I	2025.824	−6	0.110	222±9	1	Overlaps with Zn II 2025.512
	2852.126	−4	1.77	668±14	1	
Mg II	1239.925	+1	0.00027	82±6	5	
	1240.395	+1	0.00013	60±6	5	
	2795.528	−2	0.592	1197±17	1	
	2802.704	−6	0.295	1142±17	1	
Al II	1670.787	−8	1.88	521±11	1	
Al III	1854.716	+3	0.539	167±13	1	
	"	−57	"	117±11		High velocity component
	1862.790	+0	0.268	101±7	1	
	"	−62	"	67±7		High velocity component
Si I	1845.520	+0	0.152	24±6	2	
Si II	1190.416	−5	0.291	407±27	3	
	1193.289	−11	0.582	676±30	3	
	1260.421	−10	1.122	476±10	3	
	1304.372	−16	0.093	396±10	3	
	1526.708	−3	0.119	478±13	3	
	1808.012	+3	0.00225	294±6	3	

Table 3.11 (continued)

Observed interstellar lines in the mean spectrum of WR136

Ion	λ_{lab} (Å)	V_{LSR} (km s^{-1})	f	W_λ (mÅ)	Ref.	Comments
Si II*	1264.737	−9	0.860	46±2	2	
	"	−53	"	54±2		High velocity component
Si III	1206.510	+21	1.66	360±41	1	
	"	−41	"	450±41		High velocity component
Si IV	1393.755	+24	0.528	349±11	1	
	"	−66	"	203±10		High velocity component
	1402.770	+21	0.262	276±6	1	
	"	−67	"	149±4		High velocity component
P II	1532.510	+5	0.0951	63±6	2	
S I	1807.341	+6	0.112	30±4	2	
S II	1250.586	−2	0.00535	204±9	1	
	1253.812	−3	0.0107	243±10	1	
	1259.520	−5	0.0159	235±9	1	
Cl I	1347.240	+10	0.112	76±4	1	
Ca II	3933.663	+15	0.688	233±14	2	
	3968.468	+17	0.341	160±9	2	
Cr II	2055.596	−2	0.167	65±9	7	
	2065.501	+2	0.0798	68±9	7	
Mn II	1197.184	+3	0.096	88±8	1	
	2576.107	+1	0.288	365±20	1	
	2593.731	+2	0.223	386±17	1	
	2605.697	−1	0.158	324±23	1	
Fe II	1608.456	−5	0.0963	347±13	6	
	2373.733	+3	0.0419	363±72	6	
	2382.035	+3	0.398	677±64	6	
	2585.878	−5	0.0846	591±29	6	
	2599.396	−8	0.294	658±24	6	
Ni II	1317.217	+6	0.0759	54±5	8	
	1370.136	+11	0.0725	91±5	8	
	1454.842	+4	0.0256	85±1	8	Blend
	1741.547	+4	0.0851	95±4	8	
	1751.910	+3	0.0419	59±6	8	
Cu II	1358.773	−13	0.460	52±5	1	
Zn II	2025.512	−6	0.412	400±10	1	
	2062.016	−3	0.202	206±13	1	Blend with Cr II 2061.575
CO	(v'=4←v''=0)	...	0.0251	54±4	9	Vibrational bands
	(v'=3←v''=0)	...	0.0360	37±7	9	of the
	(v'=2←v''=0)	...	0.0429	24±2	9	$A^1\Pi$–$X^1\Sigma^+$
	(v'=1←v''=0)	...	0.0380	64±5	9	transitions

(1) Morton (1978); (2) Morton & Smith (1973); (3) Dufton *et al.* (1983); (4) Morton (1975);

(5) Hibbert *et al.* (1983); (6) Nussbaumer, Pettini & Storey (1981);

(7) Morton, York & Jenkins (1988); (8) Butler & Storey (personal communication);

(9) Lassettre and Skerbele (1971).

spectra and thereby effectively removing much of the fixed pattern noise. For the LWP wavelength range, the signal-to-noise is lowest ($\sim$ 10) for $\lambda < 2400$Å and peaks at $\sim$ 45 near 2800Å. The velocities quoted in Table 3.11 have been corrected to the LSR frame of reference by assuming that the neutral species (C I, C I*, C I**, Cl I and S I) in the SWP wavelength range are at $V_{LSR} = +9$ km s^{-1}, as deduced from the Na I lines. For the LWP wavelength range, the correction factor was determined by matching the mean velocity of lines from singly ionised species in both the SWP and LWP wavelength ranges. The accuracy of the LSR velocity correction can be assessed by considering the velocity agreement between the optical and UV high velocity components. From Table 3.11, the mean velocity of the UV components is -64 ± 5 km s^{-1} compared to -65 km s^{-1} for Na I; I am therefore confident that the adopted velocity scale is the correct one.

Excluding the high velocity components which will be discussed in Section 3.7.3.3, three distinct velocity groups can be identified. The first consists of the neutral species C I, C I*, C I**, Cl I and S I (16 lines; $V_{LSR} = +9.0 \pm 1.7$ km s^{-1}). A second group containing species commonly found in H I clouds (C II, C II*, N I, O I, Mg I, Mg II, Al II, Si I, Si II, Si II*, P II, S II, Cr II, Mn II, Fe II, Ni II, Cu II and Zn II) is found at $V_{LSR} = -1.6 \pm 4.8$ km s^{-1}(40 lines). The main components of the highly ionised species of C IV, Al III, Si III and Si IV are observed at different velocities and form the third group: Si III and Si IV are at +21 km s^{-1}; C IV at +15 km s^{-1} and Al III at +2 km s^{-1}. I defer discussion of this group until Section 3.7.3.3 but note that the velocity of Al III indicates that it may consist of contributions from Groups 2 and 3. The velocities of the Ca II lines (+15, +17 km s^{-1}) are quite different from those of the Group 1 and 2 species but agree with those of C IV. The accuracy of the velocity measurements depends ultimately on the overall wavelength calibration of IUE high dispersion images. The small r.m.s. dispersion of 1.7 km s^{-1} that was derive for the 16 narrow lines arising from neutral species (1200–1800 Å) indicates that the overall wavelength calibration is good. I obtain a r.m.s. dispersion of 4.8 km s^{-1} for the 40 SWP lines arising from HI-type species. This larger value is mainly due to measurement uncertainties because many of the lines are broad and saturated; it is reduced to 2.9 km s^{-1} if the narrower, less saturated lines are selected. I have also searched for systematic effects arising from possible inaccuracies in the IUE wavelength calibration by

examining all the measured velocities as a function of wavelength. I find only a random distribution. Overall, I therefore find that the velocity measurements are dominated by measurement uncertainties rather than deficiencies in the IUE wavelength calibration. I will adopt the conservative value of $\pm$ 5 km s^{-1} for the error in the measured velocities.

Total column densities along the line of sight to WR 136 have been determined for the H I-type species forming Group 2. I have assumed that these absorption lines have a Maxwellian velocity distribution and that the species are distributed over the absorbing clouds with the same relative abundances. Empirical curves of growth have been constructed by plotting $\log(W_\lambda/\lambda)$ against $\log(f\lambda)$ and horizontally shifting the points for each ion until a smooth curve was defined. The resulting curve of growth is presented in Figure 3.18 where the error bars along the ordinate reflect the uncertainties in the measured equivalent widths as given in Table 3.11. The observed curve was then compared to theoretical ones in order to determine the range in the Doppler parameter b which can be used to describe the data. In evaluating these theoretical curves, I have assumed an instrumental resolution function with b_{inst}=18 km s^{-1}. This value was empirically determined from a group of relatively blend-free interstellar lines towards the WR star HD 50896 by Howarth and Phillips (1986) and is consistent with the value given by Boggess *et al.* (1978b) when describing the performance of the IUE scientific instruments. The large number of points, covering a wide range in oscillator strength, tightly constrains b to the value of 20 ± 1 km s^{-1}. The theoretical fit is shown in Figure 3.18 where the horizontal axis has been labelled for Mg II λ2802.704.

Single-component curve of growth studies like the one performed here have certain limitations since the line of sight intersects numerous clouds and representation by one smooth Maxwellian velocity distribution can lead to errors. For example, Routly & Spitzer (1952) first pointed out that weak, higher velocity components will increase the equivalent width of the stronger lines but not that of the weaker lines. This induces an overestimate of the b parameter and an underestimate of the column density. However, Jenkins (1986) carried out an analysis of the effects of a single component curve of growth on the determination of column densities for lines of sights formed by numerous clouds. He concluded that if the line centre optical depth ($\tau_0 = \pi^{1/2}e^2\lambda f N/m_e cb$) of

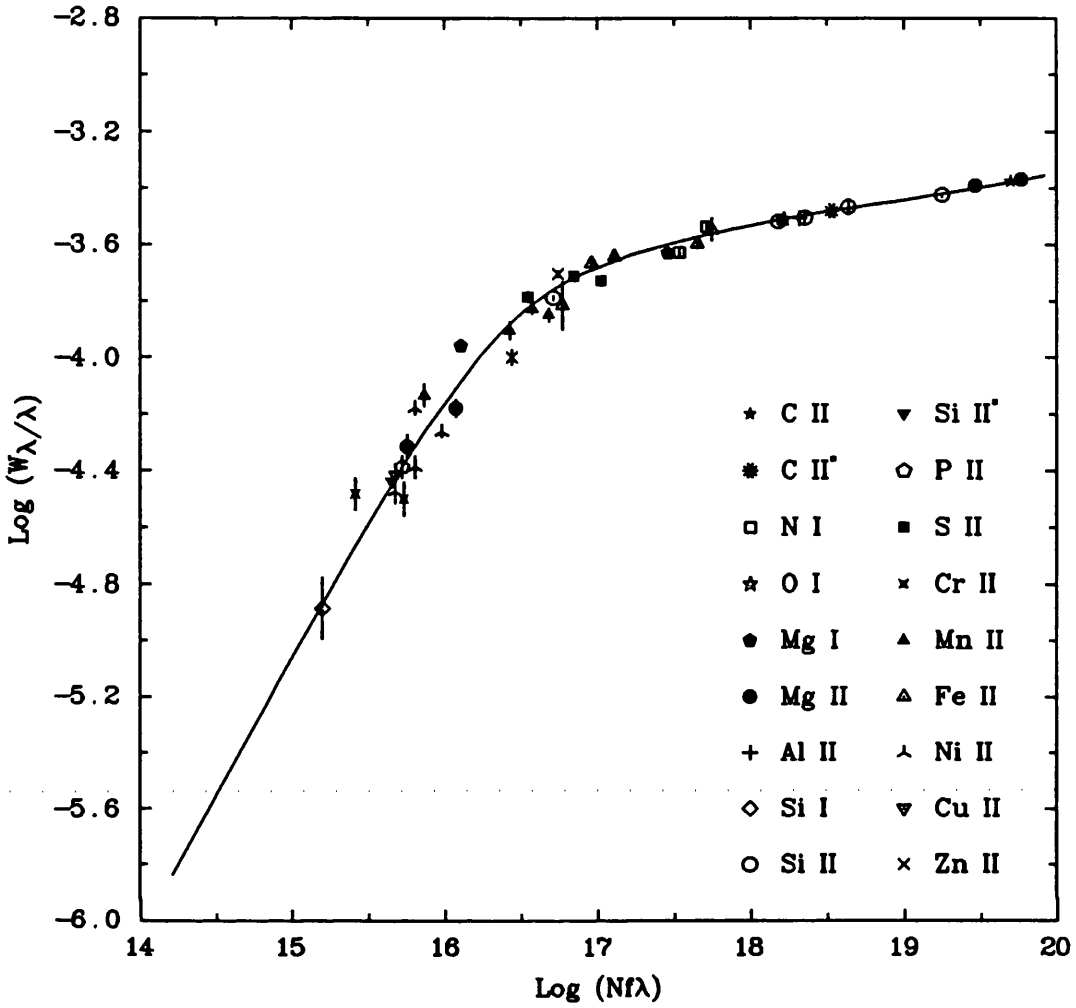

Figure 3.18 : Empirical curve of growth for the low-velocity H I-type species observed towards WR 136. The continuous line is a theoretical curve of growth for a single cloud model with b=20 km s^{-1}. The horizontal axis has been labelled for Mg II λ2802.704.

the weakest line for a given ion did not exceed 5, the column densities were accurate to within 20%. I have therefore calculated the line centre optical depths for each line observed and found that for all ions except C II, N I, O I and Al II this condition is satisfied These four ions will therefore not be considered in the remainder of this Section. The resulting column densities are given in Table

Table 3.12

Column Densities (N) and Depletion Values (δ) for the H I-type Species towards WR 136 (log $N(\mathrm{H})_\odot = 12.0$, log $N(\mathrm{H}) = 21.63$)

Ion	log $N_\odot$	log N(Observed)	δ(Observed)	δ(predicted)	Ref.
Mg I+II	7.58	16.50 – 16.55	−0.71 to −0.66	−0.52 ± 0.02	2
Si I+II	7.55	15.90 – 16.27	−1.28 to −0.91	−1.15 ± 0.03	1
P II	5.45	14.52 – 14.61	−0.49 to −0.40	−0.49 ± 0.04	2
S II	7.21	15.64 – 15.80	−1.20 to −1.04	−0.83 ± 0.06	1
Cr II	5.67	13.04 – 13.39	−2.19 to −1.84	...	...
Mn II	5.45	13.77 – 13.91	−1.31 to −1.17	−1.29 ± 0.02	1
				−1.13 ± 0.03	2
Fe II	7.67	14.65 – 14.87	−2.65 to −2.43	−2.14 ± 0.03	1
				−1.96 ± 0.06	2
Ni II	6.25	13.74 – 13.99	−2.14 to −1.89	...	...
Cu II	4.21	12.85 – 12.94	−0.93 to −0.83	...	...
Zn II	4.60	13.69 – 13.95	−0.54 to −0.28	−0.31 ± 0.06	1

1. Van Steenberg & Shull (1988)
2. Jenkins, Savage & Spitzer (1986)

3.12 where the range reflects the interval in b which gives an acceptable fit to the observed curve of growth.

The depletion factor of element i on interstellar grains compared to solar abundances, δ_i, is given by the following expression:

$$\delta_i = \log[N_i/N_H] - \log[N_i/N_H]_\odot \ .$$

In order to calculate these values I need to evaluate the total hydrogen column density N_H along the line of sight towards WR 136. Bohlin, Savage & Drake (1978) found a relatively good correlation between N(H I) and E(B−V) for 100 stars observed with the *Copernicus* satellite. The H I column density was determined by multiplying the region of the *Lyα* line by $exp(+\sigma_\lambda N(\mathrm{H\,I}))$, where σ_λ was assumed to be a Lorentzian profile, for various values of N(H I) until a flat spectrum was restored. This technique cannot used here because of the possible presence of a stellar P Cygni profile for He II λ1215.2 (*cf.* Howarth & Phillips 1986). Bohlin *et al.* (1978) found that $<N(\mathrm{H\,I})/E(\mathrm{B-V})> = 4.8 \times 10^{21}$ cm^{-2} mag^{-1}. Shull & Van Steenberg (1985) found a comparable value of $<N(\mathrm{H\,I})/E(\mathrm{B-V})> = 5.2 \times 10^{21}$ cm^{-2} mag^{-1} in a more extensive survey of 244

early-type stars with IUE. I will adopt this latter value. With $E(B-V)= 0.59$ (Table 3.8), this yields a H I column density of $N(H\,I)= 3.1 \times 10^{21}$ cm^{-2}.

I need to determine the contribution of H_2 to the total hydrogen column density. Savage *et al.* (1977) used an equivalent procedure to the one used for *Lyα* on the $J = 0$ and 1 rotational levels of the $v'' = 0$ vibrational state of H_2 to evaluate the molecular hydrogen column density towards 109 stars observed with *Copernicus*. These column densities are reasonably well correlated with the colour excess. I used the empirical correlation (*cf.* their Figure 4), extrapolated to $E(B-V)= 0.59$, to deduce a column density of $N(H_2)= 0.6 \times 10^{21}$ cm^{-2}. Therefore, I will adopt for the total hydrogen column density towards WR 136: $N_H = N(H\,I)+2N(H_2)= 4.3 \times 10^{21}$ cm^{-2}. As pointed out by Van Steenberg & Shull (1988), the 1σ dispersion in the correlation between H column density and colour excess leads to an error on the H column density of ± 0.25 dex.

Depletion values, calculated using the solar abundances of Grevesse (1984), are listed in Table 3.12 and shown in Figure 3.19. I have assumed that all the dominant stages of ionisation have been observed and I have neglected contributions from H II regions along the line of sight. The given range reflects the interval in column density allowed by the data as well as the error for N_H. No error estimate was included for the solar abundances.

Correlations have been found between the depletions of certain elements and the mean density along the line of sight $< n_H >= N_H/R$ where R is the distance to the star. Using the H column density deduced above and the distance to WR 136 from Table 3.8 (1.8 kpc) a mean H density of $< n_H > = 0.65$ cm^{-3} is found. Jenkins, Savage & Spitzer (1986) present formulae for calculating the expected depletions of Mg, P, Mn and Fe for a given mean hydrogen density. Likewise, Van Steenberg & Shull (1988) provide best-fit straight line coefficients for the depletions of Si, S, Mn, Fe and Zn as a function of mean hydrogen density. In Table 3.12 and Figure 3.19, I compare the observed values of the depletions with the values predicted by Jenkins *et al.* (1986) and Van Steenberg & Shull (1988) for the observed mean hydrogen density. Within the observational errors, the observed depletion values for Si, P, Mn and Zn agree well with the predicted ones while for Mg, S and Fe they are only slightly higher. The interstellar line of sight towards WR 136 can thus be characterised as having a relatively "normal" depletion pattern.

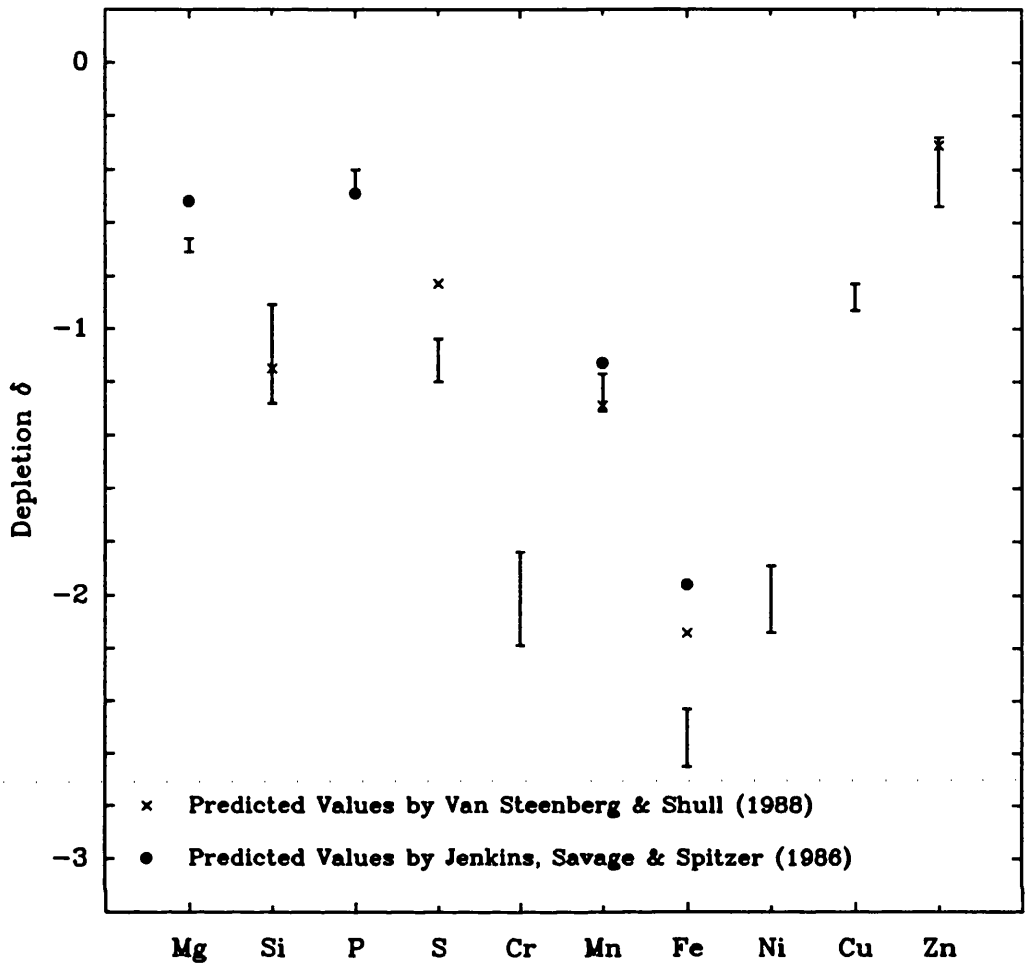

Figure 3.19 : Range of depletion values for the low-velocity H I-type species compared to values predicted from the mean H density, $< n_H >=0.65\ cm^{-3}$.

3.7.3.3 Stars in Cygnus

The 13 stars in the two Cygnus OB associations are highly reddened and thus the IUE SWP spectra in general contain broad, saturated, low velocity interstellar absorption lines. High velocity absorption components are detected towards all the stars in the sample except P Cygni.

In order to characterise the velocity distribution of the interstellar gas towards the sample of stars, I have calculated the mean velocity of a selection of lines arising from neutral species (C I, C I*, C I**, Cl I, S I); H I-type species; and individual velocities and equivalent widths of the highly ionised species

(C IV, Si III, Si IV and Al III). These velocities have been converted to the LSR frame of reference by assuming that the IUE neutral species are formed at the same velocity as the Na I lines (*cf.* Section 3.7.3.1). I have also measured the velocities of all the high velocity components detected in the SWP spectra. The LSR velocities of the components detected in the H I-type species are given in Table 3.13 for the 9 stars which show such components. In Table 3.14, I list the LSR velocities and total equivalent widths of all the components detected in the highly ionised species for each star in this study. The mean LSR velocities of the low velocity neutral and HI-type species are also listed in Table 3.14; the scatter in the r.m.s deviations reflect the difficulty of measuring broad, unresolved lines. The spectral region covering the interstellar C IV doublet is shown in Figures 3.20(a) and (b) for the WR and OB stars respectively. Each line has been rectified by applying a low-order polynomial fit to selected continuum regions and successive spectra have been shifted by 1 ordinate unit. I now discuss each star in turn.

WR 134

This star is a member of the Cygnus OB3 association and has very strong, broad interstellar lines which are probably blends of several unresolved components. Two low-ionisation interstellar lines (O I λ1302 and Si II λ1526) show strong, partially resolved components at -50 km s^{-1}. Si II* λ1265 is clearly present and split into two components at -22 and $+35$ km s^{-1}. The highly ionised species C IV, Si IV and Al III have asymmetric blue wings and a component is marginally resolved in C IV λ1550 at -25 km s^{-1}, in agreement with Si II*. The velocities of the main components of C IV and Si IV ($+3$ km s^{-1}) agree with the mean velocity of the singly ionised species. The velocities of the Al III interstellar lines are quite different (-19, -10 km s^{-1}) and indicate that they are probably blends of the -25 km s^{-1} and $+3$ km s^{-1} components.

WR 135

This star is close to WR 134 and also a member of the Cygnus OB3 association. It has a similar interstellar spectrum with strong, broad lines. Partially resolved components are seen in three low ionisation lines at a mean velocity of -53 ± 1 km s^{-1}. This value agrees well with the -50 km s^{-1}

Table 3.13

LSR Velocities (km s^{-1}) of Components in H I-type Species

Ion	λ_{vac}(Å)	WR 134	WR 135	HD 191456	WR 137	HD 192639	WR 138	WR 136	HD 193514
C II*	1335.703			−63	−56		−33		−69,−24
O I	1302.168	−51	−52	−57	−52				−69
Al II	1670.787			−57	−54				
Si II	1193.289								
	1260.421						−37		
	1304.372		−53	−62	−58	−47			
	1526.708	−49		−64					
	1808.012				−57	−46			
Si II*	1264.737	−22,+35	−36			−64	−41	−53	
S II	1250.586				−58	−51			−27
	1253.812				−59	−52			−33
	1259.520				−60	−53			
Fe II	1608.456		−54		−61				

Table 3.14
LSR Velocities (km s^{-1}) and Equivalent Widths (mÅ) of Components in Highly Ionised Species

Ion	λ_{vac} (Å)	WR 134 V	WR 134 W_λ	WR 135 V	WR 135 W_λ	HD 191456 V	HD 191456 W_λ	WR 137 V	WR 137 W_λ	HD 192639 V	HD 192639 W_λ	WR 138 V	WR 138 W_λ	HD 192303 V	HD 192303 W_λ
C IV	1548.188	−1	604	+4 −45	480	+13 −55	725	+14 −22 −67	431	+25 −54	374	+12 −43	306	+24	
	1550.762	+8 −25	541	−3 −44	455	+20 −63	579	+18 −23 −62	311	+20 −51	349	+17 −43	280	+24 −49	
Si IV	1393.755	+4	483	+0 −44	359	+15 −60		+18 −23 −70	332			+13 −47	252		
	1402.770	+1	420	−1 −46	316	+21 −63		+19 −19 −68	240	+19 −54	280	+14 −50	180		
Al III	1854.716	−19	556	−15	417	+22 −44	903	−1 −64	232	+9 −53	586	+14 −33	340	+14 −68	713
	1862.790	−10	430	−11	358	+13 −46	678	+13 −16 −62	158	+0 −56	395	+13 −40	177	+18 −75	575
Si III	1206.510			−1 −52	377	+7 −48		+19 −24 −69	425	+20 −48	487				
N V	1238.808					+15	70								
	1242.796					+8	31								
Mean Velocity of Neutral Species		+9.0±2.7		+12.5±3.4		+10.5±1.9		+9.0±2.7		+3.0±3.0		+6.0±4.2		+2.0±4.0	
Mean Velocity of HI-type Species		+2.5±3.0		+1.9±3.4		+7.4±2.6		+6.1±2.0		+1.1±4.1		−4.0±3.7		−2.8±3.4	

Table 3.14 (continued)
LSR Velocities (km s^{-1}) and Equivalent Widths (mÅ) of Components in Highly Ionised Species

Ion	λ_{vac} (Å)	WR 136 V	WR 136 W_λ	P Cygni V	P Cygni W_λ	HD 193443 V	HD 193443 W_λ	HD 228519 V	HD 228519 W_λ	WR 139 V	WR 139 W_λ	HD 193514 V	HD 193514 W_λ
C IV	1548.188	+17	365	+2	378	+2	335			−10	122	−1	496
		−61	167			−28				−44			
	1550.762	+14	277	+6	376	+7	321			−10	119	−5	564
		−61	108			−32				−44		−59	
Si IV	1393.755	+24	349	+4	273	+3	279			−14	115		
		−66	203			−24				−47			
	1402.770	+21	276	+5	211	+11	205			−6	61	−4	440
		−67	149			−17				−44		−63	
Al III	1854.716	+ 3	167	−8	171	−5	387	+13	630	−6	91	−7	607
		−57	117			−34							
	1862.790	+ 0	101	−7	96	−6	270	+13	473	−11	42	−4	436
		−62	67			−30		−31					
Si III	1206.510	+21	360										
		−41	450										
N V	1238.808	−72	29										
	1242.796	−65	15										
Mean Velocity of Neutral Species		+9.0±1.7		+3.0±3.2		+3.0±3.6		+1.5±3.4		+6.0±4.1		+1.0±2.2	
Mean Velocity of HI-type Species		−1.6±4.8		−5.8±5.7		+3.3±3.6		+1.3±3.8		−0.8±4.4		−2.4±3.9	

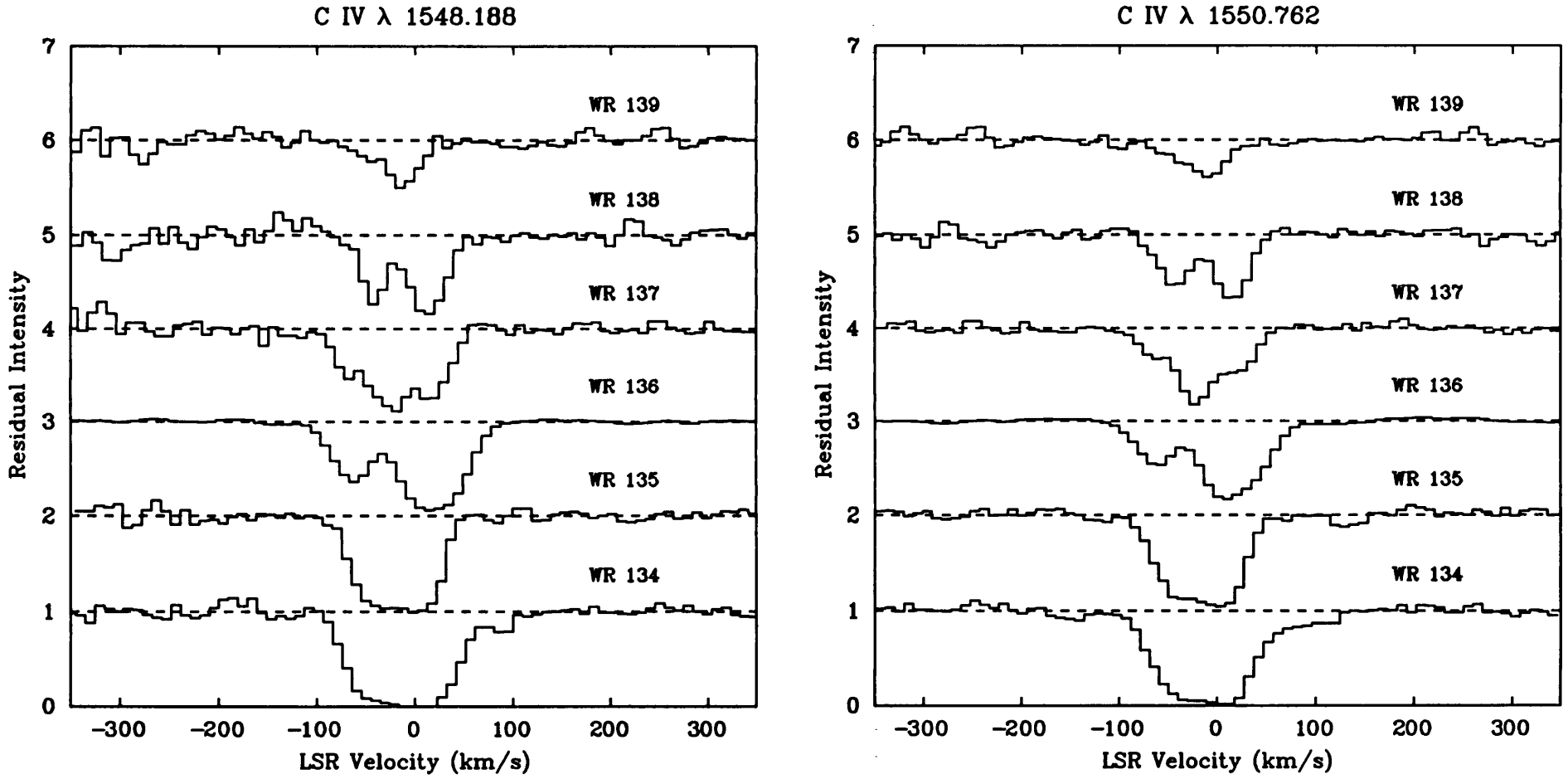

Figure 3.20 (a) : Rectified ultraviolet C IV profiles for the WR stars in the sample. Each component of the doublet is shown in LSR velocity space. Successive spectra have been shifted by 1 ordinate unit.

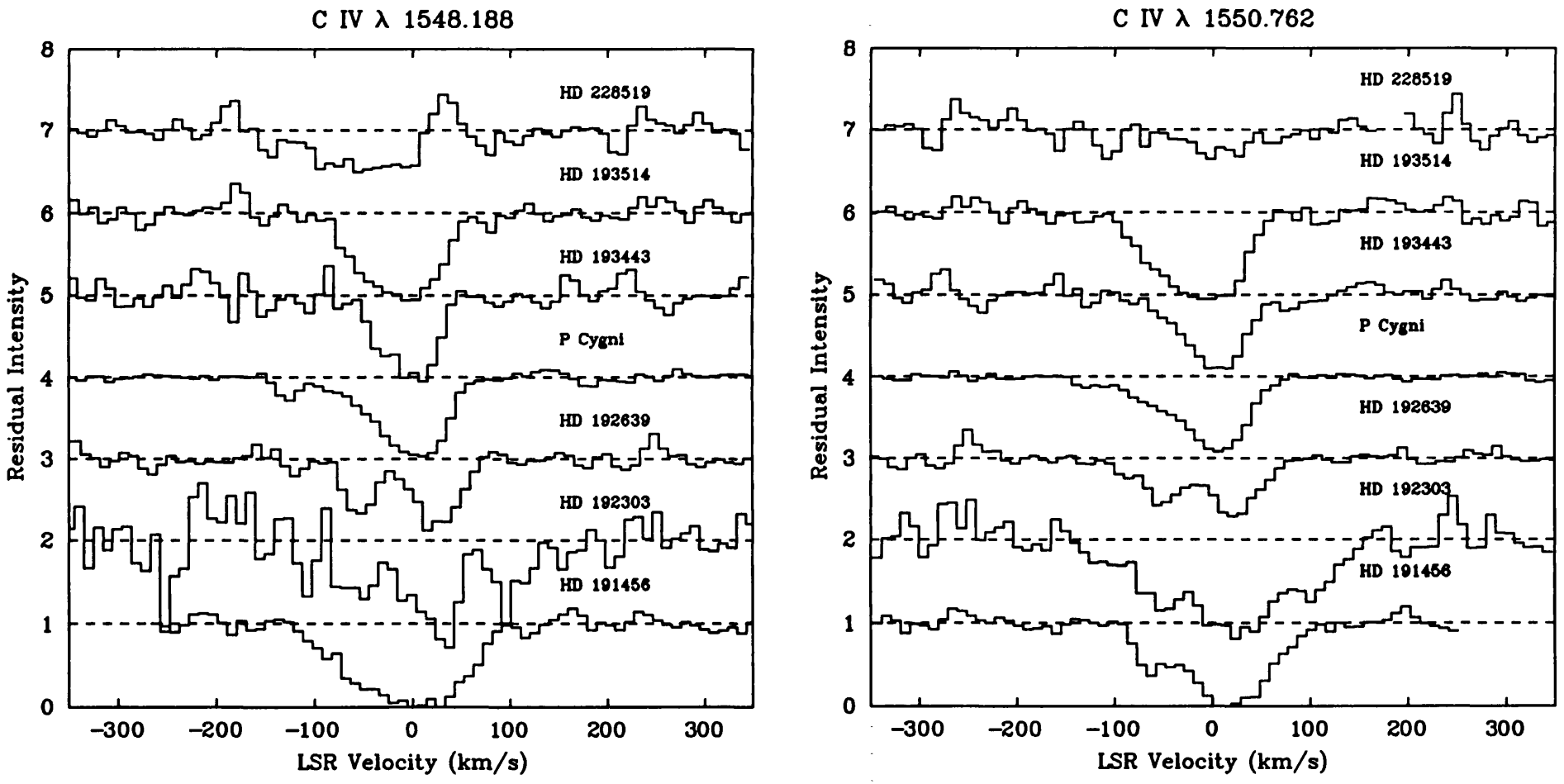

Figure 3.20 (b) : Rectified ultraviolet C IV profiles for the O stars in the sample. Each component of the doublet is shown in LSR velocity space. Successive spectra have been shifted by 1 ordinate unit.

component observed in Na I and also with the two components observed in the low ionisation species in WR 134. Si II* λ1265 has a single component at -37 km s^{-1}. The C IV and Si IV lines show components near -45 km s^{-1}. The main components of Si III, C IV and Si IV occur near zero velocity in agreement with the main components of the more lowly ionised species. Al III, as in WR 134, occurs at a more negative velocity and is probably a blend of the two components seen in C IV.

HD 191456

This star is the third member of the Cygnus OB3 association in the sample and has similar broad interstellar lines, although the high-velocity components are better resolved. These can be classified into two distinct groups. The first includes the low ionisation species of C II*, O I, Al II and Si II as well as the higher ionisation species of C IV and Si IV and is at a mean velocity of -61 ± 3 km s^{-1}, slightly higher than the velocity of the low ionisation components in WR 134 and WR 135. The second group contains Al III and Si III at a mean velocity of -46 km s^{-1} which is in better agreement with the -50 km s^{-1} component of WR 134 and WR 135. The main component of Si III agrees well with the main component of the lower ionisation species but the other highly ionised species C IV , Si IV , Al III and N V are at a higher mean velocity of $+16 \pm 5$ km s^{-1} . This is the only star for which I detect N V in low velocity gas.

WR 137

A large number of strong components are observed in the line of sight to this star. They are fairly well resolved in all ions. Most of the low ionisation species (C II*, O I, Al II, Si II, S II and Fe II) show components with a mean velocity of -57 ± 3 km s^{-1}, in good agreement with the -55 km s^{-1} component observed in Na I. The highly ionised species have a more complex velocity structure. Three components with mean velocities of -66 ± 3 km s^{-1}, -21 ± 3 km s^{-1} and $+17 \pm 3$ km s^{-1} are clearly visible. I associate the $+17$ km s^{-1} feature with the main interstellar component and note that the velocity is higher than that of the low ionisation species but in very good agreement with the main component of the highly ionised gas observed towards HD 191456.

HD 192639

This star has strong high velocity components, clearly resolved in the C IV, Si IV, Si III and Al III lines, and partially resolved in Si II and S II with a mean velocity of -51 ± 3 km s^{-1}, in good agreement with other components observed towards WR 134, WR 135 and HD 191456. HD 192639 was first studied by PWP. My measured velocities agree well with theirs for Si IV but differ by ~ 10 km s^{-1} for C IV and ~ 15 km s^{-1} for Al III. I also detect a component at a somewhat higher velocity of -64 km s^{-1} in Si II*. The main components of C IV, Si IV and Si III are at a mean velocity of $+21 \pm 3$ km s^{-1} which is similar to the corresponding velocities in HD 191456 and WR 137. Al III occurs at the same velocity as the low ionisation species.

WR 138

The C IV, Si IV and Al III lines towards this star show clearly resolved components while the low ionisation lines of C II*, Si II and Si II* have partially resolved components. The mean velocity is -41 km s^{-1} with a relatively large scatter of 6 km s^{-1} . Many singly ionised lines have blue wings extending to ~ -50 km s^{-1}, indicating that this component is probably present in a broader range of lines than is apparent from Tables 3.13 and 3.14. The main components of C IV, Si IV and Al III are again at a velocity which is higher than that of the low ionisation species, with a mean of $+14 \pm 2$ km s^{-1} .

HD 192303

This star is very close to WR 136 on the plane of the sky but unfortunately the single spectrum available is very noisy. Moreover, the interstellar lines are broad and may contain some contamination from the photospheric lines of this B1 III star. Nevertheless, weak, partially resolved components are detected at -68 and -75 km s^{-1} in the Al III doublet and at -49 km s^{-1} in C IV λ1550. No components are resolved in the singly ionised lines. Again, the main component of the highly ionised species of C IV and Al III ($\sim +20$ km s^{-1}) is at a higher velocity than the singly ionised species.

WR 136

As can be seen from Tables 3.13 and 3.14, ten high velocity components are detected in the line of sight towards this star. The C IV, Si IV and Al III doublets have a very clear double structure which was first reported by Huber *et al.* (1979) who attributed the high velocity gas to the nebula NGC 6888, surrounding the star. In addition, I detect a high velocity component in the N V doublet, seen only at this velocity. The mean velocity of the components is $-64\pm$ 5 km s^{-1} which agrees well with the velocity of the component detected in Na I at -65 km s^{-1}. Components are also detected in the Si II*λ1265 line at -53 km s^{-1} and in the Si III λ1206 line at -41 km s^{-1} . In general, many of the singly ionised lines are wide and clearly have asymmetric blue wings, suggesting the presence of unresolved high velocity components. The main components of C IV, Si IV and Si III are at a mean velocity of $+19 \pm 4$ km s^{-1} and that of Al III agrees with the lower ionisation species.

P Cygni

No high velocity gas is detected towards this star. The velocity of the highly ionised species is consistent with that of the singly ionised species, although in both cases the scatter is high. In general, the lines are relatively narrow ($\sim$ 60 km s^{-1}) and do not show any obvious asymmetries, indicating a real absence of components.

HD 193443

This star shows partially resolved components at an intermediate velocity of $\sim -$ 30 km s^{-1} in the C IV and Si IV doublets and an asymmetric blue wing, hinting at a similar component in the Al III doublet. No gas at higher velocities is present. My velocities agree well with those given by PWP who first reported the presence of these components in the line of sight towards this star. The velocity of the main component of the highly ionised species is consistent with that of the singly ionised species, although the scatter is quite high because of the unresolved nature of the components.

HD 228519

This star has only one spectrum available and it is relatively noisy. Only one partially resolved component is detected in the Al III λ1862 line at ~ -31 km s^{-1}. It is clearly present in the other component of the doublet although it is not resolved. Some singly ionised species have asymmetric blue wings, hinting at the presence of weak unresolved intermediate velocity components. The velocity of the main component of Al III is estimated at +13 km s^{-1}, which is higher than the mean velocity of the H I-type species.

WR 139

WR 139 is a well known WR+O spectroscopic binary system (V444 Cygni). Great care was therefore taken when adding spectra to form the mean, as flux levels are known to change significantly as a function of orbital phase. For each of the high ionisation lines of C IV, Si IV and Al III, I have selected fixed continuum regions and rectified the spectra by fitting a low order polynomial to this continuum. All the rectified spectra were then aligned and added together. This procedure has revealed weak high velocity components in the C IV and Si IV lines but not in the Al III lines. The mean velocity of these components is $-45\pm$ 2 km s^{-1}. No high velocity components are detected from singly ionised gas but the signal-to-noise in the individual spectra is lower. The main component of C IV, Si IV and Al III is at a velocity of -10 ± 3 km s^{-1} which is more negative than that found for the low ionisation species.

HD 193514

The interstellar lines formed along the line of sight towards this star are generally very broad and strong, indicating the presence of several unresolved components. High velocity components are partially resolved in C II* λ1335 and O I λ1302 at -69 km s^{-1} . Gas at the intermediate velocity of ~ -28 km s^{-1} is detected in the singly ionised lines of C II* λ1335, S II λ1250 and S II λ1253. Partially resolved components are also detected in C IV λ1550 and Si IV λ1402 at ~ -61 km s^{-1} while C IV λ1548, Si IV λ1393, as well as the Al III doublet, have very strong asymmetric blue wings, strongly suggesting the presence of this component in these lines. These measurements are very similar to the ones

previously found by PWP when they first noted the presence of high velocity gas towards this star. The mean velocity of the main component of the highly ionised species is consistent with the mean velocity of the H I-type gas.

3.7.4. DISCUSSION AND CONCLUSIONS

One fact that clearly emerges from the analysis of the IUE interstellar spectra formed in the line of sight towards the stars in the sample is that this region of Cygnus is dynamically very active. I have detected low, intermediate and high velocity components, formed in gas with varying degrees of ionisation, towards most of the stars I have studied. These lines are undoubtedly the result of several phenomena, some very energetic, which I will attempt to identify in this section.

In order to try to gain more insight into the origin of the various components detected towards the stars in the sample, I have obtained column densities, velocity dispersions and velocities by fitting theoretical profiles to the high velocity components detected in the HI-type gas and to all the high ionisation components. The theoretical line profiles were calculated and adjusted to fit the observed profiles following the procedure described in Section 3.7.3.1. The results are presented in Tables 3.15 and 3.16. For some stars, the fitted velocities are slightly different to the measured values because of the difficulties associated with measuring blended lines. As a consequence of the broad instrumental profile of IUE (FWHM$\approx$30 km s^{-1}), the b values determined for the low velocity components are generally not very well constrained. These lines almost certainly consist of a number of individual components blended together. In this case, the implicit assumption of a single absorbing cloud is not correct and the derived column densities should be viewed as lower limits. Conversely, the weaker, high velocity components appear single and thus their b and N values are well constrained. I have excluded WR 134 from Table 3.16 because its components are too blended to produce satisfactory profile fits.

3.7.4.1 Low Velocity Gas

As mentioned in Section 3.7.3.1, the velocities of the main components for the neutral gas (Na I, C I, C I*, C I**, Cl I and S I) reflect the spatial distribution of the stars in the sample. For the four southernmost stars WR 134, WR 135, WR 137 and HD 191456 as well as for WR 136 the velocity is $\sim$ +10

Table 3.15

Column Densities (Log$N$, cm^{-2}), Velocity Dispersions (b, km s^{-1}) and Mean Velocities (V, km s^{-1}) of Components in HI-type Species

Ion	WR 134		WR 135		HD 191456		WR 137		HD 192639		WR 138		HD 193514			
	log$N$	b	log$N$	b	log$N$	b	log$N$	b	log$N$	b	log$N$	b	log$N$	b	log$N$	b
C II*					14.10	15	14.30	15			14.13	15	13.93	10	15.15	12
O I	14.60:	33:	14.88	20	14.21	18	14.75	7					14.30	10		
Al II					12.70	18	13.30	7								
Si II	14.15:	33:	14.60	10	13.95	10	14.05	15	15.25	7	13.45	14				
S II							14.75	8	14.73	13					15.30	10
Fe II			14.30	10			13.97	7								
V	−50		−53		−61		−57		−51		−37		−69		−28	

Note : A colon indicates that the component is badly blended and the derived parameters are uncertain.

Table 3.16

Column Densities (log N, cm^{-2}), Velocity Dispersions (b, km s^{-1}) and Velocities (V, km s^{-1}) of Components in Highly Ionised Species

Star	C IV			Si IV			Al III			Si III			N V			$\frac{C\,IV}{Si\,IV}$	$\frac{Si\,IV}{Al\,III}$	$\frac{Si\,IV}{Si\,III}$
	V	log N	b	V	log N	b	V	log N	b	V	log N	b	V	log N	b			
(a) High Velocity Components																		
WR 135	−47	14.30	15	−45	13.60	15				−54	13.50	15				6.3		1.3
HD 191456	−60	14.05	15	−61			−50	13.35	20	−47	12.85	9						
WR 137	−66	13.60	10	−69	12.80	13	−63	12.50	10	−67	13.50	8				6.3	2.0	0.2
HD 192639	−54	14.05	10	−54	13.47	13	−58	13.40	10	−50	13.45	20				3.8	1.2	1.0
WR 138	−43	14.10	10	−48	13.30	8	−37	13.10	10							6.3	1.6	
HD 192303	−53	14.80	11				−70	13.15	10									
WR 136	−63	13.85	13	−66	13.75	15	−62	12.97	17	−45	13.50	30	−65	13.19	17	1.3	6.0	
WR 139	−47	13.10	10	−45	12.55	10										3.6		
HD 193514	−59	14.00	15	−63	13.40	15	−65	13.00	15							4.0	2.5	
(b) Intermediate Velocity Components																		
WR 137	−23	15.30	8	−20	14.40	8	−20	12.95	10	−24	14.50	8				7.9	28	1.0
HD 193443	−32	13.70	10	−32	13.60	8	−32	12.90	8							1.3	5.0	
HD 228519							−32	13.40	10									
(c) Low Velocity Components																		
WR 135	+ 0	15.20	15	+ 6	15.30	10	−12	13.70	20	− 1	13.40	17				0.8		
HD 191456	+15	14.80	30	+18			+18	14.10	30	+ 7	14.10	8	+12	13.60	20			
WR 137	+20	14.10	10	+22	13.70	10	+18	12.95	15	+22	14.20	8				2.5	5.6	0.3
HD 192639	+22	14.25	17	+19	13.87	18	+ 5	13.60	40	+22	13.70	20				2.4		1.5
WR 138	+13	14.50	10	+13	15.50	8	+16	13.25	15							0.1	178	
HD 192303	+24	15.00	30				+15	14.00	25									
WR 136	+15	14.50	24	+19	14.10	28	+ 0	13.18	18	+25	13.40	30				2.5		5.0
P Cygni	+ 2	14.55	25	+ 1	14.00	20	− 7	13.60	12							3.5		
HD 193443	+ 7	15.50	12	+10	15.10	8	− 5	13.50	20							2.5		
HD 228519							+12	13.60	15									
WR 139	−12	13.80	7	−10	13.20	10	− 5	12.80	10							4.0	2.5	
HD 193514	+ 0	16.00	15	− 4	15.30	20	− 5	14.00	22							5.0	20	

km s^{-1} while for the five northern stars HD 193514, HD 228519, HD 193443, P Cygni and HD 192303 I find a lower velocity of $\sim +2$ km s^{-1}. WR 138, WR 139 and HD 192639 have intermediate velocities and thus are not specifically included in either of these two groups. The measured velocities for these three stars are most likely the result of blending between the lines from the two groups. The velocity distribution of the HI-type gas is slightly different to that of the neutral gas. For all the stars included in the the sample, the main components are found near V_{LSR}=0 km s^{-1}. Therefore, for the stars in the northern part of the association, these lines are formed in the same clouds or in clouds of similar velocity as the neutral species. For the other stars, the velocity difference indicates that they are formed in separate clouds. Despite their different spatial distributions, all these values agree well with the velocities expected from normal galactic rotation (0–9 km s^{-1}), indicating that the main components of the neutral and HI-type interstellar lines are formed in clouds along the line of sight to Cyg OB1 and OB3. An analysis of interstellar cloud abundances in the line of sight to WR 136 (Section 3.7.3.2) shows that it is unexceptional with a fairly normal depletion pattern.

As was found for the neutral species, the main components of the highly ionised species can be separated into two distinct groups, reflecting the spatial distribution of the stars. These are not, however, the same groups. The first group, occupying the central part of our sample region, contains HD 191456, WR 137, HD 192639, WR 138, HD 192303, WR 136 and HD 228519 and is at a mean velocity of $+17\pm4$ km s^{-1} (35 lines). Lozinskaya and Sitnik (1988) using H_α interferometric observations find a mean velocity of $V_{LSR}=+12 \pm 5$ km s^{-1} for the complex of bright nebulae accompanying the Cyg OB1 association. Marston & Meaburn (1988) also find a mean value of $V_{LSR}=+13$ km s^{-1} for the ambient gas surrounding NGC 6888. These emission line velocities are consistent with my mean velocity and therefore indicate that the +17 km s^{-1} component observed in the highly ionised species towards these seven stars originates in gas local to the Cyg OB1 association. Humphreys (1978) lists the stellar radial velocities of the Cyg OB1 and Cyg OB3 association members. There is a large spread in the values; the mean LSR stellar radial velocities are $+8 \pm 10$ km s^{-1} for Cyg OB1 and $+8 \pm 9$ km s^{-1} for Cyg OB3. The mean values agree well with the values of +7 (Cyg OBI) and +9 (Cyg OB3) km s^{-1}

expected from galactic rotation. My measured velocity of +17 km s^{-1} is therefore higher than the galactic rotation value and may indicate that the gas is not at rest although the errors on the stellar radial velocities are too large to be confident of this. The velocities of the Si III and Al III lines do not always agree with those of C IV and Si IV. Similar differences have been found, for example, in the Carina nebula (Walborn, Heckathorn and Hesser 1984) and are usually explained by the fact that these ions, having lower ionisation potentials, can be formed at the interfaces of interstellar clouds, along the line of sight.

As mentioned in Section 3.7.3.1, the velocities of the main component of the Ca II optical interstellar lines are found to differ from those of Na I, which I have assumed to be at the same velocity as the lines of neutral species observed in the ultraviolet spectra. For the five stars WR 134, WR 135, WR 136, WR 137 and HD 191456 I find a mean velocity for the Ca II lines of +14±1 km s^{-1}. This is consistent with the +17±4 km s^{-1} component mentioned above and suggests that they have a common origin. It is well known that the Na I/Ca II column density ratio correlates with the radial velocity of the component in the sense that higher velocity gas has a lower Na I/Ca II ratio (Routly and Spitzer 1952, Siluk and Silk 1974). One explanation, first put forward by Routly and Spitzer (1952), is that this is a consequence of collisional ionisation of Na I by thermal electrons in high-temperature clouds. Routly and Spitzer (1952) and Pottash (1972) have shown that small ratios can be produced in gas at temperatures above a critical value of $\sim$ 7000 K. I suggest that this interpretation can be applied to the +14 km s^{-1} component, the high temperature being consistent with the fact that it is observed only in highly ionised species in the ultraviolet. I therefore conclude that the +17 km s^{-1} component arises in a large scale H II region associated with the Cygnus OB1 association.

The second group includes WR 134 and WR 135 as well as the 3 northern stars HD 193514, HD 193443 and P Cygni and is detected at the same velocity as the HI-type gas, near V_{LSR}=0 km s^{-1}. The unusually high column densities obtained from the profile fits to these lines strongly suggest that this component does not originate in the intervening interstellar medium. The few measurements that exist of the column densities of interstellar C IV and Si IV, free from contamination by circumstellar material (*e.g.* Laurent, Paul and Pettini 1982), have yielded much smaller values than those listed in Table 3.16.

The most widespread suggestion for the origin of strong, highly ionised interstellar lines is that they originate in disturbed circumstellar H II regions (*e.g.* Smith, Willis & Wilson 1980). I therefore suggest that the component observed in the highly ionised gas near V_{LSR}=0 km s^{-1} towards this second group of stars also originates in material local to the Cygnus OB1 and OB3 associations. For the remaining star, WR 139, the mean velocity for the main components of the highly ionised species is -9 ± 3 km s^{-1}. This value does not fit easily in either of the two groups mentioned above as it is more negative than the mean velocity of the H I-type species (-1 ± 4 km s^{-1}).

3.7.4.2 High-Velocity Components

3.7.4.2.1 *Intermediate-Velocity Gas*

Evidence for the presence of intermediate-velocity material in the lines of sight towards the Cygnus stars in my sample is found for species with varying degrees of ionisation. For the neutral gas a weak, blended component is observed in the Na I optical interstellar lines towards WR 135 and WR 136 at a velocity of ~ -20 km s^{-1}. HI-type gas is detected at a similar velocity of ~ -28 km s^{-1} towards HD 193514 in the transitions of C II* and S II. Most of the intermediate velocity gas is, however, observed in the highly ionised or excited species. Components are found in C IV, Si IV, Al III, Si III or Si II* towards WR 134 (-22, -25 km s^{-1}), WR 137 (-21 ± 3 km s^{-1}, 6 lines), HD 193443 (-27 ± 6 km s^{-1}, 6 lines) and HD 228519 (-27 km s^{-1}). These detections are not, however, correlated with the spatial distribution of the stars in the sample. It is difficult to determine if this effect is real or if it is simply caused by the fact that the component is not resolved towards all stars. Considering that most of the stars have very broad and saturated main components, and that the instrumental resolution function for both the optical and the ultraviolet observations is rather large, the second explanation is most likely to be the correct one. The highly ionised nature of this gas suggests that this component arises in dense, hot gas. Towards WR 137, the intermediate velocity component is particularly strong; the C IV and Si IV column densities are among the highest I have measured and, for this star, are higher than for the +17 km s^{-1} component discussed in the previous section. Clearly, data of much higher resolution are required to establish the extent and exact nature of this intermediate velocity

component. It seems likely that it arises in dense, highly ionised gas expanding away from the Cygnus OB1 association.

3.7.4.2.2 *High-Velocity Gas*

I observe high-velocity components formed in gas of varying degrees of ionisation, indicating a wide range of physical conditions. Weak components are detected in the optical Na I interstellar lines towards WR 135, WR 136 and WR 137 but not in any other neutral species. In the case of WR 135 and WR 137 the Na I velocities are similar to those observed in HI-type species while for WR 136, they are similar to the velocities of the highly ionised components. This suggests that they share a common origin while their weakness (N(Na I)$<10^{12}$ cm^{-2}) indicates that Na I is only a minor constituent. The mean velocity of the HI-type species and the fitted velocity of C IV are indicated in Figure 3.21 for the high velocity components observed towards the stars in our sample. The interpretation of these components is complicated by the fact that the velocities observed for the various ions towards a given star do not always agree and can differ by up to $\sim$20 km s^{-1}. For example, the velocities of the components for the highly ionised species observed towards WR 137 agree very well and have a mean value -66 ± 3 km s^{-1} (7 lines). However, the velocities of the components for the H I-type species observed towards this same star have a mean value of -57 ± 3 km s^{-1} (9 lines) which is significantly different from the mean velocity of the highly ionised species. I am confident that this velocity difference is real as I was not able to obtain acceptable profile fits for all the components using a single velocity. Another good example is WR 136 for which I have a mean spectrum of very high quality. The velocities of C IV, Si IV, Al III and N V are very similar with a mean of -63 ± 3 km s^{-1} but differ from the measured velocity for the Si III component which we find to be -41 km s^{-1}. The component observed in the Si II* transition towards this star has an intermediate velocity of -53 km s^{-1} which is most likely a blend between the -41 km s^{-1} and -63 km s^{-1} components. These specific examples strongly suggest that the differences between the velocities of the components observed towards a given star and between the various stars in the sample are real and not caused by measurement errors or wavelength calibration problems. The only clear spatial structure that is apparent is observed for HI-type species. The components detected towards the five stars WR 134, WR 135, HD 191456, WR 137 and

HD 192639 have similar velocities with a mean value of $-55\pm$ 5 km s^{-1} (24 lines). These stars form a compact group in the south of our sample which is reminiscent of the shell around the cluster IC 4996 described by Lozinskaya and Sitnik (1988). Using a distance of 1.8 kpc for the Cyg OB1 association yields a physical size of 27 $\times$ 37 pc for this region. The velocities of the other components range from -40 km s^{-1} to -70 km s^{-1}, with no clear grouping or systematic velocity gradients apparent across the surveyed region.

These high-velocity components detected in HI-type and highly-ionised species towards 10 out of 13 stars in my sample have two likely origins; they can either arise in gas closely associated with each individual star or they can be formed in a supershell enveloping the Cygnus OB1 association. The first possibility could correspond to O star or WR star nebulae which are either composed of gas ejected in an earlier evolutionary stage, or of ambient interstellar gas swept up by the wind of the star. Lozinskaya and Sitnik (1988) have reported the discovery of new small-scale nebulae associated with three of the stars in the sample: WR 137, HD 192639 and WR 139. There are also previously known nebulae associated with WR 134 and WR 136 (NGC 6888). In the case of WR 136, very good measurements are available for the expansion velocity of the associated nebula NGC 6888. From optical emission line spectra centred on WR 136, Chu (1988) finds $V_{neb} = -74$ km s^{-1} and Marston and Meaburn (1988) find $V_{neb} = -72$ km s^{-1} for a position very close to WR 136. These values are significantly different from the velocity of the ultraviolet absorption lines measured here (-64 km s^{-1}). Furthermore, the fact that this high velocity absorption component is detected in N V renders a nebular origin for this component very unlikely. Photoionisation models which successfully reproduce the nebular emission line strengths in NGC 6888 predict an absence of N V (Esteban and Vílchez 1991) in clear contradiction to my observations. Therefore, I conclude that the -64 km s^{-1} component detected in the line of sight towards WR 136 does not originate in NCG 6888 as previously suggested by Huber *et al.* (1979). In fact, although a nebular origin cannot be ruled out for any of the other lines of sight, the relatively narrow range in observed velocity for the high velocity gas observed towards the sample of stars (-40 to -70 km s^{-1}) suggests a common origin. Furthermore, considering the wide range in wind kinetic energies (*e.g.* between the WN 6 star WR 136 and the B1 III star HD 192303) and ages of the stars towards which I have detected high velocity

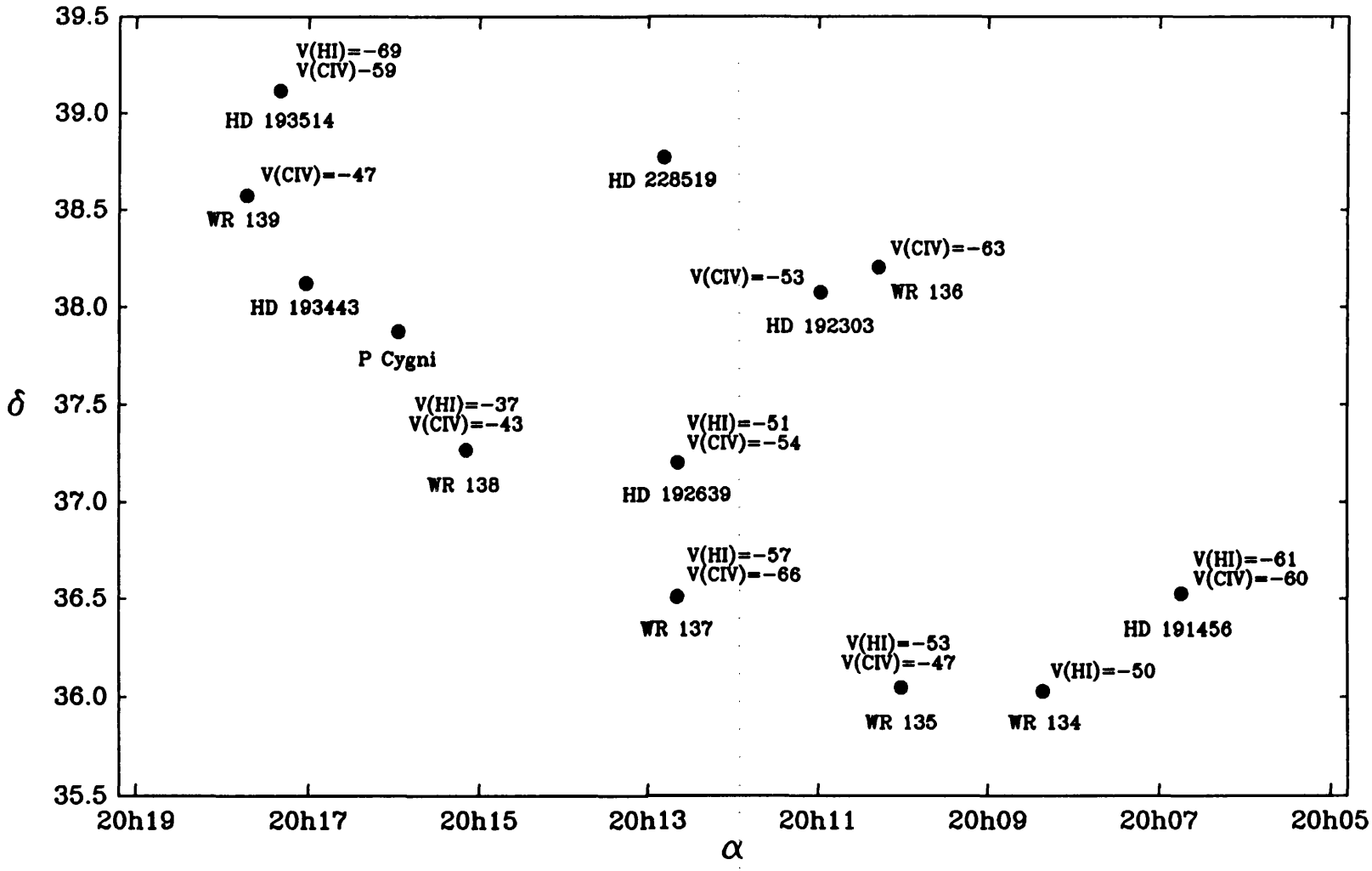

Figure 3.21 : Positions of the O and WR Cygnus stars included in this work. The mean velocity of the HI−type species and the fitted velocity of CIV are indicated for the high velocity components observed towards the stars in the sample.

gas, there is no reason to expect all individual nebulae to have similar expansion velocities. A much wider range of expansion velocities has been detected in the past for nebulae associated with WR stars (*e.g.* -87 km s^{-1} for RCW 58 (associated with WR 40); Smith *et al.* 1988 and -18 km s^{-1} for NGC 2359 (associated with WR 7); Chu, Treffers and Kwitter 1983). I therefore believe that these components are formed in an expanding supershell enveloping the Cyg OB1 association, as first proposed by PWP. Adopting a distance of 1.8 kpc for the Cyg OB1 association, I evaluate the size of the region for which high velocity gas has been detected as 68 pc $\times$ 97 pc or a radius of $\sim$ 40 pc. The energy required to produce the supershell through a supernova explosion or the maximum ambient gas density for a supershell driven by stellar winds can be determined following the procedure of PWP. From Chevalier (1974), the initial energy of a supernova for a remnant of radius R (pc), expansion velocity V (km s^{-1}) and ambient density n_0 (cm^{-3}) is given by

$$E = 5.3 \times 10^{43} n_0^{1.12} V^{1.40} R^{3.12} \text{ erg}$$

Adopting R$\approx$40 pc and V≈-55 km s^{-1}, I find energies of 0.1 x 10^{51} ergs, 1.4 x 10^{51} ergs and 19 x 10^{51} ergs for ambient densities of 0.1, 1 and 10 cm^{-3} respectively. This compares well with the typical energy produced by a type II supernova ($\sim 10^{51}$ ergs; Woltjer 1974) and therefore the supershell could have been produced by a supernova explosion. Alternatively, according to Weaver *et al.* (1977), the stellar wind power required to drive a shell of radius R (pc), expansion velocity V (km s^{-1}) in an ambient density n_0 (cm^{-3}) can be evaluated by the following expression:

$$L_w = 3.5 \times 10^{29} n_0 V^3 R^2 \text{ erg s}^{-1}$$

The total wind power produced by the stars in the Cyg OB1 association has been evaluated by Abbott (1982) as $\sim$ 1.2 x 10^{38} erg s^{-1}. This implies that in order to have been produced by the combined effect of stellar winds, the supershell must have an ambient density of $\leq$ 1.3 cm^{-3}, which is not an unreasonable value. Therefore, I conclude that the combined stellar winds from the Cyg OB1 association are also capable of driving the supershell.

In order to try to gain more insight into the origin of the gas, I have analysed in more detail the high velocity components formed in the line of sight towards WR 137. For this star, many components are observed covering a wide

range of ionisation stages. In particular, the S II lines are detected; as sulphur is usually undepleted in the interstellar medium those lines can be used as a reference to determine relative abundances. As discussed earlier, the lowly and highly ionised species occur at different velocities; therefore, I will only evaluate the depletion pattern for the high velocity HI-type gas. Using the solar abundances of Grevesse (1984) I obtain the following depletion pattern: δ_C=−1.93, δ_{Fe}=−1.24, $\delta_{Al} = -0.71$, $\delta_{Si} = -1.04$ and $\delta_O = -1.70$. This is highly puzzling as almost total grain destruction and therefore very low depletion is expected for material moving at such high velocities. A similar depletion pattern has also been observed in a high velocity component towards the Carina star HD 93205 by Laurent, Paul and Pettini (1982). One suggestion put forward by these authors is that the processes of grain destruction are not yet completed. These authors dismissed this interpretation because they found a large deficiency of Fe compared to Si and Mn. These three ions are thought to be removed from the gas in similar proportions and thus should have similar depletion values. Instead, they suggest that the component originates in a cloud which is interacting with gas generated in a recent supernova explosion, and thus heavily contaminated by freshly synthesized material, rendering the abundances far from cosmic.

The fact that I do not observe a unique velocity or a systematic velocity gradient for the numerous high velocity components detected towards the Cygnus supershell indicates that it is not a smooth, uniformly expanding structure. Such velocity differences could be produced in an inhomogeneous or fragmented expanding shell of gas in which various portions of the structure are at slightly different distances from the illuminating stars. Such fragmentation could have arisen through density inhomogeneities in the ambient interstellar gas which, given the size of the supershell, are probably to be expected.

Various mechanisms can produce highly ionised species such as C IV, Al III, Si III- IV and N V. Studies with the *Copernicus* satellite have revealed interstellar lines of O VI towards numerous lines of sight. A careful analysis of these absorption lines by Jenkins (1978a,b) has lead to the conclusion that they arise in hot, ubiquitous gas which is collisionally excited at temperatures of $T \geq 10^5$ K. However, this collisional ionisation mechanism produces large amounts of N V and very little Si IV which does not agree with our fitted column densities, listed in Table 3.16. Photoionisation models of H II regions,

using NLTE atmospheres for the exciting stars, such as those presented by de Kool and de Jong (1985) can produce column densities of C IV and Si IV of the same order of magnitude as those I detect towards my sample of Cygnus stars as well as similar C IV/Si IV column density ratios. The best agreement is found if the material in which the lines originates is depleted. de Kool and de Jong (1985) present only one such model using average depletion values, as observed towards ζ Oph (a factor of 5 for C and a factor of 40 for Si). My observations, although few, require at least this amount of depletion, if not more. This is consistent with my results from the detailed analysis of the line of sight towards WR 137, using S II as a reference ion. According to the model of de Kool and de Jong, the C IV and Si IV lines arise predominantly in photoionised clumps embedded in hot stellar wind shocked gas around the hot stars. These clumps survive the passage of the shock from the stellar wind bubble due to the fact that they were initially cold and dense. The strong depletion is easily explained by the relatively long survival time for silicon and carbon dust cores ($\sim 10^8$ yrs; Martin 1978). I therefore conclude that photoionisation is most likely the predominant production mechanism for the highly ionised species for which I have detected high velocity components. However, the presence of N V in the line of sight towards WR 136 implies that some other mechanism must be contributing to the ionisation. Since the Cygnus region is known to be a soft X-ray source (Cash *et al.* 1980), the most likely additional mechanism is X-ray photoionisation. This is probably not the dominant mechanism because we do not detect high velocity N V towards any other stars.

It would certainly be of interest to obtain IUE high resolution observations of more Cygnus stars in order to determine the extent of the postulated supershell. Moreover, higher resolution spectra using future ultraviolet instrumentation such as Lyman/FUSE would definitely provide a much improved description of the various components that arise in the line of sight towards Cygnus.

Chapter 4

New Results on the Ultraviolet Variability of HD 50896

4.1 Introduction

The WN5 star HD 50896 (WR 6 in the catalogue of van der Hucht *et al.* 1981) is presently the most promising candidate for a WR+compact binary system. A well-established period of 3.766 days has been found in the emission line fluxes and radial velocities (Firmani *et al.* 1980, Niemela and Mendez 1982); continuum light (Firmani *et al.* 1980, Cherepaschuk 1981, Lamontagne, Moffat and Lamarre 1986, van Genderen *et al.* 1987, Drissen *et al.* 1989, Balona, Egan and Marang 1989); and optical linear polarization (McClean 1980, Drissen *et al.* 1989). Furthermore, the mass function (f(m)=0.015 $M_{\odot}$) deduced from the radial velocity variations (Firmani *et al.* 1980) is low; the star is located at an unusually high distance of 356 pc above the galactic plane (Moffat 1982); and it is associated with the ring nebula S308. However, although the periodicity of 3.766 days is consistently present in most photometric and polarimetric datasets, unexplained observational features remain which prevent a definite conclusion concerning the binarity of WR 6. For example, Drissen *et al.* (1989) found that although the light and polarization curves are smooth and coherent over periods of $\sim$ 2 weeks, changes occur in their shape and amplitude over

longer timescales. Those authors suggest that the binary modulation is always present but that it occurs in conjunction with some other phenomenon with a much longer timescale, possibly caused by the precession of an accretion disk surrounding the neutron star companion. Another complication is the lack of phase-dependency of the variations observed in the ultraviolet P Cygni profiles which should be observed through the Hatchett and McCray effect in a WR + neutron star system (see Chapter 1, Section 1.1.4). However, perhaps the most serious objection against the WR + neutron star binarity of WR 6 is the absence of high levels of X-ray emission from this star. Stevens and Willis (1988) have calculated the theoretically-expected X-ray flux for WR 6 assuming that it is a binary with a neutron star companion. They found that, for a wide range of system parameters, the expected level of X-ray emission is higher by at least a factor of two than is presently observed [L_X(0.2–4.0 KeV)=1.0 $\times$ 10^{33}, L_X(2.0–6.0)$\leq$1.5 $\times$ 10^{34}, L_X(10.0–25.0)$\leq$4.8 $\times$ 10^{33}]. The only way to reconcile the lack of a strong X-ray flux from the star within the binary hypothesis would be to postulate that the neutron star companion is not accreting material from the WR wind. This could be achieved if the neutron star were spun up by the accretion of angular momentum which would consequently produce centrifugal inhibition of accretion. Finally, Schulte-Ladbeck *et al.* (1990) have recently reported the discovery of polarization changes across the He II emission lines which, when plotted in the Q-U plane, describe a loop clockwise from the blue to the red wing of the line. They interpret this as indicating that the polarized line profiles are the signature of a rotating, expanding wind around a single WR star.

Even in the event of WR 6 being proved to be a binary, intrinsic variations in the WR wind itself are not excluded. Willis *et al.* (1986a, 1989) have obtained an extensive set of 44 IUE high resolution SWP observations spread over 7 consecutive days in 1983. An analysis of those data, together with 24 archival spectra, revealed the presence of substantial variations in the absorption components of the P Cygni profiles of N V λ1240, C IV λ1550, He II λ1640 and N IV λ1718. Those variations were not found to vary in phase with the ephemeris of Lamontagne, Moffat and Lamarre (1986) (P=3.766 days, E_0=2443199.53) and thus do not provide evidence for the Hatchett and McCray effect. Instead, the variations were found to be epoch dependent. Compared to earlier observations, the 1983 dataset was found to show relatively low amplitude variations and a

subset of these spectra were added together to form a mean. Compared to this mean, the spectra drawn from the archive show very large changes with different spectral lines showing different behaviours. The timescale of the changes was tentatively determined to be of the order of one day and the line profile variations were interpreted as reflecting physical changes in the velocity, density or ionisation structures of the WR wind. Although those observations strongly suggest that the presence of a collapsed companion is not the cause of the ultraviolet variations, the temporal sampling was insufficient to determine accurately the rise and decay timescales of the changes, or any possible recurrence timescale. Therefore, as part of this work, an extensive sequence of IUE spectra was obtained in order to try to gain more insight into the nature of the ultraviolet line profile variations. The results of the analysis of those data are presented in this chapter.

4.2 Observations

In a joint NASA-Vilspa project, a total of 130 high resolution SWP (Short Wavelength Prime: $\lambda\lambda$ 1150–2050 Å; $\Delta\lambda \sim 0.1$ Å) IUE spectra of WR 6 was obtained over a period of 6 consecutive days in December 1988 (7–12/12/1988). The observations were taken in the large aperture (10×20 ″) and the exposure time for each spectrum was 4 minutes. Strong saturation effects occurred in the peak of the He II λ1640 emission line. Affected pixels were subsequently removed during the data reduction procedure. Also included in this study are 4 SWP spectra obtained ten months earlier (20–23/2/1988) with the same exposure time and aperture. A log of these observations, giving the SWP image number and the Julian Date at the beginning of the exposure, is presented in Table 4.1.

The spectra were uniformly extracted from the PHOT images provided by the ground stations using the IUEDR software described by Giddings (1983) and Giddings and Rees (1989) available on the UK Starlink network of VAX computers. The resulting spectra with intensities in flux numbers per second (FN s^{-1}) were mapped onto a fixed wavelength grid between 1150–2150 Å in intervals of 0.1 Å. Subsequent measurements and analysis were performed using the Starlink DIPSO software package (Howarth and Murray 1990).

Table 4.1

IUE SWP High Resolution Images of HD 50896

SWP Image Number	Julian Date 2440000+	SWP Image Number	Julian Date 2440000+
32948	7211.7026	34909	7503.4139
32951	7212.6993	34910	7503.4364
32957	7213.7002	34911	7503.4596
32965	7214.8104	34912	7503.4811
34878	7502.5518	34913	7503.5041
34879	7502.5763	34914	7503.5273
34880	7502.5991	34915	7503.5486
34881	7502.6205	34916	7503.5748
34882	7502.6422	34917	7503.5961
34883	7502.6645	34918	7503.6178
34884	7502.6865	34919	7503.6391
34885	7502.7078	34920	7503.6626
34886	7502.7291	34921	7503.6855
34887	7502.7538	34922	7503.7073
34888	7502.7755	34923	7503.7286
34889	7502.7969	34924	7503.7498
34890	7502.8182	34925	7503.7711
34891	7502.8396	34926	7503.7928
34892	7502.8698	34927	7503.8145
34893	7502.8943	34928	7503.8359
34894	7502.9163	34929	7503.8652
34895	7502.9390	34930	7503.8904
34896	7502.9641	34931	7503.9115
34897	7502.9895	34932	7503.9329
34898	7503.0157	34933	7503.9548
34899	7503.0389	34934	7503.9803
34900	7503.0613	34935	7504.0016
34901	7503.0858	34936	7504.0249
34902	7503.1073	34937	7504.0471
34905	7503.3209	34938	7504.0733
34906	7503.3459	34939	7504.0940
34907	7503.3683	34943	7504.3181
34908	7503.3904	34944	7504.3473

Table 4.1 (Continued)

IUE SWP High Resolution Images of HD 50896

SWP Image Number	Julian Date 2440000+	SWP Image Number	Julian Date 2440000+
34945	7504.3694	34982	7505.4404
34946	7504.3916	34983	7505.4635
34948	7504.4460	34984	7505.4885
34949	7504.4691	34985	7505.5100
34950	7504.4904	34986	7505.5331
34951	7504.5124	34987	7505.5566
34952	7504.5359	34988	7505.5819
34953	7504.5618	34989	7505.6034
34954	7504.5841	34990	7505.6247
34955	7504.6082	34991	7505.6465
34956	7504.6298	34992	7505.6684
34957	7504.6516	34993	7505.6904
34958	7504.6728	34994	7505.7122
34959	7504.6945	35001	7506.5751
34960	7504.7163	35002	7506.5984
34961	7504.7378	35003	7506.6199
34962	7504.7597	35004	7506.6412
34963	7504.7810	35005	7506.6631
34964	7504.8050	35006	7506.6848
34965	7504.8270	35007	7506.7063
34966	7504.8477	35008	7506.7281
34967	7504.8758	35009	7506.7490
34968	7504.8981	35010	7506.7702
34969	7504.9212	35011	7506.7919
34970	7504.9499	35012	7506.8136
34971	7504.9722	35013	7506.8365
34972	7504.9958	35014	7506.8581
34973	7505.0184	35016	7507.5879
34974	7505.0439	35017	7507.6125
34975	7505.0680	35018	7507.6346
34976	7505.0982	35019	7507.6581
34979	7505.3625	35020	7507.6798
34980	7505.3928	35021	7507.7021
34981	7505.4168		

4.3 Results and Discussion

After ensuring that no wavelength shift existed between the spectra by aligning a selection of narrow interstellar lines, all spectra were closely compared. Significant variability was revealed in several spectral lines. In particular, changes were found in the N V λ1240, C IV λ1550, He II λ1640 and N IV λ1718 P Cygni profiles in both the absorption and emission components. Variations were also detected in subordinate transitions between $\sim$ 1200–1500 Å, which are generally attributed to numerous lines of Fe V and Fe VI. A detailed description of these changes are presented in this section.

4.3.1 VARIATIONS IN THE ABSORPTION COMPONENTS OF THE MAJOR P CYGNI PROFILES

The changes detected in the absorption component of all major P Cygni profiles observed in the ultraviolet spectrum of WR 6 occur over a relatively broad wavelength range but seem to be mainly confined to the blue edge. The variations occur over a fixed wavelength range with no apparent movement across the profile as a function of time. In Figure 4.1, examples of the P Cygni absorption component variability occurring in this dataset are presented for the C IV λ1550, He II λ1640 and N IV λ1718 transitions for two spectra, SWP 34917 and SWP 34936, which have been obtained $\sim$ 10 hours apart. The N V λ1240 doublet is found to show the same pattern of variability as C IV λ1550 and will therefore not be discussed further.

In order to quantify these changes, I have measured the equivalent width of the absorption component of the P Cygni profiles for all three ions. For each spectrum, the profiles were rectified by fitting a low-order polynomial to fixed continuum ranges on either side of the profiles. In order to minimize the subjectivity in the measurements, the equivalent widths were evaluated over a fixed range from a wavelength shortward of the beginning of the absorption component to the maximum redward wavelength of the flat bottom absorption component ($\Delta\lambda$=1700.0–1711.4 Å for N IV, $\Delta\lambda$=1530.0–1543.50 Å for C IV and $\Delta\lambda$=1624.0–1633.0 Å for He II). The red edge of the absorption is not included in these measurements as its behaviour seems to be more closely related to the changes found in the emission component of the P Cygni profile.

The equivalent width measurements are listed in Table 4.2 and plotted as a function of Julian Date in Figure 4.2. The data for the 4 spectra obtained in

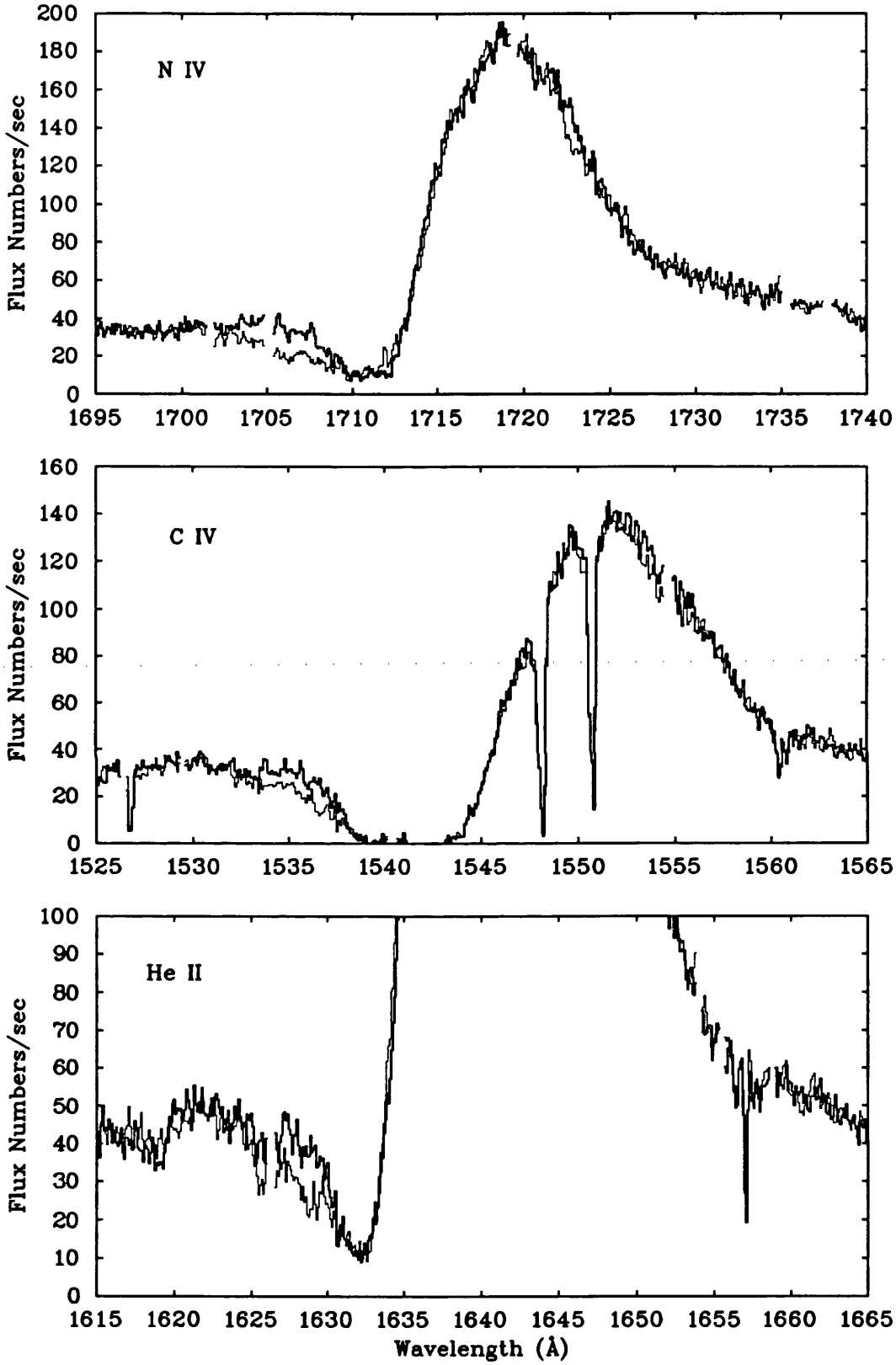

Figure 4.1 : IUE spectra SWP34917 (thin line) and SWP34936 (thick line) illustrating the variations in the absorption components of the NIV λ1718, CIV λ1550 and HeII λ1640 P Cygni profiles.

February 1988 were excluded from the latter for convenience. Although relatively noisy, the measurements are quite revealing. First, for all three lines there is a gradual increase in absorption beginning at approximately JD 2447503, followed by a gradual decrease on a similar timescale. The whole event lasts for $\sim$ 1 day which is of the order of the flow time through the wind. This is followed by a second and third event for which we only have partial coverage. The third event resembles the first, showing similar patterns of variability for all three lines. However, the second event shows different characteristics. While a decrease is observed in the strength of the absorption component for the N IV λ1718 and C IV λ1550 transitions, the He II λ1640 absorption is still increasing. The time-delay for this event is particularly noticeable during the decrease and is of the order of 6 hours. I have carried out rank correlation tests in order to verify the above statement that the three absorption components generally vary in concert. The Spearman rank-order correlation coefficient (r_s) between the N IV equivalent width measurements and the C IV and He II measurements is 0.55 and 0.60 respectively, with a confidence level in the significance of the correlation of 99.9 % in both cases. It is not clear from these tests if the small difference in the pattern of variability of the He II absorption component observed in the second event in meaningful. More observations are required to verify this.

All these measurements have been subjected to a periodicity search between ν_{min}=1/(Δt)=0.19 d^{-1} where Δt is the time interval over which the data where obtained and the Nyquist frequency ν_{max}=Δt/2(N$-$1)=12.44 d^{-1} where N is the number of data points, using the power spectrum methods described by Scargle (1982) and available in the DIPSO software package. The periodogram for the N IV equivalent width variations (reproduced in Figure 4.3 (a)) is presented in Figure 4.3 (b) and shows a very clear peak at 0.98 days. Similar results were also obtained for the other transitions (P=0.97 days for C IV and P=1.03 days for He II). These numerically produced period fits are similar to the timescale of variability evident to the eye in Figure 4.2. In order to test the significance of these periods, I have performed a Monte Carlo simulation, replacing each equivalent width measurement by a random number with a gaussian distribution; the mean value of the gaussian was set to the mean of the equivalent width measurements for the N IV absorption and σ was set to the standard deviation from this mean. The resulting random numbers are

Table 4.2

Equivalent Widths of Absorption Components

SWP Image Number	N IV (Å)	C IV (Å)	He II (Å)	SWP Image Number	N IV (Å)	C IV (Å)	He II (Å)
32948	2.995	7.423	1.101	34910	3.888	7.534	1.976
32951	2.646	7.187	1.907	34911	3.882	7.688	1.935
32957	3.313	6.949	1.206	34912	3.796	7.517	1.579
32965	2.726	6.777	1.639	34913	3.968	7.339	1.803
34878	2.602	6.896	0.775	34914	3.974	7.673	1.783
34879	2.569	6.630	1.035	34915	3.794	7.705	1.742
34880	2.548	6.758	0.806	34916	3.933	7.575	1.863
34881	2.576	6.922	0.853	34917	3.733	7.684	2.267
34882	2.759	6.845	0.812	34918	3.662	7.516	1.918
34883	2.766	7.173	1.062	34919	3.553	7.474	2.279
34884	2.810	7.194	1.281	34920	3.446	7.889	2.064
34885	2.694	6.734	0.647	34921	3.390	7.710	1.926
34886	2.730	6.943	0.850	34922	2.738	7.413	1.650
34887	2.813	6.872	1.116	34923	2.948	7.356	1.676
34888	2.718	6.977	0.764	34924	3.174	6.982	1.548
34889	2.617	6.948	0.641	34925	2.829	7.138	1.285
34890	2.643	6.944	0.656	34926	2.889	7.383	1.258
34891	2.418	6.876	0.718	34927	2.502	7.035	1.379
34892	2.565	6.952	0.541	34928	2.348	7.019	0.969
34893	2.422	6.732	0.765	34929	2.311	6.864	0.754
34894	2.678	6.858	0.810	34930	2.376	6.641	0.640
34895	2.757	6.766	0.338	34931	2.196	6.814	0.778
34896	2.893	6.902	0.698	34932	2.255	6.595	0.984
34897	2.659	7.045	0.810	34933	2.230	6.583	0.568
34898	2.948	6.920	0.971	34934	2.490	6.572	1.052
34899	3.055	6.753	0.666	34935	2.598	6.634	0.553
34900	3.108	7.065	0.872	34936	2.000	6.512	0.498
34901	3.248	6.969	0.994	34937	2.470	6.723	0.843
34902	3.405	7.301	0.692	34938	2.576	6.638	0.875
34905	4.354	7.456	1.926	34939	2.690	6.665	0.863
34906	4.069	7.763	1.703	34943	3.856	7.139	1.663
34907	4.210	7.665	1.747	34944	3.662	7.170	1.993
34908	3.985	7.409	1.703	34945	3.809	7.102	1.884
34909	4.000	7.423	1.870				

Table 4.2 (Continued)

Equivalent Widths of Absorption Components

SWP Image Number	N IV (Å)	C IV (Å)	He II (Å)	SWP Image Number	N IV (Å)	C IV (Å)	He II (Å)
34946	3.754	7.153	2.172	34982	2.943	6.797	1.203
34948	3.831	7.079	2.249	34983	2.901	6.796	1.246
34949	3.286	7.239	2.226	34984	2.750	6.669	1.411
34950	3.356	7.138	2.024	34985	2.838	6.688	1.037
34951	3.391	7.038	2.065	34986	2.776	6.726	1.214
34952	3.378	7.013	2.046	34987	2.699	6.798	1.168
34953	3.377	6.941	1.950	34988	2.888	6.531	0.692
34954	3.194	6.952	1.817	34989	2.608	6.399	1.017
34955	3.055	6.874	1.816	34990	2.390	6.555	0.724
34956	3.059	7.357	1.532	34991	2.953	6.673	0.811
34957	3.018	6.734	2.000	34992	2.605	6.174	1.004
34958	3.120	7.056	1.815	34993	2.580	6.757	0.804
34959	2.987	6.636	1.605	34994	2.654	6.397	0.535
34960	2.471	6.734	1.575	35001	2.884	7.031	0.086
34961	2.975	6.577	1.144	35002	3.305	6.881	0.646
34962	2.851	6.347	1.601	35003	3.413	6.645	0.956
34963	2.909	6.901	1.617	35004	3.487	6.809	0.793
34964	2.855	6.668	1.297	35005	3.651	6.709	1.115
34965	2.881	6.489	1.347	35006	3.714	6.555	0.835
34966	2.683	6.693	1.428	35007	3.744	7.050	0.766
34967	2.736	6.397	1.462	35008	3.761	6.933	1.125
34968	2.749	6.627	1.256	35009	3.810	6.867	1.074
34969	2.548	6.583	1.174	35010	3.805	6.608	1.052
34970	2.500	6.568	1.200	35011	3.794	6.715	0.968
34971	2.841	6.750	1.353	35012	3.669	6.847	1.187
34972	2.997	6.310	1.537	35013	3.764	6.951	1.449
34973	3.134	6.846	1.511	35014	3.779	6.843	0.843
34974	3.168	6.744	1.749	35016	3.265	7.246	1.615
34975	3.172	6.884	1.569	35017	3.016	7.269	1.178
34976	3.572	6.922	1.843	35018	2.917	7.358	1.685
34979	2.781	6.327	1.419	35019	2.792	7.448	1.430
34980	2.485	6.523	1.234	35020	2.932	6.935	1.674
34981	2.912	6.548	1.415	35021	2.775	6.979	1.101

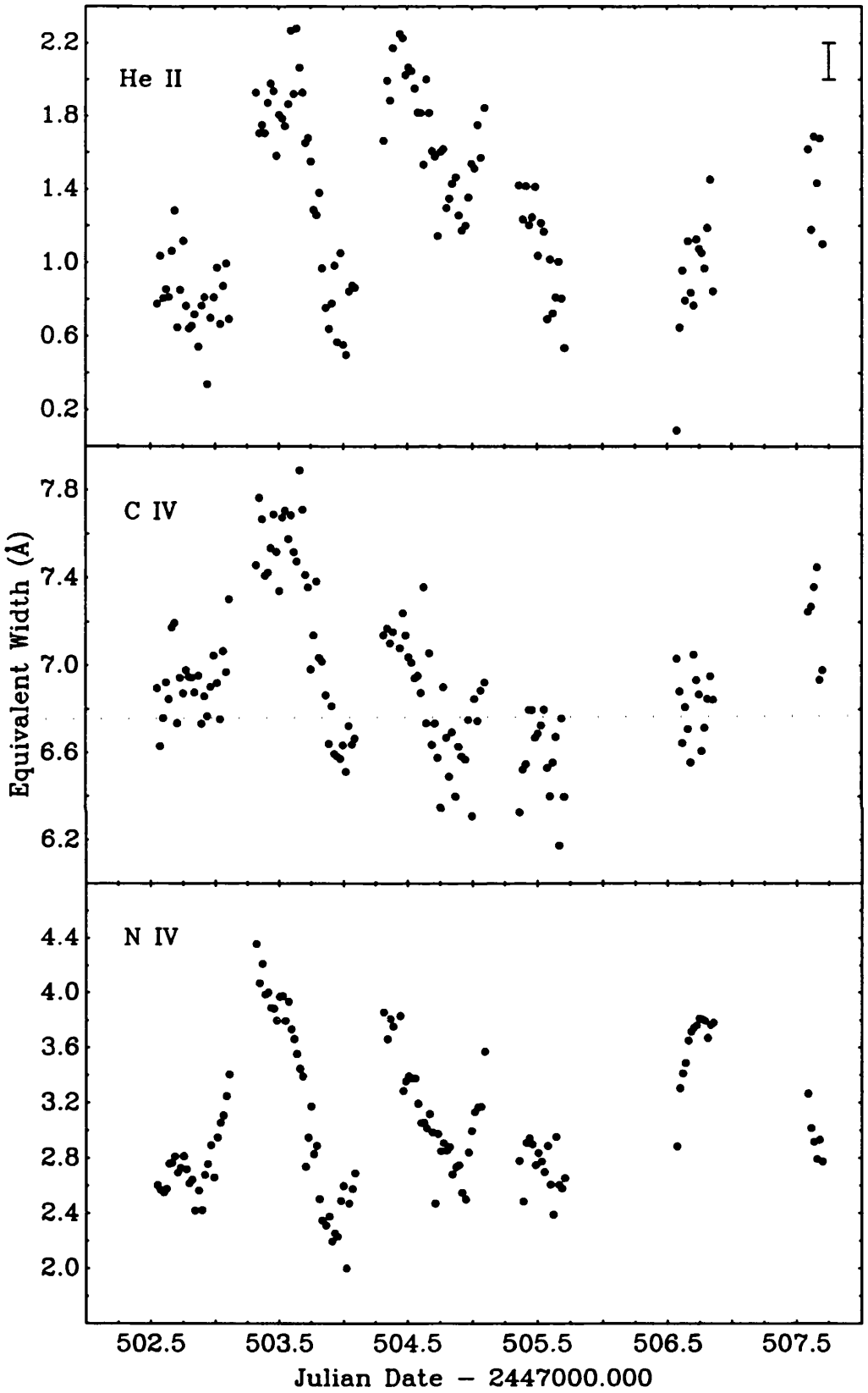

Figure 4.2 : Equivalent widths (Å) of the absorption components of N IV, C IV and He II P Cygni profiles of WR 6 as a function of Julian Date. The typical 1 σ error bar shown in the top right corner of the graph was estimated from the spectra which were judged by eye to be identical within the noise level.

plotted in Figure 4.3 (c) and the corresponding periodogram is shown in Figure 4.3 (d). The similarity between the two periodograms is striking. The 0.98 day period is also present in the periodogram of the random numbers with an amplitude which is even larger than that of the N IV equivalent width measurements. This simple experiment demonstrates that the period of $\sim$ 1 day found in the equivalent width variations, and indeed all the other possible frequencies, do not reflect solely real periodicities in the dataset but are rather an artefact of the sampling frequency. Examination of the log of the 1988 observations in Table 4.1 shows gaps of $\sim$ 5 hours in each of the three days of monitoring, where observation ceased due to the earth constraint. This arises at the same time each day, and it is clear that the periodogram program preferentially finds this window periodicity in the dataset. This highlights the importance of continuous time coverage when studying variable phenomena on these timescales; although the number of observations in a given time interval is very high for this dataset, ambiguities generated by the sampling of the data still remain.

Despite these difficulties, it is clear from Figure 4.2 that there is a recurrence timescale of $\sim$ 1 day for the variability, when it is taking place, and the 1988 observations provide the clearest measurement of the real timescale of the ultraviolet variability of this star. This does not seem, however, to be a strict periodicity. An indication of this is given by the set of observations starting at $\sim$ JD 2447506.5. Although the paucity of these data renders their interpretation insecure they do not seem to agree very well with the first three events, being slightly shifted in time. This, together with the fact that the second event displays different characteristics from the other two, strongly suggests that the nature of these variations is not truly periodic.

One important characteristic of the variations is the velocity range over which they occur. This is typically between -1600 and -2400 km s^{-1} for He II, -1800 and -2800 km s^{-1} for N IV and -2200 and -3150 km s^{-1} for C IV. Most of the variations therefore occur at velocities exceeding the normal outflow velocity of the wind, evaluated from the violet limit of the saturated absorption trough of the C IV resonance doublet as -1900 km s^{-1} (Prinja, Barlow and Howarth 1990). This is similar to the changes observed at some earlier epochs (Willis *et al.* 1989), although the amplitude of the variations seems to be much smaller. Variability at velocities exceeding the normal bulk outflow velocity of the wind has also been observed for the WN 8 star WR 40 (Smith *et al.*

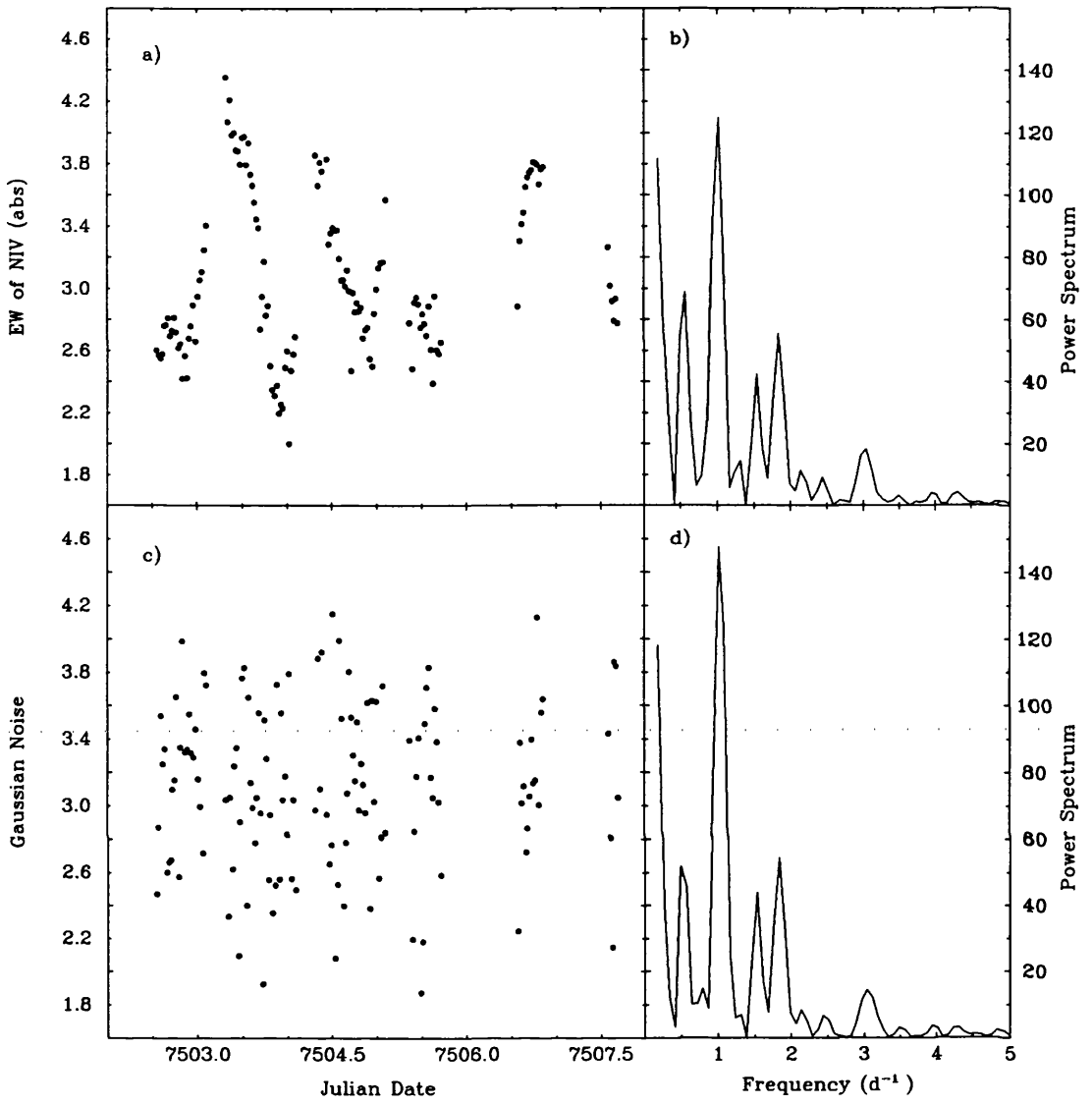

Figure 4.3 : (a) Equivalent width measurements of the absorption component of N IV λ1718 and (b) corresponding power spectrum for WR 6. For comparison, (c) set of random numbers with an identical sampling and (d) corresponding power spectrum.

1985, 1986) and for the WN 6 star WR 136 (see Chapter 3). In the case of WR 136 a similar timescale for the changes was found ($\sim$ 1 day) while for WR 40, a gradual decrease of the absorption was observed over a period of 5 days. As discussed in Chapter 3, this type of variability is reminiscent of the radiatively driven blob model of Lucy and White (1980) or the propagating shock models of Lucy (1982, 1983) and Owocki, Castor and Rybicki (1988)

which are capable, at least qualitatively, of reproducing such variations. As no significant phase-dependence is found with the proposed period of 3.766 days, the changes observed in the absorption components cannot be interpreted as being caused by the Hatchett and McCray effect and therefore an intrinsic explanation is much more plausible.

4.3.2 VARIATIONS IN THE EMISSION COMPONENTS OF THE MAJOR P CYGNI PROFILES

Inspection of the spectra reveals that the emission components of the P Cygni profiles of N V, C IV, He II and N IV also show variability, although the changes are clearly of much smaller amplitude than in the absorption components. Saturation effects occur in the peak of the He II and N V profiles and therefore much of the information concerning the emission flux of these transitions is lost. The N V P Cygni emission suffers from the additional problem of having its red wing partially blended with a subordinate transition (most likely of Fe VI) which also shows variability and therefore it is practically impossible to obtain any useful information on it emission flux variability. Equivalent width measurements have been made for the other three lines. For the He II transition, only the red wing of the profile could be measured ($\Delta\lambda$=1648–1660 Å). In the case of C IV, the complete emission component was measured ($\Delta\lambda$=1543.5–1565 Å); the strong interstellar absorption lines have been removed prior to the equivalent width measurements and the gaps replaced by a linear interpolation. The emission component of the N IV P Cygni profile appeared to show a different variability pattern in the blue and red wings than in the peak of the line. Therefore the measurements were made over three separate regions; the blue wing ($\Delta\lambda$=1711.4.0–1717.4 Å), the peak of the line ($\Delta\lambda$=1717.4–1721.9 Å) and the red wing ($\Delta\lambda$=1721.9–1740 Å). The various equivalent width measurements are listed in Table 4.3 and plotted as a function of Julian Date in Figure 4.4. As for the absorption components, the 4 February 1988 observations were excluded from this figure. The emission component equivalent width variations have a very small amplitude, typically $\lesssim$ 20 %, while for the absorption components the changes were found to range from $\sim$ 30 % for C IV, 70% for N IV and a factor of 2 for He II (see Figure 4.2).

It is clear from Figure 4.4 that the changes in the emission components occur on a much longer timescale than the changes in the absorption components. While an increase in absorption followed by a decrease was found to

Table 4.3

Equivalent Widths of Emission Components

SWP Image Number	N IV (Å) Blue Wing	N IV (Å) Peak of line	N IV (Å) Red Wing	C IV (Å)	He II (Å)
32948	-8.976	-16.053	-15.981	-26.503	-19.021
32951	-8.940	-16.601	-15.921	-25.823	-18.797
32957	-8.797	-15.899	-15.314	-27.585	-19.719
32965	-8.916	-15.937	-14.915	-27.644	-19.456
34878	-8.177	-15.857	-14.793	-26.872	-18.912
34879	-7.921	-15.990	-14.897	-27.267	-18.665
34880	-7.894	-15.784	-14.800	-26.729	-17.901
34881	-8.033	-15.860	-14.819	-26.765	-17.844
34882	-8.249	-16.588	-15.502	-27.483	-18.861
34883	-8.324	-16.678	-15.416	-26.601	-17.830
34884	-7.944	-16.309	-15.192	-27.907	-17.958
34885	-8.007	-16.276	-14.850	-27.917	-18.601
34886	-8.301	-16.558	-15.348	-26.796	-18.627
34887	-8.046	-16.099	-14.830	-27.385	-18.294
34888	-8.177	-16.863	-15.454	-26.861	-17.793
34889	-8.132	-16.639	-15.097	-26.587	-18.385
34890	-8.194	-16.879	-15.611	-25.813	-18.849
34891	-7.982	-16.435	-15.151	-27.100	-17.941
34892	-8.291		-14.871	-28.133	-18.875
34893	-8.316	-16.825	-15.158	-27.828	-18.772
34894	-7.960	-16.513	-14.446	-26.724	-18.362
34895	-7.950	-16.789	-14.332	-27.139	-18.846
34896	-8.111	-16.457	-14.644	-27.686	-17.973
34897	-8.434	-17.240	-15.428	-27.290	-18.472
34898	-8.074	-16.772	-15.058	-26.939	-18.324
34899	-8.332	-17.116	-14.988	-27.400	-19.007
34900	-8.316	-17.075	-15.089	-26.077	-18.324
34901	-8.042	-16.645	-14.907	-26.899	-18.031
34902	-7.977	-16.901	-14.799	-26.156	-19.522
34905	-7.809	-16.089	-14.122	-27.216	-19.412
34906	-8.359	-17.331	-15.360	-28.053	-19.125
34907	-8.114	-16.505	-14.481	-27.275	-18.739
34908	-8.128	-16.857	-14.967	-29.146	-19.213
34909	-8.222	-16.950	-14.878	-28.777	-18.965
34910	-7.953	-16.992	-14.882	-28.009	-19.420
34911	-8.342	-16.708	-15.230	-27.831	-19.398
34912	-8.062	-17.069	-15.045	-28.264	-19.567
34913	-8.383	-17.330	-15.290	-28.860	-18.787
34914	-8.064	-16.848	-14.877	-27.617	-19.740
34915	-8.498	-17.435	-15.156	-27.884	-19.016
34916	-8.500	-17.667	-15.579	-28.199	-19.059
34917	-8.842	-18.036	-16.211	-27.625	-20.714
34918	-8.791	-17.422	-15.656	-28.389	-20.544
34919	-8.638	-17.491	-15.235	-29.264	-19.443
34920	-8.571	-17.436	-15.553	-28.034	-20.399

Table 4.3 (Continued)

Equivalent Widths of Emission Components

SWP Image Number	N IV (Å) Blue Wing	N IV (Å) Peak of line	N IV (Å) Red Wing	C IV (Å)	He II (Å)
34921	-8.653	-17.266	-15.392	-27.520	-19.961
34922	-8.693	-17.794	-15.518	-28.418	-19.997
34923	-8.587	-17.551	-15.041	-28.746	-20.057
34924	-8.169	-16.628	-14.678	-28.581	-19.338
34925	-8.222	-17.310	-15.149	-29.080	-19.473
34926	-8.316	-17.090	-15.114	-27.623	-19.315
34927	-8.595	-17.679	-15.433	-28.914	-19.342
34928	-8.447	-17.675	-15.279	-29.388	-20.358
34929	-8.492	-17.274	-14.965	-28.867	-19.542
34930	-8.239	-17.186	-15.013	-28.425	-19.694
34931	-8.395	-17.038	-15.128	-28.280	-19.818
34932	-8.632	-17.366	-15.559	-28.601	-19.257
34933	-8.340	-17.269	-14.962	-28.588	-19.440
34934	-8.340	-17.266	-15.230	-28.660	-18.792
34935	-8.440	-17.162	-14.960	-29.251	-19.559
34936	-8.547	-17.221	-15.616	-28.585	-19.184
34937	-8.152	-16.753	-14.576	-28.309	-19.463
34938	-8.721	-17.341	-15.042	-28.087	-19.026
34939	-8.689	-17.249	-15.139	-29.161	-19.324
34943	-8.219	-16.023	-15.018	-28.868	-19.345
34944	-8.510	-16.348	-15.347	-28.964	-19.884
34945	-8.117	-16.011	-14.845	-28.761	-19.513
34946	-8.333	-15.638	-14.364	-29.706	-19.208
34948	-8.105	-15.358	-14.049	-28.930	-19.318
34949	-8.489	-15.926	-15.166	-28.166	-19.635
34950	-8.396	-15.998	-15.307	-28.553	-19.851
34951	-8.543	-15.807	-14.641	-28.445	-19.614
34952	-8.637	-15.982	-15.090	-28.928	-20.175
34953	-8.442	-15.815	-14.716	-29.794	-19.927
34954	-8.433	-15.711	-15.165	-29.558	-20.026
34955	-8.858	-15.959	-15.371	-29.117	-20.271
34956	-8.454	-15.708	-14.539	-27.180	-20.282
34957	-8.113	-15.441	-15.138	-28.631	-19.363
34958	-8.653	-15.777	-15.172	-28.937	-19.925
34959	-8.922	-16.285	-15.377	-29.640	-20.442
34960	-9.152	-16.841	-15.772	-28.469	-19.395
34961	-8.701	-15.779	-15.086	-28.626	-20.383
34962	-8.419	-15.562	-15.317	-29.263	-19.935
34963	-8.565	-15.906	-14.849	-27.889	-19.347
34964	-8.412	-15.729	-15.245	-28.659	-19.913
34965	-8.600	-16.006	-15.337	-29.076	-20.289
34966	-8.662	-15.599	-15.225	-28.216	-19.978
34967	-8.665	-15.761	-14.921	-28.672	-19.892
34968	-8.556	-15.865	-15.297	-29.446	-19.618

Table 4.3 (continued)

Equivalent Widths of Emission Components

SWP Image Number	N IV (Å) Blue Wing	N IV (Å) Peak of line	N IV (Å) Red Wing	C IV (Å)	He II (Å)
34969	-8.748	-16.169	-15.342	-28.442	-19.724
34970	-8.980	-16.275	-15.460	-28.649	-19.410
34971	-8.692	-15.841	-14.957	-28.407	-19.650
34972	-8.807	-15.874	-14.903	-28.522	-19.570
34973	-8.132	-15.557	-14.717	-28.223	-19.715
34974	-8.721	-15.941	-15.146	-28.678	-21.421
34975	-8.751	-15.933	-15.795	-29.320	-20.675
34976	-8.559	-16.003	-15.129	-29.855	-20.127
34979	-8.778	-15.745	-15.333	-29.225	-19.944
34980	-8.586	-15.657	-15.305	-29.161	-20.357
34981	-8.702	-15.984	-15.492	-28.714	-20.226
34982	-8.487	-15.642	-15.118	-28.984	-18.942
34983	-8.684	-15.881	-15.299	-28.818	-20.146
34984	-8.643	-15.618	-15.522	-29.178	-19.887
34985	-8.726	-15.976	-15.297	-28.800	-20.312
34986	-8.543	-15.830	-15.454	-27.944	-19.480
34987	-8.483	-15.522	-15.698	-28.038	-18.647
34988	-8.687	-15.802	-15.028	-28.238	-20.009
34989	-8.411	-15.850	-15.773	-28.751	-18.756
34990	-8.584	-15.741	-14.836	-28.336	-19.593
34991	-8.184	-15.346	-14.607	-29.183	-19.928
34992	-8.234	-15.428	-14.917	-28.483	-18.257
34993	-8.394	-15.774	-15.402	-26.905	-18.527
34994	-8.531	-15.712	-14.939	-28.083	-19.746
35001	-8.025	-15.754	-14.723	-26.394	-18.796
35002	-8.088	-15.947	-14.964	-27.501	-18.805
35003	-8.118	-16.044	-14.532	-27.477	-18.392
35004	-7.924	-15.885	-14.480	-28.312	-18.477
35005	-7.723	-16.064	-14.407	-27.314	-18.347
35006	-7.462	-15.772	-14.308	-27.844	-17.842
35007	-7.761	-15.958	-13.943	-26.084	-18.681
35008	-7.447	-15.581	-13.540	-26.967	-18.650
35009	-7.917	-16.238	-14.701	-27.568	-18.577
35010	-7.636	-15.997	-14.025	-26.824	-17.803
35011	-7.869	-16.421	-14.224	-27.361	-18.529
35012	-7.910	-16.121	-14.279	-26.639	-18.758
35013	-7.563	-16.022	-13.897	-27.304	-17.595
35014	-7.824	-16.252	-14.681	-27.295	-18.845
35016	-8.339	-16.522	-14.462	-28.523	-19.195
35017	-8.357	-16.925	-14.677	-28.184	-20.417
35018	-8.602	-17.361	-14.896	-27.729	-19.517
35019	-8.200	-16.668	-14.552	-27.166	-19.484
35020	-8.457	-16.739	-14.711	-28.765	-18.843
35021	-8.670	-17.075	-15.357	-27.194	-19.602

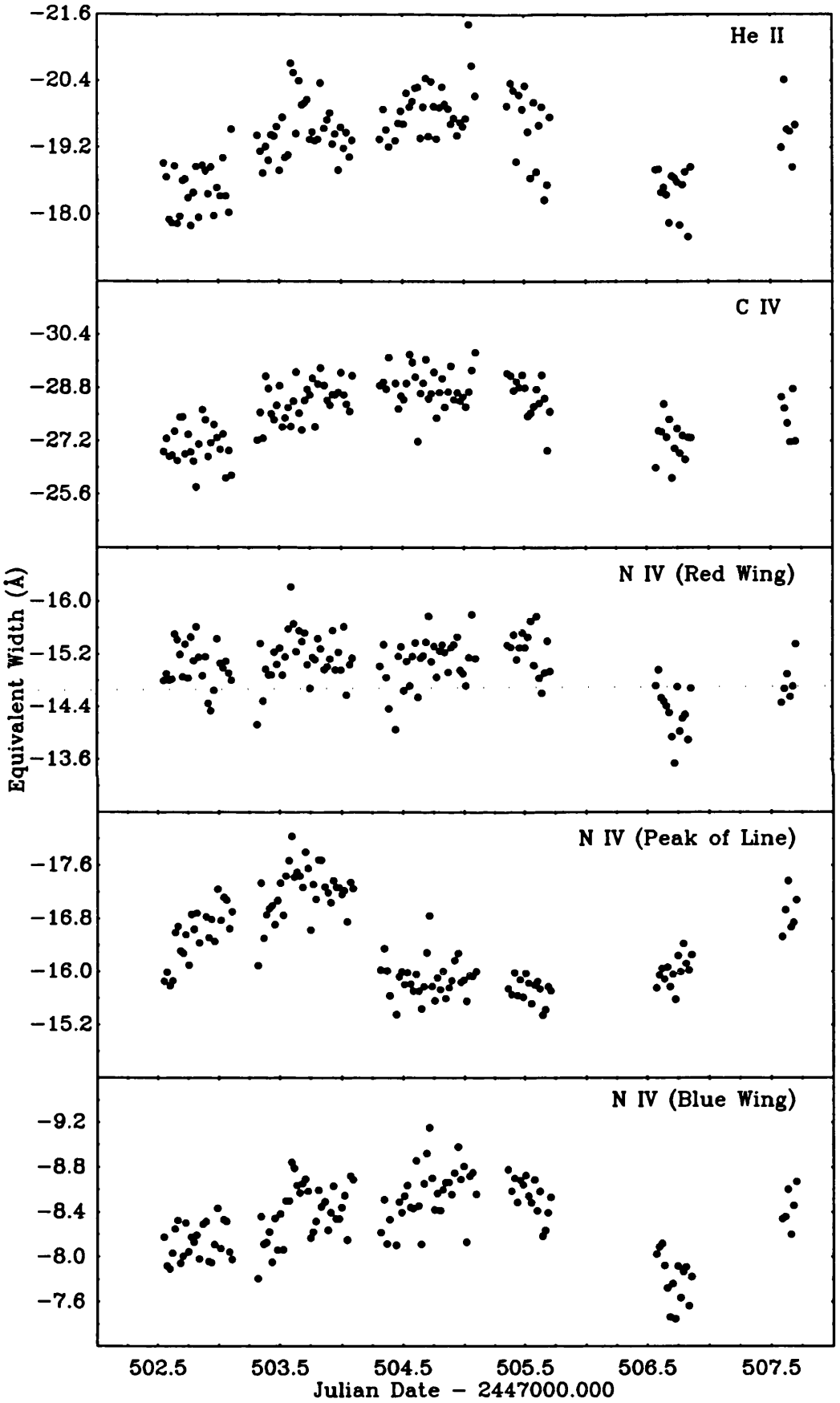

Figure 4.4 : Equivalent widths (Å) of the emission components of N IV, C IV and He II as a function of Julian Date.

take place over a period of $\sim$ 1 day, the variations in the emission fluxes occur on a timescale of the order of the data string or longer. This indicates that whatever mechanism is producing the absorption variability, the physical scale over which it is occurring is not of the order of the size of the emission forming region but is much smaller. For example, variations in the global mass-loss rate of WR 6 would produce changes in the emission and absorption components on the same timescale. Conversely, a variable phenomenon arising in the wind on the scale of the core of the WR star would be readily detectable in the absorption component while the changes in the emission component would reflect the *combined* effect of several similar phenomena, which could very well lead to a different timescale.

The emission variability is also more complex than the changes detected in the absorption components. The variations in the C IV, He II and the blue wing of the N IV emission components appear to occur in concert, increasing slowly for $\sim$ 2 days and decreasing on a similar timescale. This was verified by performing nonparametric correlation tests. The Spearman rank-order correlation coefficient (r_s) between the emission component equivalent widths of C IV and the He II and blue wing of N IV equivalent width measurements are 0.60 and 0.55 respectively with a confidence level in the significance of the correlation of 99.9 % in each case. Therefore, I conclude that the changes, although small, are significant and show a similar behaviour for the C IV, He II and part of the N IV emission components. The peak and the red wing of the N IV emission component show, however, different behaviours. Very little variability is detected in the red wing of the profile; most of the scatter in Figure 4.4 is probably caused by measurement errors. Conversely, the peak of the line shows definite changes although with a different pattern as for the C IV and He II lines. The emission increases for $\sim$ 1 day, decreases on a similar timescale and seems to remain constant for a similar time period; although the observations are sparse, there is some indication that another increase is taking place towards the end of the observing run.

According to the model of HD 50896 by Hillier (1988), the dominant excitation mechanism for the resonance transition of C IV λ1550 is collisional excitation from the the ground state. The dominant mechanism for the He II λ1640 transition is also collisional excitation but from the lower level of the

transition. Conversely, the N IV λ1718 transition has a more complex excitation mechanism with excitation from low lying states as well as continuum fluorescence contributing to the population of the upper level of the transition (Hillier 1988). It is also quite instructive to compare the formation regions for the emission components of the three P Cygni profiles. These are illustrated in Figure 4.5 and were kindly supplied to me by Paul Crowther who used the co-moving frame model atmosphere code of Dr. D.J. Hillier. The quantity ξ is a measure of the proportion of the total flux emitted at a particular radius and is defined so that the area under the curve is unity (*c.f.* Hillier 1988). It can be seen that while the formation regions for the C IV and He II are extremely similar, the N IV line is formed at much smaller radii and by different processes. Therefore, we can understand, at least qualitatively, why the variations found in the emissions components of C IV and He II are similar while the changes in the N IV transition show a different pattern of variability.

Changes in the emission component of P Cygni profiles have been observed in an earlier dataset of WR 6 (Willis *et al.* 1989) as well as for the WR stars WR 40 (Smith *et al.* 1985, 1986) and WR 136 (see Chapter 3). One similarity between all the datasets is that the amplitude of the variations is much smaller than that detected in the absorption component. With such small changes it is difficult to establish a timescale for the variations. Numerous spectra are required in order to obtain sufficient statistics to distinguish a trend. In the case of WR 136 for which sufficient data were available, the timescale of the emission variability was found to be very similar to that of the absorption component in contrast with the data described in this section.

4.3.3 VARIATIONS IN SUBORDINATE TRANSITIONS

Additional variations have also been detected in a series of spectral features in the wavelength range $\sim$ 1200–1500 Å. These lines do not have a secure identification but are generally thought to be the result of a large number of Fe V and Fe VI transitions (Willis *et al.* 1986b). Examples of the type of variability occurring for these transitions are presented in Figure 4.6 where the two spectra, SWP 34968 and SWP 35011, have been obtained $\sim$ 2 days apart.

The Fe VI lines are mainly concentrated between $\sim$ 1200–1350 Å while the Fe V lines dominate between $\sim$ 1350–1500 Å. However, it is very difficult to obtain any information concerning the velocity range over which the variability is taking place. Not only is the identification of each specific spectral feature

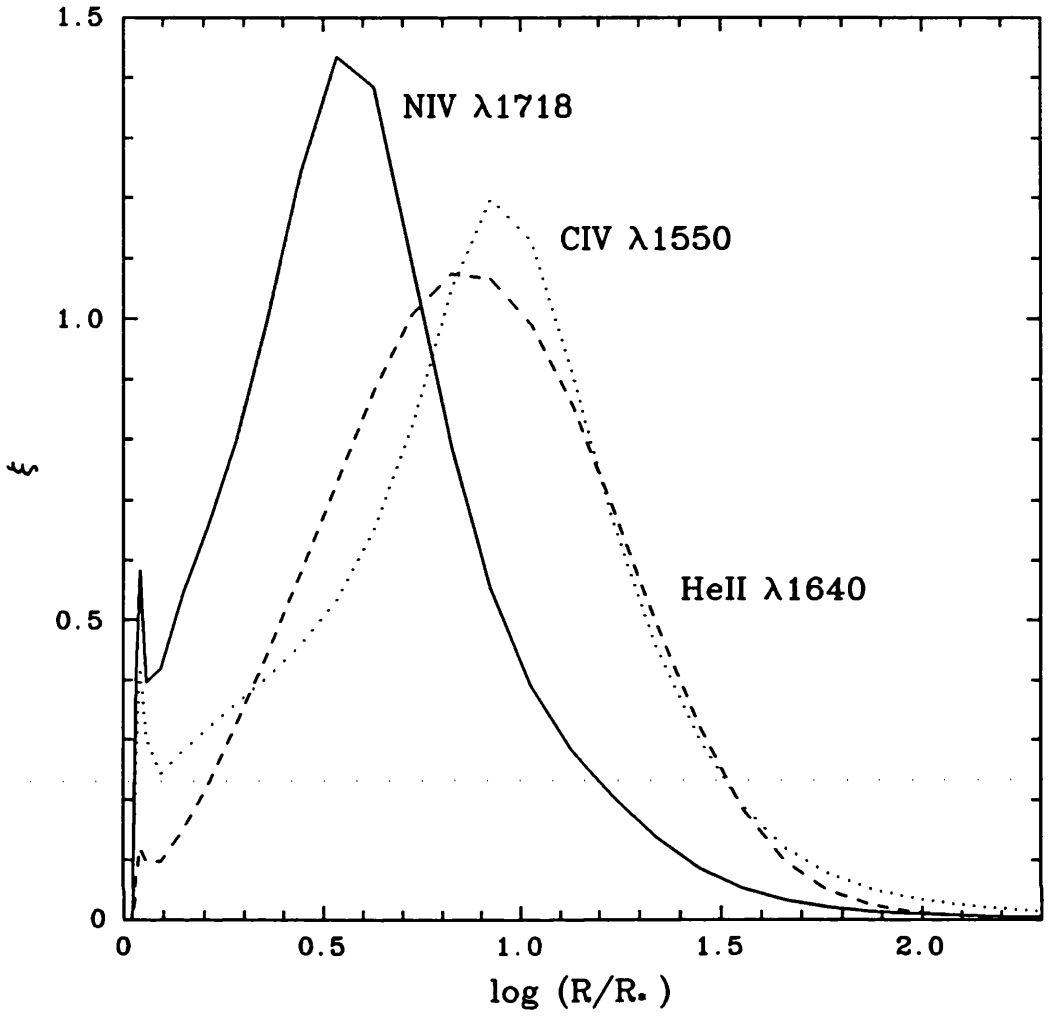

Figure 4.5 : Formation regions for the emission components of the CIV λ1550, He IIλ1640 and NIV λ1718 P Cygni profiles.

insecure, but blending effects also complicate the interpretation of the variability. The fact that there is no obvious continuum region in this spectral range renders direct equivalent width measurements almost impossible. Therefore, in order to quantify the changes, I have made use of the mean spectrum mentioned in Section 4.1 consisting of set of observations obtained in 1983 (*i.e.* Willis *et al.* 1989). First, in order to eliminate possible effects of continuum variations, I have scaled each individual spectrum in the present dataset to the mean spectrum. This was achieved by matching the flux levels in the wavelength range $\Delta\lambda = 1820 - 1900$Å where no spectral features are apparent. I have then taken the ratio of each scaled spectrum with the mean and measured the equivalent width of the excess for two wavelength ranges, $\lambda\lambda 1248 - 1330$ Å (dominated by

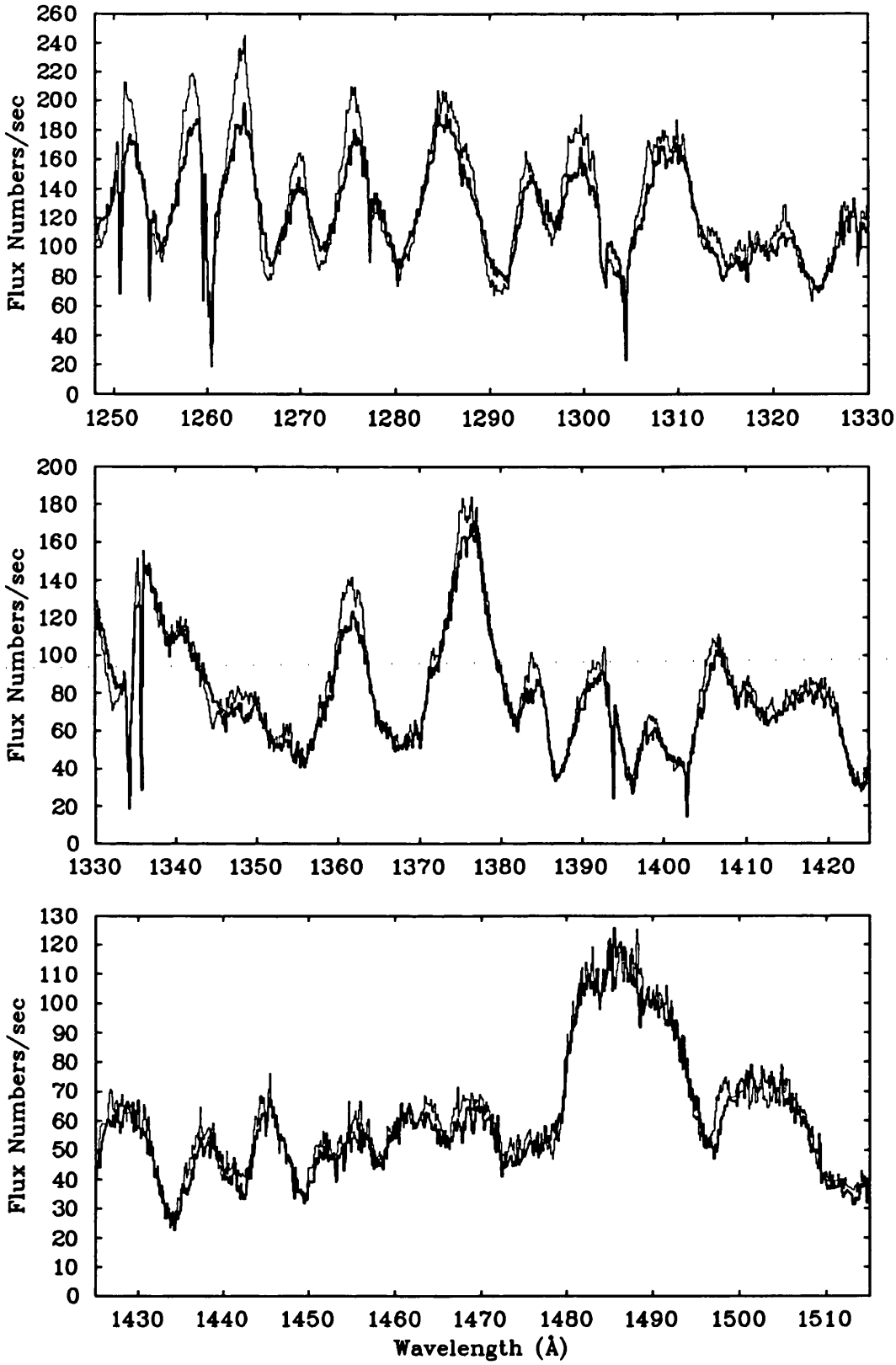

Figure 4.6 : IUE spectra SWP34968 (thin line) and SWP35011 (thick line) illustrating the variations in the wavelength range $\lambda\lambda 1248 - 1515$ *Å.*

Fe VI lines) and $\lambda\lambda 1330-1515$ Å (dominated by Fe V lines). The measurements are listed in Table 4.4 and plotted against Julian Date in Figure 4.7. Positive numbers indicate a general flux level lower than the mean (extra absorption) and negative numbers indicate a general flux level higher than the mean.

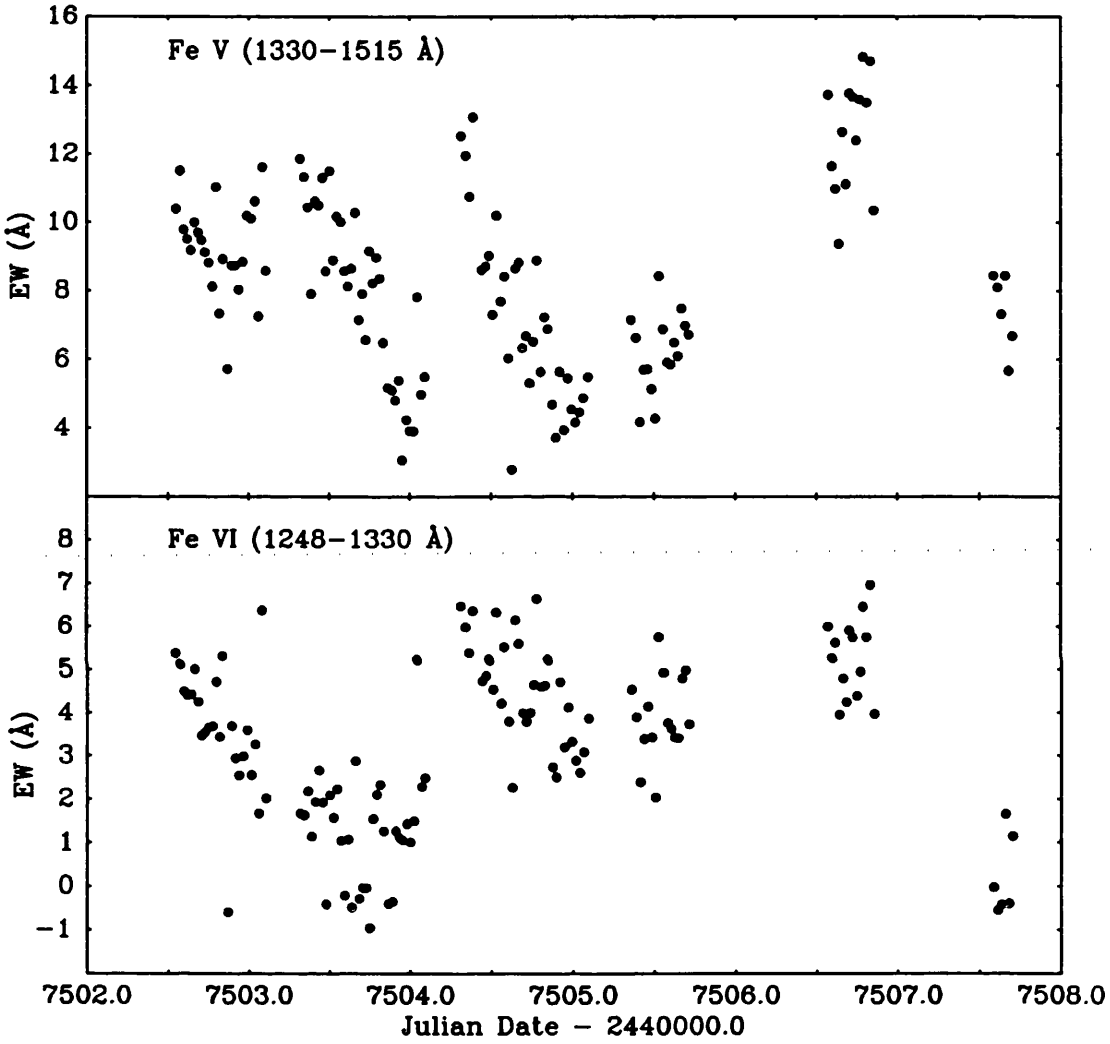

Figure 4.7 : Equivalent width measurements for the spectral ranges $\lambda\lambda 1248-1330$ *Å (Fe VI) and* $\lambda\lambda 1330-1515$ *Å (Fe V).*

The variations observed in the Fe V and Fe VI spectral features are different although some similarities do exist. A significant (99.9 %) but weak correlation is found between the two wavelength ranges with a Spearman's rank coefficient of r_s=0.43. However, stronger correlations exist between the Fe V excess equivalent widths and the absorption equivalent width measurements (*e.g.* r_s=0.54 for N IV) and between the Fe VI excess equivalent widths and the N IV

Table 4.4

Equivalent Widths Measurements for Subordinate Transitions

SWP Image Number	$\Delta\lambda$ (Å) (1248−1330)	$\Delta\lambda$ (Å) (1330−1515)	SWP Image Number	$\Delta\lambda$ (Å) (1248−1330)	$\Delta\lambda$ (Å) (1330−1515)
32948	4.592	7.515	34910	10.500	2.655
32951	2.413	6.444	34911	11.304	1.920
32957	1.500	3.781	34912	8.572	0.417
32965	2.679	6.371	34913	11.500	2.089
34878	10.396	5.369	34914	8.884	1.568
34879	11.512	5.121	34915	10.170	2.224
34880	9.785	4.487	34916	10.011	1.038
34881	9.512	4.398	34917	8.577	0.220
34882	9.186	4.426	34918	8.130	1.070
34883	9.997	5.009	34919	8.646	0.489
34884	9.699	4.252	34920	10.284	2.874
34885	9.472	3.463	34921	7.152	0.288
34886	9.121	3.548	34922	7.912	0.040
34887	8.822	3.654	34923	6.569	0.042
34888	8.128	3.676	34924	9.155	0.961
34889	11.035	4.711	34925	8.226	1.542
34890	7.334	3.432	34926	8.971	2.097
34891	8.922	5.304	34927	8.364	2.324
34892	5.718	0.597	34928	6.487	1.261
34893	8.736	3.687	34929	5.175	0.406
34894	8.735	2.945	34930	5.099	0.357
34895	8.029	2.541	34931	4.810	1.263
34896	8.838	2.983	34932	5.388	1.112
34897	10.193	3.584	34933	3.056	1.057
34898	10.110	2.548	34934	4.234	1.424
34899	10.616	3.256	34935	3.920	1.004
34900	7.252	1.666	34936	3.905	1.491
34901	11.616	6.361	34937	7.821	5.221
34902	8.577	2.016	34938	4.976	2.282
34905	11.858	1.668	34939	5.489	2.482
34906	11.329	1.627	34943	12.527	6.457
34907	10.442	2.172	34944	11.952	5.971
34908	7.910	1.136	34945	10.752	5.376
34909	10.622	1.931			

Table 4.4 (Continued)

Equivalent Widths Measurements for Subordinate Transitions

SWP Image Number	$\Delta\lambda$ (Å) (1248−1330)	$\Delta\lambda$ (Å) (1330−1515)	SWP Image Number	$\Delta\lambda$ (Å) (1248−1330)	$\Delta\lambda$ (Å) (1330−1515)
34946	13.070	6.351	34982	5.698	3.382
34948	8.608	4.733	34983	5.713	4.133
34949	8.712	4.858	34984	5.132	3.419
34950	9.017	5.222	34985	4.274	2.031
34951	7.300	4.546	34986	8.423	5.739
34952	10.195	6.308	34987	6.881	4.926
34953	7.686	4.214	34988	5.918	3.750
34954	8.418	5.514	34989	5.853	3.615
34955	6.037	3.790	34990	6.495	3.421
34956	2.786	2.260	34991	6.099	3.407
34957	8.645	6.135	34992	7.481	4.790
34958	8.814	5.588	34993	6.984	4.982
34959	6.328	3.993	34994	6.724	3.727
34960	6.678	3.793	35001	13.725	5.991
34961	5.303	3.995	35002	11.638	5.263
34962	6.522	4.650	35003	10.983	5.618
34963	8.884	6.629	35004	9.370	3.945
34964	5.634	4.598	35005	12.635	4.789
34965	7.227	4.633	35006	11.121	4.241
34966	6.886	5.222	35007	13.763	5.899
34967	4.680	2.735	35008	13.653	5.740
34968	3.709	2.507	35009	12.392	4.382
34969	5.633	4.720	35010	13.577	4.947
34970	3.932	3.201	35011	14.825	6.452
34971	5.449	4.118	35012	13.491	5.746
34972	4.540	3.322	35013	14.701	6.957
34973	4.163	2.885	35014	10.350	3.960
34974	4.454	2.608	35016	8.438	0.034
34975	4.868	3.082	35017	8.098	0.555
34976	5.482	3.864	35018	7.315	0.432
34979	7.151	4.534	35019	8.435	1.646
34980	6.631	3.889	35020	5.669	0.402
34981	4.168	2.382	35021	6.681	1.144

emission equivalent widths (r_s=−0.62). This seems to indicate that the changes observed in the Fe V and Fe VI lines take places on a different timescale. From Figure 4.6, it also appears that the variations in these two wavelength ranges have a different nature; while for a given spectrum the flux in the Fe V lines is always consistently below or above the flux in the spectrum to which it is compared, the flux in the Fe VI wavelength range can be below and above that of the comparison spectrum, even for adjacent wavelength ranges. These results should, however, be viewed with caution as the measurements described in this section reflect the combined behaviour of numerous lines and therefore are very difficult to interpret. They are likely to include several effects superimposed and therefore the correlations mentioned above only give a general indication of which effect is dominant.

4.4 Conclusion

Substantial variability has been found in the ultraviolet spectrum of the WN 5 star WR 6. Changes have been detected in the absorption and emission components of the major P Cygni profiles of N V λ1240, C IV λ1550, He II λ1640 and N IV λ1718. The variations in the absorption components occur in concert for all lines and are mainly confined to the absorption edge. As a result of the excellent time resolution of the present dataset, it was established that the changes not only take place on a timescale of ∼ 1 day but also have a recurrence timescale of a similar value. Although previous datasets had tentatively suggested similar timescales for the changes, this is the first time that more than one event (increase followed by a decrease) has been observed in a given series of observations. The variations detected in the emission components of these P Cygni profiles take place on a much longer timescale than the changes in the absorption components. This indicates that whatever in causing the variability is not occurring on the scale of the wind but is much more localised. The changes in the emission also have a much smaller amplitude and do not show the same pattern of variability in all lines. The variations in the N IV transition, although occurring on a similar timescale, do not arise in concert with the changes found in the other lines. This can be qualitatively understood in terms of differing excitation mechanisms and formation regions in the wind. Finally, variability has also been found in a series of Fe V and Fe VI transitions.

The changes for these two ions appear to differ in nature, although some similarities do exist; the variations in the Fe V lines more closely resemble the N IV absorption variations while the Fe VI lines seem to vary with a similar pattern as the N IV emission component. However, blending effects and insecure identification of particular transitions renders the interpretation of the variations found in these lines more difficult and therefore the results should be viewed with caution.

The variations detected in the absorption components of the major ultraviolet P Cygni profiles of HD 50896 do not show a significant phase-dependence with the proposed 3.766 day binary period. Therefore, the observed variability cannot be readily interpreted as being caused by the Hatchett and McCray effect, which should be observed for a WR + neutron star binary system. Consequently, although the variations do not completely rule out the binarity of this star, they do not provide support for this hypothesis. I conclude that the ultraviolet spectral variability is intrinsic to the WN5 wind, reflecting changes in its physical properties. The variations in the P Cygni absorption components are of particular interest as they arise at velocities in excess of the terminal velocity of the wind, determined from the saturated absorption trough of the C IV λ1550 resonance doublet (v_{black}). Such high-velocity material is a natural consequence of the wind models including radiative instabilities presented by Lucy (1982, 1983) or Owocki, Castor and Rybicki (1988) (see Chapter 1, Section 1.2.2). Moreover, the nature of the changes strongly suggests that the latter model is more appropriate. The variations arise as a relatively small strengthening of the blue edge of the absorption component of the strong P Cygni profiles. In view of the large oscillator strength of these transitions, the fact that the excess absorption is not saturated indicates that the material causing the changes is of low density. This is, in fact, a major difference between the two models. Lucy's model, which includes a series of forward shocks, predicts high-velocity material at *high* density, while Owocki, Castor and Rybicki's model predict high-velocity material at *low* density. In fact, variable blue absorption edges in the absorption component of strong P Cygni profiles was identified by Owocki, Castor and Rybicki as a signature of their wind model. The timescale of $\sim$ 1 day determined from the present dataset for this absorption component variability is probably not truly periodic with a unique amplitude. I hope that the results presented

in this chapter will be used to constrain the theoretical time-dependent wind models and serve as a guide for future observing programs.

Chapter 5

UV Observations of Selective Wind Eclipses in γ Velorum

5.1 Introduction

The third brightest star in the Vela constellation, γ Velorum, consists of two visual companions at an angular distance of 41 $''$ often referred to as γ^1 and γ^2 Velorum. γ^1 Velorum was found to be a single-lined spectroscopic binary system with a period of 1.48 days. The spectral type of the primary star was established as B2 III (Hernández and Sahade 1980) but the spectral type of the companion is still unknown. γ^2 Velorum is of particular interest as it includes the brightest Wolf-Rayet (WR) star in the sky. The correct nomenclature for this system of stars is γ Vel A and γ Vel B but we should refer to the WR+O system as γ Vel as it is much brighter than its visual companion and that the two components are so close (see Bidelman 1979). Therefore, I will adopt γ Vel for the WR+O binary in this work since I am not concerned with the other system here.

γ Velorum or WR 11 in the catalogue of van der Hucht *et al.* (1981) was first announced to be a double-lined spectroscopic WR binary system by Sahade (1955). The spectral type of the WR component was established as WC8 by Smith (1968) while for the O star the determination was not straightforward

having been evaluated as O6 (Smith 1955), O7.5 (Ganesh and Bappu 1967), O8 (Baschek and Scholz 1971) and finally O9 I by Conti and Smith (1972). At first, it was assumed that the WR star was the brighter component but by comparing its emission line strengths with those of another WC8 star that is believed to be single (HD 192103), Conti and Smith (1972) concluded that it is the O star that is 1.4 times brighter than the WR star at optical wavelengths. Later, the same result was found in the ultraviolet by Willis and Wilson (1976) (see also Stickland and Lloyd 1990).

The first orbital solution was obtained by Ganesh and Bappu (1967) who found a period of 78.5 days, an eccentricity e=0.17 and minimum masses ($M \sin^3 i$) of 46.3 $M_\odot$ and 13.0 $M_\odot$ for the O-type and WR stars respectively. Moffat (1977) obtained an extensive set of 74 narrow band photoelectric observations over a nearly continuous 37 day period covering the phases when the WR star is in front of the O star. He found no eclipse in the pseudo continuum light curve which lead to an upper limit for the inclination of 73°. Using Ganesh and Bappu's orbital solution, this gives minimum masses of 15 $M_\odot$ and 53 $M_\odot$ for the WC8 and O9 I stars respectively. A new orbital solution was obtained by Niemela and Sahade (1980) using optical data covering a very long time span which yielded an improved value for the period of P=78.5002 ± 0.0001 days. The value of the eccentricity that they derive, e=0.40, is much higher than the one from the previous solution. Pike, Stickland and Willis (1983), also using long timescale optical data, obtained an orbital solution which differed mainly from the Niemela and Sahade's solution by the amplitude of the O star orbit which they found to be almost 2 times smaller ($\sim$ 40 km s^{-1}compared to $\sim$ 70 km s^{-1}). This has serious consequences, mainly on the minimum masses of the stars which they find to be much smaller. In order to try to solve the controversy, Moffat *et al.* (1986) obtained a series of 50 optical spectroscopic plates distributed over 3 orbital cycles. Their observations mainly confirm the orbit obtained by Niemela and Sahade (1980) yielding very similar parameters. However, the matter is still not completely resolved because recently Stickland and Lloyd (1990) used 41 high resolution archival IUE spectra obtained between April 1978 and February 1980 to produce a new orbital solution which supports the previous low determination of the O star amplitude.

Variability in spectral line intensities has been reported by several authors. Short timescale changes (minutes and night-to-night) have often been observed

in optical emission lines such as He II λ4686 and C III– IV λ4650. The most recent report was by Jeffers, Stiff and Weller (1985) who also include a list of most previous detections. The changes they observe occur in the blue wing of the C III– IV blend at 4650 Å on a timescale of a few minutes. These authors interpret the phenomenon as being caused by the presence of a neutron star companion orbiting the WC8 star with a period of $\sim$ 5.4 days. However, this interpretation has been questioned by Moffat *et al.* (1986) as it implies radial velocity variations which they do not detect in their extensive set of spectroscopic plates. Moffat (1977) found changes in optical emission line profiles with a slightly longer timescale of $\sim$ 15–19 days which seem to be stronger for the lines of lower ionisation (C III and He I as opposed to C IV and He II). He suggests that this is because the former arise in the outermost, relatively cooler layers of the wind where perturbations of the O star are likely to have a strong effect. However, he finds no correlation between the changes and the orbital period which sheds some doubt on this interpretation.

Phase-dependent spectroscopic variations in the ultraviolet were first detected for γ Vel by Willis and Wilson (1976) using spectra obtained with the sky-survey telescope (S2/68) on the TD-1A satellite. These were attributed to selective eclipsing of the O star light by the dense WC8 wind. The changes were later confirmed by Willis *et al.* (1979) in a study of an extensive set of IUE observations. The variations were reported for a large variety of low excitation ions including C II, C III, C IV, Si II, Si III, Si IV, N IV and He II. Recently, Brandi, Ferrer and Sahade (1989) (see also Sahade and Zorec 1981) have analysed the Si IV, C IV and N V resonance profiles in the IUE archival spectra of γ Vel. The phase-dependant variations observed led them to describe these profiles as a superposition of two separate components; one stationary P Cygni profile and one absorption feature that moves back and forth in phase. This last feature is interpreted as a stream of gas moving away from the system at an angle of 110° from the direction of the line joining the WR and O stars which projects against a dense concentration of gas located between the two stars and moving away at ~ -700 km s^{-1}. This concentration of matter arises as a result of the collision between the two stellar winds. The new interpretation is considerably different from the previous one by Willis *et al.* (1976, 1979). In an attempt to shed new light on the problem I will present in this chapter an analysis of *all* IUE high

resolution spectra of γ Vel available in the archives. The study will not be limited to a restricted number of lines as in the case of Brandi, Ferrer and Sahade (1989) but will include all transitions which show phase-dependent variations in order to obtain a global view of the problem. This will be supplemented by 8 *Copernicus* satellite spectra covering the whole orbital period providing a much broader wavelength range and thus a larger number of transitions.

5.2 Observations

I have searched the IUE Merged Observing Log for all high resolution ($\Delta\lambda \sim$ 0.1–0.3 Å) spectra of γ Vel. The search yielded 40 SWP (Short Wavelength Prime, $\lambda\lambda$ 1150–2050 Å) and 30 LWR (Long Wavelength Redundant; $\lambda\lambda$ 1850–3200Å) spectra all secured with the small aperture ($\sim$ 3"). All images were uniformly extracted from the Rutherford Appleton Laboratory World Data Centre archives using the IUEDR software package, which yields improved output spectra compared to the standard IUESIPS data (see description in Chapter 2), and is available on the UK SERC STARLINK network of VAX computers. It is very important to obtain uniform data as the study involves comparing spectra in order to analyse variability and thus the instrumental effects need to be minimized. The spectra were then mapped on a uniform grid ($\Delta\lambda \sim$ 0.1 for the SWP range and at $\Delta\lambda \sim$ 0.2 for the LWR range). All subsequent analysis was performed using the DIPSO software package (Howarth and Murray, 1990) also available on STARLINK. Tables 5.1 and 5.2 list the SWP and LWR image numbers respectively obtained from the archive. Also given are the Julian Dates at the beginning of the exposure, the exposure times and the orbital phases calculated with the ephemeris of Moffat *et al.* (1986) (P=78.5002 days and E_0=2445768.96).

Also included in this analysis are 8 *Copernicus* spectra obtained in March-April 1977 and March-April 1980. *Copernicus*, the third of Nasa's very successful Orbiting Astronomical Observatories (OAO), carried the Princeton high-dispersion spectrometer designed to scan stellar spectra with a resolution of $\sim$ 0.05–0.20 Å between 950–1450 Å (U1 and U2 phototubes) and $\sim$ 0.1–0.4 Å between 1650–3000 Å (V1 and V2 phototubes). A detailed description of the instrumentation and performances of the satellite is given by Rogerson *et al.* (1973).

Table 5.1

IUE SWP High Resolution Images of γ Vel

SWP Image Number	Julian Date 2440000.000+	Exposure Time (s)	Orbital Phase P=78.5002d
1358	3612.713	3	0.532
1359	3612.850	6	0.534
1413	3623.746	5	0.673
1425	3625.695	5	0.697
1545	3643.535	5	0.925
1546	3643.599	11	0.925
1605	3651.544	5	0.027
1717	3664.304	1	0.189
1718	3664.337	3	0.190
1719	3664.398	5	0.190
1761	3671.459	5	0.280
1811	3678.537	5	0.370
2290	3734.939	5	0.089
2291	3734.966	2	0.089
2295	3735.229	2	0.093
2388	3745.097	6	0.218
2389	3745.127	12	0.219
2504	3757.840	6	0.381
2514	3758.939	5	0.395
2683	3770.156	6	0.538
2817	3782.535	5	0.695
2964	3795.450	4	0.860
3139	3807.049	4	0.008
3271	3821.361	5	0.190
3377	3830.931	3	0.312
3378	3830.968	3	0.312
3379	3830.995	4	0.313
3386	3831.657	3	0.321
3498	3843.513	3	0.472
3572	3854.554	3	0.613
3677	3865.559	3	0.753
3935	3891.867	3	0.088
4636	3947.589	3	0.798
4719	3954.349	3	0.884
5480	4035.302	5	0.915
6175	4099.226	3	0.730
6351	4118.150	3	0.971
6532	4132.760	3	0.157
7200	4200.358	3	0.018
7980	4287.725	3	0.131

Table 5.2

IUE LWR High Resolution Images of γ Vel

LWR Image Number	Julian Date 2440000.000+	Exposure Time (s)	Orbital Phase P=78.5002d
1315	3612.756	5	0.533
1316	3612.835	13	0.534
1396	3625.665	13	0.697
1497	3643.569	7	0.925
1498	3643.628	8	0.926
1543	3651.579	7	0.027
1619	3664.369	4	0.190
1651	3670.492	7	0.268
2073	3734.962	12	0.089
2074	3735.005	4	0.090
2076	3735.233	3	0.093
2167	3745.100	3	0.218
2298	3758.943	4	0.395
2596	3795.467	3	0.860
2708	3807.051	3	0.008
2882	3821.366	3	0.190
2963	3830.934	3	0.312
2964	3830.970	4	0.312
2973	3831.660	3	0.321
3075	3843.517	3	0.472
3145	3854.551	3	0.613
3240	3865.562	3	0.753
3510	3891.871	3	0.088
4026	3947.581	3	0.798
4084	3954.346	3	0.884
5340	4099.223	3	0.730
5486	4118.152	3	0.971
5601	4132.756	3	0.157
6210	4200.360	3	0.018
6952	4287.720	3	0.131

The *Copernicus* spectra used in this work were obtained with the U2 and V2 phototubes with a resolution of 0.2 and 0.4 Å respectively. Each spectrum has been corrected for charged particle background. A correction for signal pointing errors was also made using the flux from the U1 monitoring tube. For

Table 5.3

***Copernicus* Observations of γ Vel**

Julian Date 2440000.000+	Orbital Phase P=78.5002d	U2 Observed Wav. Range (Å)	V2 Observed Wav. Range (Å)
3218.5	0.510	751– 964	1481–1907
3219.5	0.523	965–1297	1909–2575
3220.5	0.536	1298–1635	2575–3252
3253.5	0.956	751–1045	1481–2069
3254.5	0.969	1045–1369	2069–2718
3255.5	0.981	1369–1644	2718–3269
4300.5	0.294	950–1263	1880–2504
4307.5	0.383	950–1274	1880–2527
4322.5	0.574	950–1273	1880–2526
4329.5	0.663	950–1261	1880–2451
4350.5	0.931	950–1262	1880–2504
4358.5	0.032	950–1262	1880–2504

the 1977 observations, the stray and scattered light has been removed from the U2 data using the standard software packages described by Bohlin (1975) but this was impossible for the 1980 observations. The stray light at given wavelength, λ is approximately 30 % of the signal at λ+20 Å averaged over a range of $\pm$ 3.5 Å. However, the wavelength range observed in 1980 is not broad enough to calculate an appropriate recurrence relation. The stray light accounts for $\sim$ 40 % of the flux but is a fairly smooth function. No such problems exist for the V2 phototube. As a consequence of this difference in reduction procedure for the 1977 and 1980 data, great care is required when attempting to compare them directly, as instrumental effects could be difficult to distinguish from real variations. Table 5.3 lists the Julian Date of the observations, the orbital phase calculated with the same ephemeris as for the IUE data and the U2 and V2 wavelength ranges observed. It is noted that the U2 spectra are only significant between 930–1450 Å because of the low sensitivity outside this spectral range and that the V2 data exhibit considerable noise shortward of 1700 Å.

5.3 Results and Discussion

5.3.1 ULTRAVIOLET SPECTRAL VARIATIONS

A thorough examination of all the ultraviolet spectra included in this study reveals that the largest spectral variations occur between phase 0.0 (when the O star is behind the dense WR wind) and phase 0.5 (when the O star is in front). This strongly suggests that the cause of the variations is an eclipse of the O star light by the WR wind. In such a situation the largest absorption column is encountered when the O star is on the far side of the WR star and it gradually decreases as the star orbits to the front, thus producing the largest changes between phases 0.0 and 0.5 as observed in our data. Another characteristic of the variations is their repeatability over different epochs. This is demonstrated in Figure 5.1 where IUE SWP spectra near phases 0.0 and 0.5 are presented for the Si IIIλ1206 transition at two different epochs. The spectra were secured in April–May 1978 and December 1978–January 1979 and are thus separated by three orbital cycles. The fact that the variations are identical from one orbital cycle to another indicates that they are truly phase-dependent and thus are related to effects in the binary system. However, this does not exclude the possibility that intrinsic variability of the type described in Chapters 2,3 and 4 could be superimposed on the binary-related changes. These would be of much smaller amplitude and would not be phase-dependent. Therefore, they would be easily distinguishable from the changes described here.

In order to illustrate which atomic species show evidence of variability, the difference between spectra at phases 0.0 and 0.5 is presented in Figure 5.2. From 950–1290 Å the 1977 U2 *Copernicus* spectra are presented while between 1280–1950 Å and 2130–2470 Å the IUE SWP and LWR spectra respectively are shown. In an attempt to improve the signal-to-noise, mean spectra were produced for the SWP and LWR wavelength ranges at both orbital phases. The SWP means consist of 3 spectra (SWP 1605, 3139, 7200) at phase 0.0 and 4 spectra (SWP 1358, 1359, 2683, 3498) at phase 0.5 while the LWR means include 4 spectra (LWR 1543, 2708, 5486, 6210) at phase 0.0 and 3 spectra (LWR 1315, 1316, 3075) at phase 0.5. No variations were found between 1950–2130 Å and longward of 2470 Å and are therefore not presented in the figure. All the spectra used in this study were obtained with a small aperture and are therefore not photometricaly calibrated. It was thus necessary to scale the

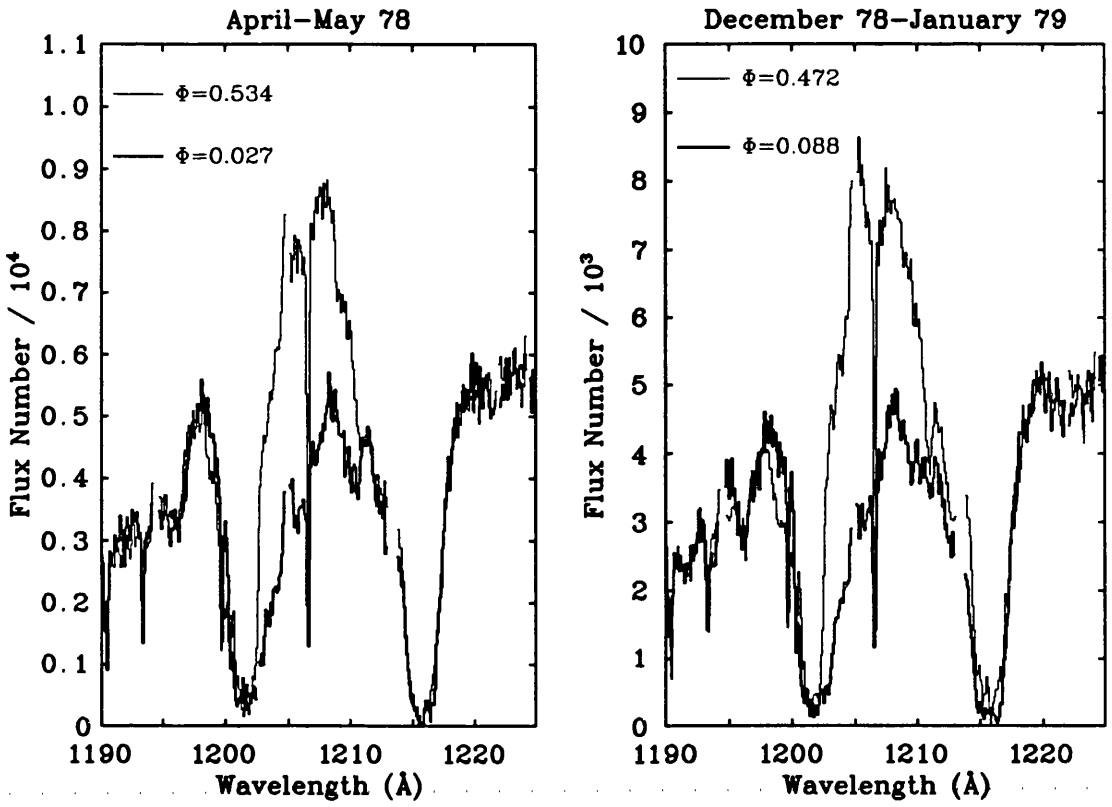

Figure 5.1 : Si III λ1206 line of γ Vel near phases 0.0 and 0.5 obtained with IUE at two different epochs

spectra to one chosen reference spectrum before adding them to form a mean. For this reason, it will not be possible to draw any conclusion concerning the presence of continuum eclipses. It will be assumed, as for optical wavelengths (Moffat 1977), that the ultraviolet continuum is constant throughout the whole orbital cycle. Support for this hypothesis is found in the work of Willis and Wilson (1976) who find only a few percent difference in the continuum level of their two S2/68 spectra.

Suggested identification of the major species that show variability are indicated in Figure 5.2 and details are given in Table 5.4. Listed are the ions, their laboratory and observed wavelengths as well as the ionisation potential. The feature at 1037 Å although most likely due to C II may include a contribution from O VI λ1037.6. The Si IV lines at $\sim$ 1725 Å are probably blended with the Fe V lines which are numerous in the spectral region.

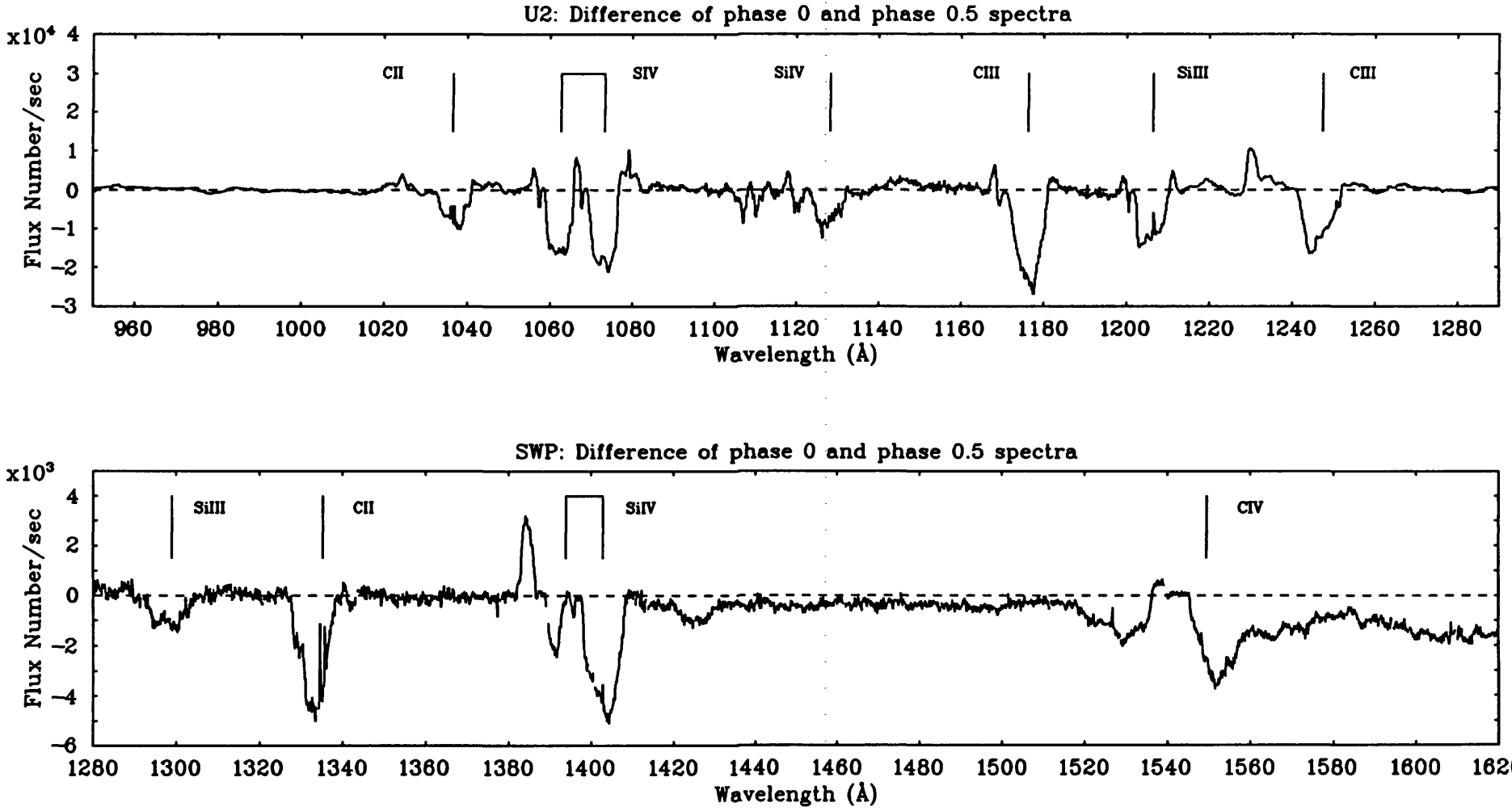

Fig 5.2 : Eclipse Spectrum of γ Velorum

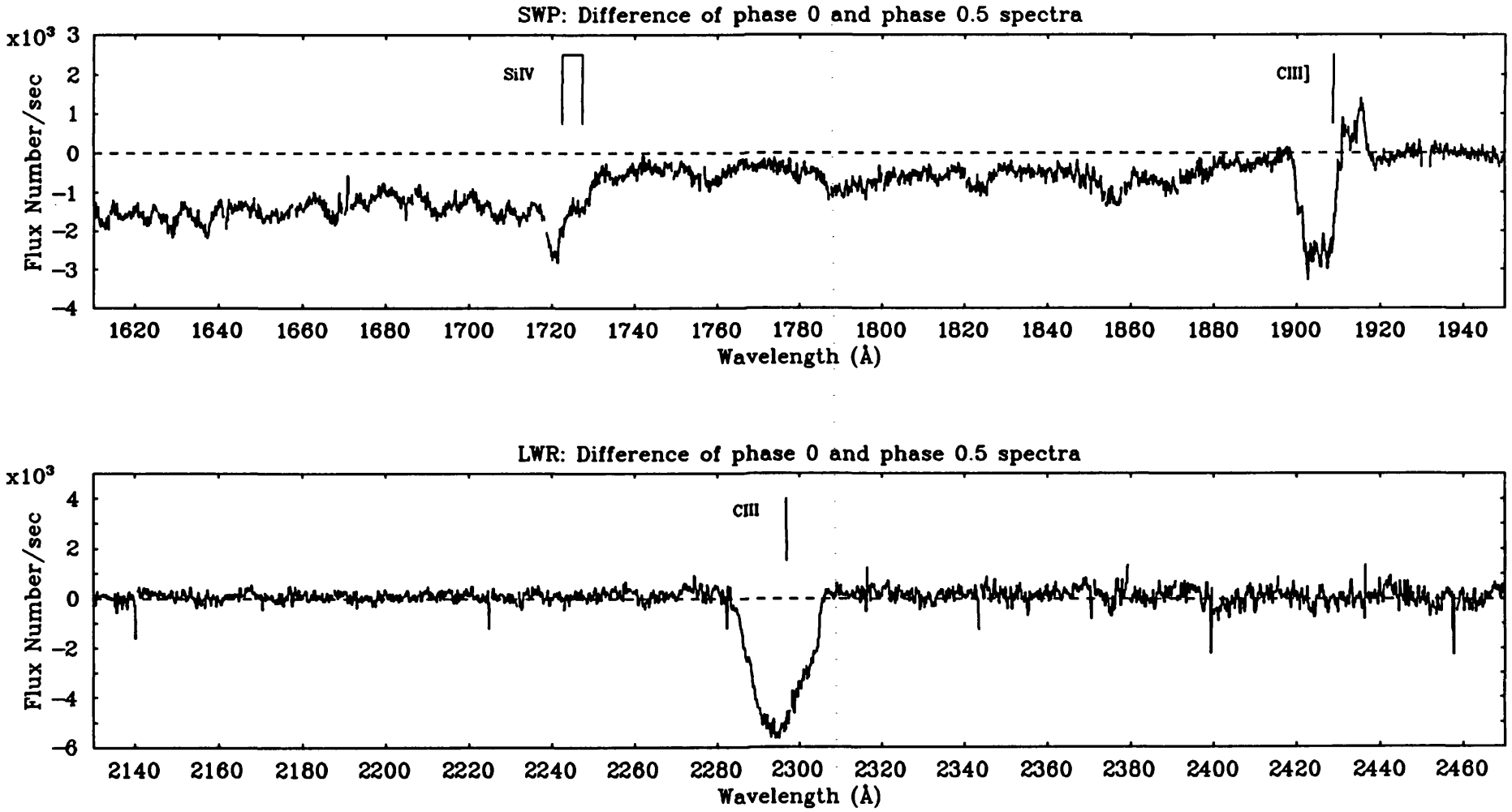

Fig 5.2 (cont.) : Eclipse Spectrum of γ Velorum

Table 5.4

Major Observed Eclipse Transitions for γ Vel

Ion	λ_{Lab}	λ_{Obs}	Ion. Pot.
C III	977.03	978.95	47.89
C II	1036.34,1037.02	1036.85	24.38
S IV	1062.67	1062.22	47.30
S IV	1072.99	1072.80	47.30
Si IV	1122.49,1128.34	1127.73	45.14
C III	1175.71	1176.29	47.89
Si III	1206.51	1206.18	33.49
C III	1247.38	1246.49	47.89
Si III	1294.54–1303.32	1298.50	33.49
C II	1334.53,1335.70	1332.96	24.38
Si IV	1393.76,1402.77	1403.16	45.14
C IV	1548.19,1550.76	1551.95	64.49
Si IV	1722.53,1727.38	1720.50,1726.90	45.14
C III	1908.73	1904.65	47.89
C III	2296.87	2294.42	47.89

The ions observed embrace a broad range of ionisation including C II, C III, C IV, Si III, Si IV and S IV. Note that the flux below 1010 Å is very weak. Therefore, on the scale presented in Figure 5.2 it is difficult to detect any variations. However, a more detailed examination reveals the presence of variability in the C III 977.2 Å transition. These identifications are very similar to the ones suggested by Willis *et al.* (1979) although one major difference is the feature near 1720Å which is attributed here to Si IV instead of N IV. No nitrogen absorption is thought to be present as generally expected in the case of absorption in WC winds. Another difference is that excluding the most obvious transitions, I will not attempt to identify any individual lines within the broad absorption observed between $\sim$ 1410–1900 Å. As in the case of CV Serpentis (Eaton, Cherepashchuk and Khaliullin 1985b), I associate this feature with a large number of Fe IV transitions between the $3d^4 4s - 3d^4 4p$ levels. The lines are broadened by the velocity dispersion in the wind and are blended together

to form a continuum–like absorption. This feature will be examined in more detail in a later section.

5.3.2 DETAILED DESCRIPTION OF THE VARIATIONS

The large number of spectra available for γ Vel allows for a detailed analysis of the variations as a function of orbital phase. The various spectral lines for which variation are found show three distinctive types of behaviour which will be discussed here in turn.

5.3.2.1 *The C III λ2297 Transition and Other Lines of Similar Behaviour*

The first group including C II λ1037, S IV λ1062,1072, Si IV λ1125, C III λ1175, Si III λ1206, C III λ1247, Si III λ1299, C II λ1334, Si IV λ1725 and C III λ2297 is well represented by the last of these transitions. This line is well isolated which prevents confusion caused by blends with other spectral features. Furthermore, it is not usually detected in O9 I spectra and thus the interpretation of the changes will be greatly facilitated. Figure 5.3 illustrates the variations for a subset of 12 orbital phases, compared to the spectrum at phase 0.534 (O star in front). In order to facilitate the comparison of one spectrum to another for these small aperture observations, each individual spectrum was scaled to LWR 2708 at phase 0.008. This was achieved by taking the ratio of LWR 2708 and a particular spectrum, fitting a low order polynomial to the resulting data points in wavelength regions where there are no line variations, and multiplying the fitted polynomial to the spectrum considered. In several cases, a constant value was sufficient to scale the data but for some spectra it was necessary to use a first order polynomial. The spectra were also corrected for orbital velocity shifts using the radial velocity curve of Moffat *et al.* (1986). Here I assumed that the spectrum at phase 0.008 was at V_r=0.0 km s^{-1} as I am not concerned with precise absolute velocities.

The line evolves from a P Cygni profile with a saturated absorption and a relatively small emission at phase 0.008 to a pure emission line at phase 0.534. Its behaviour in the second part of the orbit is very similar, as expected. The emission component is well centered on the rest wavelength near phases 0.0 and 0.5 but is significantly redshifted at most other phases. This behaviour seems to be caused by the appearance of an absorption component which gradually increases in strength and width from phase 0.5 to 0.0 and then gradually decreases from phase 0.0 to phase 0.5. The most common interpretation for line

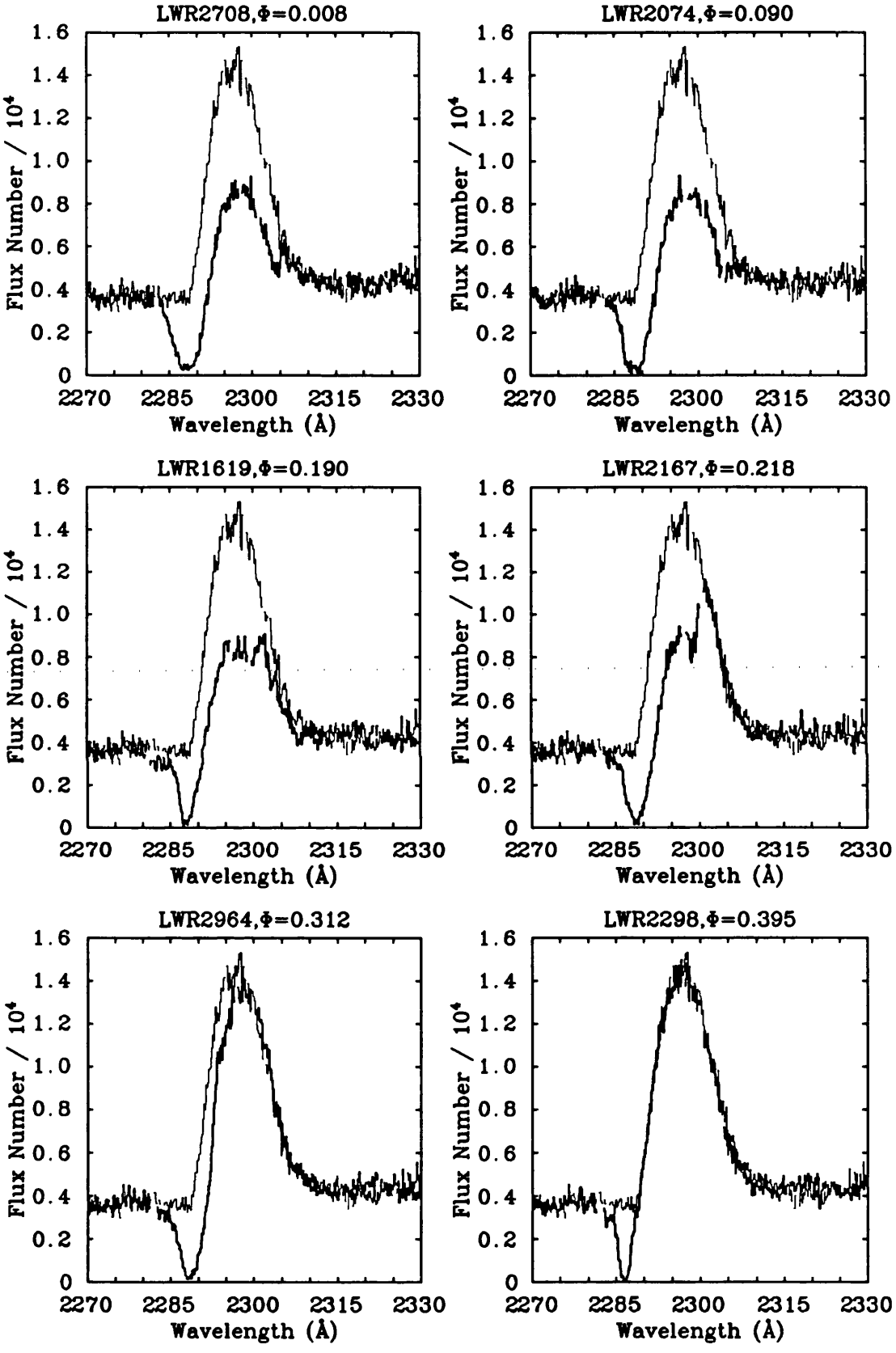

Figure 5.3 : Variations in the C III λ2297 profile with orbital phase. The thin line is LWR1316 (Φ =0.534) and the thick line is the spectrum indicated at the top of each graph.

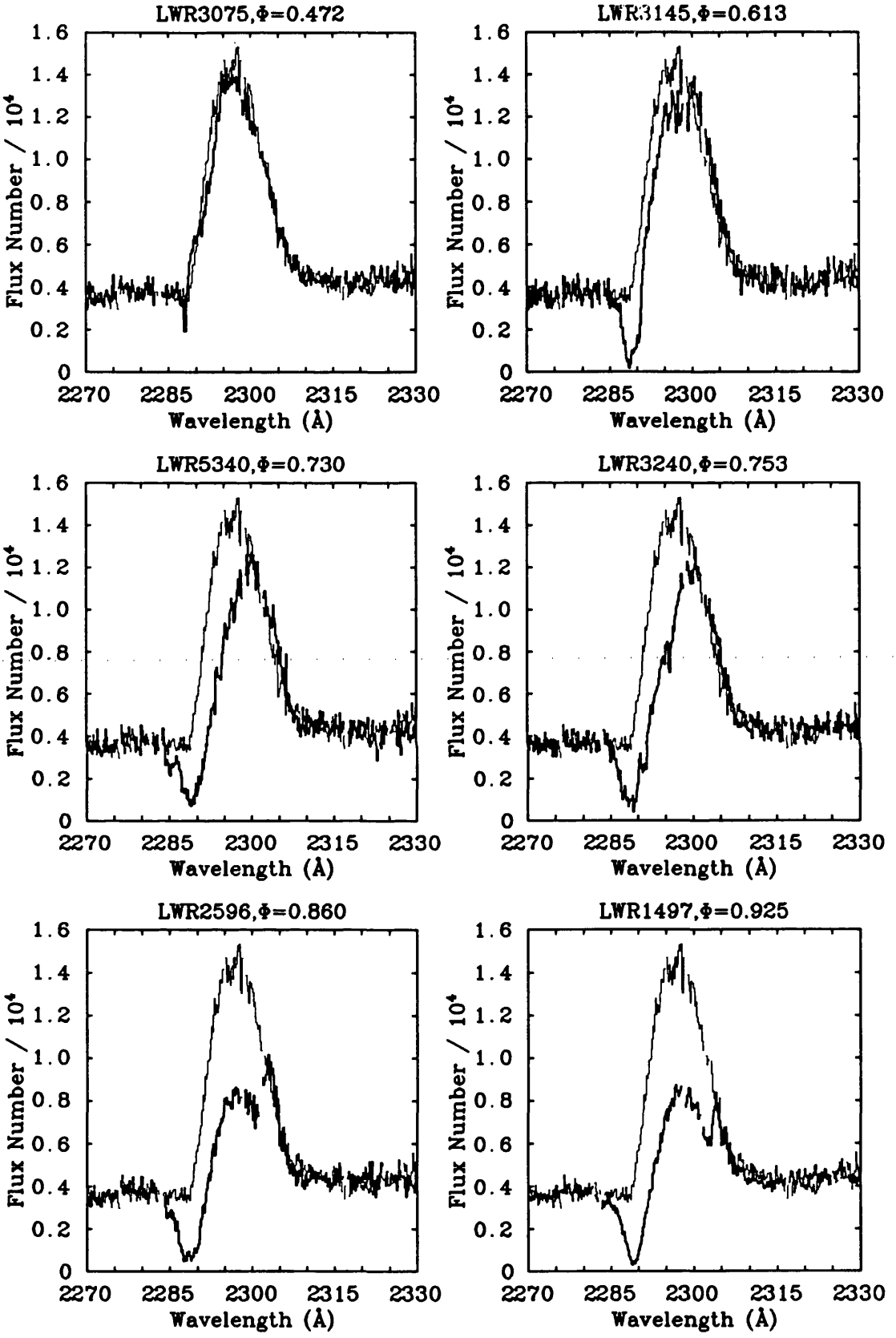

Figure 5.3 (continued) : Variations in the CIIIλ2297 profile with orbital phase. The thin line is LWR1316 (Φ=0.534) and the thick line is the spectrum indicated at the top of each graph.

variability in WR binaries is atmospheric eclipses of the O star continuum flux by the WR wind. I will begin by considering if such a simple assumption can explain the detailed behaviour of this line as a function of phase.

In such a scenario, when the O star is in front (Φ=0.5), no wind absorption occurs (or only very little if the extent of the wind is larger than the orbit). Therefore, the corresponding spectrum represents the "undisturbed" spectrum consisting only of the light from the O and WR stars. If we assume that the winds of the O and WR stars are not disrupted by interaction or collision effects, the flux from the O star (F_O) and the flux from the WR star (F_{WR}) should be constant during the whole orbital cycle and thus the spectrum at phase 0.5 can be used to compare with spectra at other phases. The flux that we expect to observe at a given wavelength for phase 0.5 should therefore be given by $F_{0.5}=F_O+F_{WR}$. At other phases, the O star light is eclipsed by the dense WR wind so the observed flux should be given by $F_\Phi=F_{WR}+F_O e^{-\tau}$ where τ is the opacity at that particular wavelength. Therefore, if we take the difference between the spectra at these two phases we will basically obtain the difference between the flux of the O star modulated by the wind absorption and the undisturbed O star flux $F_{diff}=F_O e^{-\tau}-F_O$. At least for wavelength regions where there are no wind features in the O star spectrum, the behaviour of the differenced spectra as a function of wavelength would then be the same as the eclipse spectra. As the O star orbits the WR wind, its light beam will encounter different ranges of velocities at each particular orbital phase. This can be seen in Figure 5.3 ; the width of the absorption is maximum at phase 0 and decreases towards phase 0.5. The observed limits of the absorption in velocity space for the C IIIλ2297 transition are given in Table 5.5 for each orbital phase presented in Figure 5.3.

The extent of the absorption at a particular point in the orbit can be estimated by calculating the position of the O star with respect to the WR centre and evaluating the maximum and minimum wind velocities encountered by the light beam. Presented in Figure 5.4 is a simple sketch illustrating the geometrical setting discussed here. The WR star is situated at the origin of the system of coordinates with its wind extending outwards to a very large distance. In this work, I assume that the extent of the WR wind is larger than the orbital separation. The position of the O star, which is assumed to be a point source, is indicated by the radius vector r and the observer is looking in the z direction.

Table 5.5

Range of velocities for which wind absorption is detected in the C IIIλ2297 transition.

LWR Image Number	Orbital Phase P=78.5002d	Velocity Range (km s^{-1})
2708	0.008	−1758 − +1118
2074	0.090	−1578 − +1298
1619	0.190	−2154 − +1074
2167	0.218	−2064 − +562
2964	0.312	−2019 − +192
2298	0.395	−2170 − −994
3075	0.472	...
3145	0.613	−1408 − +418
5340	0.730	−1641 − +462
3240	0.753	−1498 − +498
2596	0.860	−1651 − +768
1497	0.925	−1902 − +939

The light from the O star will encounter wind material with projected velocities given by VZ=V(r)z/r. The extent of the velocity range over which absorption will occur is determined by the position of the O star (VZ_O) and the extent of the WR wind (VZ_{wind}). If it is assumed that the ion producing the transition considered is present in the wind up to a very large radius, the latter limit can be readily estimated to $VZ_{wind}=-V(r)_{r\rightarrow\infty}=-V_\infty$ where V_∞ is the terminal velocity of the WR wind for the ion under consideration (in this case C III). From Table 5.5, I obtain an observed mean velocity of -1804 ± 170 km s^{-1} which compares relatively well with the value of the maximum bulk outflow velocity of the WR wind, 1520 ± 200 km s^{-1}, estimated from the half width of the forbiden Ne II line at 12μm (Barlow, Roche and Aitken 1988). Rigorously, this mean velocity should be compared to the terminal bulk outflow velocity of C III which is, unfortunately, unavailable. The fact that the mean of the observed velocities of C III agrees with the maximum bulk outflow velocity of the wind suggests that the observations are roughly in agreement with the model described here. Furthermore, the adopted velocity law is only a best approximation for this particular problem ; the blue absorption edge observed in all P Cygni profiles is evidence that there is some material in the wind moving

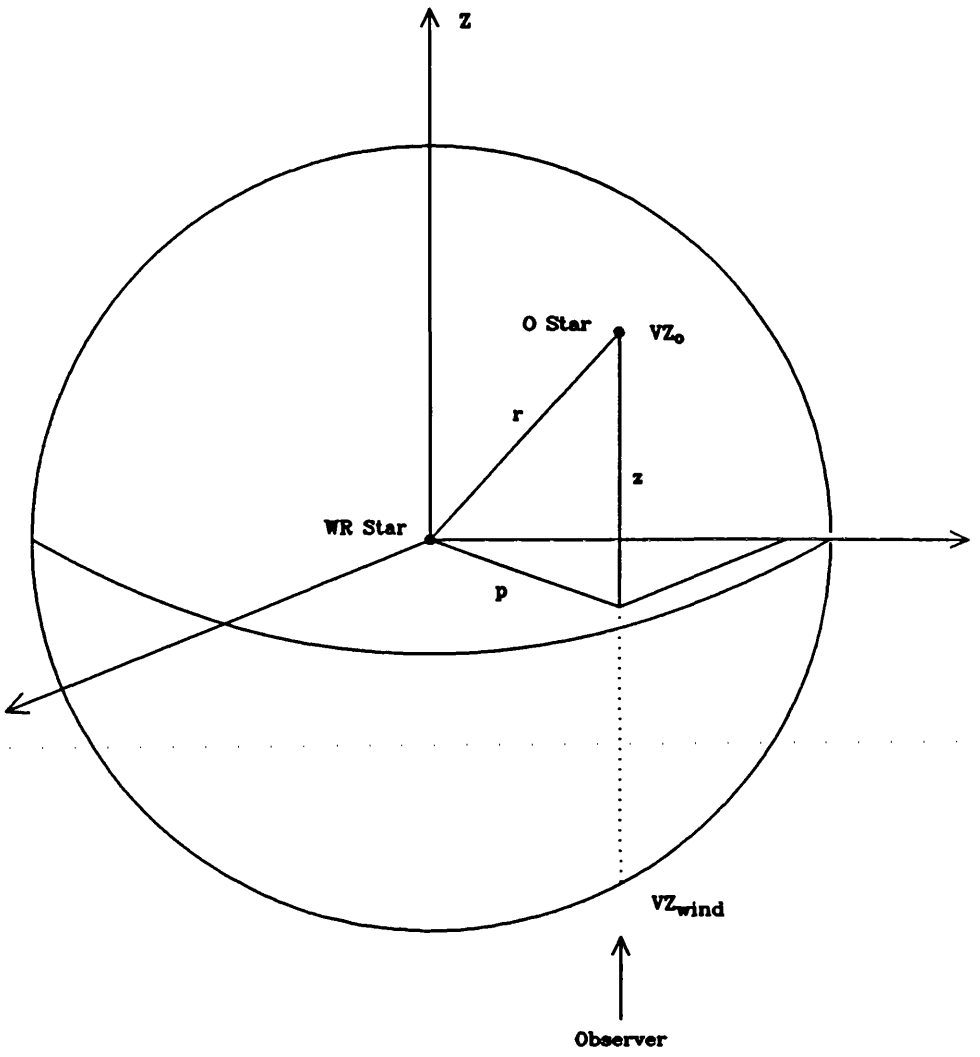

Figure 5.4 : Simplified sketch illustrating the geometrical setting of wind eclipses.

at velocities in excess of the terminal velocity. If this material were situated in the line of sight, a higher velocity may well be observed as is the case here. The other limit is given by

$$VZ_O = V(r)(r^2 - p^2)^{\frac{1}{2}}/r$$

with the impact parameter p given by the well known expression

$$p^2 = r^2(cos^2(v+\omega) + sin^2(v+\omega)cos^2 i)$$

Here v is the true anomaly, ω is the angle of periastron passage from the ascending node and i is the inclination of the orbit. I will adopt the velocity law

of Friend and Abbott (1986) $V(r)=V_\infty(1-R_{WR}/r)^{0.8}$ where R_{WR} is the radius of the WR core which I will assume to be 11 $R_\odot$ for a WC 8 core (Abbott *et al.* 1986). For V_∞, I will adopt the value of Barlow, Roche and Aitken (1988), 1520 km s^{-1}. The orbital elements of Moffat *et al.* (1986) will be used (e=0.4, ω=250°, T_o=2445802.6 and A=300 $R_\odot$) to determine the values of r and v and finally VZ_O. Figure 5.5 presents calculated values of VZ_O for various values of the inclination compared to measured values from Table 5.5.

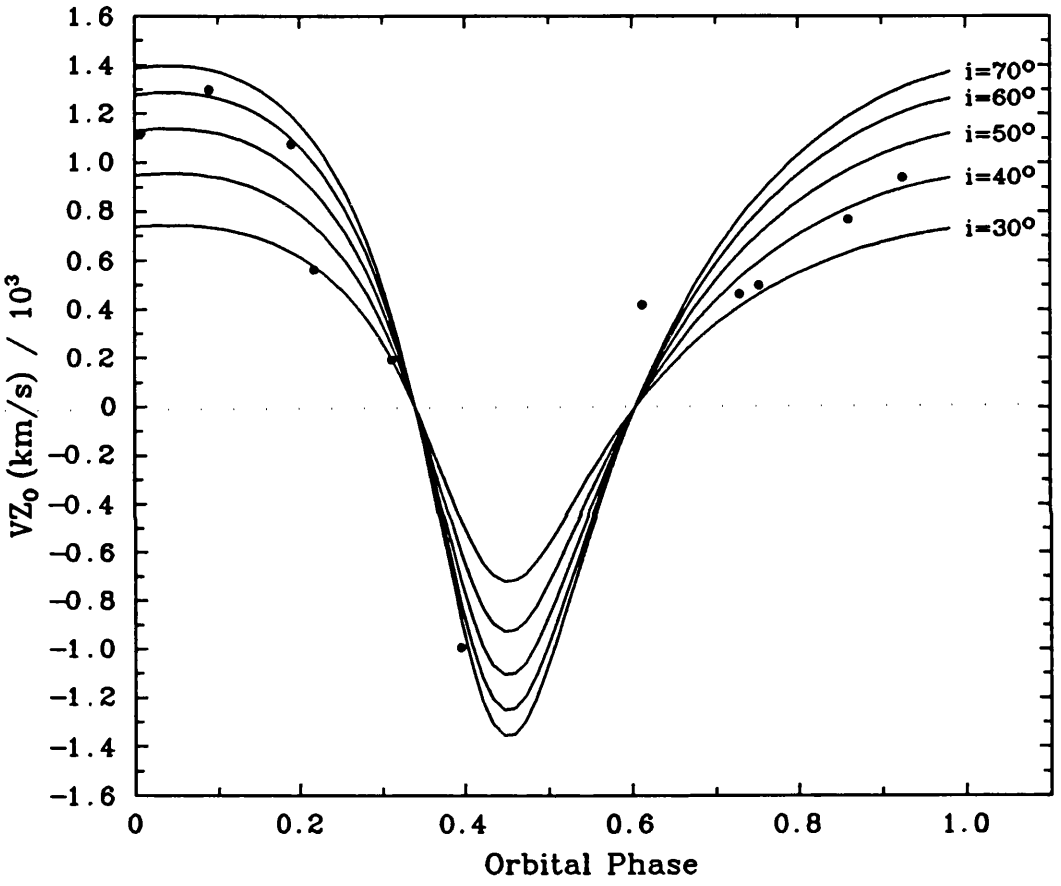

Figure 5.5 : Observed (dots) and predicted (full line) velocity range upper limits for the absorption of the O star light by the WR wind as a function of orbital phase for various values of the inclination.

For such a simple model, the agreement between the observed and calculated values is relatively good. In principle, it is possible to determine the value of the orbital inclination with this type of analysis. However, in practice the present model is probably too simple, excluding effects such as interactions

between the two stellar winds and the presence of material at velocities in excess of the terminal velocity of the WR wind.

The previous analysis indicates that on purely geometrical grounds the selective atmospheric eclipse model explains relatively well the variations observed in this group of lines. However, further investigations reveal some discrepancies. As mentioned above, the difference between the flux of a spectrum for which an eclipse occurs and the spectrum at phase 0.5 is given by $F_{diff}=F_O e^{-\tau}-F_O$. The magnitude of this value must always be smaller than F_O. But inspection of Figure 5.3 reveals that this is not always the case. For several phases, the difference between the two spectra is even larger than the combined continuum of the two stars, estimated from wavelength regions on either side of the P Cygni profile. The most likely explanation for this inconsistency is that the assumption that the spectrum at phase 0.5 consist only of the undisturbed fluxes of the two stars is wrong. Some indication that this is correct is obtained by comparing this line with a corresponding feature in a single WR star of the same spectral type. The WR star HD 192103 (WR 135) is the best candidate for such a comparison. From the atlas of high resolution IUE spectra described in Chapter 2, this line is found to have a weak blue-shifted absorption component which is not detected here in the spectrum at phase 0.5. Some additional light can be included in the spectrum at phase 0.5 by coherent backscattering or reflection of the O star continuum by the WR wind into the line of sight. This effect should occur roughly between phases 0.25 and 0.75, reaching a maximum when the O star is in front of the WR star. This light would be stronger for negative wind velocities, as this is the portion of the wind which is closer to the O star. The net effect should thus be that the absorbtion component of the P Cygni profile will be partially filled in, as seems to be observed in the data presented here. But such an effect cannot be very substantial, especially with such a large orbital separation. Inspection of Figure 5.3 reveals that, on the contrary, this amount needs to be very large in order to explain the changes. For example, the difference between the spectra at phases 0.395 and 0.534 is approximately equal to the combined continuum of the WR and O stars. Since the O star is 1.4 times brighter than the WR star, it can be deduced that to explain such a large difference, the spectra at phase 0.534 must include almost 100 % of reflected O star light and all the O star light must be removed from the spectrum at phase 0.395. The latter statement is reasonable because the wind is very dense

but the former is totally impossible since the solid angle of the wind cannot be 4π. I conclude that reflection effects, although most certainly present, cannot totally explain the discrepancies in the magnitude of the eclipses.

In this analysis, it was assumed that the emission of the WR wind is spherically symmetric and therefore that the amount of emitted light is constant with orbital phase. However it is possible that this assertion is incorrect. It is not unreasonable to speculate that effects such as interaction between the two winds could alter their state, thus creating an asymmetry in the emission with orbital phase. This, together with selective atmospheric eclipses of the O star continuum is the most likely explanation for the phase dependent variations observed in this first group of spectral lines. However, the exact nature of this asymmetry is impossible to determine from the present observations. There is some indication of the presence of a standing shock caused by the collision of the two winds from the analysis of the variations observed in the group of line discussed in the next section but only very simple models can be applied to this very complex situation.

5.3.2.2 *The Si IV λ1396 Doublet and Other Lines of Similar Behaviour*

The second group includes the resonances doublets of Si IV λ1396, C IV λ1550 and more speculatively of N V λ1240. The changes are best illustrated by the Si IV transition. Figure 5.6 presents a series of 12 spectra obtained at various orbital phases, indicated at the top of each graph, compared to the spectrum obtained when the O star is in front of the WR star (LWR 1359, Φ=0.534). Each individual spectrum was scaled to LWR 1359 and corrected for orbital motion using Moffat *et al.*'s (1986) radial velocity curve. As for the C III λ2297 transition it was assumed that the spectrum at phase 0.008 is at V_r=0 km s^{-1}.

The variations can be described as a superposition of two effects. First, the same changes occurring in the group of lines described in the last section can be detected here as a decrease of the emission component between phases 0.5 and 0.0. Simultaneously, a high velocity absorption wing becomes apparent in the blue component of the doublet at Φ=0.312, reaching a maximum when the O star is in front, and starting to disappear after Φ=0.613. Similar changes have been detected in the IUE high resolution spectra of the well-known WR+O binary V444 Cygni (Shore and Brown 1988). These authors described

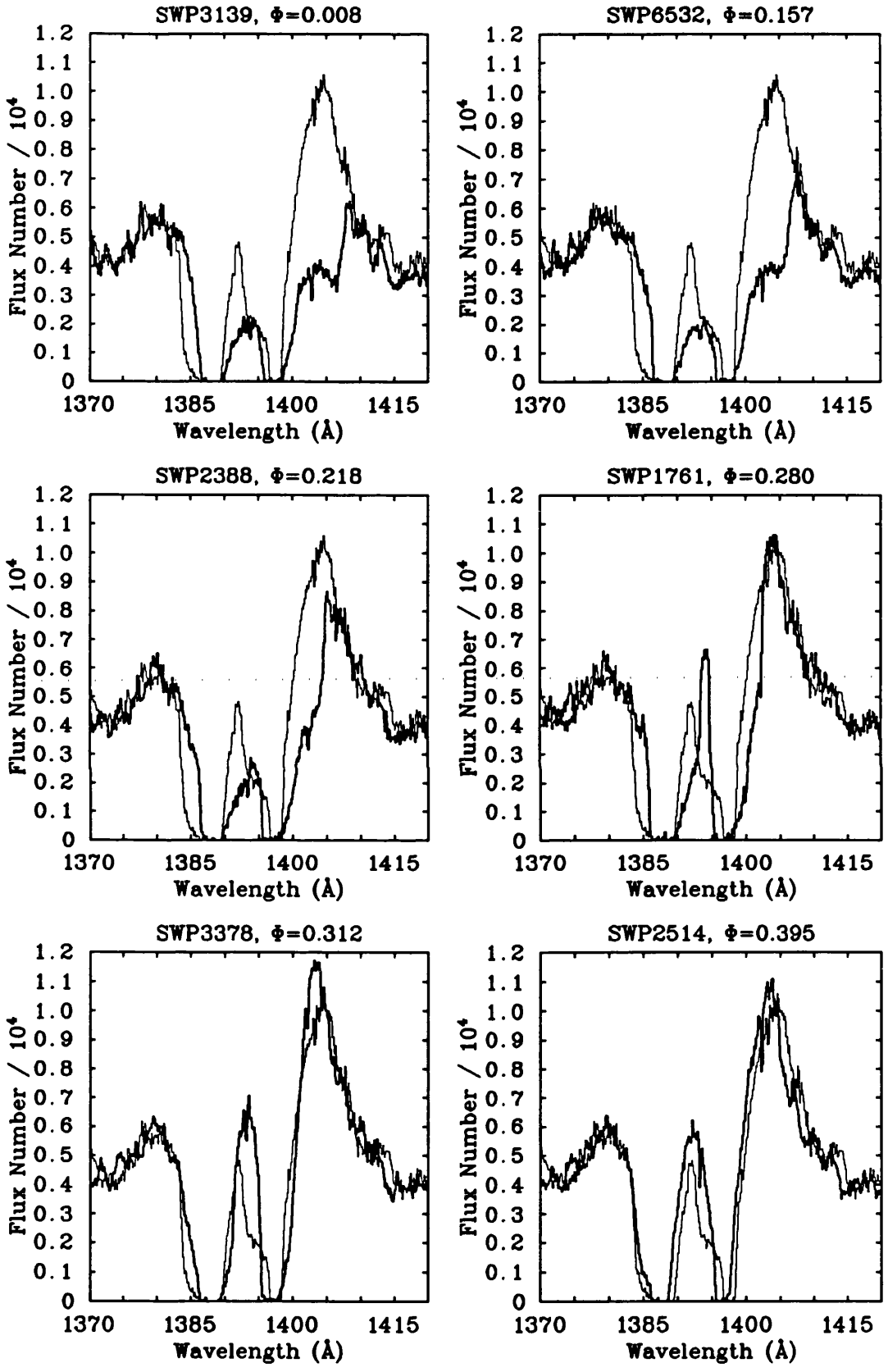

Figure 5.6 : Variations in the SiIVλ1396 doublet with orbital phase. The thin line is LWR1359 (Φ =0.534) and the thick line is the spectrum indicated at the top of each graph.

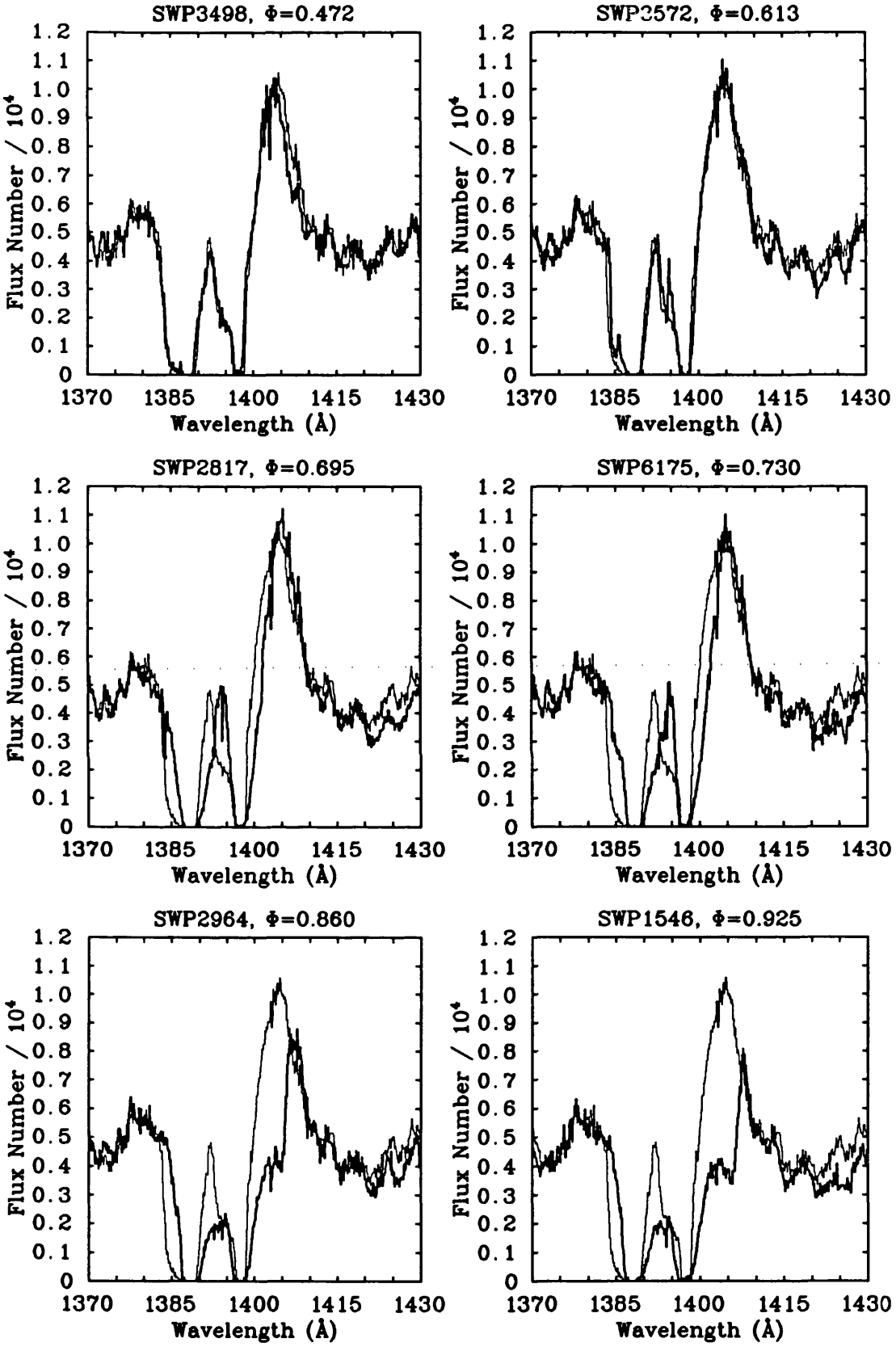

Figure 5.6 (continued) : Variations in the Si IVλ1396 doublet with orbital phase. The thin line is LWR1359 (Φ=0.534) and the thick line is the spectrum indicated at the top of each graph.

the variations as a consequence of the formation of a standing shock following the collision between the two stellar winds. In fact, a much more complex region of shocked gas is formed, consisting of two shocks separated by a contact discontinuity (see Chapter 1, Section 1.3.5). The study of such a region is beyond the scope of this work and therefore, I will adopt the thin-shell approximation and consider the shocked region as a two-dimensional surface. In the remainder of this chapter, I will refer to the shocked region as the shock surface or the shock. The shock surface surrounds the star with the less energetic outflow which in the present case is the O star. The WR wind in the region between the two stars is prevented from reaching the volume around the O star defined by the shock surface, being forced along the shock lines. Consequently, a region forms around the O star in which the density is determined by the density in the O star wind, which is much lower than that of the WR wind. In the remainder of this chapter, I will refer to this region as the "cavity". At phases when the O star is in front of the WR star, the observer is looking into this cavity and therefore sees mainly the O star wind. As the O star wind is much faster than the WR wind, a high velocity wing appears in the P Cygni profile. At phases when the WR star is in front, we see the side of the O star wind which is prevented to reach its terminal velocity by the shock surface. Consequently, the high velocity wing disappears and we see predominantly the WR wind. The maximum velocity of the observed feature appearing in the spectra between phases 0.312 and 0.613 is -2265 km s^{-1} which is consistent with the range of terminal velocities of O9 I stars (Prinja, Barlow and Howarth 1990), in agreement with the interpretation described above. Another point in favour of this interpretation is the lines for which this type of change is detected. Theoretically, this effect can only be detected in spectral lines which are seen as wind features in the O star spectra. Inspection of IUE high resolution spectra of O stars (Walborn and Nichols-Bohlin 1987, Walborn, Nichols-Bohlin and Panek 1985) reveals that the only lines that are seen as wind features in an O9 I IUE spectra are N Vλ1240, Si IVλ1396 and C IVλ1550, which is exactly the same group of lines discussed here. The N V λ1240 doublet was included in this group after careful examination of the spectra. Figure 5.7 presents the IUE SWP spectra at phases 0.008 and 0.534 in the region of the N V doublet. Confusion arises because of the dominance in this wavelength range of the C III λ1247 P Cygni profile formed in the WR wind. In the top part of the graph the spectra are plotted in the

C III λ1247.38 velocity space. The profile changes from a pure emission line at phase 0.534 to a P Cygni profile with a relatively weak emission at phase 0.008, in exactly the same way as the C III λ2297 line described in the previous section. The bottom part of the graph shows the spectra in the N V λ1238.81 velocity space. Despite the confusion with the C III λ1247 transition, it can be clearly seen that a high velocity wing with a maximum velocity consistent with the terminal velocity of the O star is present at phase 0.534 and disappears at phase 0.008. The fact that this high velocity wing appears at wavelengths corresponding to the wind velocities for the N V doublet is an indication that it is related to the O star wind since this feature is not detected in WC spectra.

In an attempt to try to confirm that this is indeed the correct interpretation, I have used a program kindly provided by Dr. I.R Stevens to calculate the approximate shape of the shock surface. This is achieved by determining the positions for which the ram pressures of both winds are equal. For simplicity, the calculation are made only in the plane of the orbit. The first parameter that needs to be determined is the location of the stagnation point on the line joining the two stars. For a constant velocity law, this is readily determined by:

$$\frac{r_1}{D} = \frac{1}{1 + \lambda_0^{-0.5}}$$

where r_1 is the radial distance from star 1, which is chosen to be the star with the highest momentum flux, D is the stellar separation and λ_0 is the momentum ratio, $\lambda_0 = \dot{M}_1 v_{1\infty}/\dot{M}_2 v_{2\infty}$. For an accelerating velocity law of the type $v(r) = v_\infty(1\text{–}R_*/r)^\beta$, the solution involves numerically solving a simple differential equation in r_1. Once the position of the stagnation point is determined, the problem of calculating the shape of the shock in the x–y plane with star 1 at the center of the system of coordinates reduces to solving the following first order linear differential equation:

$$\frac{dx}{dy} = \frac{\lambda(x/r_1) - (D-x)/r_2}{\lambda(y/r_1) + y/r_2}$$

where λ is the general expression for the momentum ratio :

$$\lambda^2 = \frac{\dot{M}_1 v_1(r_1) r_2^2}{\dot{M}_2 v_2(r_2) r_1^2}$$

and the position of the stagnation point on the x axis is used as a boundary condition.

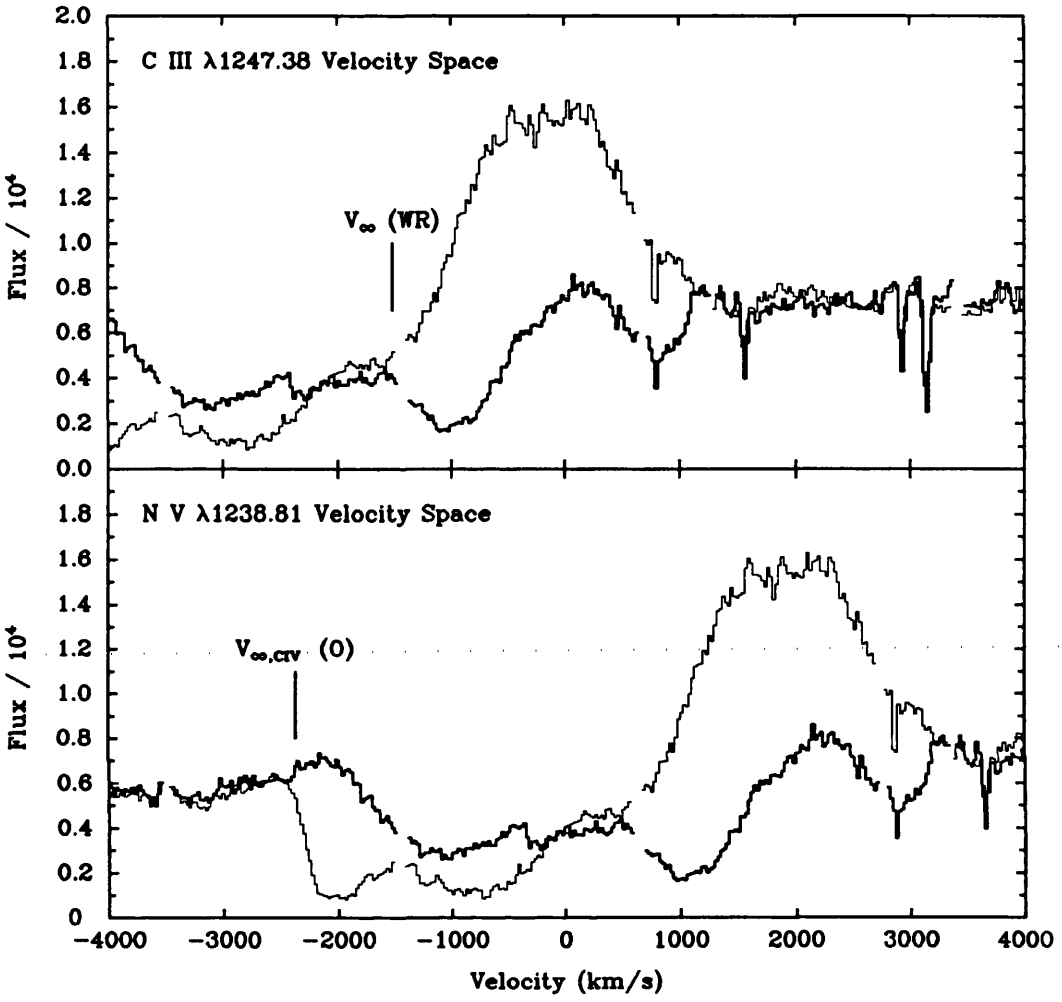

Figure 5.7 : γ Vel IUE SWP spectra at phases 0.008 (thick line) and 0.534 (thin line) in the C III λ1247.38 and N V λ1238.81 velocity spaces. The terminal velocities of the WR (−1520 km s^{-1}) and O stars (−2370 km s^{-1}, from the C IV P Cygni profile) are indicated on the graph.

The input parameters that need to be specified include the terminal velocity (v_∞), the mass-loss rate ($\dot{M}$) and the radius (R_*) of each star as well as the orbital separation. I will adopt the terminal velocity of the WR star determined from the rectangular profile of the forbidden Ne II 12 μm line (−1520 km s^{-1}) by Barlow, Roche and Aitken (1988) and the terminal velocity of the O star determined from the saturated absorption of the C IV resonance doublet

at phase 0.5 (-2370 km s^{-1}) by Prinja, Barlow and Howarth (1990). This last value is consistent with the range of terminal velocities found for single O9 I stars by these same authors. The mass loss rate of the WR star was determined from the radio flux to 8.8x10^{-5} $M_\odot$/yr by Barlow, Roche and Aitken (1988) and for the O star I will adopt a typical mass-loss for an O9 I star of 1.3x10^{-6} $M_\odot$/yr (Howarth and Prinja 1989). Typical values for the radius of each star were chosen; 11 $R_\odot$ for the WR star (Abbott *et al.* 1986) and 21 $R_\odot$ for the O star (Howarth and Prinja 1989). Finally, the stellar separation for each orbital phase will be evaluated from the orbital elements of Moffat *et al.* (1986) (e=0.4, ω=250° and A=300 $R_\odot$)

Because the shape of the shock depends on the stellar separation and the orbit of γ Vel is highly eccentric, a calculation is required for each orbital phase. For certain sets of parameters, the shock is found to be crushed on the surface of the star with the smallest flux, in this case the O star. For accelerating velocity laws ($\beta > 0$), I found that, with the set of parameters adopted here, this occurred for distances close to periastron passage. Unfortunately, the program is not designed to deal with such a situation and I was therefore forced to adopt a constant velocity law. However, for large distances where the shock is not crushed on the surface of the O star, I have compared the shock obtained for constant winds with the one obtained for accelerating winds with β=0.8. The differences were found to be relatively small with the opening angle of the shock surface being only slightly smaller in the case of the accelerating wind. Therefore, adopting constant velocity laws should not have a great influence on the final conclusions. Figure 5.8 presents examples of shock surfaces for a subset of the orbital phases. The position of the stars at each orbital phase is indicated as well as the line of sight of the observer.

This Figure illustrates that, given the present set of parameters, only the spectra obtained at phase Φ=0.472 can be easily explained. Indeed this is the only phase among the ones illustrated in Figure 5.6 for which the observer is looking directly into the lower density cavity formed by the shock surface around the O star. However, it can be shown that reducing the momentum ratio by a reasonable amount increases the opening angle of the shock, therefore allowing this to be true for phases 0.395 and 0.534 as well. However, it is very difficult with this model alone to understand the presence of the high velocity wing in the spectra obtained at phases 0.312 and 0.613. Indeed at these phases, the shock

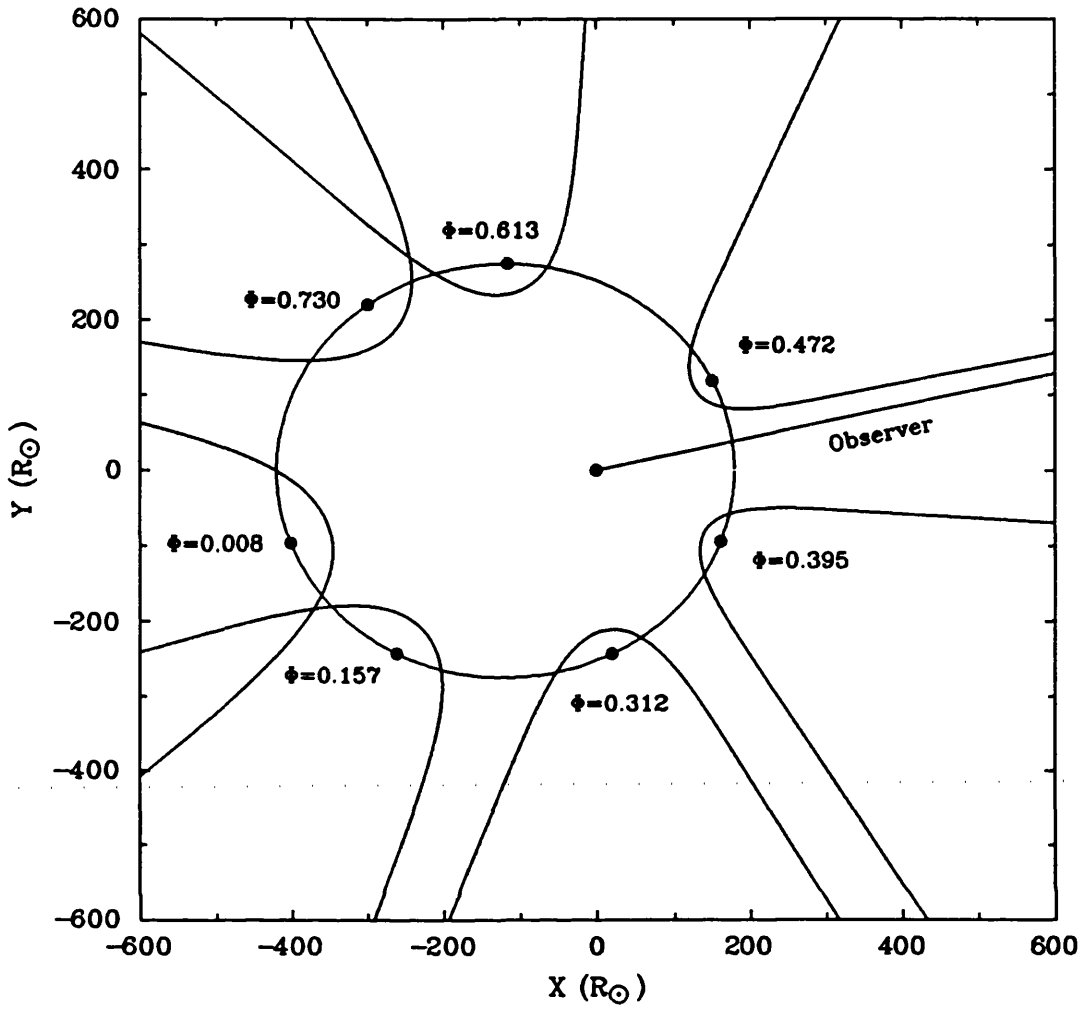

Figure 5.8 : Shock surfaces evaluated by calculating the position of equal ram pressures for a selection of orbital phases. The WR star is at the centre of the system of coordinates and the position of the O star is indicated for each phase. The line of sight of the observer is also indicated.

cone would have to be reversed, implying that the O star would be the star with the highest momentum flux, which is highly unlikely. Using accelerating winds would make matters even worse as the opening of the shock cones would be smaller. However, this model is only a very simple one. Effects such as movement of material *along* the shock surface cannot be evaluated. If there were material moving at very high velocities along the shock front it is possible that absorption would become visible when the observer's line of sight to the O star would intercept the shock surface. This absorption would be visible at

the velocity of the material projected along the line of sight to the observer. It is also difficult to evaluate how the formation of this low density cavity around the O star affects the symmetry of the WR wind emission. Certainly, the emission between the two stars will be disrupted by the formation of the shock surface, which may well lead to effects compatible with the observations described in the last section, but the present model is insufficient to provide a detailed description of the phenomenon taking place.

Williams *et al.* (1990b) have searched for the signature of a collision between the two stellar winds in the form of non-thermal emission at 1100 μm. They have found no evidence for such emission. However, this is not a very strong constraint against the existence of a shock as the geometry at the time the observations were obtained (Φ=0.75) was unfavourable. Indeed at this orbital phase, the absorption by the WR wind is large, which can cause the source to be undetected. These observations should be repeated at an orbital phase where the absorption in the wind is minimized.

Therefore I conclude that considering it's simplicity this interpretation of the appearance of the high velocity wing at phases when the O star is in front of the WR star is fairly successful. However, comparison with theoretical models based on proper hydrodynamic calculations is required to obtain a complete understanding of this very complex situation.

5.3.2.3 *The FeIV Continuum-like Absorption and the CIII] λ1909 Transition.*

The last group of lines includes the continuum-like absorption between $\sim$ 1410–1900 Å and the semi-forbiden transition of C III at 1908.73 Å. As demonstrated when discussing the variations observed in the first group of lines, the absorption in the spectrum at phase 0.0 due to selective eclipses of the O star continuum by the WR wind should be approximately centered on the rest wavelength of the transition, with a width corresponding roughly to twice the terminal velocity of the WR wind. For this group of lines, however, the absorption is found to be significantly blue shifted.

In an attempt to verify if the broad absorption between $\sim$ 1410–1900 Å is indeed due to a large number of FeIV lines, I have constructed a very simple semi-empirical model spectrum by using the experimental wavelengths and intensities for the transitions between the $3d^4 4s - 3d^4 4p$ levels from Ekberg and Edlén (1978). Each of the 561 lines were broadened to a Gaussian profile

and added together to form a broad absorption. I found that in order to fit the observations, the FWHM of the gaussian profiles must be relatively narrow compared to what is expected for selective eclipses and that the entire broad absorption must be blue-shifted. Figure 5.9 shows the adopted model with a gaussian profile width of FWHM=850 km s^{-1} and a shift of -950 km s^{-1} compared to the ratio of the observed spectra at phases 0.0 and 0.5. The model was simply chosen by judging 'by eye' which parameters best fitted the observations. The model was scaled to the observations using a constant value. In order to try to improve the signal to noise of the observations, the two spectra used to produce the ratio in this figure are means consisting of 3 spectra at phase 0.0 (SWP 3139,1605,7200) and 4 spectra at phase 0.5 (SWP 1358,1359,2683,3498). The wavelength range corresponding to the saturated absorption trough of the C IV λ1550 P Cygni profile was removed from the observations due to large spikes caused by taking the ratio of two numbers near zero. As can be seen from the figure, the agreement between the model and the observations is remarkable in view of the simple approach adopted.

Inspection of Figure 5.2 reveals that the C III]λ1909 absorption is also blue shifted. The shift, however, is different with a value of only -600 km s^{-1}. The width of the absorption on the other hand is larger than the one used to model the Fe IV lines, the absorption ranging from ~ -1600 to $+300$ km s^{-1}. Figure 5.10 illustrates the variation of this line for a subset of 6 orbital phases, indicated on the top of each plot, compared to the spectrum obtained at phase 0.532 (SWP 1358). The changes are quite complex with little absorption occurring at positive velocities. Instead, there is a slight excess in the red part of the emission

The behaviour of this last group of lines seems to indicates that the distribution, in the WR wind, of the ions producing these transitions is asymmetric. Only material in front of the WR star, which we observe at negative velocities seems to be absorbing the O star continuum. This may well be another consequence of the formation of the shock front following the collision between the two winds. However, as mentioned in the previous section, the present model for the shock is far too simple to provide any satisfactory explanation. Finally, it is worth mentioning, that a similar effect could also be observed if the ions producing these transitions were only present at radii larger than the

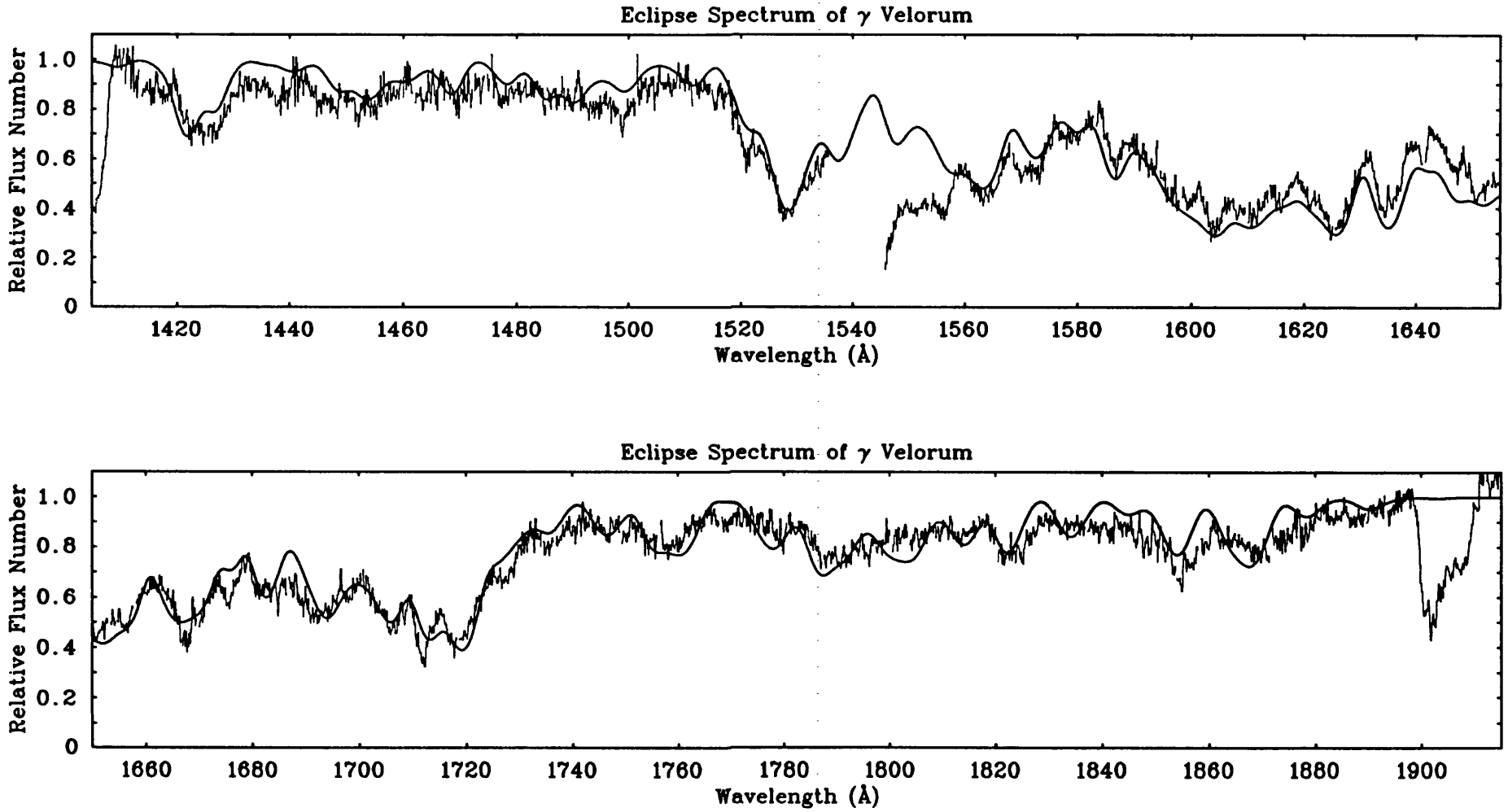

Fig 5.9 : Fe IV Empirical model (thick line) compared to the ratio of SWP spectra at phases 0.0 and 0.5 (thin line).

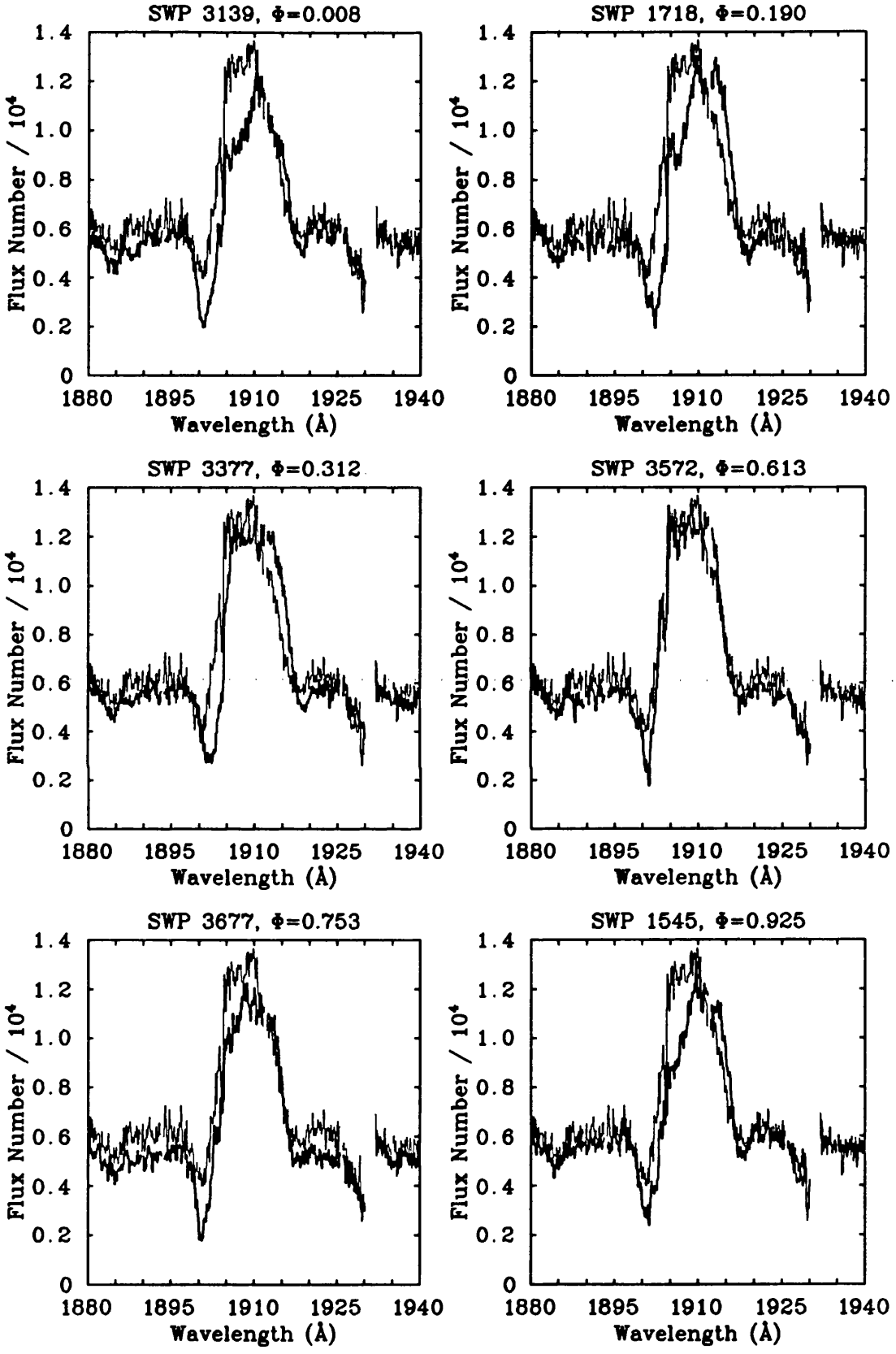

Figure 5.10 : Variations in the CIII]λ1908.73 doublet with orbital phase. The thin line is SWP 1358 (Φ =0.532) and the thick line is the spectrum indicated at the top of each graph.

orbit of the O star (Koenigsberger 1990). However, in the case of the observations described in this section it would be difficult to understand the presence of absorption at low negative velocities and especially the absorption at positive velocities observed in the C III]λ1909 line (-1600 to $+300$ km s^{-1}). With a semi-major axis of 300 $R_\odot$, the material at distances larger than the orbit of the O star is expected to be already moving at relatively high velocities.

5.4 Related Variations in V444 Cygni and CV Serpentis

5.4.1 V444 CYGNI

As briefly mentioned in the last section, changes similar to the ones described here for γ Velorum have been found for the well-known WR+O binary system V444 Cygni. Shore and Brown (1988), in a study of a series of high resolution IUE spectra of this star, concluded that the variations observed in the He II, N IV and C IV P Cygni profiles are evidence of an interaction region separating the winds of the O and WR stars. However, there was no mention in this work of the behaviour of the broad absorption shortward of $\sim$ 1500 Å which is thought to be caused by a large number of Fe V and Fe VI lines. This feature was first mentioned by Koenigsberger and Auer (1985) in a study of a series of low resolution IUE spectra. These low resolution observations do not allow for a detailed study of the absorption as a function of wavelength. In order to determine if the behaviour of these lines is similar to the one found for the Fe IV lines in γ Velorum, I have retrieved a series of high resolution SWP archival spectra of V444 Cygni near phases 0.0 and 0.5 from the World Data Center at the Rutherford Appleton Laboratory. Table 5.6 gives a log of these observations. Listed are the SWP image number, the Julian Date at the beginning of the exposure, the exposure time and the orbital phase calculated from the ephemeris of Cherepashchuk and Khaliullin (1973) (P=4.212424, E_0=2441164.332).

The spectra were extracted from the PHOT images in the same way as the spectra for γ Vel as described in Section 5.2. In order to obtain improved signal-to-noise, means were formed at both orbital phases. The difference of these two spectra is presented in Figure 5.11. The absorptions due to C IV

Table 5.6

IUE SWP High Resolution Archival Spectra of V444 Cygni Near Phases 0.0 and 0.5

SWP Image Number	Julian Date 2440000.000+	Exposure Time (s)	Orbital Phase P=4.212424d
25904	6195.817	12000	0.456
25905	6195.976	12300	0.494
25994	6208.819	12000	0.543
26007	6210.818	12000	0.017
26008	6210.976	12300	0.055
26030	6214.821	12000	0.967
26031	6214.980	12300	0.005
26041	6216.980	12120	0.480

λ1550, He II λ1640 and N IV λ1718 are clearly visible as well as the broad depression between 1250–1500 Å.

I have used experimental intensities and wavelengths of 353 lines of Fe V between the $3d^3 4s$–$3d^3 4p$ levels (Ekberg 1975a) and 121 lines of Fe VI between the $3d^2 4s$–$3d^2 4p$ levels (Ekberg 1975b) to produce a semi-empirical model spectrum. The lines were broadened to a Gaussian profile with a FWHM=1000 km s^{-1} and added together with the Fe VI lines being given a weight of twice that of the Fe V lines. I found that in order to fit the observations, the model had to be shifted by ~ -1100 km s^{-1}. The final model is presented superimposed on the ratio of the mean spectra at phases 0.0 and 0.5 in Figure 5.12. As a reference, the tick marks at the top of the graph indicate the unshifted positions of the Fe V and Fe VI lines, with the length of the tick being proportional to the experimental intensity. As in the case of the Fe IV lines for γ Vel, the agreement is very good.

5.4.2 CV SERPENTIS

CV Serpentis (WC8+O9III–IV) is a well known double-lined spectroscopic binary with an orbital period of 29.7 days. It was first discovered by Hiltner (1945) and a definitive orbit was obtained by Massey and Niemela (1981). There has been several inconsistent reports of eclipses in optical spectroscopy (*cf.* Hiltner 1945) and photometry (*cf.* Gaposchkin 1949). In particular, Hjellming & Hiltner (1963) reported a very deep 0.5 magnitude eclipse; this has never been reobserved and is believed to be an isolated event. For some years, several papers

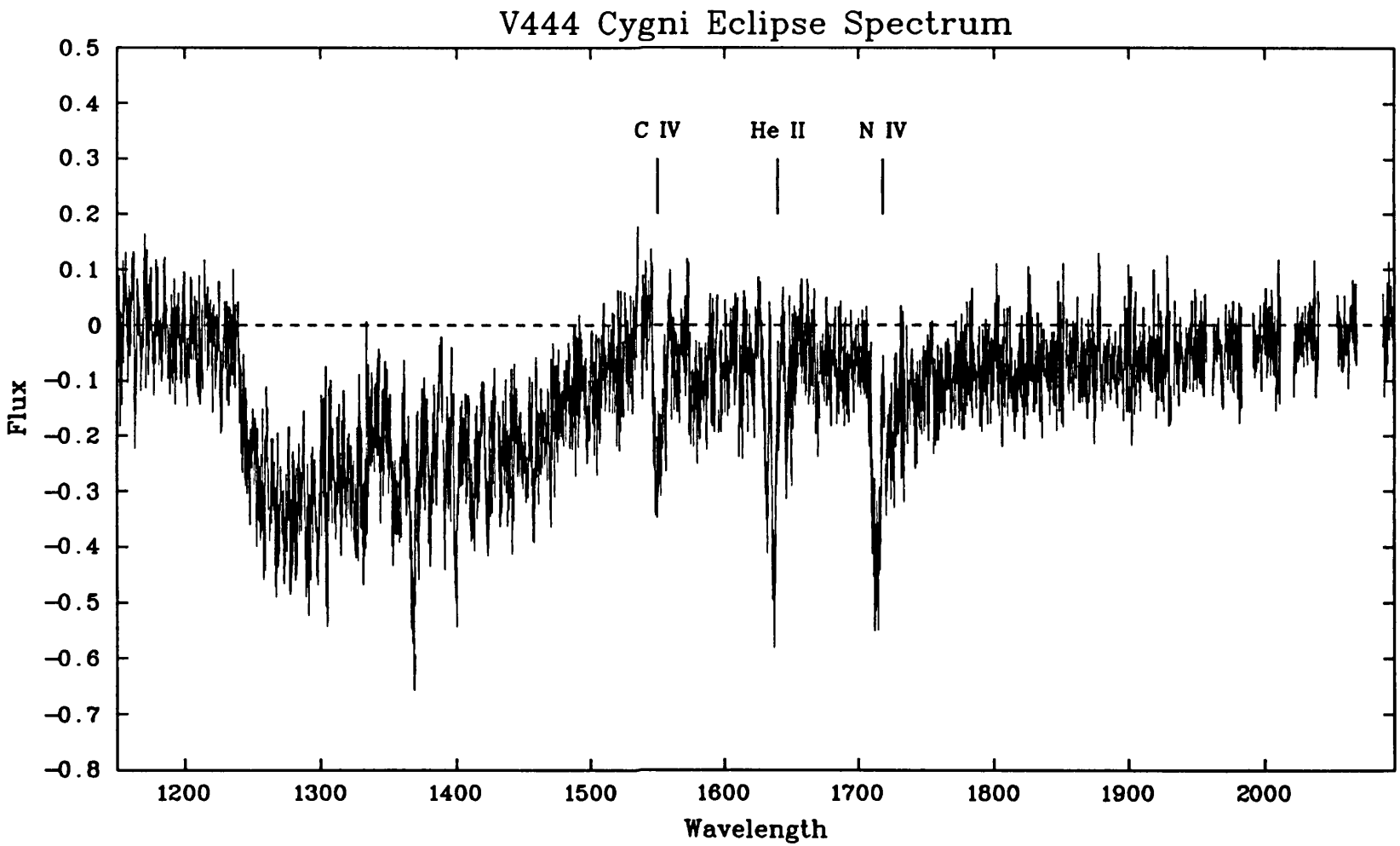

Figure 5.11 : Difference of the mean spectra at phases 0.0 and 0.5

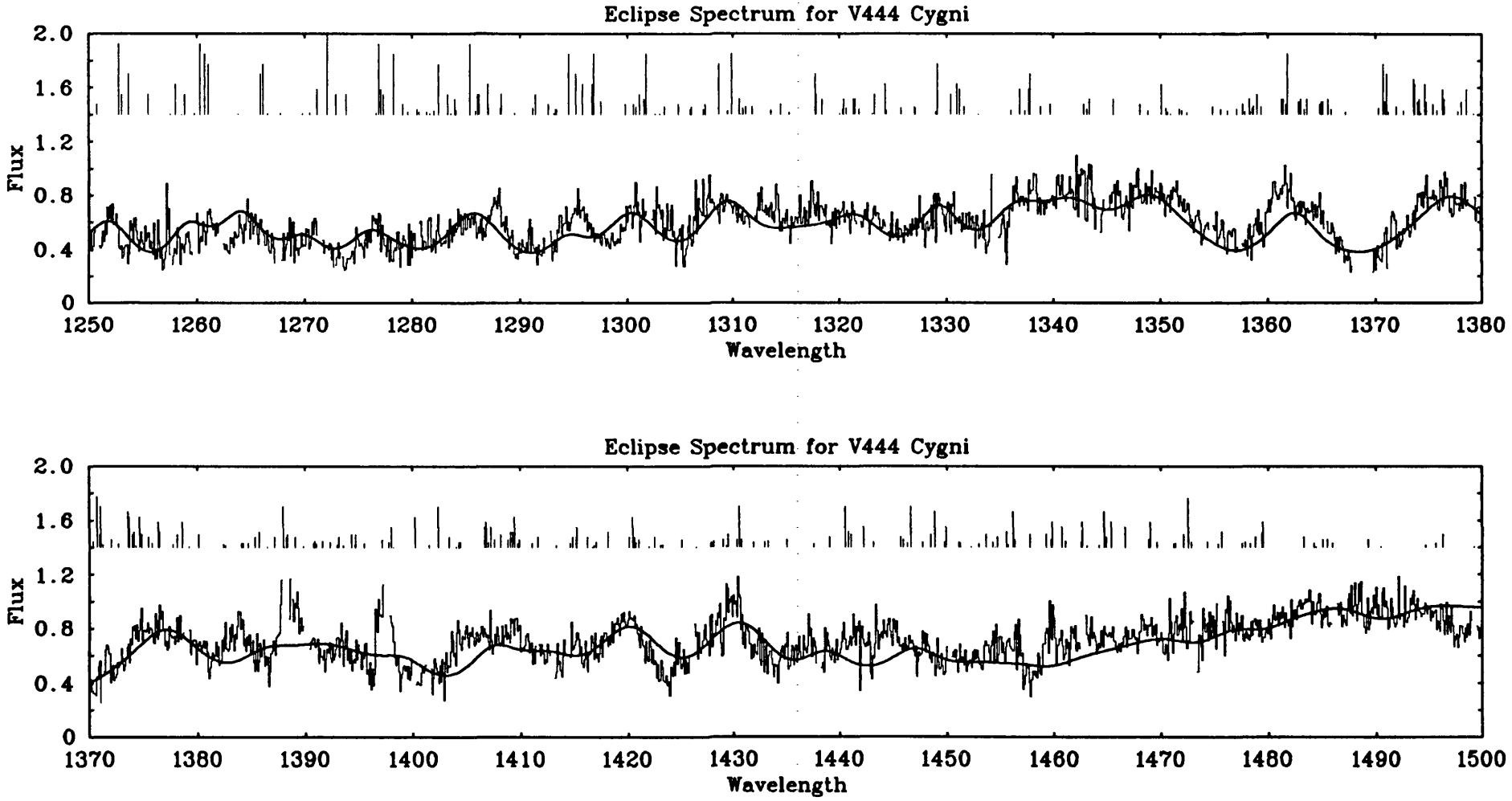

Fig 5.12 : FeV + FeVI empirical model (thick line) compared to the ratio of SWP mean spectra at phases 0.0 and 0.5.

reported that the system had essentially stopped eclipsing (Kuhi & Schweizer (1970), Stepién (1970), Cherepashchuk (1972), Morrison & Wolff (1972) and Schild & Liller (1975)).

Variations associated with atmospheric eclipses of the O star light by the dense WR wind were later found using IUE low resolution spectra by Howarth, Willis & Stickland (1982) and Eaton, Cherepashchuk and Khaliullin (1985b). These changes were discovered in a number of ultraviolet spectral lines such as Si IV λ1400, C IV λ1550 and C III] λ1909 as well as in a broad wavelength band between $\sim$ 1500–1730Å. As for γ Velorum, this broad absorption is associated with a large number of $3d^4 4s$-$3d^4 4p$ Fe IV transitions broadened by the velocity dispersion in the wind and blended together to form an unresolved feature. These low resolution ultraviolet studies included limited details on the velocity structure of the absorption. Therefore, in August 1988 as part of this work, two SWP high resolution spectra were obtained at both orbital conjunctions, with the aim of securing information of this nature. Although the exposure times were long, 428 minutes at phase 0.0 (SWP 34037) and 337 minutes at phase 0.5 (SWP 34121), the spectra are both extremely noisy. Variations are detected in Si IV λ1396, C IV λ1550 and C III]λ1909 transitions as well as in the broad band between $\sim$ 1410–1910 Å.

As in the case of γ Vel I have produced a simple synthetic model spectrum for the broad absorption using the Fe IV experimental wavelength and intensities of Ekberg and Edlén (1978) with each line broadened to a Gaussian profile with FWHM=1000 km s^{-1}. This model is shown in Figure 5.13 superimposed to the ratio of the spectra at phases 0.0 and 0.5. Because of the poor quality of the data, this spectra was smoothed using a Gaussian filter with σ=0.1 and obvious noise spikes have been removed. In order to fit the observations the synthetic spectrum had to be blue-shifted by $\sim$ 1000 km s^{-1}. In this figure, the rest wavelength of the C III λ1908.73 transition is also indicated. It can be seen that this line is also shifted by $\sim$ -1000 km s^{-1} and that the width is similar to that of the Fe IV lines. The resonances doublets of Si IV and C IV have saturated absorption profiles which precludes obtaining a complete velocity profile of the absorption. However, absorption is detected at positive

wavelengths which suggests that the true profile is more symmetric around the rest wavelength of the transition.

In summary, I have found that the eclipse profiles of the C III] λ1909 and Fe IV transitions for CV Serpentis are similar to the ones observed in γ Vel, which suggests a similar origin. Conversely, no high velocity wing appears at phase 0.5 when the O star is in front of the WR star. This may indicate that in this case the interaction of the two stellar winds does not produce a shock but may also be a consequence of similar terminal velocities of the O and WR stellar winds. The spectral type of the O star in this case indicates that its terminal velocity is likely to be smaller than for γ Vel. From Prinja, Barlow and Howarth (1990) the mean terminal velocities for O9 III and O9 V stars are 1875 km s^{-1} and 1365 km s^{-1} respectively. The terminal velocity of the WC8 star is unknown but as it is of the same spectral type as the WR star in γ Vel we can expect a value of $\sim$ 1500 km s^{-1}. Therefore, the second interpretation for the absence of the high velocity wing at phase 0.5 is plausible. It would be interesting to study the behaviour as a function of phase of the well-isolated C III λ2297 transition for CV Serpentis. Unfortunately, up to date, no high resolution IUE spectra has been obtained in the LWP wavelength region.

5.5 Conclusions

The analysis presented in this chapter of the phase-dependent variations observed in the IUE high resolution spectra of γ Velorum has revealed that previous interpretations of these changes were only partially correct. Although it is found that selective eclipses of the O star continuum by the WR wind play an important role in producing the changes, they are insufficient to provide a complete explanation. The appearance of a high velocity wing in the P Cygni absorption components of lines which are seen as wind features in O9 I spectra at phases when the O star companion is in front of the WR star has led to the suggestion that the formation of a shock front following the collision between the two stellar winds is also a vital component for a full understanding of the ultraviolet spectroscopic variations. Finally, it is confirmed that the broad absorption between $\sim$ 1410–1910 Å is due to a large number of Fe IV transitions. However, it was found that the eclipse profile of these lines was significantly blue-shifted suggesting that the distribution of the ions in the WR wind is asymmetric. A blue-shifted eclipse profile was also found for a large number of

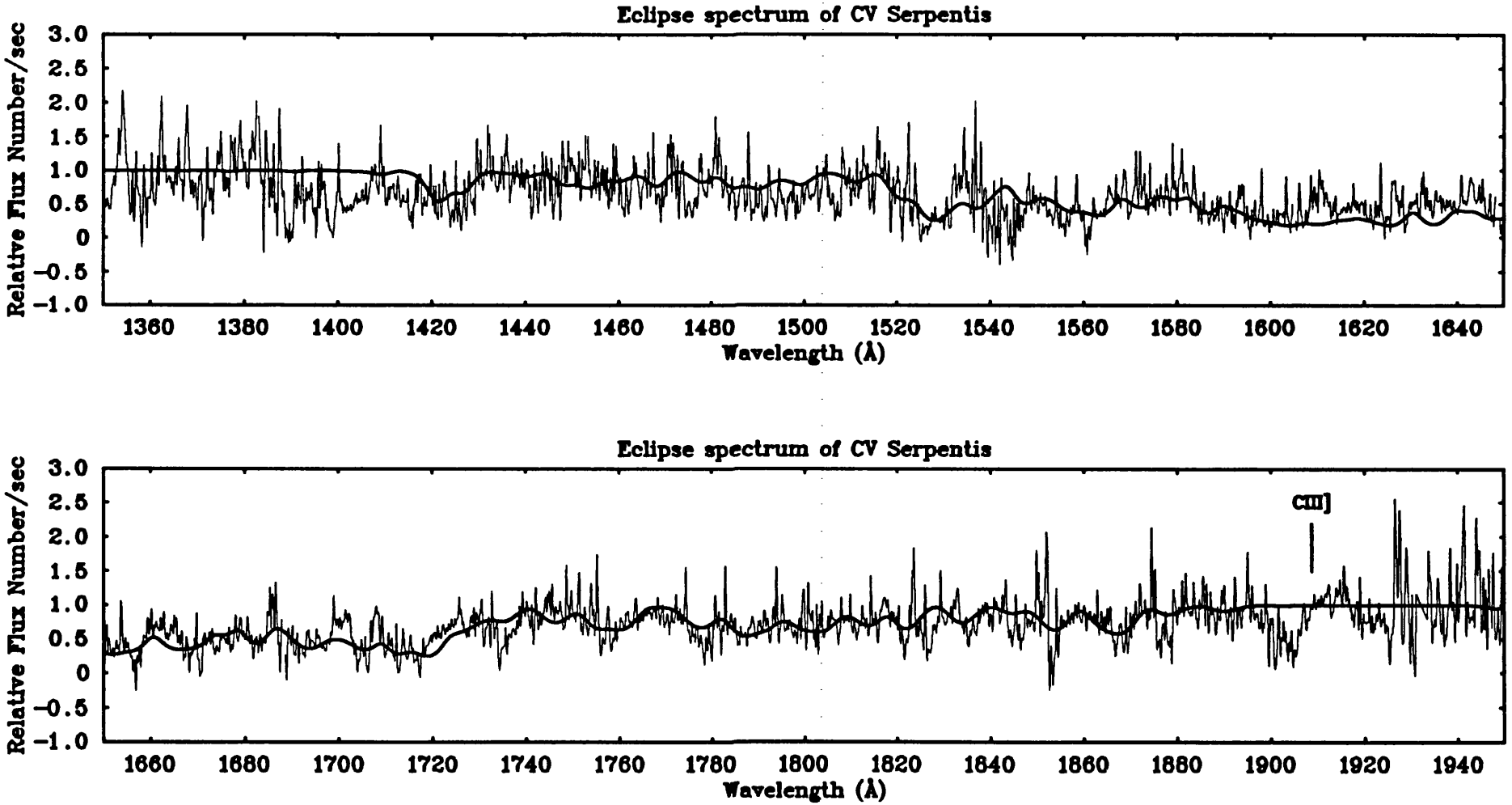

Fig 5.13 : Empirical Fe IV model (thick line) compared to ratio of phase 0.0 and 0.5 spectra

Fe V and Fe VI transitions in the case of V444 Cygni and for Fe IV transitions in CV Serpentis. The similar behaviour of these Fe lines in the eclipse spectra of these three very different WR+O binary systems suggests a common origin. This may well be a consequence of the formation of a shock front although specific details still remain to be determined from a comparison of the observations with proper hydrodynamics calculations. γ Vel does not qualify as a *close* binary system, where interaction effects between the two stellar winds are known to be a common phenomenon. Nevertheless, this study has shown that such effects must not be neglected for these systems as they still can play an important role.

Summary and Future Work

In the first part of this work, the results of an archival search for ultraviolet spectroscopic variability in the spectra of all galactic WR stars observed more than once at high resolution with IUE were presented. A total of 17 stars were included in this study, of which 6 were shown to be variable: WR 6, WR 24, WR 25, WR 40, WR 78 and WR 136. Marginal evidence for variability was also found for two additional stars, WR 23 and WR 111. This result indicates that variability is an ubiquitous phenomenon in the ultraviolet spectra of WR stars, a conclusion which is similar to that of previous studies in the optical, in which a large fraction of WR stars were found to show variability in photometry, spectroscopy and polarimetry. Excluding HD 50896 (WR 6) and HD 192163 (WR 136), discussed in detail in other parts of this work, and HD 96548 (WR 40) studied elsewhere, the available datasets are not very extensive and consequently it was not possible to determine accurately the nature and timescale of the observed changes. It would certainly be of interest to obtain further high resolution IUE observations of these stars, with the specific aim of searching for variability. Previous studies have demonstrated that the best results for this type of investigation are obtained with datasets with a good time resolution and which extend over several days. This allows to properly map out the variability and prevents the introduction of window periodicities in the observations. WR 25 is a particularly good candidate for future ultraviolet spectroscopic variability studies, in view of its exceptionally high X-ray flux and of the variability found in the radial velocities, X-ray flux and linear polarization.

In Chapter 3, a study of 77 high resolution IUE spectra of the WN6+c candidate HD 192163 (WR 136) was presented. Of these spectra, 48 (24 SWP and 24 LWP) were obtained over 48 hours in 1987 and the remaining 29 spectra, obtained from the IUE archive, cover various epochs from 1978–1987. The 1987 series of spectra show significant variability in the N IV λ1718, C IV λ1550 and He II λ1640 P Cygni profiles over a period of 24 hours. Enhanced P Cygni absorption is observed at velocities exceeding the usual maximum wind outflow velocity, as determined from archive spectra. The strength of this excess absorption is observed to increase at the same rate for all three ions and then decrease for N IV and C IV while He II continues to increase in strength. The rise and decay timescales for N IV and C IV are approximately 1 day. Weak variability is

also observed at low outflow velocities for N IV and at high positive velocities for He II and C IV. These features are only observed to increase in strength in contrast to the behaviour of the high negative velocity absorption enhancements. The possible causes of these variations in terms of binary-induced changes due to a compact companion and intrinsic stellar wind variations were considered. All the published optical radial velocity data have been re-analysed and a period of 4.55 days was adopted, although it is questionable whether the variations are periodic. The neutron star hypothesis was tested by computing the expected X-ray luminosity as a function of phase allowing for wind attenuation. It was found that these values are incompatible with the lack of observed X-rays from HD 192163, which suggests that a neutron star is not present. It was also found that the ultraviolet variations do not have the required phase dependence to be caused by the Hatchett and McCray effect and that this effect cannot explain the observed variations at velocities in excess of the normal maximum wind velocity. Therefore, an intrinsic explanation for the observed ultraviolet variability is much more plausible.

In Chapter 4, a similar study of the WN5+compact candidate, HD 50896 (WR 6), was conducted. A total of 130 high resolution IUE spectra, obtained over a period of 6 consecutive days, were analysed. Significant variability was found in the absorption and emission components of the P Cygni profiles of N V λ1240, C IV λ1550, He II λ1640 and N IV λ1718. As for HD 192163, the variations detected in the absorption components were found to be mainly confined to the blue edge, at velocities in excess of the normal outflow velocity of the wind. The changes occur in concert for all lines. As a result of the excellent time resolution of the dataset for this star, it was established that the variability, when it is taking place, not only has a timescale of $\sim$ 1 day but also has a recurrence timescale of a similar value. This is the best measurement so far of the real timescale of the ultraviolet spectroscopic variability for HD 50896. The changes detected in the emission components have a much smaller amplitude than the changes detected in the absorption components and occur on a much longer timescale, of the order of the data string or longer. This clearly indicates that the mechanism causing the variations does not occur on the scale of the wind but is much more localised. The changes detected in the emission component of N IV λ1718 are complex and have a different behaviour from that of the other emission components. Although the variations have a

similar timescale, they do not occur in concert with the changes detected in the C IV λ1550 and He II λ1640 lines. This is explained qualitatively by the fact the N IV line is formed at much smaller radii and by different processes than the C IV and He II lines. The variability is not confined to the strong P Cygni profiles; significant changes have been detected for a series of subordinate transitions, generally attributed to lines of Fe V and Fe VI. Although some similarities exist between the variations detected for these two ions, the Fe V lines have a behaviour that more closely resembles the N IV absorption variations while the Fe VI lines seem to vary with a similar pattern as the N IV emission component. However, this results remains speculative, due to blending effects and insecure identifications of particular transitions. In summary, the variability observed in the ultraviolet spectrum of HD 50896 is complex and cannot be readily explained by the effects of a compact companion orbiting in the WR wind. In particular, the well-determined timescale of the changes detected in the absorption components as well as the fact that the variations occur at velocities in excess of the terminal velocity of the wind, is not compatible with the behaviour predicted by the Hatchett and McCray effect. It is much more likely that the variability is intrinsic to the WR wind.

Therefore for both HD 192163 and HD 50896, an intrinsic interpretation for the variability is preferred. Models incorporating radiatively driven wind instabilities are found to, at least qualitatively, account for the ultraviolet variations that we observe at the highest outflow velocities. In future studies it would be of interest to try to establish if there are any links between the changes observed in the ultraviolet spectra of these stars and variations detected in the optical photometry, spectroscopy and polarimetry. As optical emission lines usually have smaller opacities than the ultraviolet lines, they provide information on the inner parts of the wind. Conversely, the ultraviolet resonance and low-excitation lines have large opacities and therefore provide information on the outermost regions of the wind. Hence, through simultaneous observations in the optical and ultraviolet, we should be able to monitor the propagation of line-driven instabilities or shocks through the wind.

A study of the interstellar medium in the line of sight towards HD 192163 and other stars in Cygnus, using high resolution IUE spectra, has been presented in the latter part of Chapter 3. It was found that this region is dynamically very active. Low, intermediate and high-velocity components, formed in gas

with varying degrees of ionisation, have been detected towards most of the 13 stars in the sample. The resolution of this dataset was insufficient to establish the exact nature and extent of the intermediate velocity gas but it seems likely that it arises in dense, highly-ionised gas expanding away from the Cyg OB1 association. The high-velocity gas is interpreted as arising in an expanding supershell enveloping the Cyg OB1. Previous claims that the high-velocity components observed in the highly-ionised species of C IV λ1550, Si IV λ1396, and Al III λ1854 towards HD 192163 arise in the nebula surrounding the star, NGC 6888, are not supported by this study. The velocities measured in the ultraviolet spectrum do not agree with the velocity of the nebula, obtained from optical emission lines. The supershell is at least 68 pc $\times$ 97 pc in size and could have been produced by a supernova explosion or by the combined stellar winds from the Cyg OB1 association. It would certainly be of interest, in future studies, to establish the extent of the supershell by obtaining IUE high resolution spectra of additional stars in Cygnus. Higher resolution spectra, from future ultraviolet instrumentation such as Lyman/FUSE, would certainly lead to a more detailed description of the various components observed in the line of sight towards the stars in this region.

In the last part of this work, a study of the phase-dependent variations observed in the *Copernicus* and IUE spectra of the well-known WR+O binary γ Velorum has been presented. Although selective eclipses of the O star continuum by the WR wind are confirmed as causing at least part of the variations, they were found to be insufficient to provide a complete explanation. While the velocity range over which the eclipses occur agree relatively well with the range predicted by simple geometric considerations, the amplitude of the variations cannot be readily understood. The appearance of a high-velocity wing in the N V λ1240, Si IV λ1396 and C IV λ1550 P Cygni absorption components are interpreted as being a consequence of the formation of a region of shocked gas, following the collision of the two stellar winds. The approximate shape of the shocked region is evaluated by determining the positions for which the ram pressures of both winds are equal. Considering its simplicity, it is found that this model is fairly successful in reproducing the observed variations. A broad absorption in the eclipse spectrum of γ Vel between $\sim$ 1410–1910 Å is attributed to a large number of Fe IV transitions between the $3d^4 4s - 3d^4 4p$ levels. A simple semi-empirical model spectrum has been constructed by using

experimental wavelengths and intensities. Each line is broadened by a Gaussian profile and all lines are added together to form a broad absorption. It is found that, in order to fit the observations, the model spectrum must be blue-shifted by $\sim$ 850 km s^{-1}. This indicates that the distribution of these ions in the WR wind is asymmetric. This may be a result of the formation of the region of shocked gas which would certainly disrupt the WR wind. However, the model used in this work are too simple to provide a satisfactory explanation. Similar blue-shifted absorptions were observed for the same Fe IV transitions in the WC8+O9 binary CV Serpentis and for a series of Fe V and Fe VI transitions in the WN5+O5 binary V444 Cygni. In future work, it would be of interest to construct a more realistic model spectrum for the Fe IV, Fe V and Fe VI lines by using the newly available oscillator strengths for these transitions (Fawcett 1990) and simple absorption spectroscopy assumptions. Future developments of such model may provide information on the relative abundances of these ions and on excitation conditions in the wind. Futhermore, the advent of the Lyman/FUSE satellite will allow observations in the 200–400 Å wavelength region, which also contains a series of Fe transitions.

References

Abbott, D.C. 1980, *Astrophys. J.*, **242**, 1183 .

Abbott, D.C. 1982, *Astrophys. J.*, **263**, 723 .

Abbott, D.C., Bieging, J.H., and Churchwell, E. 1984, *Astrophys. J.*, **280**, 671 .

Abbott, D.C., Bieging, J.H., Churchwell, E., and Torres, A.V. 1986, *Astrophys. J.*, **303**, 239 .

Abbott, D.C., and Conti, P.S. 1987, *Ann. Rev. Astr. Astrophys.*, **25**, 113 .

Antokhin, I.I., Aslanov, A.A., and Cherepashchuk, A.M. 1982, *Soviet Astron. Lett.*, **8**, 156 .

Antokhin, I.I., and Cherepashchuk, A.M. 1984, *Soviet Astron. Lett.*, **10**, 155 .

Antokhin, I.I., and Cherepashchuk, A.M. 1985, *Soviet Astron. Lett.*, **11**, 355 .

Antokhin, I.I., Kholtygn, A.F., and Cherepashchuk, A.M. 1988, *Sov. Astron.*, **32**, 285 .

Antokhin, I.I., and Volkov, I.M. 1987, *Inf. Bull. Variable Stars*, **2973** .

Aslanov, A.A. 1982, *Astron. Tsirk.*, **1238**, 5 .

Aslanov, A.A., and Cherepashchuk, A.M. 1981, *Soviet Astron. Lett.*, **7**, 265 .

Auer, L.H., Colomé, C., and Koenigsberger, G. 1988, in *A Decade of UV Astronomy with the IUE Satellite*, (ESA SP-281), p193 .

Auer, L.H., and Koenigsberger, G. 1982, *Bull. A. A. S.*, **14**, 634 .

Baade, D. 1988, in *O Stars and Wolf-Rayet Stars*, eds. P.S. Conti, A.B. Underhill, NASA SP-497, p137 .

Balona, L.A., Egan, J., and Marang, F. 1989, *Mon. Not. R. astr. Soc.*, **240**, 103 .

Barbier, M. 1962, *Publ. Obs. Hte-Provence*, **6**, 57 .

Barlow, M.B., Roche, P.F., and Aitken, D.K. 1988, *Mon. Not. R. astr. Soc.*, **239**, 821 .

Baschek, B., and Scholz, M. 1971, *Astr. Astrophys.*, **11**, 83 .

Beals, C.S., and Oke, F.B. 1953, *Mon. Not. R. astr. Soc.*, **113**, 530 .

Bianchi, L., and Bohlin, R. 1983, *ESA/IUE Newsletter*, No 16, p17 .

Bidelman, W.P. 1979, in *Mass Loss and Evolution of O-type stars*, IAU Symposium No. 83, eds. P. S. Conti and C. W. H. de Loore, Reidel, Dordrecht, Holland, p137 .

Bocharev, N.G. 1988, *Nature*, **332**, 518 .

Bocharev, N.G., and Sitnik, T.G. 1985, *Astrophys. Space Sci.*, **108**, 237 .

Boggess, A., *et al.* 1978a, *Nature*, **275**, 2 .

Boggess, A., *et al.* 1978b, *Nature*, **275**, 7 .

Bohlin, R.C. 1975, *Astrophys. J.*, **200**, 402 .

Bohlin, R.C., Savage, B.D., and Drake, J.F. 1978, *Astrophys. J.*, **224**, 132 .

Bouigue, R., Boulon, J., and Pedoussaut, A. 1963, *Ann. Toulouse*, **29**, 17 .

Brand, P.W.J.L., and Zealey, W.J. 1975, *Astr. Astrophys.*, **38**, 363 .

Brandi, E., Ferrer, O.E., and Sahade, J. 1989, *Astrophys. J.*, **340**, 1091 .

Brown, J.C., McLean, I.S., and Emslie, A.G. 1978, *Astr. Astrophys.*, **68**, 415 .

Butler, K., and Storey, P.J., personal communication.

Carlberg, R.G. 1980, *Astrophys. J.*, **241**, 1131 .

Carnochan, D.J. 1982, *Mon. Not. R. astr. Soc.*, **201**, 1139 .

Cash, W., Charles, P., Bowyer, S., Walter, F., Garmire, G., and Reigler, G. 1980, *Astrophys. J. (Letters)*, **238**, L71 .

Castor, J.I., Smith, L.F., and van Blerkom, D. 1970, *Astrophys. J.*, **159**, 1119 .

Cherepashchuk, A.M. 1972, *Soviet Astron. Lett.*, **15**, 955 .

Cherepashchuk, A.M. 1976, *Soviet Astr. Letters*, **2**, 138 .

Cherepashchuk, A.M. 1981, *Mon. Not. R. astr. Soc.*, **194**, 755 .

Cherepashchuk, A.M., and Khaliullin, Kh.F. 1973, *Soviet Astron.*, **17**, 330 .

Chevalier, R.A. 1974, *Astrophys. J.*, **188**, 501 .

Chu, Y.–H. 1988, *Publ. Astr. Soc. Pacif.*, **100**, 986 .

Chu, Y.–H., Treffers, R.R., and Kwitter, K.B. 1983, *Astrophys. J. Suppl.*, **53**, 937 .

Conti, P.S., and Niemela, V.S., and Walborn, N.R. 1979, *Astrophys. J.*, **228**, 206 .

Conti, P.S., Roussel-Dupree, D., Massey, P, and Rensing, M. 1984, *Astrophys. J.*, **282**, 693 .

Conti, P.S., and Smith, L.F. 1972, *Astrophys. J.*, **172**, 623 .

Cowie, L.L., Songaila, A., and York, D.G. 1979, *Astrophys. J.*, **230**, 469 .

Cowie, L.L., Hu, E.M., Taylor, W., and York, D.G. 1981, *Astrophys. J. (Letters)*, **250**, L25 .

Cox, A.N., and Cahn, J.H. 1988, *Astrophys. J.*, **326**, 804 .

Dickel, H.R., Habing, H.J., and Isaacman, R. 1980, *Astrophys. J. (Letters)*, **238**, L39 .

Dickel, H.R., Wendker, H., and Bieritz, J.H. 1969, *Astr. Astrophys.*, **1**, 270 .

Drissen, L., Robert, C., Lamontagne, R., Moffat, A.F.J., and St-Louis, N. 1989, *Astrophys. J.*, **343**, 426 .

Drissen, L., St-Louis, N., Moffat, A.F.J., and Bastien, P. 1987, *Astrophys. J.*, **322**, 888 .

Dufton, P.L., Hibbert, A., Kingston, A.E., and Tully, J.A. 1983, *Mon. Not. R. astr. Soc.*, **202**, 145 .

Dupree, A.K., *et al.* 1980, *Astrophys. J.*, **238**, 969 .

Eaton, J.A., Cherepashchuk, A.M., and Khaliullin, Kh.F. 1985a, *Astrophys. J.*, **297**, 266 .

Eaton, J.A., Cherepashchuk, A.M., and Khaliullin, Kh.F. 1985b, *Astrophys. J.*, **296**, 222 .

Ekberg, J.O. 1975a, *Phys. Scripta*, **12**, 42 .

Ekberg, J.O. 1975b, *Phys. Scripta*, **11**, 23 .

Ekberg, J.O., and Edlen, B. 1978, *Phys. Scripta*, **18**, 107 .

Esteban, C., and Vílchez, J.M. 1991, in *IAU Symposium 143, Wolf-Rayet Stars and Interrelations with Other Massive Stars in Galaxies*, eds. K.A. van der Hucht and B. Hidayat, (Kluwer:Dordrecht), in press. .

Fawcett, B. 1989, *Atomic Data and Nuclear Data Tables*, **41**, 181 .

Firmani, C., Koenigsberger, G., Bisiacchi, G.F., Moffat, A.F.J., Isserstedt, J. 1980, *Astrophys. J.*, **239**, 607 .

Friend, D.B., and Abbott, D.C. 1986, *Astrophys. J.*, **311**, 701 .

Ganesh, K.S., and Bappu, M.K.V. 1968, *Kodaikanal Obs. Bull.*, No. 183 .

Gaposchkin, S. 1949, *Peremennye Zvezdy*, **7**, 36 .

van Genderen, A.M., van der Hucht, K.A., and Larsen, I. 1990, *Astr. Astrophys.*, **229**, 123 .

van Genderen, A.M., van der Hucht, K.A., and Steemers, W.J.G. 1987, *Astr. Astrophys.*, **185**, 131 .

Giaretta, D., Mead, J.M., and Benvenuti, P. 1987, in *Exploring the Universe with the IUE Satellite*, ed. Y. Kondo, D. Reidel, p. 759 .

Giddings, J.R. 1983, *ESA IUE Newsletter*, No. 17, p. 53 .

Giddings, J.R., and Rees, P.C.T. 1989, *SERC Starlink User Note*, No 37.7 .

Girard, T., and Willson, L.A. 1987, *Astr. Astrophys.*, **183**, 247 .

Giuliani, J.L. 1982, *Astrophys. J.*, **256**, 624 .

Grevesse, N. 1984, *Phys. Scripta.*, **T8**, 49 .

Hatchett, S.P., and McCray, R. 1977, *Astrophys. J.*, **211**, 552 .

Hernández, C.A., and Sahade, J. 1980, *Publ. Astr. Soc. Pacif.*, **92**, 819 .

van den Heuvel, E.P.J. 1976, in *IAU Symposium No. 73*, eds P. Eggleton *et al.*, p35 .

Hibbert, A., Dufton, P.L., Murray, M.J., and York, D.G. 1983, *Mon. Not. R. astr. Soc.*, **205**, 535 .

Hillier, D.J. 1984, *Astrophys. J.*, **280**, 744 .

Hillier, D.J. 1987, *Astrophys. J. Suppl.*, **63**, 965 .

Hillier, D.J. 1988, *Astrophys. J.*, **327**, 822 .

Hiltner, W.A. 1945, *Astrophys. J.*, **102**, 492 .

Hiltner, W.A. 1949, *Astrophys. J.*, **110**, 95 .

Hiltner, W.A. 1956, *Astrophys. J. Suppl.*, **2**, 389 .

Hjellming, R.M. and Hiltner, W.A. 1963, *Astrophys. J.*, **137**, 1080 .

Hogg, D.E. 1989, *Astron. J.*, **98**, 282 .

Howarth, I.D., and Murray, J 1990, *SERC Starlink User Note*, No 50 .

Howarth, I.D., and Phillips, A.P. 1986, *Mon. Not. R. astr. Soc.*, **222**, 809 .

Howarth, I.D., and Prinja, R.K. 1989, *Astrophys. J. Suppl.*, **69**, 527 .

Howarth, I.D., Willis, A.J., and Stickland, D. 1982, in *3rd European IUE Conference*, Esa Sp-176, p331 .

Huber, M.C.E., Nussbaumer, H., Smith, L.J., Willis, A.J., and Wilson, R. 1979, *Nature*, **278**, 697 .

van der Hucht, K.A., Conti, P.S., Lundström, I., and Stenholm, B. 1981, *Space Sci. Rev.*, **28**, 227 .

van der Hucht, K.A., Hidayat, B., Admiranto, A.G., Supelli, K.R., and Doom, C. 1988, *Astr. Astrophys.*, **199**, 217 .

Humphreys, R. M. 1978, *Astrophys. J. Suppl.*, **38**, 309 .

Ikhsanov, R.N. 1961, *Soviet Astronomy - A.J.*, **4**, 923 .

Jeffers, S.J., Stiff, T., and Weller, W.G. 1985, *Astron. J.*, **90**, 1852 .

Jenkins, E.B. 1978a, *Astrophys. J.*, **219**, 845 .

Jenkins, E.B. 1978b, *Astrophys. J.*, **220**, 107 .

Jenkins, E.B. 1986, *Astrophys. J.*, **304**, 739 .

Jenkins, E.B., Savage, B.D., and Spitzer, L. 1986, *Astrophys. J.*, **301**, 355 .

Kallman, T.R., and McCray, R. 1982, *Astrophys. J. Suppl.*, **50**, 263 .

Koenigsberger, G. 1990, *Astr. Astrophys.*, **235**, 282 .

Koenigsberger, G., and Auer, L.H. 1985, *Astrophys. J.*, **297**, 255 .

Koenigsberger, G., Firmani, C., and Bisiacchi, G.F. 1980, *Rev. Mexicana Astron. Astrofiz.*, **5**, 45 .

Koenigsberger, G., Moffat, A.F.J., and Auer, L.H. 1987, *Astrophys. J. (Letters)*, **322**, L41 .

Koenigsberger, G., Moffat, A.F.J., and Auer, L.H. 1988, in *A decade of UV Astronomy with the IUE Satellite*, Vol. 1, ESA SP-281, p197 .

de Kool, M., and de Jong, T. 1985, *Astr. Astrophys.*, **149**, 151 .

Kopal, Z., and Shapley, M.B. 1946, *Astrophys. J.*, **104**, 160 .

Kuhi, L.V. 1968, *Astrophys. J.*, **152**, 89 .

Kuhi, L.V., and Schweizer, F. 1970, *Astrophys. J. (Letters)*, **160**, L185 .

Lafler, K., and Kinman, T.D. 1965, *Astrophys. J. Suppl.*, **11**, 199 .

Lamers, H.J.G.L.M., de Groot, M, and Cassatella, A. 1983, *Astr. Astrophys.*, **128**, 299 .

Lamers, H.J.G.L.M., Snow, T.P., de Jager, C., and Langerwerf, A. 1988, *Astrophys. J.*, **325**, 342 .

Lamontagne, R. 1983, *Ph.D. Thesis*, Université de Montréal .

Lamontagne, R., and Moffat A.F.J. 1987, *Astron. J.*, **94**, 1008 .

Lamontagne, R., Moffat, A.F.J., and Lamarre, A. 1986, *Astron. J.*, **91**, 925 .

Lamontagne, R., Moffat, A.F.J., and Seggewiss, W. 1984, *Astrophys. J.*, **277**, 258 .

Lamontagne, R., Robert, C., Grandchamps, A., Lapierre, N., Moffat, A.F.J., Drissen, L., and Shara, M. 1991, in Proc. IAU Symposium 143, *Wolf-Rayet Stars and Interrelations with Other Massive Stars in Galaxies*, eds. K.A. van der Hucht and B.Hidayat, (Kluwer: Dordrecht), in press .

Lassettre, E.N., and Skerbele, A. 1971, *J. Chem. Phys.*, **54**, 1957 .

Laurent, C., Paul, J.A., and Pettini, M. 1982, *Astrophys. J.*, **260**, 163 .

Losinskaya, T.A., and Sitnik, T.G. 1988, *Sov. Astron. Lett.*, **14**, 100 .

Lucy, L.B. 1982, *Astrophys. J.*, **255**, 278 .

Lucy, L.B. 1983, *Astrophys. J.*, **274**, 372 .

Lucy, L.B. 1984, *Astrophys. J.*, **284**, 351 .

Lucy, L.B., and White, R.L. 1980, *Astrophys. J.*, **241**, 300 .

Luna, H.G. 1982, *Publ. Astr. Soc. Pacif.*, **94**, 695 .

Lundström, I. and Stenholm, B. 1984, *Astr. Astrophys. Suppl.*, **35**, 303 .

Luo, D., McCray, R., and MacLow, M.-M. 1990, *Astrophys. J.*, **362**, 267 .

MacGregor, K.B., Hartmann, L., and Raymond, J.C. 1979, *Astrophys. J.*, **231**, 514 .

Maeder, A. 1985, *Astr. Astrophys.*, **147**, 300 .

Marston, A.P., and Meaburn, J. 1988, *Mon. Not. R. astr. Soc.*, **235**, 391 .

Martin, P.G. 1978, in *Cosmic Dust*, Oxford University Press, Oxford. .

Massey, P., Niemela, V.S. 1981, *Astrophys. J.*, **245**, 195 .

Matthews, J.M., and Beech, M. 1987, *Astrophys. J. (Letters)*, **313**, L25 .

McCandliss, S.R. 1988, *Ph. D. Thesis*, University of Colorado .

McDonald, J.K. 1947, *Publs. Dominion astr. Obs.*, **7**, 311 .

McLean, I.S. 1980, *Astrophys. J. (Letters)*, **236**, L149 .

Moffat, A.F.J. 1977, *Astr. Astrophys.*, **57**, 151 .

Moffat, A.F.J. 1978, *Astr. Astrophys.*, **68**, 41 .

Moffat, A.F.J. 1982, in *IAU Symposium No. 99*, eds. C. de Loore and A.J. Willis, Reidel, Dordrecht, p263 .

Moffat, A.F.J. 1983, in Paris Workshop on *WR Stars; Progenitors of Supernovae ?*, eds M.C. Lortet and A. Pitault (Observatoire de Paris, Meudon) p VII.19 .

Moffat, A.F.J., Drissen, L., Lamontagne R., and Robert, C. 1988, *Astrophys. J.*, **334**, 1038 .

Moffat, A.F.J., Firmani, C., McLean, I.S., and Seggewiss, W. 1982, in *IAU Symposium No. 99*, eds. C. de Loore and A.J. Willis, (Reidel: Dordrecht, p577 .

Moffat, A.F.J., and Isserstedt, J. 1980, *Astr. Astrophys.*, **91**, 147 .

Moffat, A.F.J., Koenigsberger, G., and Auer, L.H. 1989, *Astrophys. J.*, **344**, 734 .

Moffat, A.F.J., Lamontagne, R., Williams, P.M., Horn, J., and Seggewiss, W. 1987, *Astrophys. J.*, **312**, 807 .

Moffat, A.F.J., and Robert, C. 1991, in IAU Symposium 143, *Wolf-Rayet Stars and Interrelations with Other Massive Stars in Galaxies*, eds K.A. van der Hucht and B. Hidayat, (Kluwer: Dordrecht), in press .

Moffat, A.F.J., and Seggewiss, W. 1978, *Astr. Astrophys.*, **70**, 69 .

Moffat, A.F.J., and Shara, M.M. 1986, *Astron. J.*, **92**, 952 .

Moffat, A.F.J., Vogt, N., Paquin, G., Lamontagne, R., and Barrera, L.H. 1986, *Astron. J.*, **91**, 1386 .

Monderen, P., De Loore, C.W.H., van der Hucht, K.A., and van Genderen, A.M. 1988, *Astr. Astrophys.*, **195**, 179 .

Morrison, N.D., and Wolff, S.C. 1972, *Publ. Astr. Soc. Pacif.*, **84**, 635 .

Morton, D.C. 1975, *Astrophys. J.*, **197**, 85 .

Morton, D.C, 1978, *Astrophys. J.*, **222**, 863 .

Morton, D.C., and Smith, W.H. 1973, *Astrophys. J. Suppl.*, **26**, 333 .

Morton, D.C., York, D.G., and Jenkins, E.B. 1988, *Astrophys. J. Suppl.*, **68**, 449 .

Nicolet, B. 1978, *Astr. Astrophys. Suppl.*, **34**, 1 .

Niemela, V.S., and Mendez, R.H. 1982, in *Proc. IAU Symp. No 99*, eds C. de Loore and A.J. Willis, (D Reidel), p295 .

Niemela, V.S., and Sahade, J. 1980, *Astrophys. J.*, **238**, 244 .

Noels, A., and Scuflaire, R. 1986, *Astr. Astrophys.*, **161**, 125 .

Nussbaumer, H., Pettini, M., and Storey, P.J. 1981, *Astr. Astrophys.*, **102**, 351 .

Owocki, S.P., Castor, J.I., and Rybicki, G.B. 1988, *Astrophys. J.*, **335**, 914 .

Owocki, S.P., Poe, C.H., and Castor, J.I. 1990, in *Properties of Hot Luminous Stars*, ed. C.D. Garmany (San Francisco: ASP), p283 .

Owocki, S.P., and Rybicki, G.B. 1984, *Astrophys. J.*, **284**, 337 .

Owocki, S.P., and Rybicki, G.B. 1985, *Astrophys. J.*, **299**, 265 .

Pauldrach, A., Puls, J., Hummer, D.G., and Kudritzki, R.P. 1985, *Astr. Astrophys.*, **148**, L1 .

Pérez, M.R., Oliversen, N., Garhart, M., and Teays, T. 1991, in *IUE in the ERA of New Space Missions*, ESA Sp-310, in press .

Phillips, A.P., Welsh, B.Y., and Pettini, M. 1984 (PWP), *Mon. Not. R. astr. Soc.*, **206**, 55 .

Piirola, V., and Linnaluoto, S. 1988, in *Polarized Radiation of Circumstellar Origin*, eds. G.V. Coyne *et al.* (Vatican: Vatican Observatory), p655 .

Pike, C.D., Stickland, D.J., and Willis, A.J. 1983, *The Observatory*, **103**, 154 .

Poe, C.H., Owocki, S.P., and Castor, J.I. 1990, *Astrophys. J.*, **355**, in press .

Pollock, A.M.T. 1987, *Astrophys. J.*, **320**, 283 .

Pollock, A.M.T. 1989, *Astrophys. J.*, **347**, 409 .

Pollock, A.M.T., Blondin, J.M., and Stevens, I.R. 1991, in Proc. IAU Symposium 143, *Wolf-Rayet Stars and Interrelations with Other Massive Stars in Galaxies*, eds. K.A. van der Hucht and B.Hidayat, (Kluwer: Dordrecht), in press .

Pottash, S.R. 1972, *Astr. Astrophys.*, **20**, 245 .

Prilutskii, O.F., and Usov, U.V. 1976, *Soviet Astr.*, **210**, 236 .

Prinja, R.K., Barlow, M.J., and Howarth, I.D. 1990, *Astrophys. J.*, **361**, 607 .

Prinja, R.K., and Howarth, I.D. 1986, *Astrophys. J. Suppl.*, **61**, 357 .

Prinja, R.K., and Howarth, I.D. 1988, *Mon. Not. R. astr. Soc.*, **233**, 123 .

Robert, C., and Moffat, A.F.J. 1989, *Astrophys. J.*, **343**, 902 .

Robert, C., Moffat, A.F.J., Bastien, P., Drissen, L., and St-Louis, N. 1989, *Astrophys. J.*, **347**, 1034 .

Robert, C., Moffat, A.F.J., Bastien, P., St-Louis, N., and Drissen, L. 1990, *Astrophys. J.*, **359**, 211 .

Rogerson, J.B., Spitzer, L., Drake, J.F., Dresler, K., Jenkins, E.B., Morton, D.C., and York, D.G. 1973, *Astrophys. J. (Letters)*, **181**, L97 .

Routly, P.M., and Spitzer, L. 1952, *Astrophys. J.*, **115**, 227 .

Sahade, J. 1955, *Publ. Astr. Soc. Pacif.*, **67**, 348 .

Sahade, J., and Zorec, J. 1981, *Mem. Soc. Astr. Italiana*, **52**, 23 .

St-Louis, N., Drissen, L., Moffat, A.F.J., Bastien, P., and Tapia, S. 1987, *Astrophys. J.*, **322**, 870 .

St-Louis, N., Moffat, A.F.J., Drissen, L., Bastien, P., and Robert, C. 1988, *Astrophys. J.*, **330**, 286 .

Savage, B.D., Bohlin, R.C., Drake, J.F., and Budich, W. 1977, *Astrophys. J.*, **216**, 291: .

Scargle, J.D. 1982, *Astrophys. J.*, **263**, 835 .

Schild, R., and Liller, W. 1975, *Astrophys. J.*, **199**, 432 .

Schmidt, G.D. 1988, in *Polarized Radiation of Circumstellar Origin*, eds G. V. Coyne et al. (Vatican: Vatican Observatory), p641 .

Schmutz, W., Hamann, W.-R., snd Wessolowski, U. 1989, *Astr. Astrophys.*, **210**, 236 .

Schulte-Ladbeck, R.E. 1989, *Astron. J.*, **97**, 1471 .

Schulte-Ladbeck, R.E., and van der Hucht, K.A. 1989, *Astrophys. J.*, **337**, 872 .

Schulte-Ladbeck, R.E., Nordsieck, K.H., Nook, M.A., Magalhães, A.M., Taylor, M., Bjorkman, K.S., and Anderson, C.M. 1990, *Astrophys. J. (Letters)*, submitted .

Seggewiss, W. 1974, *Publ. Astr. Soc. Pacif.*, **86**, 670.

Seggewiss, W. and Moffat, A.F.J. 1979, *Astr. Astrophys.*, **72**, 332.

Shore, S.N., and Brown, D.N. 1988, *Astrophys. J.*, **334**, 1021 .

Shull, J.M., and Van Steenberg, M.E. 1985, *Astrophys. J.*, **294**, 599 .

Siluk, R.S., and Silk, J. 1974, *Astrophys. J.*, **192**, 51 .

Smith, H.J. 1955, *Ph.D. Dissertation*, Harvard University, p72 .

Smith, L.F. 1968, *Mon. Not. R. astr. Soc.*, **140**, 409 .

Smith, L.J., Lloyd, C., and Walker, E.N. 1985, *Astr. Astrophys.*, **146**, 307 .

Smith, L.J., Pettini, M., Dyson, J.E., and Hartquist, T.W. 1988, *Mon. Not. R. astr. Soc.*, **234**, 625 .

Smith, L.J., Willis, A.J., Garmany, C.D., and Conti, P.S. 1986, in *New Insights in Astrophysics — 8 years of UV Astronomy with IUE*, ESA Sp-263, p. 389 .

Smith, L.J., Willis, A.J., and Wilson, R. 1980, *Mon. Not. R. astr. Soc.*, **191**, 339 .

Stepién, K. 1970, *Acta Astr.*, **20**, 13 .

Stevens, I.R. 1988, *Mon. Not. R. astr. Soc.*, **232**, 199 .

Stevens, I.R., and Willis, A.J. 1988, *Mon. Not. R. astr. Soc.*, **234**, 783 .

Stickland, D.J., and Harvey, A.S. 1987, *SERC Starlink User Note*, No. 58 .

Stickland, D.J., and Lloyd, C. 1990, *The Observatory*, **110**, 1 .

Strömgren, B. 1948, *Astrophys. J.*, **108**, 242 .

Turner, D.G. 1982, in *Proc. IAU Symp. No 99*, eds C. de Loore and A.J. Willis, (D Reidel), p27 .

Underhill, A.B., Gilroy, K.K., Hill, G.M., and Dinshaw, N. 1990, *Astrophys. J.*, **351**, 666 .

Vanbeveren, D., Van Rensbergen, W., and de Loore, C. 1982, *Astr. Astrophys.*, **115**, 69 .

Van Steenberg, M.E., and Shull, J.M. 1988, *Astrophys. J.*, **330**, 942 .

Vreux, J.-M. 1985, *Publ. Astr. Soc. Pacif.*, **97**, 274 .

Vreux, J.-M. 1987, in Proc. Workshop in Honour of C. de Jager, *Instabilities in Luminous Early Type Stars*, eds H. Lamers and C. de Loore (Dordrecht: Reidel), p81 .

Vreux, J.M., Andrillat, Y., and Gosset, E. 1985, *Astr. Astrophys.*, **149**, 337 .

Vreux, J.-M., Magain, P., Manfroid, J. and Scuflaire, R. 1987, *Astr. Astrophys.*, **180**, L17 .

Walborn, N.R. 1971, *Astrophys. J. Suppl.*, **23**, 257 .

Walborn, N.R. 1972, *Astron. J.*, **77**, 312 .

Walborn, N.R., Heckathorn, J.N., and Hesser, J.E. 1984, *Astrophys. J.*, **276**, 524 .

Walborn, N.R., and Nichols-Bohlin, J. 1987, *Publ. Astr. Soc. Pacif.*, **99**, 40 .

Walborn, N.R., Nichols-Bohlin, J., and Panek, R.J. 1985, *NASA Reference Publication*, No 1155 .

Weaver, R., McCray, R., Castor, J, Shapiro, P., and Moore, R. 1977, *Astrophys. J.*, **218**, 377 .

White, R.L., and Long, K.S. 1986, *Astrophys. J.*, **310**, 832 .

Williams, P.M., Beattie, D.H., Lee, T.J., Stewart, J.M., and Antonopoulou, E. 1978, *Mon. Not. R. astr. Soc.*, **185**, 467 .

Williams, P.M., van der Hucht, K.A., Pollock, A.M.T., Florkowski, D.R., van der Woerd, H., and Wamsteker, W.M. 1990a, *Mon. Not. R. astr. Soc.*, **243**, 662: .

Williams, P.M., van der Hucht, K.A., Sandell, G., and Thé, P.S. 1990b, *Mon. Not. R. astr. Soc.*, **244**, 101 .

Williams, P.M., van der Hucht, K.A., van der Woerd, H., Wamsteker, W.M., Geballe, T.R, Garmany, C.D., and Pollock, A.M.T. 1987, in *Instabilities in Luminous Early Type Stars*, eds. H.J.G.L.M Lamers and C.W.H. De Loore (Dordrecht: Reidel), p221 .

Williams, P.M., and Smith, M.G. 1985, IAU Circular, No 4056 .

Willis, A.J. 1982, *Mon. Not. R. astr. Soc.*, **198**, 897 .

Willis, A.J., Howarth, I.D., Conti, P.S., Garmany, C.D. 1986a, in *IAU Symp. No 116*, eds. C. de Loore, A. J. Willis, P. Laskarides, D Reidel, p. 259 .

Willis, A.J., Howarth, I.D., Smith, L.J., Conti, P.S., and Garmany, C.D. 1989, *Astr. Astrophys. Suppl.*, **77**, 269 .

Willis, A.J., van der Hucht, K.A., Conti, P.S., and Garmany, C.D. 1986b, *Astr. Astrophys. Suppl.*, 63: 417 .

Willis, A.J., and Wilson, R. 1976, *Astr. Astrophys.*, **47**, 429 .

Willis, A.J., Wilson, R., Macchetto, F., Beeckmans, F., van der Hucht, K.A., and Stickland, D.J. 1979, in *The first year of IUE*, ed. A.J. Willis (University College London), p304 .

Woltjer, L. 1974, in *Supernova and Supernova Remnants*, ed C.B. Cosmovici, (Reidel:Dordrecht), p323 .

APPENDIX

An Atlas of High Resolution IUE Spectra for 28 Galactic Wolf-Rayet Stars

Table A1

An Atlas of High Resolution IUE Spectra of 28 Galactic Wolf-Rayet Stars

WR Number	HD Number	Spectral Type	v Magnitude	E(B-V)†	SWP	LWR	LWP	Figure Number
2	6327	WN 2	11.33	0.48	1			A1
6	50896	WN 5	6.94	0.24	16		3	A2-A3
8	62910	WN 6 - WC 4	10.56	0.82	1	1		A4-A5
10	65865	WN 4.5	11.08	0.57	1			A6
14	76536	WC 6	9.42	0.51	4			A7
16	86161	WN 8	8.43	0.63	1			A8
22	92740	WN 7 + abs (SB1)	6.44	0.28	6	3		A9-A10
23	92809	WC 6	9.71	0.38	4	3		A11-A12
24	93131	WN 7 + abs	6.49	0.24	28	2		A13-A14
25	93162	WN 7 + abs	8.17	0.68	5	1		A15-A16
40	96548	WN 8	7.85	0.46	4		4	A17-A18
52	115473	WC 5	9.98	0.51	1			A19
57	119078	WC 7	10.11	0.59	3			A20
69	136488	WC 9	9.43	0.67	1		1	A21-A22
71	143414	WN 6	10.22	0.41	1			A23
77	150136	WC 8	13.16	1.19		1		A24
78	151932	WN 7	6.61	0.52	16	4	3	A25-A26
90	156385	WC 7	7.45	0.23	4	3		A27-A28
92	157451	WC 9	10.60	0.57	1		2	A29-A30
103	164270	WC 9	9.01	0.53	2	1		A31-A32
111	165763	WC 5	8.23	0.30	2	2*		A33-A34
128	187282	WN 4	10.54	0.32	2			A35
134	191765	WN 6	8.23	0.58	14	2		A36-A37
135	192103	WC 8	8.36	0.42	3	2		A38-A39
136	192163	WN 6	7.65	0.59	31		35	A40-A41
138	193077	WN 6 + abs	8.10	0.63	6		1	A42-A43
148	197406	WN 7 (SB1)	10.46	0.76			1	A44
155	214419	WN 7 (SB1)	8.75	0.76	1	1		A45-46

† E(B–V)=1.212 E(b–v), from Turner (1982).

* LWR 10490 was not included in the mean spectrum due to its poor quality.

Figure A1 : WR 2 (HD 6327), WN 2, v=11.33

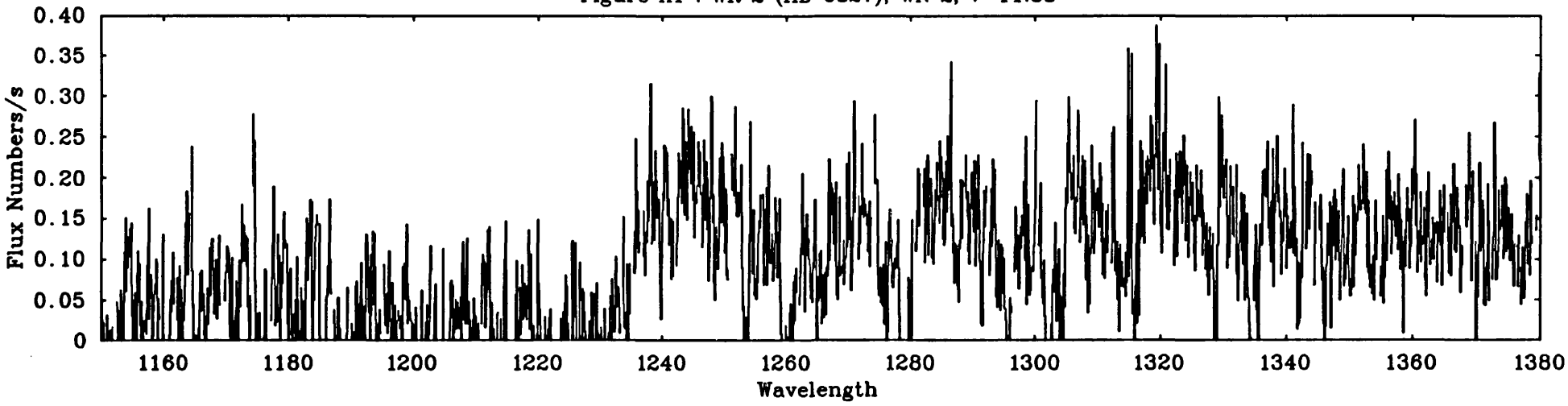

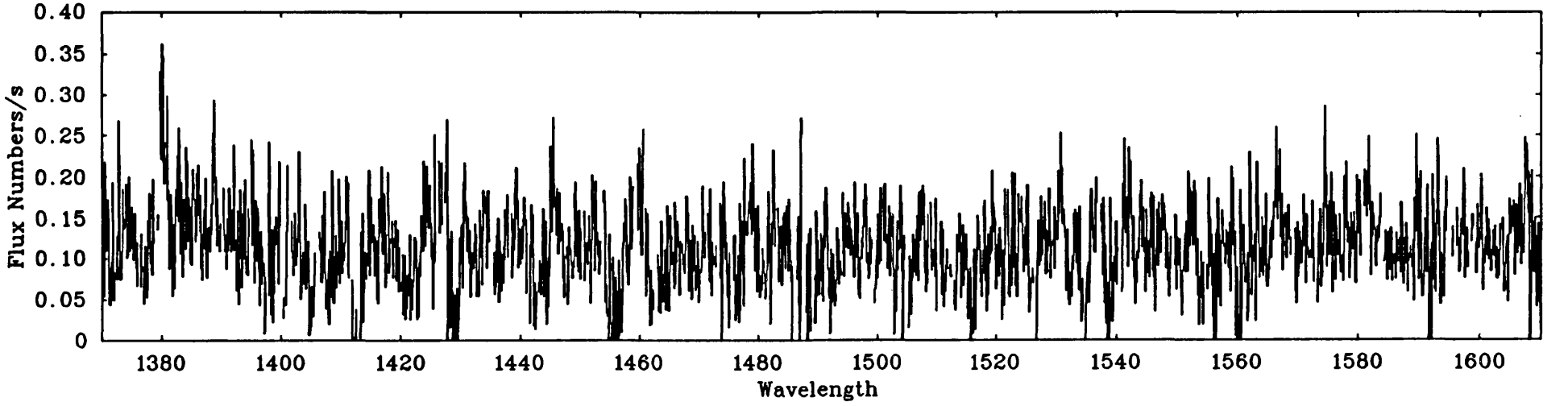

Figure A1 (continued) : WR 2 (HD 6327), WN 2, v=11.33

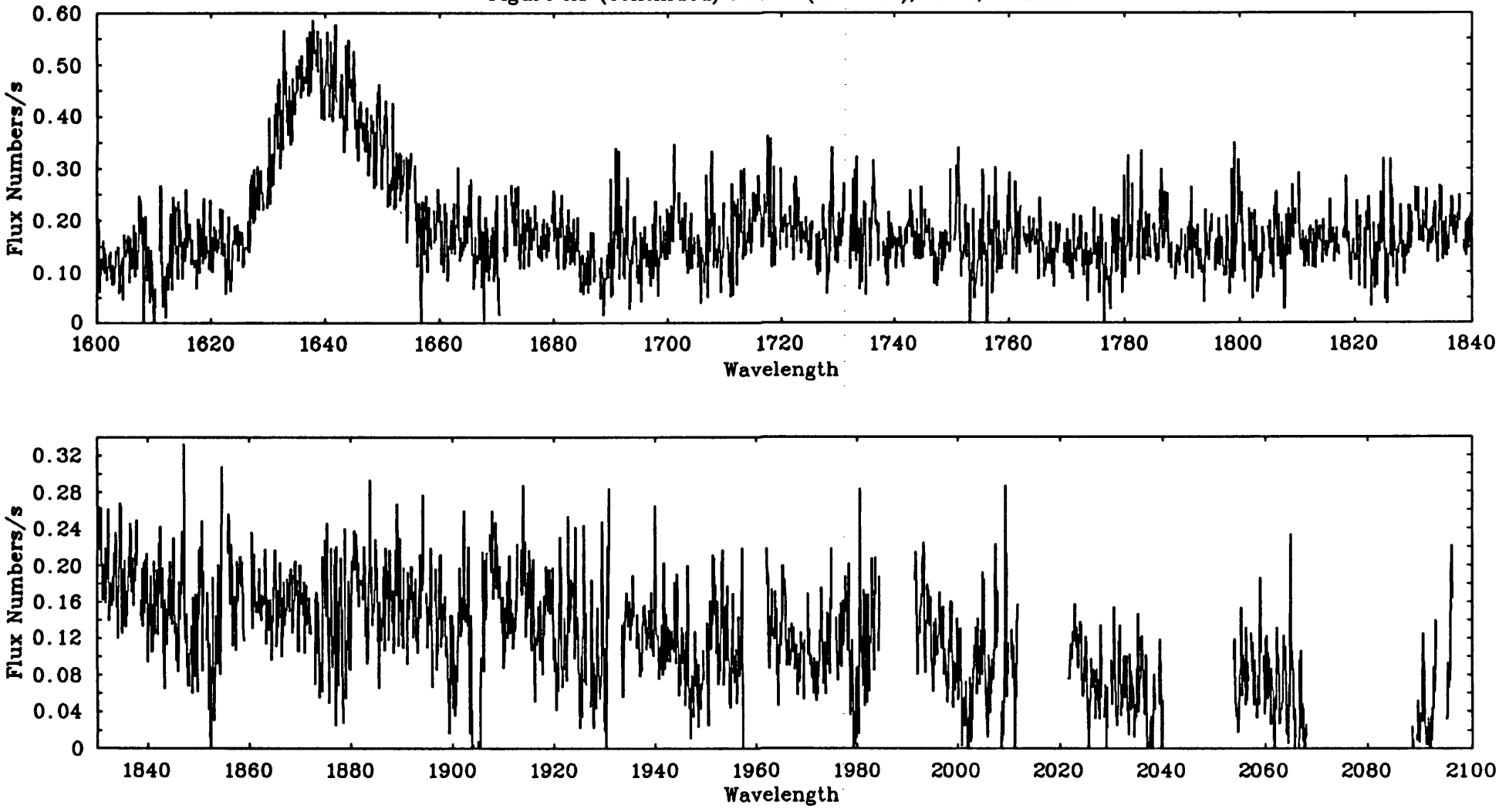

Figure A2 : WR 6 (HD 50896), WN 5, v=6.94

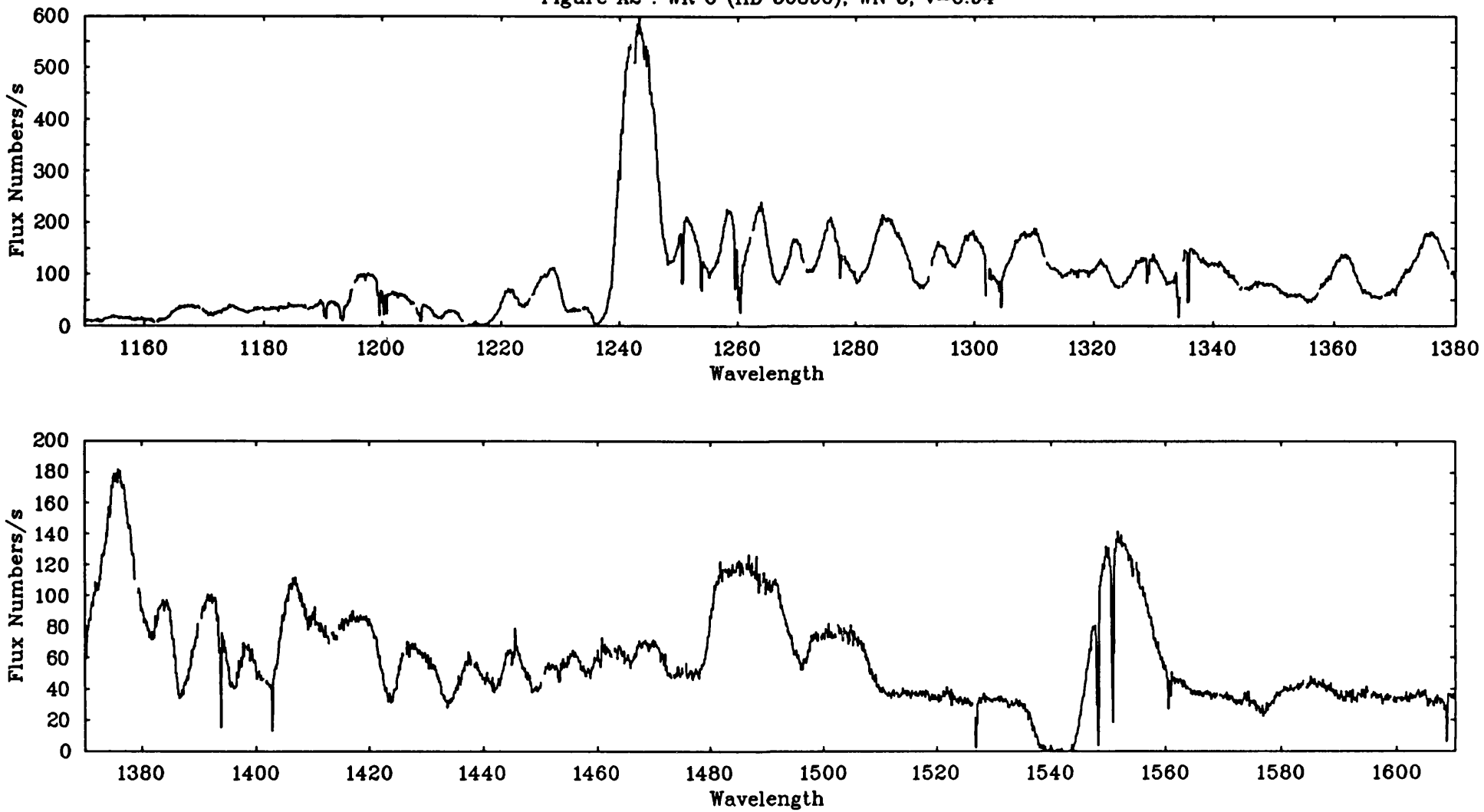

Figure A2 (continued) : WR 6 (HD 50896), WN 5, v=6.94

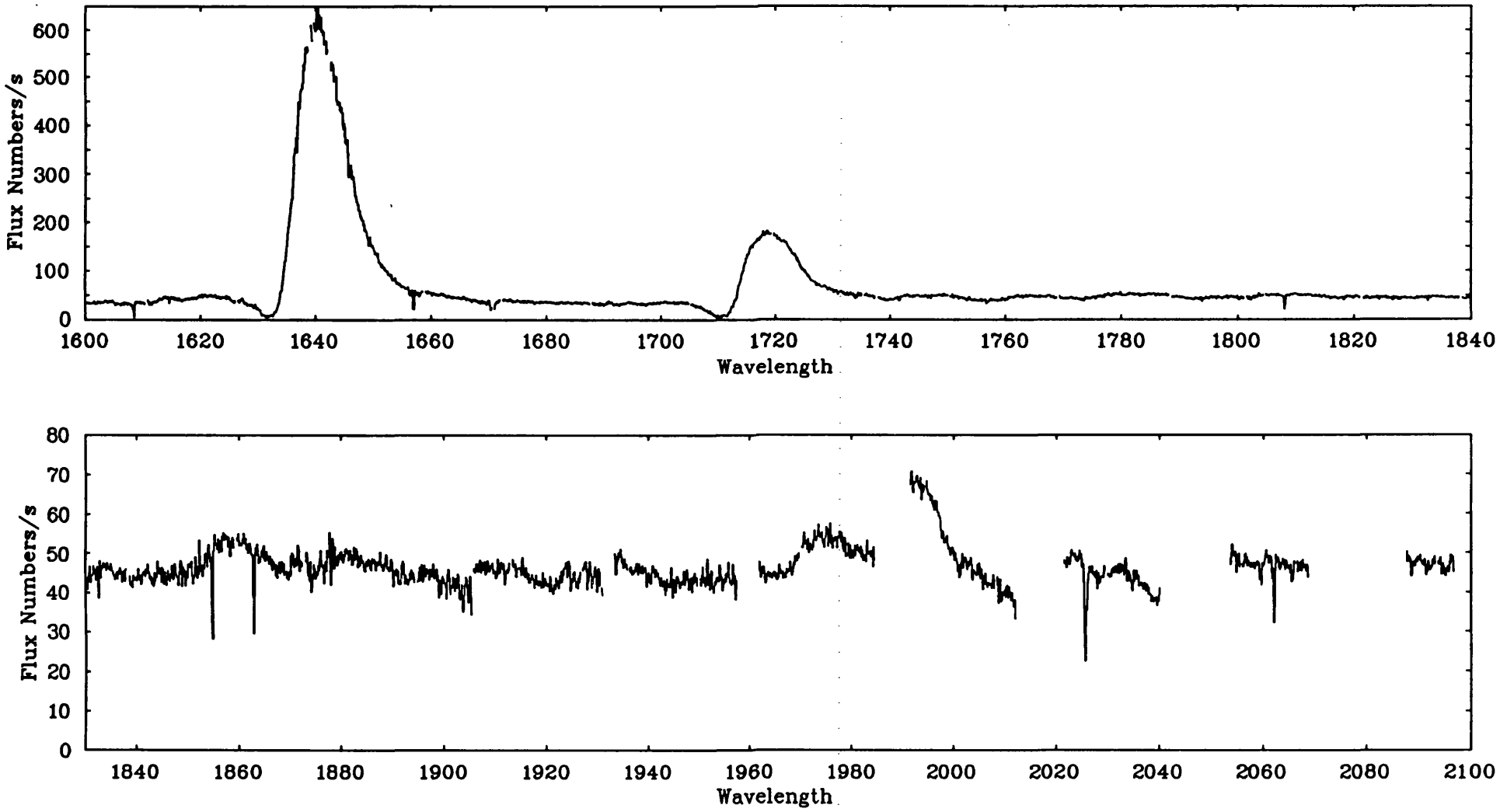

Figure A3 : WR 6 (HD 50896), WN 5, v=6.94

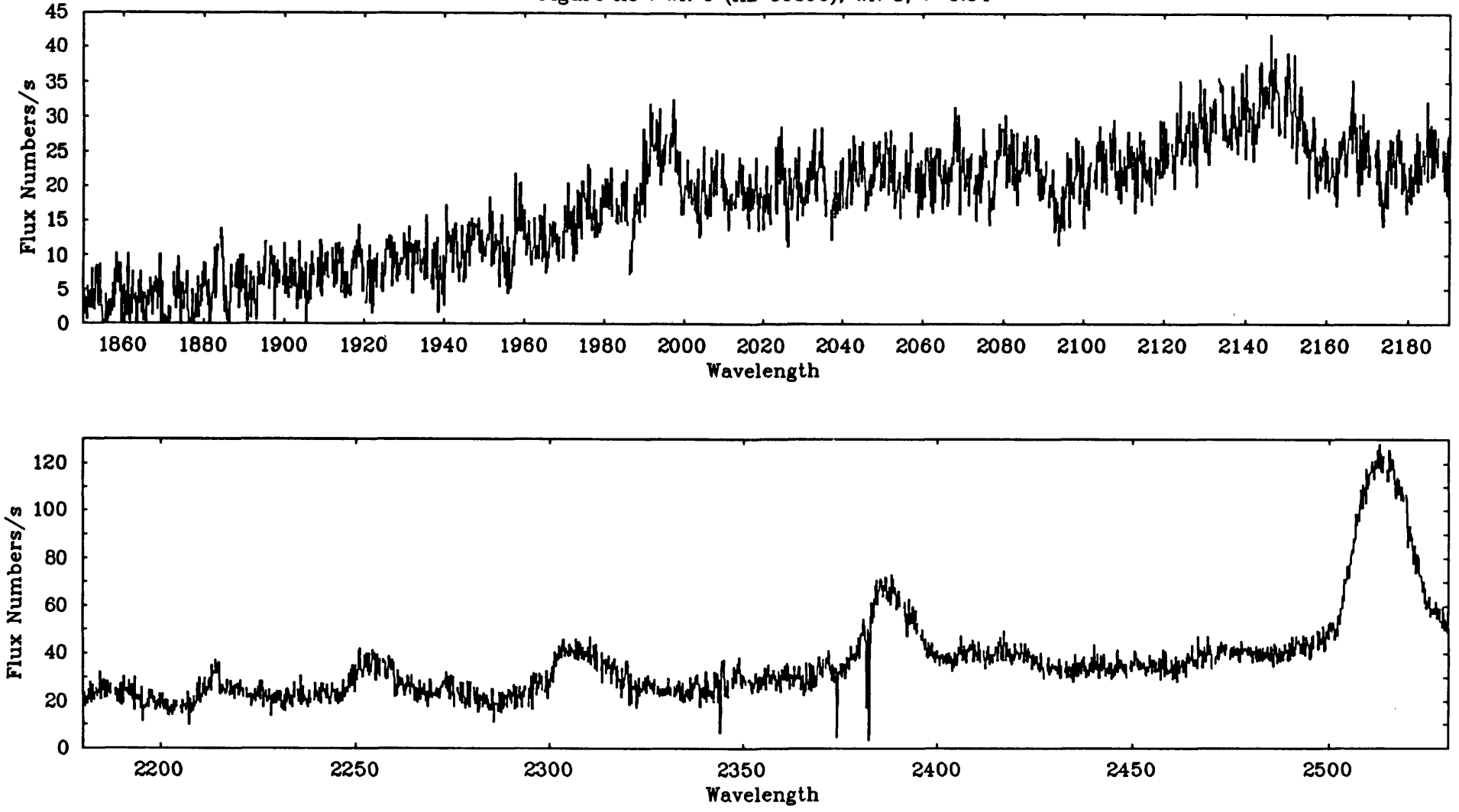

Figure A3 (continued) : WR 6 (HD 50896), WN 5, v=6.94

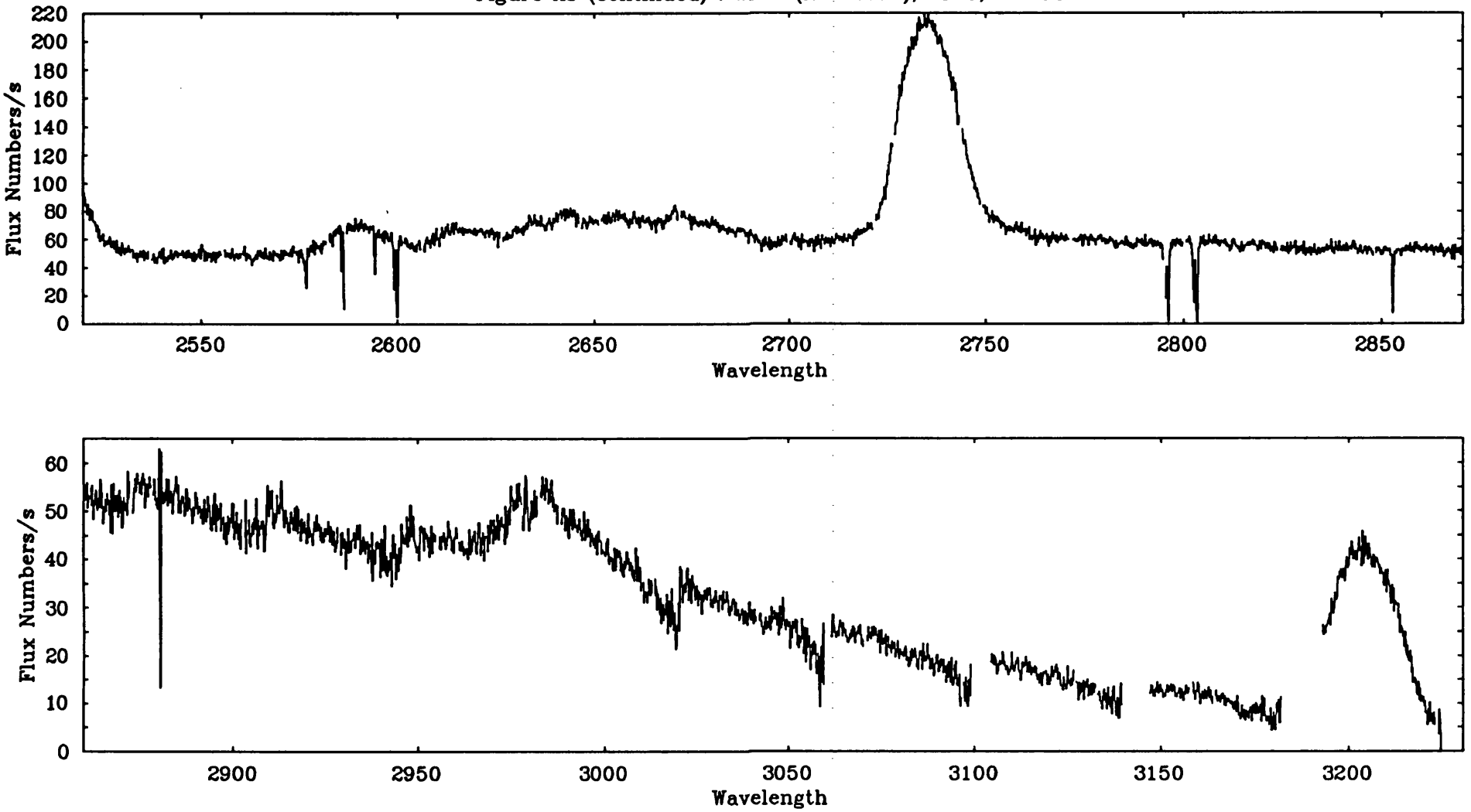

Figure A4 : WR 8 (HD 62910), WN 6 – WC 4, v=10.56

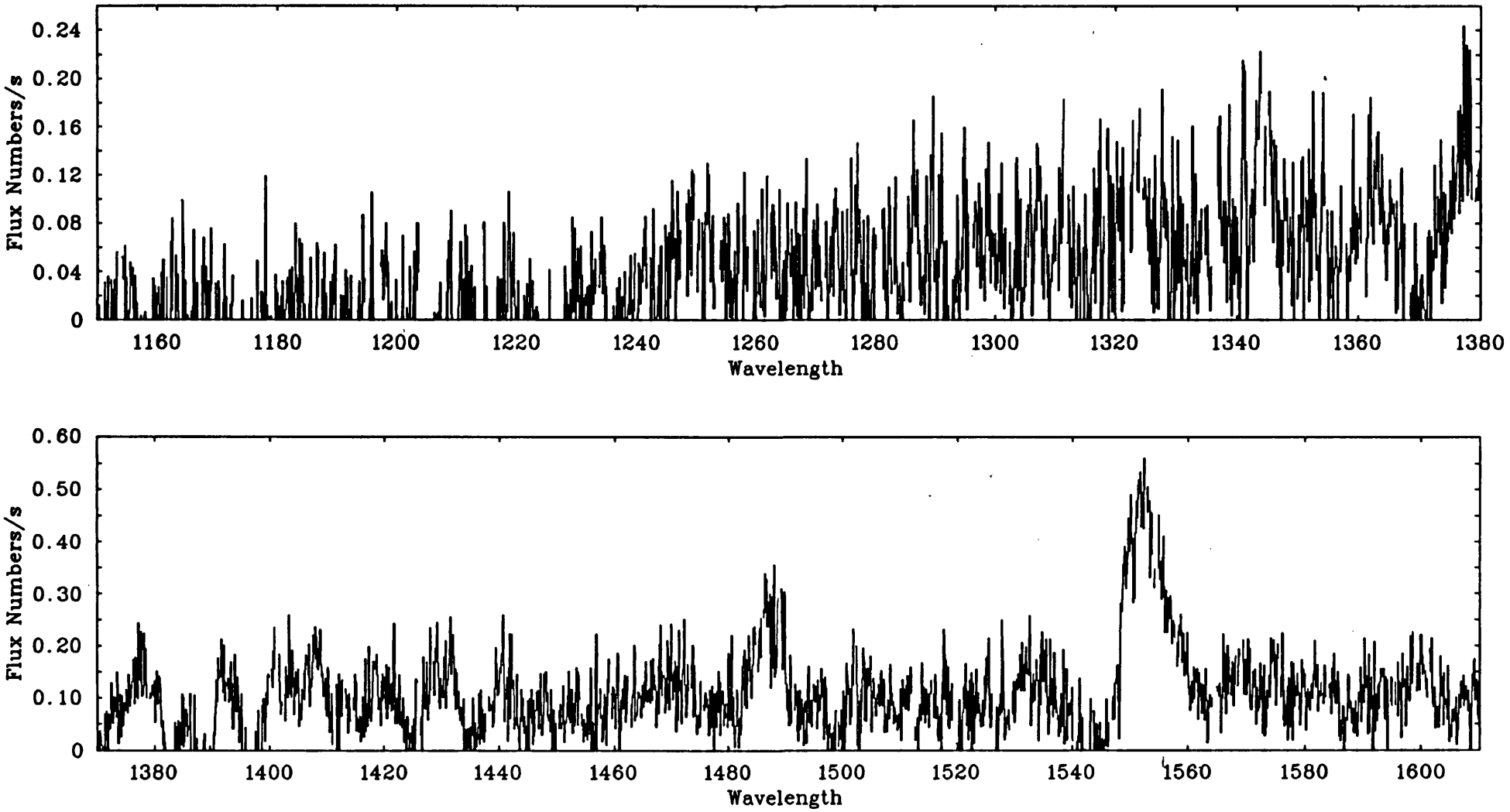

Figure A4 (continued) : WR 8 (HD 62910), WN 6 – WC 4, v=10.56

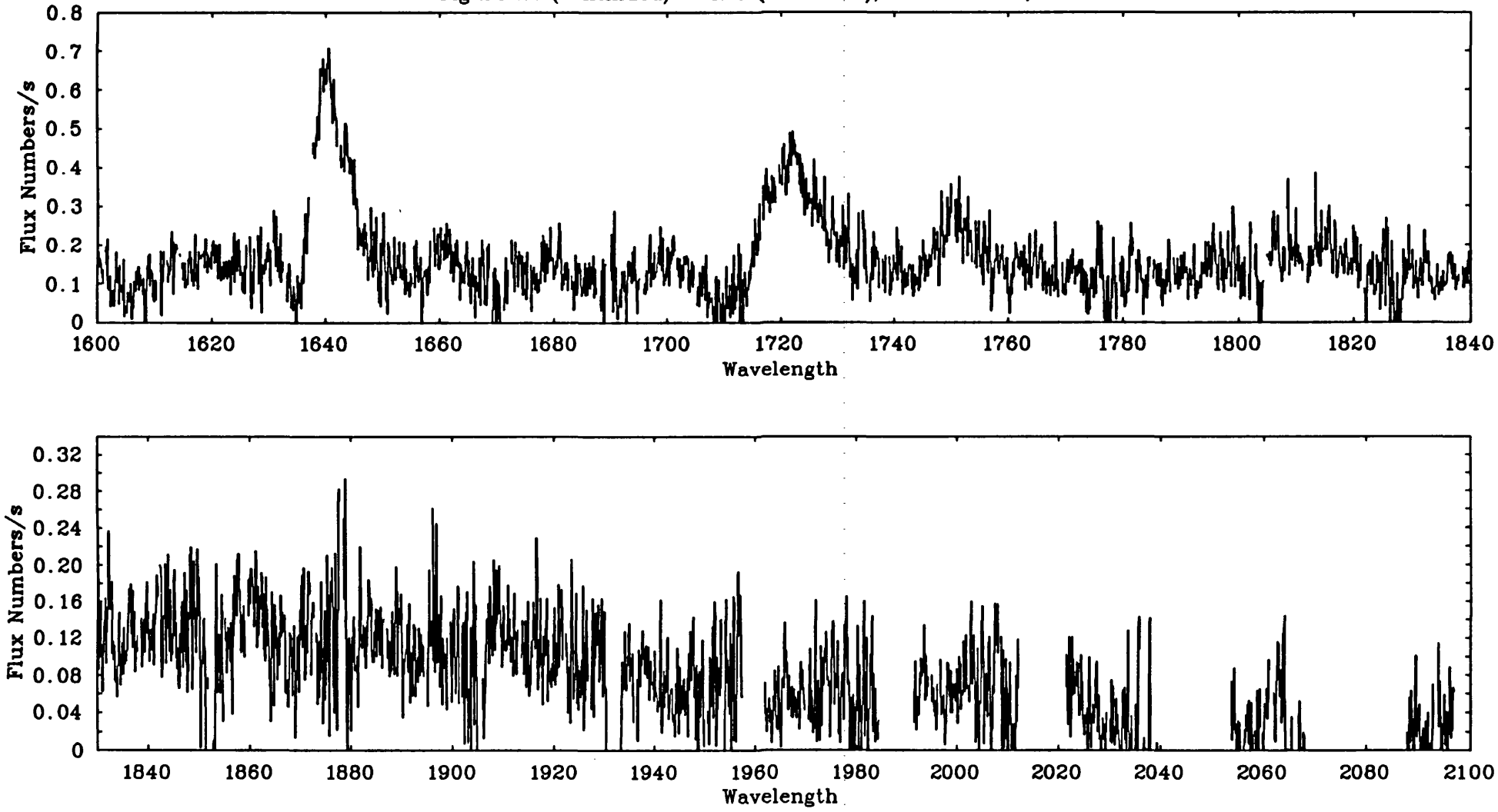

Figure A5 : WR 8 (HD 62910), WN 6 – WC 4, v=10.56

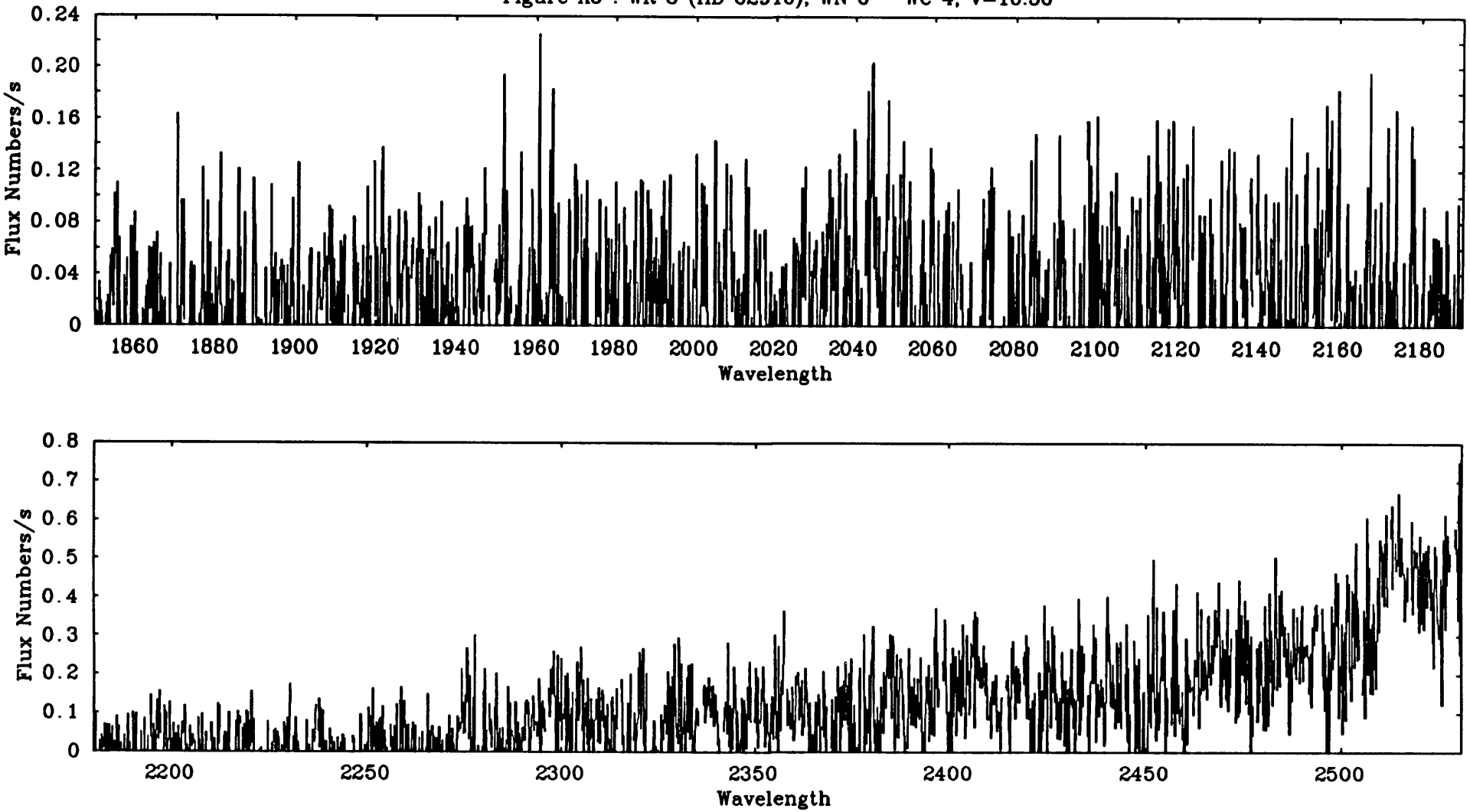

Figure A5 (continued) : WR 8 (HD 62910), WN 6 - WC 4, v=10.56

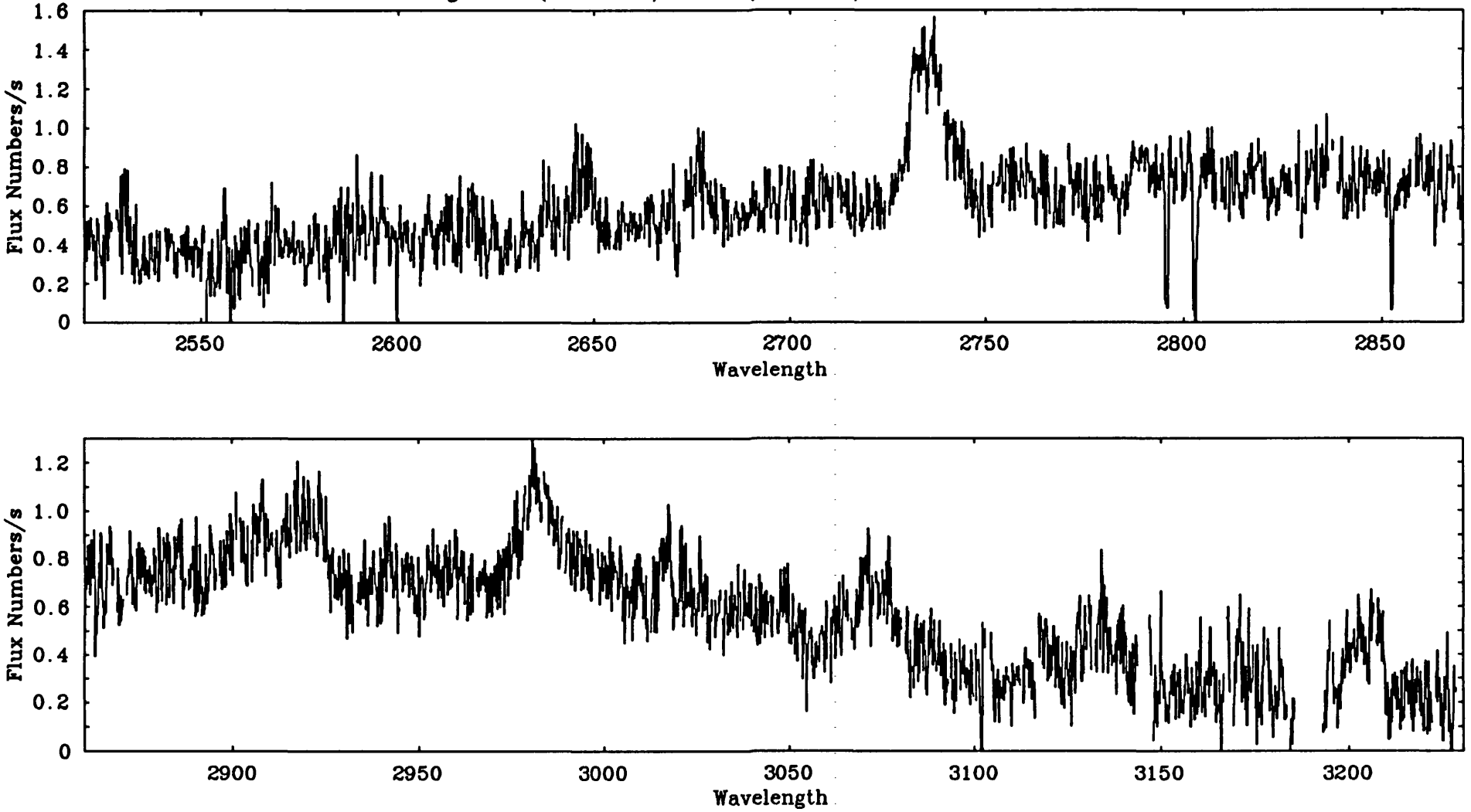

Figure A6 : WR 10 (HD 65865), WN 4.5, v=11.08

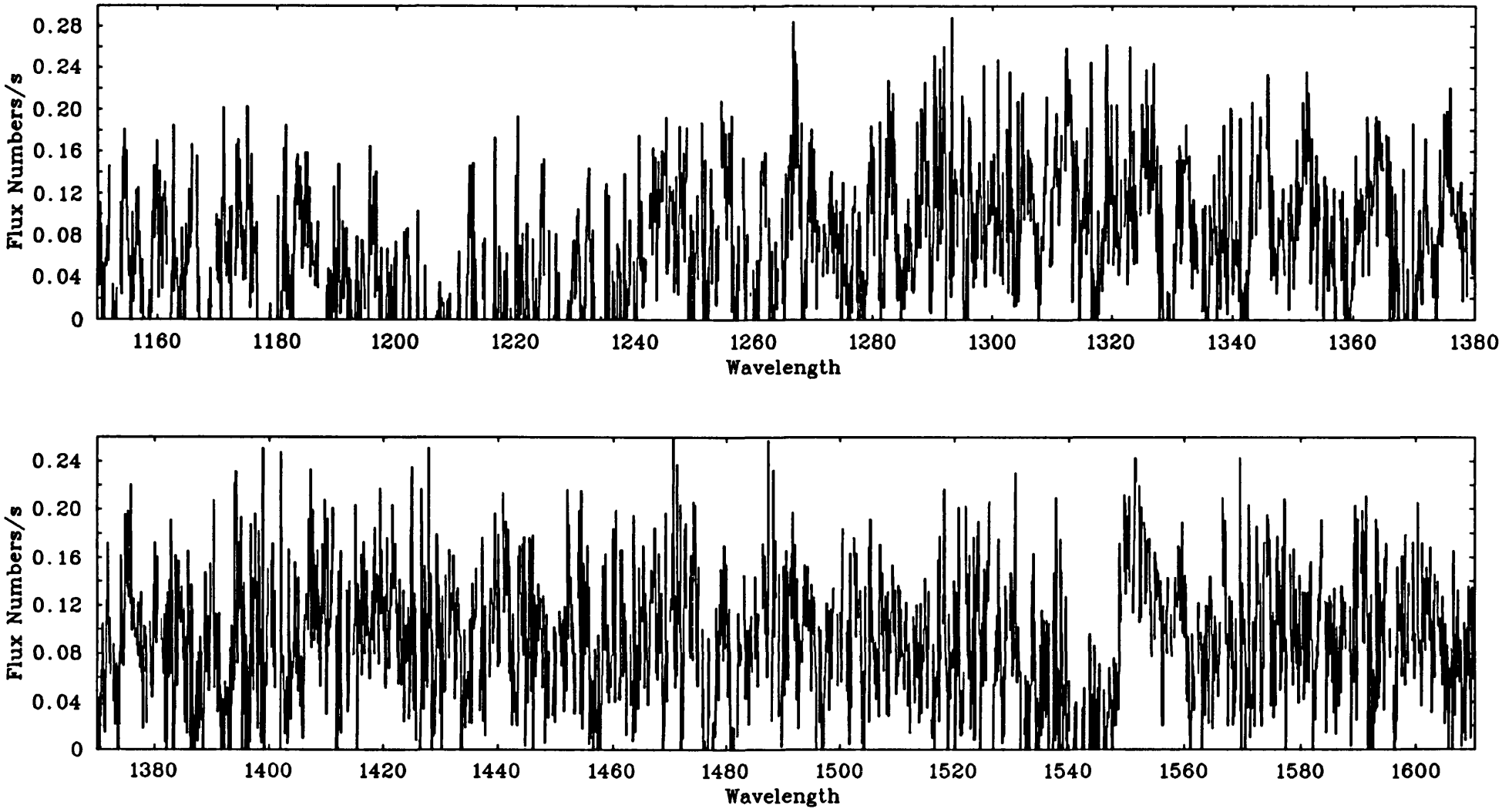

Figure A6 (continued) : WR 10 (HD 65865), WN 4.5, v=11.08

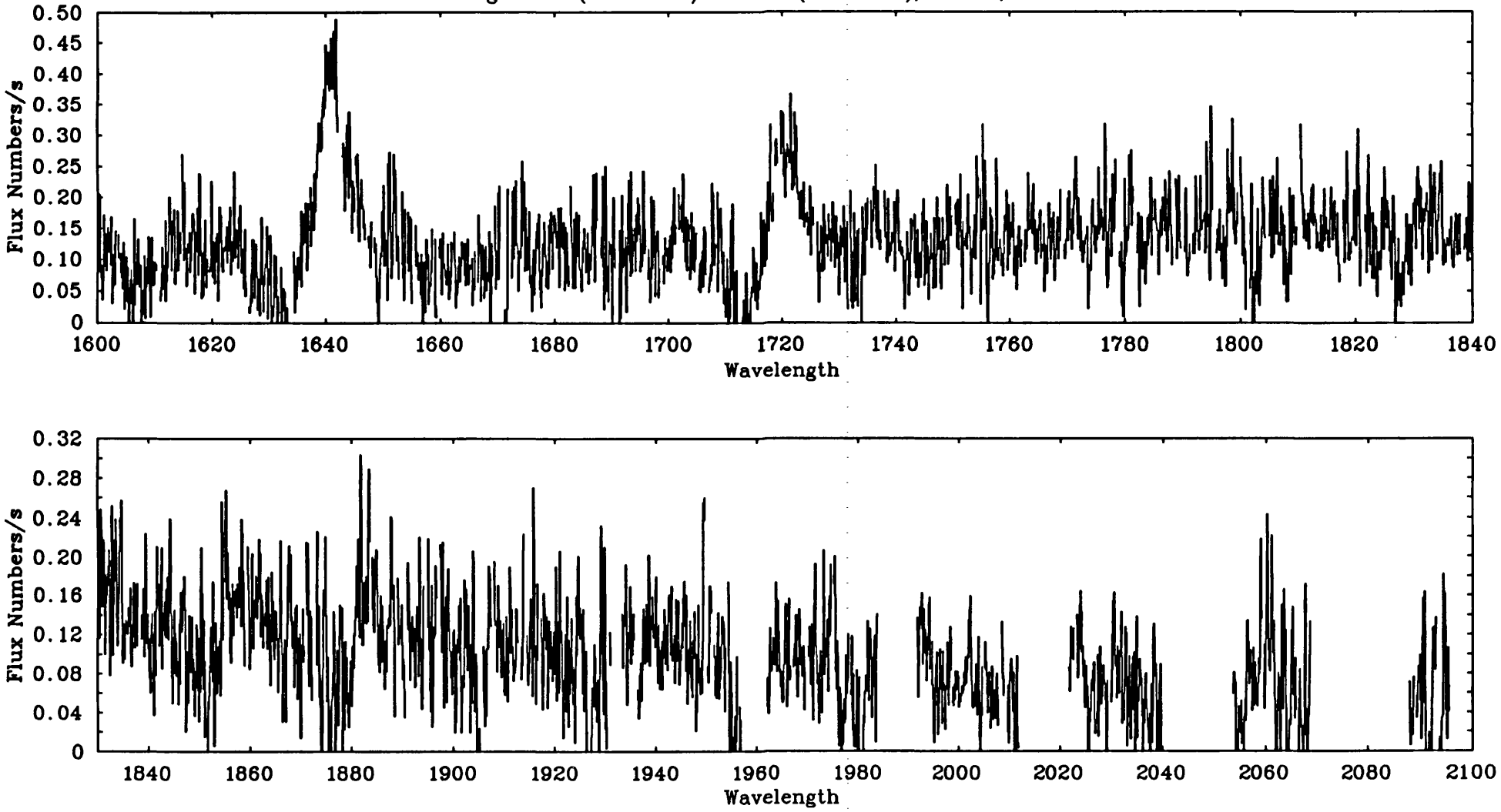

Figure A7 : WR 14 (HD 76536), WC 6, v=9.42

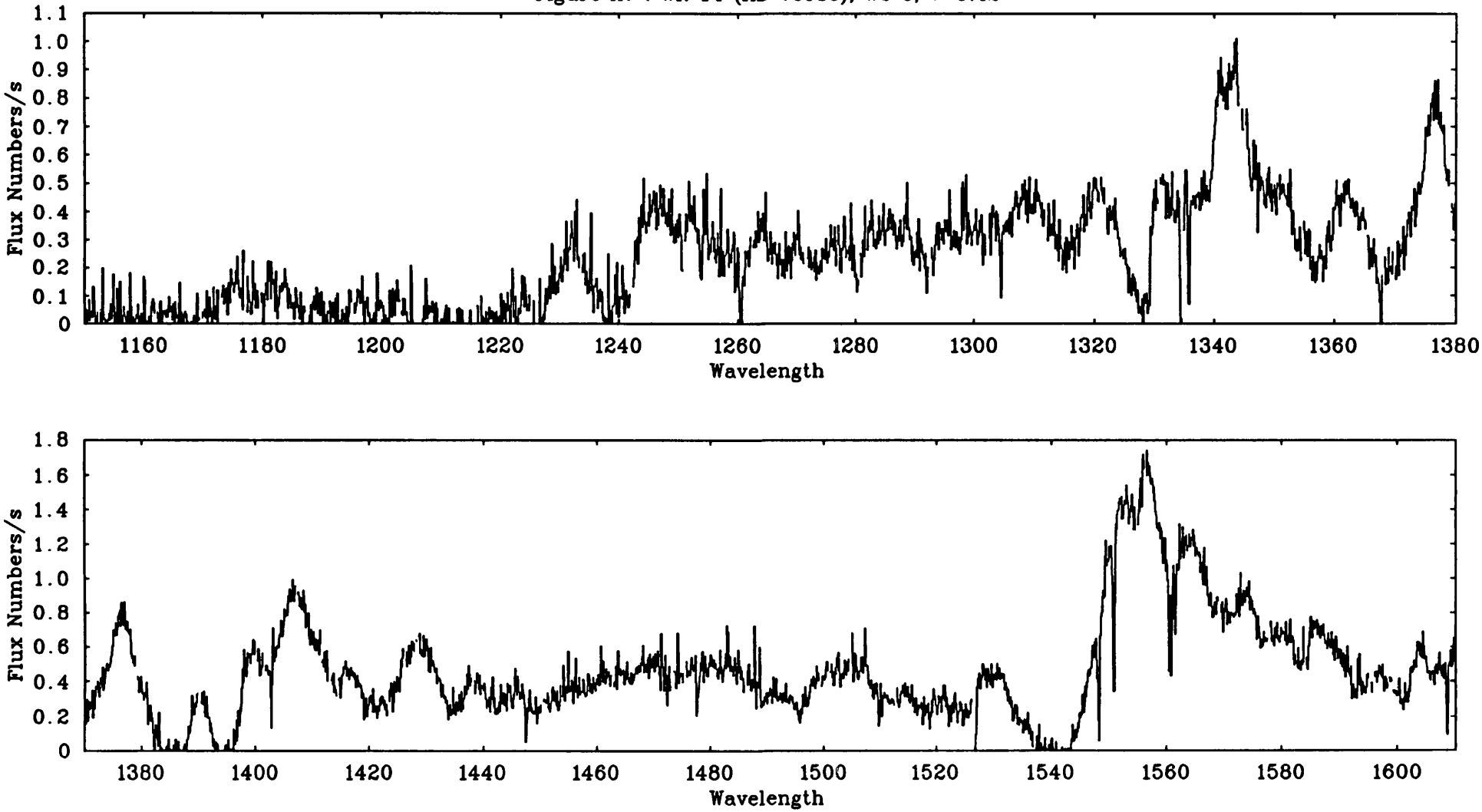

Figure A7 (continued) : WR 14 (HD 76536), WC 6, v=9.42

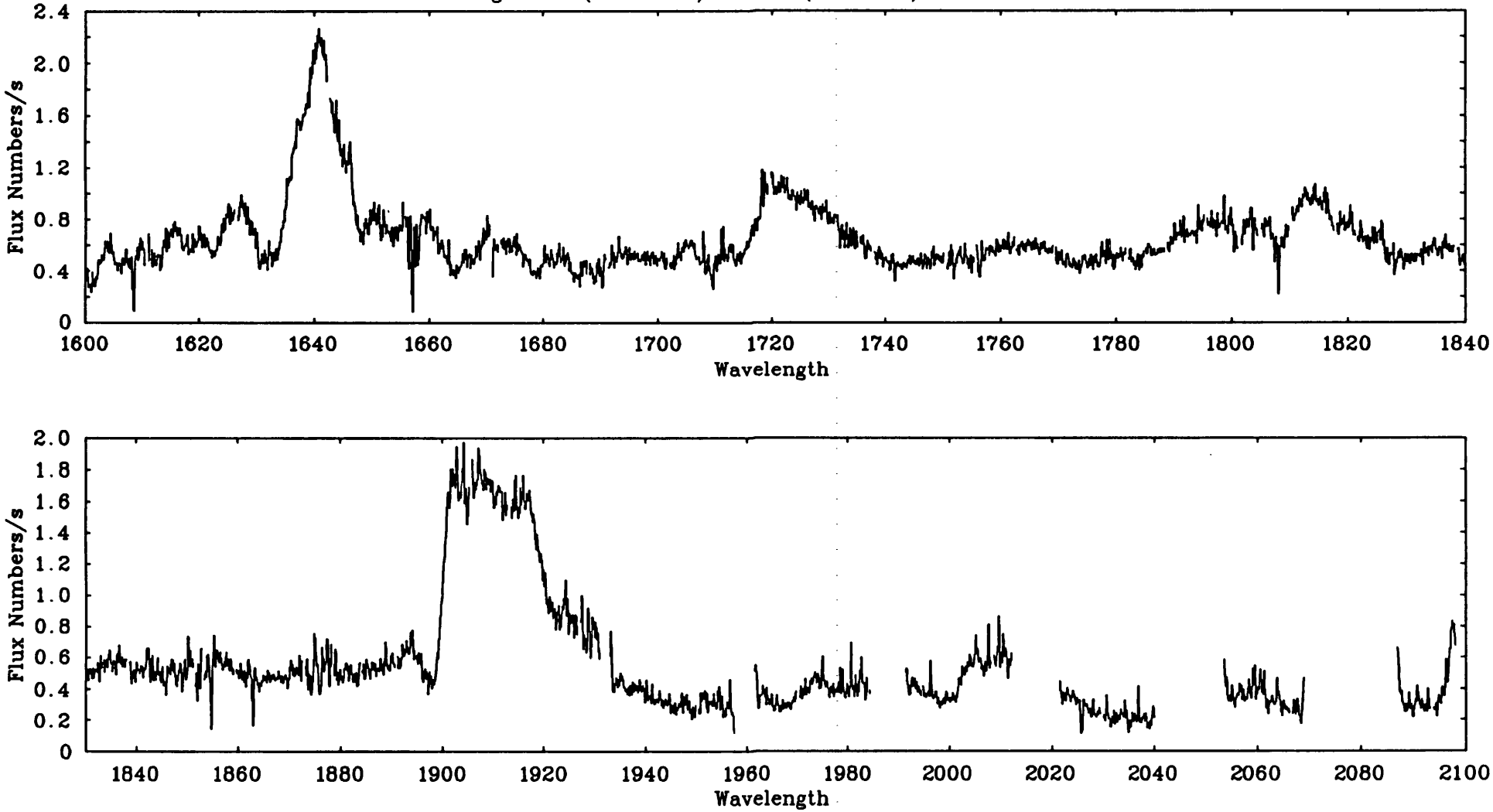

Figure A8 : WR 16 (HD 86161), WN 8, v=8.43

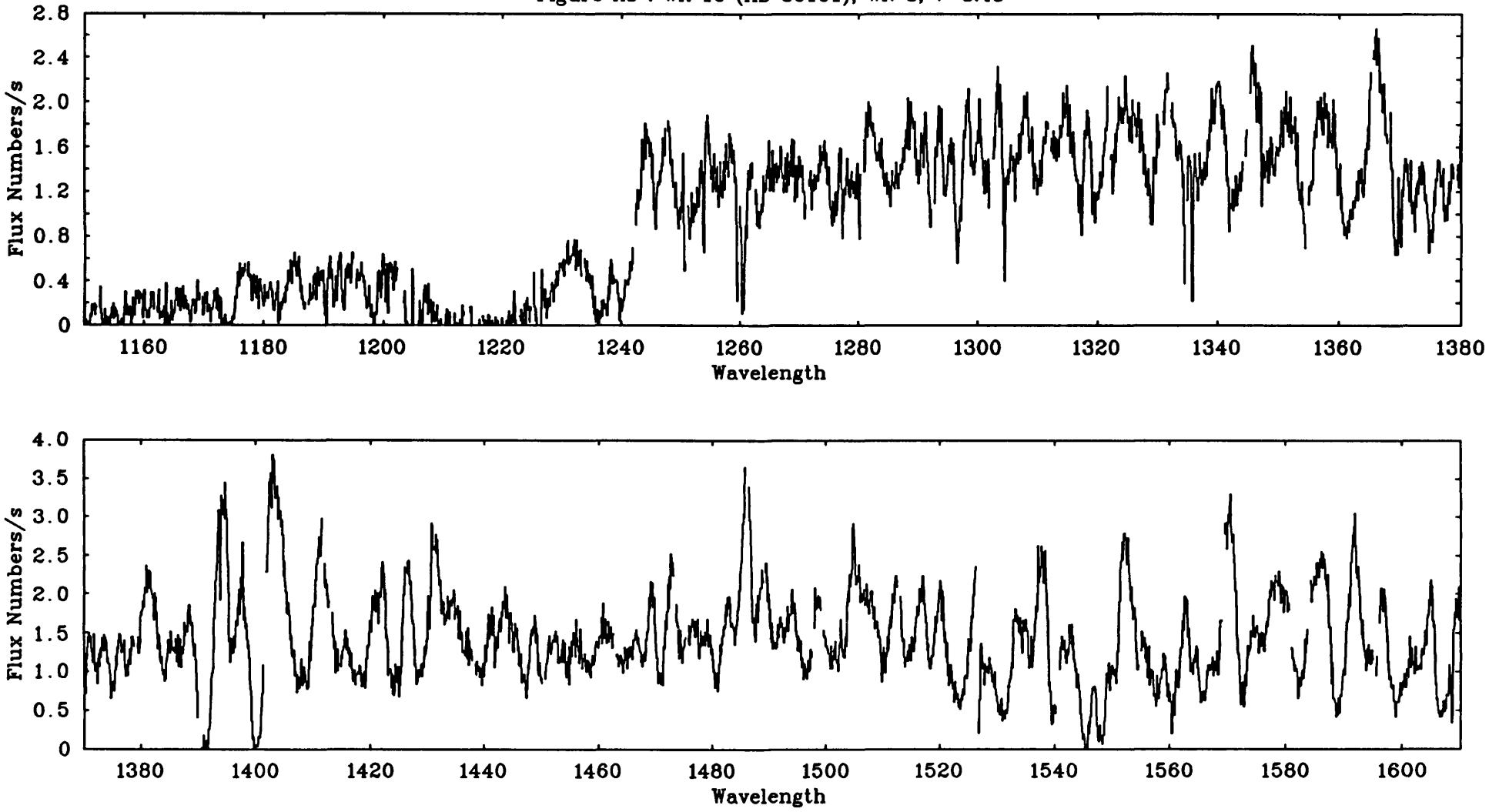

Figure A8 (continued) : WR 16 (HD 86161), WN 8, v=8.43

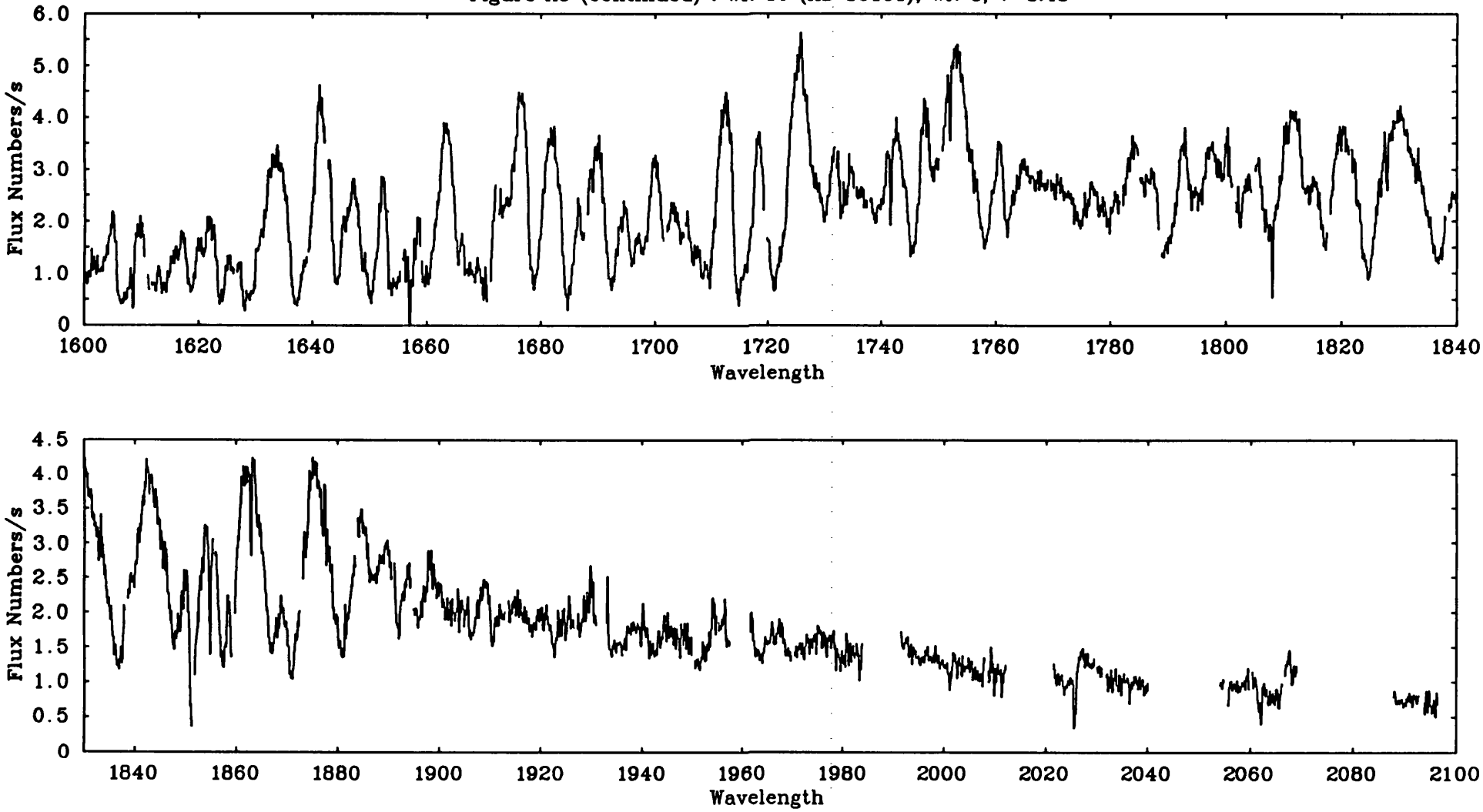

Figure A9 : WR 22 (HD 92740), WN 7 + abs (SB1), v=6.44

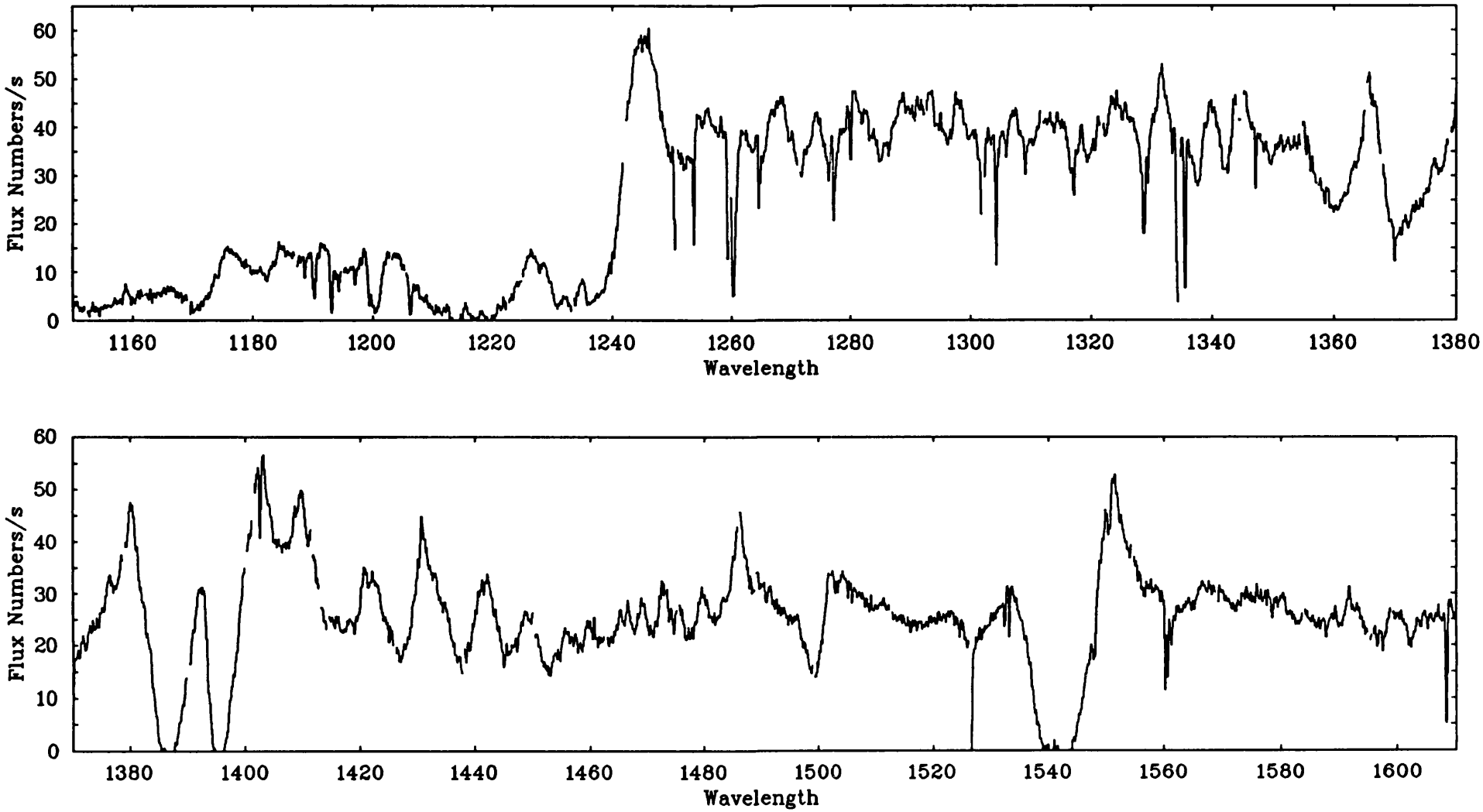

Figure A9 (continued) : WR 22 (HD 92740), WN 7 + abs (SB1), v=6.44

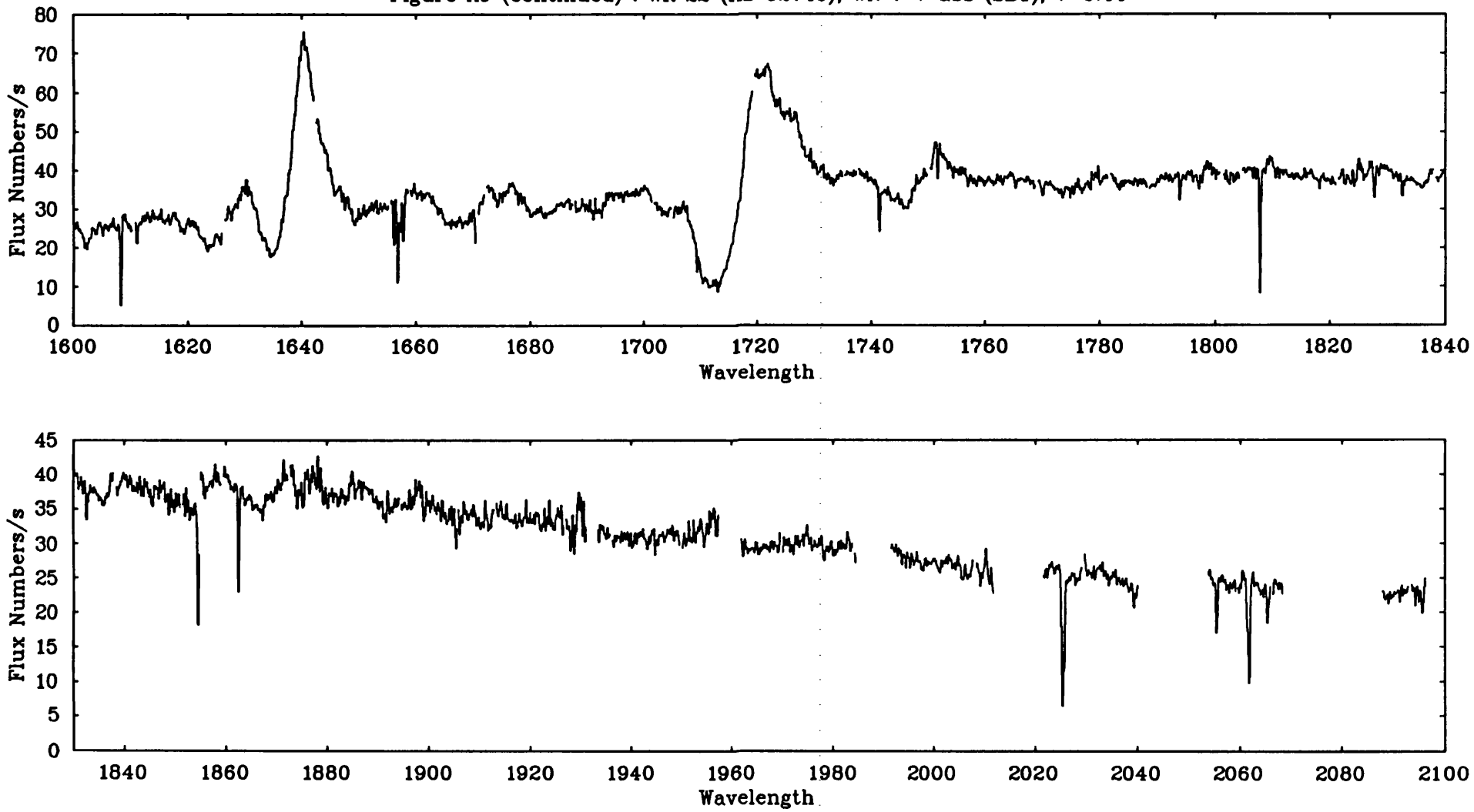

Figure A10 : WR 22 (HD 92740), WN 7 + abs (SB1), v=6.44

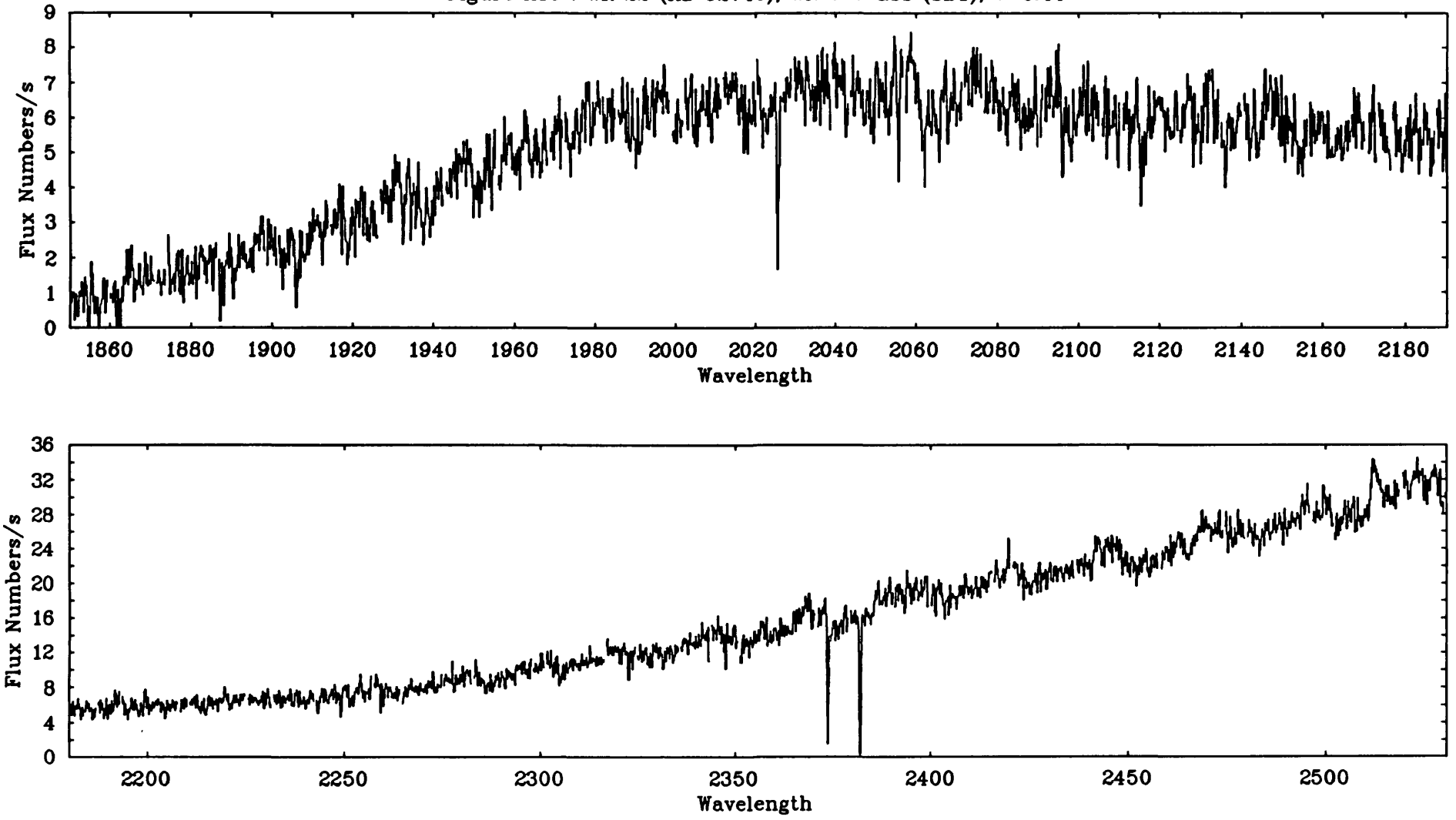

Figure A10 (continued) : WR 22 (HD 92740), WN 7 + abs (SB1), v=6.44

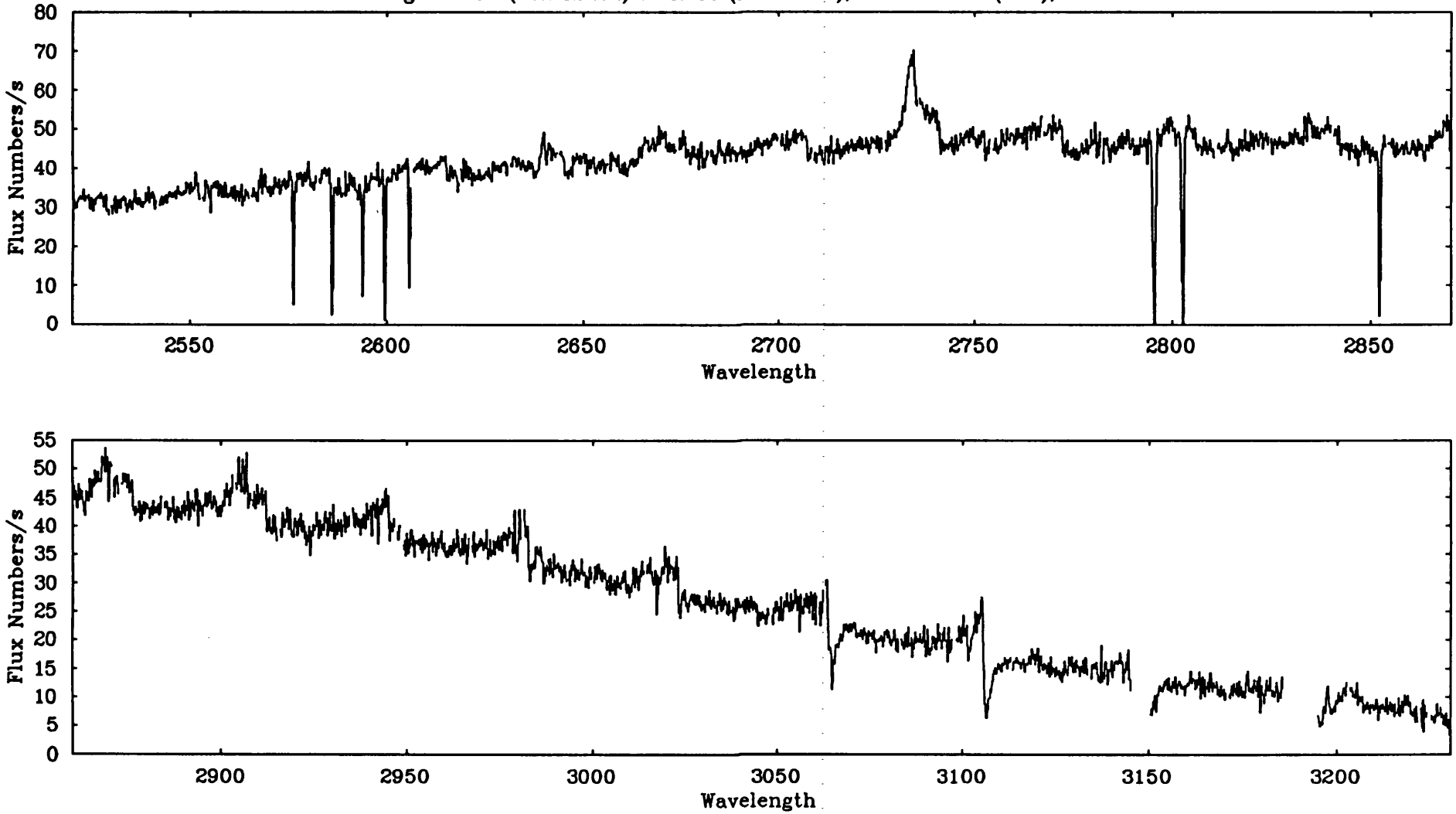

Figure A11 : WR 23 (HD 92809), WC 6, v=9.71

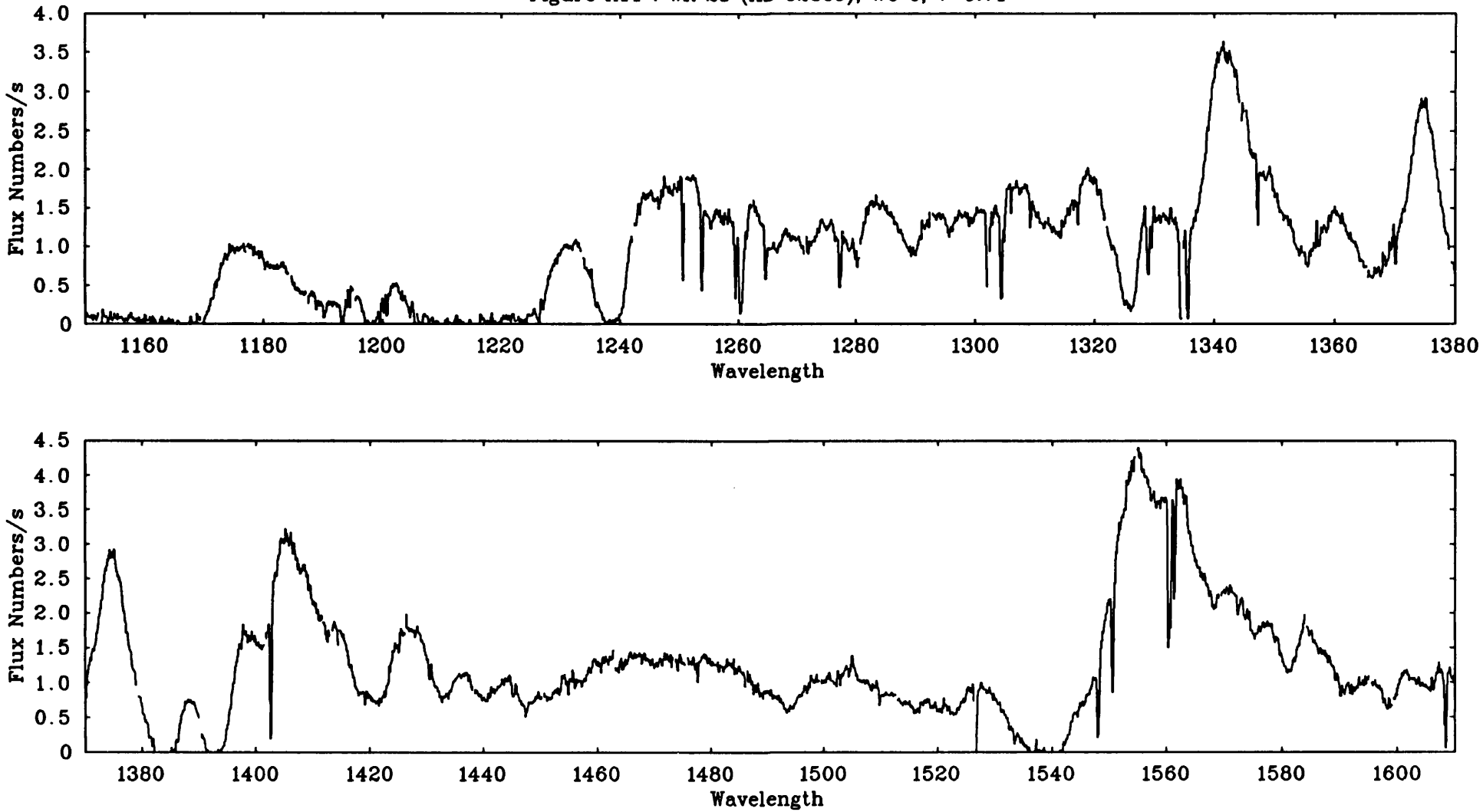

Figure A11 (continued) : WR 23 (HD 92809), WC 6, v=9.71

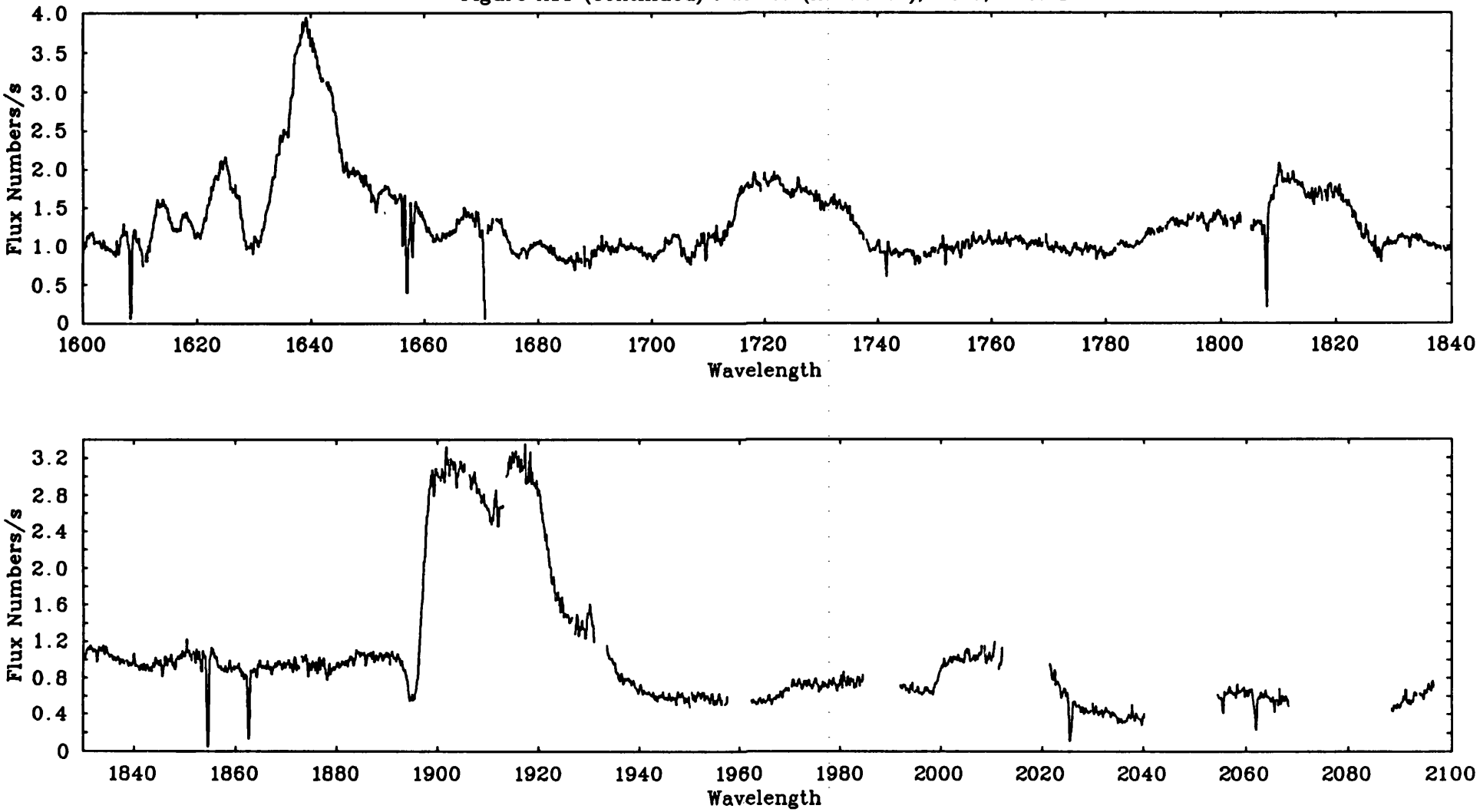

Figure A12 : WR 23 (HD 92809), WC 6, v=9.71

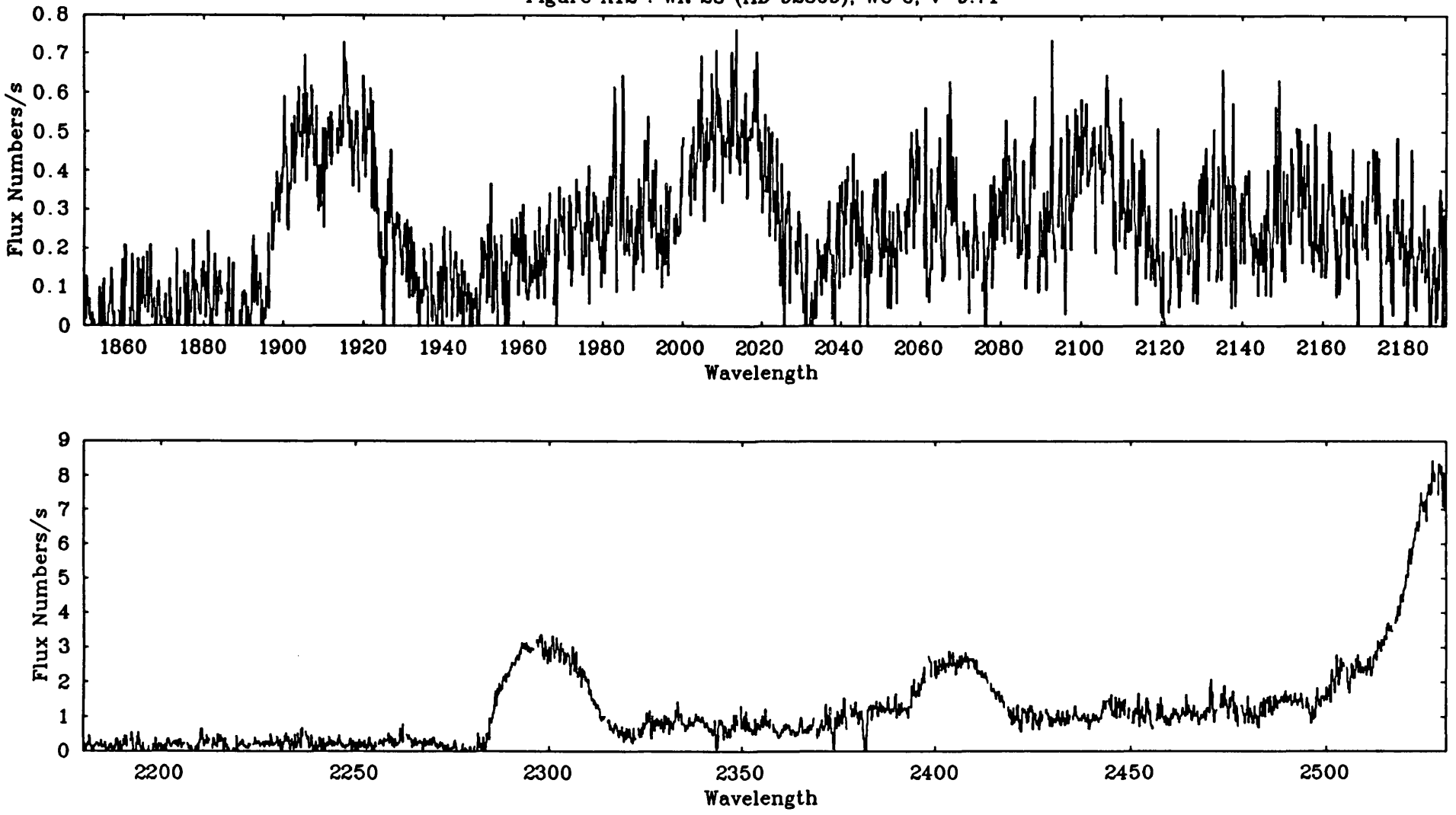

Figure A12 (continued) : WR 23 (HD 92809), WC 6, v=9.71

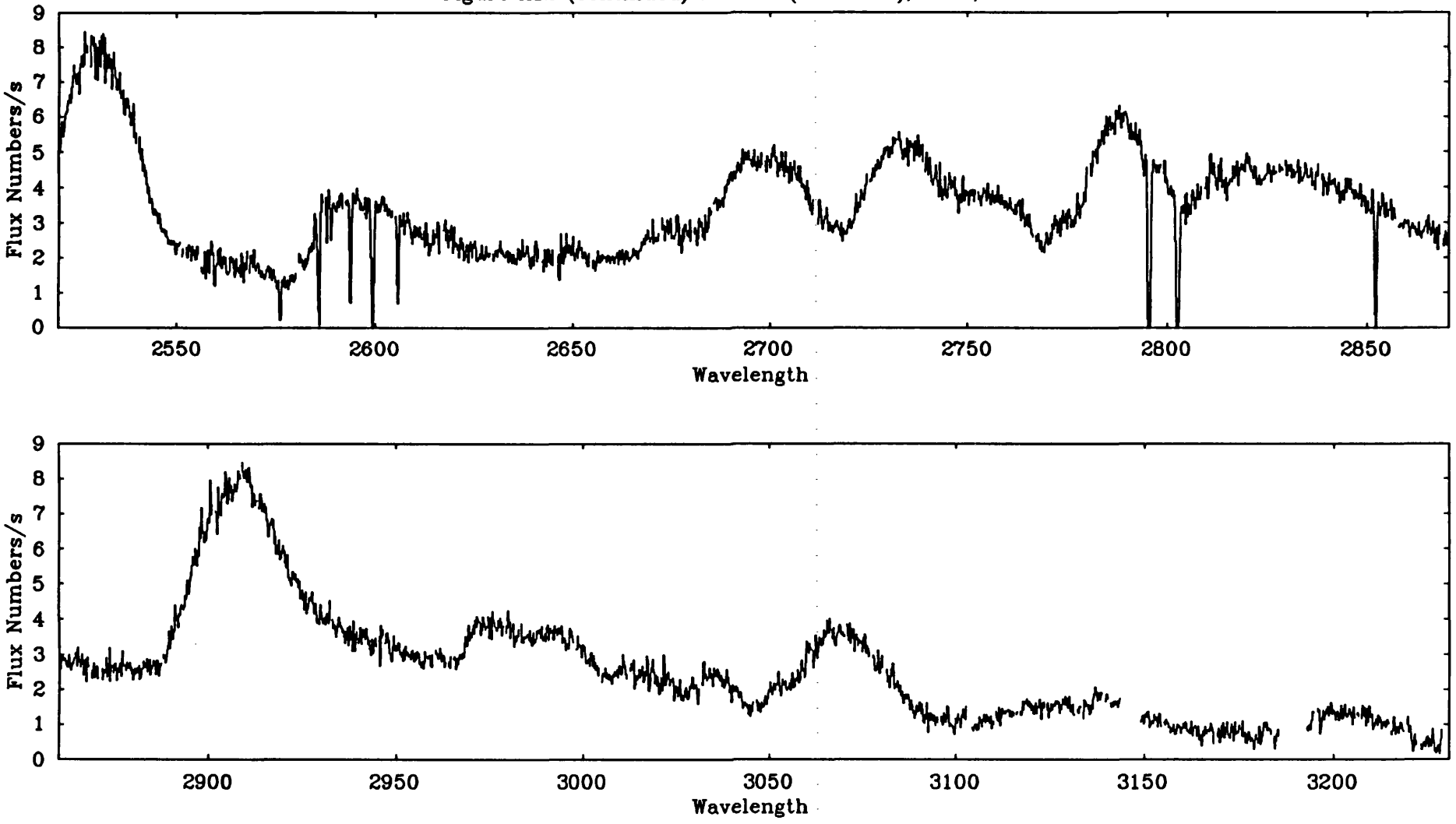

Figure A13 : WR 24 (HD 93131), WN 7 + abs, v=6.49

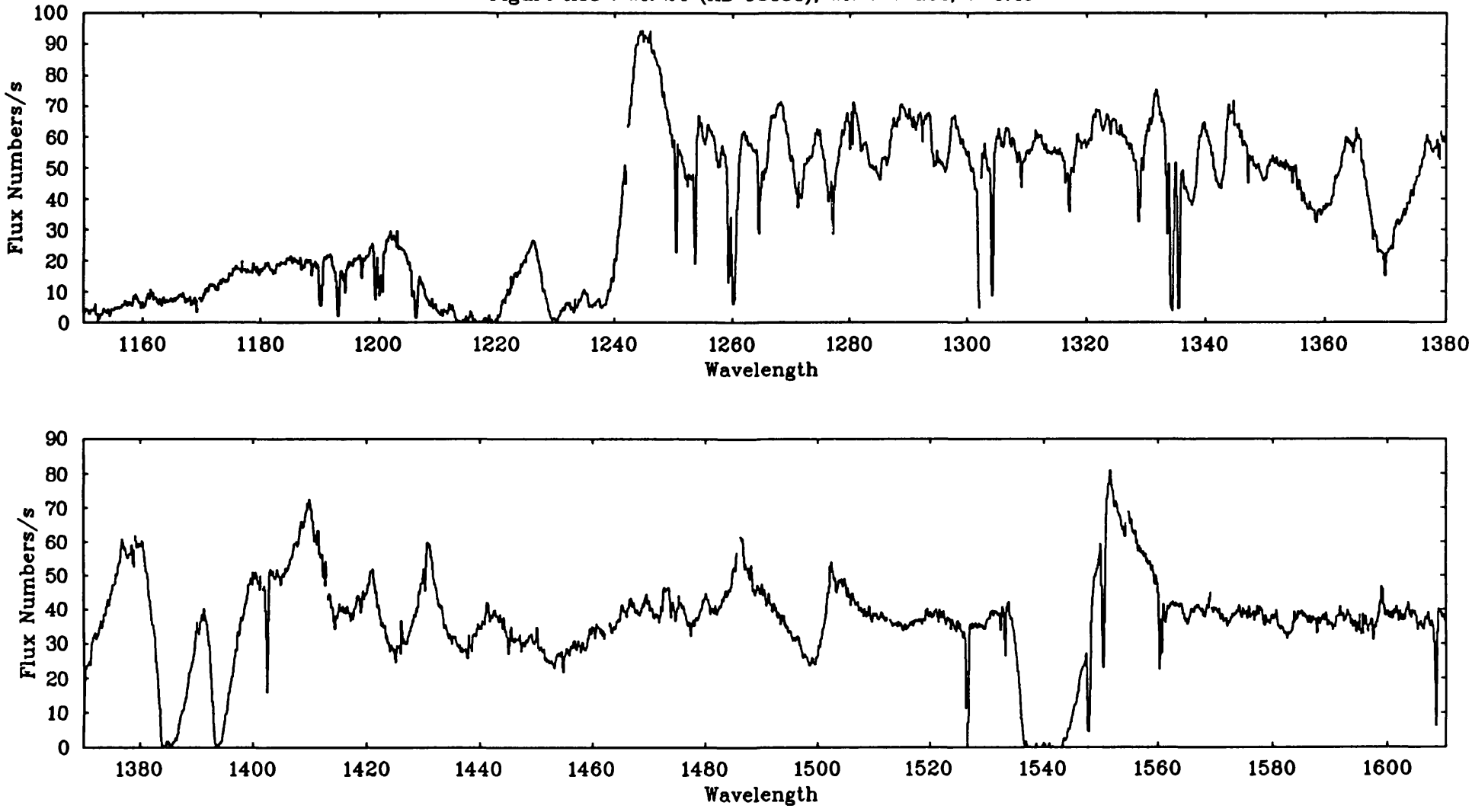

Figure A13 (continued) : WR 24 (HD 93131), WN 7 + abs, v=6.49

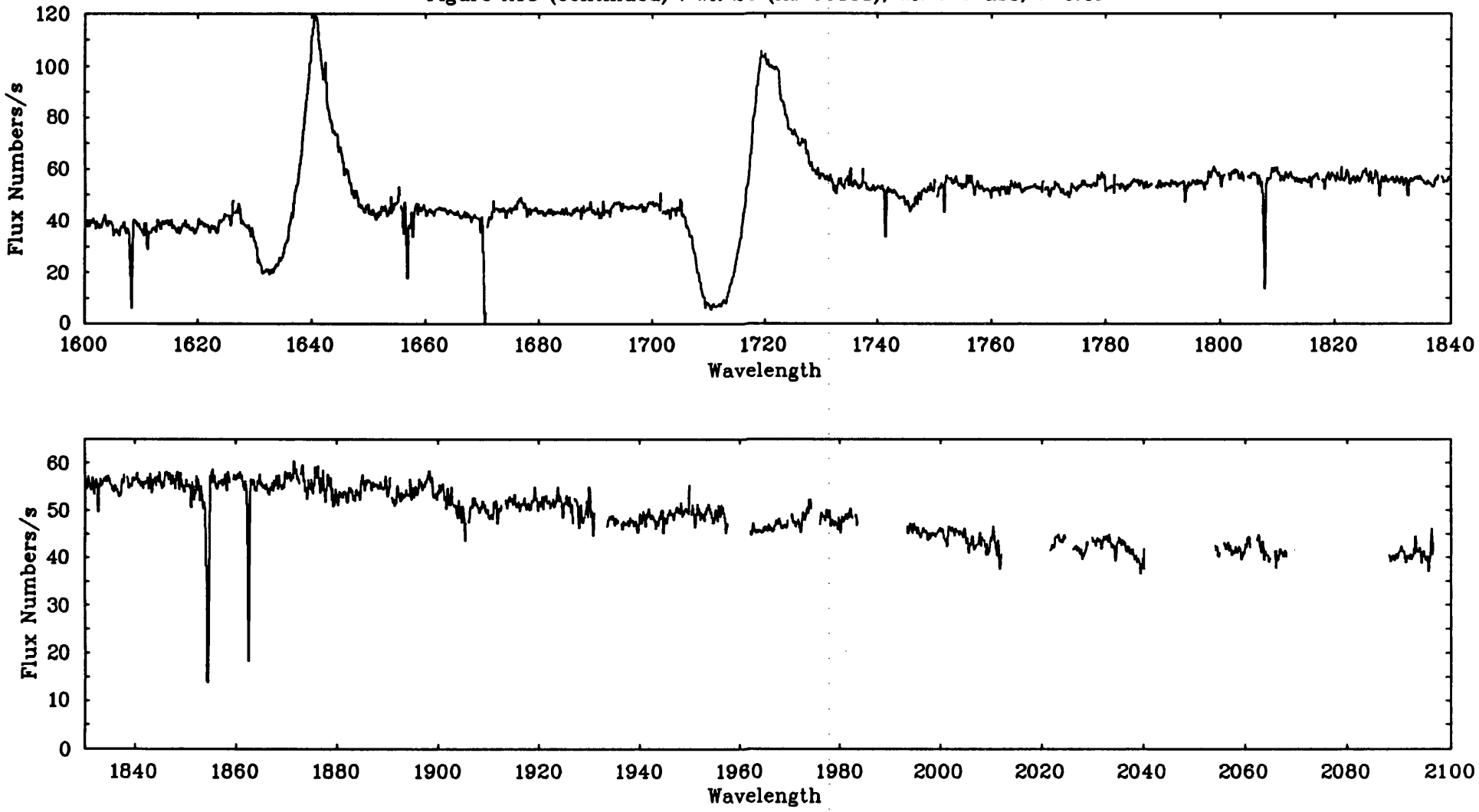

Figure A14 : WR 24 (HD 93131), WN 7 + abs, v=6.49

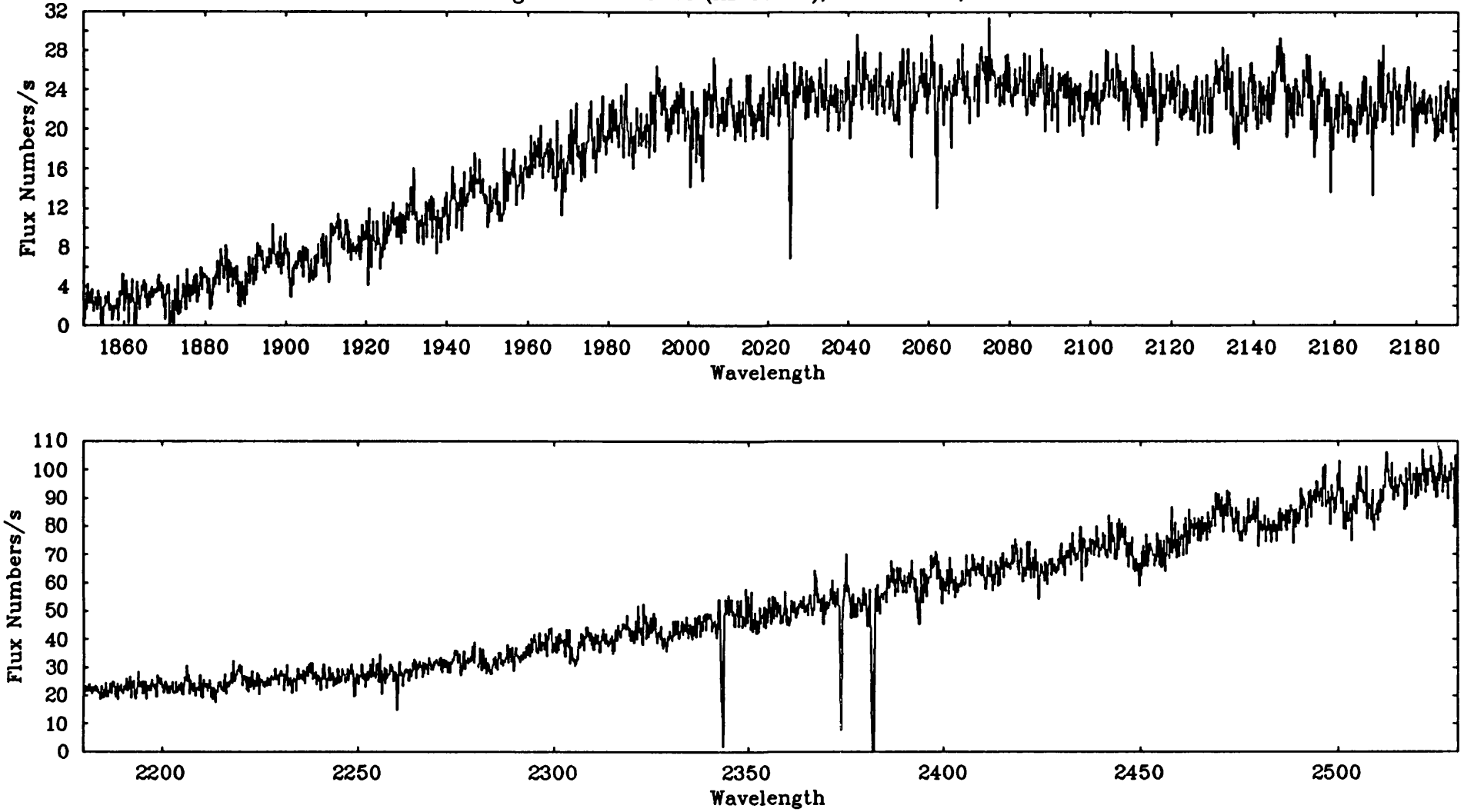

Figure A14 (continued) : WR 24 (HD 93131), WN 7 + abs, v=6.49

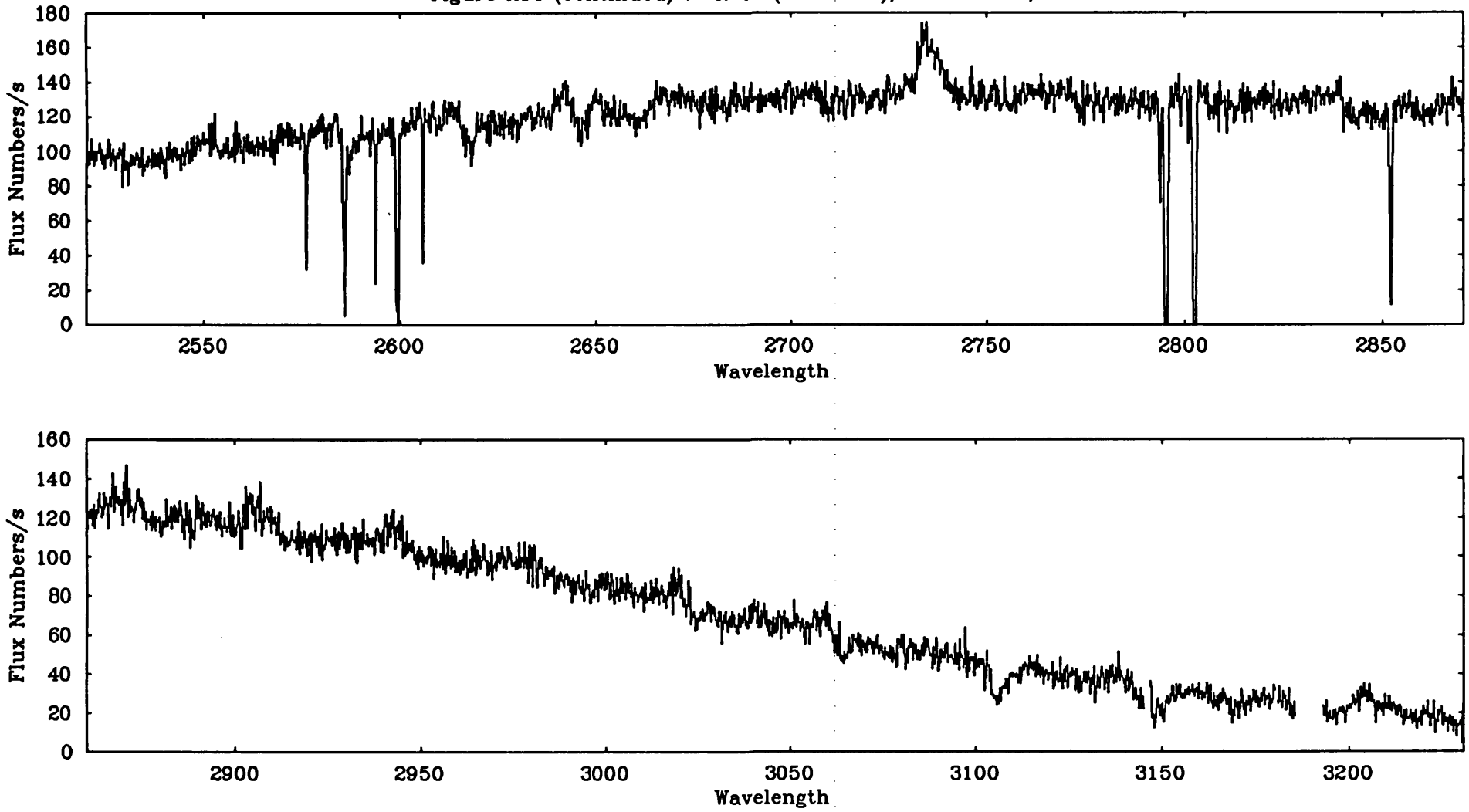

Figure A15 : WR 25 (HD 93162), WN 7 + abs, v=8.17

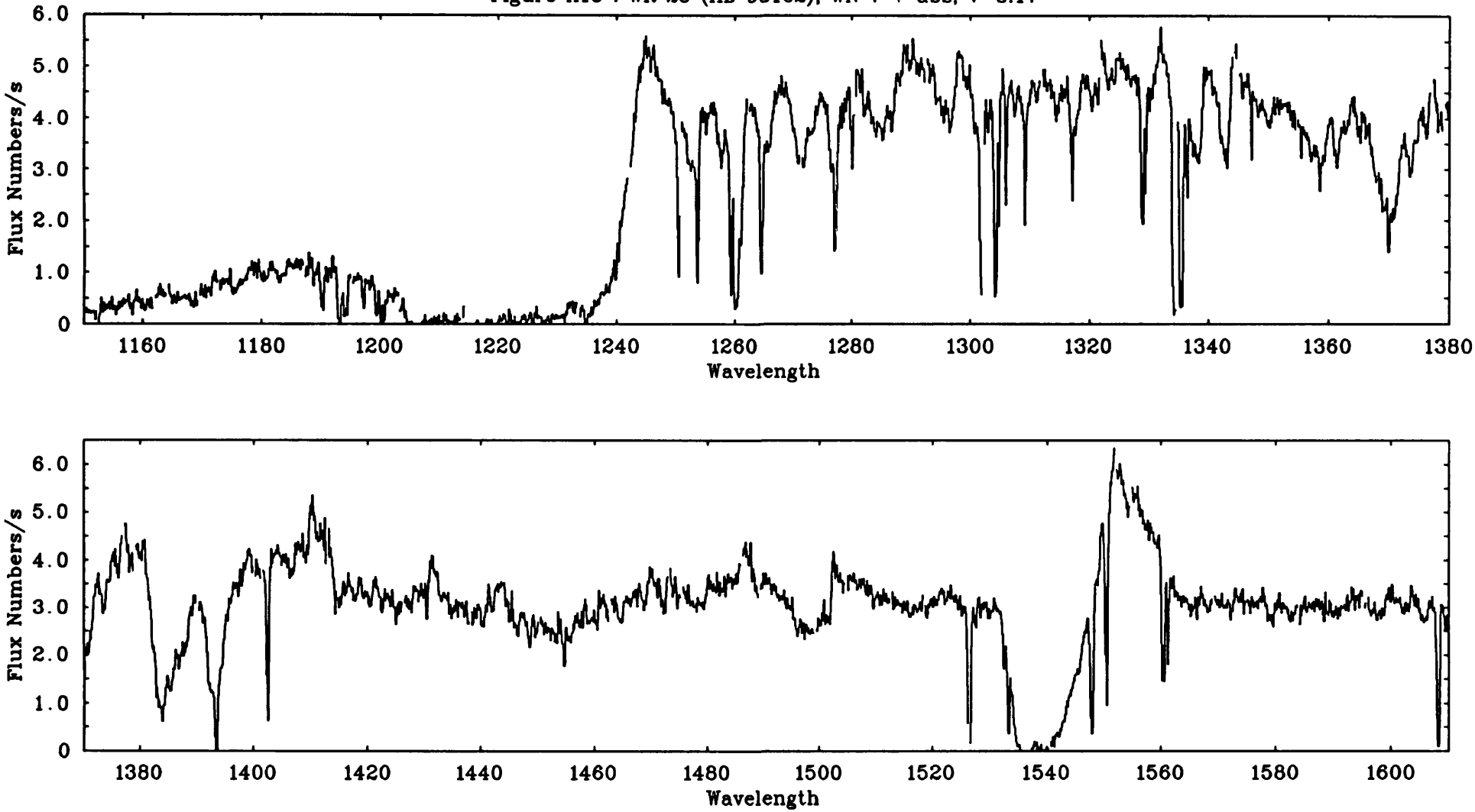

Figure A15 (continued) : WR 25 (HD 93162), WN 7 + abs, v=8.17

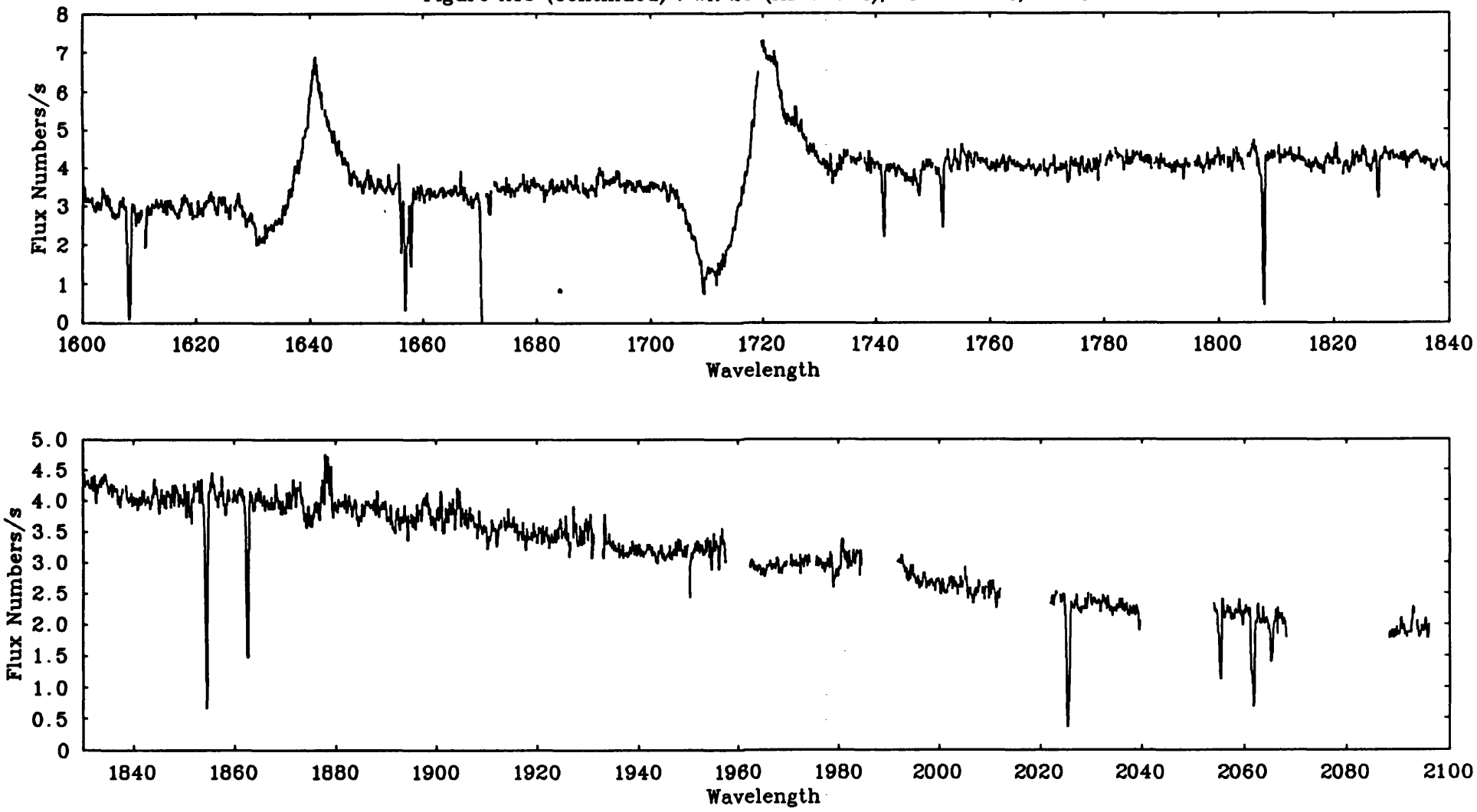

Figure A16 : WR 25 (HD 93162), WN 7 + abs, v=8.17

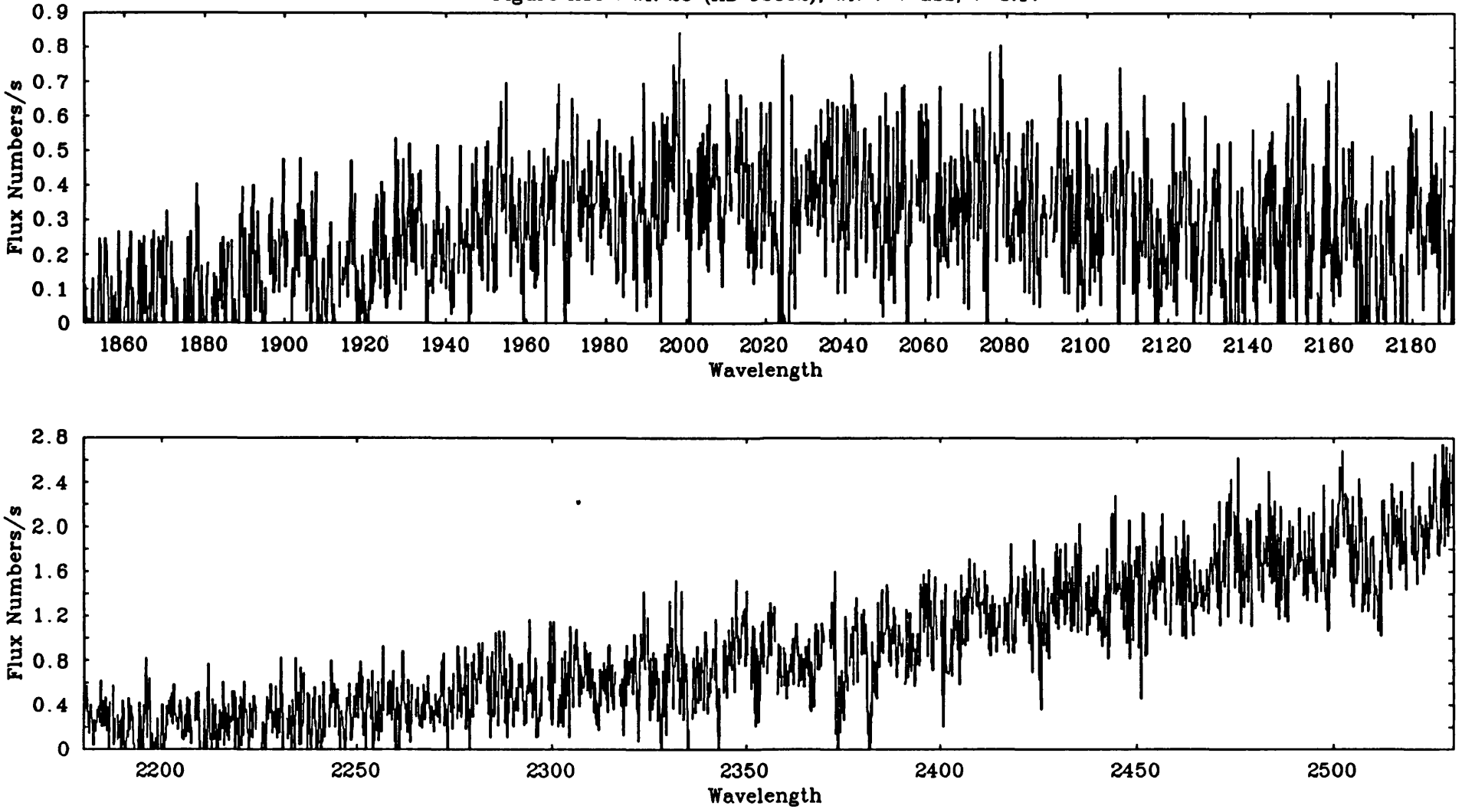

Figure A16 (continued) : WR 25 (HD 93162), WN 7 + abs, v=8.17

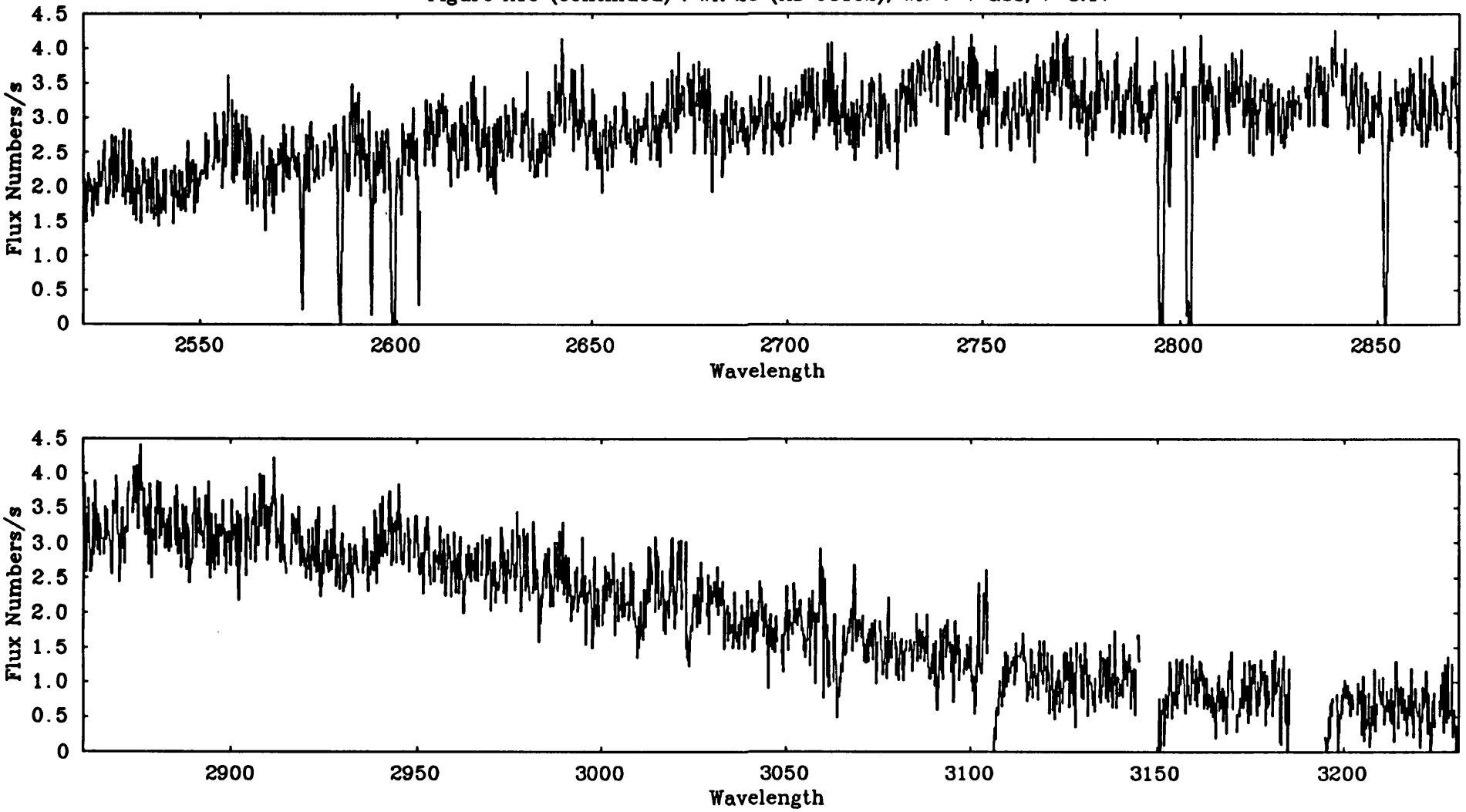

Figure A17 : WR 40 (HD 96548), WN 8, v=7.85

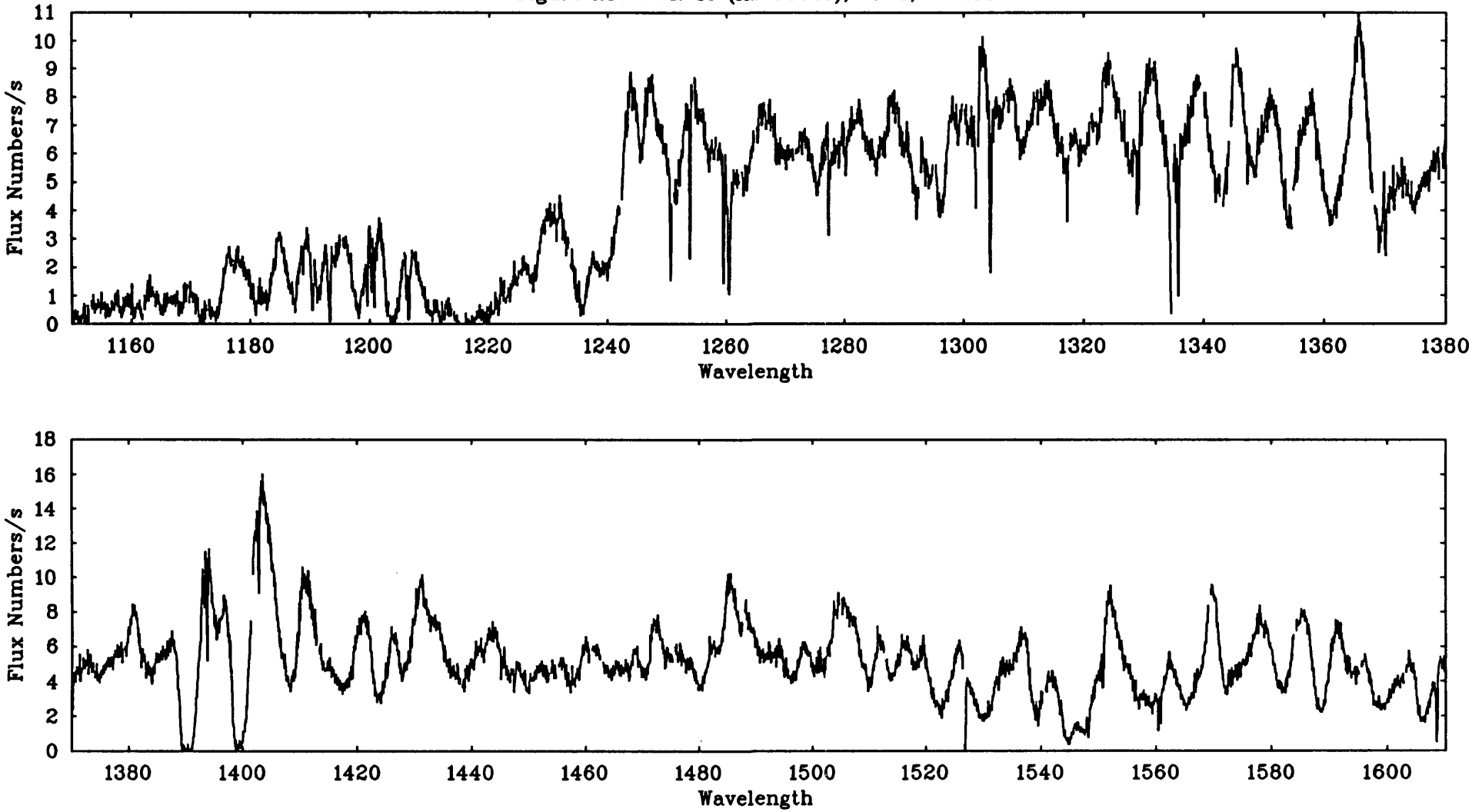

Figure A17 (continued) : WR 40 (HD 96548), WN 8, v=7.85

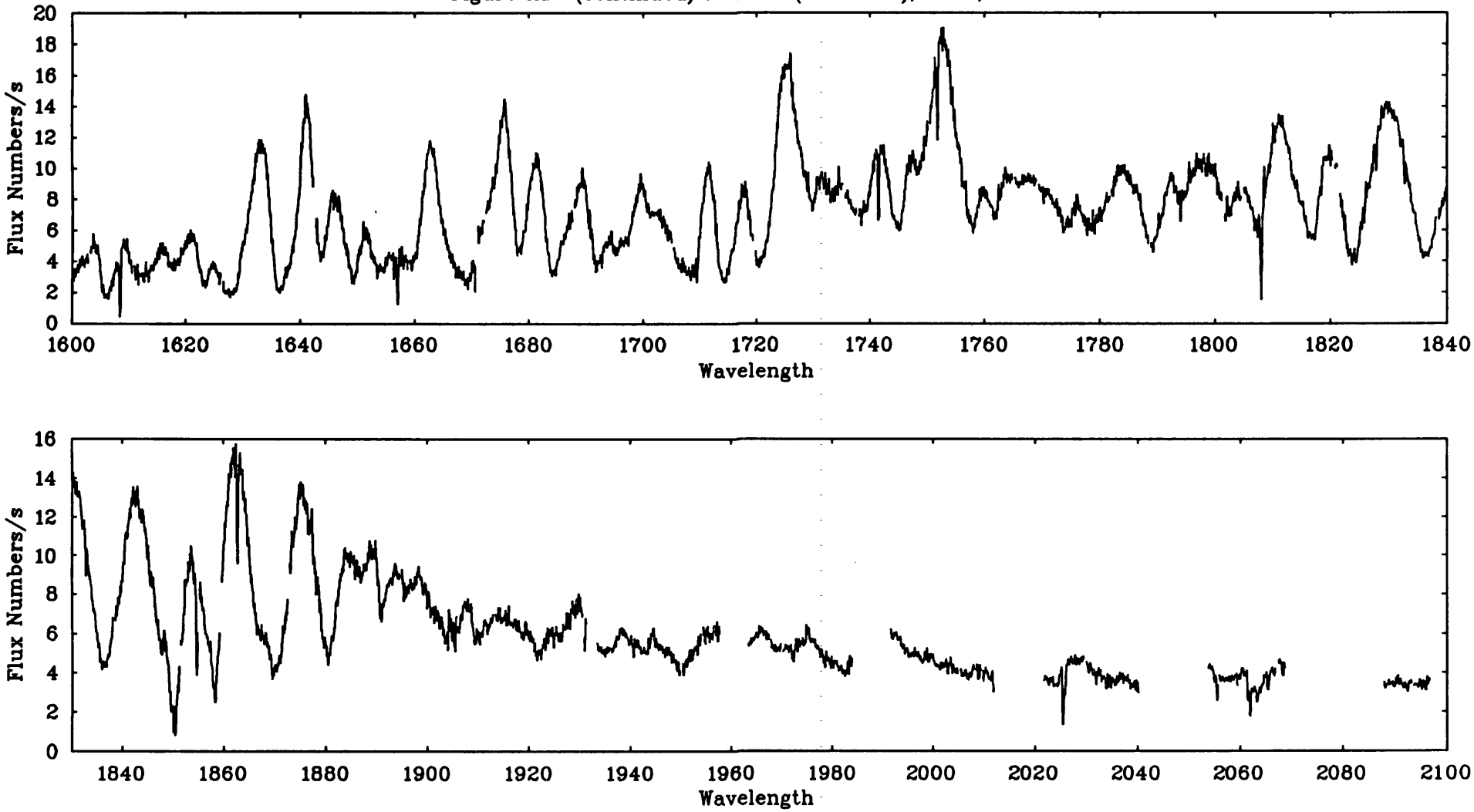

Figure A18 : WR 40 (HD 96548), WN 8, v=7.85

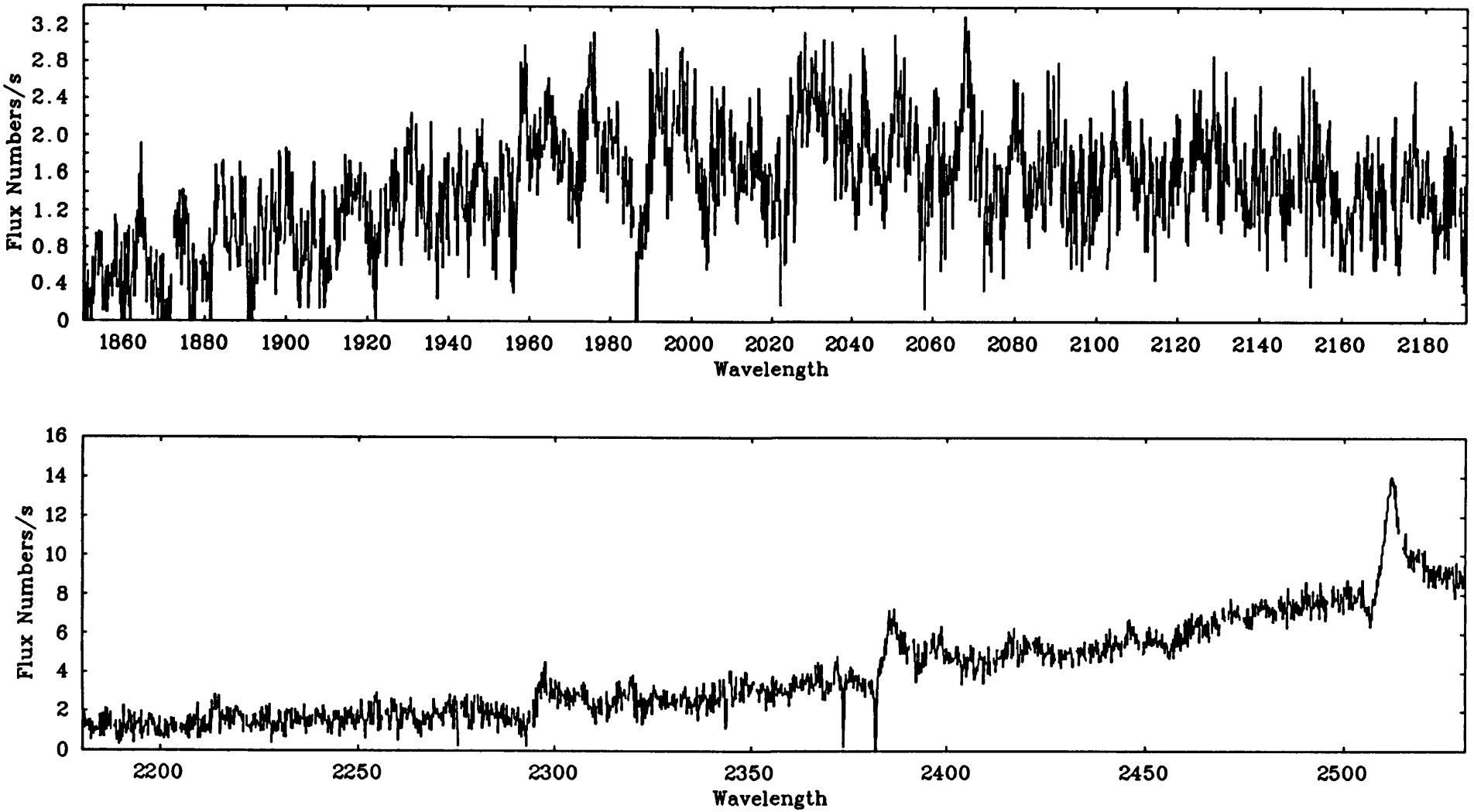

Figure A18 (continued) : WR 40 (HD 96548), WN 8, v=7.85

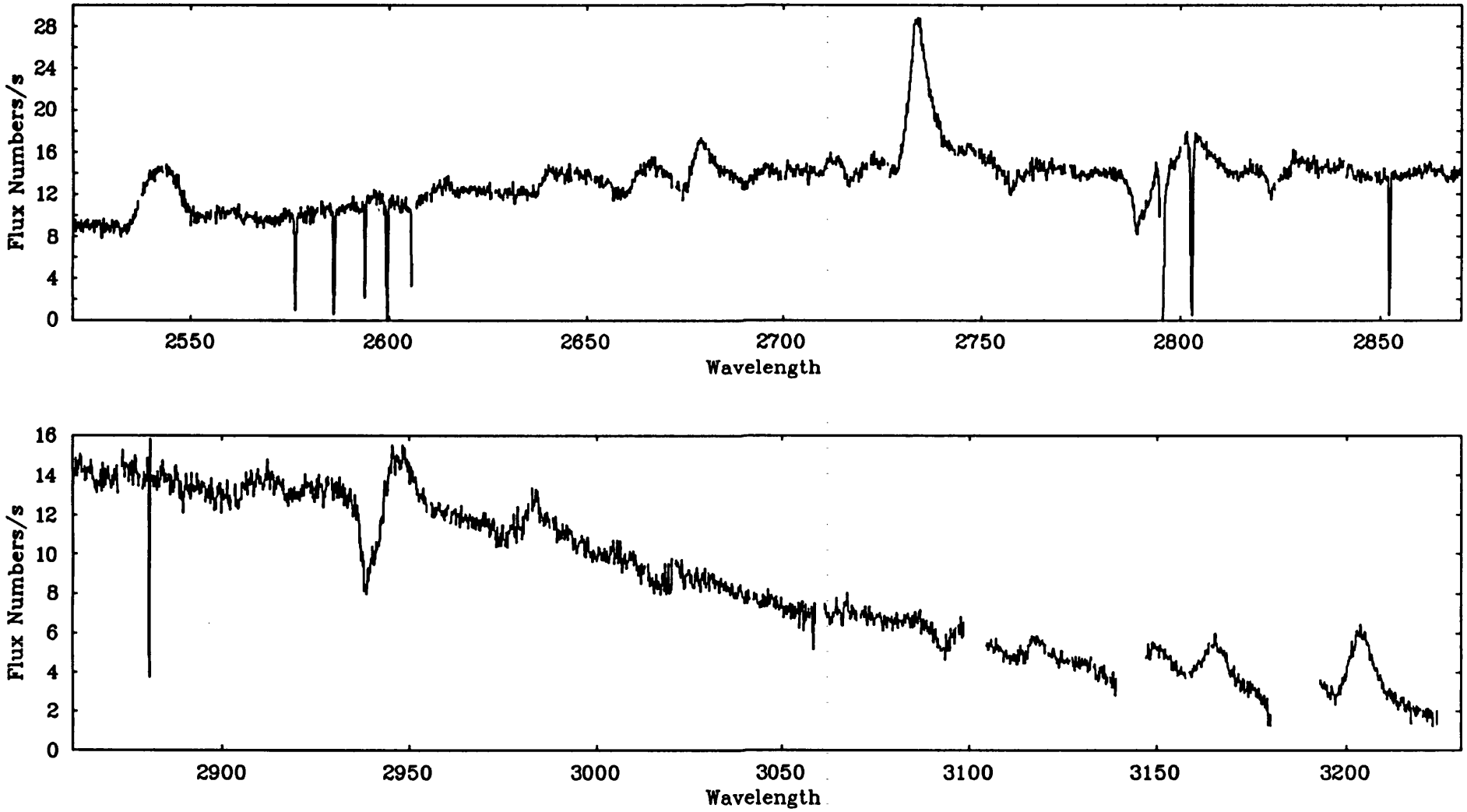

Figure A19 : WR 52 (HD 115473), WC 5, v=9.98

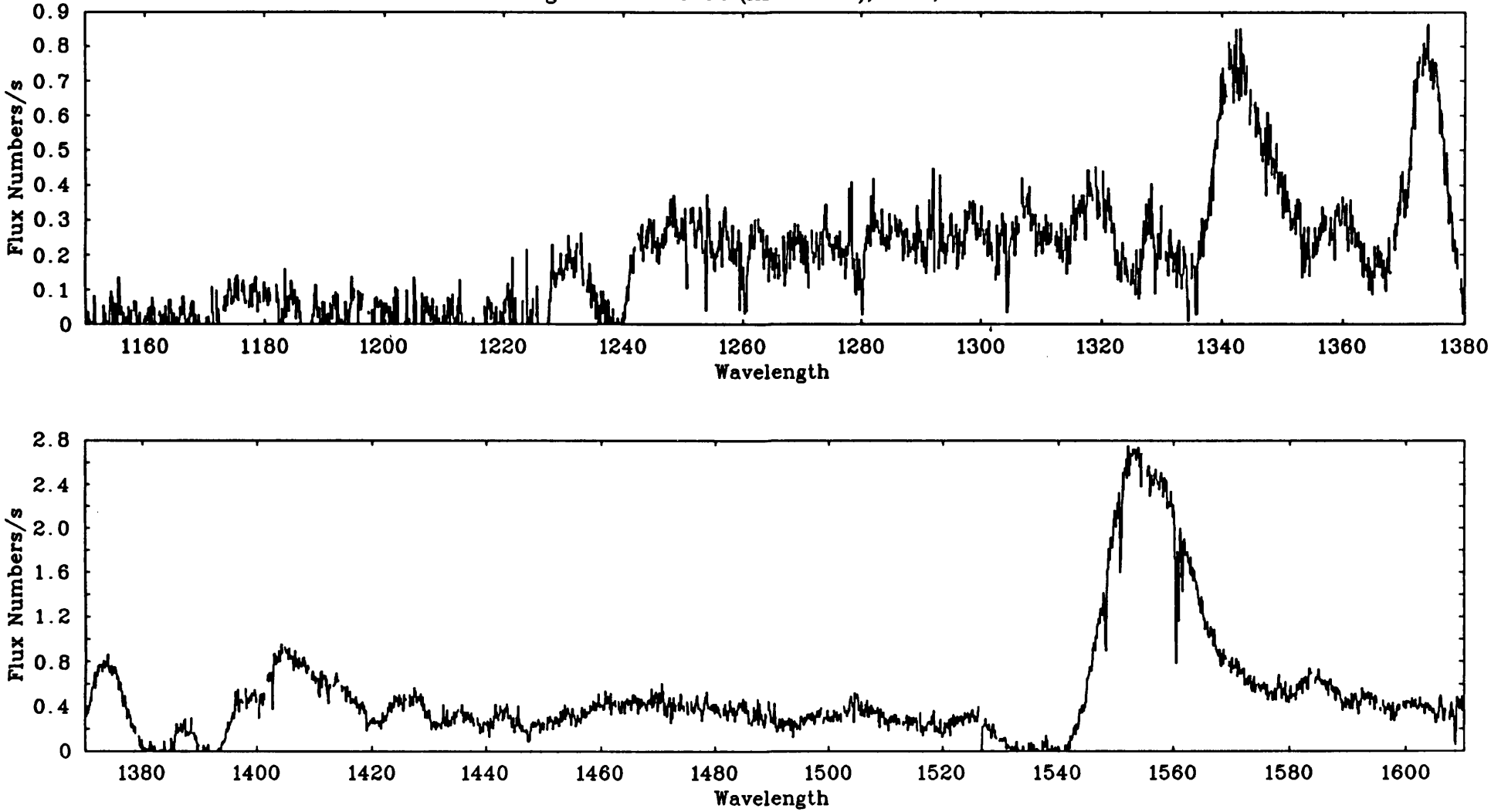

Figure A19 (continued) : WR 52 (HD 115473), WC 5, v=9.98

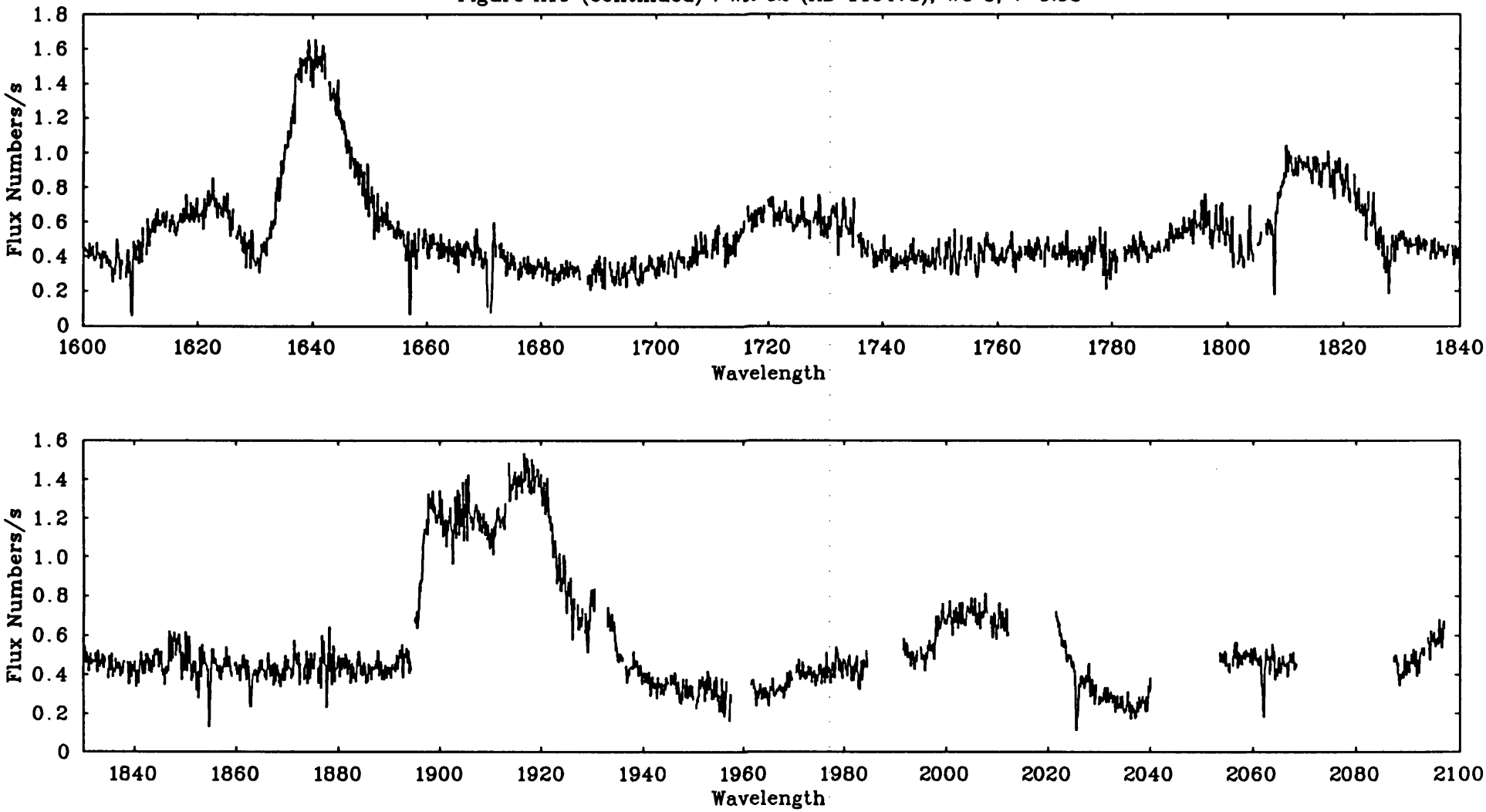

Figure A20 : WR 57 (HD 119078), WC 7, v=10.11

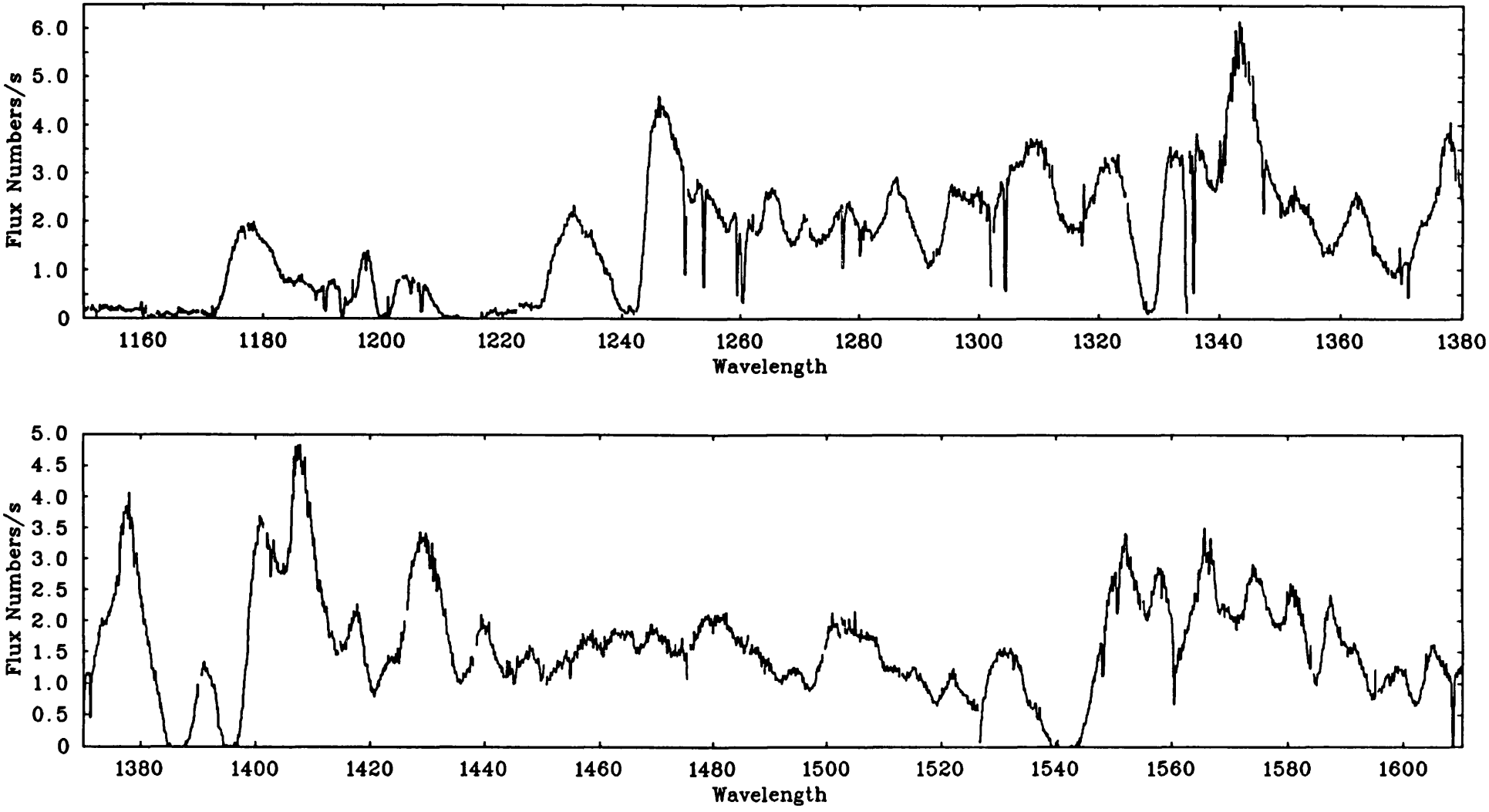

Figure A20 (continued) : WR 57 (HD 119078), WC 7, v=10.11

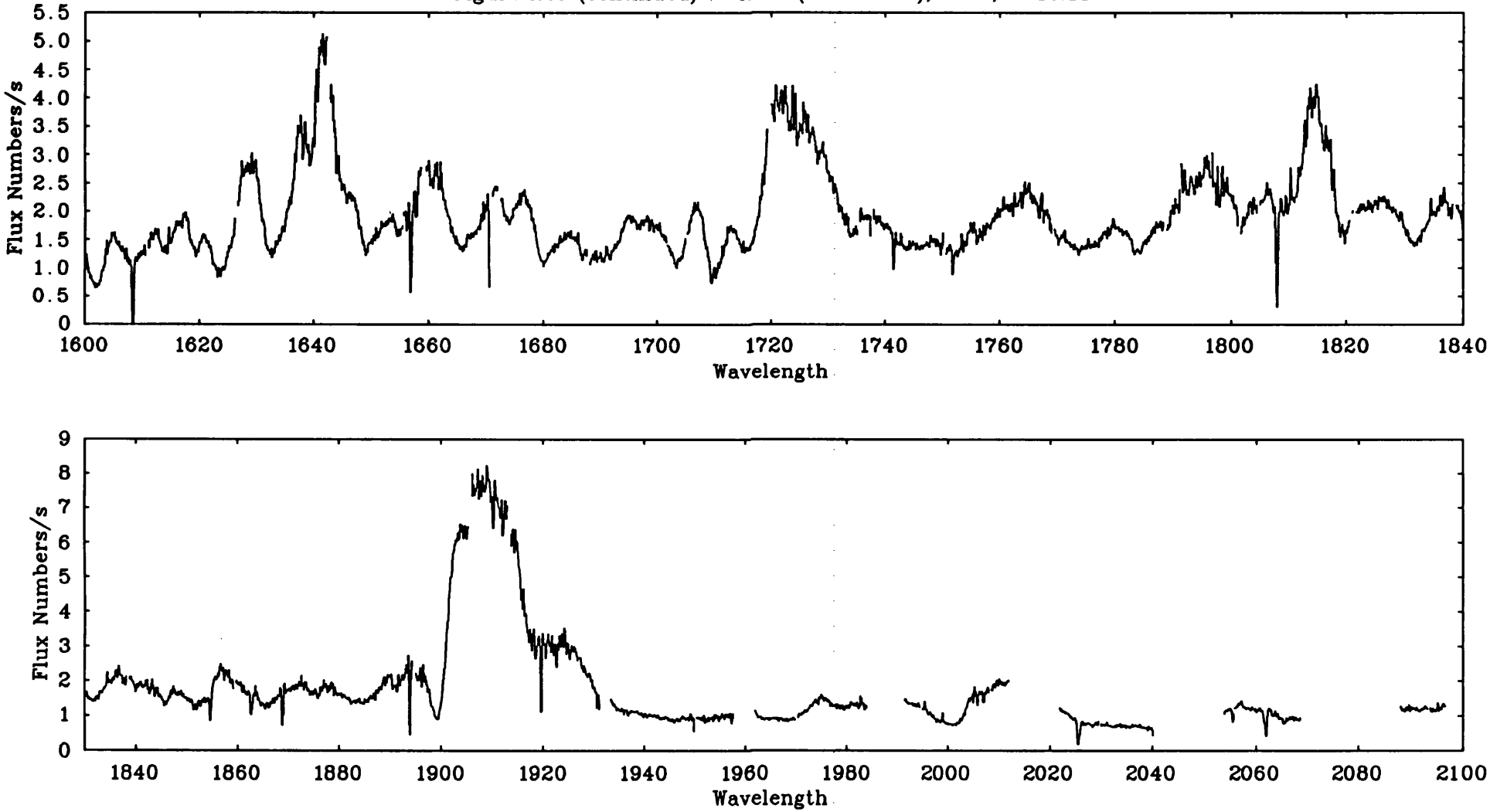

Figure A21 : WR 69 (HD 136488), WC 9, v=9.43

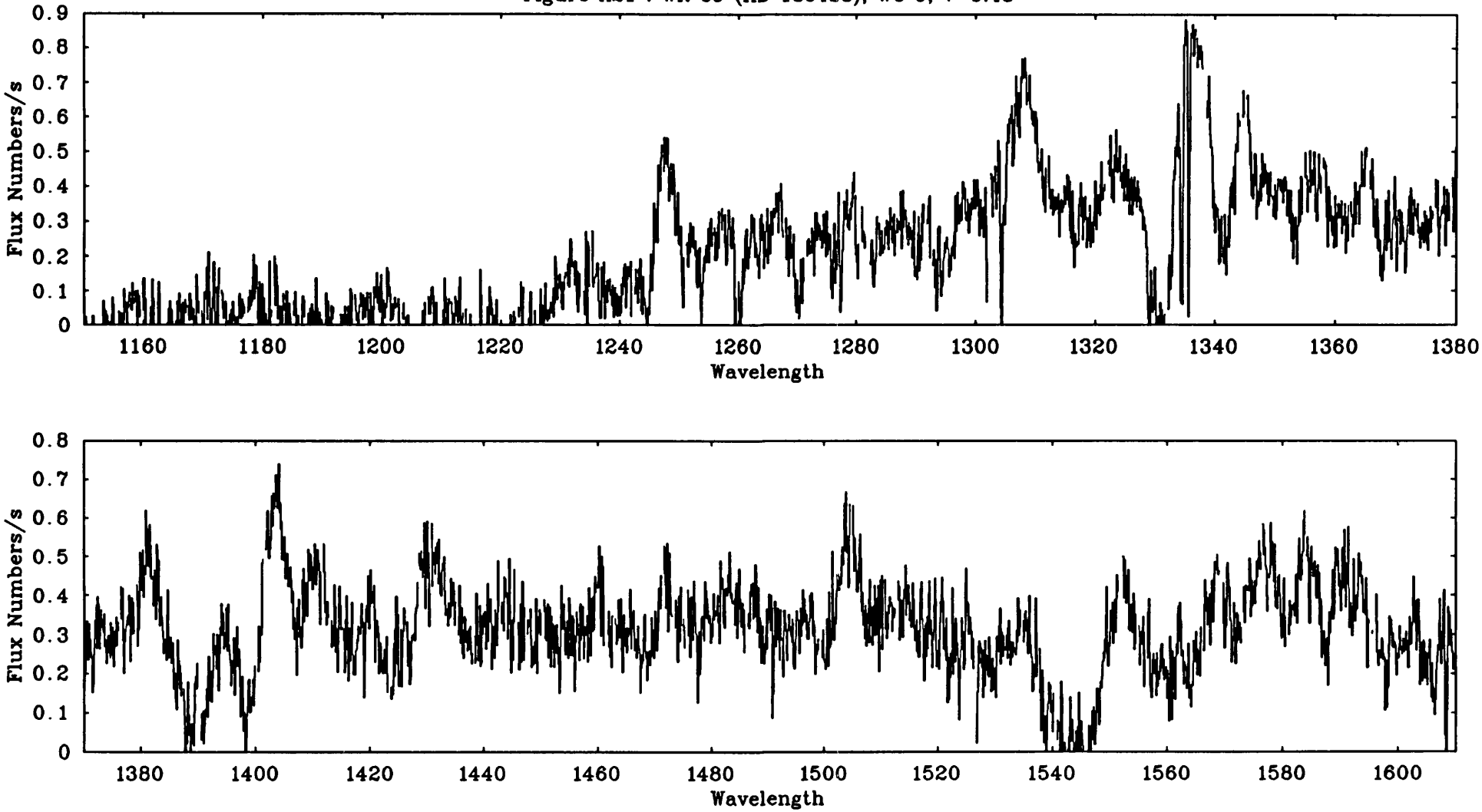

Figure A21 (continued) : WR 69 (HD 136488), WC 9, v=9.43

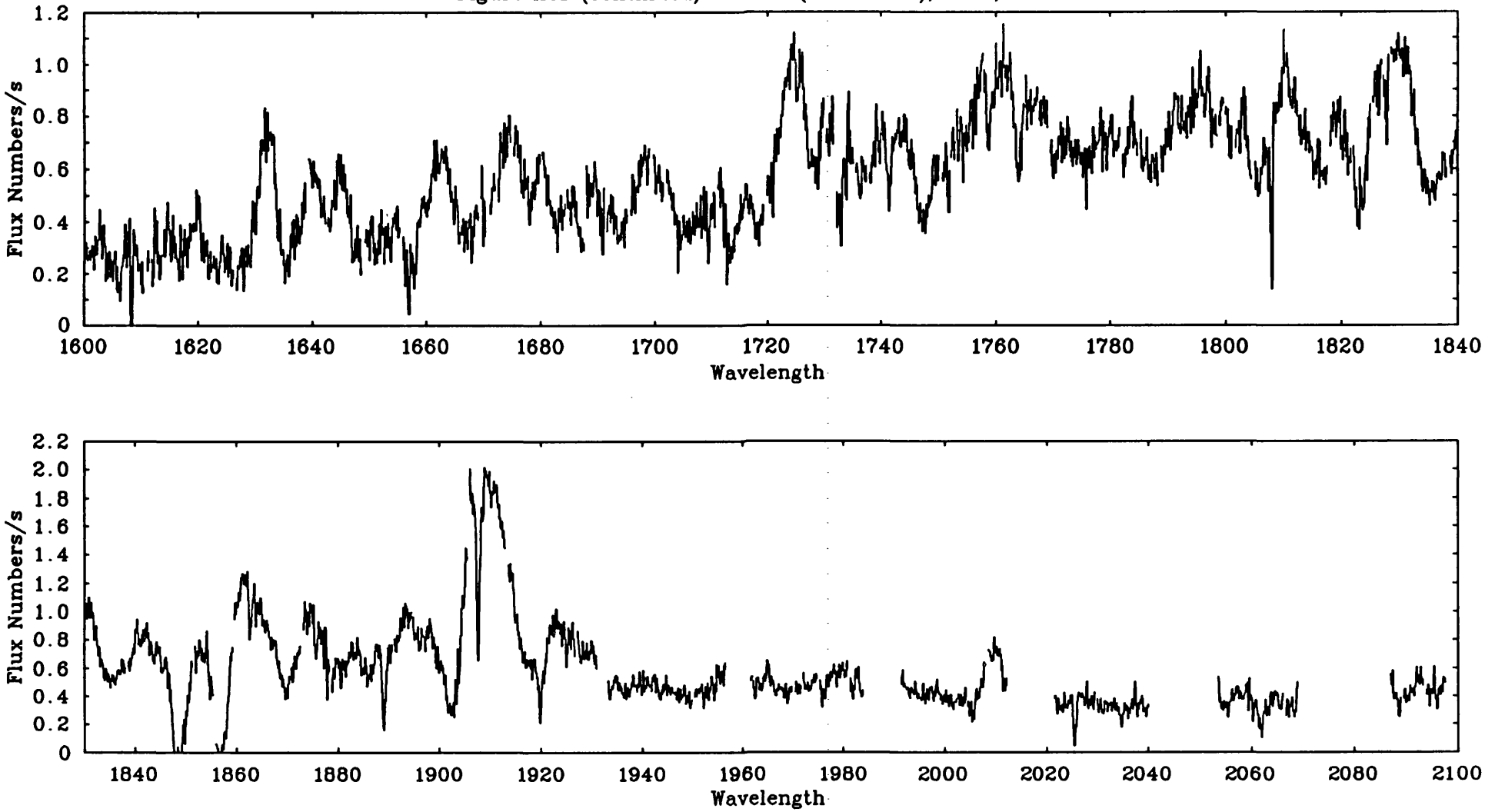

Figure A22 : WR 69 (HD 136488), WC 9, v=9.43

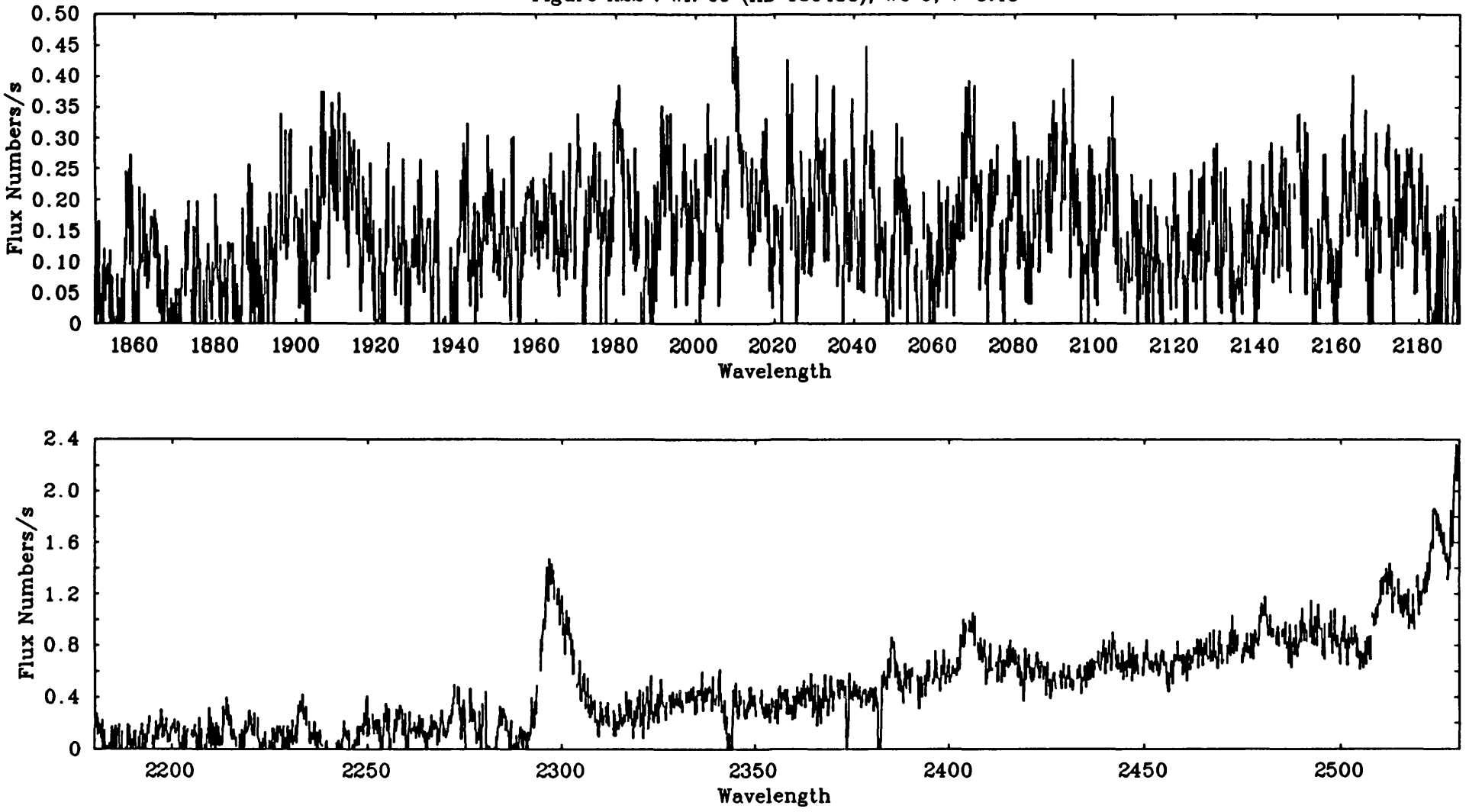

Figure A22 (continued) : WR 69 (HD 136488), WC 9, v=9.43

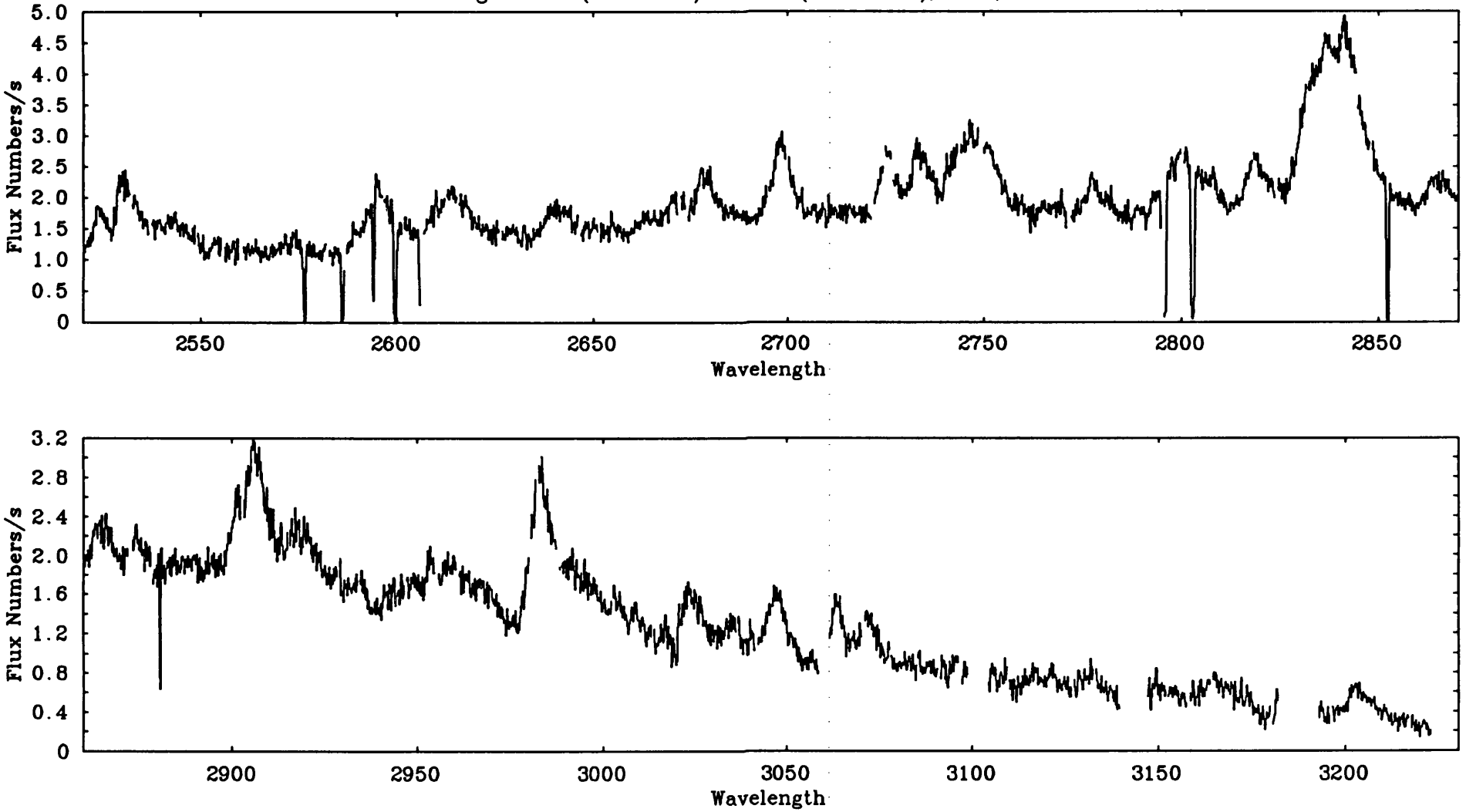

Figure A23 : WR 71 (HD 143414), WN 6, v=10.22

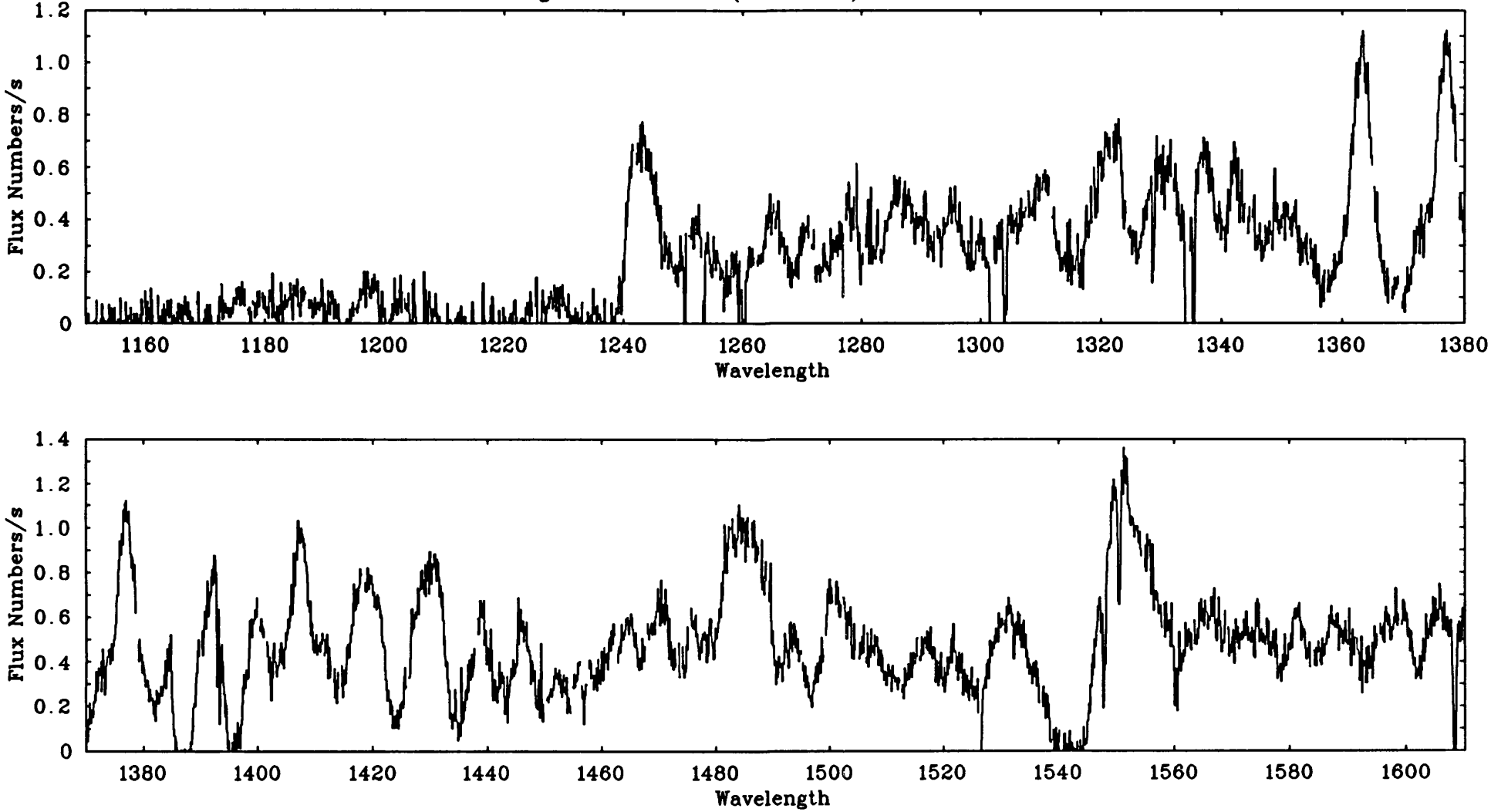

Figure A23 (continued) : WR 71 (HD 143414), WN 6, v=10.22

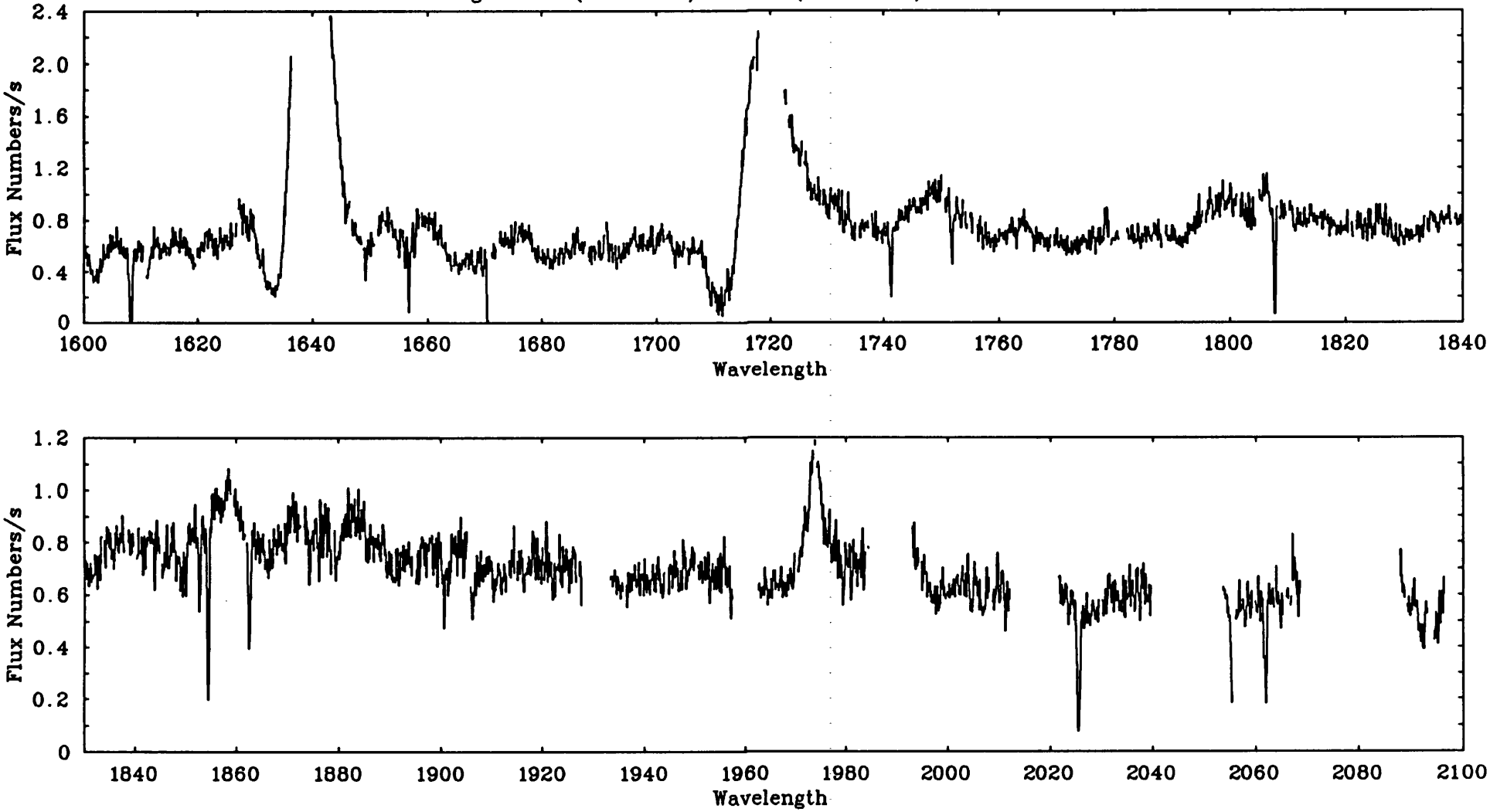

Figure A24 : WR 77 (HD 150136), WC 8, v=13.16

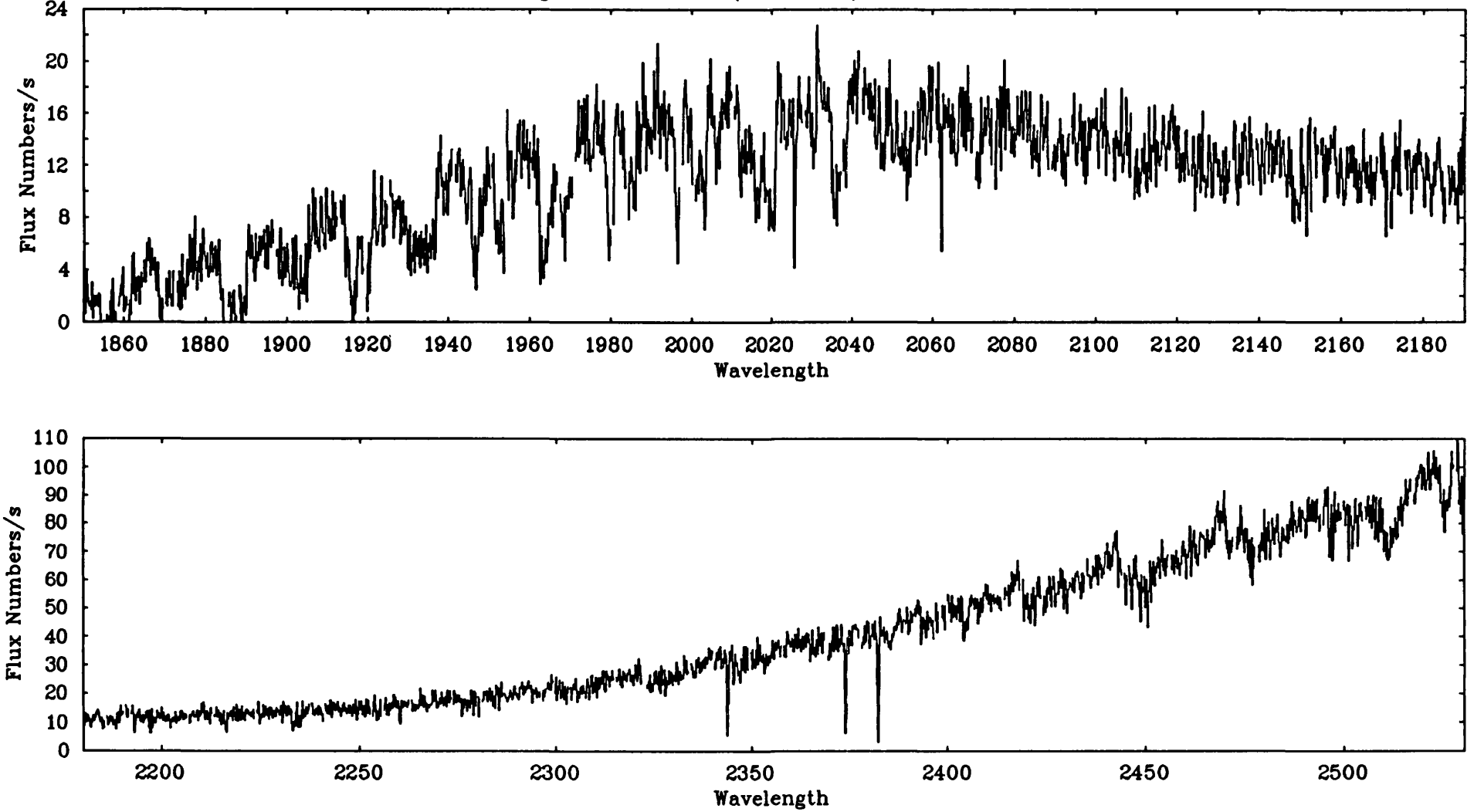

Figure A24 (continued) : WR 77 (HD 150136), WC 8, v=13.16

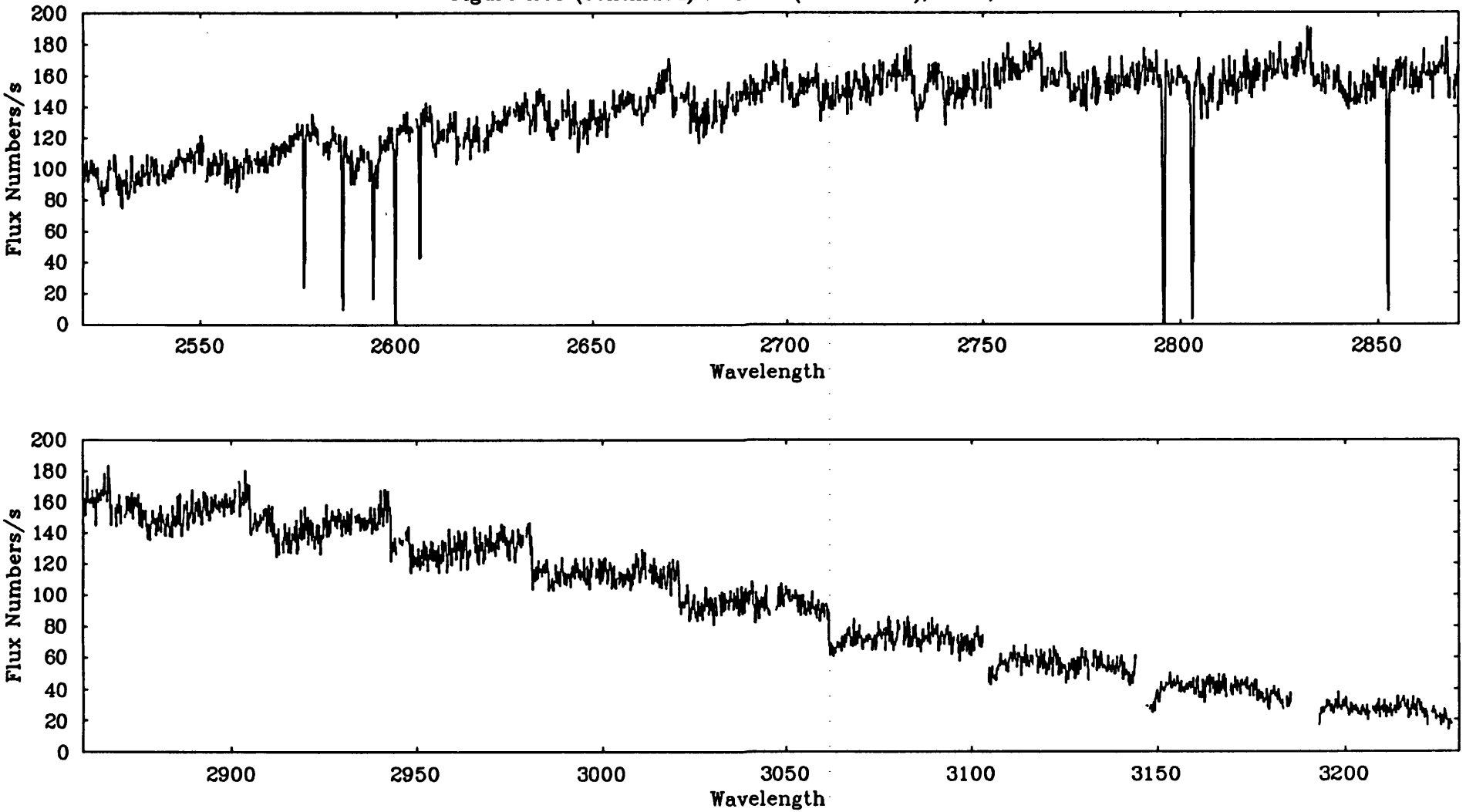

Figure A25 : WR 78 (HD 151932), WN 7, v=6.61

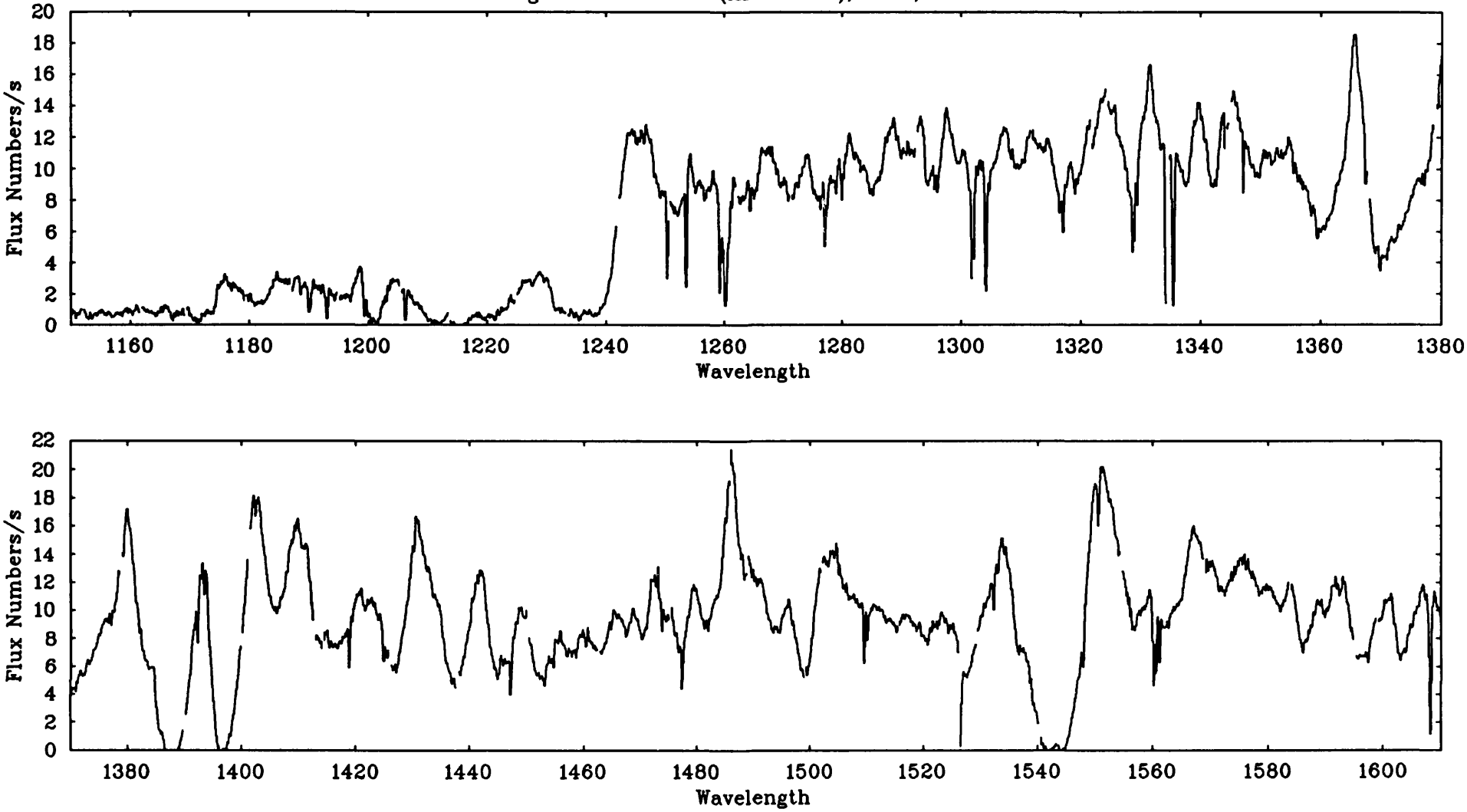

Figure A25 (continued) : WR 78 (HD 151932), WN 7, v=6.61

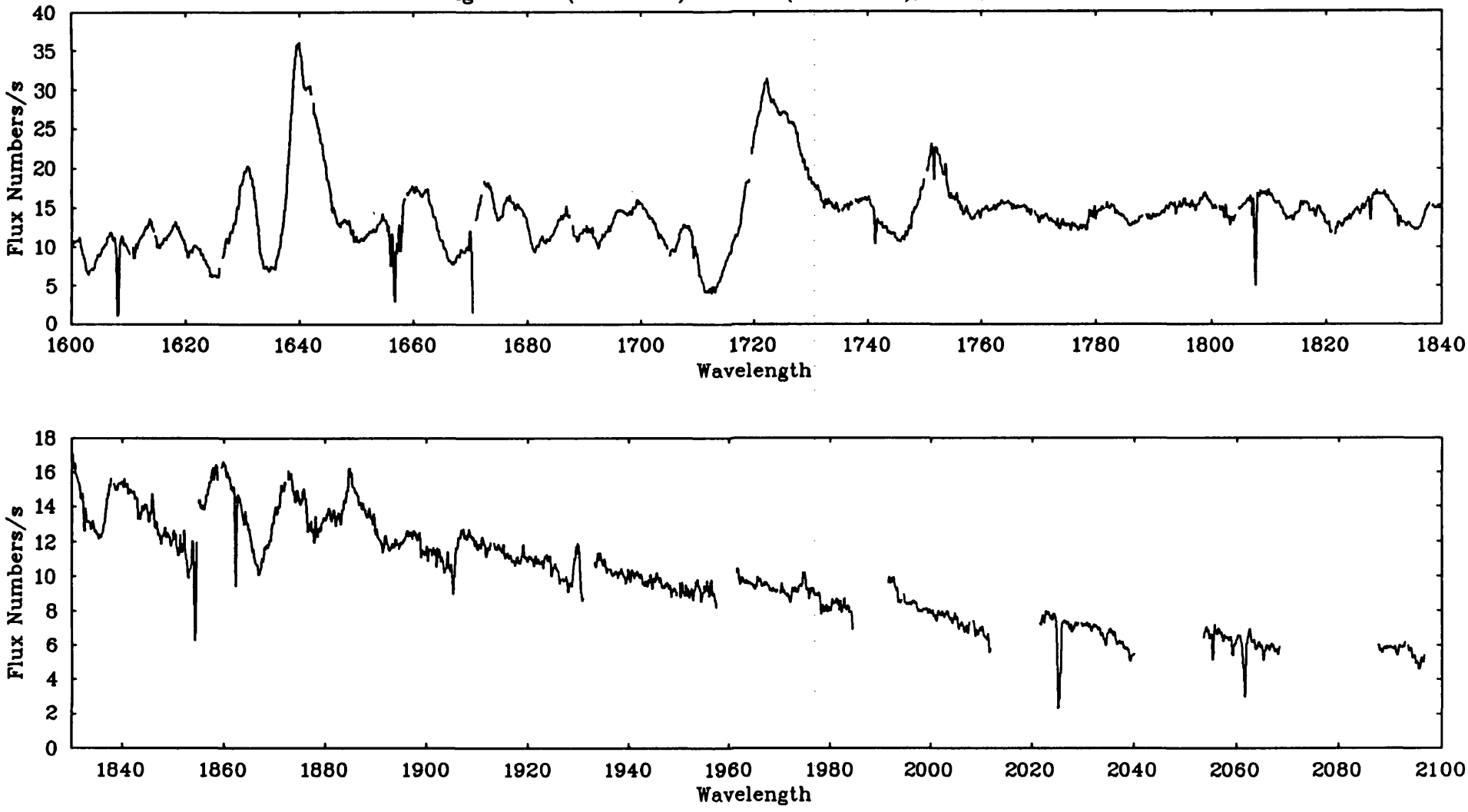

Figure A26 : WR 78 (HD 151932), WN 7, v=6.61

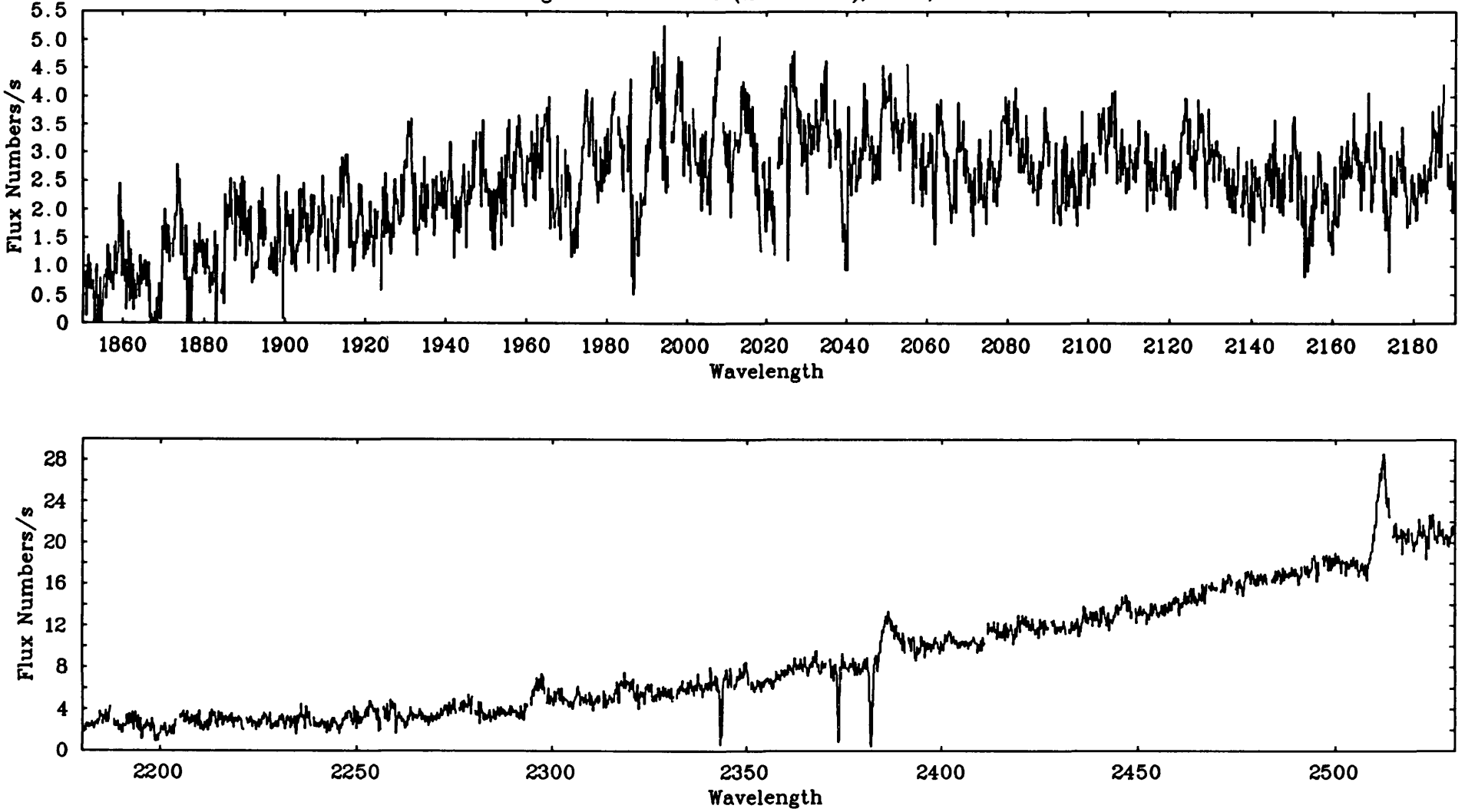

Figure A26 (continued) : WR 78 (HD 151932), WN 7, v=6.61

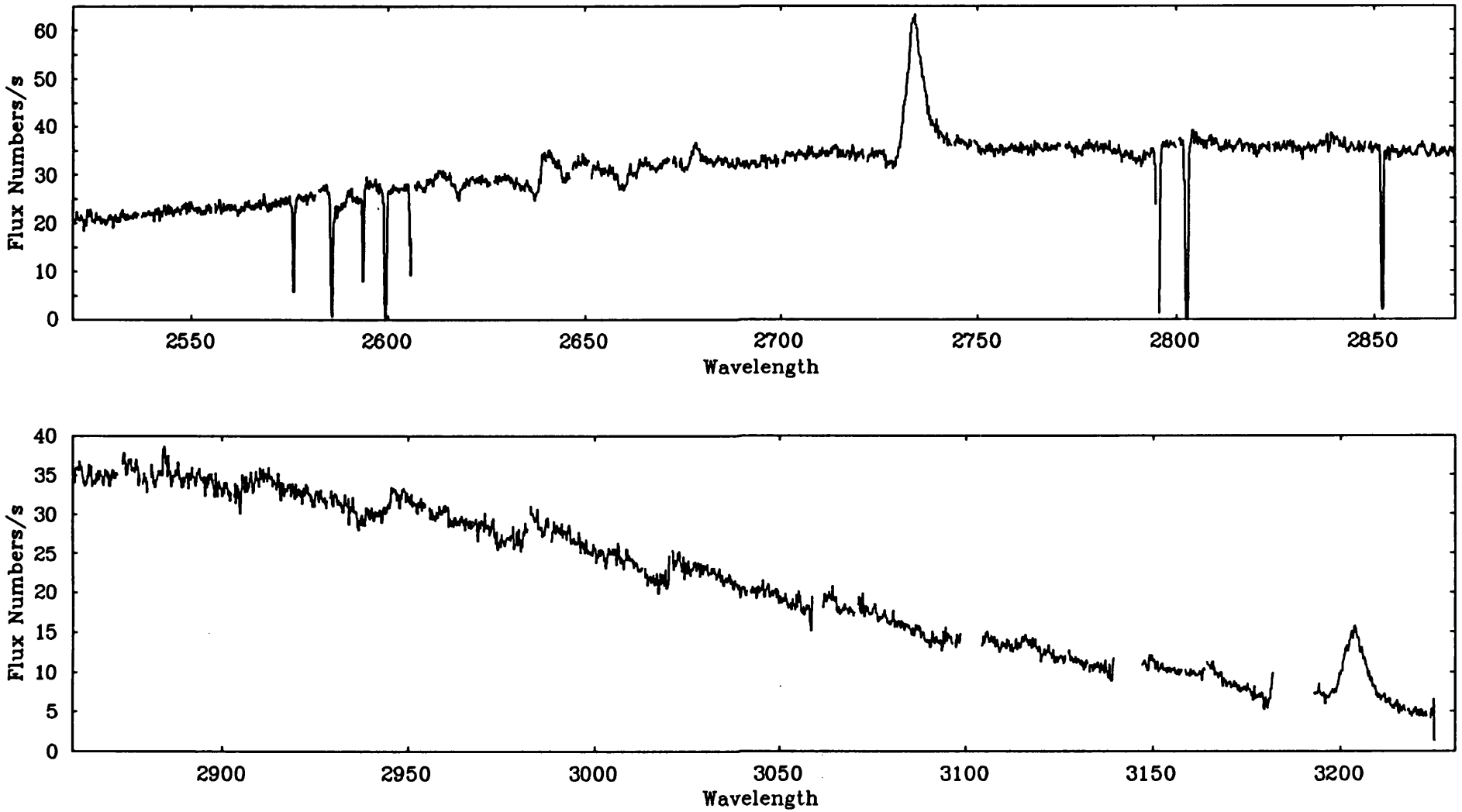

Figure A27 : WR 90 (HD 156385), WC 7, v=7.45

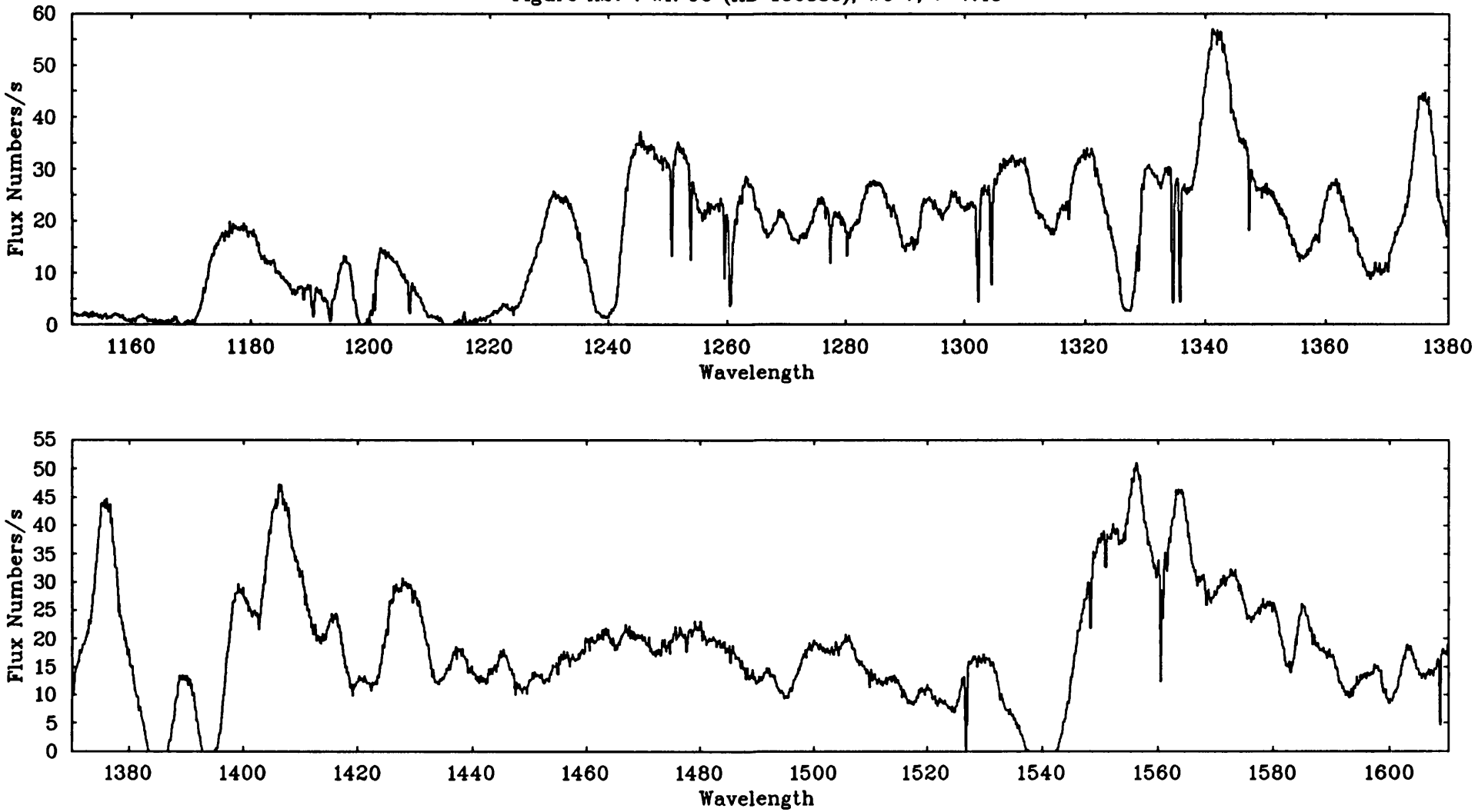

Figure A27 (continued) : WR 90 (HD 156385), WC 7, v=7.45

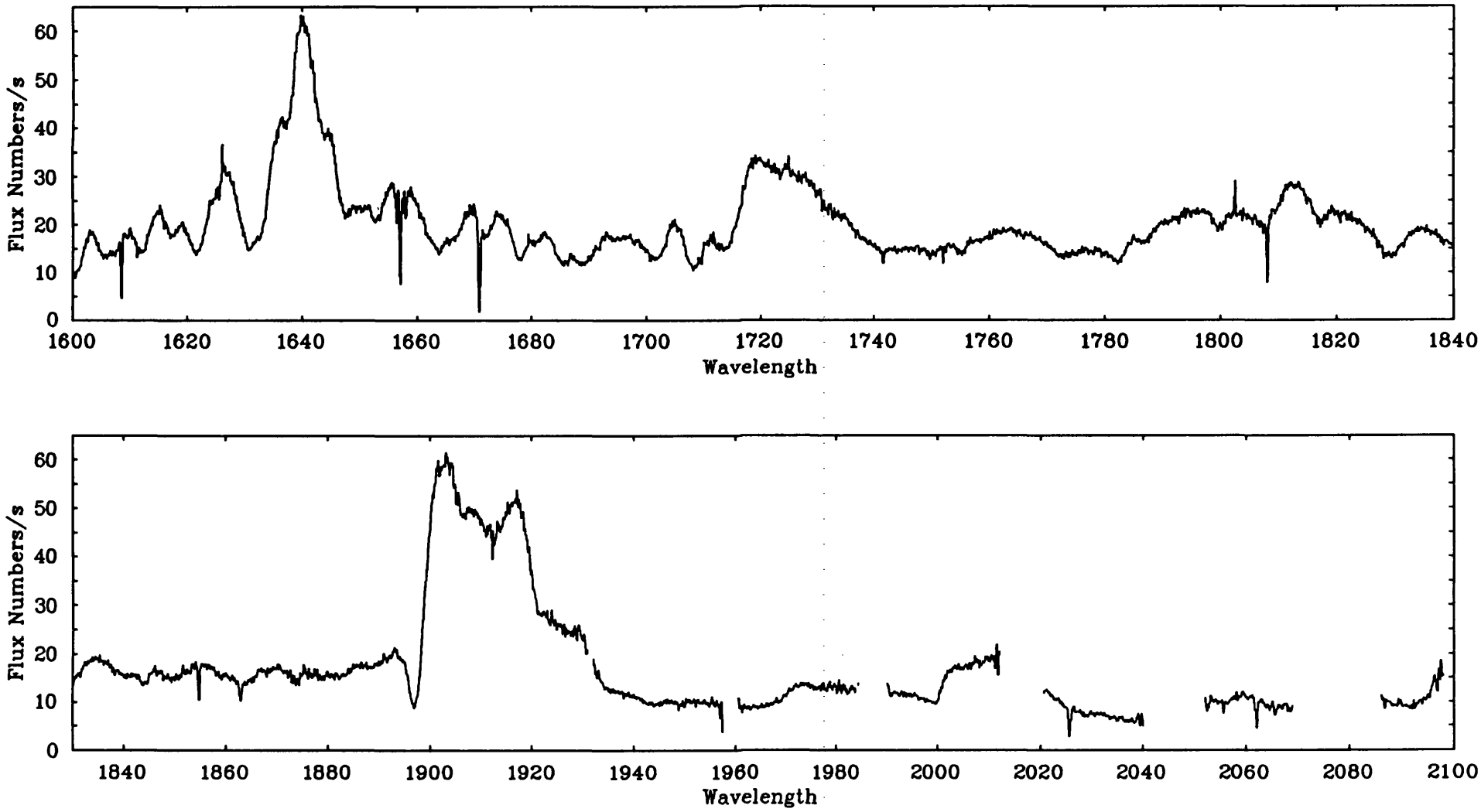

Figure A28 : WR 90 (HD 156385), WC 7, v=7.45

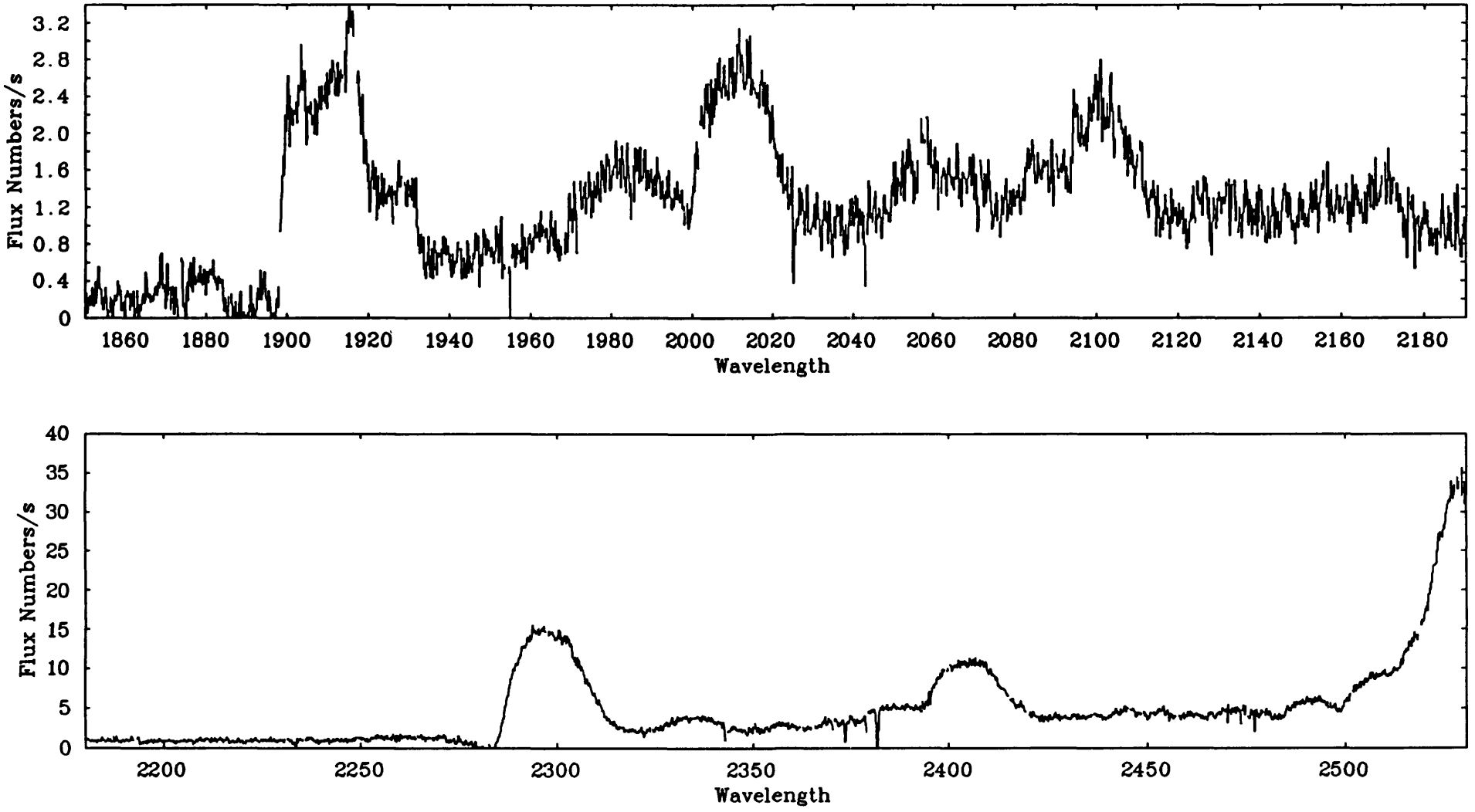

Figure A28 (continued) : WR 90 (HD 156385), WC 7, v=7.45

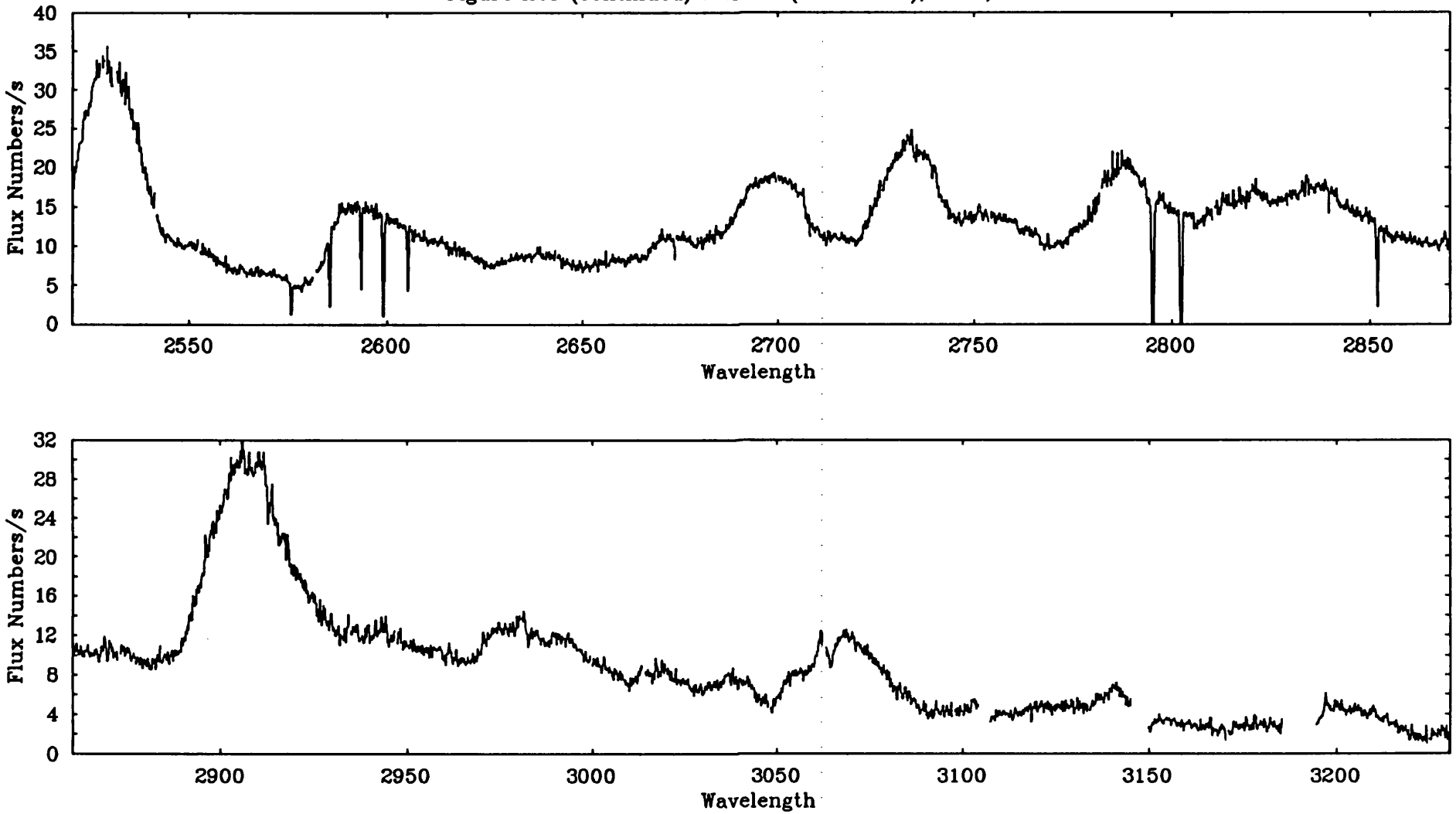

Figure A29 : WR 92 (HD 157451), WC 9, v=10.60

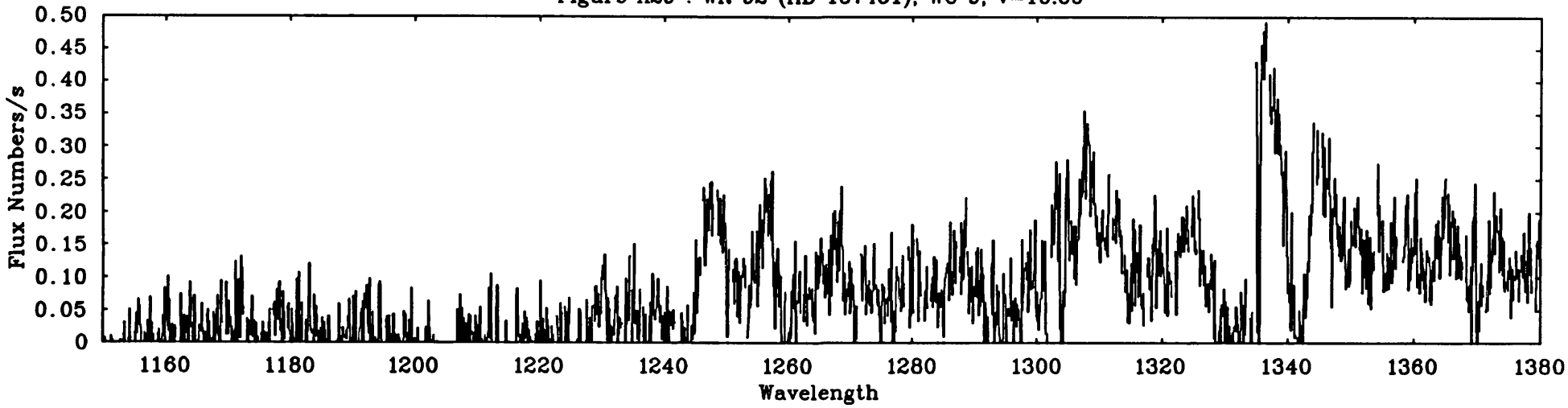

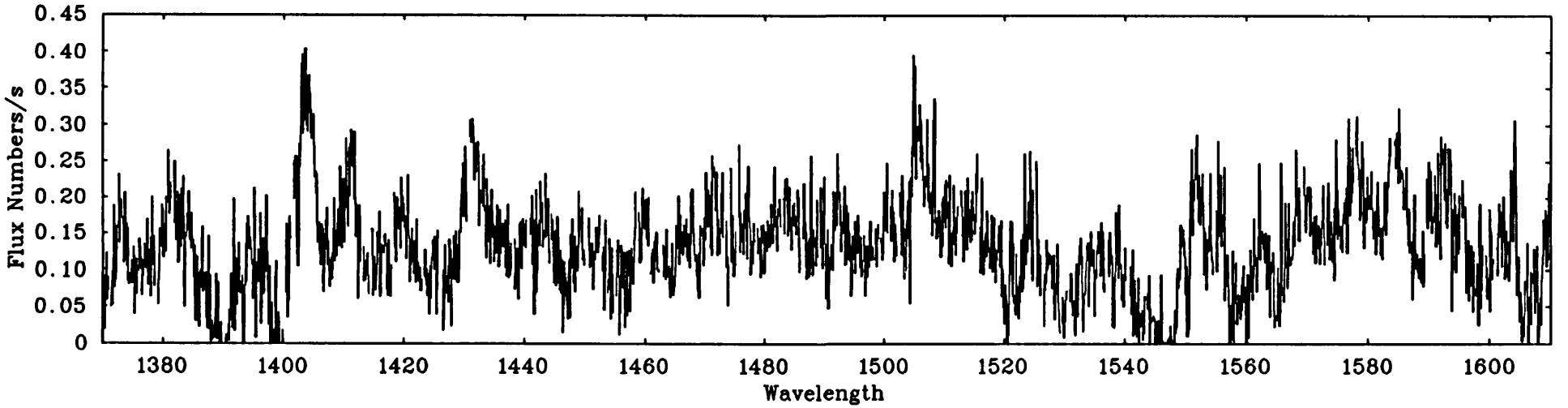

Figure A29 (continued) : WR 92 (HD 157451), WC 9, v=10.60

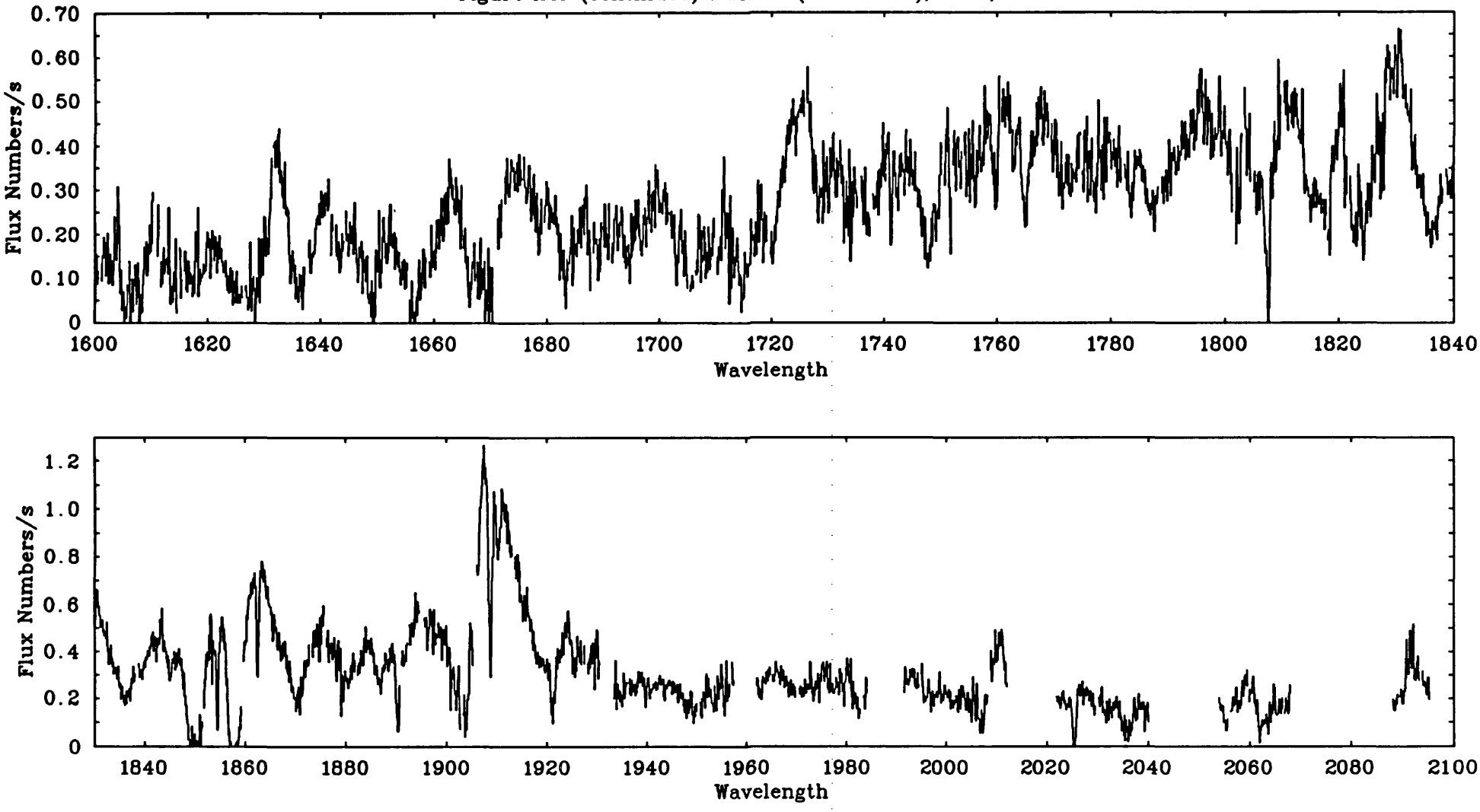

Figure A30 : WR 92 (HD 157451), WC 9, v=10.60

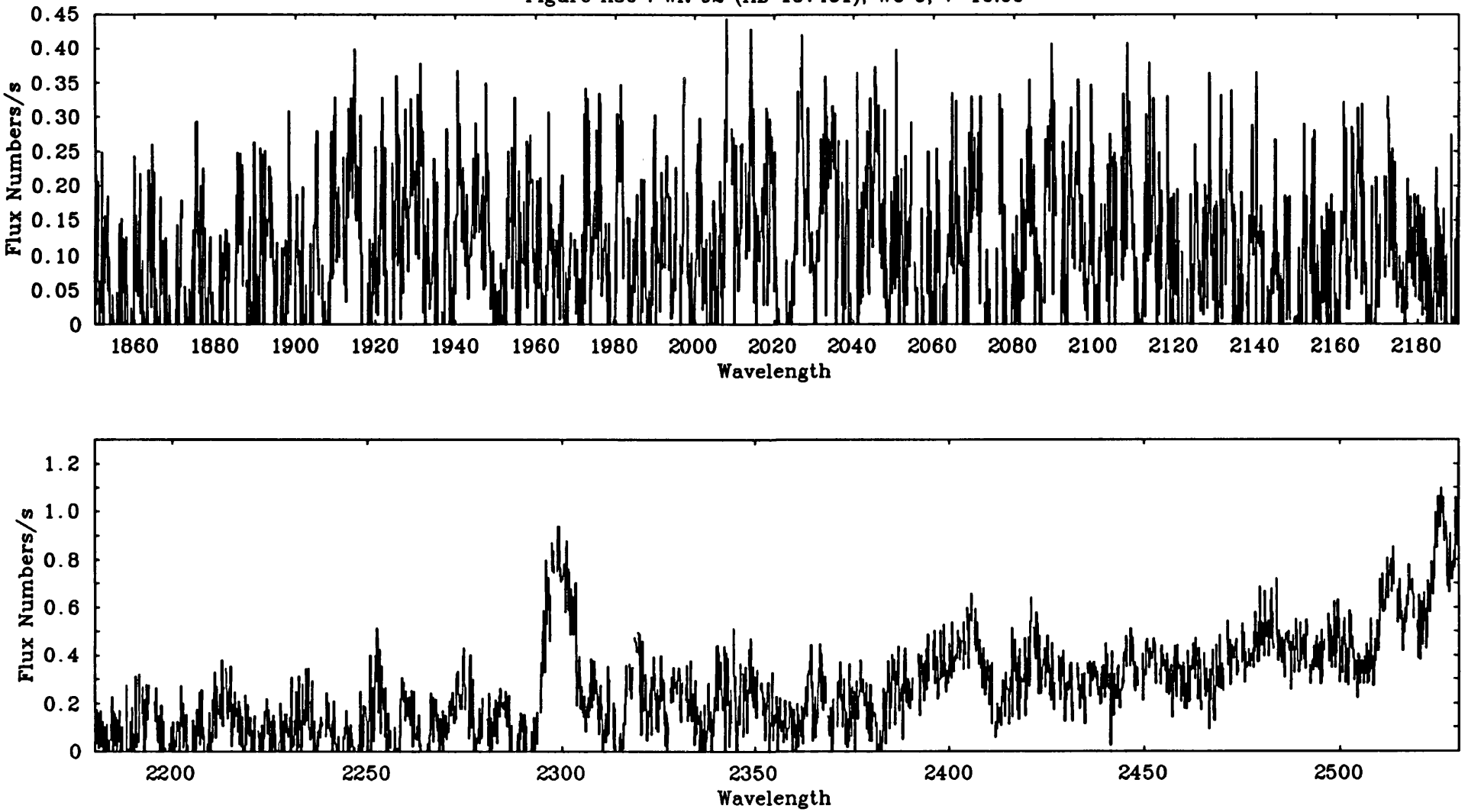

Figure A30 (continued) : WR 92 (HD 157451), WC 9, v=10.60

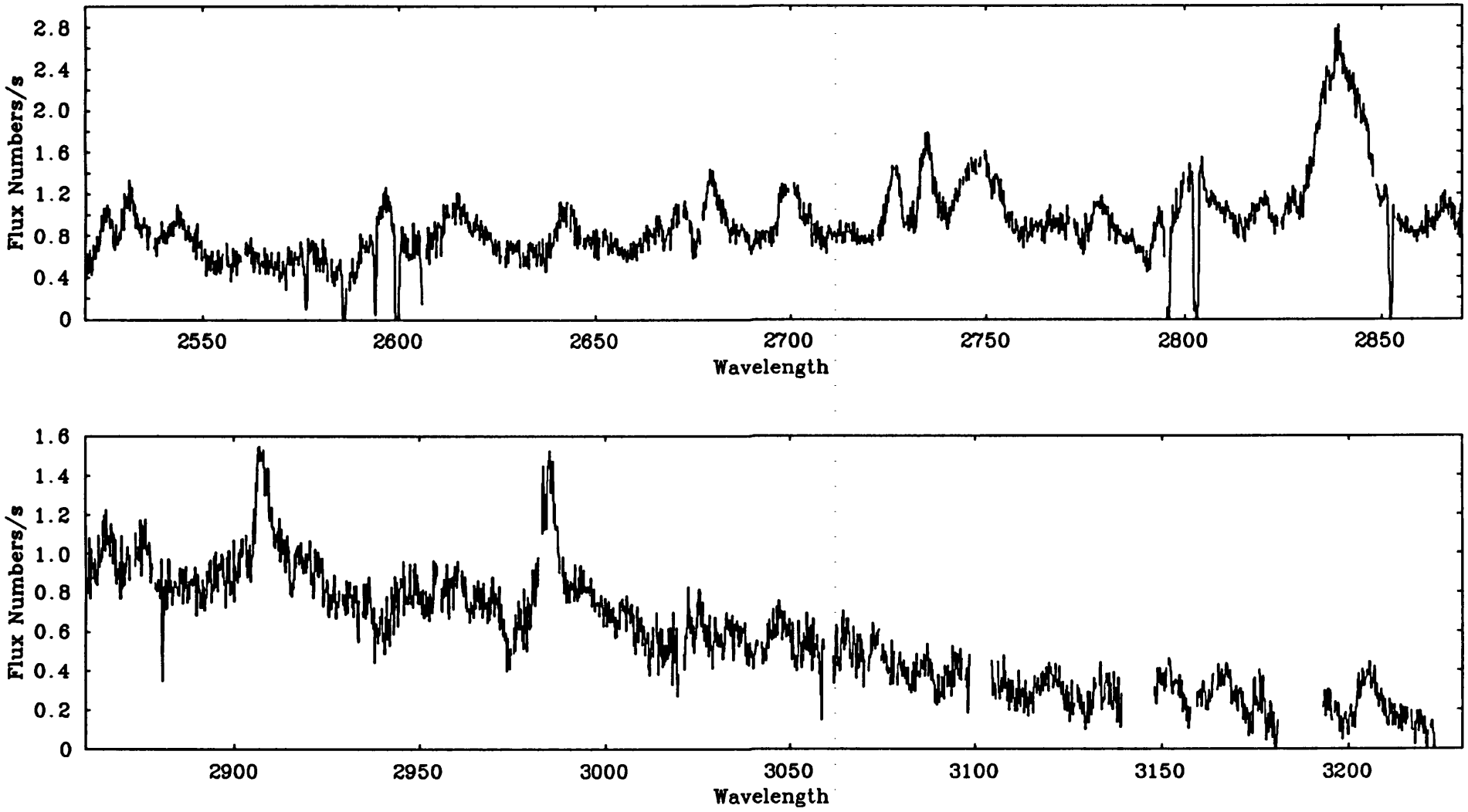

Figure A31 : WR 103 (HD 164270), WC 9, v=9.01

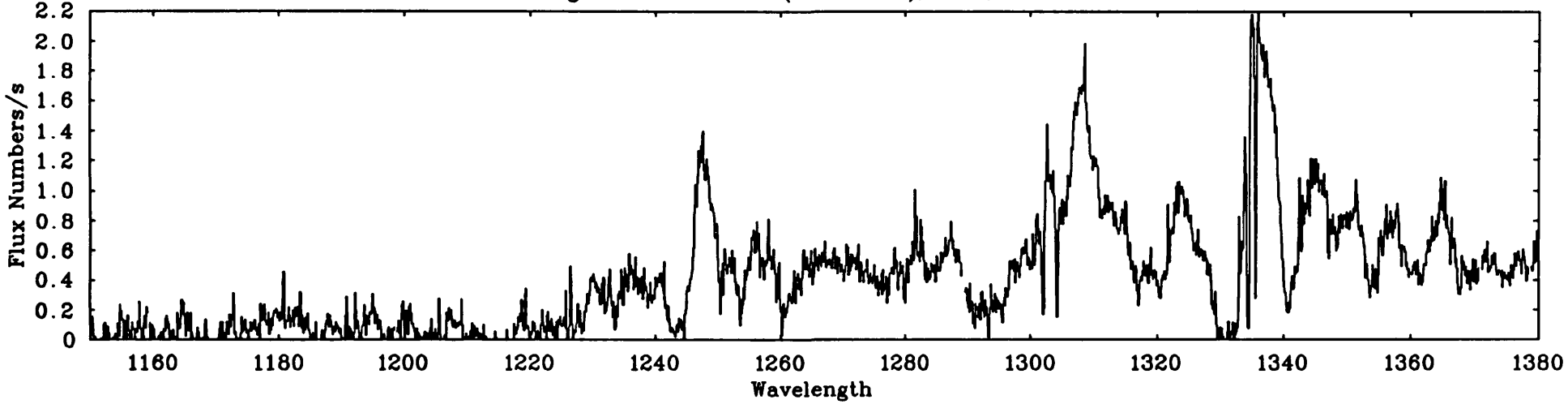

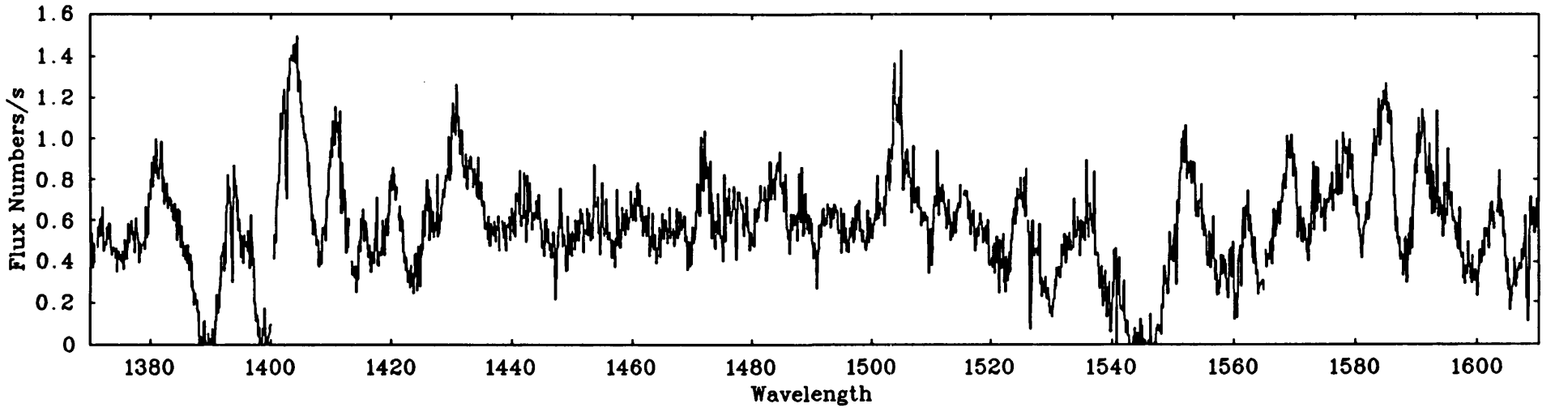

Figure A31 (continued) : WR 103 (HD 164270), WC 9, v=9.01

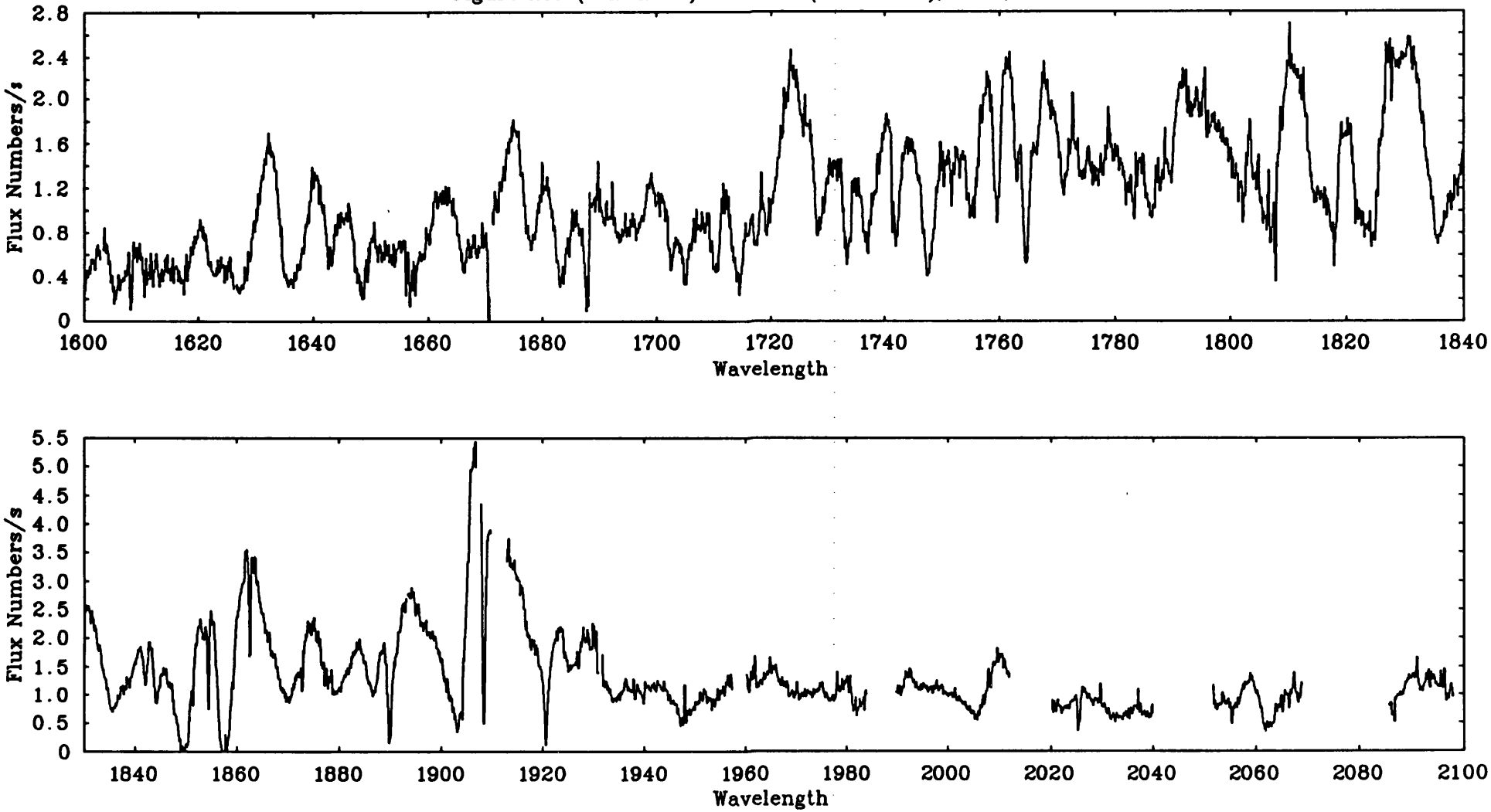

Figure A32 : WR 103 (HD 164270), WC 9, v=9.01

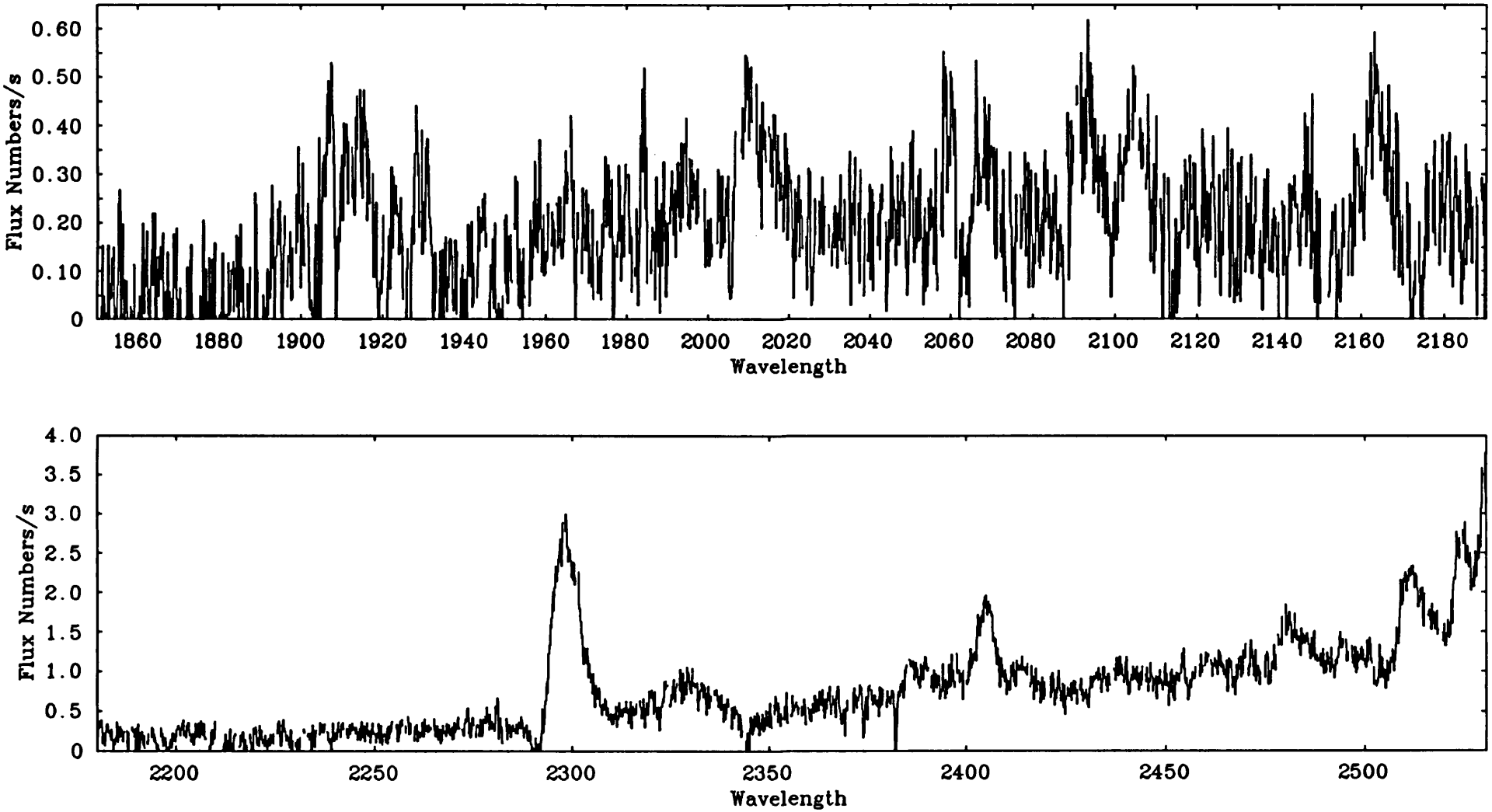

Figure A32 (continued) : WR 103 (HD 164270), WC 9, v=9.01

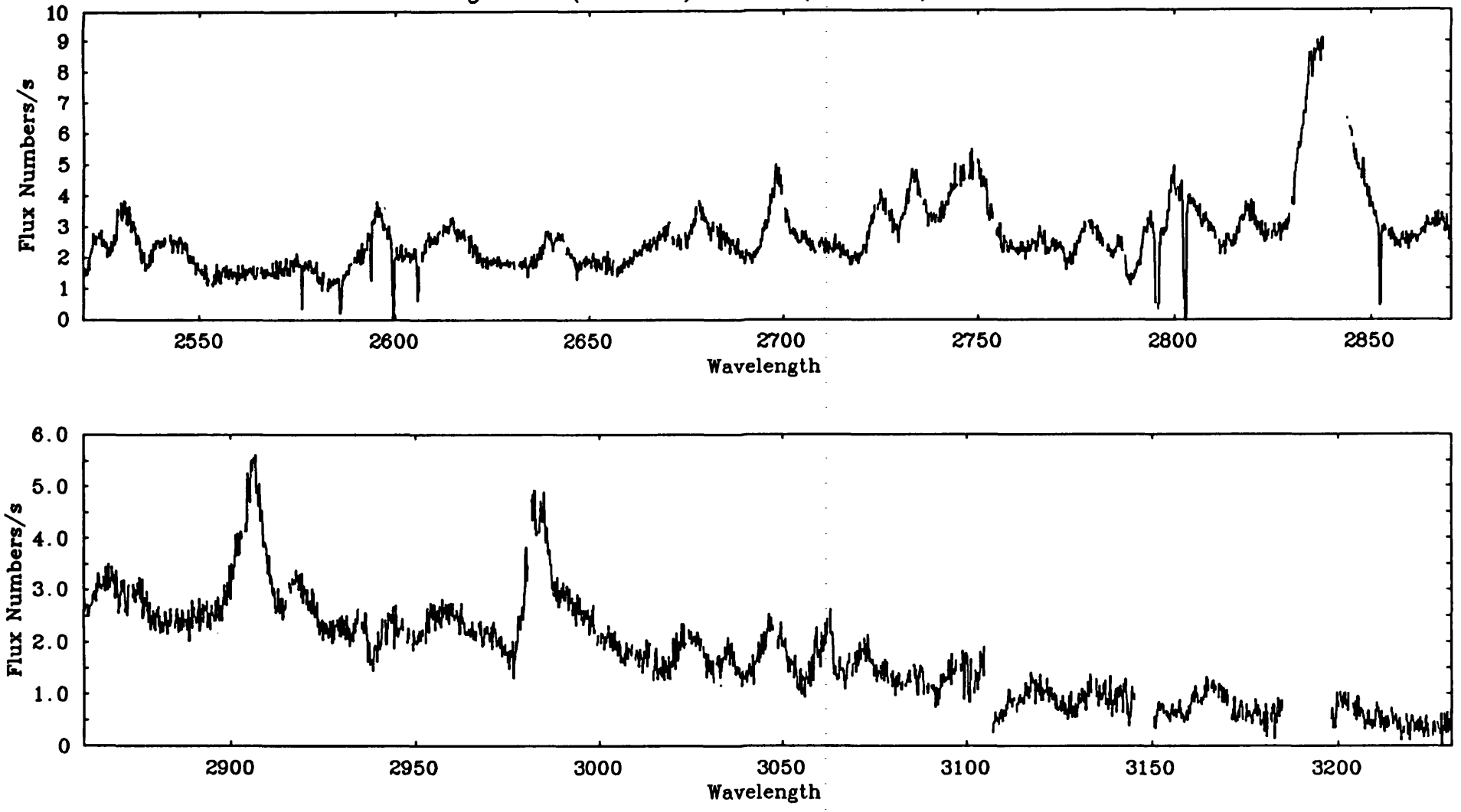

Figure A33 : WR 111 (HD 165763), WC 5, v=8.23

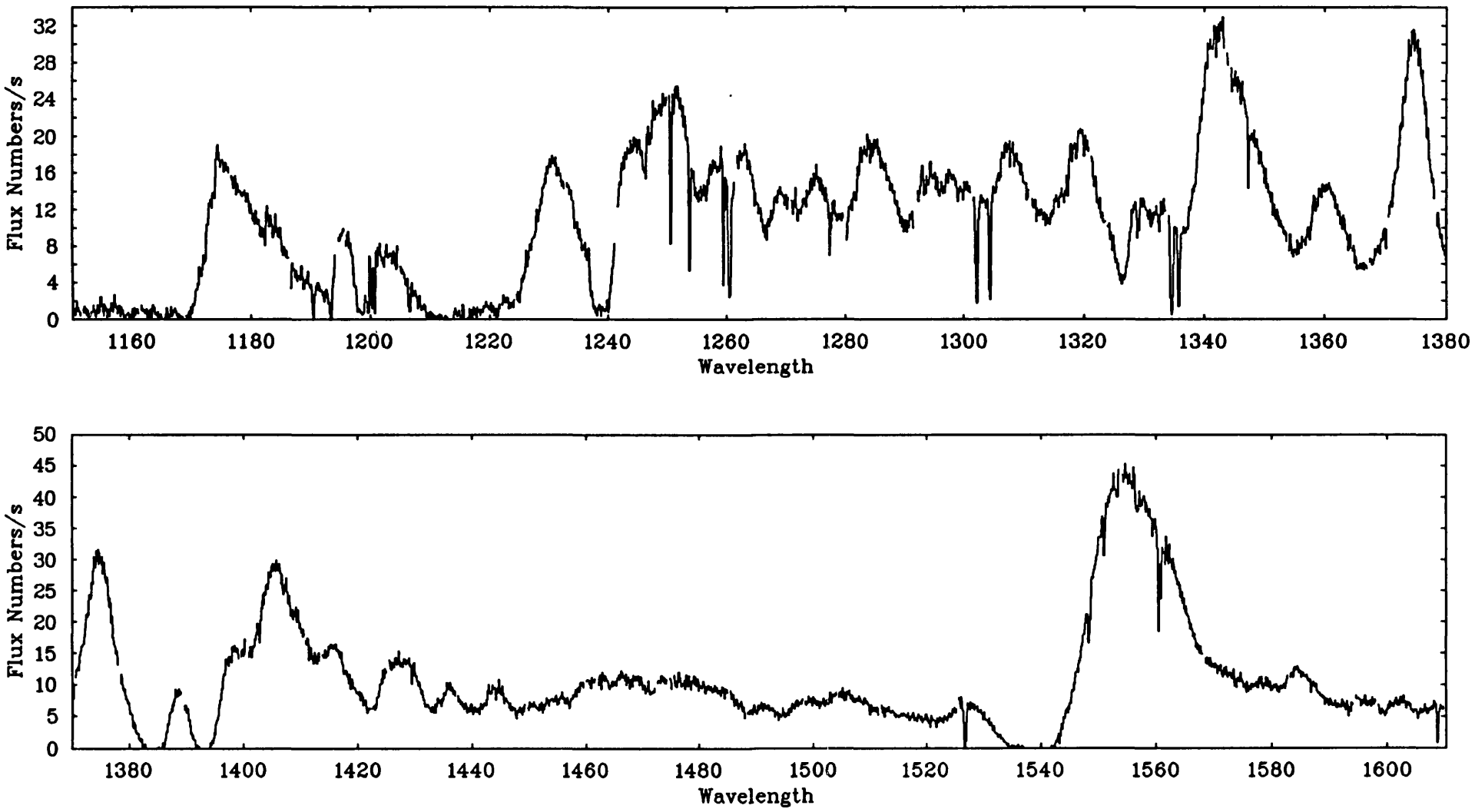

Figure A33 (continued) : WR 111 (HD 165763), WC 5, v=8.23

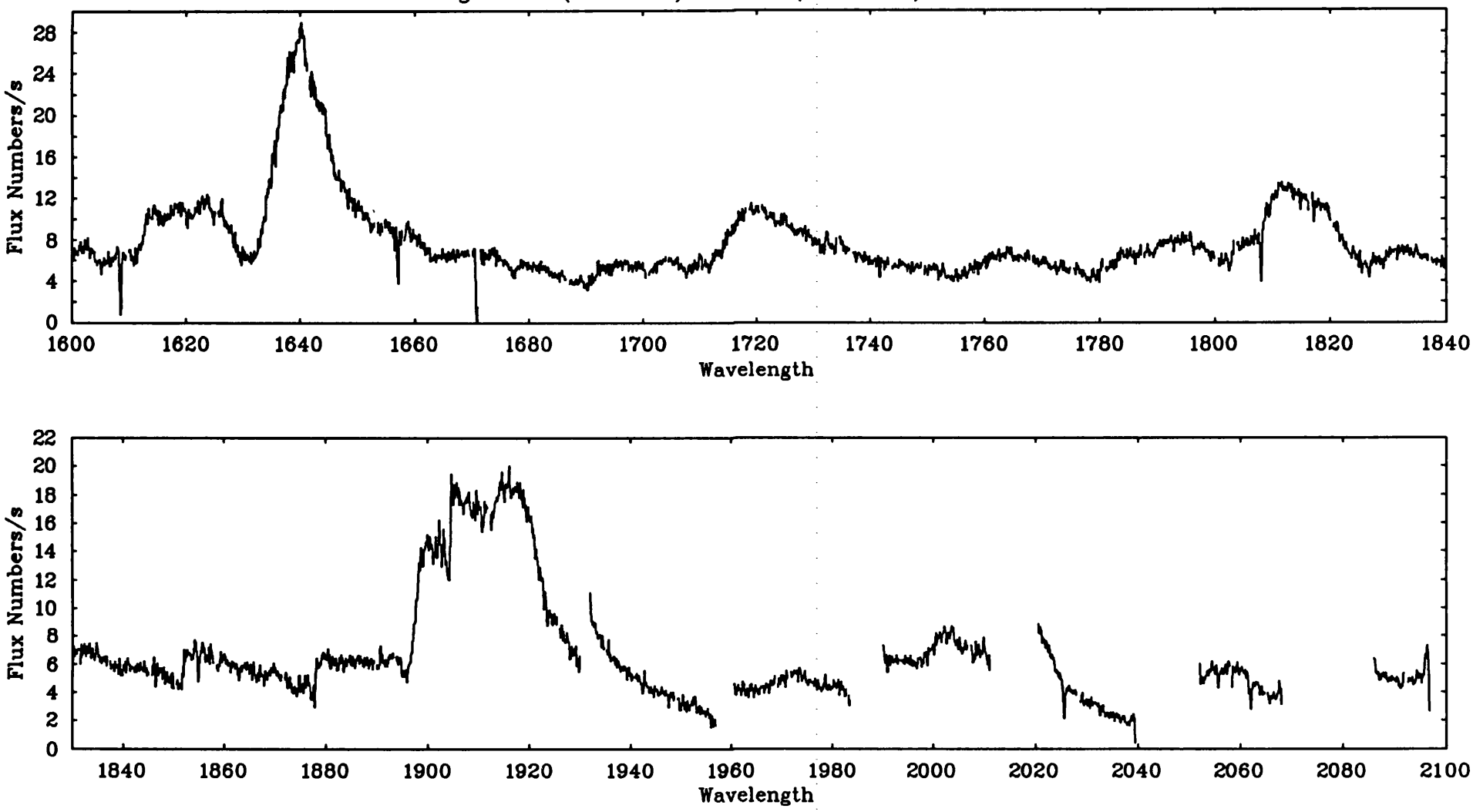

Figure A34 : WR 111 (HD 165763), WC 5, v=8.23

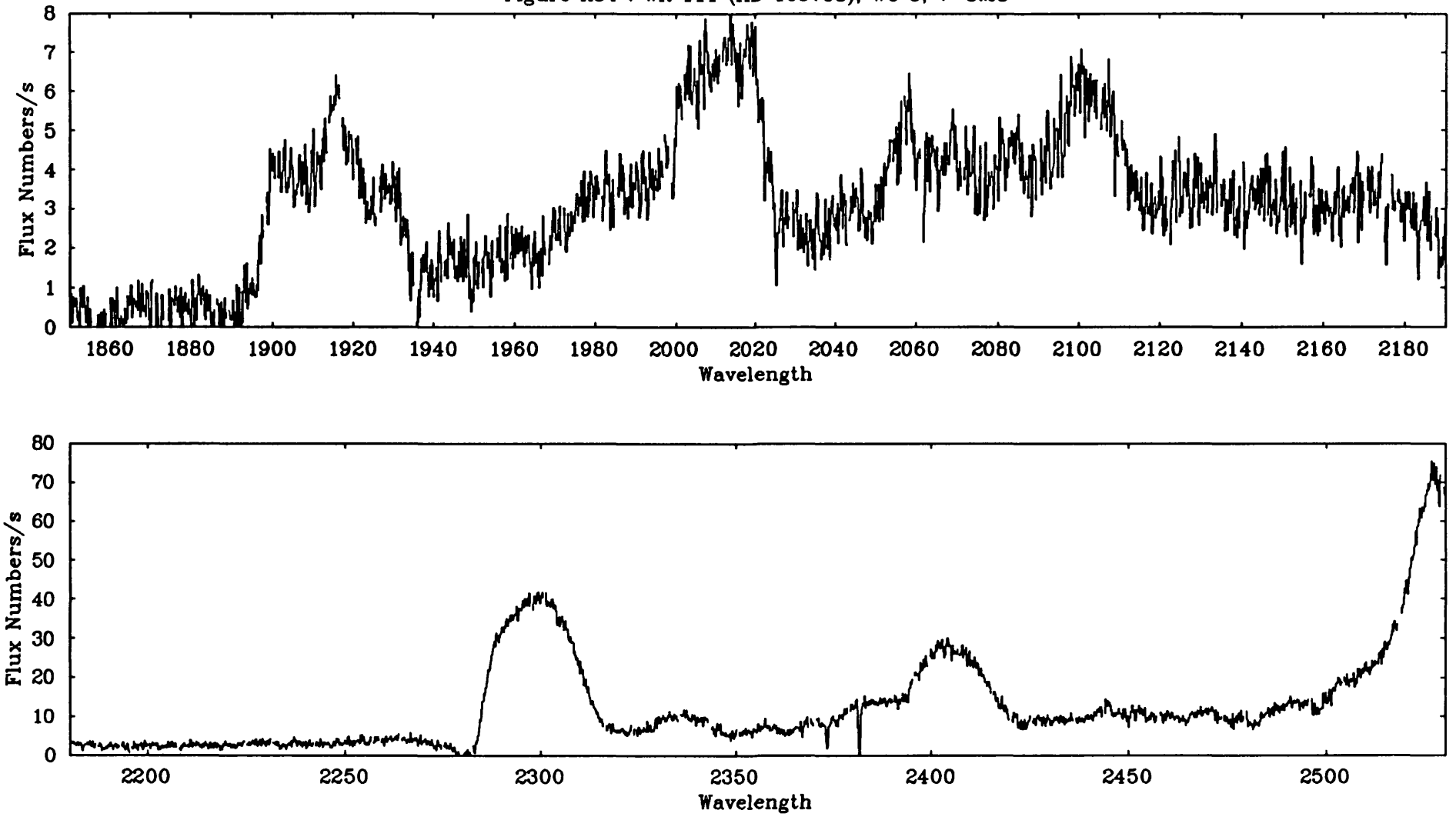

Figure A34 (continued) : WR 111 (HD 165763), WC 5, v=8.23

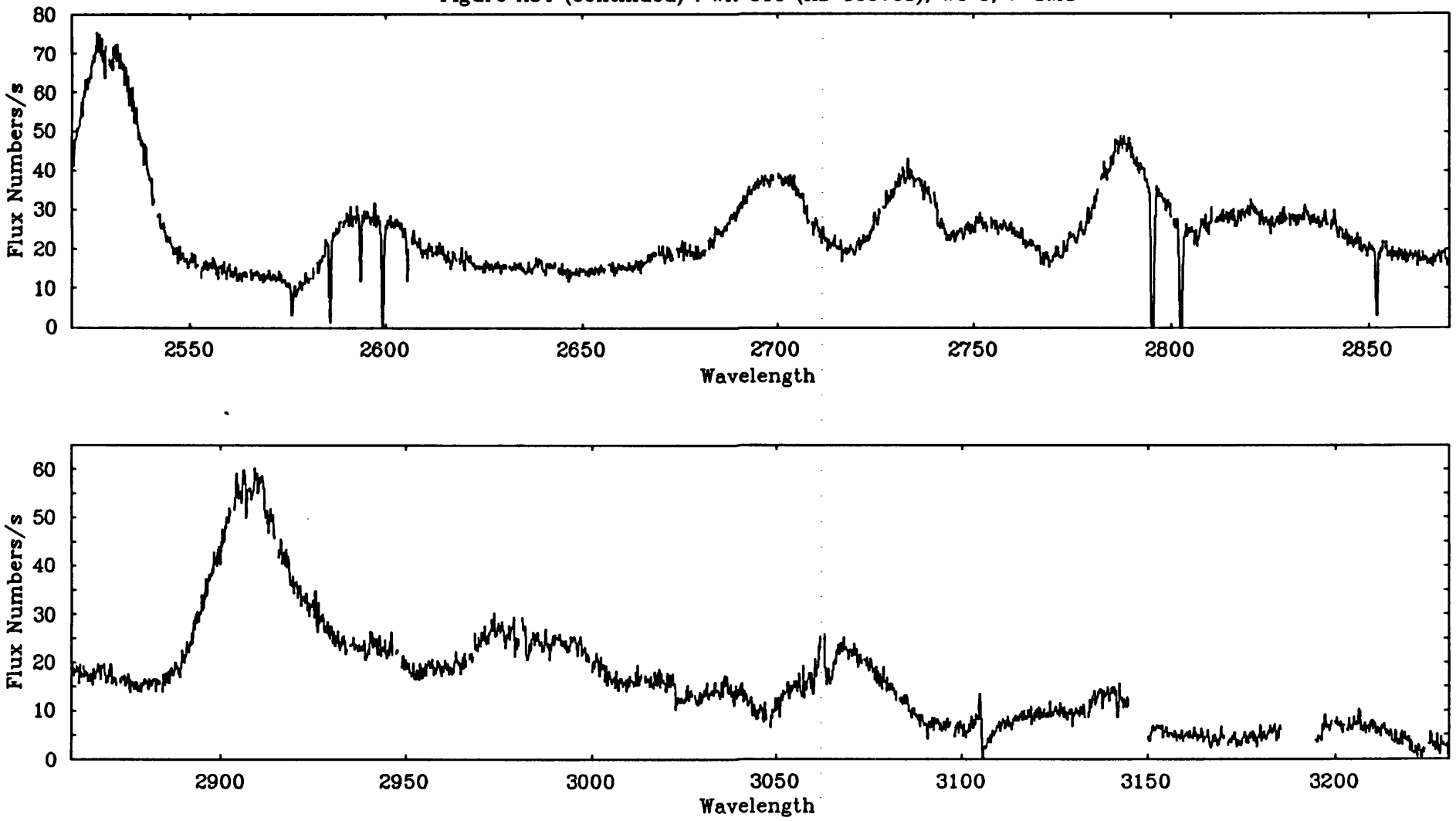

Figure A35 : WR 128 (HD 187282), WN 4, v=10.54

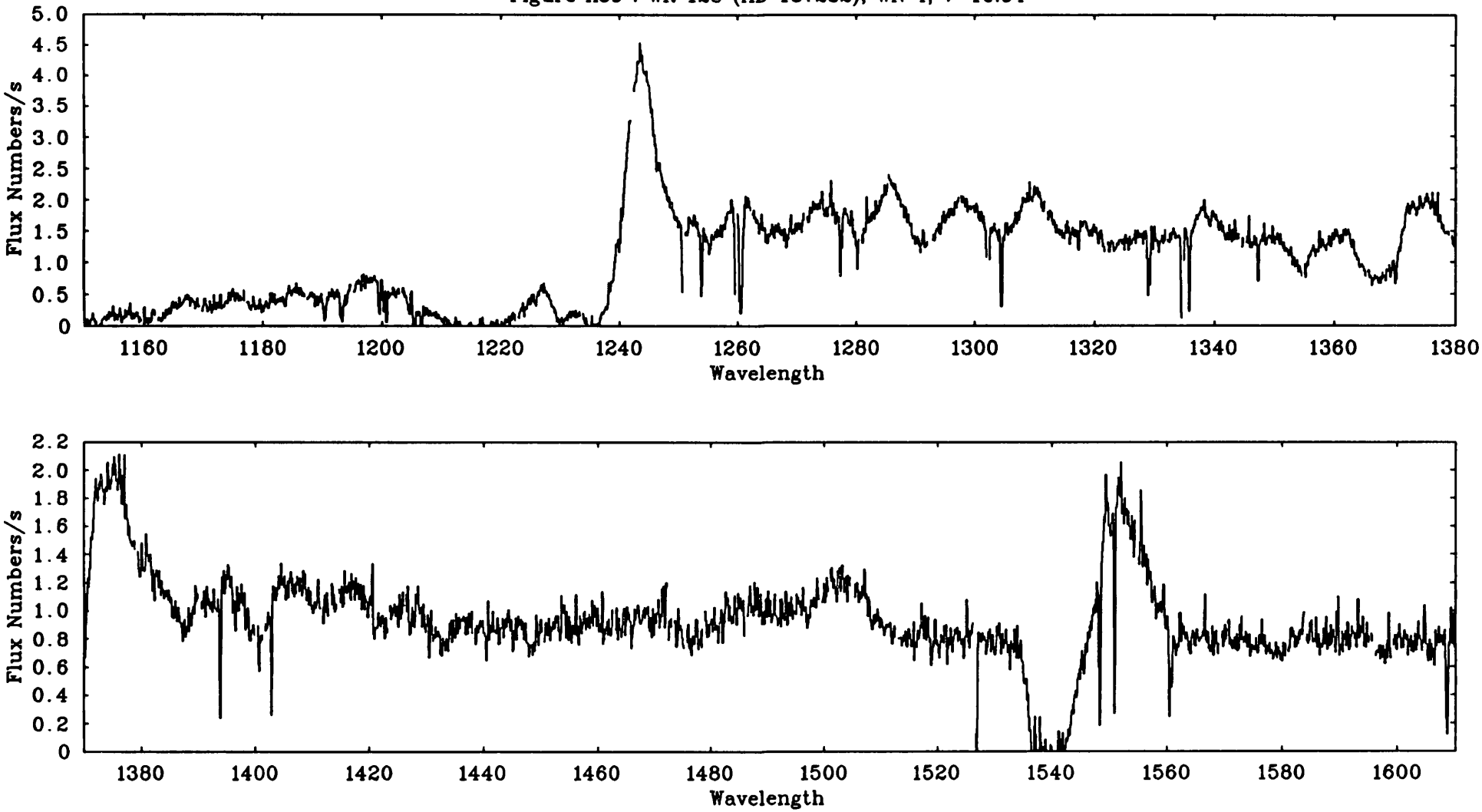

Figure A35 (continued) : WR 128 (HD 187282), WN 4, v=10.54

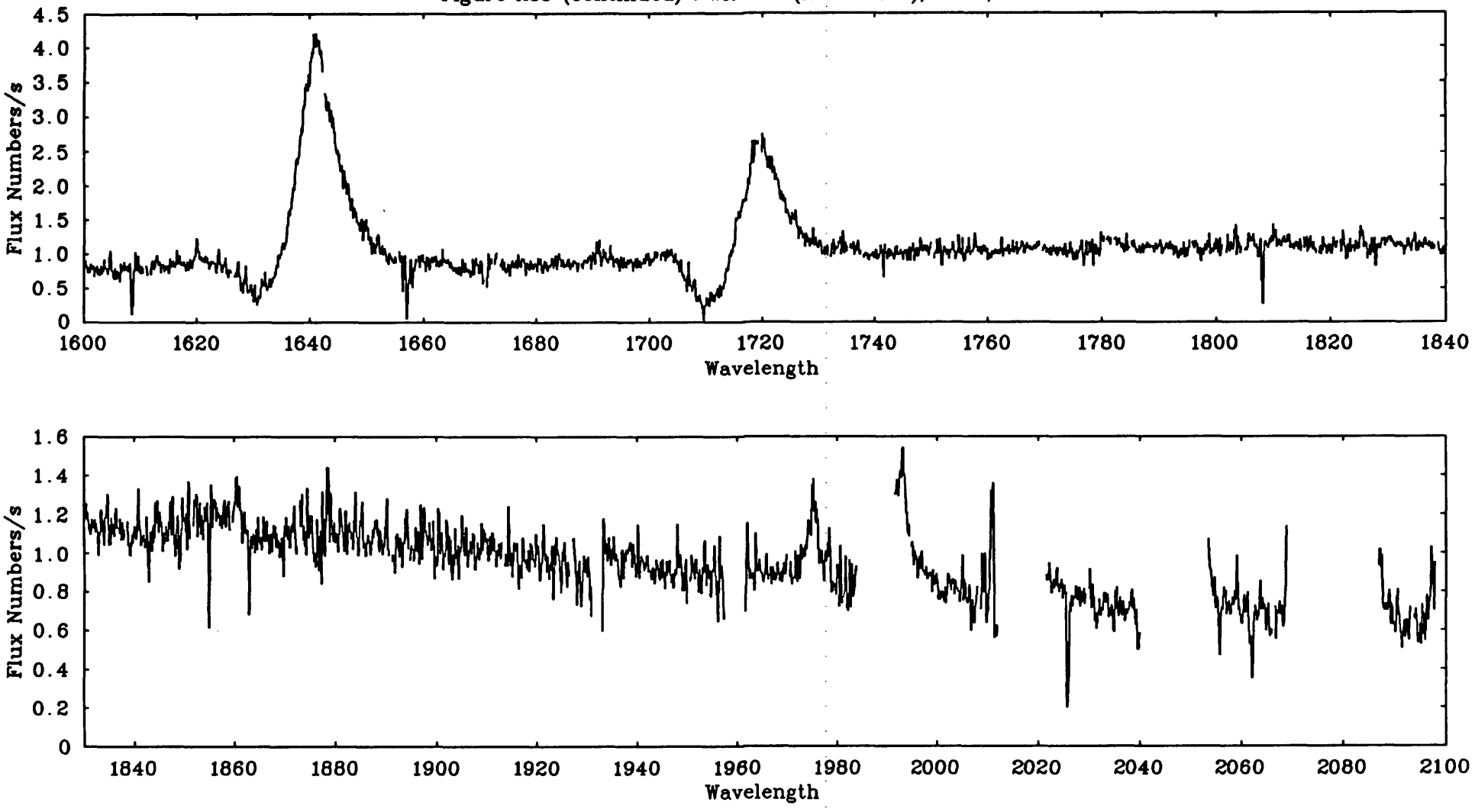

Figure A36 : WR 134 (HD 191765), WN 6, v=8.23

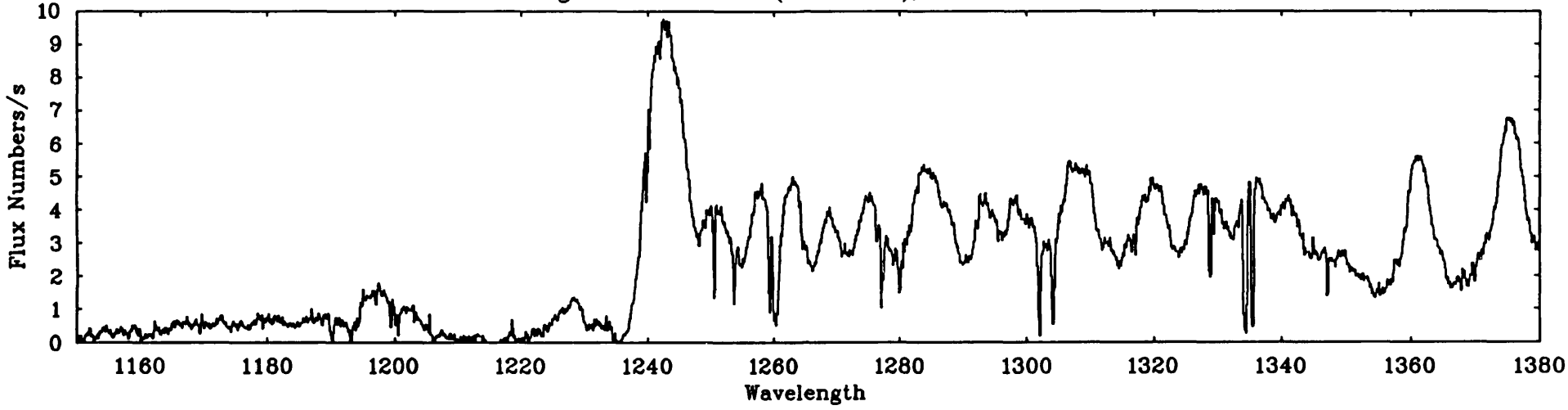

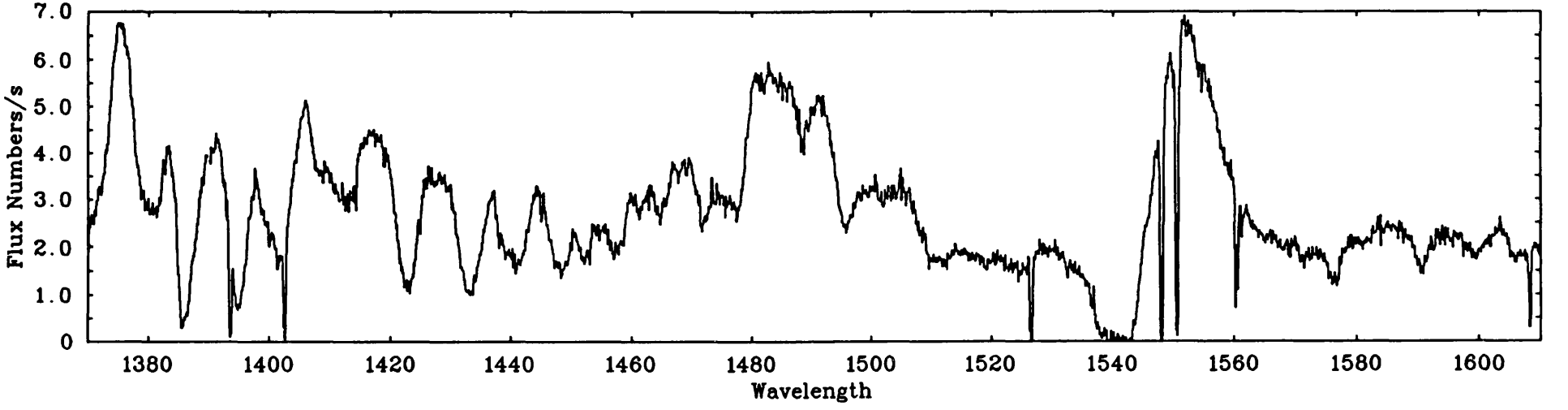

Figure A36 (continued) : WR 134 (HD 191765), WN 6, v=8.23

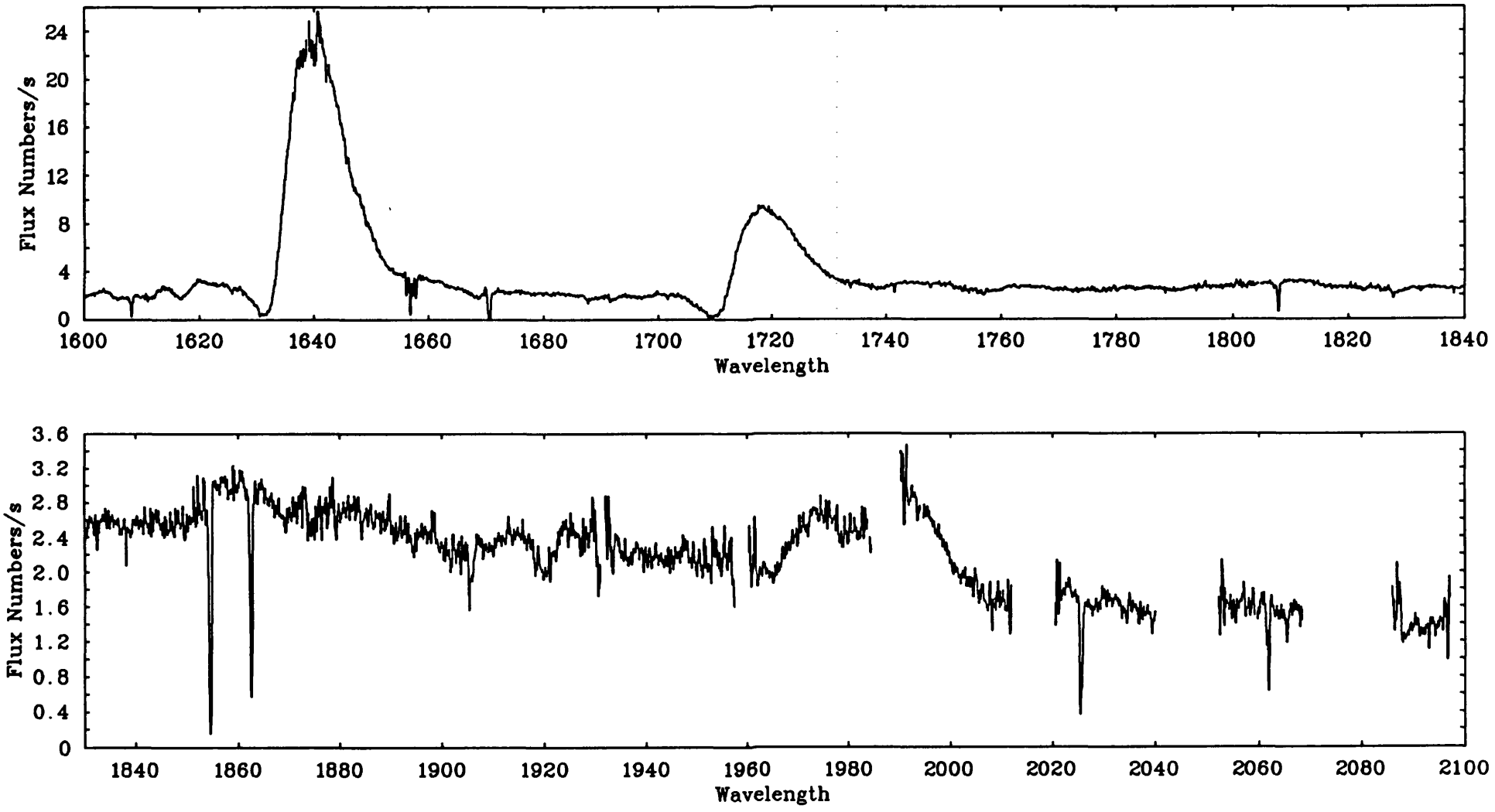

Figure A37 : WR 134 (HD 191765), WN 6, v=8.23

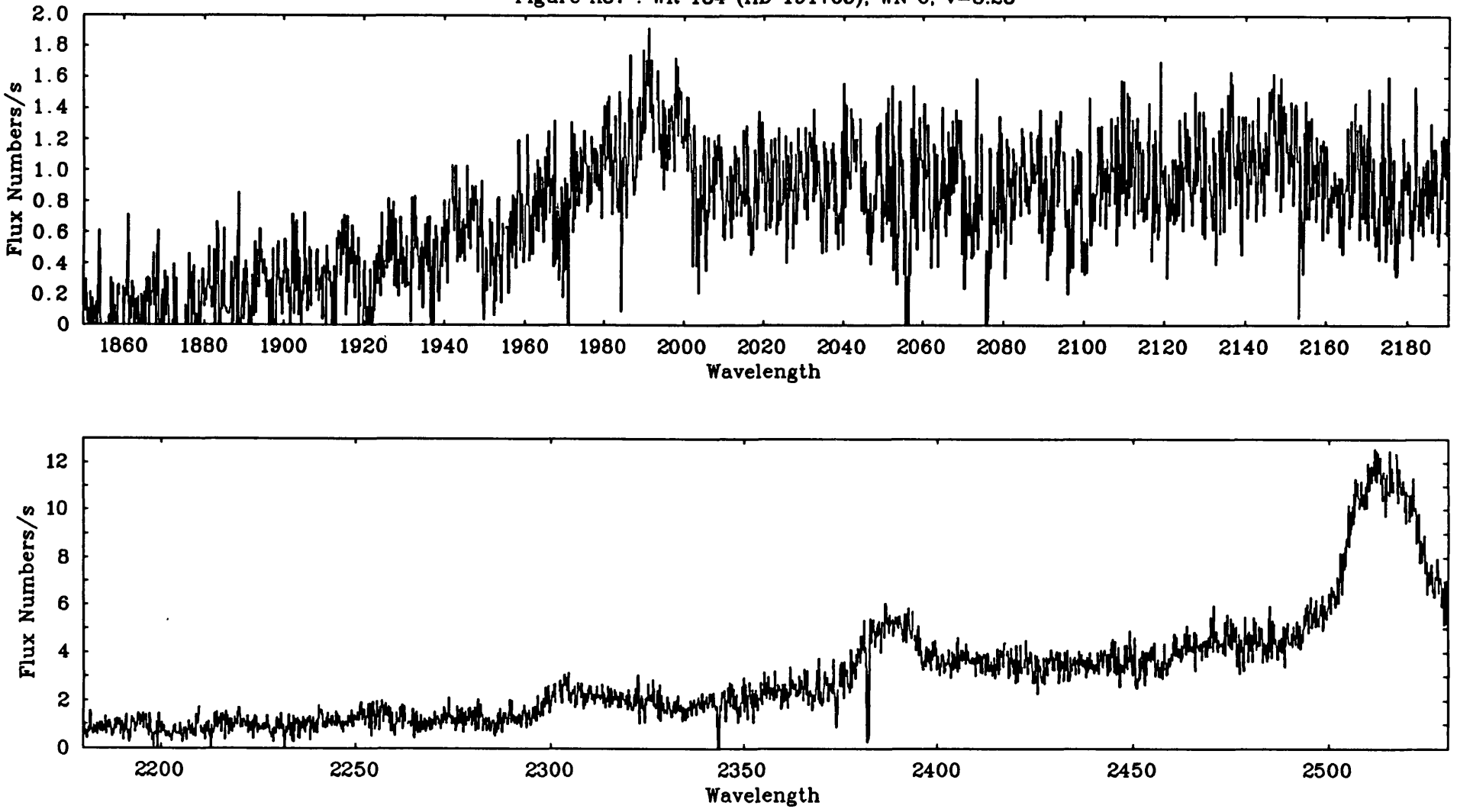

Figure A37 (continued) : WR 134 (HD 191765), WN 6, v=8.23

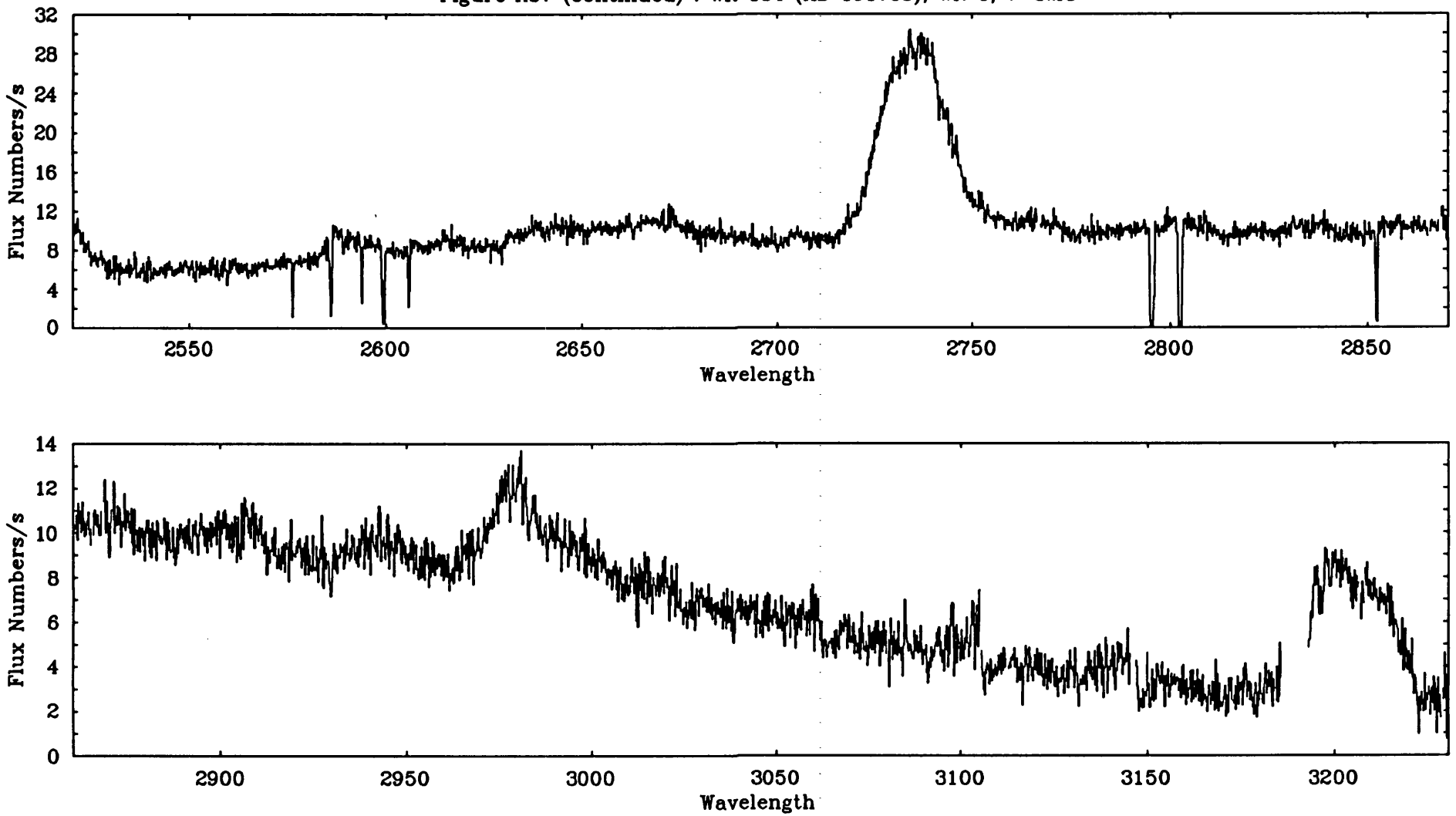

Figure A38 : WR 135 (HD 192103), WC 8, v=8.36

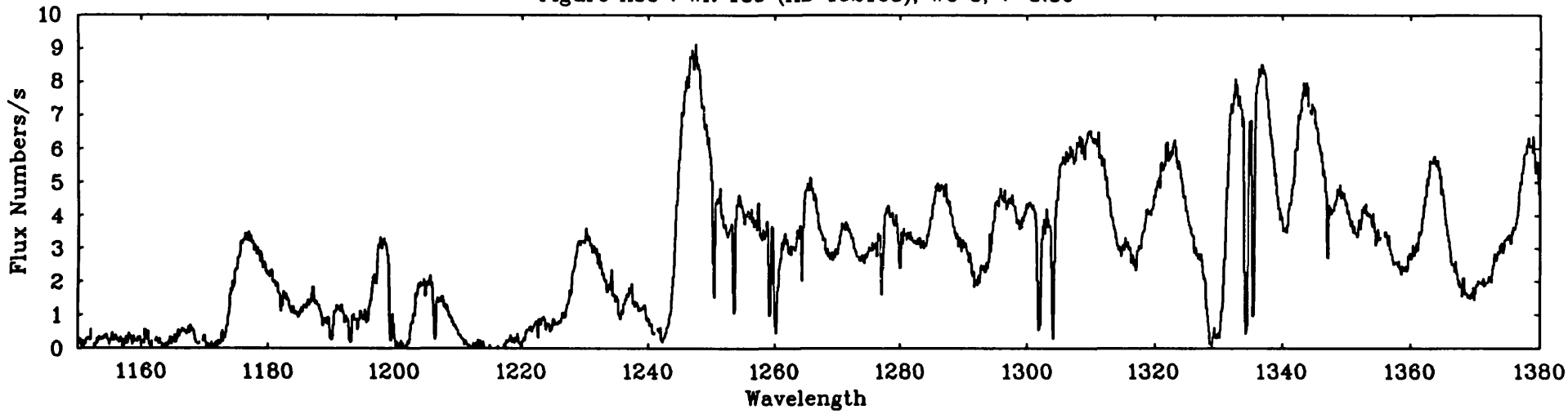

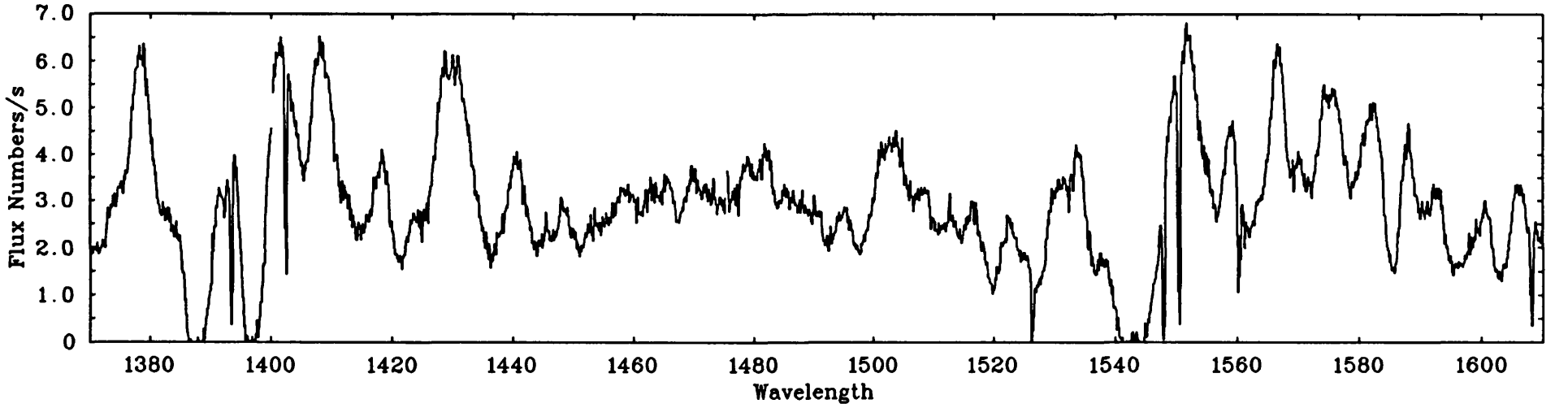

Figure A38 (continued) : WR 135 (HD 192103), WC 8, v=8.36

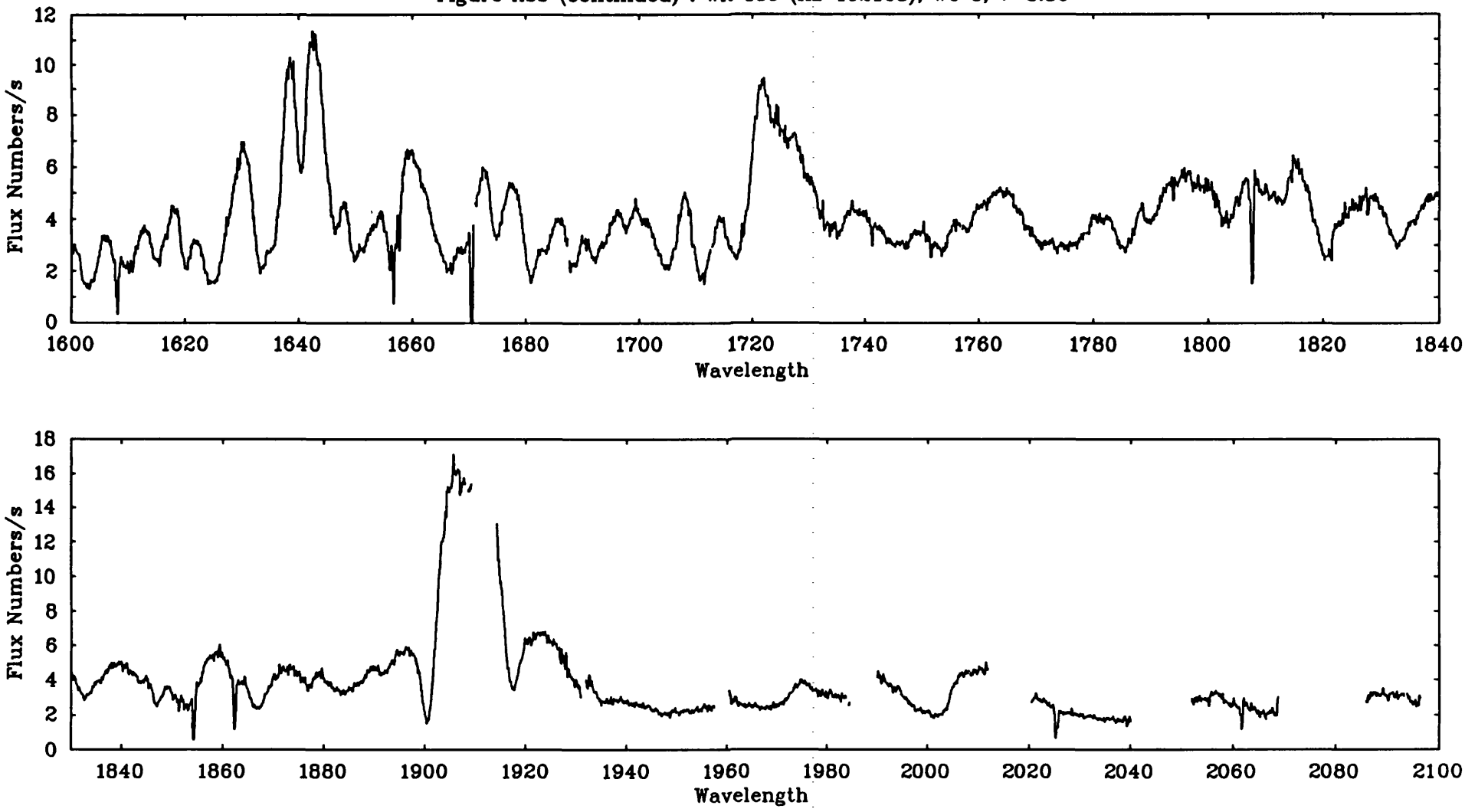

Figure A39 : WR 135 (HD 192103), WC 8, v=8.36

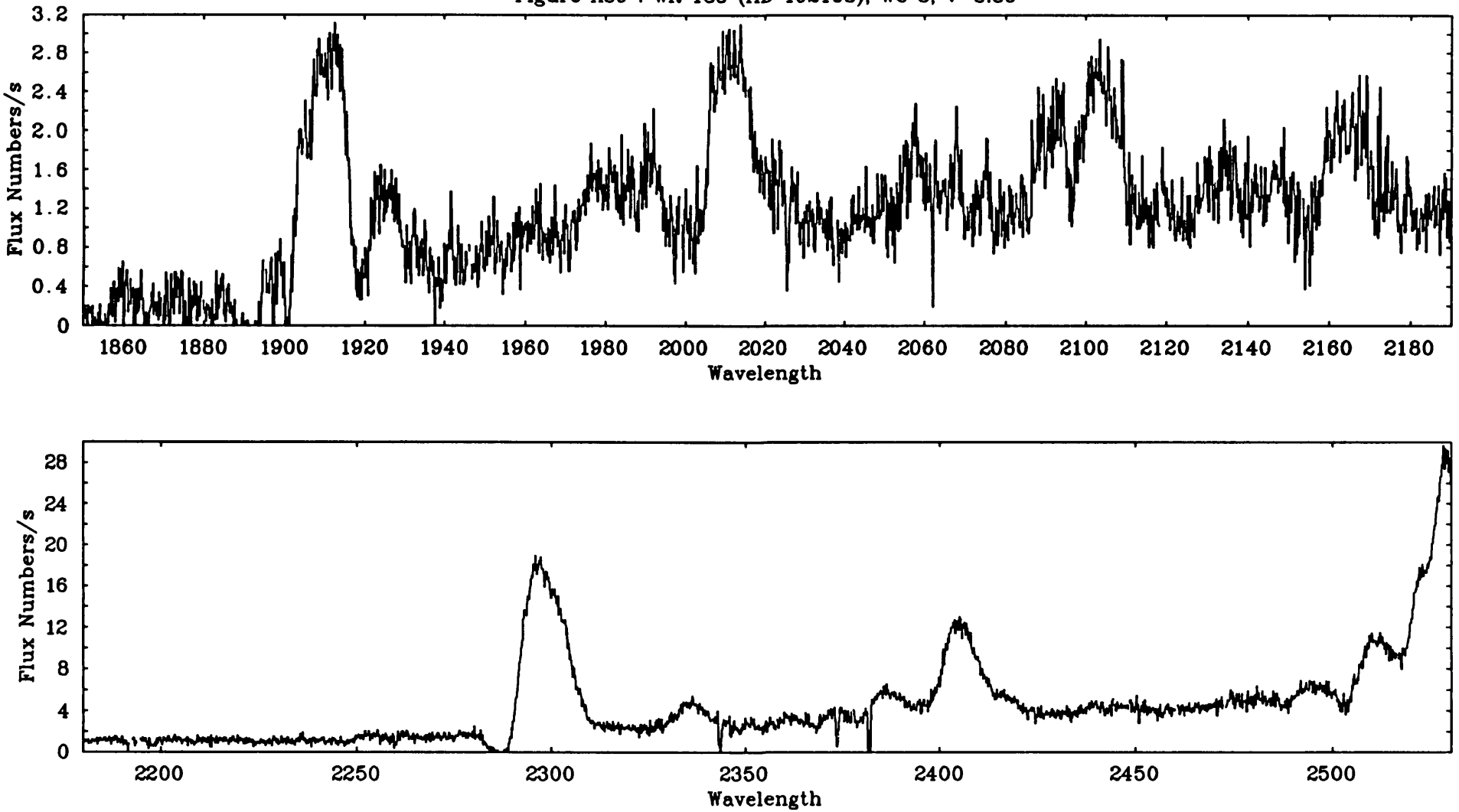

Figure A39 (continued) : WR 135 (HD 192103), WC 8, v=8.36

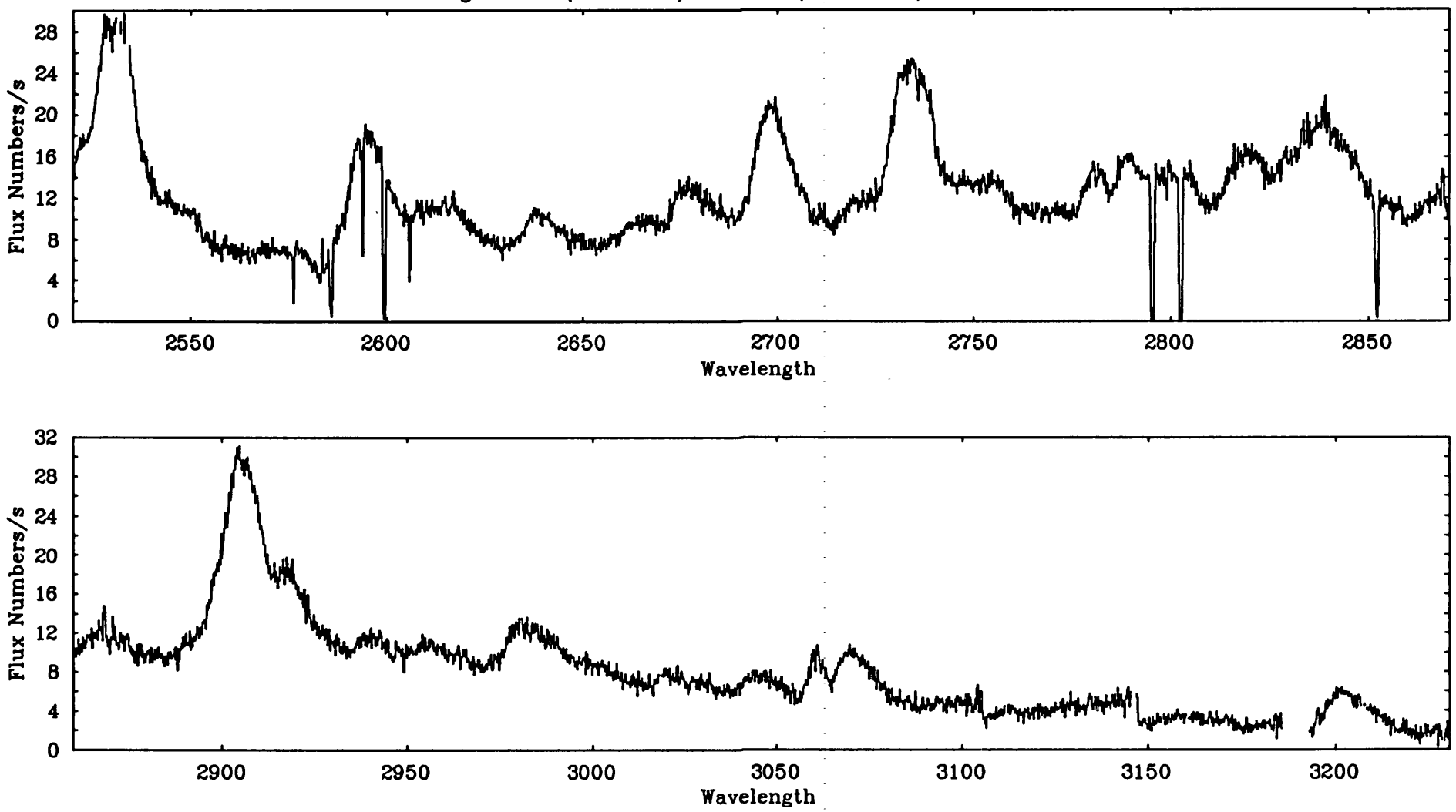

Figure A40 : WR 136 (HD 192163), WN 6, v=7.65

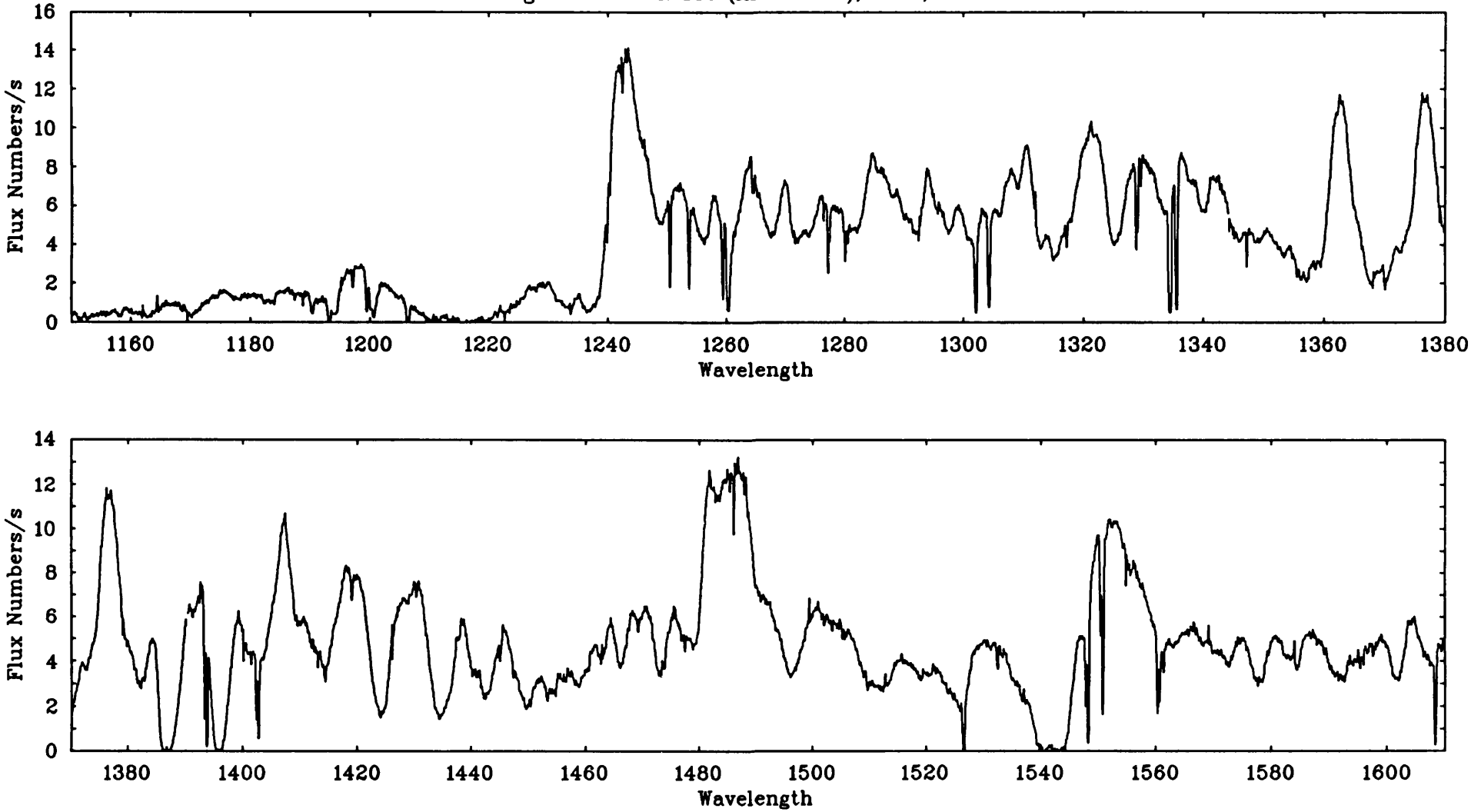

Figure A40 (continued) : WR 136 (HD 192163), WN 6, v=7.65

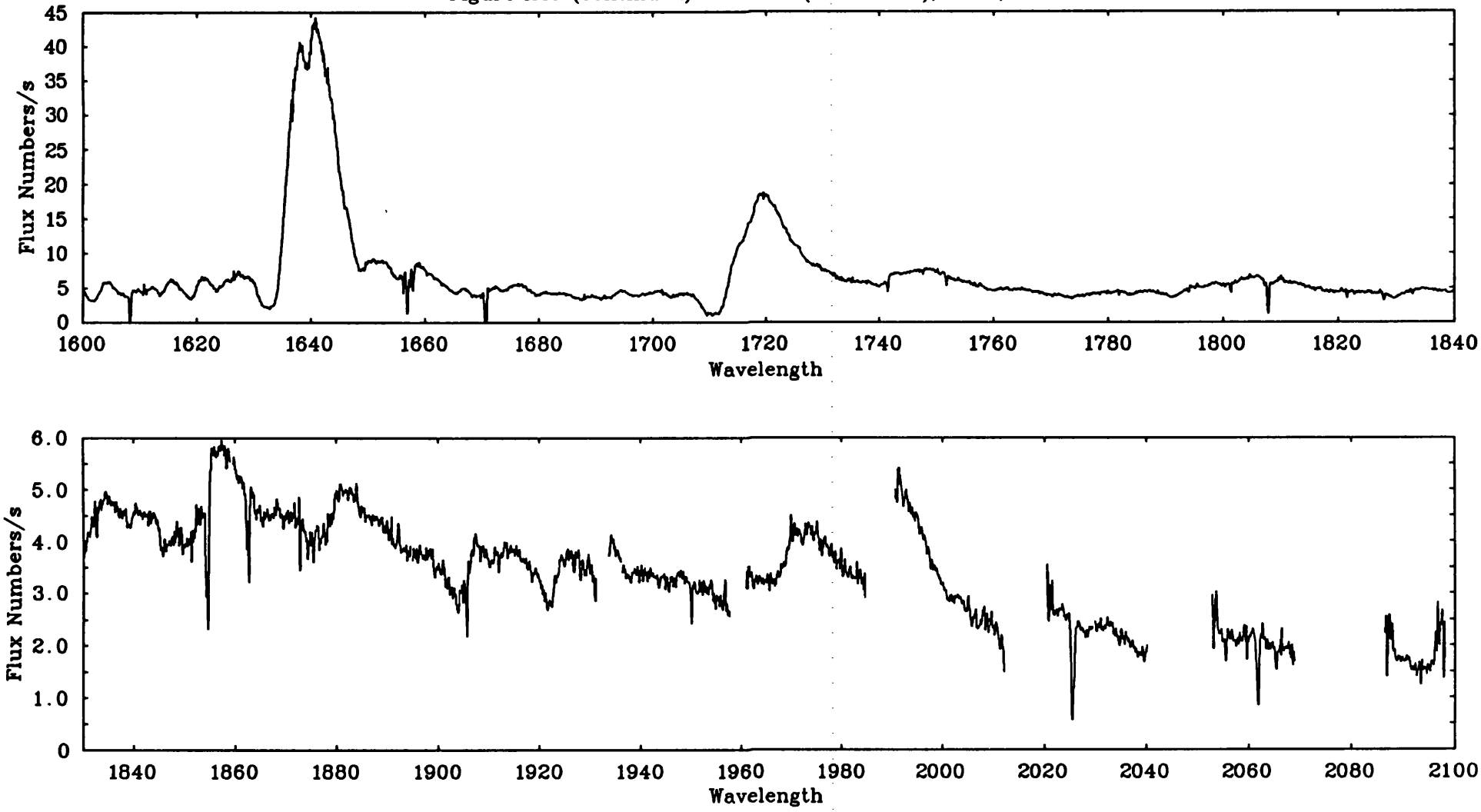

Figure A41 : WR 136 (HD 192163), WN 6, v=7.65

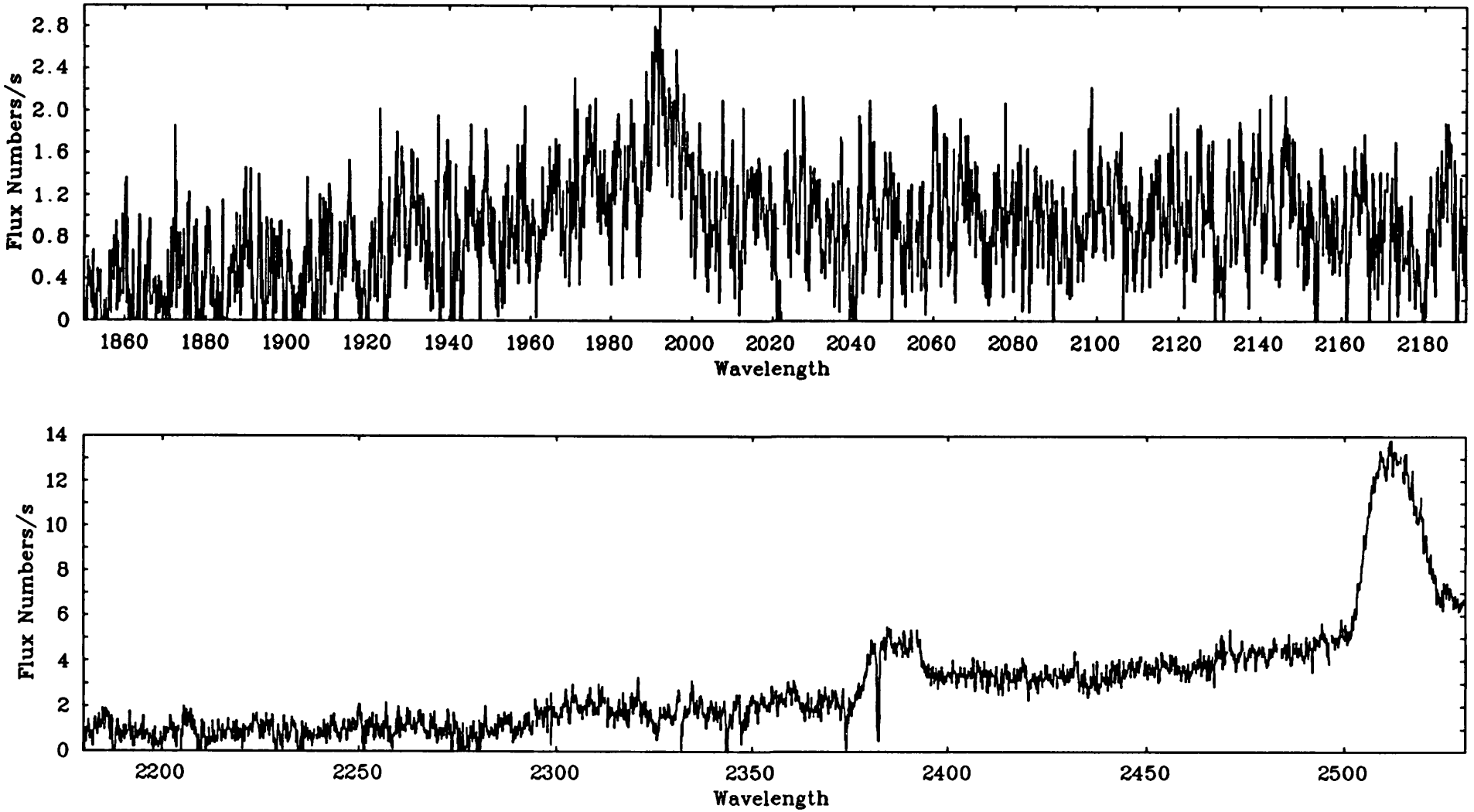

Figure A41 (continued) : WR 136 (HD 192163), WN 6, v=7.65

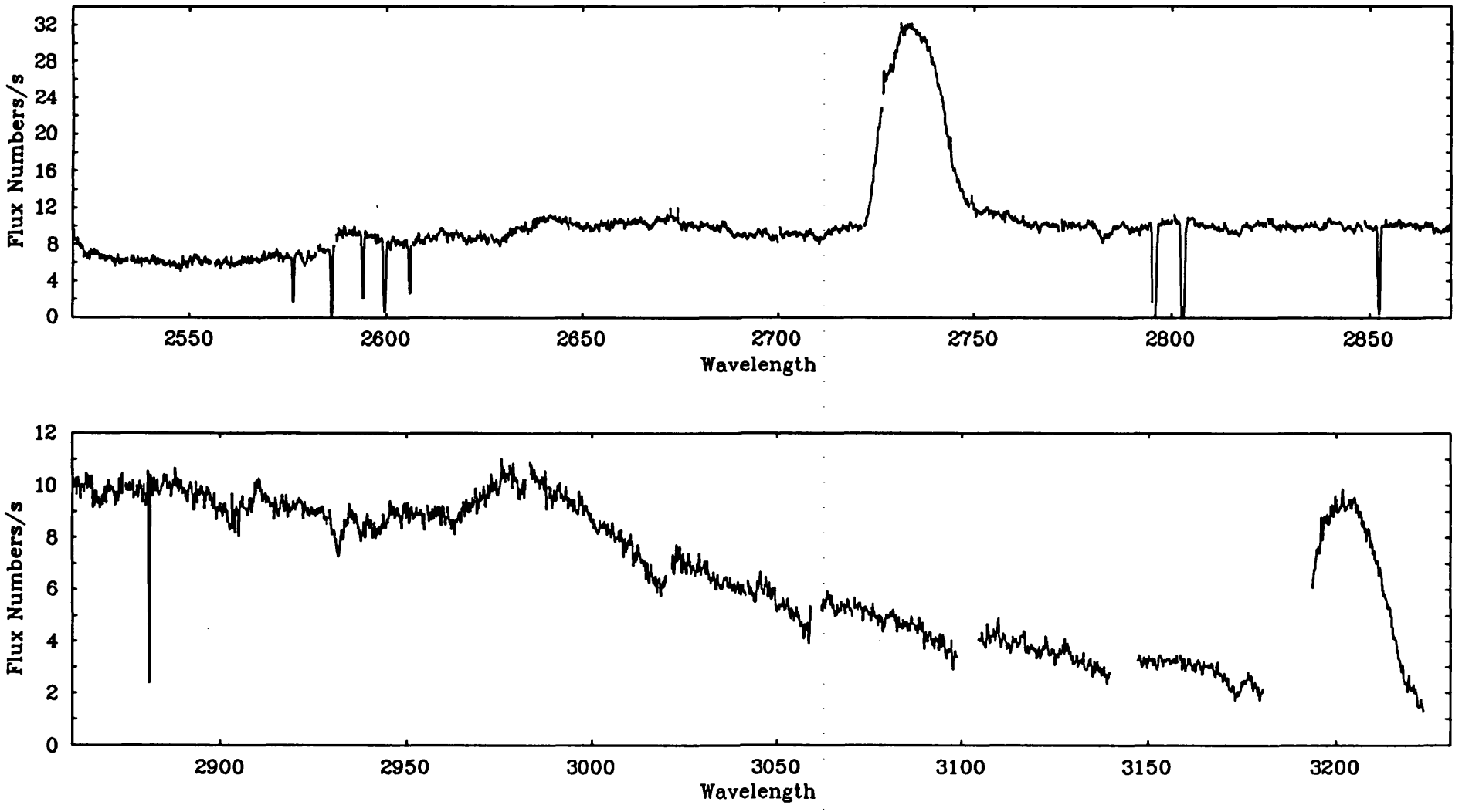

Figure A42 : WR 138 (HD 193077), WN 6 + abs, v=8.10

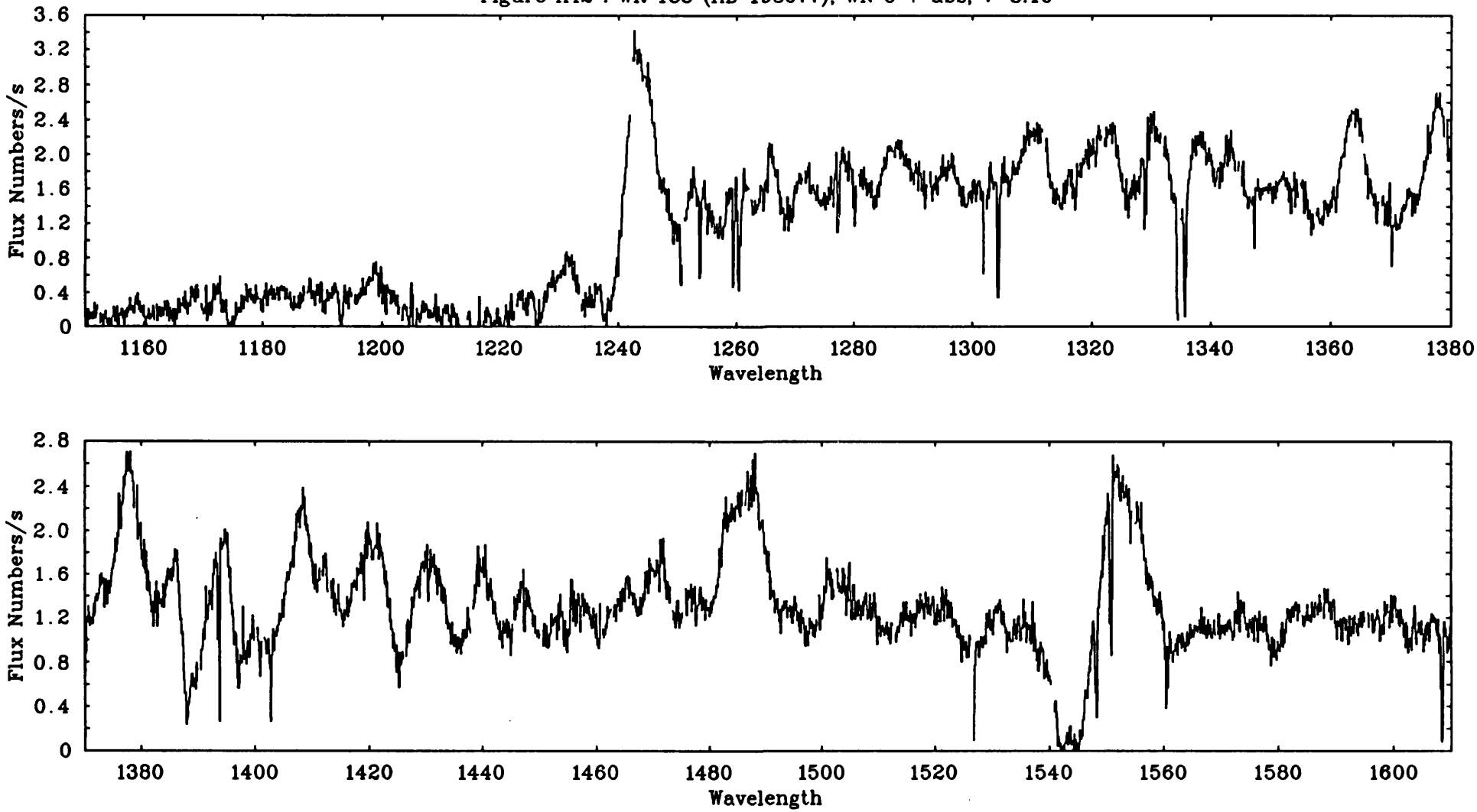

Figure A42 (continued) : WR 138 (HD 193077), WN 6 + abs, v=8.10

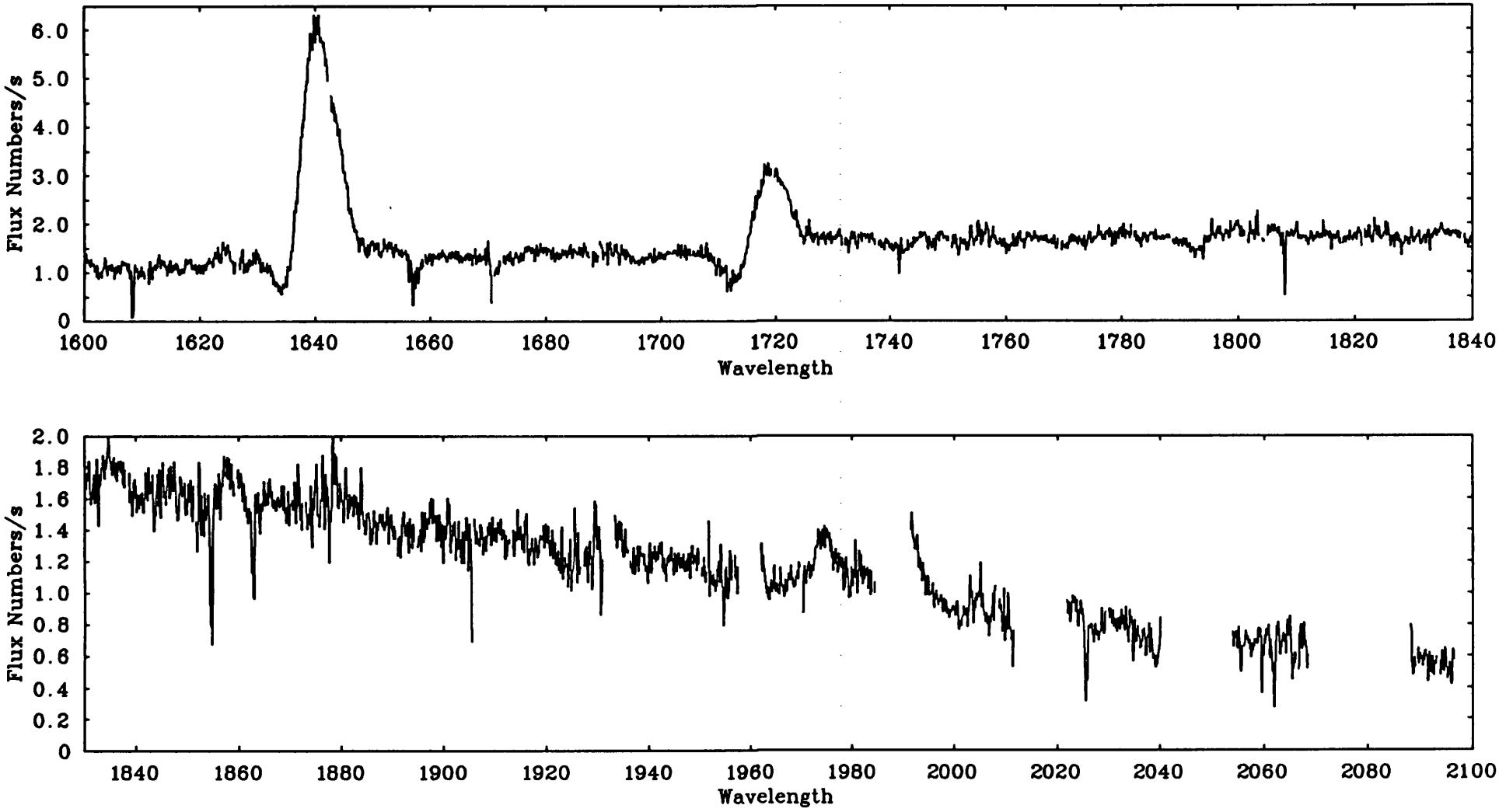

Figure A43 : WR 138 (HD 193077), WN 6 + abs, v=8.10

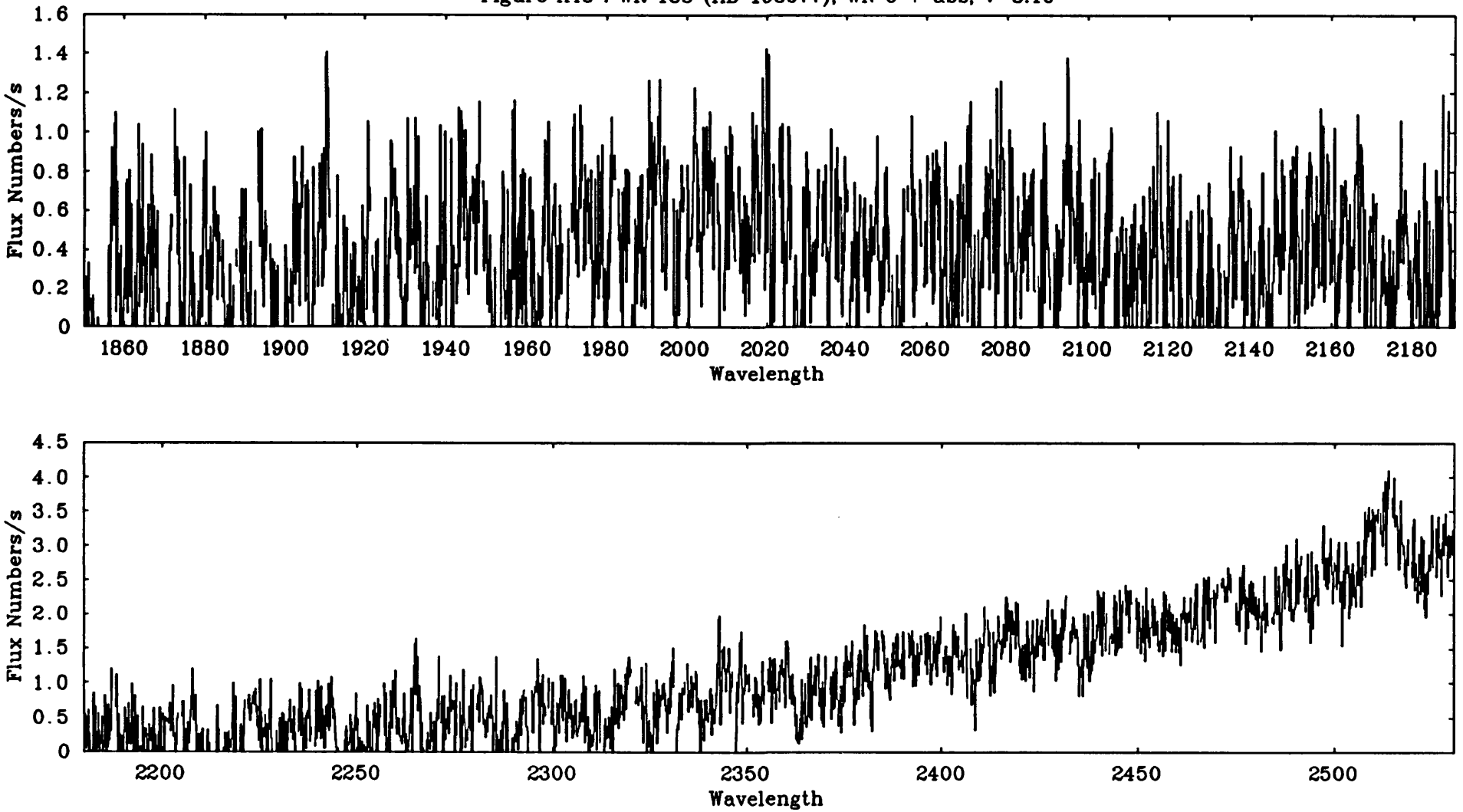

Figure A43 (continued) : WR 138 (HD 193077), WN 6 + abs, v=8.10

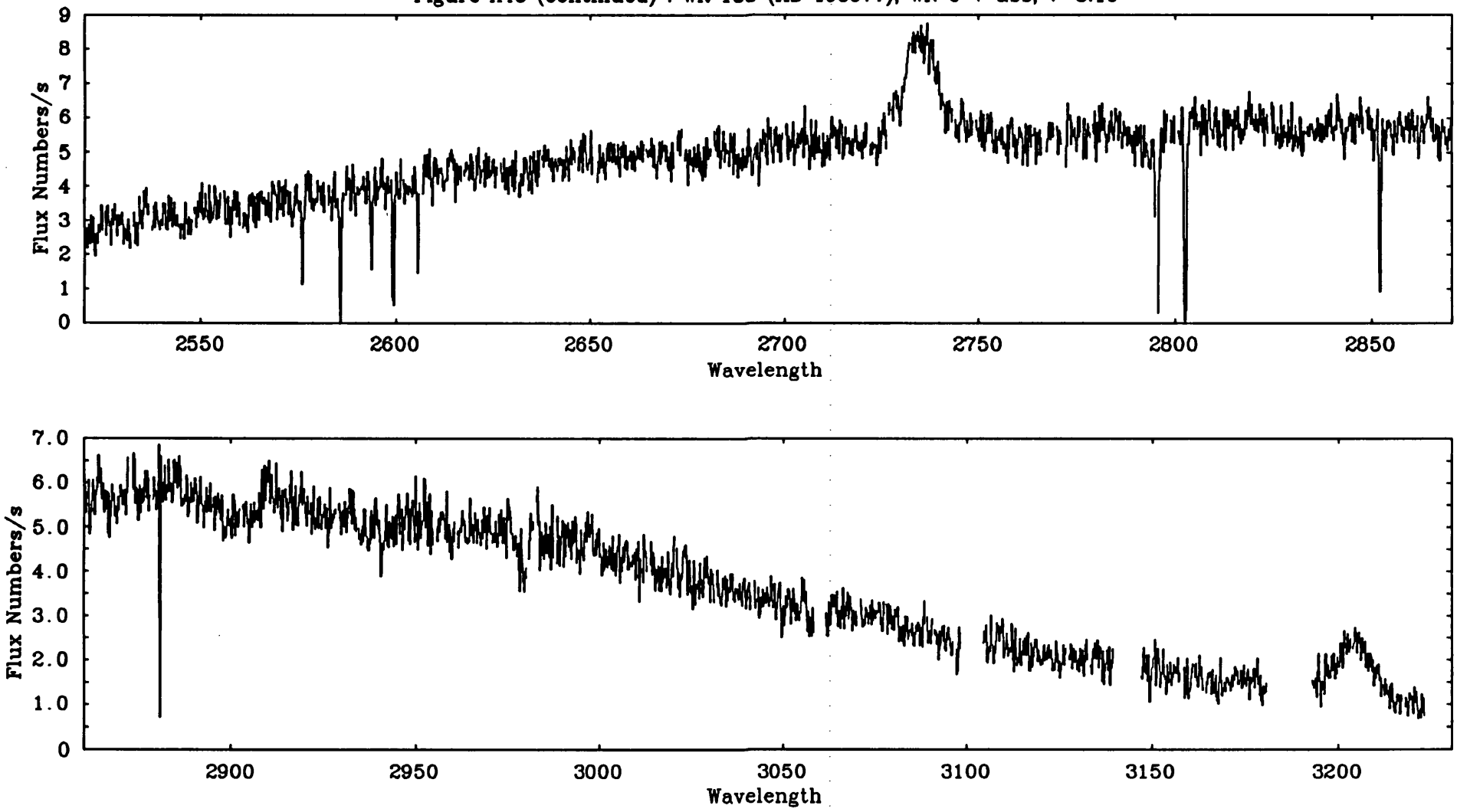

Figure A44 : WR 148 (HD 197406), WN 7 (SB1), v=10.46

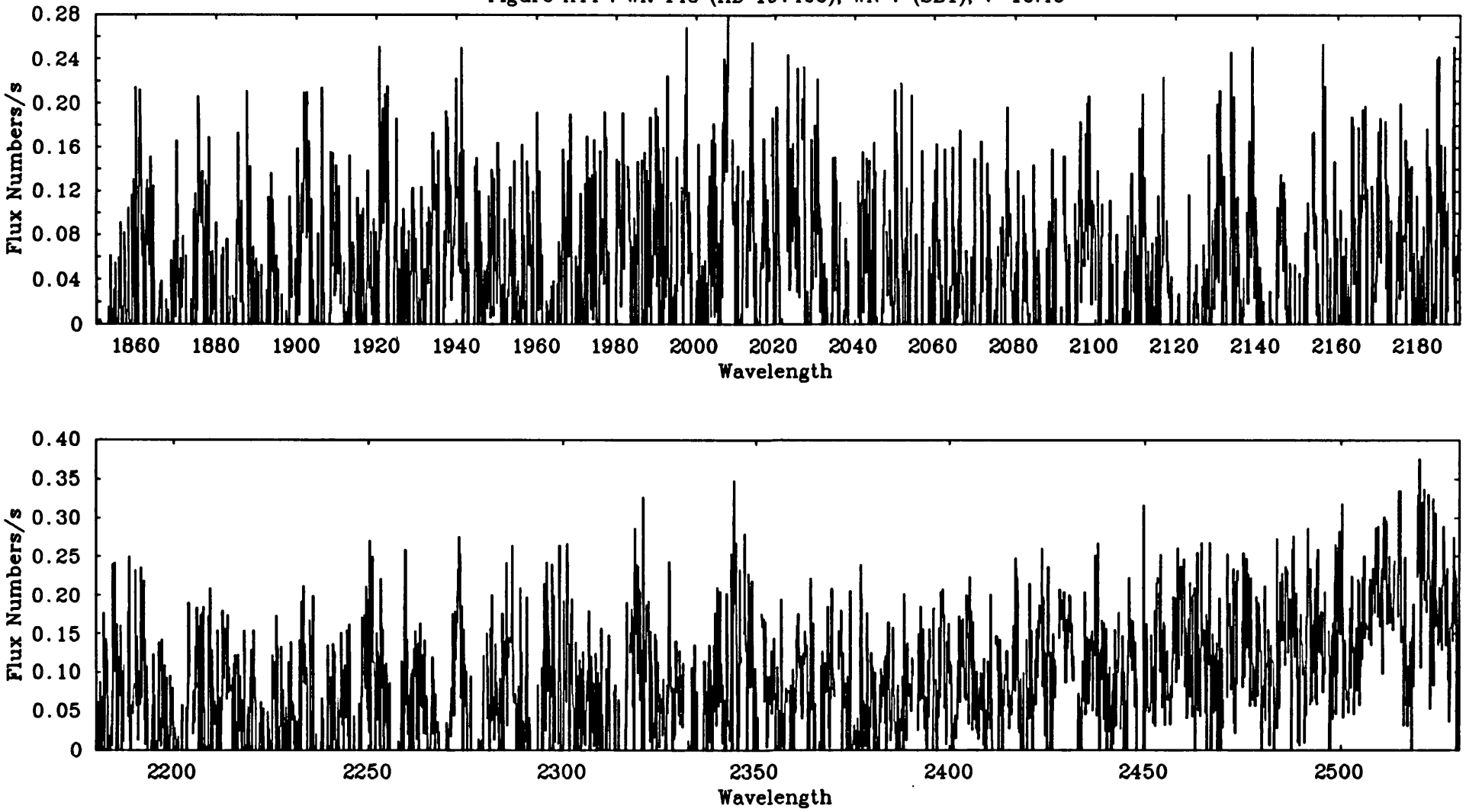

Figure A44 (continued) : WR 148 (HD 197406), WN 7 (SB1), v=10.46

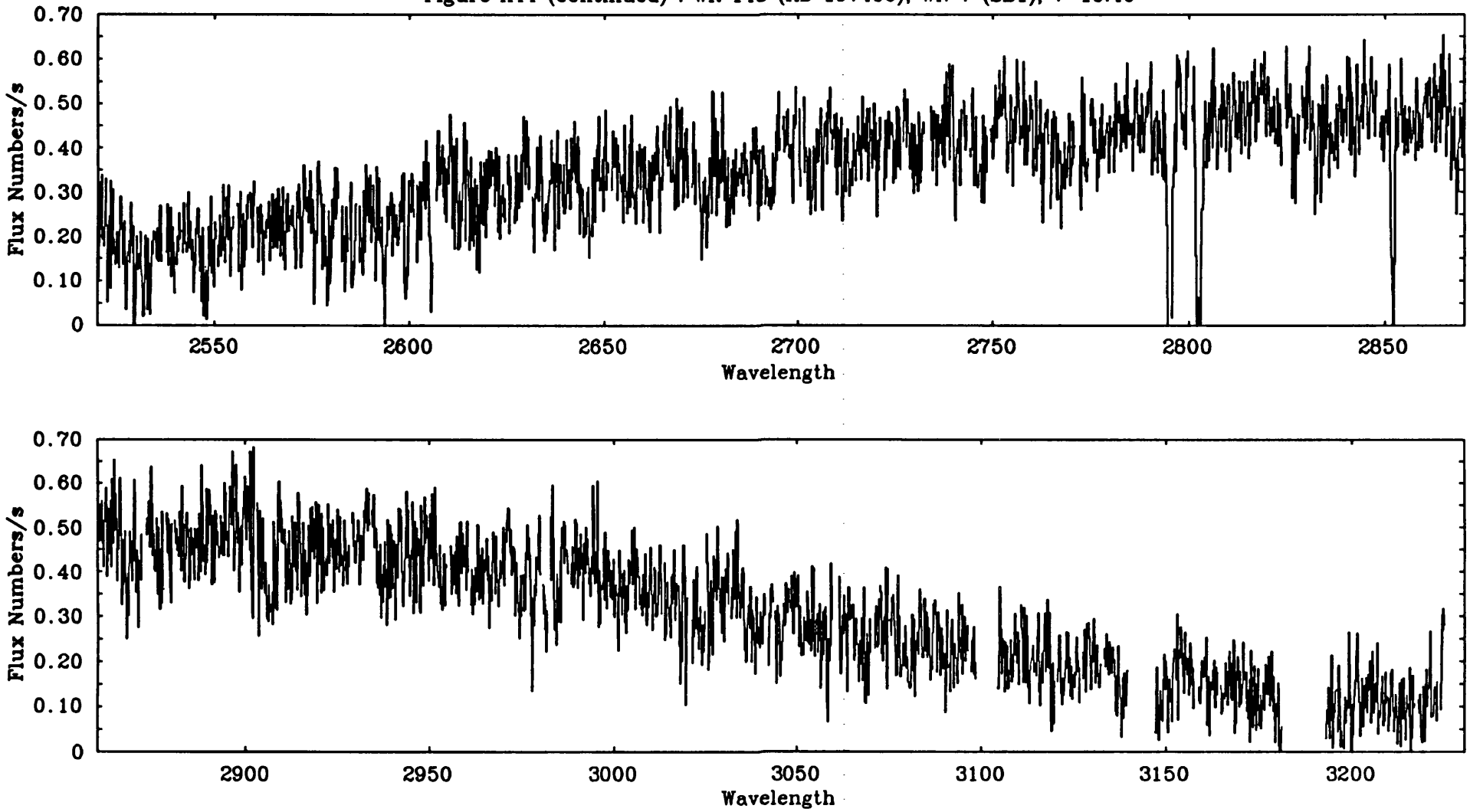

Figure A45 : WR 155 (HD 214419), WN 7 (SB1), v=8.75

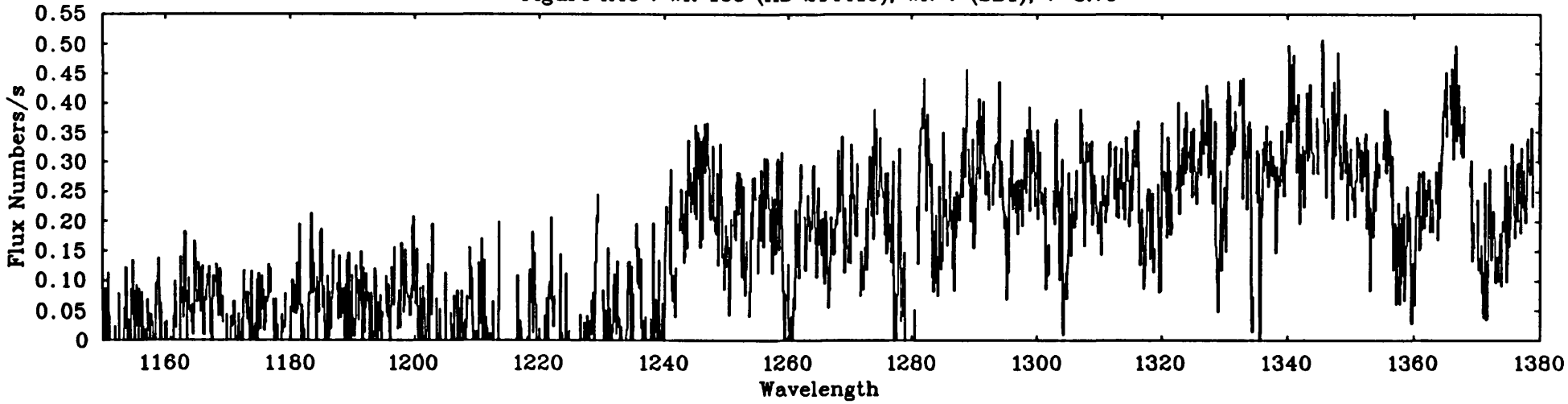

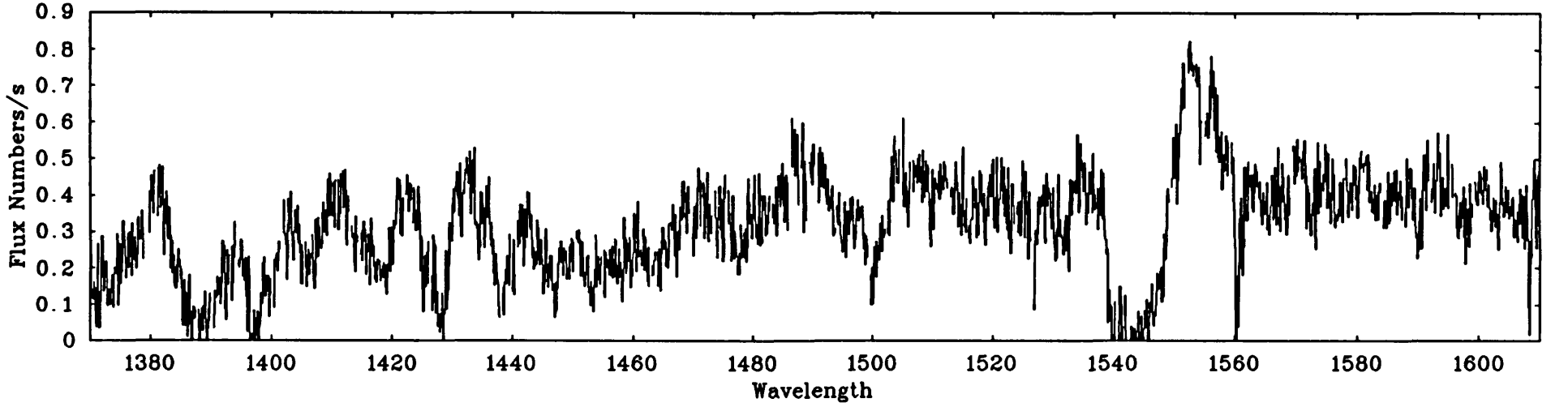

Figure A45 (continued) : WR 155 (HD 214419), WN 7 (SB1), v=8.75

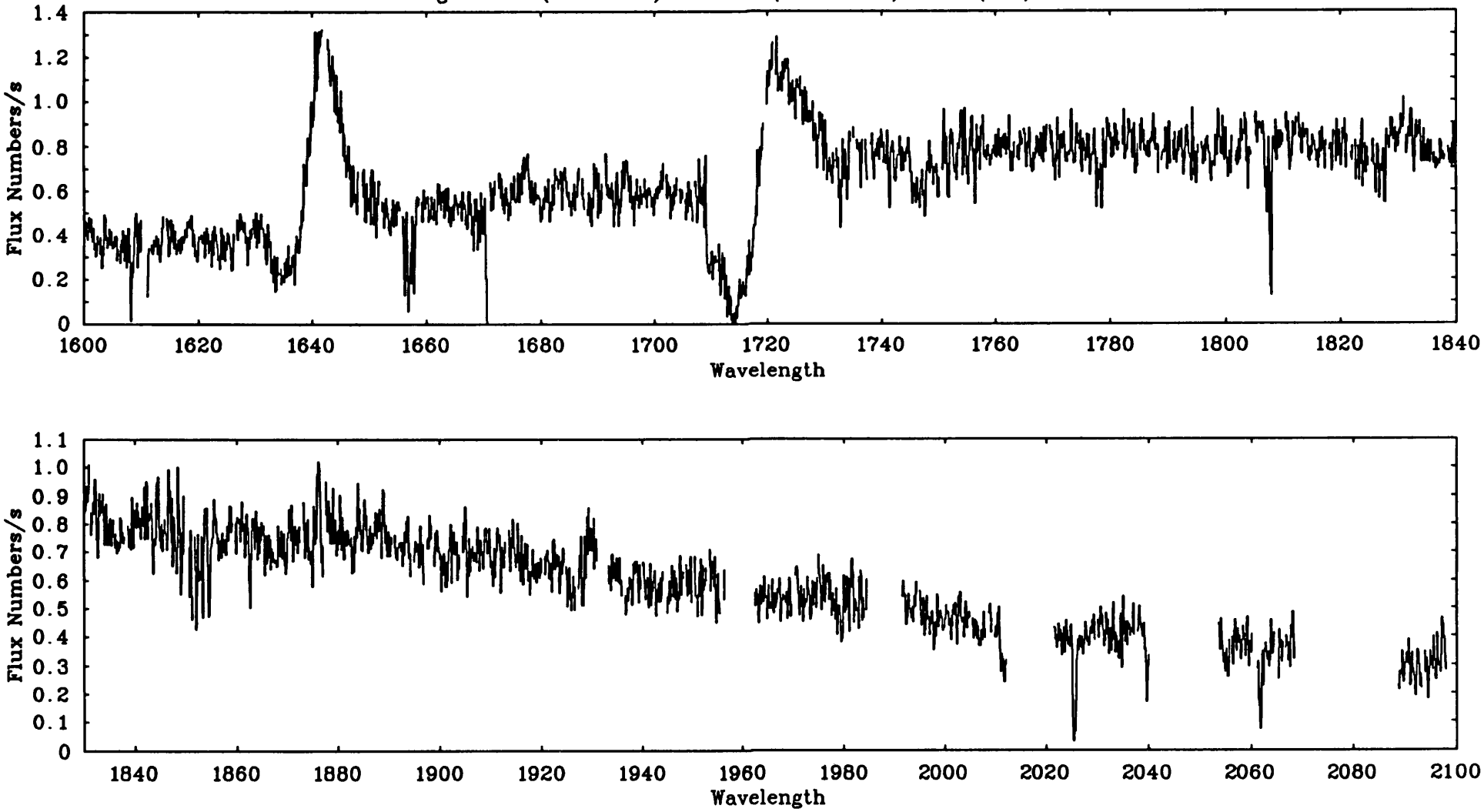

Figure A46 : WR 155 (HD 214419), WN7 (SB1), v=8.75

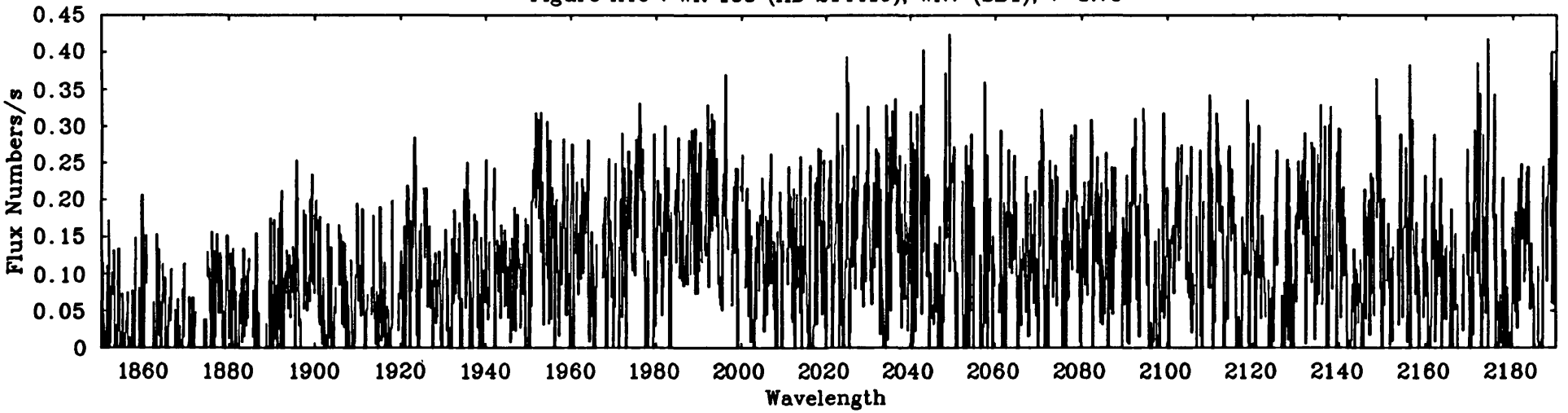

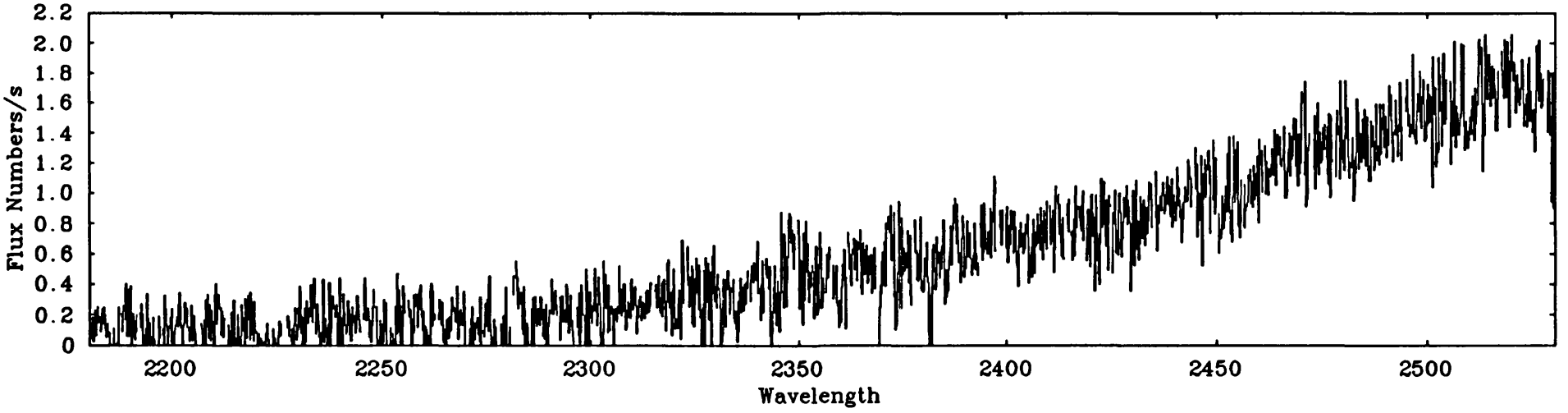

Figure A46 (continued) : WR 155 (HD 214419), WN7 (SB1), v=8.75